Intramolecular (3+2) cycloaddition reactivity between heteroatom-substituted alkynes and tethered alkynes: thermal and catalytic routes

Dominic Marcel Campeau

Thesis submitted to the University of Ottawa in partial fulfillment of the requirements for the Doctorate in Philosophy degree in Chemistry

Department of Chemistry and Biomolecular Sciences

Faculty of Science

University of Ottawa

© Dominic Marcel Campeau, Ottawa, Canada, 2024

Abstract

While 1,3-dipolar three-atom components are widely used in (3+2) cycloaddition chemistry, their exotic counterparts of *neutral* three-atom components are significantly less studied. These *neutral* three-atom components have a large synthetic potential, as their resulting (3+2) cycloadducts are zwitterionic and unstable in nature, providing new opportunities for functionalization and diversification.

In this thesis, the participation of heteroatom-substituted alkynes, a unique class of *neutral* three-atom components, in intramolecular (3+2) cycloadditions with tethered alkyne is described and further explored.

Specifically, alkyne-tethered ynamides and alkynyl sulfides were found to produce fused pyrroles and thiophenes, respectively. On the basis of experimental and theoretical studies, this thermally promoted process is proposed to occur through the stepwise formation of a (3+2) cycloadduct via diradical intermediates. These zwitterionic cycloadducts are highly reactive and provide a diverse array of pyrroles and thiophenes depending strongly on both scaffold substitution and reaction conditions.

Additionally, similar (3+2) cycloaddition processes involving ynamides or alkynyl sulfides tethered with *terminal alkynes* can be catalyzed at much lower temperatures in the presence of copper and silver salts. This catalytic process is suggested to employ mechanisms reminiscent of that of copper-catalyzed azide-alkyne couplings.

Acknowledgments

I am indebted most of all to Fabien. Your passion for organic chemistry is what convinced me to join the field in the first place, and I do not expect in my lifetime to get to work with a more enthusiastic chemist. I thank you for providing great opportunities all along my studies and pushing me to do my very best. I know that a large part of the success I have had came from the motivation you have provided over the years. I am quite proud of the work we have accomplished together and look forward to many future conversations over coffee about life and chemistry!

I have had the luck to spend multiple years in the Gagosz group working alongside our dependable postdoc David. Learning from your expertise on the subject, I have upgraded from being a curious undergrad to a confident organic chemist. I am very thankful for all the times you have provided guidance and answered my million questions as I learned to be a scientist. I can attest you have done the impressive job of keeping the lab both running and fun! I am very happy to have developed a friendship with you over the years, and I look forward to making many new memories together still in the future!

As I was trudging in the lab trying to understand this curious new chemistry we had stumbled upon, Alice bravely joined into that journey. It has been a blast to make new discoveries in the lab with you Alice, and you have been a wonderful colleague.

I have been quite fortunate that my graduate studies in the group overlapped over multiple years with Ali and Karim. I have really enjoyed my daily chemistry discussions on the board with you Ali: your literature knowledge is truly baffling. Karim: it has been a blessing to spend long hours with you in the lab. You have a very adventurous attitude towards chemistry that has been really fun to both watch and join into. I really hope to find again in the future such wonderful colleagues as yourselves!

I would also like to thank all the members of the Barriault group I have had the chance to overlap with over the years. The greatest improvement in my understanding of reaction mechanisms happened in our joint group meetings, where I have learned a lot from senior members of the Barriault group. I am really happy to have developed a sense of camaraderie with many fellow grad students in the Barriault group over the past several years.

A large thank you is also deserved by my dear parents and family. You have given me a lot of support throughout the years as I have figured out my own path in my studies and in life. Thank you for having

given me the freedom to make all of these choices and unequivocally supporting the decisions I have made. I know that it is because of your support that I have felt comfortable following my passion.

Finally, I would like to express all of the gratitude I possibly can to my partner in life, Ria. While our own journeys may have taken us to different places during our studies, I have been very fortunate to count on your love, friendship and support even from afar. Despite my choice of a topic of research that is quite difficult to discuss, I thank you for providing an immense amount of emotional support during this time.

Concerning the style of the thesis

The contents of Chapters 2,3 and 4 consist mainly of results previously published in three full research articles, whose manuscripts were originally written by myself. The figures and discussion used in this thesis are directly adapted from these articles, modified to follow the style of a thesis, and each article is properly referenced at the beginning of every chapter.

Statement of contributions

The three articles adapted herein consist of joint experimental results obtained by myself, Alice Pommainville, and Mila Gorodnichy. Major contributions to the work in Chapters 3 and 4 were performed by Alice Pommainville. Minor contributions by Alice Pommainville in Chapter 2 and Mila Gorodnichy in Chapter 4 are also included. All results contributed by A.P. and M.G. are clearly indicated in the concerned figures. All of the remaining results presented herein has been accomplished by myself unless otherwise noted.

Table of contents

1. Chapter 1 – Introduction

1.1. Thermal cycloadditions

Cycloadditions are a class of cyclization reaction involving the formation of two new bonds from two unsaturated fragments **1.001** to generate cycloadducts **1.003** (Figure 1-1). Thermally-allowed (and pericyclic) cycloadditions, as introduced by Woodward and Hoffmann,[1] possess cyclic transition states **1.002** involving [4n+2] π electrons. While the Diels-Alder reaction is a classical example of [4+2] cycloadditions (where n=1), 1,3-dipolar cycloadditions also involve [4+2] π electrons, yet only (3+2) atoms.

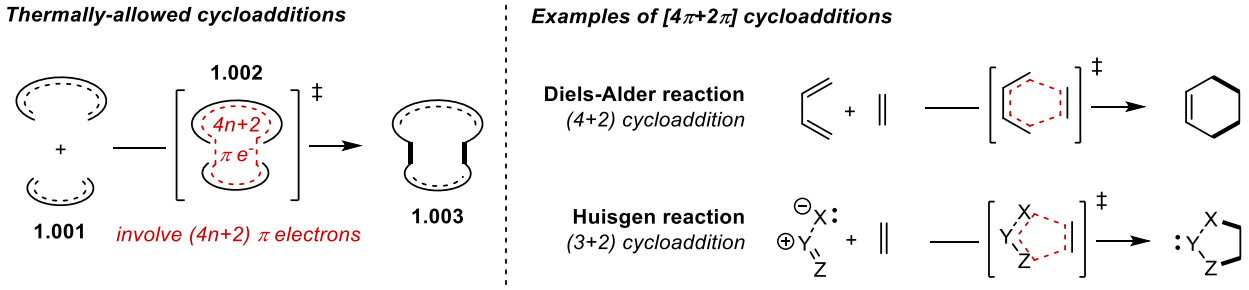

Figure 1-1. Examples of relevant thermally allowed cycloadditions.

1.2. Thermal 1,3-dipolar cycloadditions

The (3+2) cycloaddition of "1,3-dipoles" is a very well-studied area in synthetic organic chemistry. While sporadic instances of relevant (3+2) additions had been reported as early as the 1880s,[2] this class of cycloaddition was first conceptualized by Rolf Huisgen in the 1960s as "1,3-dipolar cycloadditions".[3-4] These cycloadditions, which are now sometimes dubbed "Huisgen cycloadditions", involve the reaction between a 1,3-dipole **1.004** and a "dipolarophile" **1.005** bearing a reactive unsaturation (Figure 1-2). A (3+2) cycloaddition occurs between these two reactants to provide a 5-membered cycle **1.006** devoid of partial charges in its Lewis structure, with varying degrees of saturation, depending on whether allyl-type **1.007** or propargyl-allenyl type **1.008** 1,3-dipoles are utilized. Although they are overall neutral, the name of "1,3-dipole" was given to this class of structures, as the only way to satisfy the octet rule while drawing their Lewis structures is to assign charges. It has been noted by Breugst and Reissig[5] that Huisgen later regretted the name of "1,3-dipoles", as these species do not possess high dipole moments, which may be misleading.

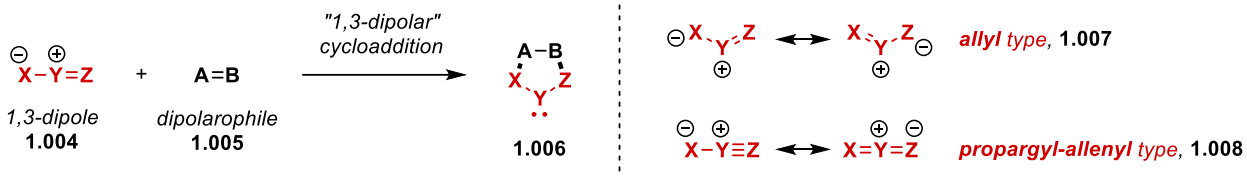

Figure 1-2. The 1,3-dipolar cycloaddition (or the Huisgen reaction)

1,3-Dipolar cycloadditions have had a monumental impact in the field of chemistry, and the topic is much too large to be covered herein. Many reviews, books and chapters have however been written on the topic, covering its history[5] and its wide-reaching applications, such as in the fields of natural product synthesis,[6] material science[7-8] and biorthogonal chemistry.[9-10]

1.2.1. The evolving mechanistic understanding of 1,3-dipolar cycloadditions

Backing his original review of the topic in 1963,[4] Huisgen also published on the kinetics and mechanism of the 1,3-dipolar cycloaddition, based on a series of results obtained by his laboratory.[11] He proposed that 1,3-dipolar cycloadditions generally proceed through a concerted mechanism, directly leading from reactants to the observed cycloadducts through a 5-membered transition state **1.009** (Figure 1-3).

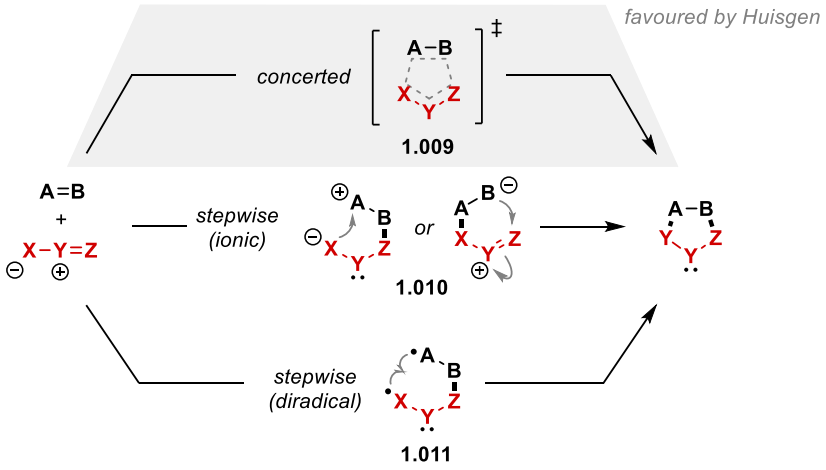

Figure 1-3. Original possible mechanisms evoked for 1,3-dipolar cycloadditions.

This mechanism, as opposed to the alternate mechanisms involving ionic **1.010** and biradical **1.011** intermediates, was based on many observations: high stereoselectivity, low dependence on solvent polarity, high entropic contribution to the activation energy, to name a few.

Huisgen recognized early on that a bent geometry is necessary at the transition state to favour a concerted process, explaining the significantly higher rates of reactivity within the allyl class of 1,3-dipoles.[11] He proposed that, at the "activated complex" with dipolarophiles, propargyl-allenyl type dipoles **1.012** take a bent conformation **1.013**, associated with electronic reconfiguration to place a lone pair of electrons on the central nitrogen atom (Figure 1-4). This optimal overlapping of the participating pi systems in the 1,3-dipole and dipolarophile would permit a concerted (3+2) cycloaddition to take place, associated with a reorganization of the cycloadduct to a more favourable planar geometry **1.014**.

Huisgen's molecular orbitals considerations (1963):

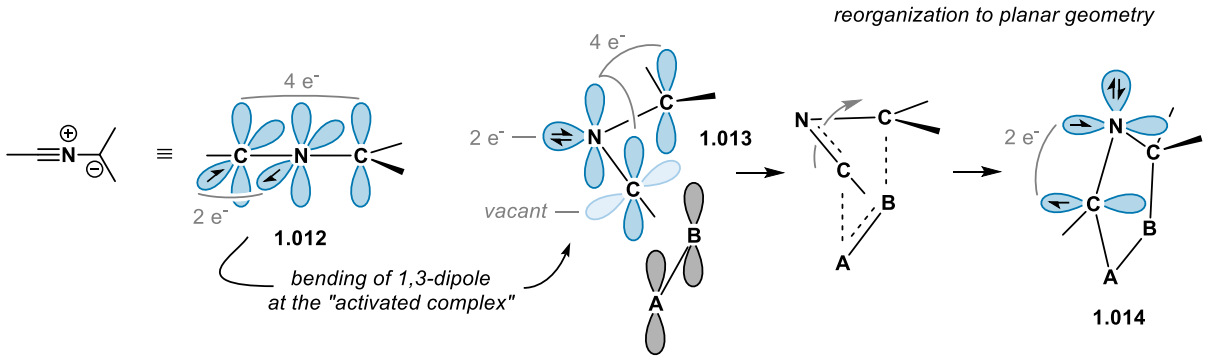

Figure 1-4. Huisgen's early MO drawings describing 1,3-dipolar cycloadditions.

In order to explain substituent effects which seemed to vary in different classes of 1,3-dipoles, Sustmann later evaluated the multiple frontier molecular orbital (FMO) interactions possible with perturbation theory, and separated cycloadditions as either type I, II or III (Figure 1-5).[12-13] In type I, the main contributing interaction at the activated complex is between the HOMO of the dipole and the LUMO of the dipolarophile are involved. In type III, it is the inverse: involving mainly the LUMO of the 1,3-dipole and the HOMO of the dipolarophile. In type II, both of these interactions participate significantly.

Classification of 1,3-dipolar cycloadditions by Sustmann (1971-1974):

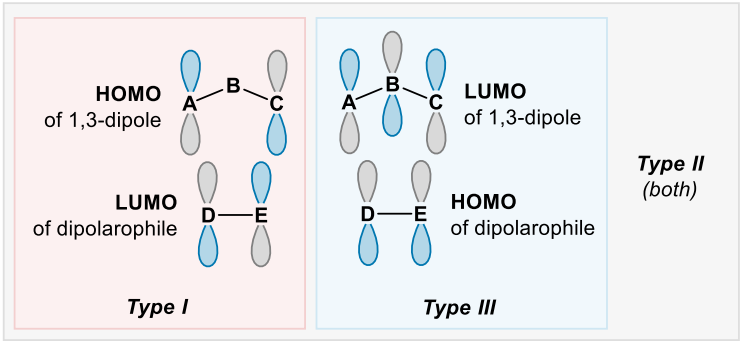

Figure 1-5. Type I, II and III 1,3-dipolar cycloadditions.

This classification was used by Sustmann to qualitatively explain the curious case of phenyl azides, where adding either electron-donating or electron-withdrawing substituents on the dipolarophile both increase the rate of cycloaddition (i.e. a type II cycloaddition).[14]

In the meantime, some scientific disagreement took place in the late 1960s involving back-to-back communications between Firestone[15] and Huisgen[16] concerning the possible intermediacy of diradical intermediates. Firestone argued that some trends observed, such as low dependency on solvent polarity and reactivity differences between alkyne and alkene dipolarophiles, could be rationalized by a diradical mechanism. Yet it seems that the concerted mechanism has been favoured over time, and is covered in textbook materials to this date.

Although the concept has changed little from then until now, there are several contributions that divulge interesting facets of the 1,3-dipolar cycloaddition. For example, Houk and Ess reported in 2007 having found a linear correlation between the "distortion energy" (previously described as "deformation energy" by Morokuma[17] and "activation strain" by Bickelhaupt[18]) of the 1,3-dipole at the transition state, and the activation energy itself (Figure 1-6).[19] Within this frame of thought, the authors calculated the difference in enthalpy between the ground state structure of the 1,3-dipoles **1.015** and its "distorted" shape **1.016** extracted from the transition state **1.017**, this difference in enthalpy was called the "distortion energy" (ΔH_D). The smaller difference between the transition state enthalpy (ΔH_T) and the distortion enthalpy was found to be relatively constant across the series of 1,3-dipoles studied and was called the "interaction energy".

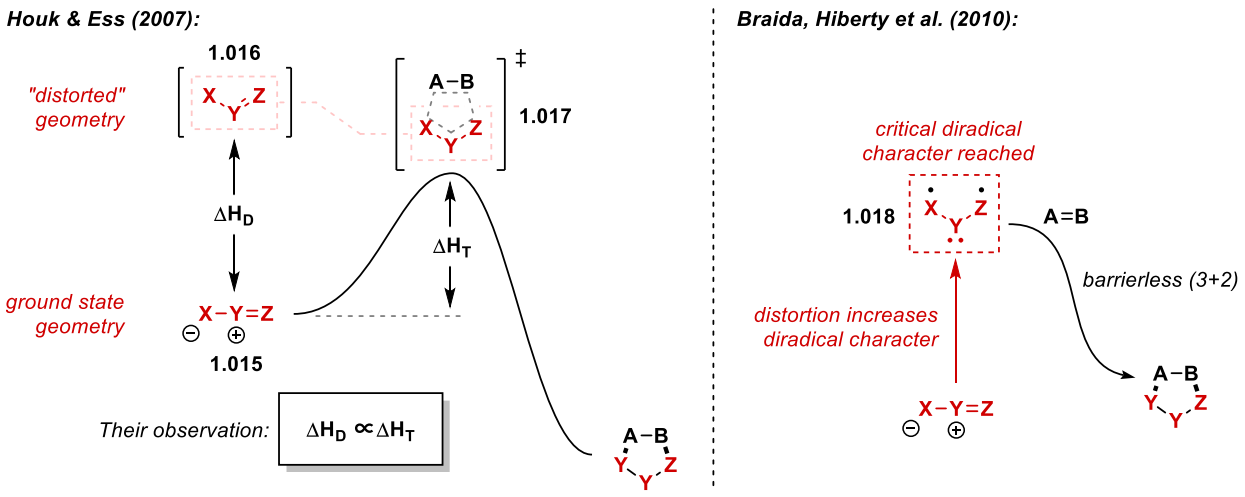

Figure 1-6. The distortion-interaction model of 1,3-dipolar cycloadditions invoked by Houk & Ess, and Braida & Hiberty's modification taking in account diradical character.

Taking it one step further, Braida, Hiberty and coworkers found that the distorted geometries investigated by Houk et al. possess a high and consistent diradical character when analyzed through a breathing orbital valence bond (BOVB) framework (Figure 1-6).[20] So, they supplemented Houk's model by proposing that, in their reactive conformation, 1,3-dipoles are distorted to a shape possessing a certain critical level of diradical character **1.018**, which then undergoes a barrierless (3+2) cycloaddition with dipolarophiles. This correlates well with the "concerted diradical" mechanism proposed earlier by Harcourt in the 1970s, which was also attained through the lens of valence bond theory.[21-22]

Additional approaches that do not necessarily involve analysis through frontier molecular orbital (FMO) models are also worthy of note. Domingo has alternatively applied the molecular electron density theory (MEDT) framework he developed to 1,3-dipolar cycloadditions.[23] MEDT rather consists of the analysis of how the electron density distributed within a system changes along multiple points of a reaction pathway, and using this to explain chemical reactivity. While the chemistry described herein will not be analyzed through Domingo's MEDT, his introduction of the term three-atom components (TACs), "a neutral species whose core framework is constituted by three continued heavy nuclei sharing an electron density of at least 8 electrons",[23] is particularly fitting and will be used throughout this thesis.

1.3. "Neutral" 3+2 cycloadditions

In the case of 1,3-dipolar cycloadditions, 1,3-dipoles **1.019** react with a dipolarophile in (3+2) cycloaddition to provide neutral cycloadducts **1.020**, which is often the reaction endpoint (Figure 1-7). By removing the formal charges on the three-atom component, one could envisage the presence of an analogous class of "neutral" (3+2) cycloadditions. In this case, neutral three-atom components **1.021** (isoelectronic to their dipolar counterparts) would react with a certain π unsaturation in a (3+2) cycloaddition to provide *zwitterionic* cycloadducts **1.022**. Considering that 1,2-zwitterionic species are often reactive, these zwitterionic cycloadducts may be reaction intermediates, rather than endpoints, and could lead to subsequent chemistry.

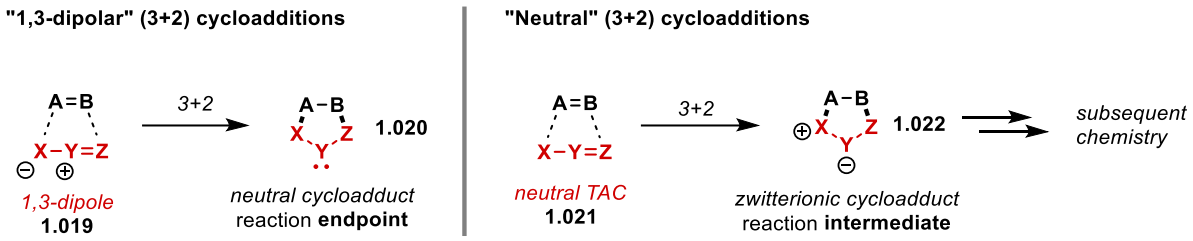

Figure 1-7. The difference between "1,3-dipolar" and "neutral" (3+2) cycloadditions.

Anticipating that these "neutral" (3+2) cycloadditions are likely to be much less exothermic than 1,3-dipolar cycloadditions, the mechanism by which these could take place may vary significantly.

> *NOTE: 1,3-Dipoles could also be considered as "neutral", since they possess a net charge of 0. It would be, however, superfluous to refer to simple TACs possessing no formal charges as "non-dipolar" or "non-zwitterionic". So, the term "neutral" TAC has been kept for the sake of convenience in this thesis.*

A thorough search of literature did not produce any review on the topic of "neutral" three-atom components in (3+2) cycloadditions. This is perhaps unsurprising due to the potentially unstable nature of the zwitterionic species produced. Unless mechanistic studies are involved, a portion of the literature analysis has to be done indirectly, by attributing observed and isolated products to a potential origin from a zwitterionic (3+2) cycloadduct.

Nevertheless, herein is compiled a series of reported chemistry involving "neutral" three-atom components in (3+2) cycloadditions with alkenes and alkynes, where the cycle formed from the (3+2) cycloaddition is maintained in the isolated product.

1.3.1. (3+2) Cycloadditions of allyl-type "neutral" TACs with carbon π systems

The "criss-cross" cycloaddition of azines with alkenes is a classical example of "1,3-dipolar" character in a formally neutral molecule (Figure 1-8). In this case, azines **1.023**, a class of diaza-butadienes react once with a two-atom component, typically alkenes, to form a zwitterionic cycloadduct **1.024**. This reactive intermediate is an azomethine imine, a classical 1,3-dipole which is prone to undergo a (3+2) cycloaddition as well, which ultimately provides a neutral bicycle **1.025**. These two consecutive (3+2) cycloadditions taking place across the 1,3 and 2,4 positions of the azine explains the "criss-cross" name given to this transformation. Developments in the use of azine-based criss-cross cycloadditions have been recently reviewed.[24-25]

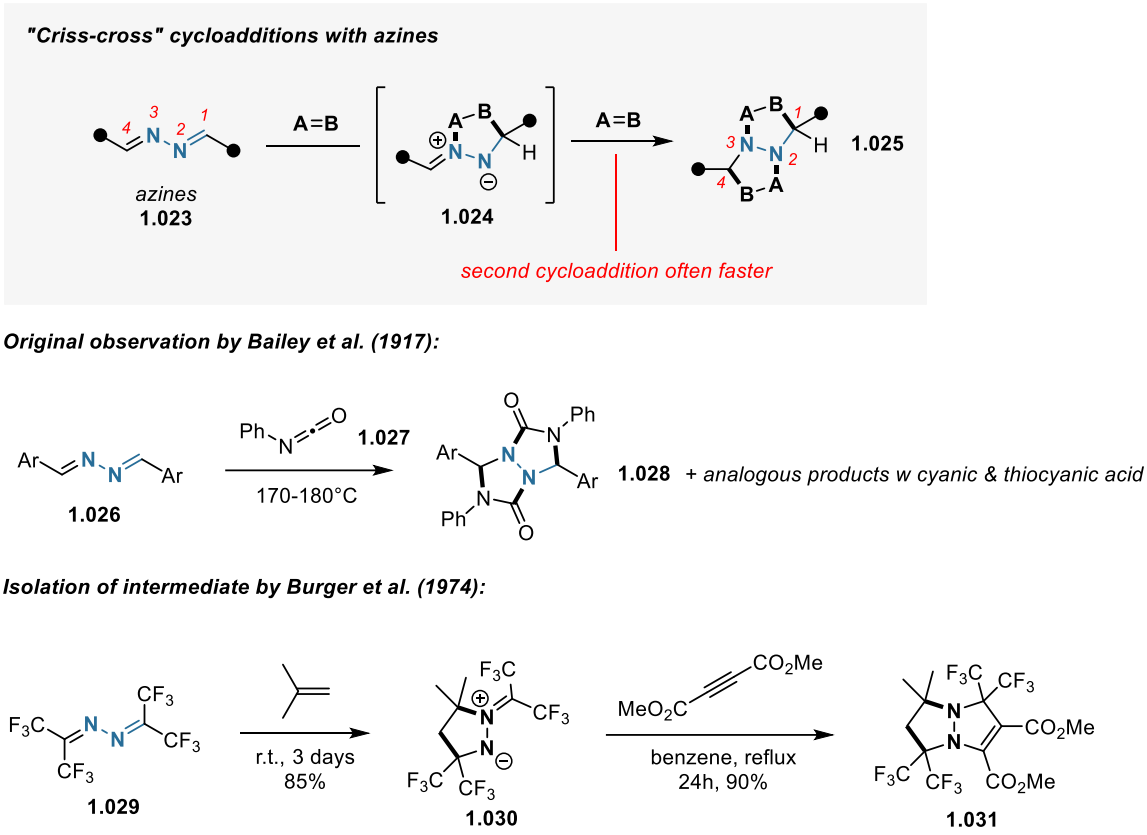

Figure 1-8. Early contributions on the criss-cross cycloaddition of azines.

In 1917, Bailey and coworkers reported on the reactivity between azines **1.026** and isocyanate derivatives **1.027**, demonstrating the formation of bis-cycloadducts with structure **1.028**.[26-27] While early work on this transformation focused on isocyanates as two-atom components, work on the use of alkene and alkyne partners was later achieved. Specifically, Burger and coworkers were able to make use of the tetra(trifluoromethyl)azine **1.029** to isolate a stable azomethine imine intermediate **1.030**.[28-30] While confirming the intermediacy of a zwitterionic cycloadduct, it also demonstrated that "mixed" criss-cross cycloadditions were also possible, where the two units of two-atom components incorporated in the final product **1.031** are different.

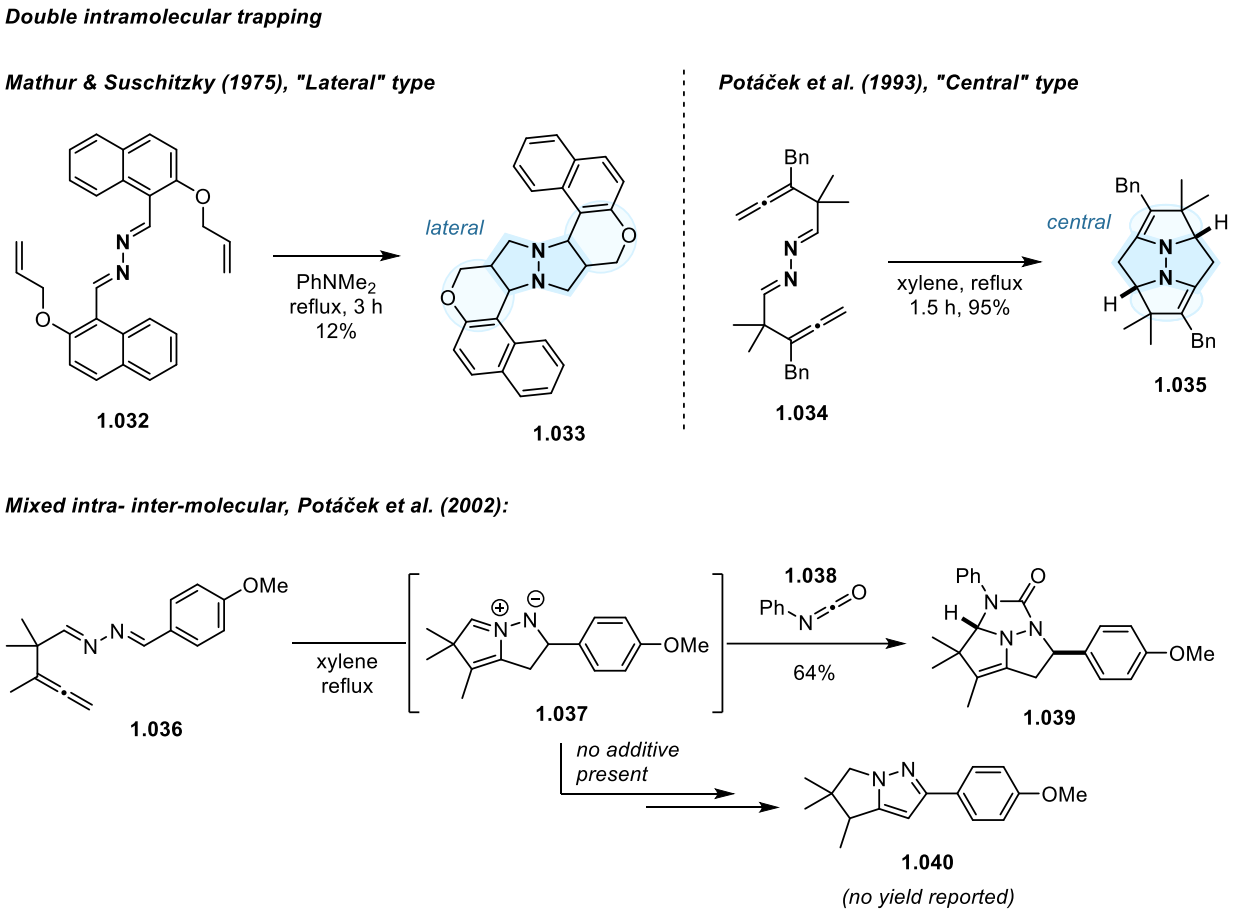

Figure 1-9. Intramolecular versions of the criss-cross cycloaddition with azines.

Further extension of the chemistry to intramolecular variants permitted to generate quite complex polycyclic motifs (Figure 1-9). The first intramolecular criss-cross cycloaddition was reported by Mathur and Suschitzky,[31] where a doubly allylated azine **1.032**, upon heating, was seen to undergo a criss-cross addition to the polycycle **1.033**. Later, Potáček, Viehe and coworkers reported a different type of criss-cross adduct **1.035** produced from bis-allenyl azine **1.034**, where the hydrazine moiety is "centralized" in the bis-cycloadduct.[32] These two types of connectivity were dubbed "central" and "lateral", preference to which was suggested to be predicated by geometrical constraints and electronic variations within the azine starting materials. Potáček and coworkers later explored their system in a single allenyl-functionalized azine **1.036**.[33] In this case, a mixed criss-cross product **1.039** could be observed in the presence of an isocyanate trap **1.038**, while aromatization to a fused pyrazole **1.040**, presumably via multiple proton-transfer sequences, was observed in the absence of any additive.

The criss-cross reactivity originally observed in azines was later observed in other aza-butadienes. Closely related to the case of azines is that of imino-substituted isocyanates (Figure 1-10). In a short communication in 1982, Jones reported observing that triazolinedione-derived ylide **1.041**, upon boiling in toluene in the presence of alkenes and alkynes, produces analogous azomethine imines **1.043**. Jones proposed the intermediacy of an imino isocyanate **1.042**, through initial release of phenyl isocyanate. Despite its synthetic potential, this reactivity was not further investigated for several decades. In a series of reports starting in 2012, the Beauchemin group developed multiple useful methodologies which permit to take advantage of this reactivity. [34-38] The highly reactive imino iso(thio)cyanates **1.045**, having a tendency to dimerize, were slowly generated at low concentrations through the thermal and reversible release of alcohols from imino carbamates **1.044**. When done in the presence of alkenes and imines, zwitterionic (3+2) cycloadducts **1.046** of the azomethine imine type are generated. In many cases, the authors found that these species could be directly isolated, but have also subsequently involved them in various transformations towards valuable nitrogen-containing scaffolds.

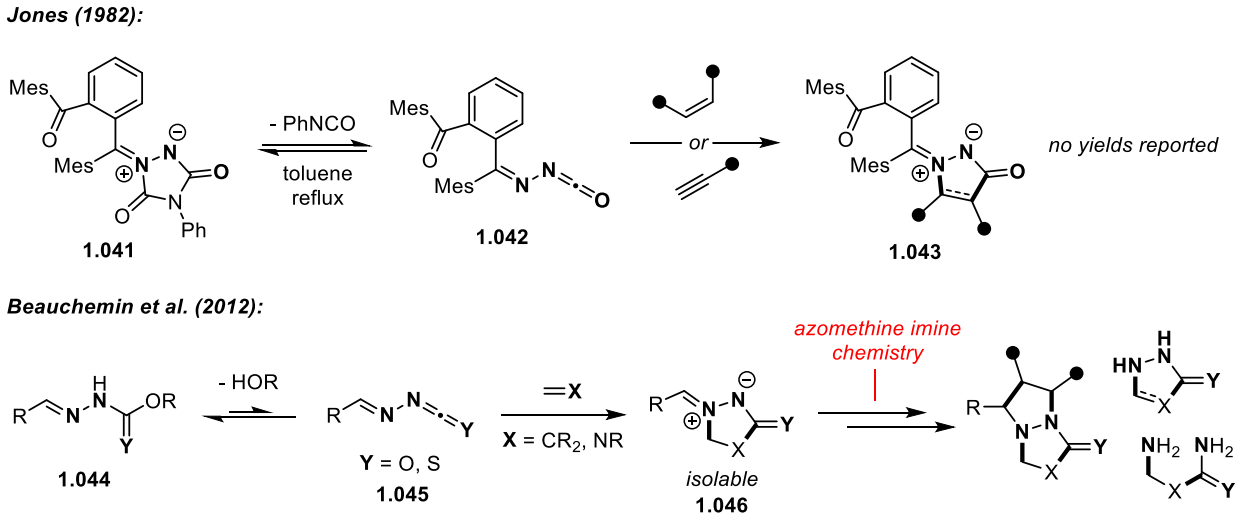

Figure 1-10. Imino isocyanates in neutral (3+2) cycloadditions.

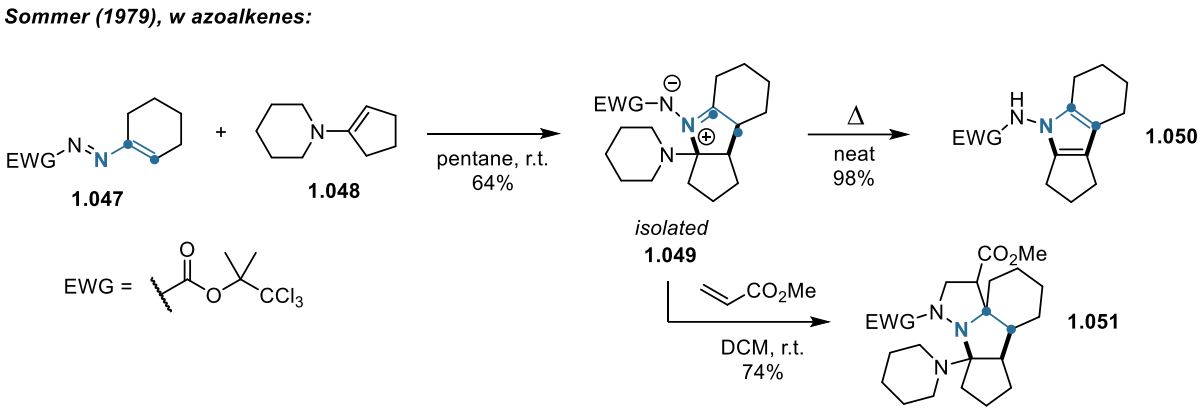

Figure 1-11. Azoalkenes in neutral (3+2) cycloadditions.

In 1979, Sommer observed the formation of a precipitate when mixing a 1:1 ratio of azoalkene **1.047** and enamine **1.048** (Figure 1-11).[39] Upon heating this precipitate, the N-aminopyrrole **1.050** was obtained. This was explained by ascribing the azomethine imine structure **1.049** to the precipitate, which was confirmed through spectroscopic evidence and trapping experiments with methyl acrylate leading to **1.051**.

The nature of this curious cycloaddition was proposed, a few years later, to be concerted yet asynchronous by Gilchrist et al.[40] The (3+2) reactivity between azoalkenes and electron-rich alkenes has however been very little used, except in a few thermal and catalyzed methodologies more recently developed by the groups of Favi and Lu towards the synthesis of pyrroles and pyrrolines.[41-47]

The oxygen-substituted analogs of aza-alkenes, nitrosoalkenes, preferentially undergo (4+2) cycloadditions with alkenes, yet zwitterionic species deriving from (3+2) cycloadditions have been observed as very minor by-products by Gilchrist et al in 1983.[48-49]

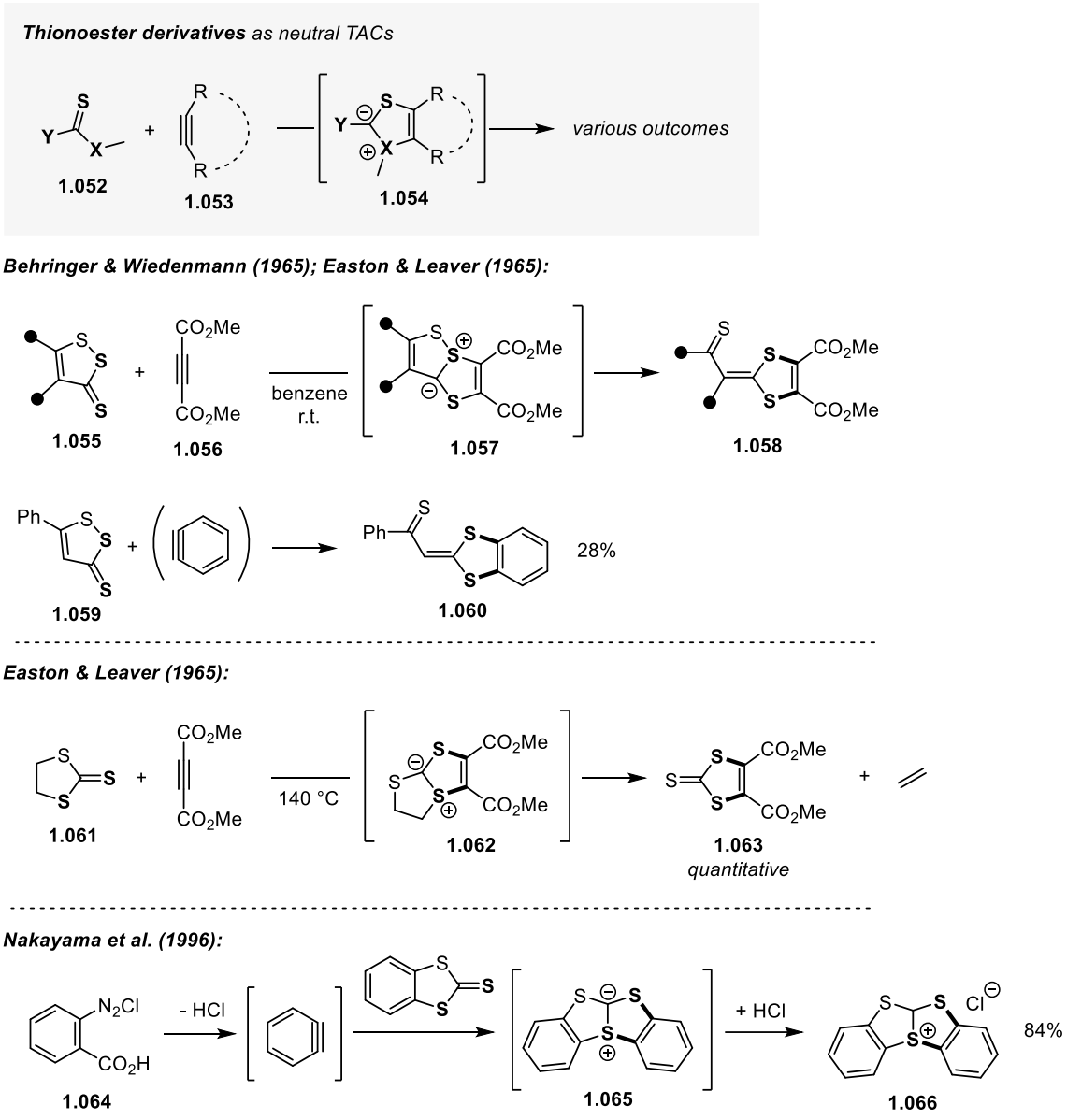

Figure 1-12. Thionoester derivatives as neutral TACs in (3+2) cycloadditions.

The reaction between disulfide thione **1.055** and dimethylacetylene dicarboxylate (DMAD) to give **1.058** was first reported by Behringer and Wiedenmann in 1965 (Figure 1-12).[50] In the same year, Easton and Leaver published their investigations on the same class of organosulfur compounds, where they observed the same (3+2) reactivity.[51-52] In addition to **1.058**, they also observed that **1.059** reacts with in-situ generated benzyne to give the analogs **1.060**. Easton and Leaver also observed that trithiocarbonates **1.061** behave similarly with DMAD to provide **1.063** in near-quantitative yields. By observing ethylene as a by-product of the reaction, the authors suggested that (3+2) cycloadduct ylide **1.062** was a probable intermediate to this transformation.

Analogous chemistry between DMAD and selenodithiocarbonate was studied by Cava and coworkers.[53-54]

By working with diazonium salt **1.064** as a benzyne precursor in the absence of base, Nakayama and coworkers were able to isolate the hydrochloride salt **1.066** of the proposed zwitterionic adduct **1.065**.[55]

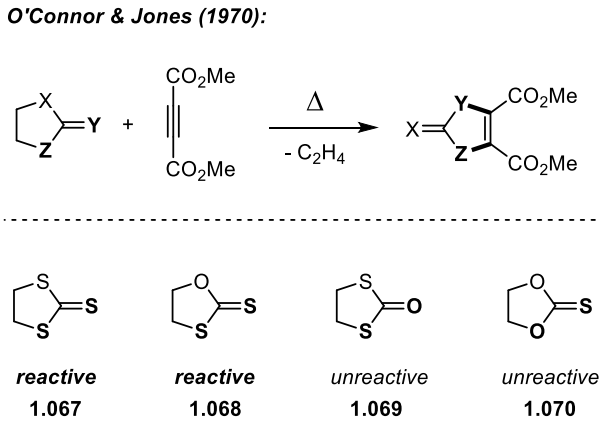

Figure 1-13. Identifying the reactive thiocarbonate derivatives.

Subsequent investigations by O'Connor and Jones in 1970 showed the importance of the S-C=S motif for the success of this reactivity,[56] as S,S'-dithiocarbonate **1.069** was unreactive, and O,O'-thiocarbonate **1.070** decomposed more quickly than any (3+2) reactivity could be observed (Figure 1-13).

Other (3+2) cycloadditions with aza-analogs of the above described thiocarbonates have also been sporadically reported in literature.[57-58]

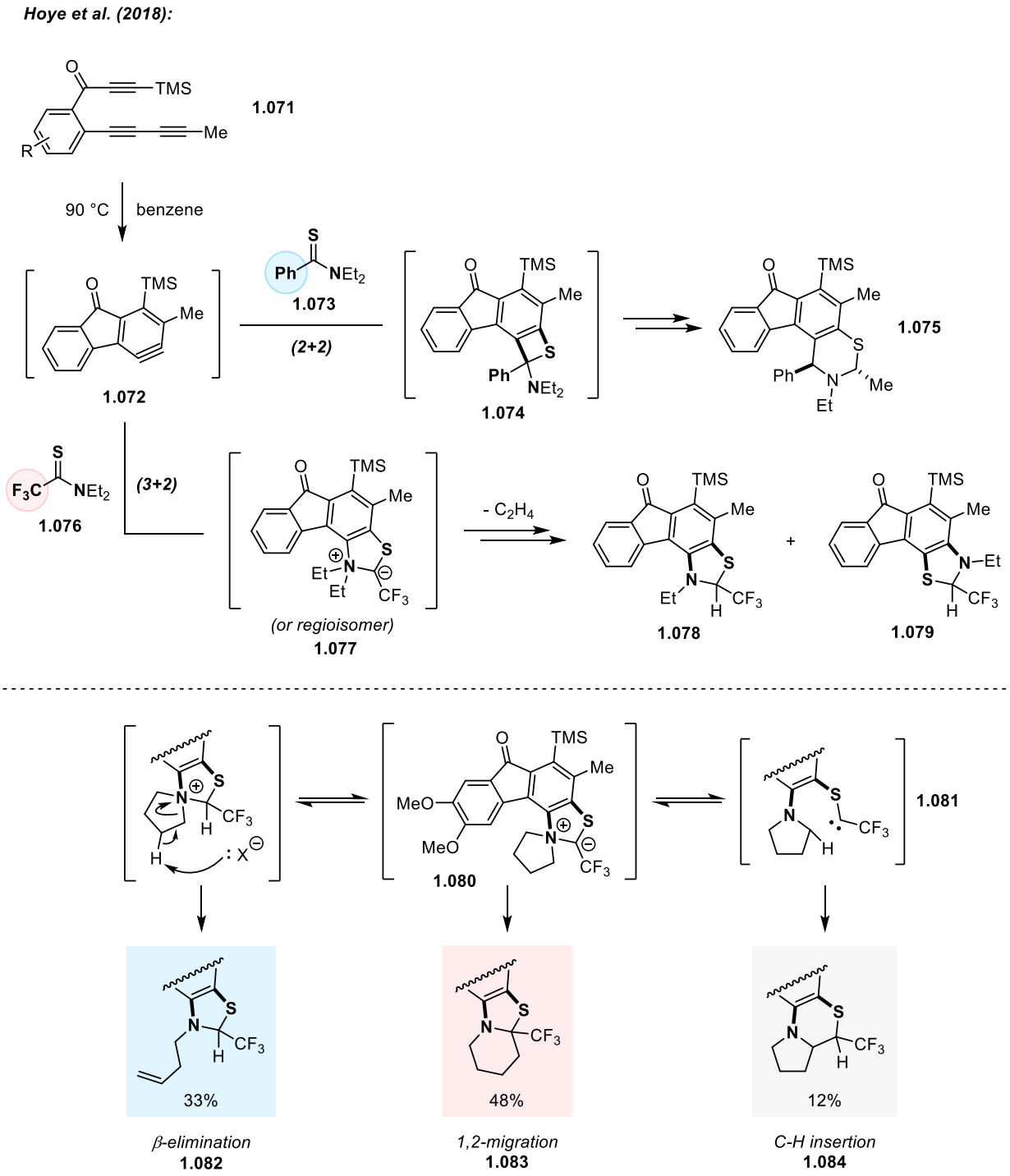

Figure 1-14. Thionoamides in (3+2) cycloadditions with complex benzynes.

As part of their research program on the formation of reactive benzyne species **1.072** from triyne scaffolds **1.071**, the Hoye group discovered an unexpected set of reactivity when attempting trapping with thionoamides (Figure 1-14).[59] When using alkyl or aryl-substituted thionoamides **1.073**, the

thiocarbonyl moiety acts as a classical 2π partner in a (2+2) cycloaddition given the proposed intermediate **1.074**. A reaction cascade then leads to the thiazine derivative **1.075**. To their surprise, when using EWG-substituted thionoamides **1.076**, they observed instead 5-membered adducts **1.078** and **1.079**, which they proposed came from the two possible regioisomers of zwitterionic (3+2) cycloadduct **1.077**. The diversity of products that could be obtained from this reactivity is well exemplified in a pyrrolidine-derived scaffold leading to zwitterion **1.080**. In this case, beta-elimination product **1.082**, 1,2-migration product **1.083** and C-H insertion product **1.084** (via formation of carbene **1.081**) could all be observed in the reaction mixture. DFT studies performed by the authors suggested a concerted but asynchronous (3+2) cycloaddition step, where significantly more C-S bond is present at the transition state.

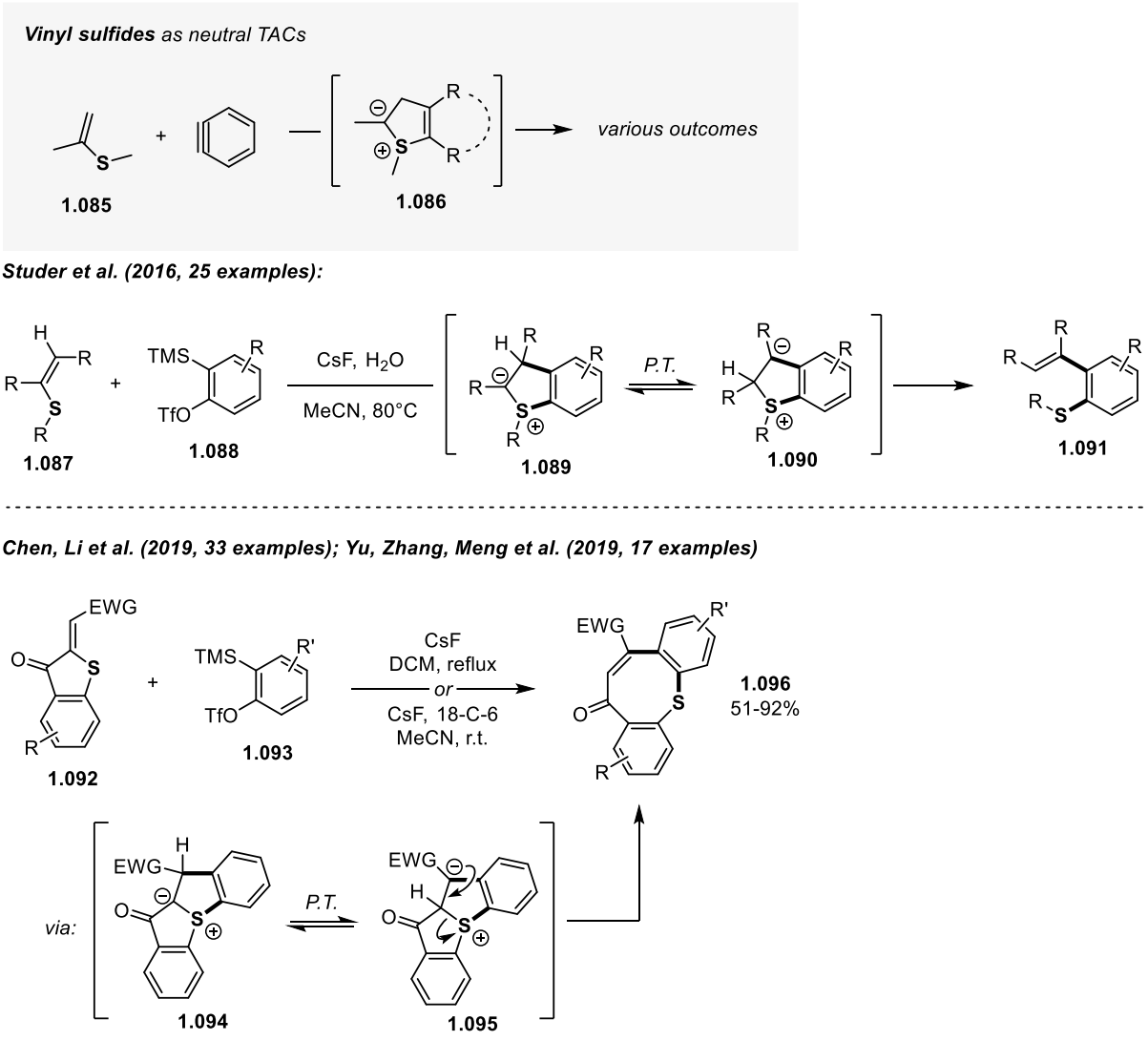

Figure 1-15. Vinyl sulfides in neutral (3+2) cycloadditions.

Vinyl sulfides may also be seen as electronic analogs of the thioesters. Studer and coworkers reported, more recently in 2016, on the reactivity between linear vinyl sulfides **1.087** and benzyne precursors **1.088** (Figure 1-15).[60] Following a proposed (3+2) cycloaddition step leading to zwitterion **1.089**, a proton shift event can occur leading to **1.090**, permitting breakage of the C-S bond to provide the observed alkenyl phenyl thioether derivatives **1.091**.

Very similar reactivity was later reported independently by Chen & Li and Yu, Zhang & Meng in 2019.[61-62] In these cases, the vinyl sulfide derivatives used, **1.092**, were cyclic in nature. An equivalent series of steps involving a (3+2) cycloaddition to **1.094**, proton shift to **1.095**, and C-S breakage explains the formation of dibenzothiocine derivatives **1.096**.

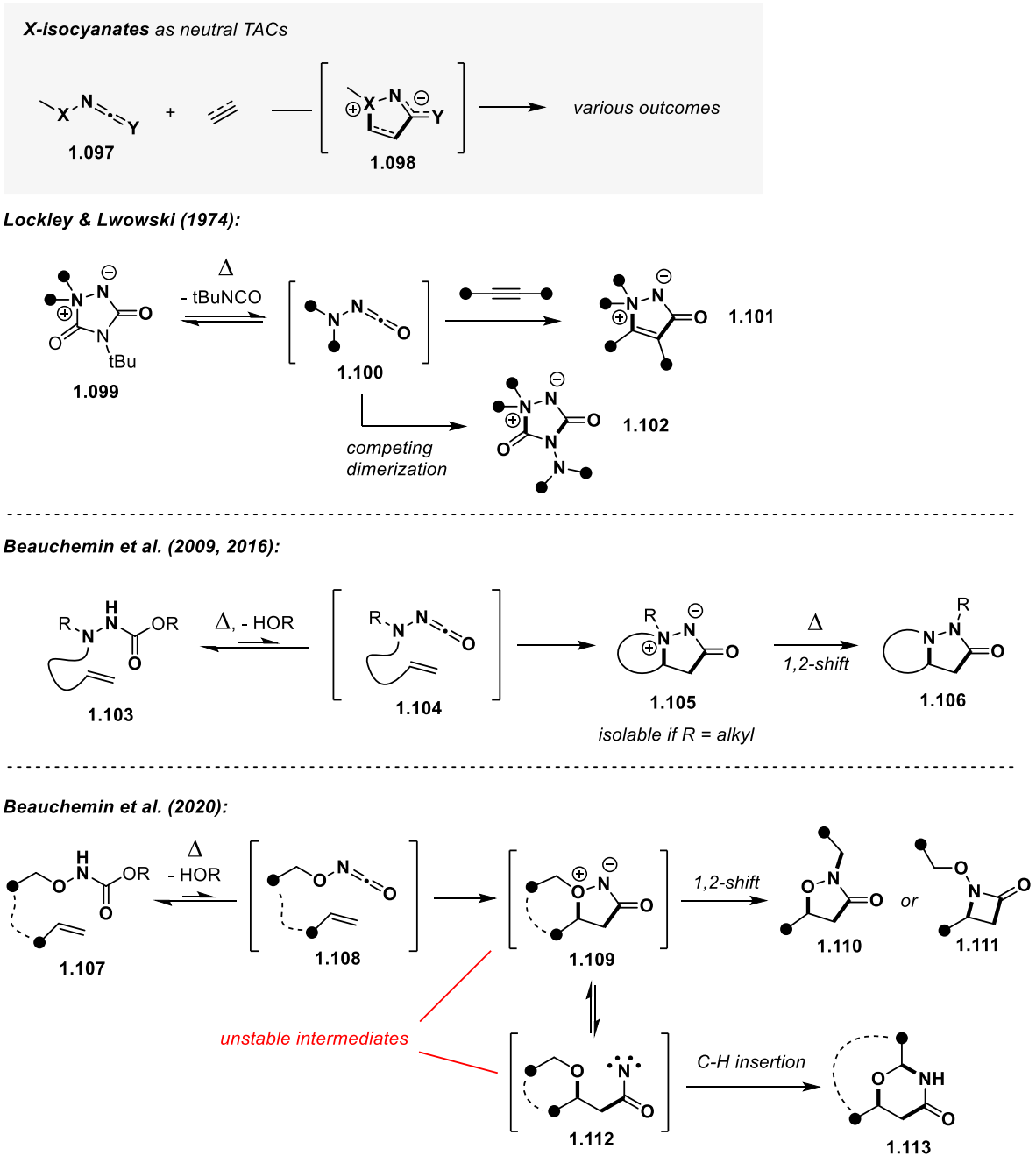

Figure 1-16. X-isocyanates in neutral (3+2) cycloadditions.

To the best of my knowledge, simple hydrazones have never been reported to produce zwitterionic (3+2) cycloadducts. Lockley and Lwowski have however, in 1974, made the interesting observation that N-aminoisocyanates **1.100**, thermally generated from amidimine precursors **1.099**, could be intercepted in the presence of alkynes to produce zwitterionic cycloadducts **1.101** (Figure 1-16).[63] The authors made use of large crystals of the starting material **1.099**, poorly soluble in the chosen

tetrachloroethylene solvent, in order to keep low concentrations of the N-aminoisocyanate intermediate **1.100**, which would otherwise irreversibly dimerize to **1.102**.

The Beauchemin group has more recently explored this chemistry by making use of more accessible and versatile isocyanate precursors.[64-66] Interestingly, by tethering carbazates **1.103** with alkenes, the group was able to reversibly generate tethered N-aminoisocyanate derivatives **1.104** under thermal conditions. These species could then undergo a (3+2) cycloaddition to generate zwitterionic aminimides **1.105**. While in some cases these species could be isolated, upon further heating, these zwitterions underwent 1,2-shift (or proton transfer if R=H) to provide neutral pyrazolone derivatives **1.106**.

The same group later expanded this chemistry to intra- and intermolecular reactions between alkenes and N-alkoxyisocyanates **1.108** using an analogous strategy from precursors **1.107**.[67] In this case, the zwitterionic (3+2) cycloadduct **1.109** is significantly less stable than in previous cases, and readily undergo either 1,2-shift chemistry to **1.110** or **1.111**, or O-N fragmentation to nitrene **1.112**, permitting to observe C-H insertion products **1.113**.

1.3.2. (3+2) Cycloadditions of propargyl-allenyl-type "neutral" TACs with carbon π systems

Some interesting structural limitations take place when looking at the propargyl-allenyl class of (3+2) cycloadditions (Figure 1-17). Both propargyl and allenyl types of 1,3-dipoles, **1.114** and **1.115**, possess a central atom that is both tetravalent and cationic. So, when looking at the C,N,O-based series of TACs, the central atom is limited only to nitrogen. This has been noted by Huisgen in his original review on the topic.[4] A similar analysis of potential propargyl-allenyl TACs of the neutral type leads to the conclusion that the central atom can only be carbon (without considering third-row elements).

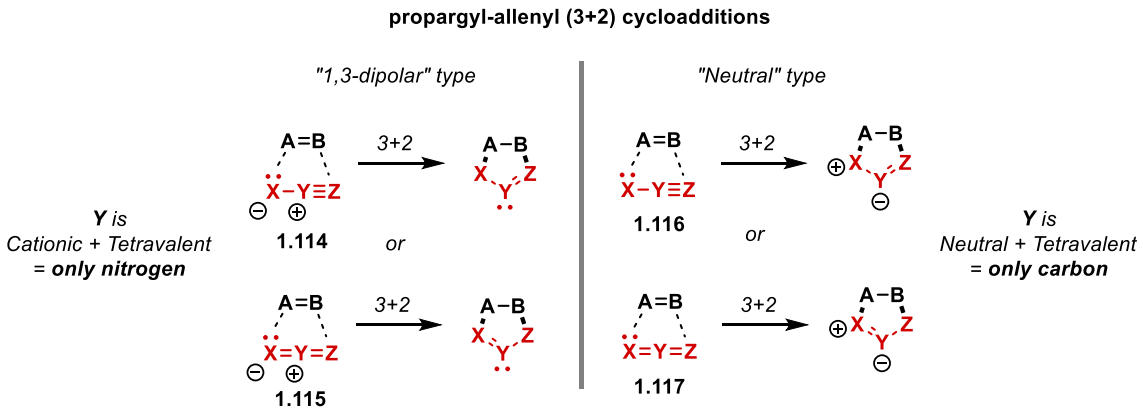

Figure 1-17. Structural restrictions in propargyl-allenyl TACs.

This is interesting, since only a handful of known structures fit this requirement. These are summarized in Figure 1-18. Although conceptually interesting, there are some practical aspects which would render the participation of many of these proposed TACs in (3+2) cycloadditions difficult. First, the resulting lone pair of electrons located on the central atom in these cycloadducts is not stabilized on carbon as well as it is on nitrogen and oxygen, posing a thermodynamic challenge to this process. Second, many of these proposed TACs have their π unsaturations polarized in a direction opposite as what is required to displace a pair of electrons onto the central atom. Third, many of these proposed TACs (especially of the allenyl type) are well-known to participate in (2+2) cycloadditions with 2π counterparts, which could surely be a competing pathway when attempting to promote 3+2 processes.

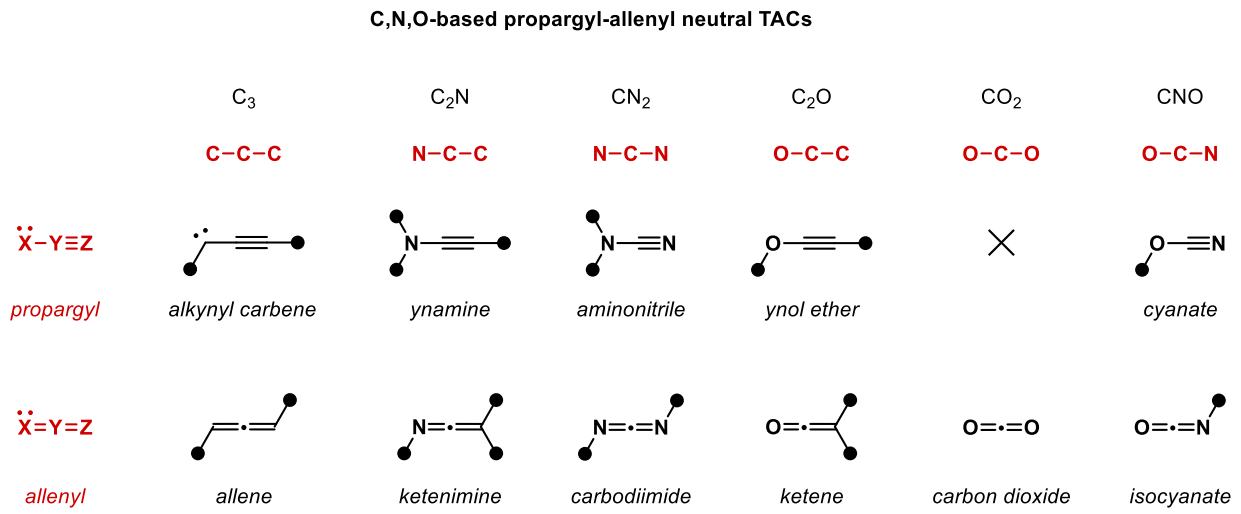

Figure 1-18. Possible structures of propargyl-allenyl type neutral TACs.

Nevertheless, some products deriving from thermal (3+2) processes of these proposed TACs have been reported in literature. To date, these reports seem to be limited only to the X-alkynyl class of propargyl-allenyl neutral TACs (such as ynamine derivatives and ynol ethers, as well as their third-row counterparts), some of which has been recently reviewed in our perspective article on the subject.[68] This limitation is perhaps expected, when considering points 2 and 3 described above. Reports of this chemistry are described in the next section.

1.3.2.1. X-Alkynyl species as neutral TACs in (3+2) cycloadditions

Likely the first use of X-alkynyl species in neutral (3+2) cycloadditions was observed by Boonstra and Arens in 1960, in their broad studies of chalcogen-substituted alkynes (Figure 1-19).[69] When the authors heated alkynyl sulfide **1.118** neat, they observed the generation of ethylene gas and of a major product **1.119**, which was isolated upon distillation of the reaction mixture. While the authors did not speculate on the mechanism of this transformation, it is reasonable to suggest, based on our current understanding of the reactivity of alkynyl sulfides, that a (3+2) cycloaddition leading to zwitterionic dimer **1.120** may explain their observation.

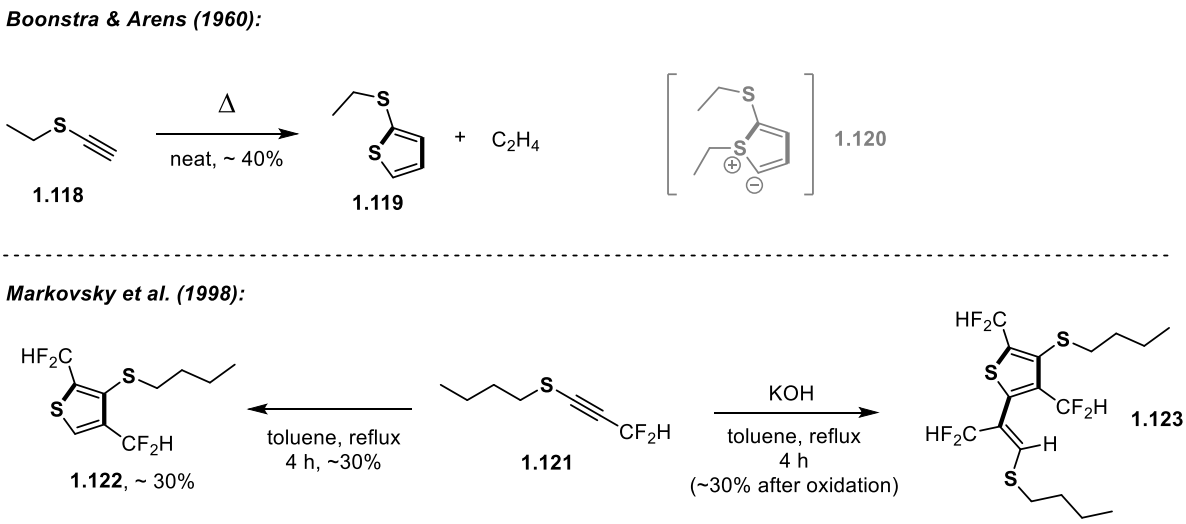

Figure 1-19. (3+2) Cycloadducts in alkynyl sulfides dimerizations.

Later in 1998, Markovsky and coworkers observed that fluoroalkylated alkynyl sulfides **1.121** lead to analogous thiophenes **1.122** via a certain dimerization process.[70] Under basic, conditions, the trimer **1.123** was instead obtained as the major product. The mechanism the authors proposed involved the heterolysis of the alkynyl sulfides starting material to product an alkynyl sulfide anion **1.124** (Figure 1-20). This anion would then undergo addition to another equivalent of starting material to provide thienyl anion **1.125**. The latter could undergo either protonation towards **1.122**, or further addition to a third equivalent of starting material under basic conditions to ultimately provide trimer **1.123**. In light of the studies reported in this thesis, an alternative mechanism involving a neutral (3+2) cycloaddition is proposed in section 3.10.

Mechanism proposed by Markovsky et al. (1998):

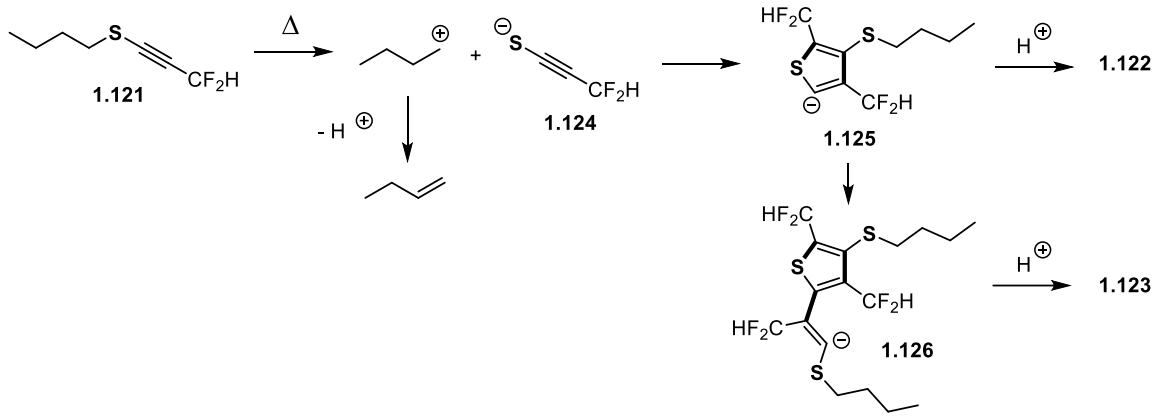

Figure 1-20. Original mechanism proposed by Markovsky and coworkers.

While the reaction between alkynyl sulfides and alkyne derivatives was not further reported in the literature, other instances of the use of alkynyl sulfides as TACs briefly appear. In 1968, Wasserman and Fernandez reported some of their observations on the reactivity between chalcogen-substituted alkynes and benzyne (Figure 1-21).[71] When generating benzyne **1.128** from precursor **1.127** in the presence of alkynyl sulfides, the authors observed the formation of benzothiophenes **1.129** and *ortho*-alkynyl phenyl thioethers **1.130**, in addition to a few other minor products. Analogous reactivity was observed with ynol ethers. They proposed that the process is initiated by nucleophilic attack of the heteroatom to the electrophilic benzyne to generate the zwitterion **1.131**. Then a divergence would occur, attack at the alpha carbon would ultimately provide **1.130**, while attack at the beta carbon would generate the cyclic zwitterion **1.132**, explaining the formation of cyclic product **1.129**. It is worthy to note that the formation of **1.130** could instead be explained by the same cyclic zwitterion **1.132**, which can also be seen as a stabilized vinylidene species **1.133**, through a Fritsch–Buttenberg–Wiechell (FBW)-type 1,2-shift. While Wasserman & Fernandez' work provide a more complete picture of the mixture obtained when reacting ynol ethers with benzyne, the formation of formal C-O insertion product **1.130** in this reaction was earlier observed by Stiles and coworkers in 1962.[72]

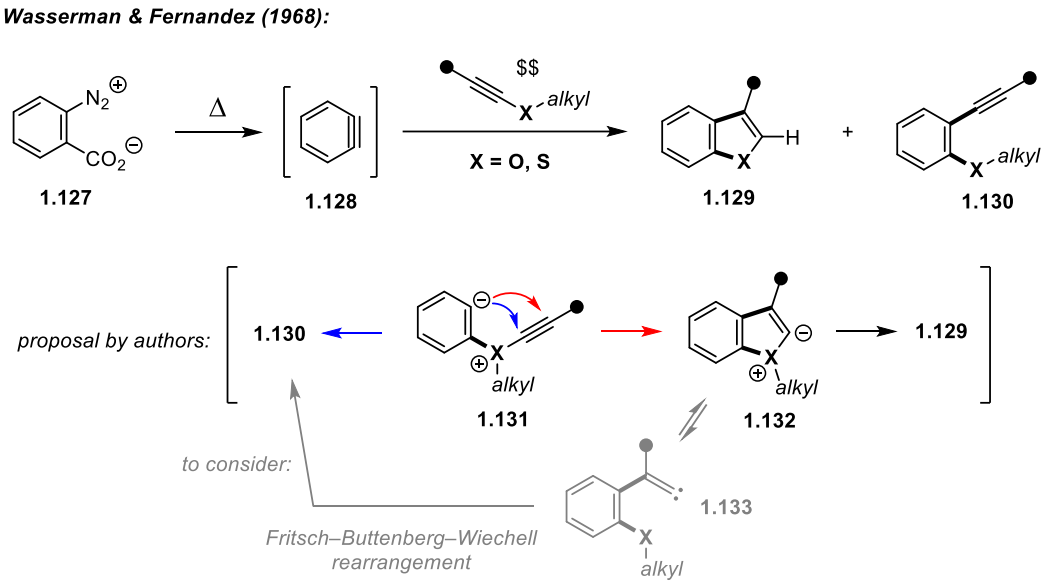

Figure 1-21. Original observations of (3+2) reactivity between alkynyl (thio)ethers and benzyne.

Interestingly, the C-X insertion product has also been observed by McAusland, as part of his PhD studies in the Greaney group, when generating benzyne intermediates in the presence of ynamides **1.136** (Figure 1-22).[73] The mechanism proposed in the thesis involved a series of steps, seemingly quite difficult, initiated by nucleophilic attack of the ynamide by its β-carbon to the benzyne. An alternative mechanism proceeding through (3+2) cycloaddition followed by Fritsch–Buttenberg–Wiechell rearrangement, as earlier proposed in Figure 1-21, would be important to consider as well here. The chemistry was described by the author as difficult to optimize due to a very complex reaction mixture, and no work on the topic has been published by the group to date.

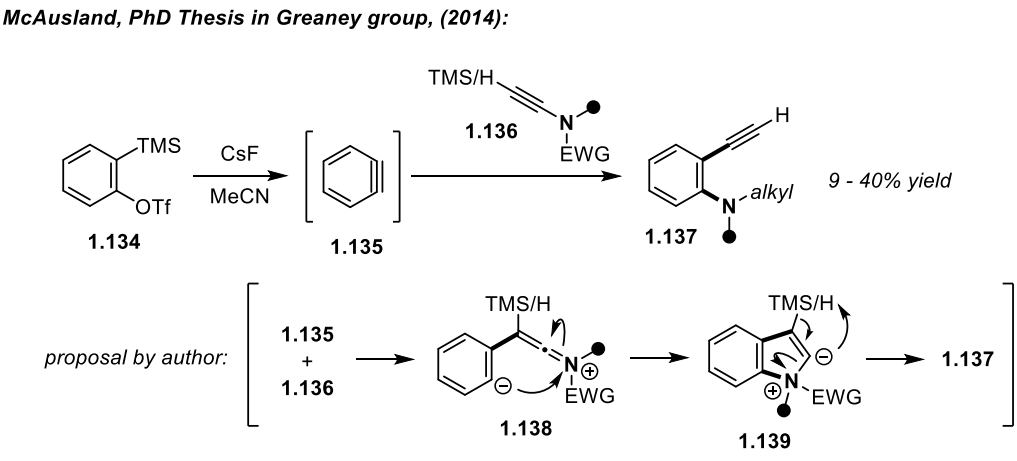

Figure 1-22. Benzyne C-N insertion products that could be explained via (3+2) cycloadditions.

The scope of reactivity between alkynyl sulfides and benzynes for the formation of benzothiophenes was further explored by the group of Yoshida in 2020 (Figure 1-23).[74] In their case, the use of Kobayashi-type aryne precursors **1.140** permitted a swift access to a wide variety of substituted aryne species **1.141**. Using the aryne distortion model by Houk and coworkers,[75] the regiochemistry of a series of (3+2) cycloadditions leading to benzothiophenes products **1.144** could be explained, assuming the sulfide would act as an initial nucleophile onto the electrophilic aryne.

In a special case, Yoshida and coworkers demonstrated that the proposed zwitterionic cycloadduct **1.143** could be trapped by carbon dioxide, leading to the benzothiophene analog **1.146**.

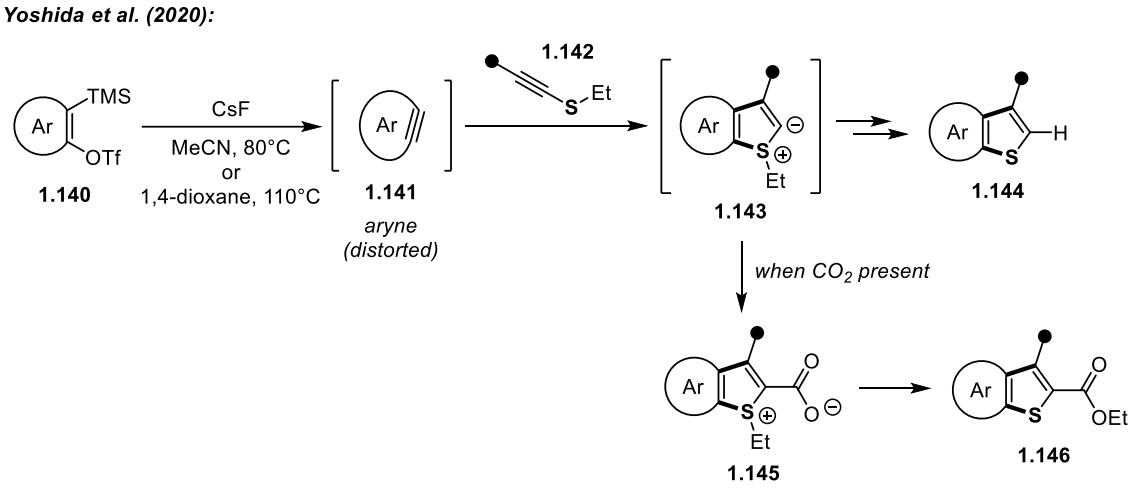

Figure 1-23. Methodology developments into the (3+2) cycloaddition between alkynyl sulfides and arynes by the Yoshida group.

Among the different X-alkynyl species known, alkynyl phosphines are somewhat more exotic species. Their involvement in (3+2) cycloaddition cascades have, however, been reported (Figure 1-24). Specifically, the criss-cross reaction involving alkynyl diphosphines **1.147** and dialkyl acetylenedicarboxylates was observed by Latscha *et al.* in 1997:[76]

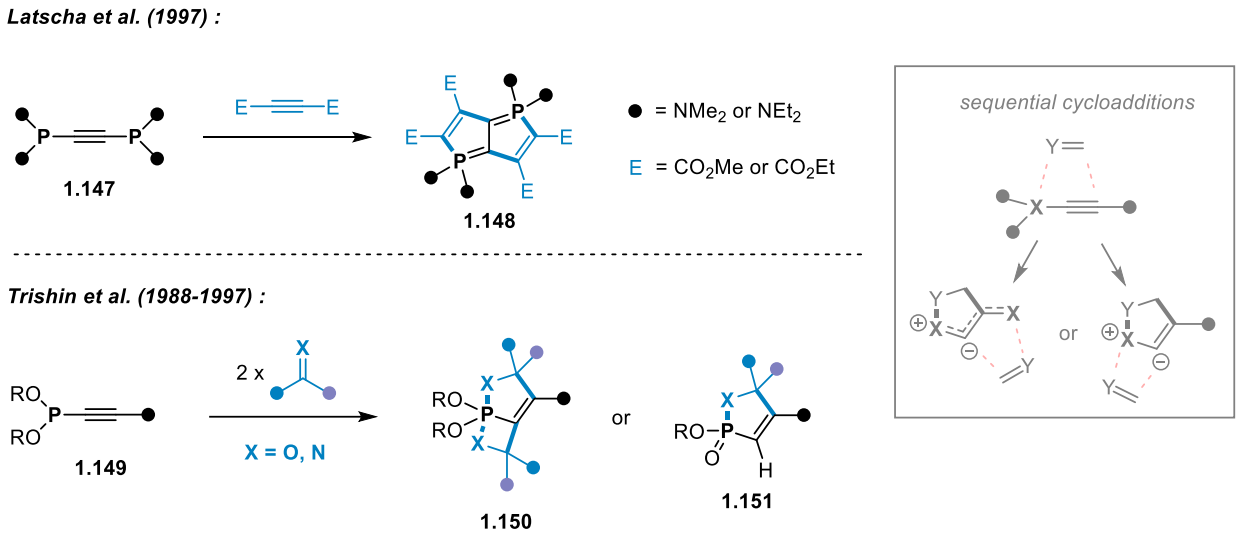

Figure 1-24. Exotic phosphacycles from alkynyl phosphine derivatives as neutral TACs.

Although not strictly involving carbon-based π partners, it is worthy of note that the group of Trishin earlier reported a series of communications between 1988-1997 showing a very similar set of criss-cross (3+2) reactivity between alkynylphosphonite esters **1.149** and carbonyl or imine derivatives to give interesting bicyclic phospholene derivatives **1.150** and **1.151**.[77-91] The reported transformations involving alkynyl phosphines have led to unusual bicyclic structures due to the possibility for phosphorus to adopt stable higher valencies.

In addition to our own efforts described in this thesis,[92-94] a few contributions to the topic have been published by the Anderson group[95] and the Takasu and Takikawa group[96] since our initial forays in this chemistry. These are described and further discussed in section 5.1.

1.4. Introduction to coinage metal-catalyzed 1,3-dipolar cycloadditions involving terminal alkynes

The broad use of catalysis has permitted the use of milder conditions while achieving higher regio- and stereoselectivities than could be reached in classical thermal 1,3-dipolar cycloadditions. This field of research is quite broad and advances on the subject are periodically reviewed.[97]

In particular relevance to the chemistry that will be discussed in Chapter 4, the involvement of *terminal alkynes* in metal-catalyzed azide-alkyne couplings, nitrile oxide alkyne couplings and the Kinugasa reaction will be selectively introduced here.

1.4.1. The copper-catalyzed azide-alkyne coupling (CuAAC)

The (3+2) cycloaddition between azides **1.153** and alkynes **1.152** to give triazoles **1.154/1.155** is one of the first 1,3-dipolar cycloadditions to have been observed (Figure 1-25).[98] While a wide variety of transition metals were later found to catalyze this cycloaddition to provide only one of the two possible regioisomers,[99] its most famous variant is surely the copper-catalyzed azide-alkyne coupling (CuAAC), which was independently reported by the groups of Meldal and Fokin/Sharpless in 2002.[100-101] This copper-catalyzed variant and the use of the strained-alkyne version applied by Bertozzi in 2004 towards bioorthogonal applications[102] have become eponymous with the concept of "click chemistry". This topic was the theme of the Nobel Prize in Chemistry in 2022.[103]

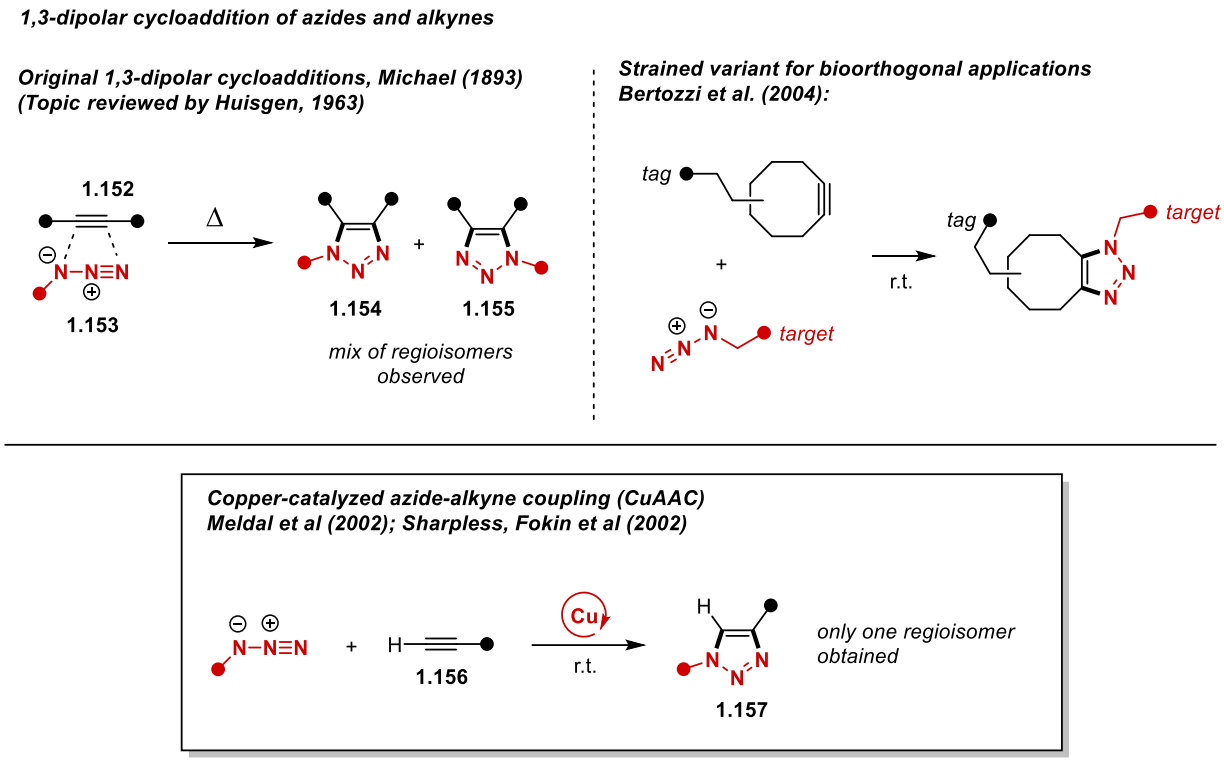

Figure 1-25. Selected contributions towards the 1,3-dipolar cycloaddition of azides and alkynes.

The CuAAC is particularly interesting, because it permits to involve terminal alkynes **1.156**, many of which are typically sluggish dipolarophiles, in a (3+2) cycloaddition at surprisingly low temperatures. In addition, it exclusively produces the **1.157** regioisomer, which permits a much cleaner reaction profile than under classical thermal conditions.

The mechanism of CuAAC has been extensively studied in the decade following its discovery, and progresses in its general mechanistic understanding has been reviewed.[104]

In their seminal articles on the topic, both Meldal and Fokin/Sharpless independently observed that this reactivity was only observed for *terminal* alkynes, and that catalysis only occurred from copper(I) (and not from copper(II)).[100-101] This led both groups to propose stepwise mechanisms (rather than concerted) involving the complexation of azides to copper(I) acetylides.

The original mechanism drawn up by Sharpless and Fokin involved mononuclear intermediates (Figure 1-26).[100] They proposed the initial formation of copper acetylides **1.159**. Rather than a direct (3+2) event taking place, which would not explain well the exclusive regioselectivity observed, they proposed the formation of a complex **1.161** between the azide's internal nitrogen atom and the copper unit. Based on preliminary DFT calculations, they proposed that a metallacycle **1.162** would take form, generating the first C-N bond. Then, a ring contraction to the copper triazole **1.163** would follow, providing the observed triazole **1.164** after protodemetallation.

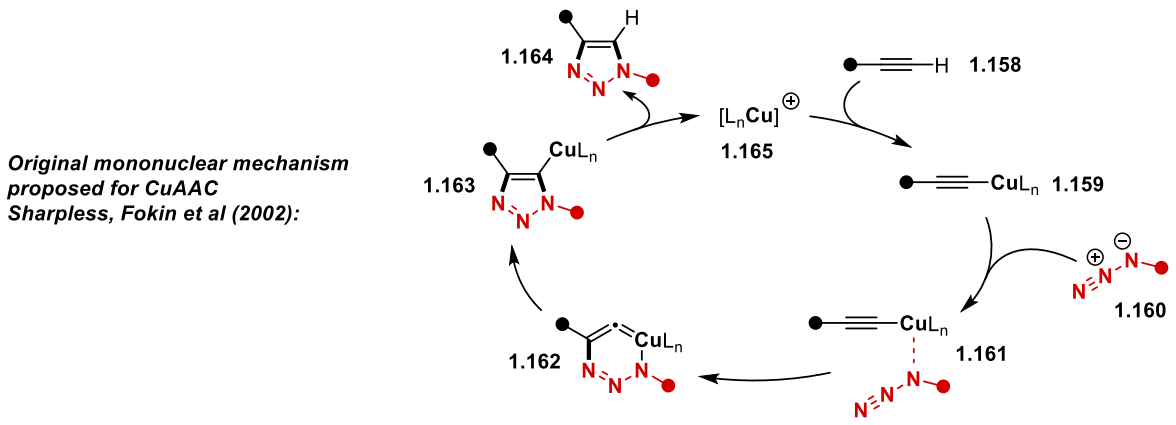

Figure 1-26. Original mononuclear mechanism proposed for CuAAC.

This first mechanistic draft was amended over time as more experimental data was obtained. After initial reaction kinetics investigations by Fokin and Sharpless displayed a second-order dependence on the copper catalyst (Figure 1-27),[105] Fokin soon after shared computational studies demonstrating that dinuclear copper complexes provide additional lowering of the reaction activation barrier.[106] Fokin later demonstrated experimentally that isolated mono copper acetylide species **1.167** were unreactive towards azides until exogeneous copper(i) salt is added.[107] Additionally, use of isotopically enriched copper salts led to enriched copper triazole adducts **1.169**, suggesting that multiple copper units are involved in the cycloaddition process (control experiments ruled out independent copper exchange in **1.167** and **1.168**). Finally, Bertrand and coworkers were able, for the first time, to isolate dinuclear acetylide complex **1.172** using a special class of cyclic alkyl amino

carbene (CAAC) ligand.[108] They showed that these had cycloaddition rates with azides orders of magnitude above that of their mononuclear equivalent **1.170**.

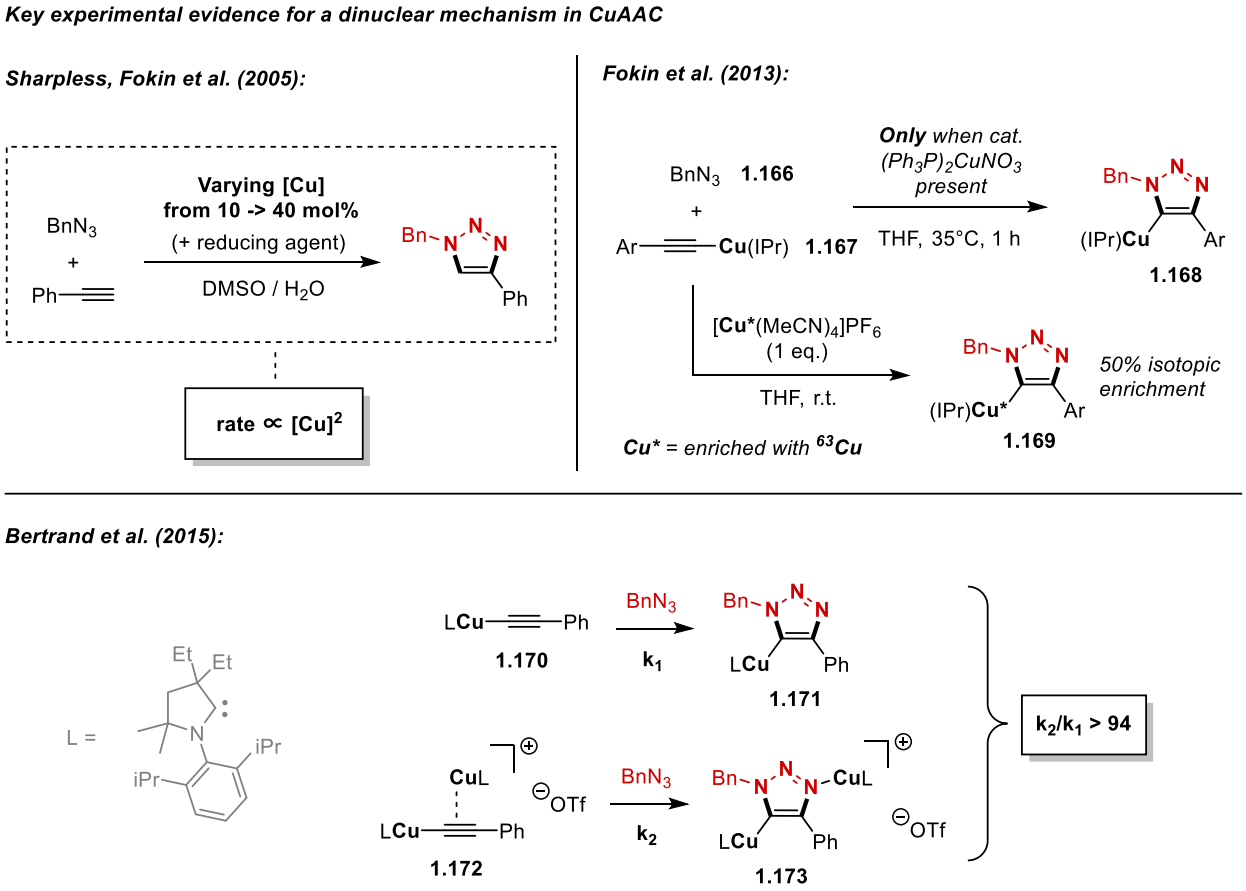

Figure 1-27. Experimental evidence for the participation of dinuclear copper species in CuAAC.

To this date, the dinuclear mechanism (Figure 1-28) seems to be generally accepted and has been backed up by multiple computational studies of the possible reaction pathways.[109-112]

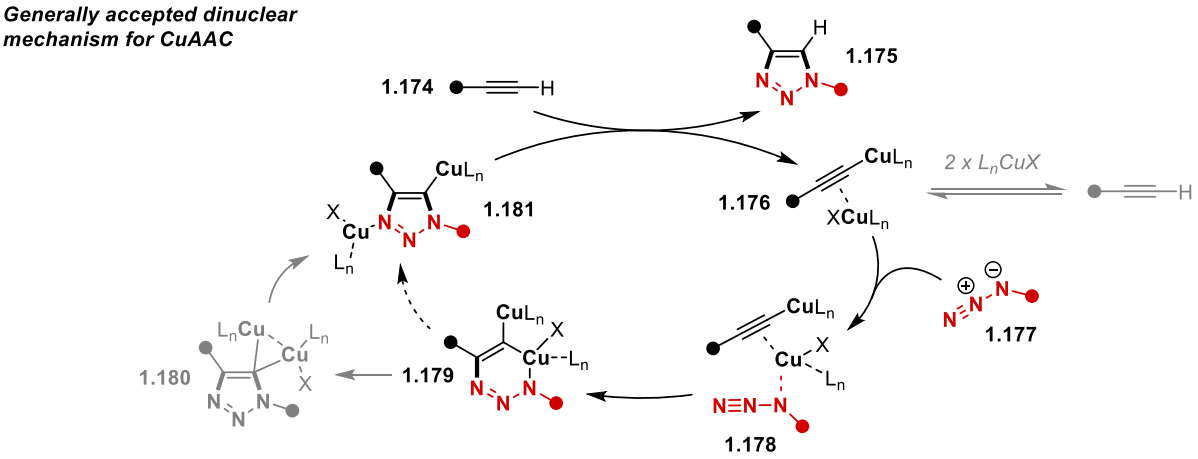

Figure 1-28. The updated dinuclear mechanism generally accepted for CuAAC.

1.4.2. The silver-catalyzed azide-alkyne coupling (AgAAC)

This catalytic activity leading regioselectively to 1,4-substituted triazole is not only observed with copper, but also its nearest periodic table neighbour in group 11, silver. This can be perhaps reasoned considering the shared structural and reactivity profiles of silver and copper acetylides.[113-114]

The silver-catalyzed azide-alkyne coupling (AgAAC) had first been observed by the group of McNulty in 2011, where they used well-defined silver(i) complexes bearing bidentate ligands **1.182** to catalyze the cycloaddition (Figure 1-29).[115-116] Various sets of reaction conditions making use of silver salts to catalyze azide-alkyne couplings were later reported,[117-120] some of which are highlighted here.

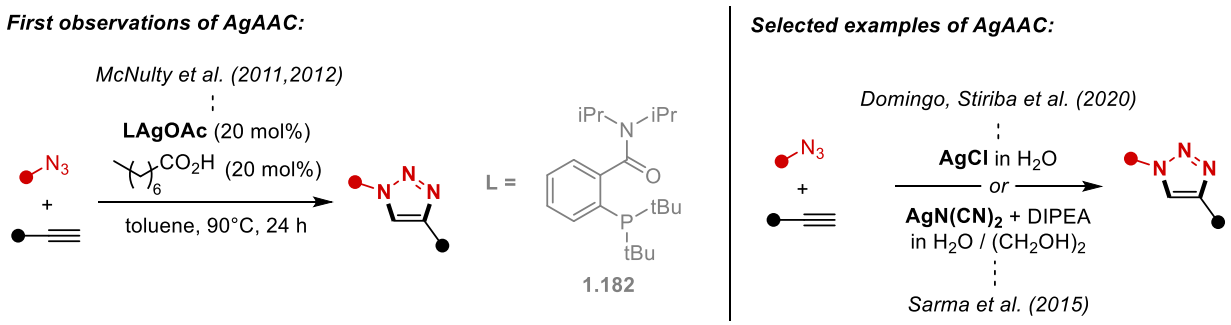

Figure 1-29. Use of silver in the azide-alkyne coupling (AgAAC).

Multiple computational studies on the AgAAC suggest that a dinuclear mechanism, analogous to that proposed for the CuAAC, likely takes place.[118, 121-122]

Other than (3+2) additions involving *inorganic* azides,[123-124] there is no convincing example to date demonstrating the use of gold(I) for catalyzing the (organic) azide-alkyne coupling.

1.4.3. The copper-catalyzed nitrile oxide azide coupling (NOAC)

Early mechanistic studies on the CuAAC performed by Sharpless and Fokin permitted the group to predict similar reactivity in nitrile oxides.[125] Although the thermal 1,3-dipolar cycloaddition between nitrile oxides **1.183** and alkynes typically form the 3,5-regioisomer exclusively,[11] it is not always the case. In a model reaction showcased by Sharpless and Fokin making use of aryl nitrile oxide precursor **1.185** and phenylacetylene **1.184**, the thermal cycloaddition requires heating, an extended reaction time, lower overall yields, and exhibits low regioselectivity between the two possible regioisomers **1.186** and **1.187** (Figure 1-30). On the other hand, by applying their copper-catalyzed conditions (originally developed for CuAAC), they could see high yields after a short period of time at room temperature, and exclusive formation of the 3,5-substituted regioisomer **1.186**.

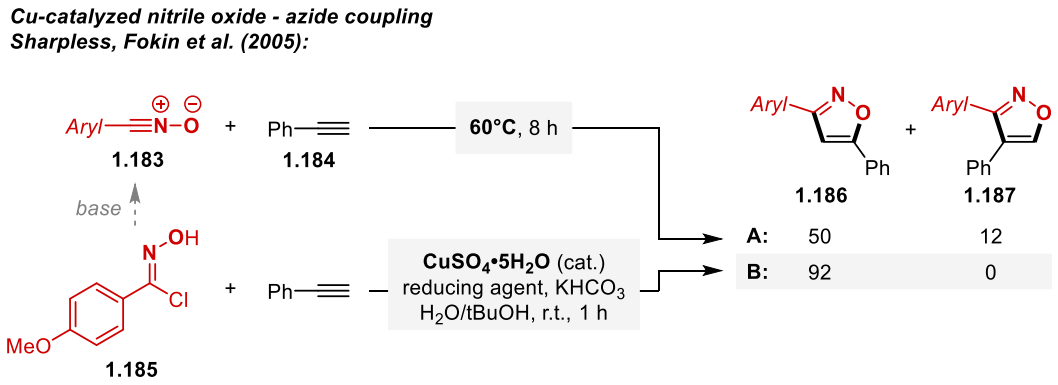

Figure 1-30. Copper catalysis applied to the nitrile oxide alkyne coupling.

Although the use of catalyzed nitrile oxide azide coupling did not find as widespread use as the CuAAC, it has become a recognized tool in bioconjugation chemistry.[126]

1.4.4. The Kinugasa reaction

A catalyzed variant of 1,3-dipolar cycloadditions of particular relevance to this section is the Kinugasa reaction. This process involves the conversion of terminal alkynes **1.192** and nitrones **1.191** in the presence of a copper catalyst to form beta-lactams **1.193** (Figure 1-31). Due to the medicinal relevance of the products obtained, this reaction is of particular interest to the pharmaceutical industry.[127]

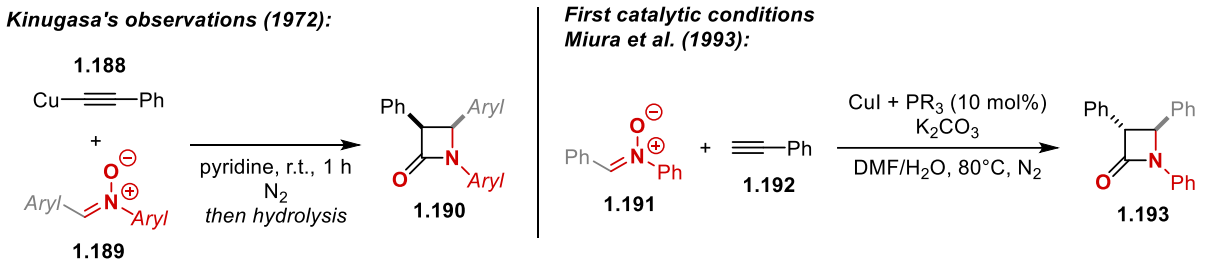

Figure 1-31. Initial works on the Kinugasa reaction.

The original report by Kinugasa in 1972 actually involved the reaction between copper acetylides **1.188** and nitrones **1.189**, which provided beta-lactams **1.190** upon workup.[128] The first catalytic conditions were reported much later by Miura and coworkers in 1993.[129]

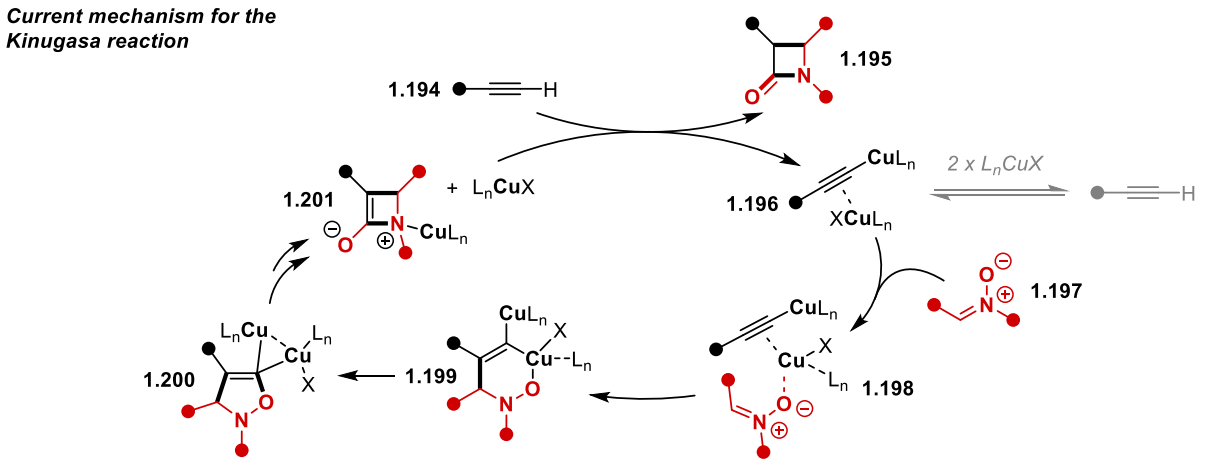

Figure 1-32. Current mechanism of the Kinugasa reaction.

Although early mechanistic ideas involved mono nuclear pathways, on the basis of new evidence provided from the CuAAC, Himo and coworkers reported in 2015 a lower reaction barrier when involving two copper units when performing computational studies on the Kinugasa reaction (Figure 1-32).[130] The mechanism they proposed involved an initial sequence of steps quite similar to the CuAAC, where a complex **1.198** between dinuclear copper acetylide **1.196** and nitrone **1.197** is first formed. The formation of a metallacycle **1.199** ensues, followed by ring contraction to **1.200**. From here, the mechanism diverges (from CuAAC) in order to explain the formation of the observed lactam **1.195**.

A second-order dependence on the copper catalyst within kinetic studies on the reaction by the Hein group later provided some experimental evidence that a dinuclear mechanism may be involved.[131]

Subtleties on the conversion of bis metallated cycloadduct **1.200** to the observed lactam **1.195** were more recently investigated computationally by Himo *et al*.[132]

1.5. Motivation for further investigations in (3+2) cycloaddition chemistry

The literature reviewed herein points to several gaps in our current knowledge within the broad topic of (3+2) cycloadditions.

First, the use of heteroatom-substituted alkynes as TACs in "neutral" (3+2) cycloadditions is extremely sparse. Upon the beginning of our studies on this topic, only a few scattered observations of this reactivity had been reported, and no useful methodology had been developed making use of it. Yet these (3+2) cycloadditions produce reactive intermediates of high interest, as they are potential precursors to valuable, highly functionalized heterocycles.

Second, relatively new principles uncovered from catalytic variants of 1,3-dipolar cycloadditions have potential to be applied towards other classes of (3+2) cycloadditions, such as the "neutral" type introduced herein.

With these opportunities in mind, a series of broad objectives could be elaborated:

1) Investigate the propensity of synthetically useful heteroatom-substituted alkynes towards (3+2) cycloadditions within an intramolecular context.
2) Gain a better mechanistic understanding of neutral (3+2) cycloadditions involving heteroatom-substituted alkynes through experimental and computational studies.
3) Evaluate the scope of these (3+2) cycloadditions and identify catalytic systems that may promote this chemistry under milder conditions.

1.6. Chapter references

1. Hoffmann, R.; Woodward, R. B., Conservation of orbital symmetry. *Acc. Chem. Res.* **1968,** *1* (1), 17-22.
2. Buchner, E., Einwirkung von Diazoessigäther auf die Aether ungesättigter Säuren. *Berichte der deutschen chemischen Gesellschaft* **1888,** *21* (2), 2637-2647.
3. Huisgen, R., 1,3-Dipolar Cycloadditions. *Proc. Chem. Soc.* **1961,** (October), 357-369.
4. Huisgen, R., 1,3-Dipolar Cycloadditions. Past and Future. *Angew. Chem. Int. Ed. Engl.* **1963,** *2* (10), 565-598.
5. Breugst, M.; Reissig, H.-U., The Huisgen Reaction: Milestones of the 1,3-Dipolar Cycloaddition. *Angew. Chem. Int. Ed.* **2020,** *59* (30), 12293-12307.

6. Padwa, A.; Pearson, W. H., *Synthetic applications of 1, 3-dipolar cycloaddition chemistry toward heterocycles and natural products*. John Wiley & Sons: 2003; Vol. 59.
7. Goodall, G. W.; Hayes, W., Advances in cycloaddition polymerizations. *Chem. Soc. Rev.* **2006,** *35* (3), 280-312.
8. Lutz, J.-F., 1,3-Dipolar Cycloadditions of Azides and Alkynes: A Universal Ligation Tool in Polymer and Materials Science. *Angew. Chem. Int. Ed.* **2007,** *46* (7), 1018-1025.
9. Lutz, J.-F.; Zarafshani, Z., Efficient construction of therapeutics, bioconjugates, biomaterials and bioactive surfaces using azide–alkyne "click" chemistry. *Adv. Drug Delivery Rev.* **2008,** *60* (9), 958-970.
10. Moses, J. E.; Moorhouse, A. D., The growing applications of click chemistry. *Chem. Soc. Rev.* **2007,** *36* (8), 1249-1262.
11. Huisgen, R., Kinetics and Mechanism of 1,3-Dipolar Cycloadditions. *Angewandte Chemie International Edition in English* **1963,** *2* (11), 633-645.
12. Sustmann, R., A simple model for substituent effects in cycloaddition reactions. I. 1,3-dipolar cycloadditions. *Tetrahedron Lett.* **1971,** *12* (29), 2717-2720.
13. Sustmann, R., Orbital energy control of cycloaddition reactivity. *Pure Appl. Chem.* **1974,** *40* (4), 569-593.
14. Sustmann, R.; Trill, H., Substituent Effects in 1,3-Dipolar Cycloadditions of Phenyl Azide. *Angewandte Chemie International Edition in English* **1972,** *11* (9), 838-840.
15. Firestone, R. A., Mechanism of 1,3-dipolar cycloadditions. *J. Org. Chem.* **1968,** *33* (6), 2285-2290.
16. Huisgen, R., Mechanism of 1,3-dipolar cycloadditions. Reply. *J. Org. Chem.* **1968,** *33* (6), 2291-2297.
17. Nagase, S.; Morokuma, K., An ab initio molecular orbital study of organic reactions. The energy, charge, and spin decomposition analyses at the transition state and along the reaction pathway. *J. Am. Chem. Soc.* **1978,** *100* (6), 1666-1672.
18. Bickelhaupt, F. M., Understanding reactivity with Kohn–Sham molecular orbital theory: E2–SN2 mechanistic spectrum and other concepts. *J. Comput. Chem.* **1999,** *20* (1), 114-128.
19. Ess, D. H.; Houk, K. N., Distortion/Interaction Energy Control of 1,3-Dipolar Cycloaddition Reactivity. *J. Am. Chem. Soc.* **2007,** *129* (35), 10646-10647.
20. Braida, B.; Walter, C.; Engels, B.; Hiberty, P. C., A Clear Correlation between the Diradical Character of 1,3-Dipoles and Their Reactivity toward Ethylene or Acetylene. *J. Am. Chem. Soc.* **2010,** *132* (22), 7631-7637.
21. Harcourt, R. D., Valence formulae and 1,3 dipolar cycloaddition reactions. *J. Mol. Struct.* **1972,** *12* (3), 351-366.
22. Harcourt, R. D., A re-statement of the concerted-diradical mechanism for 1,3-dipolar cycloaddition reactions. *Tetrahedron* **1978,** *34* (20), 3125-3127.
23. Ríos-Gutiérrez, M.; Domingo, L. R., Unravelling the Mysteries of the [3+2] Cycloaddition Reactions. *Eur. J. Org. Chem.* **2019,** *2019* (2-3), 267-282.
24. Ali, R.; Hasan, A., The Criss-Cross Cycloaddition: A Simple Access to Valuable Heterocycles and Polymers. *ChemistrySelect* **2022,** *7* (47), e202203610.
25. Rádl, S., Crisscross cycloaddition reactions. *Aldrichimica Acta* **1997,** *30*, 97-100.
26. Bailey, J. R.; McPherson, A. T., THE CRISSCROSS ADDITION ON CONJUGATE SYSTEMS. THE ACTION OF CYANIC ACID, THIOCYANIC ACID AND ISOCYANATES ON AZINES. *J. Am. Chem. Soc.* **1917,** *39* (7), 1322-1338.
27. Bailey, J. R.; Moore, N. H., The Use of Cyanic Acid in Glacial Acetic Acid. II. The Addition of Cyanic Acid on Benzalazine. *J. Am. Chem. Soc.* **1917,** *39* (2), 279-291.

28. Burger, K.; Thenn, W.; Gieren, A., The 1:1 Intermediate of the "Criss-Cross" Cycloaddition of Isobutylene to Hexafluoroacetone Azine. *Angew. Chem. Int. Ed. Engl.* **1974,** *13* (7), 474-475.
29. Burger, K.; Thenn, W.; Rauh, R.; Schickaneder, H., [3+2]-Cycloadditions to Trifluoromethyl-Substituted Azomethinimines. *Angew. Chem. Int. Ed. Engl.* **1974,** *13* (7), 477-478.
30. Gieren, A.; Narayanan, P.; Burger, K.; Thenn, W., X-Ray Structure Analysis of the 1:1 Intermediate of the "Criss-Cross" Cycloaddition of Isobutylene to Hexafluoroacetone Azine. *Angew. Chem. Int. Ed. Engl.* **1974,** *13* (7), 475-476.
31. Mathur, S. S.; Suschitzky, H., Syntheses of heterocyclic compounds. Part XXXII. Intramolecular 1,3-dipolar cycloadditions of 2-allyloxy- and 2-prop-2-ynyloxy-aromatic aldehyde azines. *J. Chem. Soc., Perkin Trans. 1* **1975,** (23), 2479-2483.
32. Potáček, M.; Marek, R.; Žák, Z.; Trottier, J.; Janoušek, Z.; Viehe, H. G., Novel thermal tetracyclization by intramolecular azine "criss-cross" addition. *Tetrahedron Lett.* **1993,** *34* (51), 8341-8344.
33. Man, S.; Kulhánek, P.; Potáček, M.; Nečas, M., New fused heterocycles by combined intra-intermolecular criss-cross cycloaddition of nonsymmetrical azines. *Tetrahedron Lett.* **2002,** *43* (36), 6431-6433.
34. Bongers, A.; Clavette, C.; Gan, W.; Gorelsky, S. I.; Betit, L.; Lavergne, K.; Markiewicz, T.; Moon, P. J.; Das Neves, N.; Obhi, N. K.; Toderian, A. B.; Beauchemin, A. M., Intermolecular Aminocarbonylation of Alkenes using Concerted Cycloadditions of Iminoisocyanates. *J. Org. Chem.* **2017,** *82* (2), 1175-1194.
35. Bongers, A.; Ranasinghe, I.; Lemire, P.; Perozzo, A.; Vincent-Rocan, J.-F.; Beauchemin, A. M., Synthesis of Cyclic Azomethine Imines by Cycloaddition Reactions of N-Isocyanates and N-Isothiocyanates. *Org. Lett.* **2016,** *18* (15), 3778-3781.
36. Clavette, C.; Gan, W.; Bongers, A.; Markiewicz, T.; Toderian, A. B.; Gorelsky, S. I.; Beauchemin, A. M., A Tunable Route for the Synthesis of Azomethine Imines and β-Aminocarbonyl Compounds from Alkenes. *J. Am. Chem. Soc.* **2012,** *134* (39), 16111-16114.
37. Gan, W.; Moon, P. J.; Clavette, C.; Das Neves, N.; Markiewicz, T.; Toderian, A. B.; Beauchemin, A. M., Synthesis and Reactivity of Unsymmetrical Azomethine Imines Formed Using Alkene Aminocarbonylation. *Org. Lett.* **2013,** *15* (8), 1890-1893.
38. Lavergne, K.; Bongers, A.; Betit, L.; Beauchemin, A. M., Modular Synthesis of Pyrazolones Using an Alkene Aminocarbonylation Reaction. *Org. Lett.* **2015,** *17* (14), 3612-3615.
39. Sommer, S., [3+2]-Cycloadditions of Azoalkenes to Enamines-Criss-Cross Cycloadditions to Azoalkenes. *Angew. Chem. Int. Ed.* **1979,** *18* (9), 695-696.
40. Clarke, S. J.; Davies, D. E.; Gilchrist, T. L., Competing [4 + 2] and [3 + 2] cycloaddition in the reactions of nucleophilic olefins with ethyl 3-(toluene-p-sulphonylazo)but-2-enoate. *J. Chem. Soc., Perkin Trans. 1* **1983,** (0), 1803-1807.
41. Attanasi, O. A.; Favi, G.; Filippone, P.; Golobič, A.; Stanovnik, B.; Svete, J., Unexpected Behavior of the Reaction between 1,2-Diaza-1,3-Butadienes and 3-Dimethylaminopropenoates: A Useful Entry to New Pyrrolines, Pyrroles, and Oxazolines. *J. Org. Chem.* **2005,** *70* (11), 4307-4313.
42. Attanasi, O. A.; Favi, G.; Mantellini, F.; Moscatelli, G.; Santeusanio, S., A Novel Assembly of Substituted Pyrroles by Acid-Catalyzed Sequential Three-Component Reaction of Amines, Alkynoates, and 1,2-Diaza-1,3-dienes. *Adv. Synth. Catal.* **2011,** *353* (9), 1519-1524.
43. Attanasi, O. A.; Favi, G.; Mantellini, F.; Moscatelli, G.; Santeusanio, S., Synthesis of Functionalized Pyrroles via Catalyst- and Solvent-Free Sequential Three-Component Enamine−Azoene Annulation. *J. Org. Chem.* **2011,** *76* (8), 2860-2866.
44. Ciccolini, C.; Mari, G.; Gatti, F. G.; Gatti, G.; Giorgi, G.; Mantellini, F.; Favi, G., Synthesis of Polycyclic Fused Indoline Scaffolds through a Substrate-Guided Reactivity Switch. *J. Org. Chem.* **2020,** *85* (17), 11409-11425.

45. Mari, G.; Catalani, S.; Antonini, E.; De Crescentini, L.; Mantellini, F.; Santeusanio, S.; Lombardi, P.; Amicucci, A.; Battistelli, S.; Benedetti, S.; Palma, F., Synthesis and biological evaluation of novel heteroring-annulated pyrrolino-tetrahydroberberine analogues as antioxidant agents. *Biorg. Med. Chem.* **2018,** *26* (18), 5037-5044.
46. Mari, G.; Crescentini, L. D.; Favi, G.; Lombardi, P.; Fiorillo, G.; Giorgi, G.; Mantellini, F., Heteroring-Annulated Pyrrolino-Tetrahydroberberine Analogues. *Asian J. Org. Chem.* **2017,** *6* (6), 720-727.
47. Mei, G.-J.; Zheng, W.; Gonçalves, T. P.; Tang, X.; Huang, K.-W.; Lu, Y., Catalytic Asymmetric Formal [3+2] Cycloaddition of Azoalkenes with 3-Vinylindoles: Synthesis of 2,3-Dihydropyrroles. *iScience* **2020,** *23* (2), 100873.
48. Davies, D. E.; Gilchrist, T. L., Investigation of the retro-Diels–Alder reaction as a method for the generation of nitroso-olefins. *J. Chem. Soc., Perkin Trans. 1* **1983,** (0), 1479-1481.
49. Davies, D. E.; Gilchrist, T. L.; Roberts, T. G., The cycloaddition of α-nitrosostyrenes to olefins. Investigations of the scope and mechanism of the reaction. *J. Chem. Soc., Perkin Trans. 1* **1983,** (0), 1275-1281.
50. Behringer, H.; Wiedenmann, R., Isomere der thiathiophthene aus trithionen und acetylenen. *Tetrahedron Lett.* **1965,** *6* (41), 3705-3712.
51. Easton, D. B. J.; Leaver, D., 1,3-Dipolar reactivity of 1,2-dithiole-3-thiones and 1,3-dithiolan-2-thiones. *Chem. Commun. (London)* **1965,** (22), 585-586.
52. Easton, D. B. J.; Leaver, D.; Rawlings, T. J., The dithiole series. Part V. Reactions of 1,2-dithiole-3-thiones and 1,3-dithiolan-2-thiones with acetylenic esters and with benzyne. *J. Chem. Soc., Perkin Trans. 1* **1972,** (0), 41-45.
53. Lakshmikantham, M. V.; Cava, M. P., Isomeric ethylene selenodithiocarbonates. *J. Org. Chem.* **1976,** *41* (5), 879-881.
54. Lakshmikantham, M. V.; Cava, M. P., Alternate synthesis of tetraselenafulvalene. *J. Org. Chem.* **1976,** *41* (5), 882-882.
55. Nakayama, J.; Kimata, A.; Taniguchi, H.; Takahashi, F., Reactions of 1,3-benzodithiole-2-thione and ethylene trithiocarbonate with benzyne generated from 2-carboxybenzenediazonium chloride: preparation of novel bicyclic sulfonium salts by trapping 1,3-dipolar cycloaddition intermediates. *Chem. Commun.* **1996,** (2), 205-206.
56. O'Connor, B. R.; Jones, F. N., Reactions of ethylene di- and trithiocarbonates with acetylenes. Anomalous reaction with bromocyanoacetylene to give a thioacyl bromide. *J. Org. Chem.* **1970,** *35* (6), 2002-2005.
57. Akiba, K.-y.; Ochiumi, M.; Tsuchiya, T.; Inamoto, N., Formation of 2-arylaminothiazoles by 1,3-dipolar cycloaddition of "Hector's base" with acetylenes. *Tetrahedron Lett.* **1975,** *16* (7), 459-462.
58. Oliver, J. E.; Brown, R. T., Imino-1,2,4-dithiazoles. II. Dipolar additions. *J. Org. Chem.* **1974,** *39* (15), 2228-2233.
59. Zhang, J.; Page, A. C. S.; Palani, V.; Chen, J.; Hoye, T. R., Atypical Mode of [3 + 2]-Cycloaddition: Pseudo-1,3-dipole Behavior in Reactions of Electron-Deficient Thioamides with Benzynes. *Org. Lett.* **2018,** *20* (18), 5550-5553.
60. Li, Y.; Mück-Lichtenfeld, C.; Studer, A., Sulfonium Ylides by (3+2) Cycloaddition of Arynes with Vinyl Sulfides: Stereoselective Synthesis of Highly Substituted Alkenes. *Angew. Chem. Int. Ed.* **2016,** *55* (46), 14435-14438.
61. Ding, W.; Yu, A.; Zhang, L.; Meng, X., Construction of Eight-Membered Cyclic Diaryl Sulfides via Domino Reaction of Arynes with Thioaurone Analogues and DFT Study on the Reaction Mechanism. *Org. Lett.* **2019,** *21* (22), 9014-9018.

62. Xiao, P.; Su, S.; Wang, W.; Cao, W.; Chen, J.; Li, J.; Chen, Y., Sequential cycloaddition and ring expansion reaction of arynes and methylenebenzothiopheneones: synthesis of a benzo-fused eight-membered ring via sulfonium ylides. *RSC Advances* **2019,** *9* (67), 39119-39123.
63. Lockley, W. J. S.; Lwowski, W., Cyclic aminimides containing the pyrazolone skeleton. *Tetrahedron Lett.* **1974,** *15* (48), 4263-4266.
64. Ivanovich, R. A.; Clavette, C.; Vincent-Rocan, J.-F.; Roveda, J.-G.; Gorelsky, S. I.; Beauchemin, A. M., Intramolecular Alkene Aminocarbonylation Using Concerted Cycloadditions of Amino-Isocyanates. *Chem. - Eur. J.* **2016,** *22* (23), 7906-7916.
65. Ivanovich, R. A.; Quartus, J. A. M.; Das Neves, N.; Loiseau, F.; Raymond, M.; Beauchemin, A. M., Aminimide Synthesis Using Concerted Amination Reactions of Alkenes: Scope and Mechanistic Information. *J. Org. Chem.* **2019,** *84* (15), 9792-9800.
66. Roveda, J.-G.; Clavette, C.; Hunt, A. D.; Gorelsky, S. I.; Whipp, C. J.; Beauchemin, A. M., Hydrazides as Tunable Reagents for Alkene Hydroamination and Aminocarbonylation. *J. Am. Chem. Soc.* **2009,** *131* (25), 8740-8741.
67. Allen, M. A.; Ivanovich, R. A.; Beauchemin, A. M., O-Isocyanates as Uncharged 1,3-Dipole Equivalents in [3+2] Cycloadditions. *Angew. Chem. Int. Ed.* **2020,** *59* (51), 23188-23197.
68. Campeau, D.; Gagosz, F., Heteroatom-substituted alkynes as three-atom components in (3+2) cycloadditions. *Cell Rep. Phys. Sci.* **2023,** *4* (1).
69. Boonstra, H. J.; Arens, J. F., Chemistry of acetylenic ethers XLII: A simplified method for the preparation of acetylenic thioethers; a number of new reactions of these compounds. *Recl. Trav. Chim. Pays-Bas* **1960,** *79* (8), 866-887.
70. Shermolovich, Y. G.; Timoschenko, V. M.; Musyanovich, R. Y.; Povolotsky, M. I.; Pirozhenko, V. V.; Markovsky, L. N., 1-(alkylthio)-polyfluoroalkynes. Reactions with mercaptans and thermal transformations. *Heteroat. Chem* **1998,** *9* (2), 151-154.
71. Wasserman, H. H.; Fernandez, J. M., Novel reactions of benzyne with acetylenic ethers. *J. Am. Chem. Soc.* **1968,** *90* (19), 5322-5323.
72. Stiles, M.; Burckhardt, U.; Haag, A., Reaction of Benzyne with Acetylenic Compounds. *J. Org. Chem.* **1962,** *27* (12), 4715-4716.
73. McAusland, D. Arynes in synthesis; New reaction and precursor development. PhD Dissertation, University of Manchester, Manchester, 2014.
74. Matsuzawa, T.; Hosoya, T.; Yoshida, S., One-step synthesis of benzo[b]thiophenes by aryne reaction with alkynyl sulfides. *Chem. Sci.* **2020,** *11* (35), 9691-9696.
75. Medina, J. M.; Mackey, J. L.; Garg, N. K.; Houk, K. N., The Role of Aryne Distortions, Steric Effects, and Charges in Regioselectivities of Aryne Reactions. *J. Am. Chem. Soc.* **2014,** *136* (44), 15798-15805.
76. Merk, B.; Fath, M.; Pritzkow, H.; Latscha, H. P., Synthese und Untersuchung neuer 1λ5, 4λ5-Diphosphapentalen- und 1λ5,4λ5 - sowie 1λ5,5λ5-Diphosphaazulen-Systeme / Synthesis of New 1λ5,4λ5-Diphosphapentalene- and 1λ5,5λ5-Diphosphaazulene Systems. *Z. Naturforsch. B* **1997,** *52* (1), 1-8.
77. Burangulova, R. N.; Trishin, Y. G.; Konovalova, I. V.; Burnaeva, L. A.; Chistokletov, V. N.; Pudovik, A. N., Reaction of dialkyl alkynylphosphonites with benzoyl cyanide and benzoylformate esters. *Zh. Obshch. Khim.* **1989,** *59* (9), 1979.
78. Dokuchaeva, I. S.; Konovalova, V. I.; Trishin, Y. G.; Burnaeva, L. A.; Kazanina, T. Y.; Chistokletov, V. N.; Pudovik, A. N., Reactions of dialkyl alkynylphosphonites with diethyl mesoxalate in the presence of proton donors. *Zh. Obshch. Khim.* **1991,** *61* (3), 611.
79. Drozd, V. N., Reaction of ethyl propiolate and benzoylacetylene with allyl and benzyl esters of dithiobenzoic acid. *Zh. Org. Khim.* **1989,** *25* (7), 1559.

80. Gaumont, A.-C.; Simon, A.; Denis, J.-M., Uncatalyzed hydrophosphination of multiple bonds by alkenyl- or alkynyl-phosphine-oxides; evidence for a P-H activation. *Tetrahedron Lett.* **1998,** *39* (9), 985-988.
81. Huang, Y.; Bentrude, W. G., Conformational Equilibria of Phosphoranes with 5-Alkyl-Substituted 1,3,2-Dioxaphosphorinane Rings Attached Diequatorially to Five-Coordinated Phosphorus. Are Boat/Twist Conformations Populated? *J. Am. Chem. Soc.* **1995,** *117* (50), 12390-12396.
82. Konovalova, I. V.; Dokuchaeva, I. S.; Trishin, Y. G.; Burnaeva, L. A.; Chistokletov, V. N.; Pudovik, A. N., Reaction of dimethyl alkynylphosphonites with trifluoromethyl carbonyl compounds, chloral, and bromal. *Zh. Obshch. Khim.* **1989,** *59* (8), 1726.
83. Konovalova, I. V.; Trishin, Y. G.; Burnaeva, L. A.; Dokuchaeva, I. S.; Chistokletov, V. N.; Pudovik, A. N. Method of producing 1,3-dioxa-2,2-dimethoxy-4,7-bis(alkoxycarbonyl)-6-phenyl-2-phosphabicyclo[3.2.0]heptenes. SU1439106, 1988.
84. Konovalova, I. V.; Trishin, Y. G.; Burnaeva, L. A.; Khusnutdinova, E. K.; Chistokletov, V. N.; Pudovik, A. N., Reaction of diphenyl isocyanatophosphite and dimethyl alkynylphosphonites with diphenylcarbodiimide and N-(2,2,2-trichloroethyl)acetamide. *Zh. Obshch. Khim.* **1988,** *58* (6), 1292.
85. Konovalova, I. V.; Trishin, Y. G.; Dokuchaeva, L. A.; Burnaeva, L. A.; Efremov, Y. Y.; Kazanina, T. Y.; Chistokletov, V. N.; Pudovik, A. N., Reaction of dialkyl alkynylphosphonites with diethyl mesoxalate and trimethyl pyruvonitrile. *Zh. Obshch. Khim.* **1990,** *60* (8), 1706.
86. Mironov, V. F.; Dimukhametov, M. N.; Mironova, E. V.; Krivolapov, D. B.; Abdrakhmanova, L. M., Caged C-P phosphoranes based on 2-(2-methyl-4-oxopent-2-yloxy)- and 2-[2-(methylcarbonyl)-1-phenoxy]-1,3,2-benzodioxaphospholes and diethyl mesoxalate. *Russ. J. Gen. Chem.* **2015,** *85* (2), 441-449.
87. Trishin, Y. G.; Konovalova, I. V.; Burangulova, R. N.; Burnaeva, L. A.; Chistokletov, V. N.; Pudovik, A. N., Reaction of dialkyl alkynylphosphonites with pyruvate esters. *Zh. Obshch. Khim.* **1988,** *58* (11), 2434.
88. Trishin, Y. G.; Mingazova, B. F.; Konovalova, I. V., Preparation of 1-methyl-3-methoxy-3-oxo-2,5-diphenyl-Δ4-1,3-azaphospholine by reaction of methyl (2-phenylethynyl)phosphonite with N-benzylidenemethylamine. *Zh. Obshch. Khim.* **1995,** *65* (1), 161.
89. Trishin, Y. G.; Vorob'ev, M. V.; Namestnikov, V. I., Synthesis of 3-oxo-3-ethoxy-2-p-fluorophenyl-5-tert-butyl-Δ4-1,3-oxaphospholene. *Zh. Obshch. Khim.* **1995,** *65* (1), 164.
90. Trishin, Y. G.; Vorob'ev, M. V.; Nemestnikov, V. I., Preparation of 4-benzoyl-1-methoxy-1-oxo-3,5-diphenyl-Δ2-phospholene by reaction of methyl (2-phenylethynyl)phosphonite with benzylideneacetophenone. *Zh. Obshch. Khim.* **1996,** *66* (6), 1049-1050.
91. Trishin, Y. G. V. e., M. V.; Namestnikov, V. I., Cyclization of Ethyl (3,3-Dimethyl-1-butynyl)-(1-hydroxy-1-phenyl-2,2,2-trifluoroethyl)phosphinate. *Zh. Obshch. Khim.* **1997,** *67* (12), 2057-2058.
92. Campeau, D.; Pommainville, A.; Gagosz, F., Ynamides as Three-Atom Components in Cycloadditions: An Unexplored Chemical Reaction Space. *J. Am. Chem. Soc.* **2021,** *143* (25), 9601-9611.
93. Campeau, D.; Pommainville, A.; Gorodnichy, M.; Gagosz, F., Copper and Silver Catalysis in the (3 + 2) Cycloaddition of Neutral Three-Atom Components with Terminal Alkynes. *J. Am. Chem. Soc.* **2023,** *145* (34), 19018-19029.
94. Pommainville, A.; Campeau, D.; Gagosz, F., The Synthetic Potential of Thiophenium Ylide Cycloadducts**. *Angew. Chem. Int. Ed.* **2022,** *61* (32), e202205963.
95. Smith, P. J.; Jiang, Y.; Tong, Z.; Pickford, H. D.; Christensen, K. E.; Nugent, J.; Anderson, E. A., Synthesis of Polysubstituted Fused Pyrroles by Gold-Catalyzed Cycloisomerization/1,2-Sulfonyl Migration of Yndiamides. *Org. Lett.* **2021,** *23* (16), 6547-6552.

96. Tawatari, T.; Kato, R.; Kudo, R.; Takasu, K.; Takikawa, H., Intramolecular Ynamide–Benzyne (3+2) Cycloadditions. *Angew. Chem. Int. Ed.* **2023,** *62* (19), e202300907.
97. Hashimoto, T.; Maruoka, K., Recent Advances of Catalytic Asymmetric 1,3-Dipolar Cycloadditions. *Chem. Rev.* **2015,** *115* (11), 5366-5412.
98. Michael, A., Ueber die Einwirkung von Diazobenzolimid auf Acetylendicarbonsäuremethylester. *J. Prakt. Chem.* **1893,** *48* (1), 94-95.
99. Wang, C.; Ikhlef, D.; Kahlal, S.; Saillard, J.-Y.; Astruc, D., Metal-catalyzed azide-alkyne "click" reactions: Mechanistic overview and recent trends. *Coord. Chem. Rev.* **2016,** *316*, 1-20.
100. Rostovtsev, V. V.; Green, L. G.; Fokin, V. V.; Sharpless, K. B., A Stepwise Huisgen Cycloaddition Process: Copper(I)-Catalyzed Regioselective "Ligation" of Azides and Terminal Alkynes. *Angew. Chem. Int. Ed.* **2002,** *41* (14), 2596-2599.
101. Tornøe, C. W.; Christensen, C.; Meldal, M., Peptidotriazoles on Solid Phase: [1,2,3]-Triazoles by Regiospecific Copper(I)-Catalyzed 1,3-Dipolar Cycloadditions of Terminal Alkynes to Azides. *J. Org. Chem.* **2002,** *67* (9), 3057-3064.
102. Agard, N. J.; Prescher, J. A.; Bertozzi, C. R., A Strain-Promoted [3 + 2] Azide–Alkyne Cycloaddition for Covalent Modification of Biomolecules in Living Systems. *J. Am. Chem. Soc.* **2004,** *126* (46), 15046-15047.
103. The Nobel Prize in Chemistry 2022: It just says click – and the molecules are coupled together. The Royal Swedish Academy of Sciences: Stockholm, Sweden, 2022.
104. Berg, R.; Straub, B. F., Advancements in the mechanistic understanding of the copper-catalyzed azide–alkyne cycloaddition. *Beilstein J. Org. Chem.* **2013,** *9*, 2715-2750.
105. Rodionov, V. O.; Fokin, V. V.; Finn, M. G., Mechanism of the Ligand-Free CuI-Catalyzed Azide–Alkyne Cycloaddition Reaction. *Angew. Chem. Int. Ed.* **2005,** *44* (15), 2210-2215.
106. Ahlquist, M.; Fokin, V. V., Enhanced Reactivity of Dinuclear Copper(I) Acetylides in Dipolar Cycloadditions. *Organometallics* **2007,** *26* (18), 4389-4391.
107. Worrell, B. T.; Malik, J. A.; Fokin, V. V., Direct Evidence of a Dinuclear Copper Intermediate in Cu(I)-Catalyzed Azide-Alkyne Cycloadditions. *Science* **2013,** *340* (6131), 457-460.
108. Jin, L.; Tolentino, D. R.; Melaimi, M.; Bertrand, G., Isolation of bis(copper) key intermediates in Cu-catalyzed azide-alkyne "click reaction". *Science Advances* **2015,** *1* (5), e1500304.
109. Özkılıç, Y.; Tüzün, N. Ş., A DFT Study on the Binuclear CuAAC Reaction: Mechanism in Light of New Experiments. *Organometallics* **2016,** *35* (16), 2589-2599.
110. Straub, B. F., μ-Acetylide and μ-alkenylidene ligands in "click" triazole syntheses. *Chem. Commun.* **2007,** (37), 3868-3870.
111. Ben El Ayouchia, H.; Bahsis, L.; Anane, H.; Domingo, L. R.; Stiriba, S.-E., Understanding the mechanism and regioselectivity of the copper(i) catalyzed [3 + 2] cycloaddition reaction between azide and alkyne: a systematic DFT study. *RSC Advances* **2018,** *8* (14), 7670-7678.
112. Calvo-Losada, S.; Pino-González, M. S.; Quirante, J. J., Rationalizing the Catalytic Activity of Copper in the Cycloaddition of Azide and Alkynes (CuAAC) with the Topology of ∇2ρ(r) and ∇∇2ρ(r). *J. Phys. Chem. B* **2015,** *119* (4), 1243-1258.
113. Halbes-Letinois, U.; Weibel, J.-M.; Pale, P., The organic chemistry of silver acetylides. *Chem. Soc. Rev.* **2007,** *36* (5), 759-769.
114. Sladkov, A. M.; Lev Yu, U., Copper and Silver Acetylides in Organic Synthesis. *Russian Chemical Reviews* **1968,** *37* (10), 748.
115. McNulty, J.; Keskar, K., Discovery of a Robust and Efficient Homogeneous Silver(I) Catalyst for the Cycloaddition of Azides onto Terminal Alkynes. *Eur. J. Org. Chem.* **2012,** *2012* (28), 5462-5470.
116. McNulty, J.; Keskar, K.; Vemula, R., The First Well-Defined Silver(I)-Complex-Catalyzed Cycloaddition of Azides onto Terminal Alkynes at Room Temperature. *Chem. - Eur. J.* **2011,** *17* (52), 14727-14730.

117. Ali, A. A.; Chetia, M.; Saikia, B.; Saikia, P. J.; Sarma, D., AgN(CN)2/DIPEA/H2O-EG: a highly efficient catalytic system for synthesis of 1,4-disubstituted-1,2,3 triazoles at room temperature. *Tetrahedron Lett.* **2015,** *56* (43), 5892-5895.
118. Ben El Ayouchia, H.; Bahsis, L.; Fichtali, I.; Domingo, L. R.; Ríos-Gutiérrez, M.; Julve, M.; Stiriba, S.-E. Deciphering the Mechanism of Silver Catalysis of "Click" Chemistry in Water by Combining Experimental and MEDT Studies *Catalysts* **2020**, *10* (9), 956.
119. Ferretti, A. M.; Ponti, A.; Molteni, G., Silver(I) oxide nanoparticles as a catalyst in the azide–alkyne cycloaddition. *Tetrahedron Lett.* **2015,** *56* (42), 5727-5730.
120. Ortega-Arizmendi, A. I.; Aldeco-Pérez, E.; Cuevas-Yañez, E., Alkyne-Azide Cycloaddition Catalyzed by Silver Chloride and "Abnormal" Silver N-Heterocyclic Carbene Complex. *The Scientific World Journal* **2013,** *2013* (1), 186537.
121. Boz, E.; Tüzün, N. Ş., Ag-catalyzed azide alkyne cycloaddition: a DFT approach. *Dalton Trans.* **2016,** *45* (13), 5752-5764.
122. Khairbek, A. A.; Badawi, M. A. A.-H., Mechanism of Ag(I)-catalyzed azide-alkyne cycloaddition reaction: a quantum mechanical investigation. *Reaction Kinetics, Mechanisms and Catalysis* **2023,** *136* (1), 69-81.
123. Del Castillo, T. J.; Sarkar, S.; Abboud, K. A.; Veige, A. S., 1,3-Dipolar cycloaddition between a metal–azide (Ph3PAuN3) and a metal–acetylide (Ph3PAuC≡CPh): an inorganic version of a click reaction. *Dalton Transactions* **2011,** *40* (32), 8140-8144.
124. Powers, A. R.; Ghiviriga, I.; Abboud, K. A.; Veige, A. S., Au-iClick mirrors the mechanism of copper catalyzed azide–alkyne cycloaddition (CuAAC). *Dalton Trans.* **2015,** *44* (33), 14747-14752.
125. Himo, F.; Lovell, T.; Hilgraf, R.; Rostovtsev, V. V.; Noodleman, L.; Sharpless, K. B.; Fokin, V. V., Copper(I)-Catalyzed Synthesis of Azoles. DFT Study Predicts Unprecedented Reactivity and Intermediates. *J. Am. Chem. Soc.* **2005,** *127* (1), 210-216.
126. Heaney, F., Nitrile Oxide/Alkyne Cycloadditions – A Credible Platform for Synthesis of Bioinspired Molecules by Metal-Free Molecular Clicking. *Eur. J. Org. Chem.* **2012,** *2012* (16), 3043-3058.
127. Stecko, S.; Furman, B.; Chmielewski, M., Kinugasa reaction: an 'ugly duckling' of β-lactam chemistry. *Tetrahedron* **2014,** *70* (43), 7817-7844.
128. Kinugasa, M.; Hashimoto, S., The reactions of copper(I) phenylacetylide with nitrones. *J. Chem. Soc., Chem. Commun.* **1972,** (8), 466-467.
129. Okuro, K.; Enna, M.; Miura, M.; Nomura, M., Copper-catalysed reaction of arylacetylenes with C,N-diarylnitrones. *J. Chem. Soc., Chem. Commun.* **1993,** (13), 1107-1108.
130. Santoro, S.; Liao, R.-Z.; Marcelli, T.; Hammar, P.; Himo, F., Theoretical Study of Mechanism and Stereoselectivity of Catalytic Kinugasa Reaction. *J. Org. Chem.* **2015,** *80* (5), 2649-2660.
131. Malig, T. C.; Yu, D.; Hein, J. E., A Revised Mechanism for the Kinugasa Reaction. *J. Am. Chem. Soc.* **2018,** *140* (29), 9167-9173.
132. Santoro, S.; Himo, F., Mechanism of the Kinugasa Reaction Revisited. *J. Org. Chem.* **2021,** *86* (15), 10665-10671.

2. Chapter 2 – The intramolecular (3+2) reactivity between ynamides and alkynes

Reprinted (adapted) with permission from [Campeau, D.; Pommainville, A.; Gagosz, F., Ynamides as Three-Atom Components in Cycloadditions: An Unexplored Chemical Reaction Space. *J. Am. Chem. Soc.* **2021**, *143* (25), 9601-9611]. Copyright 2021 American Chemical Society.

This report involves results by both D. Campeau and A. Pommainville. Results in this chapter were obtained by D. Campeau unless otherwise noted with "*Results in this figure obtained by …*".

2.1. Ynamides as synthons in cycloaddition chemistry

Ynamides **2.002** are the stabilized analogs of ynamines **2.001** (Figure 2-1). Although unstabilized ynamines were the first N-alkynyl species studied,[1-2] their high reactivity made them particularly difficult to isolate and work with, making them little-used synthons to this date. Renewed interest in the N-alkynyl synthon quickly followed from breakthroughs in cross-coupling methods permitting to access them, such as those of Danheiser,[3] Hsung,[4] Stahl[5] and Evano.[6]

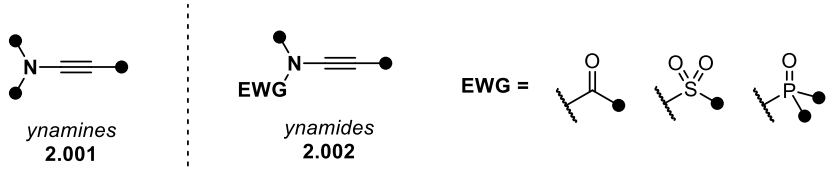

Figure 2-1. Ynamines and ynamides.

A cursory look at possible cycloaddition events involving any other synthon with ynamides provides only three outcomes (Figure 2-2, excluding (n+1) cycloadditions). The α,β outcome can be readily explained by treating ynamides as simple functionalized alkynes. The N,α and N,β outcomes are, on the other hand, less trivial and make direct use of the nitrogen atom to form new N-heterocycles.

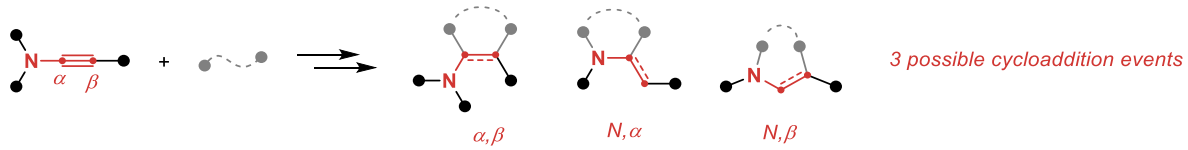

Figure 2-2. Possible cycloaddition events involving ynamides.

Ynamides are classically understood to be nucleophilic from their β-carbon, and consequently electrophilic from their α-carbon, as suggested by their mesomeric form **2.004** (Figure 2-3). This logic

has largely guided the early use of ynamides in synthetic organic chemistry, which has predominantly involved the α,β functionalization of ynamides.[7-8]

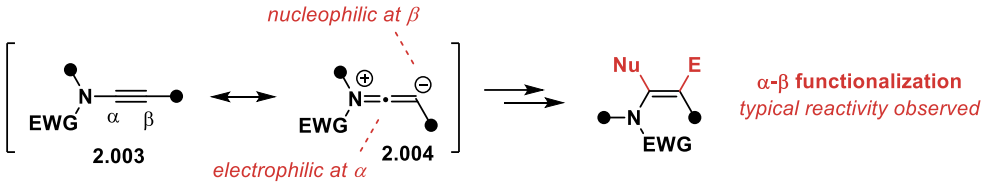

Figure 2-3. The classical α-β reactivity of ynamides.

The α,β cycloaddition reactivity of ynamides, more specifically, is vast enough to have already been reviewed multiple times,[9-10] comprising of many examples of (2+2), (3+2), (4+2) cycloadditions amongst more.

The direct use of the nitrogen atom in ynamides to form new bonds is comparatively quite rare. This is perhaps unsurprising, as the nitrogen atom in amides is not particularly nucleophilic, and the linear nature of ynamides renders it difficult to induce reactivity at nitrogen even with strategies involving geometrical constraints.

A well-studied outcome of chemistry directly involving the N-atom of ynamides **2.005** is the formation of ketenimine species **2.006** (Figure 2-4). Some of the typical routes to ketenimines from ynamides involve deprotection of the EWG and 1,3-transposition of allyl groups. These strategies have been previously reviewed by Cariou.[11] A unique radical-based method involving chain polymerization has also been reported.[12]

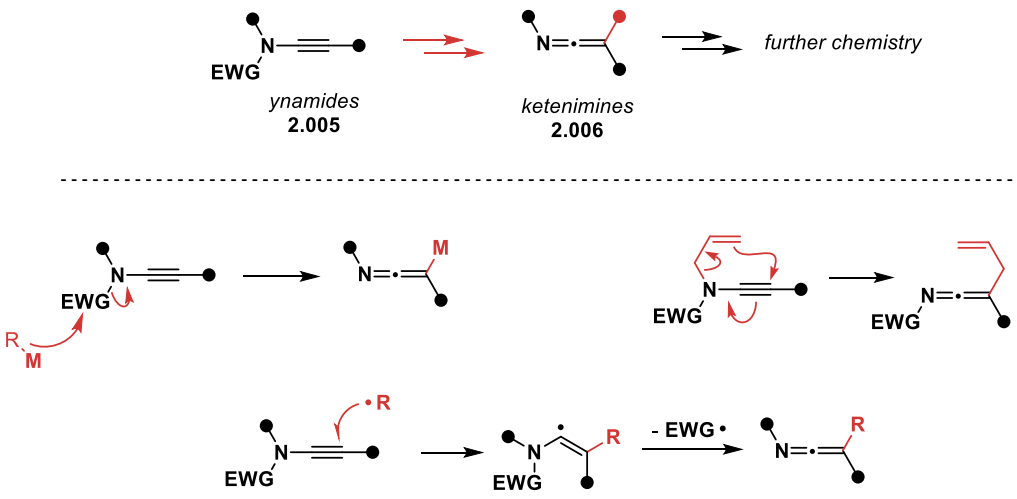

Figure 2-4. Conversion of ynamides to ketenimines.

The N,α cycloaddition of ynamides is best observed through the intermediate generation of such ketenimine species. A particularly fitting example can be found in the Cariou group's studies on the base-mediated generation of ketenimines **2.009** from ynamides **2.007** (Figure 2-5).[13] When these ketenimines are generated alongside aza-allyl anions **2.010** upon heating, formal (3+2) products **2.011** are obtained.

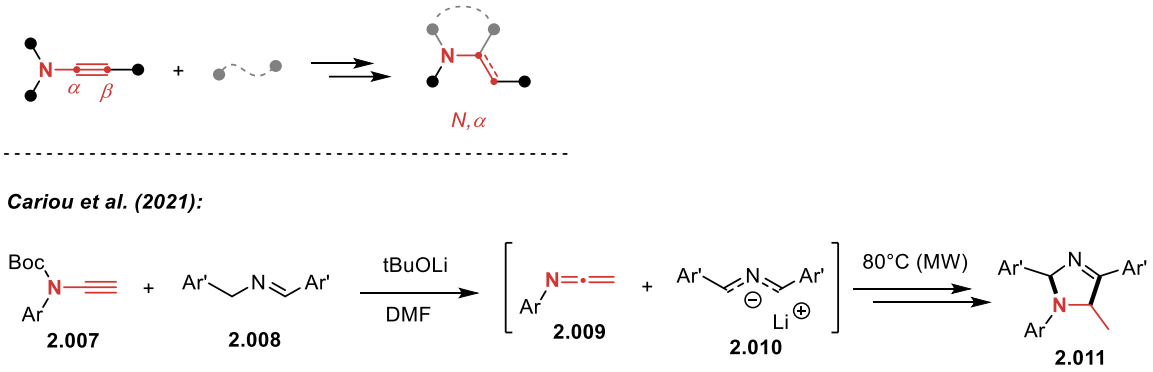

Figure 2-5. N,α cycloaddition products via ketenimine intermediates.

While N,α products have been observed, it is interesting to note that possible N,β cycloaddition products, on the other hand, had never been reported prior to our investigations on the topic (Figure 2-6). The N,β reactivity would in fact imply use of ynamides as *neutral three-atom components* in a cycloaddition reaction.

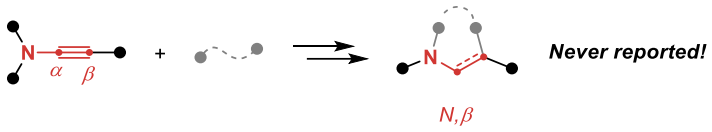

Figure 2-6. Lack of literature precedents for the N,β-cycloadditions of ynamides.

Although ynamides may be used as synthons to form new N-containing heterocycles, these cases are rarer exceptions to the typically reported reactivity of ynamides. New ways of making use of all three atoms of the ynamide synthon could lead to valuable N-containing heterocycles. N,β cycloaddition products may be a potential gap in the cycloaddition chemistry of ynamides.

2.2. Unexpected results and discovery of a new mode of reactivity in ynamides

Our first foray into the "neutral" (3+2) chemistry of ynamides came serendipitously when attempting to access the yne-ynamide scaffold **2.014a**. Upon submitting bromoalkyne **2.012** and sulfonamide **2.013** to Hsung's cross-coupling conditions[4] overnight, a minor product **2.015a** was observed

alongside the expected product **2.014a** (Figure 2-7). Although these two products eluted quite closely by silica gel chromatography, the minor product was quite crystalline, and could be observed to precipitate out of some of the collected fractions. This was a curious observation, since the expected yne-ynamides of the type **2.014a** tend to manifest as thick oils. These two products were ultimately isolated, and upon heating the yne-ynamide **2.014a** under similar conditions overnight, without any of the reagents used in the copper catalysis, a mixture of **2.014a** and **2.015a** was obtained. This meant that **2.015a** is the product of a thermal isomerization occurring in yne-ynamide **2.014a**.

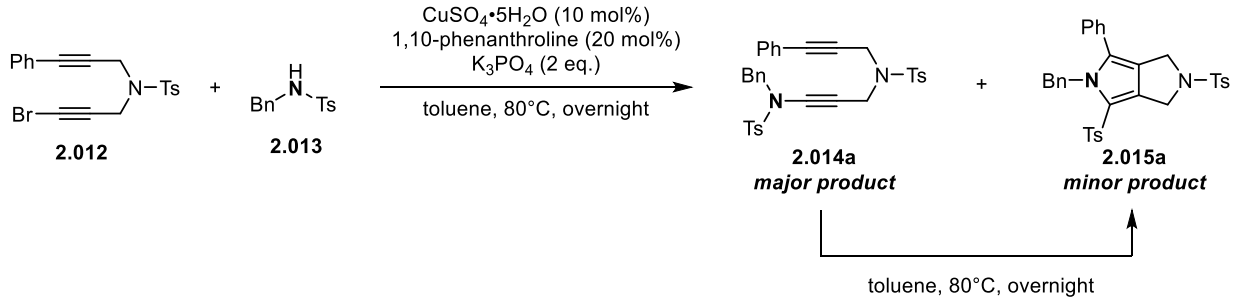

Figure 2-7. Initial observations of the unexpected by-product **2.015a**.

Although its curious structure could be ascertained through the use of 2D NMR (see Supporting Information, section 6.2.9), it was ultimately confirmed through single crystal x-ray diffraction (SCXRD) studies of a sample co-crystallized with DMSO (Figure 2-8).

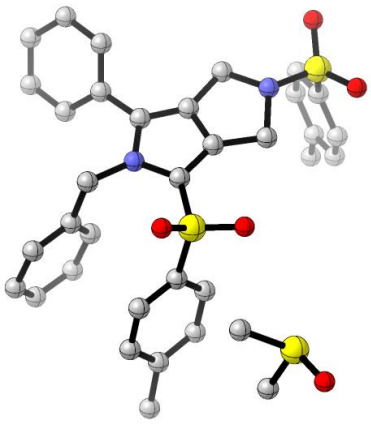

Figure 2-8. SCXRD structure of **2.015a** co-crystallized with DMSO (hydrogens omitted). See CCDC deposition # 2062485 for acquisition data.

Extensive literature search at the time did not produce any report of the use of ynamides as three-atom synthons towards the formation of 5-membered cycloadducts through simple thermal means.

It was quite clear that we had stumbled on an interesting and yet unexplored facet of ynamide chemistry, so the choice was made to investigate the mechanism and scope of this intramolecular cyclization.

2.3. Optimization of the reaction conditions

To access reasonable reaction times, the temperature was increased to 130 °C, where full conversion of the starting material was observed after 2 hours (Entry 2, Table 2-1). While this provided a reasonable NMR yield of 72%, approximately a quarter of the material was degraded towards other products. When obtaining this range of yields, a complex mixture of small signals were observed from the NMR spectrum of the crude reaction mixture, and no specific by-product could ever be isolated in large enough quantity to be characterized. Considering that there was no initial purging of the oxygen in the sealed tubes employed and that the material was heated at high temperatures, purging with argon was attempted (Entry 3). This did not cause any significant deviation to the observed yield.

A literature search done in parallel during these initial studies provided some suggestions on what additives may be beneficial. In particular, Danheiser and coworkers observed in multiple studies involving the intramolecular thermal cycloaddition of analogous poly-yne systems that phenol additives tend to increase their observed yields.[14-15] The authors also noted that the yields were augmented without significantly affecting the rates of the reactions, and suggested that the role of phenols may be to suppress polymerization of the starting material.

So, butylated hydroxy toluene (BHT), a cheap phenol-type additive, was tested under our reaction conditions (Entries 4-7). An improvement in yield was gratifyingly achieved by increasing the amount of BHT up to 1 equivalent, where an NMR yield of 96% (isolated 90%) was obtained. Another hydrogen atom donor, γ-terpinene, was also tested (Entry 8) but was not as effective as BHT. It was interesting to observe, similarly to Danheiser and coworkers, that the addition of BHT did not significantly affect the rate of the reaction, as the same reaction times were needed for full conversion of the starting material, regardless of the quantity of BHT used.

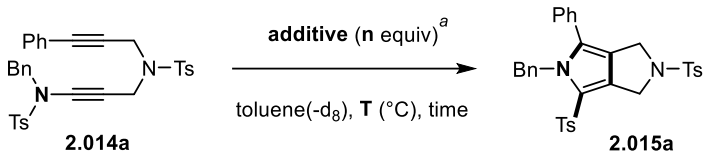

Entry	T (°C)	additive	n (equiv)	time (h)	conversion (%)[b]	yield (%)[b]
1[c]	80	—	—	15	42	13
2	130	—	—	2	100	72
3[d]	130	—	—	2	100	69
4	130	BHT	0.1	2	100	79
5	130	BHT	0.25	2	100	86
6	130	BHT	0.5	2	100	90
7	130	BHT	1	2	100	96 (90)[e]
8	130	γ-terpinene	1	2	100	77

Table 2-1. Optimization of the reaction conditions.

[a] Unless otherwise noted, reactions were performed with 0.05 mmol of **2.014a** in screw-cap NMR tubes in toluene-d_8 (0.1 M) under air and monitored by ^{1}H NMR spectroscopy. [b] Conversions and yields were determined by ^{1}H NMR spectroscopy using mesitylene as internal standard. [c] In a sealed vial in toluene (0.1 M). Conversion and yield were determined by analysis of the crude reaction mixture using mesitylene as a standard. [d] NMR tube was purged with argon. [e] Isolated yield.

It is also interesting to note that the reaction was very selective towards the migration of the tosyl group, i.e. no other major pyrrole product was obtained, and that no alternative (4+2) dehydro Diels–Alder cycloadduct[16] derived from **2.014a** could be observed.

2.4. Synthesis of the yne-ynamide substrates

The model yne-ynamide **2.014a** was constructed linearly beginning from propargylamine (Figure 2-9). Amine group protection and Sonogashira cross-coupling provided the functionalized propargyl tosylamide **2.017**. Then, propargylation and subsequent bromination of the crude intermediate diyne permitted to access bromo-diyne **2.018** in good yields. Finally, copper-catalyzed cross-coupling[4] with benzyl tosylamide provided the desired yne-ynamide **2.014a**. Note that the last step in this synthetic route requires heating. So, this route requires careful monitoring of the final C-N cross-coupling step if one desires to minimize the formation of thermal (3+2) cycloaddition products. For

this particular yne-ynamide, substrate consumption was observed after approximately 2 hours, and therefore stopped immediately.

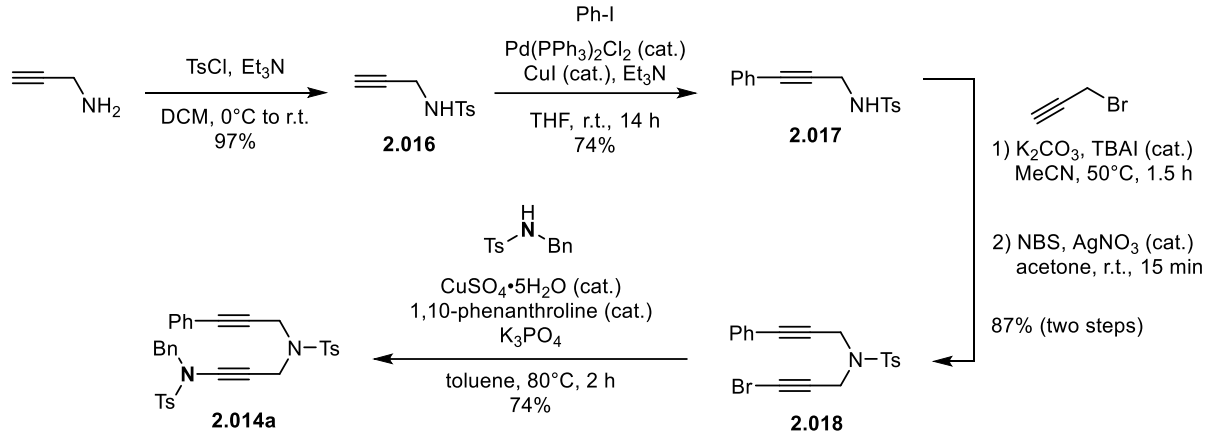

Figure 2-9. Representative procedure for the synthesis of yne-ynamides.

Although multiple substrates were produced using a very similar route to that above, a variety of strategies were employed in the synthesis of the yne-ynamide substrates in order to vary the substitution pattern on the ynamide, the alkyne moiety, and the nature of the chain tethering them (Figure 2-10). The ynamide moiety was generated either through Hsung's C-N coupling method,[4] Stahl's C-N coupling,[5] or Anderson's route via dichloroenamides.[17] The tethered alkyne was derivatized to various analogs either by generating lithium acetylides, or via one of multiple classical (Sonogashira, Cadiot-Chodkiewicz) or specialized[18] cross-coupling methods. The linker structure was generally constructed via substitution or condensation reactions between two appropriate functional groups.

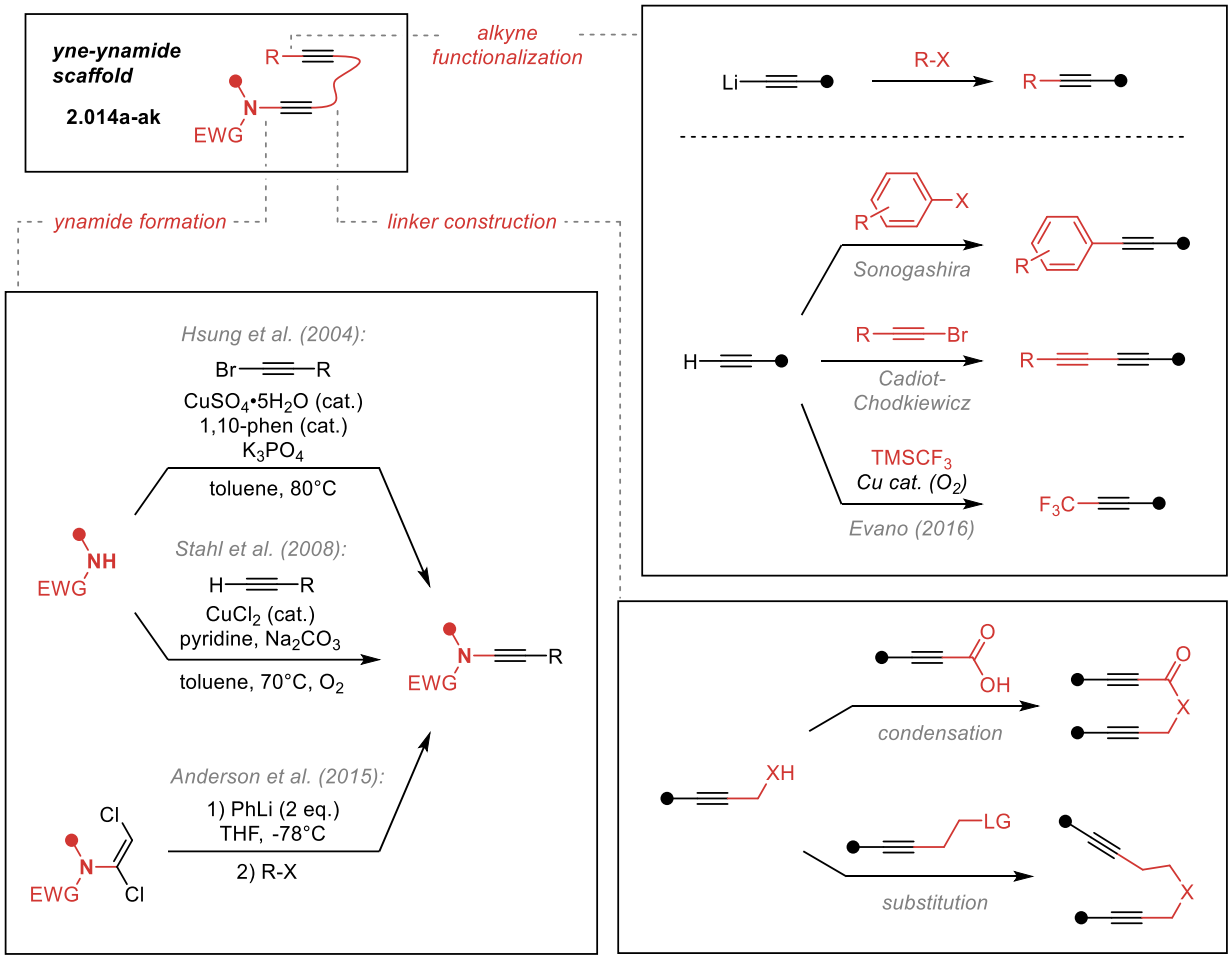

Figure 2-10. Synthetic strategies employed herein to construct yne-ynamide scaffolds.

Various combinations of any of these strategies were used to access a library of yne-ynamides possessing specific desired functionalities.

2.5. Scope of the yne-ynamide (3+2) cycloaddition cascade

As seen from the results compiled in Figures 2-11 to 2-15, the reaction exhibits good functional group compatibility and a variety of bicyclic cycloadducts could be obtained from yne-ynamides.

As for the nature of the alkyne terminus (Figure 2-11), the reaction proceeded rapidly and cleanly for all screened aryl derivatives **2.014a-j**. An array of electron-donating (EDG) and electron-withdrawing groups (EWG) were well tolerated on the aromatic moiety leading to the desired pyrroles in yields ranging from 79 to 97% after only 1 h of reaction at 130 °C. Heteroaromatic substituents were also shown to be compatible as attested by the conversion of thiophene and pyridine derivatives **2.014i-j** into pyrroles **2.015i-j** with respective 82% and 90% yields. Pleasingly, a C-sp^2 hybridized alkenyl

substituent was also tolerated and cyclohexenyl derivative **2.015k** could be formed in 83% yield after 2 h of reaction. The use of a conjugated 1,3-diyne unit was, however, detrimental to the yield of the reaction. In the case of substrate **2.014l**, the major product obtained was **2.015l** with a modest yield of 33%, and by-products derived from a potential (4+2) hexadehydro Diels-Alder reaction, if present, were only minor.[19] While the reaction of alkyl-substituted derivative **2.014m** and terminal alkyne **2.014n** proceeded very slowly, and with low yields (15-20%), that of TMS-substituted alkyne **2.014o** was comparatively very efficient (80%), yet slow. This result demonstrated that increasing the steric demand around the alkyne does not affect the efficiency of the cycloaddition process but considerably decreases its rate. Finally, the electron poor trifluoromethylated alkyne **2.014p** did not prove to be an appropriate reaction partner and only a low 13% of the desired pyrrole **2.015p** was observed.

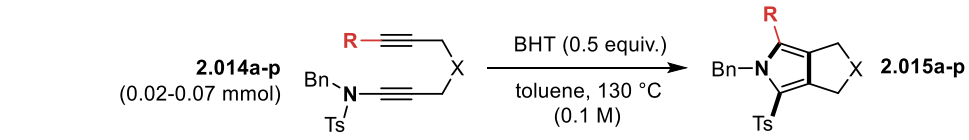

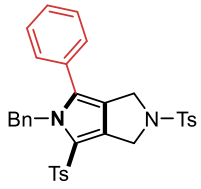

2.015a, 90%, 1.5 h

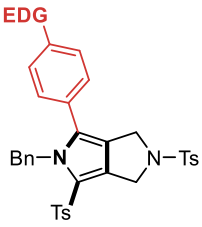

EDG = | Me_2N- **2.015b**, 79%, 1 h; H_2N- **2.015c**, 91%, 1 h; MeO- **2.015d**, 93%, 1 h; Me- **2.015e**, 97%, 1 h

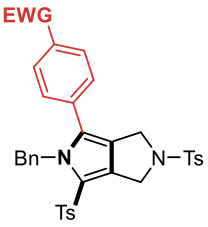

EWG = | Cl- **2.015f**, 97%, 1 h; F_3C- **2.015g**, 96%, 1 h; NC- **2.015h**, 93%, 1 h

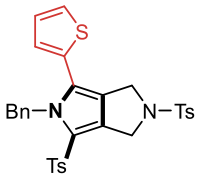

2.015i, 82%, 1 h

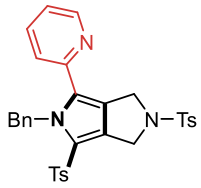

2.015j, 90%, 15 min

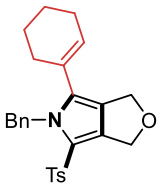

2.015k, 83%, 2 h

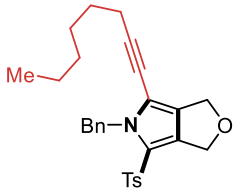

2.015l, 33%, 30 min[a]

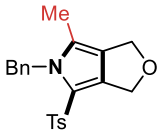

2.015m, 15%, 16 h[a]

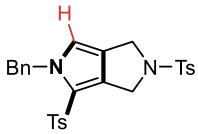

2.015n, 20%, 16 h[a]

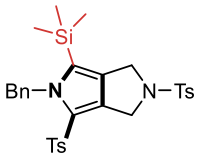

2.015o, 80%, 51 h

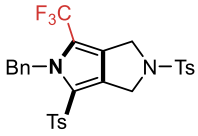

2.015p, 13%, 4 h[a]

Figure 2-11. Yne-ynamide (3+2) rearrangement: reaction scope of alkynes. [a] A complex mixture of products was observed; yield assessed by ^{1}H NMR of reaction crude.

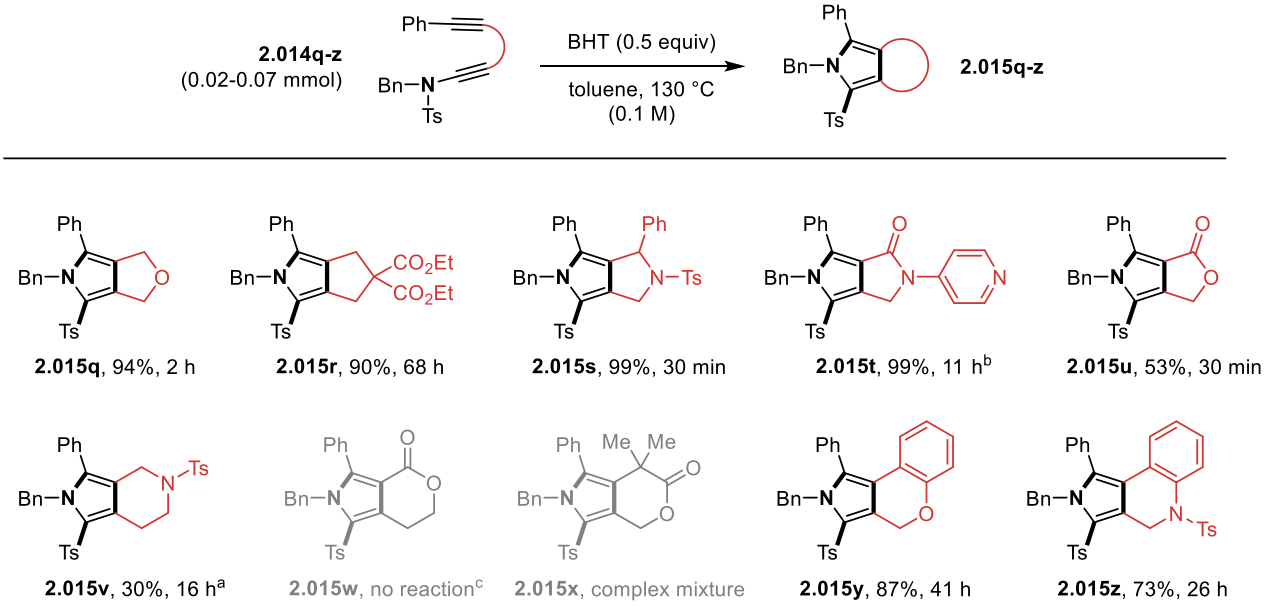

Figure 2-12. Yne-ynamide (3+2) rearrangement: reaction scope of linkers. [a] A complex mixture of products was observed; yield assessed by ^{1}H NMR of reaction crude; [b] Reaction run at 60 °C in $CDCl_3$ without BHT; [c] No reaction was observed up to 160 °C (using microwave irradiation), degradation of substrate at 200 °C.

A variety of linker structures proved capable of promoting the intramolecular (3+2) cycloaddition process (Figure 2-12). In general, substrates with a 3-membered linker led to the formation of cycloadducts similarly to model substrate **2.014a**, as exemplified by the formation of **2.015q** in 94% from a substrate possessing an ether linkage. Amide and ester tethers were both compatible (see **2.015u** and **2.015t**). Notably, the reaction of **2.015t** could even be performed at a lower temperature of 60 °C. The all-carbon malonate derivative **2.015r** also reacted well (90%), although surprisingly slowly. This is interesting as very similar rate effects have been observed by Hoye and coworkers for tri-yne scaffolds promoting HDDA reactions.[20] The introduction of a phenyl substituent in the tether had a pronounced effect on the rate of the reaction as attested by the rapid and efficient formation of pyrrole **2.015s** (>90% yield, <0.5 h). 4-Membered linkers were also investigated but the cycloaddition process proved to be less efficient in this case. Derivative **2.014v**, which only differs from model substrate **2.014a** by the presence of an extra CH_2 unit in its linker, led to a poor yielding (30%) and very unselective reaction. No reaction or only degradation was observed for carboxylic

ester derivatives **2.014w** and **2.014x**. In contrast, excellent yields were obtained for geometrically restricted phenol and aniline derivatives **2.014y** and **2.014z** (87% and 73%). These variations in tether length, nature, and substitution (Figure 2-12) clearly demonstrate that higher yields and shorter reaction times can be attained when the cyclization conformation can be easily accessed.

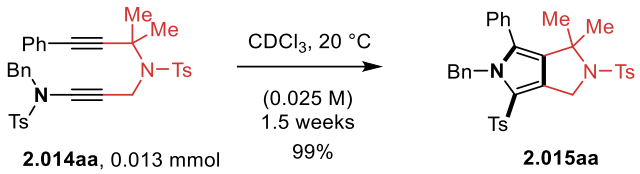

Figure 2-13. Room temperature (3+2) rearrangement of **2.014aa**.

3-Membered linkers leading to the formation of 5,5-fused bicyclic products and geometric restrictions imposed by linker substitution are favorable kinetic factors. As an example, merging the favorable three-atom tosylamide linker and a dimethyl-induced Thorpe–Ingold effect in **2.014aa** led to an extremely efficient transformation that proceeded at room temperature (Figure 2-13).

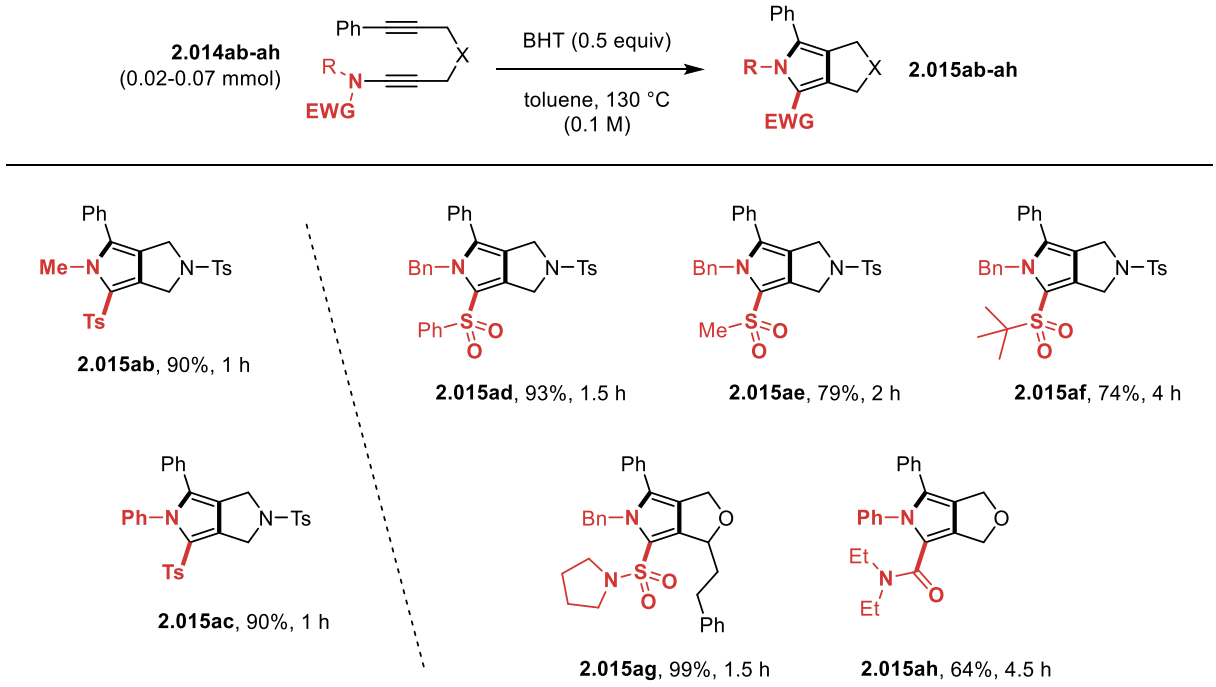

Figure 2-14. Yne-ynamide (3+2) rearrangement: reaction scope of acyclic amides.

We finally investigated the scope of amides and their corresponding electron withdrawing groups (EWGs) that could participate in the N to C migration step of the rearrangement (Figure 2-14). Pleasingly, the benzyl group in model substrate **2.014a** could be replaced by a methyl or phenyl group

without noticeable change in efficiency. N-Me and N-Ph pyrroles **2.015ab** and **2.015ac** were both isolated in 90% yield after 1 h of reaction. Alkylsulfones **2.015ae** and **2.015af**, as well as sulfonamide **2.015ag** were obtained with similar efficiency to aryl-sulfones (**2.015ad** and model **2.015a**). Carbonyl-based EWGs were also very well tolerated in this transformation. For instance, urea derivative **2.014ah** efficiently rearranged into pyrrole **2.015ah** (64%) via a migration of the carboxamide moiety.

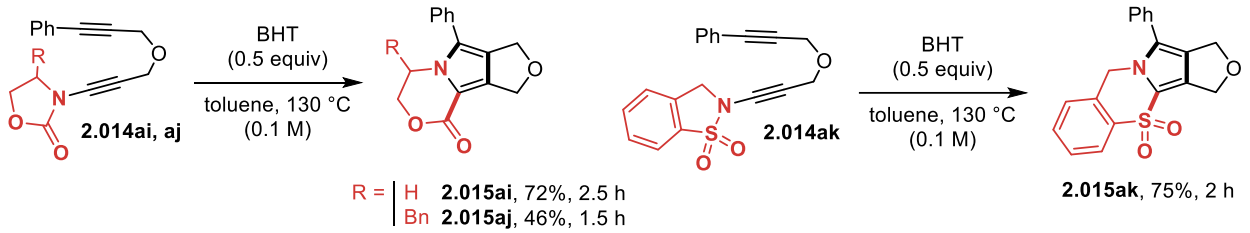

Figure 2-15. Yne-ynamide (3+2) rearrangement: use of cyclic amides.

In the case of cyclic carbamate derivatives, such as oxazolidinones **2.014ai** and **2.014aj**, the shifting of the EWG resulted in a ring expansion, providing novel tricyclic structures (Figure 2-15). This strategy could also be applied to saccharin-derived ynamide **2.014ak** that could be readily converted into polycyclic pyrrole **2.015ak**.

Overall, examples collected in Figures 2-11 to 2-15 testify to the broad applicability of this cycloisomerization process, which allows for a rapid increase of structural complexity under simple experimental conditions and from relatively easily accessible substrates.

2.6. Applications of the yne-ynamide (3+2) chemistry and derivatizations of products

To further highlight the synthetic potential of the method, the reaction of model substrate **2.014a** was conducted at a gram scale starting from bromoalkyne **2.012** and tosylamide **2.013** (Figure 2-16). A two-step procedure involving copper catalysis and thermal rearrangement with minimum intermediate workup successfully yielded 1.97 g of pyrrole **2.015a** (50% yield). Conveniently, the white product precipitates out of solution once cooled to room temperature. This single preliminary result is highly encouraging when considering developing a cascade transformation from haloalkynes and diverse amides.

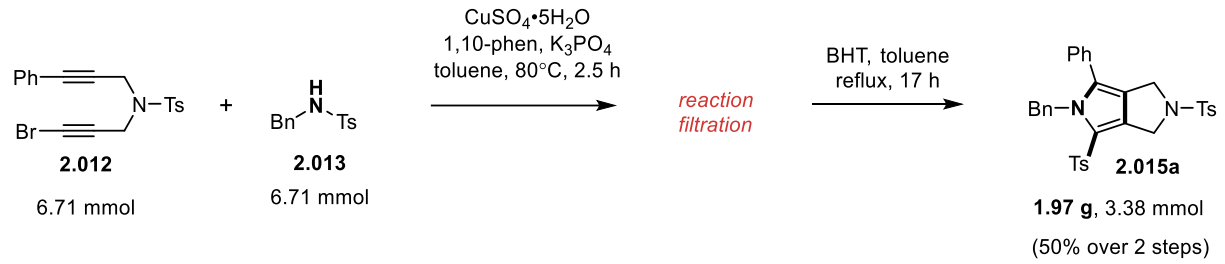

Figure 2-16. Telescoped copper-coupling and (3+2) at the gram scale with no chromatography.

Structural diversification in pyrrole products could also be further expedited in the development of a one-pot coupling / cyclization sequence (Figure 2-17). The coupling strategy devised here relies on the in-situ formation of an imine as the bridging functionality between the cycloaddition partners. By simply mixing and matching propargyl amines **2.016** with amidopropynals **2.017** in the presence of molecular sieves, followed by mild heating, a small library of bicyclic pyrroles **2.018** could be rapidly obtained in moderate yields. No large amount of any specific by-product is obtained in these reactions, despite the relatively low yields obtained. It is possible that the amidopropynals **2.017** or intermediate imine condensates have a higher propensity towards oligomerization than simple ynamides.

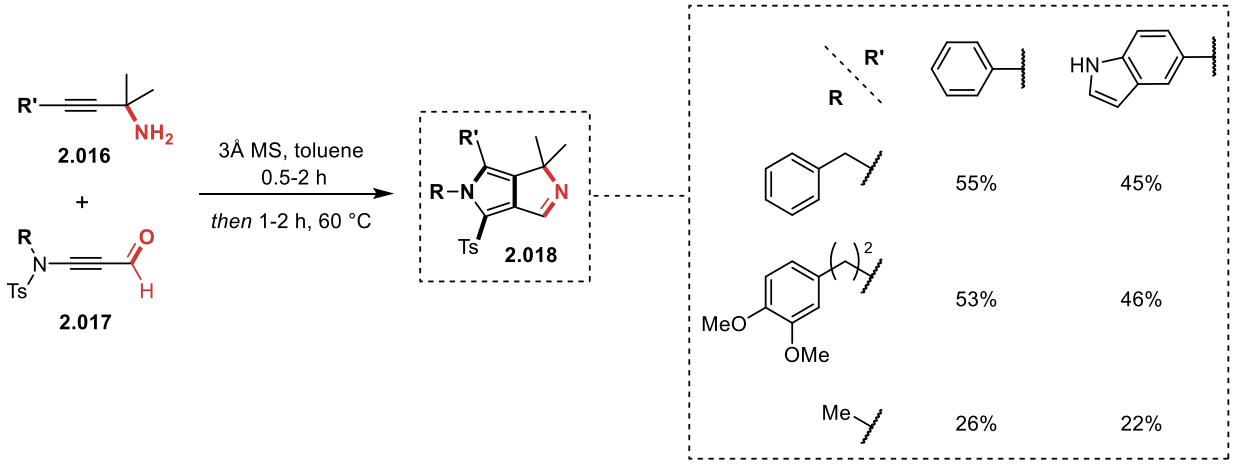

Figure 2-17. One-pot condensation / (3+2) for the generation of a small library of fused pyrroles. *Results in this figure obtained by Alice Pommainville.*

In addition to the structural diversity that can be achieved by varying the nature of the migrating EWG (vide supra) the presence of this group at position 2 of the pyrrole ring can also be advantageously employed to operate functional group interconversions. The tosyl group, in particular, was found to be easily cleaved in an oxidative dearomatization process on the pyrrole (Figure 2-18). As an example,

treatment of pyrrole **2.015a** with a mixture of Oxone and KBr in methanol led to the formation of 5-methoxypyrrol-2-one derivative **2.019** in 58% yield. This permitted direct access to γ-lactams, a structural motif found in a large array of bioactive compounds.[21] Sequential reductions of **2.019** allows for the synthesis of pyrrolone **2.020** and then lactam **2.021** in a stereoselective manner. This rapid redox sequence highlights the synthetic usefulness of the migrating sulfonyl group that can be easily manipulated to access various oxidation levels of the pyrrolo[3,4-c]pyrrole core, whose fully reduced version is a privileged motif in medicinal chemistry (contained in Seltorexant[22] and A-582941[23]).

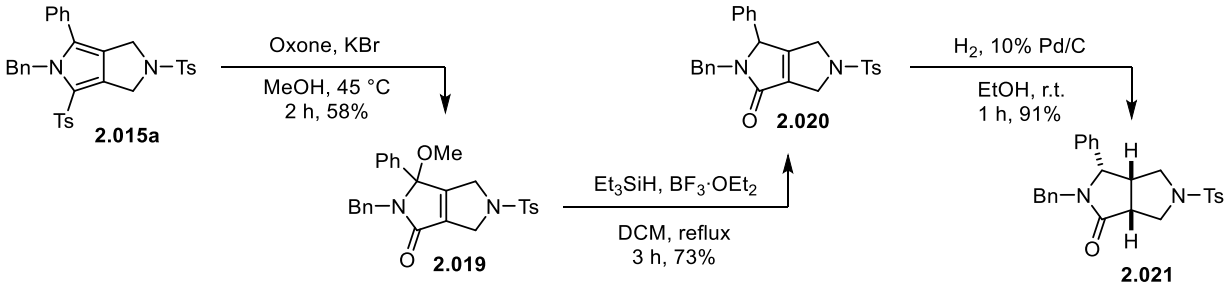

Figure 2-18. Accessing various oxidation levels of the pyrrolo[3,4-c]pyrrole core via key pyrrolone derivatives.

2.7. Early mechanistic considerations

Aside from investigating the synthetic potential of the transformation, experimental and theoretical studies were performed in tandem to gain knowledge on its mechanism and the parameters that may influence its course.

A first observation, expected yet still important, is the first-order dependence on the concentration of all yne-ynamide substrates. Representative NMR kinetic studies on **2.014h** makes this clear in Figure 2-19.

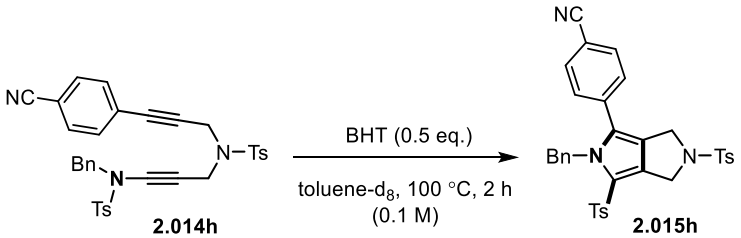

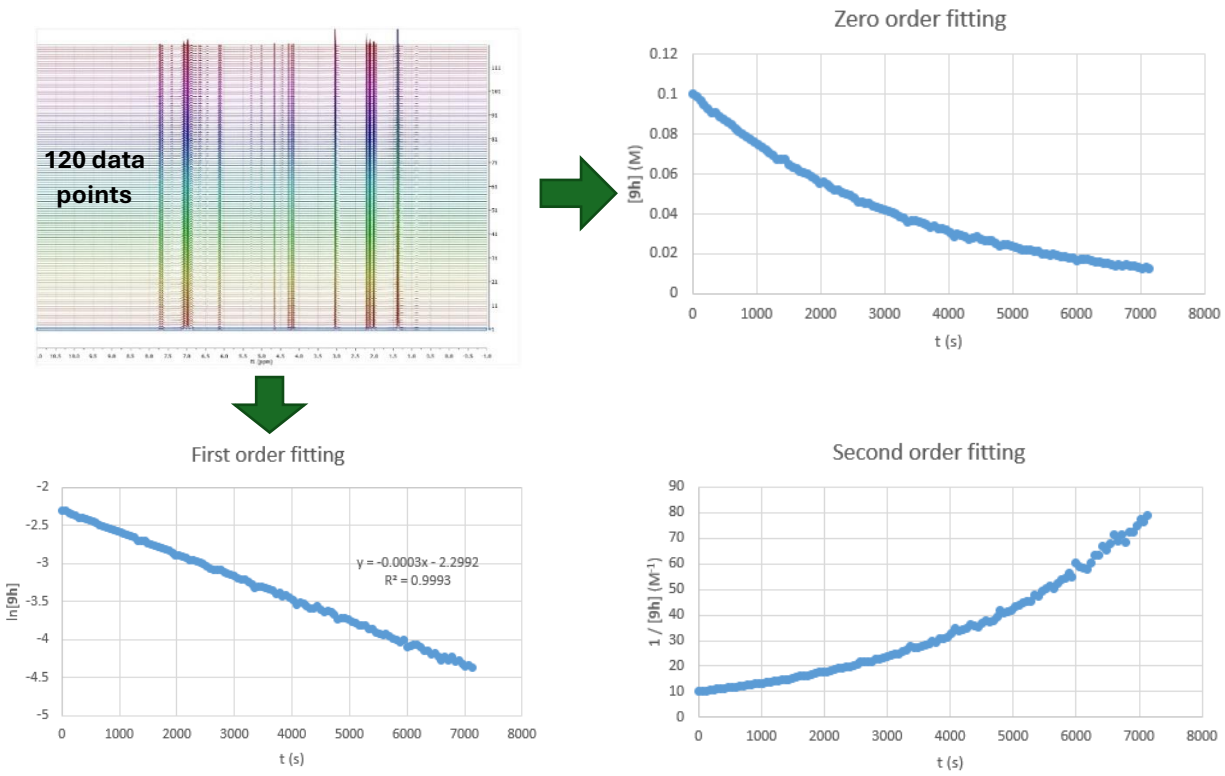

Figure 2-19. Representative procedure of NMR kinetic data processing for rearrangement of 2.014h – First order dependence on the yne-ynamides. Using the MestreNova processing software from stacked spectra, an integrals graph is produced including all 120 spectra collected (See Figure 2-24 for details on reaction conditions and collection of data). The integral values are then normalized against the internal NMR standard peak for: (peak integral of S at t_0) = $[S]_0$. Zero, first, and second order fittings were tested. The linear slope, obtained only with first order fitting, shows a first order dependence on all substrates **2.014a**-**h** (shown above here with representative data from **2.014h**). The corresponding rate constants **k** were obtained via linear regression of the processed data.

Although qualitatively observed during optimization studies, it was still of interest to ascertain, in a quantitative manner, the effect of BHT on the reaction kinetics (or more specifically the lack thereof). In early investigations on this topic during the project, the model substrate **2.014a** was heated under optimized conditions in the presence of either 0.5 or 1.0 equivalents of BHT (Figure 2-20). As can be seen from Figure 2-20, doubling the amount of BHT has little effect on the observed rate constant. In fact, it seems to very slightly slow down the consumption of starting material. This is in direct

correlation with the suggestion by Danheiser and coworkers[15] that the degradation minimized by BHT in poly-yne systems is oligo/polymeric in nature.

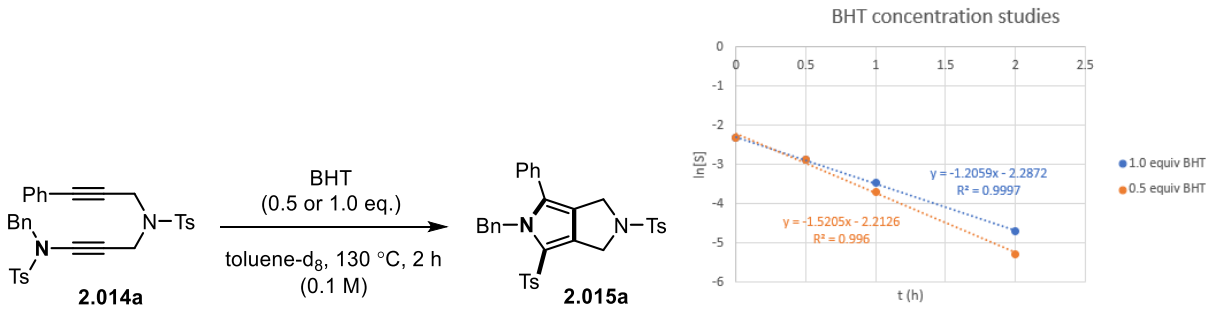

Figure 2-20. BHT concentration study. NMR kinetic studies were performed on substrate **2.014a** at 130°C (oil bath) in the presence of 0.5 equiv. and 1.0 equiv. of BHT. The NMR reaction tubes were cooled to room temperature at given intervals using 5-minute periods for data collection. As can be observed from above graph, no significant enough change in reaction rate can be observed when doubling the concentration of BHT.

The first order dependence on the yne-ynamide substrates and the lack of kinetic dependence on the BHT additive together suggest (unsurprisingly) a *unimolecular rate-limiting step*.

With this knowledge, the transformation can be simplified into two main events: a (3+2) cycloaddition event and a 1,2-migration of the EWG with the involvement of a common pyrrolium ylide intermediate (Figure 2-21). Considering that products derived from a spontaneous 1,2-shift of the EWG on ynamides have never been observed to date, the cyclization event is much more likely to occur first.

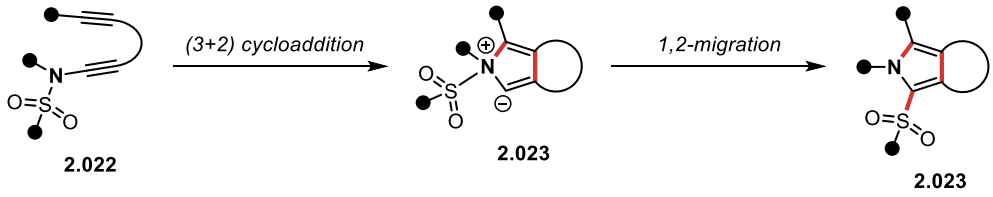

Figure 2-21. General mechanistic proposal.

This initial mechanistic proposal was heavily influenced by computational studies performed in early stages of this project. Preliminary DFT studies at the B3LYP/6-31G(d) level of theory on the model scaffold **2.024** demonstrated the clear presence of a cycloadduct **2.025** on the potential energy surface (PES) at short scan distances between the ynamide and alkyne fragments (Figure 2-22). NBO analysis of the obtained cycloadduct confirmed the Lewis structure proposed here.

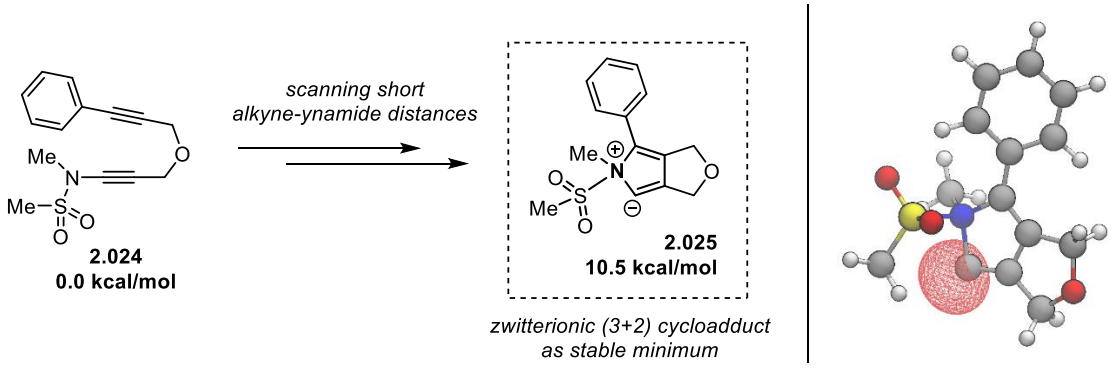

Figure 2-22. Identification of zwitterionic (3+2) cycloadducts as stable minima on the PES. Geometric optimization and vibrational frequencies calculated at the B3LYP/6-31G(d) level of theory, at the gas phase. Gibbs free energies reported in the figure. NBO analysis of the cycloadduct **2.025** locates a lone pair of electrons at position 2 of the pyrrole core, suggesting an endocyclic pyrrolium ylide configuration.

The discovery of this stable minimum in the PES strongly suggested that zwitterionic (3+2) cycloadducts are the key intermediates bridging the yne-ynamide substrates to the observed fused pyrrole products.

2.8. Studies on the (3+2) cycloaddition step

Several mechanistic considerations can be made leading to the zwitterionic (3+2) cycloadducts (Figure 2-23). The simplest explanation would involve a concerted (3+2) mechanism, with a single transition state **2.027** leading from the yne-ynamide **2.026** to the pyrrolium ylide **2.030**. Another reasonable explanation would entail the formation of an intermediate diradical species **2.028**. Recombination of the diradical species through the nitrogen atom would provide the cycloadduct **2.030**. A third route would rather involve an ionic intermediate **2.029**, which could then undergo rapid closure to **2.030**. Note that the directionality of the stepwise ionic process is important: the alternative ionic process than that chosen in Figure 2-23 would lead to a the keteniminium species **2.031**, which has improper geometry to promote a ring closure to the (3+2) cycloadduct. Yet, for an ionic process, **2.031** is a more plausible outcome than **2.029**, since ynamides are nucleophilic from their β-carbon. This consideration may be a first indication that the stepwise ionic pathway is unlikely to take part.

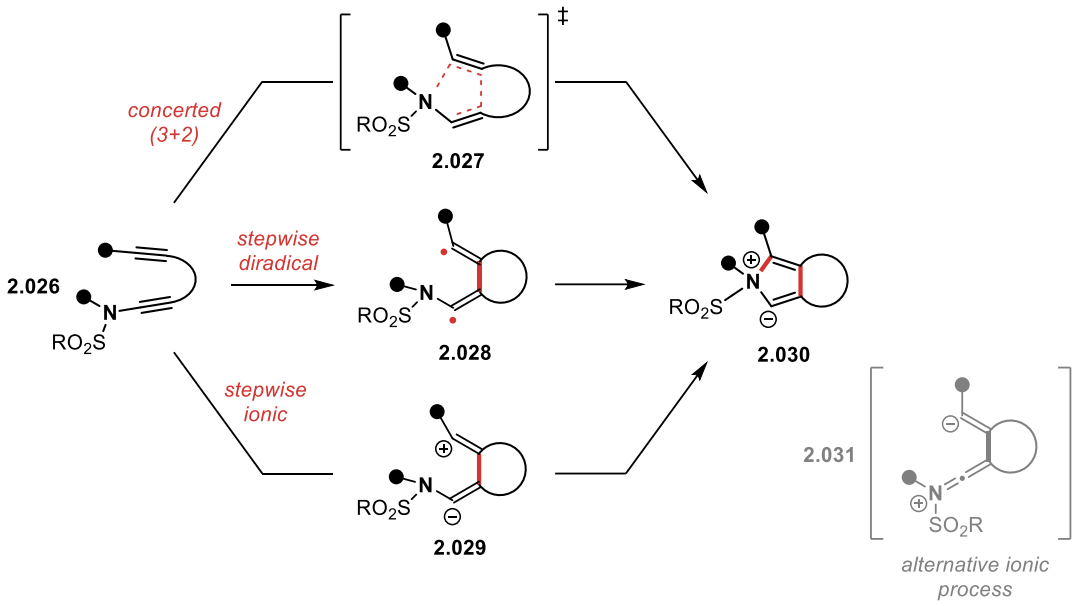

Figure 2-23. Potential pathways leading to zwitterionic (3+2) cycloadducts.

These possibilities are reminiscent of the debated mechanisms of classical 1,3-dipolar cycloadditions involving either concerted[24] or diradical[25] pathways. While ynamides are typically used in two-electron processes, radical addition to ynamides to obtain enamine radical intermediates has seen a growing interest.[26] In order to gain more information on this transformation, a series of para-substituted phenyl-derived substrates **2.014a-h** were investigated to probe electronic effects on the alkyne moiety (Figure 2-24).

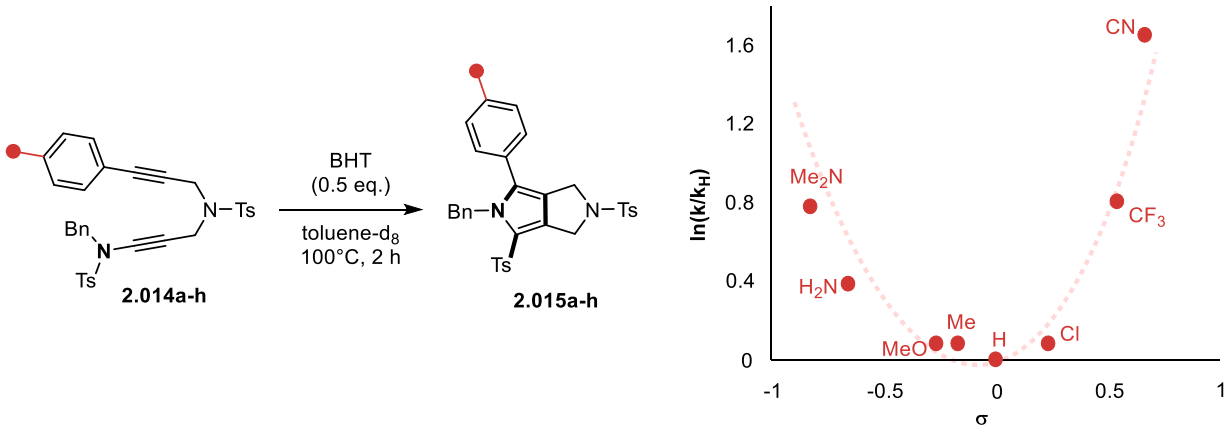

		Slope Data				
●	σ[1]	k (s^{-1})	(± SE) (s^{-1})	R^2	ln(k/k_H)	(± SE)
Me_2N-	-0.83	1.219E-04	(± 4.37E-07)	0.9985	0.7774	(± 6.83E-03)

[1] σ parameters obtained from: Hansch, C.; Leo, A.; Taft, R.W. *Chem. Rev.* **1991**, 91 (*2*), 165–195.

H_2N-	-0.66	8.220E-05	(± 3.82E-07)	0.9975	0.3835	(± 7.44E-03)
MeO-	-0.27	6.088E-05	(± 1.80E-07)	0.9990	0.0833	(± 6.52E-03)
Me-	-0.17	6.109E-05	(± 2.56E-07)	0.9979	0.0867	(± 7.17E-03)
H-	0	5.602E-05	(± 3.26E-07)	0.9960	0	-
Cl-	0.23	6.102E-05	(± 2.65E-07)	0.9978	0.0856	(± 7.26E-03)
F_3C-	0.54	1.254E-04	(± 4.24E-07)	0.9987	0.8056	(± 6.73E-03)
NC-	0.66	2.912E-04	(± 6.99E-07)	0.9993	1.6483	(± 6.29E-03)

Figure 2-24. Processed kinetic data for Hammett analysis. Reaction repeated with each indicated substrate in toluene-d_8 (0.1 M) with 0.5 eq BHT at the 0.05 mmol scale. 2.0 µL of 1,2-DBE was added as internal NMR standard. Reactions were done in sealed NMR tubes and heated to 100.0 °C in a Bruker Avance II 300 instrument. ^{1}H NMR spectra were collected every 60 seconds for 2 h, giving a stack of 120 spectra. Data was processed as indicated in Figure 2-19.

Plotting the experimentally determined rate constants in a Hammett plot (Figure 2-24) resulted in an interesting U-shaped curve. Such a shape suggests three possibilities: the cyclization event may proceed (a) via a type II cycloaddition process,[27] (b) via a diradical species, or (c) via divergent mechanisms.[28]

With this curious outcome in mind, a deeper analysis of the (3+2) cycloaddition pathway was done via DFT studies.

Characterization of the potential energy surface for the closed shell (3+2) cycloaddition was possible using DFT calculations at both the B3LYP/6-31G(d) and M06-2X/6-31+G(d) levels of theory[29-32] (Figure 2-25). For the phenyl-derived model **2.032-Ph**, the (3+2) cycloaddition step was found rate-limiting with a transition state **2.033-Ph** calculated to be 30.3 kcal/mol higher than **2.032-Ph** using the M06-2X method. No real transition state (possessing a stable wave function) corresponding to **2.033-Ph** could be located using the restricted B3LYP method. The methyl-derived model **2.032-Me** required a higher energy of around 35 kcal/mol for the corresponding transition state **2.033-Me**. It is worth noting that in both cases, the (3+2) cycloaddition step was quite asynchronous, with significantly more C–C bond having been formed at the transition state.

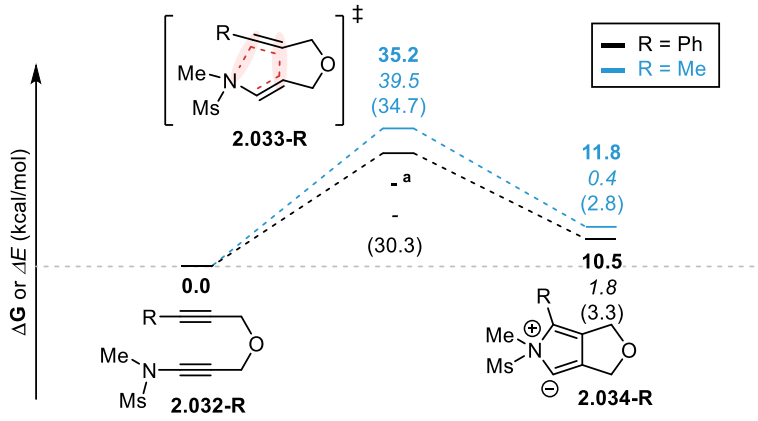

Figure 2-25. DFT calculations of closed shell potential energy surface for the (3+2) cycloaddition step. All calculations were done under the following parameters: gas phase, 1 atm, 298 K. Intrinsic reaction coordinate (IRC) calculations were performed to connect the transition states to their corresponding local minima (dotted lines). Values in bold: Relative Gibbs free energy at the B3LYP/6-31G(d) level of theory. Values in italics: Relative electronic energy at the B2PLYPD/aug-cc-pVDZ//B3LYP/6-31G(d) level of theory. (Values in parentheses): Relative Gibbs free energy at the M06-2X/6-31+G(d) level of theory. [a] Stable closed shell **2.033-Ph** could only be located using the M06-2X functional

The proposed pyrrolium ylide intermediates **2.034-Ph** and **2.034-Me** were convincingly located as stable minima in this pathway using both B3LYP (10-12 kcal/mol) and M06-2X (~3 kcal/mol) methods.

The plausibility of a closed shell process, as supported by DFT calculations, does not rule out an open shell pathway for the cycloaddition step. In fact, even within classical 1,3-dipolar cycloadditions, high-level computational studies have shown energetically lower pathways involving diradical species for the (3+2) cycloaddition between nitrile oxides and aryl acetylenes.[33]

To probe the possibility of an open shell process and the involvement of radical species, the reaction of model substrate **2.014a** was performed in the presence of TEMPO (Figure 2-26). No TEMPO-derived product could be detected. The transformation proceeded smoothly and produced **2.015a** in the same reaction time and with an even better yield than without any additive. TEMPO is likely to behave similarly to BHT in intercepting runaway radicals. A similar observation was made when the sealed reaction tube was purged with O_2 gas before heating (Figure 2-26). No oxidized product derived from **2.014a** was observed and the yield in **2.015a** was almost unchanged. It should be noted,

however, that particularly short-lived diradicals would unlikely be affected by other molecules in the reaction medium.

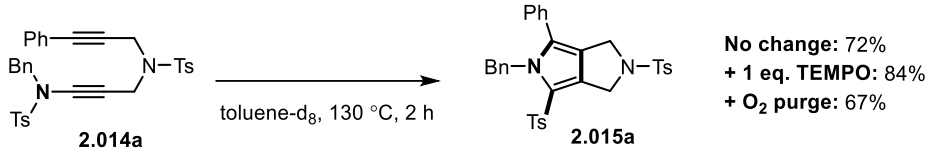

Figure 2-26. Attempting radical trapping. No by-product and no significant lowering of yield was observed in the presence of TEMPO or at high concentration of O_2.

Therefore, an intramolecular radical probe **2.014al** that features a syn-disubstituted cyclopropyl alkynyl group was prepared (Figure 2-27). 2-Phenylcyclopropyl carbinyl radicals are known to undergo very rapid ($k_{20°C}$ = 2.7 x 10^{11} s^{-1}) ring opening[34] and would therefore probe the involvement of radical species in the process. A significant amount of isomeric product was observed in the rearrangement of **2.014al** to **2.015al**, which may indicate that the formation of a radical at the α position of the cyclopropyl group is participating.

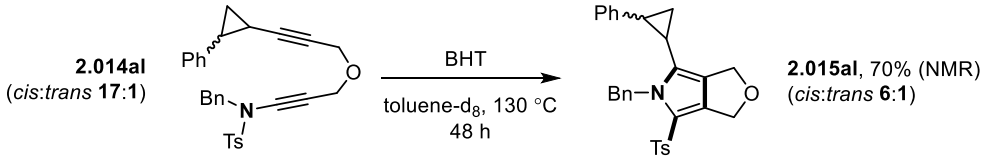

Time (h)	(*cis*)-2.014al (%)	(*trans*)- 2.014al (%)	(*cis*)- 2.015al (%)	(*trans*)- 2.015al (%)
0	100	6	0	0
2.25	87	5	16	1
6.25	60	3	40	2
60	-	-	60	11

Figure 2-27. Kinetic data for reaction of substrate 2.014al. Reaction completed with **2.014al** (29.9 mg, 0.0637 mmol) and BHT (7.0 mg, 0.0318 mmol) in toluene-d_8 (0.64 mL). 2.0 µL of 1,2-DBE was added as internal NMR standard. Reaction was completed in a sealed NMR tube and heated in an oil bath set to 130 °C. The reaction was followed by ^{1}H NMR at given time intervals until completion. Data above is represented using relative percentage (%).

NMR kinetic analyses during the reaction (Figure 2-27) and a control experiment (Figure 2-28) suggest minimal cis/trans isomerization to be occurring at the cyclopropyl motif in either the starting material or the product.

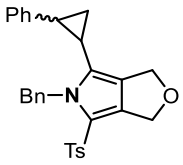

2.015al
(*cis*:*trans* **6**:**1**)

BHT
toluene-d_8, 130 °C
24h

no degradation or isomerization observed

Time (h)	(*cis*)-2.015al (%)	(*trans*)-2.015al (%)
0	100	17
24	100	19

Figure 2-28. Kinetic data for heating of pyrrole 2.015al. Mixture prepared with **2.015al** (15.0 mg, 0.0319 mmol) and BHT (7.0 mg, 0.0318 mmol) in toluene-d_8 (0.60 mL). 2.0 µL of 1,2-DBE was added as internal NMR standard. Reaction was completed in a sealed NMR tube and heated in an oil bath set to 130 °C. The reaction mixture was analyzed by ^{1}H NMR after 24 h. Data above is represented using relative percentage (%).

Attention was then turned towards identifying diradical intermediates through computational studies. The open shell potential energy surface for the phenyl acetylene derived model **2.032-Ph** was characterized at the unrestricted UB3LYP/6-31G(d) level of theory (Figure 2-29). Interestingly, the phenyl-derived model led to a transition state **2.035-Ph** of about 25 kcal/mol for the C–C bond forming and rate-limiting conversion of **2.032-Ph** into diradical intermediate **2.036-Ph**, found at 18.8 kcal/mol. The barrier for the C–N bond formation (**2.037-Ph**) was only slightly higher at 22.8 kcal/mol.

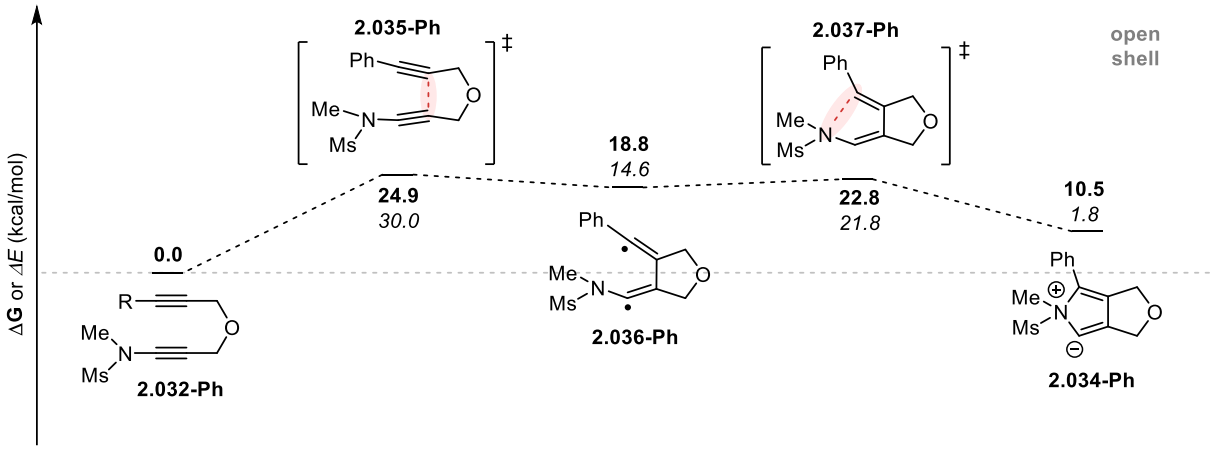

Figure 2-29. DFT calculations of the open shell potential energy surfaces for the (3+2) cycloaddition step for model **2.032-Ph**. All calculations were done under the following parameters: gas phase, 1 atm, 298 K. Intrinsic reaction coordinate (IRC) calculations were performed to connect the transition states to their corresponding local minima (dotted lines). Values in bold: Relative Gibbs free energy at the uB3LYP/6-31G(d) level of theory. Values in italics: Relative electronic energy at the uB2PLYPD/aug-cc-pVDZ//B3LYP/6-31G(d) level of theory.

In the case of methyl-derived model **2.032-Me**, a slightly more complex pathway can be observed, due to the inability of the methyl substituent to significantly stabilize the adjacent alkenyl radical (Figure 2-30). For this model, an open shell transition state **2.038-Me** could be located slightly higher at 33.9 kcal/mol. The minima associated with diradicals **2.039-Me** and **2.041-Me** could also be located with respective free energies of 29.2 and 28.1 kcal/mol. The small barrier **2.040-Me** of radical center inversion allows to access the right conformation for the cyclization to occur. The subsequent C–N bond formation has a barrier **2.042-Me** at 29.9 kcal/mol to produce the cyclic ylide. Although differing slightly in magnitude, single point energy calculations done along the open shell pathway using the more accurate B2PLYPD/*aug*-cc-pVDZ level of theory show a very similar qualitative picture for the diradical process. This method has previously shown good correlation with high-level computations regarding the formation of diradical species from diynes[35] and diradical (3+2) processes.[33]

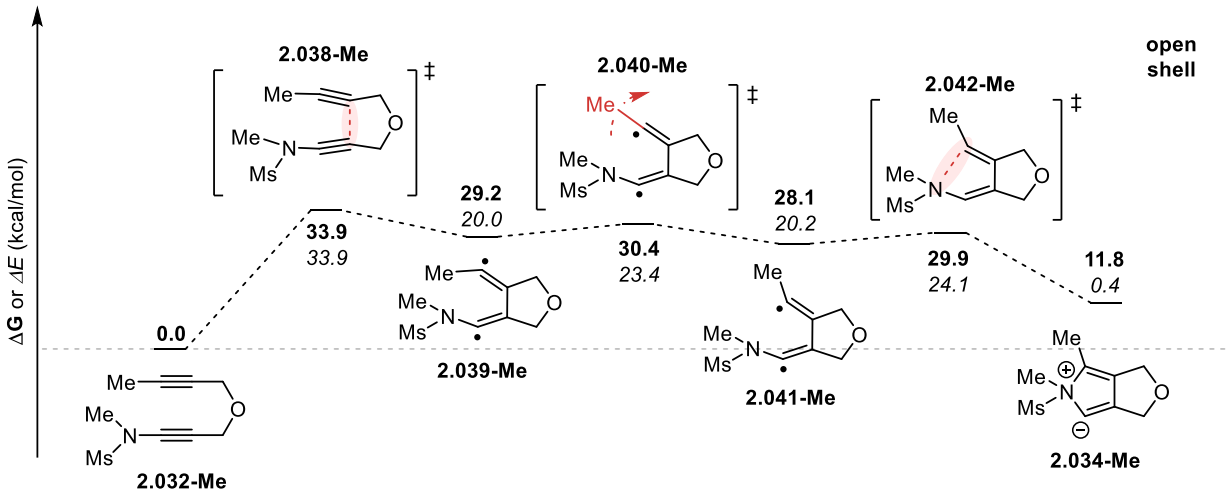

Figure 2-30. DFT calculations of the open shell potential energy surfaces for the (3+2) cycloaddition step for model **2.032-Me**. All calculations were done under the following parameters: gas phase, 1 atm, 298 K. Intrinsic reaction coordinate (IRC) calculations were performed to connect the transition states to their corresponding local minima (dotted lines). Values in bold: Relative Gibbs free energy at the uB3LYP/6-31G(d) level of theory. Values in italics: Relative electronic energy at the uB2PLYPD/aug-cc-pVDZ//B3LYP/6-31G(d) level of theory.

Considering both experimental observations and DFT calculations, a divergence in open or closed shell processes may happen for the (3+2) cycloaddition step depending on the substitution at the alkyne terminus. The clear U-shaped Hammett plot obtained along with the radical probe

experiments support such a possibility. While DFT studies show a slight favour for the open shell pathway, neither pathway can be completely ruled out yet. At the moment, both closed shell and open shell processes are still on the table. In any case, the cyclization step was found to be asynchronous, and intermediates, if formed, are extremely short-lived. A common point observed in the computation of both pathways, nevertheless, is a higher activation energy for alkyl-substituted alkynes, which fits with the significantly slower reaction times observed for scope examples **2.015m** and **2.015n**.

2.9. Studies on the 1,2-migration step

The second step of the process, the N to C migration of the EWG, may occur via an intramolecular 1,2-migration involving a single transition state **2.043** (Figure 2-31). It may also occur via fragmentation/recombination sequences involving either an ionic pair **2.044** or a radical pair **2.046**.

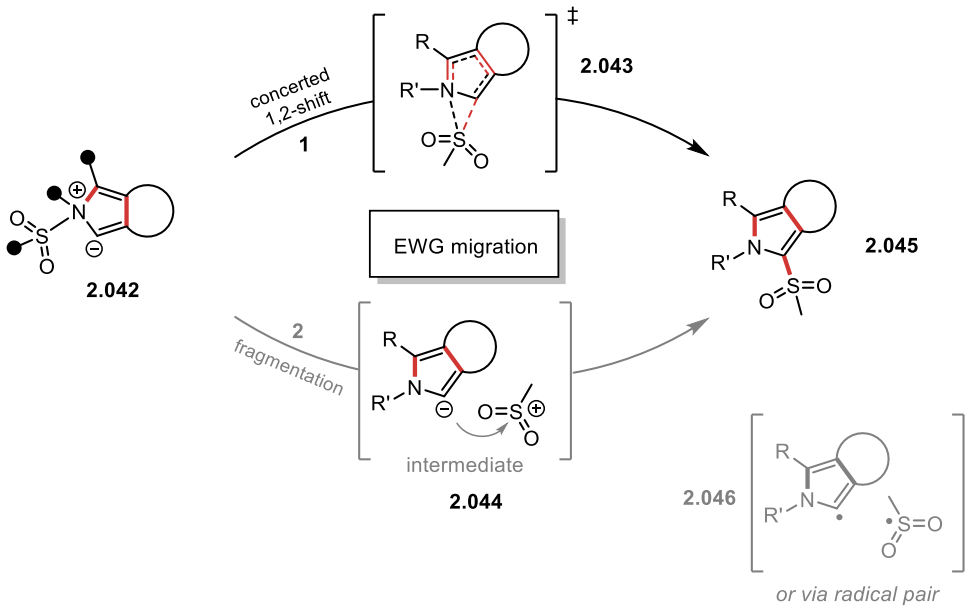

Figure 2-31. Possible mechanisms for the 1,2-migration event.

These two possibilities could be distinguished in a cross-over experiment as shown in Figure 2-32. When an equimolar mixture of structurally comparable **2.014e** and **2.014ad** substrates was heated, only the respective pyrroles **2.015e** and **2.015ad** were obtained. Since no cross-over product was observed, an intermolecular process could be ruled out (with the exception of a solvent cage taking place), thus leaving an intramolecular 1,2-shift of the EWG as the most probable pathway.

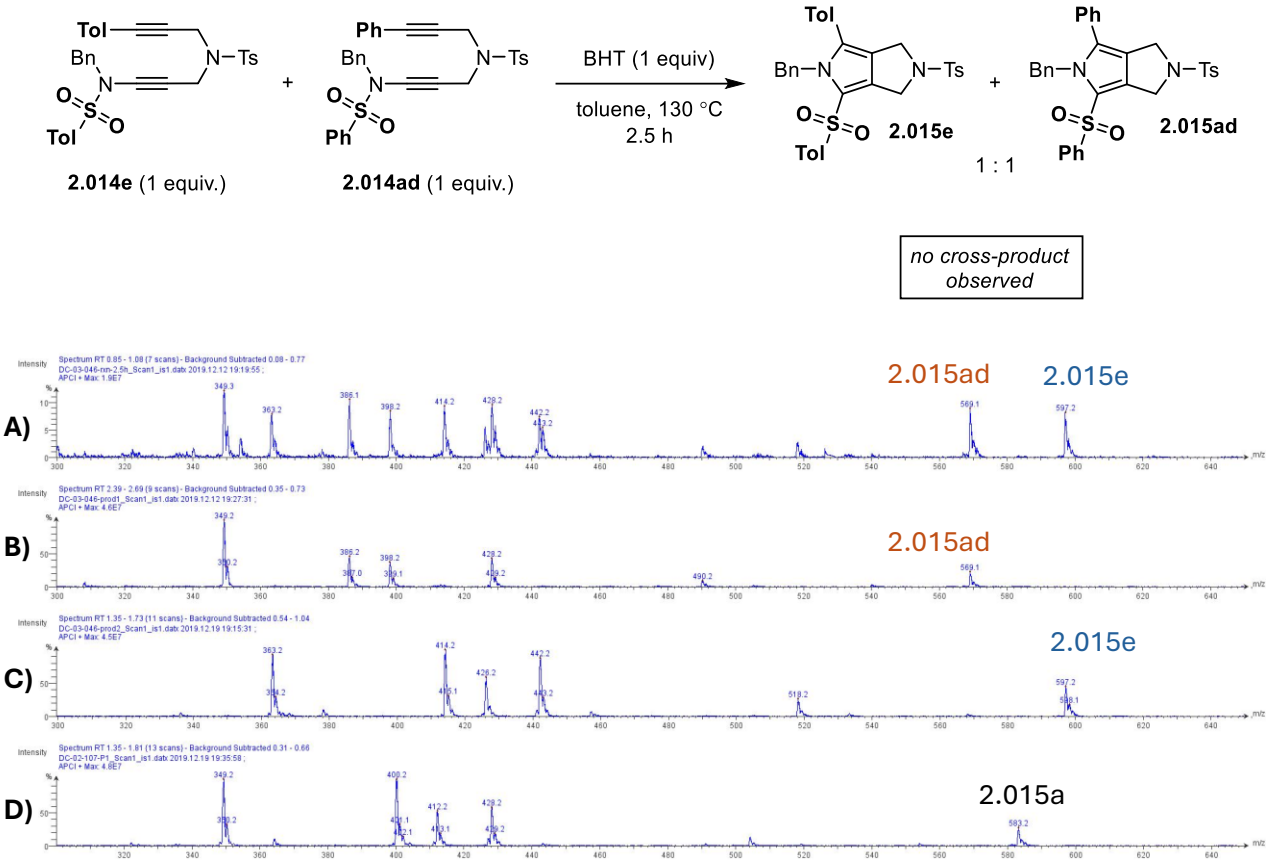

Figure 2-32. Cross-over experiment. Reaction was performed at 0.05 mmol scale in a sealed tube with 1 equiv BHT in toluene (0.1 M) under air. Analyses of the reaction crude as well as all isolated products were done by MS-APCI. **A)** Reaction mixture after complete conversion of substrates; **B)** Isolated product **2.015ad**; **C)** Isolated product **2.015e**; **D)** Isolated product **2.015a** (theoretical cross-over product).

The likelihood of an intramolecular 1,2-migration was further confirmed through computational studies. A very low barrier **2.047-Ph** ranging from ~1 to 5 kcal/mol was found across multiple levels of theory for the migration of the sulfonyl group in model zwitterionic cycloadduct **2.034-Ph** (Figure 2-33).

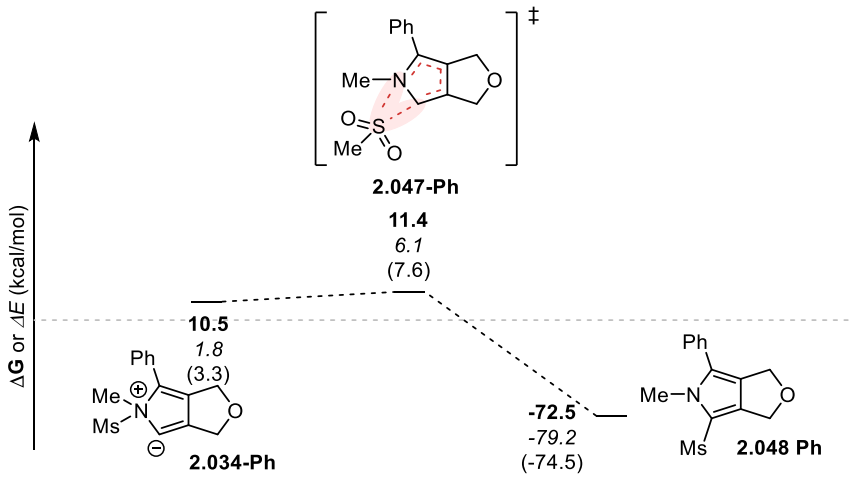

Figure 2-33. DFT calculations of the potential energy surface for the 1,2-migration step. All calculations were done under the following parameters: gas phase, 1 atm, 298 K. Intrinsic reaction coordinate (IRC) calculations were performed to connect the transition states to their corresponding local minima (dotted lines). Values in bold: Relative Gibbs free energy at the B3LYP/6-31G(d) level of theory. Values in italics: Relative electronic energy at the B2PLYPD/aug-cc-pVDZ//B3LYP/6-31G(d) level of theory. (Values in parentheses): Relative Gibbs free energy at the M06-2X/6-31+G(d) level of theory.

This migration event can rather be described as a [1,5]-sigmatropic rearrangement of the sulfonyl group along the π-system of the pyrrolium cycle, immediately followed by relaxation to the final "flat" aromatic structure (Figure 2-34).

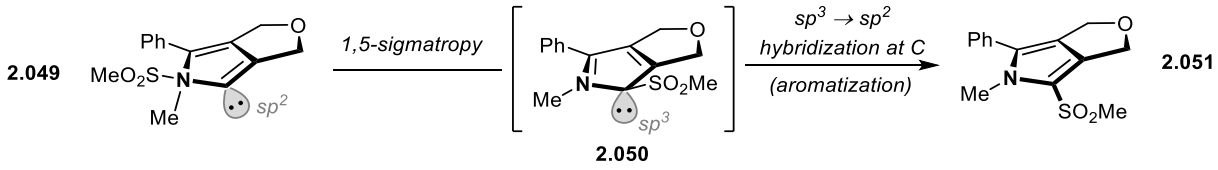

Figure 2-34. Schematic representation of the 1,2-migration step.

This can be observed upon a closer look at the intrinsic reaction coordinate (IRC) diagram calculated along the 1,2-migration transition state (Figure 2-35). The IRC seems to gradually plateau to a geometry indicative of a 1,5-sigmatropic shift. Submitting this set of coordinates directly to a geometric optimization leads to a quick "flattening" of the structure, presumably aromatizing the pyrrole core.

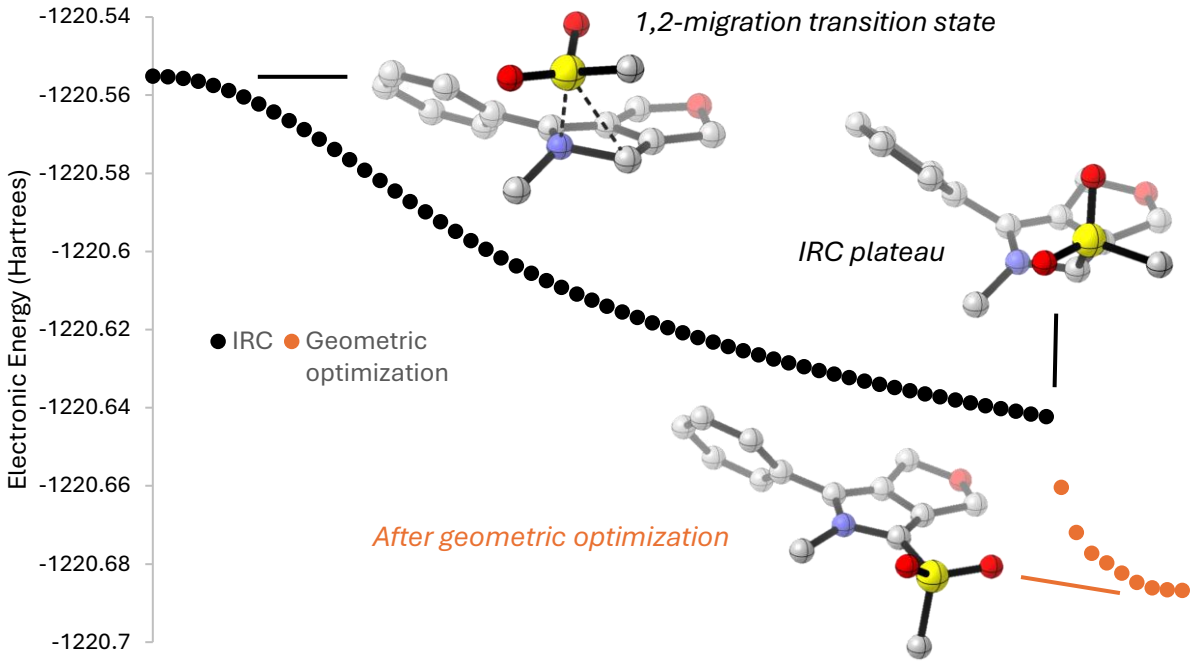

Figure 2-35. Post-transition state geometries for the 1,2-migration step.

2.10. Conclusion

In summary, an efficient and easy-to-perform thermal (3+2) rearrangement of yne-ynamide derivatives into polycyclic pyrroles has been developed, expanded, and mechanistically investigated. Aside from the large variety of substituted alkynes and linkers that were shown to efficiently promote the cyclization reaction, a notable observation remains that all the ynamides investigated herein efficiently behaved as TACs in cycloaddition reactions to form pyrroles. The (3+2) cycloaddition step may occur through a diverging concerted or a singlet diradical pathway, depending on the substitution of the reacting alkyne. A subsequent 1,2-migration of the EWG likely proceeds in a concerted intramolecular fashion from a pyrrolium ylide intermediate.

This previously unreported reactivity fills the "gap" of N,β cycloaddition products that are theoretically possible from ynamides (discussed in section 2.1), and shows that ynamides can behave as *neutral* three atom components in (3+2) cycloadditions.

2.11. Chapter references

1. Ficini, J., Ynamine: A versatile tool in organic synthesis. *Tetrahedron* **1976,** *32* (13), 1449-1486.
2. Zificsak, C. A.; Mulder, J. A.; Hsung, R. P.; Rameshkumar, C.; Wei, L.-L., Recent advances in the chemistry of ynamines and ynamides. *Tetrahedron* **2001,** *57* (36), 7575-7606.
3. Dunetz, J. R.; Danheiser, R. L., Copper-Mediated N-Alkynylation of Carbamates, Ureas, and Sulfonamides. A General Method for the Synthesis of Ynamides. *Org. Lett.* **2003,** *5* (21), 4011-4014.
4. Zhang, Y.; Hsung, R. P.; Tracey, M. R.; Kurtz, K. C. M.; Vera, E. L., Copper Sulfate-Pentahydrate-1,10-Phenanthroline Catalyzed Amidations of Alkynyl Bromides. Synthesis of Heteroaromatic Amine Substituted Ynamides. *Org. Lett.* **2004,** *6* (7), 1151-1154.
5. Hamada, T.; Ye, X.; Stahl, S. S., Copper-Catalyzed Aerobic Oxidative Amidation of Terminal Alkynes: Efficient Synthesis of Ynamides. *J. Am. Chem. Soc.* **2008,** *130* (3), 833-835.
6. Coste, A.; Karthikeyan, G.; Couty, F.; Evano, G., Copper-Mediated Coupling of 1,1-Dibromo-1-alkenes with Nitrogen Nucleophiles: A General Method for the Synthesis of Ynamides. *Angew. Chem. Int. Ed.* **2009,** *48* (24), 4381-4385.
7. DeKorver, K. A.; Li, H.; Lohse, A. G.; Hayashi, R.; Lu, Z.; Zhang, Y.; Hsung, R. P., Ynamides: A Modern Functional Group for the New Millennium. *Chem. Rev.* **2010,** *110* (9), 5064-5106.
8. Evano, G.; Coste, A.; Jouvin, K., Ynamides: Versatile Tools in Organic Synthesis. *Angew. Chem. Int. Ed.* **2010,** *49* (16), 2840-2859.
9. Iftikhar, R.; Mazhar, A.; Iqbal, M. S.; Khan, F. Z.; Askary, S. H.; Sibtain, H., Ring forming transformations of ynamides via cycloaddition. *RSC Advances* **2023,** *13* (16), 10715-10756.
10. Wang, X.-N.; Yeom, H.-S.; Fang, L.-C.; He, S.; Ma, Z.-X.; Kedrowski, B. L.; Hsung, R. P., Ynamides in Ring Forming Transformations. *Acc. Chem. Res.* **2014,** *47* (2), 560-578.
11. Dodd, R. H.; Cariou, K., Ketenimines Generated from Ynamides: Versatile Building Blocks for Nitrogen-Containing Scaffolds. *Chem. - Eur. J.* **2018,** *24* (10), 2297-2304.
12. Shen, J.; Wu, Z.; Liu, Y.; Bai, Y.; Qiu, J.; Zhang, Z.; Yuan, Z.; Zhu, G., Radical Chain Isomerization of N-Sulfonyl Ynamides to Ketenimines and Its Application to Furan Dearomatization. *Org. Lett.* **2021,** *23* (23), 9321-9326.
13. D'Hollander, A. C. A.; Romero, E.; Vijayakumar, K.; Le Houérou, C.; Retailleau, P.; Dodd, R. H.; Iorga, B. I.; Cariou, K., Base-Mediated Generation of Ketenimines from Ynamides: [3+2] Annulation with Azaallyl Anions. *Adv. Synth. Catal.* **2021,** *363* (11), 2903-2908.
14. Danheiser, R. L.; Gould, A. E.; de la Pradilla, R. F.; Helgason, A. L., Intramolecular [4+2] Cycloaddition Reactions of Conjugated Enynes. *J. Org. Chem.* **1994,** *59* (19), 5514-5515.
15. Dunetz, J. R.; Danheiser, R. L., Synthesis of Highly Substituted Indolines and Indoles via Intramolecular [4 + 2] Cycloaddition of Ynamides and Conjugated Enynes. *J. Am. Chem. Soc.* **2005,** *127* (16), 5776-5777.
16. Shibata, T.; Fujiwara, R.; Takano, D., Thermal and Au(I)-Catalyzed Intramolecular [4+2] Cycloaddition of Aryl-Substituted 1,6-Diynes for the Synthesis of Biaryl Compounds. *Synlett* **2005,** *2005* (13), 2062-2066.
17. Mansfield, S. J.; Campbell, C. D.; Jones, M. W.; Anderson, E. A., A robust and modular synthesis of ynamides. *Chem. Commun.* **2015,** *51* (16), 3316-3319.
18. Guissart, C.; Dolbois, A.; Tresse, C.; Saint-Auret, S.; Evano, G.; Blanchard, N., A Straightforward Entry to γ-Trifluoromethylated Allenamides and Their Synthetic Applications. *Synlett* **2016,** *27* (18), 2575-2580.
19. Fluegel, L. L.; Hoye, T. R., Hexadehydro-Diels–Alder Reaction: Benzyne Generation via Cycloisomerization of Tethered Triynes. *Chem. Rev.* **2021,** *121* (4), 2413-2444.
20. Woods, B. P.; Baire, B.; Hoye, T. R., Rates of Hexadehydro-Diels–Alder (HDDA) Cyclizations: Impact of the Linker Structure. *Org. Lett.* **2014,** *16* (17), 4578-4581.

21. Caruano, J.; Muccioli, G. G.; Robiette, R., Biologically active γ-lactams: synthesis and natural sources. *Org. Biomol. Chem.* **2016,** *14* (43), 10134-10156.
22. Letavic, M.; Rudolph, D. A.; Savall, B. M.; Shireman, B. T.; Swanson, D. Disubstituted octahydropyrrolo[3,4-c]pyrroles as orexin receptor modulators and their preparation. WO2012145581A1, 2012.
23. Redrobe, J. P.; Nielsen, E. Ø.; Christensen, J. K.; Peters, D.; Timmermann, D. B.; Olsen, G. M., α7 nicotinic acetylcholine receptor activation ameliorates scopolamine-induced behavioural changes in a modified continuous Y-maze task in mice. *Eur. J. Pharmacol.* **2009,** *602* (1), 58-65.
24. Huisgen, R., Mechanism of 1,3-dipolar cycloadditions. Reply. *J. Org. Chem.* **1968,** *33* (6), 2291-2297.
25. Firestone, R. A., Mechanism of 1,3-dipolar cycloadditions. *J. Org. Chem.* **1968,** *33* (6), 2285-2290.
26. Mahe, C.; Cariou, K., Ynamides in Free Radical Reactions. *Adv. Synth. Catal.* **2020,** *362* (22), 4820-4832.
27. Sustmann, R., Orbital energy control of cycloaddition reactivity. *Pure Appl. Chem.* **1974,** *40* (4), 569-593.
28. Exner, O., The Hammett Equation—the Present Position. In *Advances in Linear Free Energy Relationships*, Chapman, N. B.; Shorter, J., Eds. Springer US: Boston, MA, 1972; pp 1-69.
29. Becke, A. D., Density-functional thermochemistry. III. The role of exact exchange. *J. Chem. Phys.* **1993,** *98* (7), 5648-5652.
30. Lee, C.; Yang, W.; Parr, R. G., Development of the Colle-Salvetti correlation-energy formula into a functional of the electron density. *Phys. Rev. B* **1988,** *37* (2), 785-789.
31. Miehlich, B.; Savin, A.; Stoll, H.; Preuss, H., Results obtained with the correlation energy density functionals of becke and Lee, Yang and Parr. *Chem. Phys. Lett.* **1989,** *157* (3), 200-206.
32. Zhao, Y.; Truhlar, D. G., The M06 suite of density functionals for main group thermochemistry, thermochemical kinetics, noncovalent interactions, excited states, and transition elements: two new functionals and systematic testing of four M06-class functionals and 12 other functionals. *Theor. Chem. Acc.* **2008,** *120* (1), 215-241.
33. Haberhauer, G.; Gleiter, R.; Woitschetzki, S., anti-Diradical Formation in 1,3-Dipolar Cycloadditions of Nitrile Oxides to Acetylenes. *J. Org. Chem.* **2015,** *80* (24), 12321-12332.
34. Newcomb, M.; Johnson, C. C.; Manek, M. B.; Varick, T. R., Picosecond radical kinetics. Ring openings of phenyl-substituted cyclopropylcarbinyl radicals. *J. Am. Chem. Soc.* **1992,** *114* (27), 10915-10921.
35. Haberhauer, G.; Gleiter, R., Interplay between 1,3-Butadien-1,4-diyl and 2-Buten-1,4-dicarbene Derivatives: The Quest for Nucleophilic Carbenes. *J. Am. Chem. Soc.* **2013,** *135* (21), 8022-8030.

3. Chapter 3 – The intramolecular (3+2) reactivity between alkynyl sulfides and alkynes

Copyright (2022) Wiley. Used with permission from [Pommainville, A.; Campeau, D.; Gagosz, F., The Synthetic Potential of Thiophenium Ylide Cycloadducts. *Angew. Chem. Int. Ed.* **2022**, *61* (32), e202205963].

This report involves results by both D. Campeau and A. Pommainville. Results in this chapter were obtained by D. Campeau unless otherwise noted with "*Results in this figure obtained by …*".

3.1. Alkynyl sulfides in thermal cycloaddition chemistry

An analysis of thermal cycloadditions reported for alkynyl sulfides, similar to that done in section 2.1, shows chemistry almost exclusively limited to the α,β outcome (Figure 3-1). The N,α outcome has not been reported to date. The N,β outcome, as discussed in the introduction chapter (section 1.3.2.1) is limited only to a few reports.[1-4]

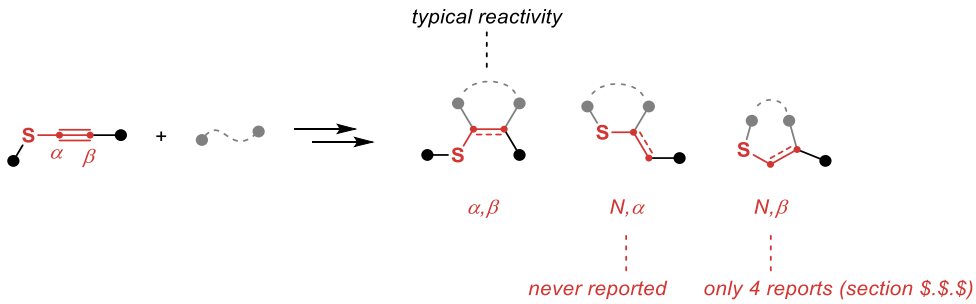

Figure 3-1. Possible outcomes of cycloadditions involving alkynyl sulfides.

There has not been any systematic study of the reactivity of simple alkynyl sulfides with cycloaddition partners. Haas and Krächter, however, did investigate the propensity of a special alkynyl disulfide **3.001** they could access towards cycloaddition with a wide variety of 4π partners, two of which are presented here (Figure 3-2).[5] These cycloadditions were successful, yet sluggish, requiring high temperatures even when done under neat conditions. More recently, alkynyl sulfides **3.004** were found to also participate in (2+2) reactions with PTAD **3.005** under thermal conditions.[6]

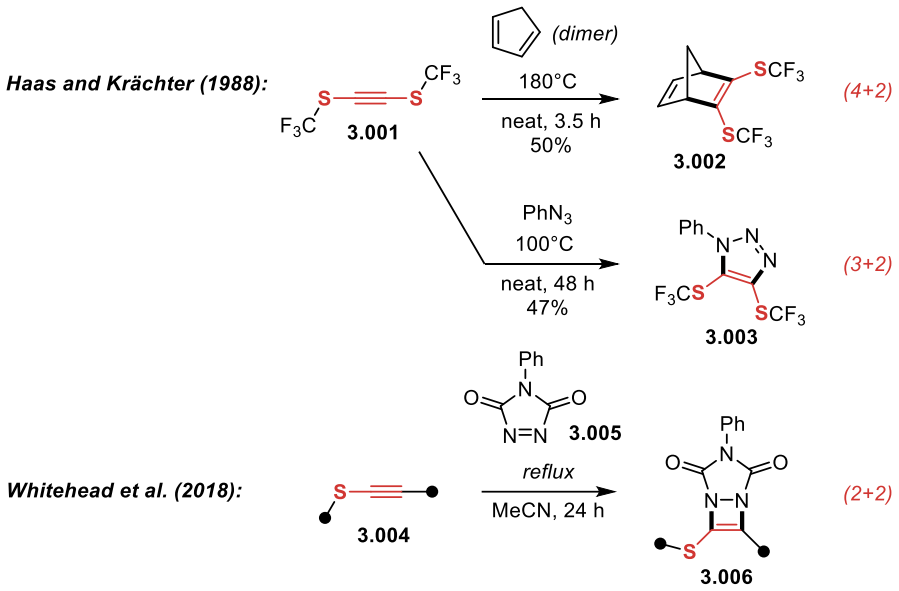

Figure 3-2. Selected α,β-based cycloadditions of alkynyl sulfides.

Despite their use as functionalized alkynes in cycloaddition reactions, alkynyl sulfides have the potential to participate in more complex cycloadditions involving the sulfur atom. The few reports on the use of alkynyl sulfides as *neutral* TACs[1-4] indicated good potential in transferring the (3+2) chemistry observed for the yne-ynamide scaffold (described in Chapter 2) to alkynyl sulfide derivatives.

An important line of inquiry that was not tackled in Chapter 2 would address the outcome of other hypothetical heteroarylium intermediates *not* containing electron-withdrawing groups such as **3.008** and **3.009** (Figure 3-3).

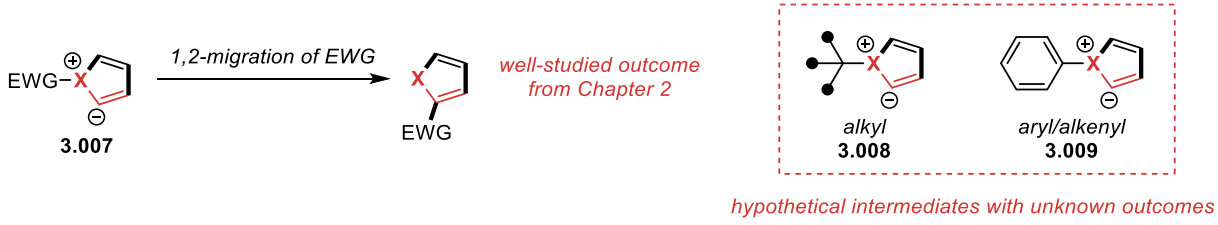

Figure 3-3. New lines of inquiry involving hypothetical heteroarylium ylides.

Unfortunately, this would not be easily studied with the N-alkynyl class of neutral three-atom components, since ynamine derivatives **3.011** which are not stabilized by an EWG are quite sensitive to hydration and even mild protic sources (Figure 3-4). Alkynyl sulfides **3.012** bearing alkyl or aryl substituents, on the other hand, have been successfully employed under a wide variety of

conditions. Alkynyl sulfides may then be a good avenue to access and study these newly hypothesized heteroarylium ylide intermediates.

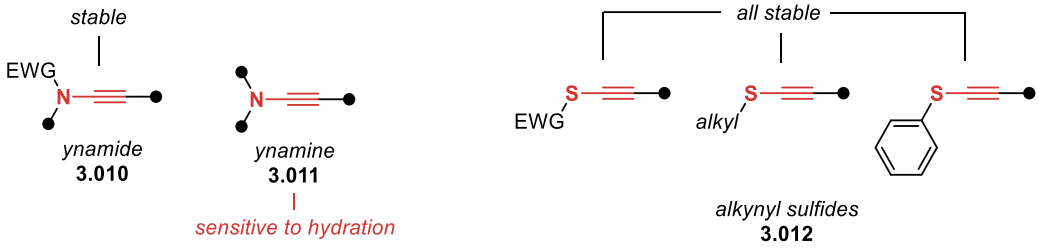

Figure 3-4. Larger space of synthetically relevant X-alkynyl species found in alkynyl sulfides.

For this reason, analogous yne-alkynyl sulfide scaffolds were targeted for further investigations.

3.2. Synthesis of yne-alkynyl sulfide substrates

The scaffolds studied in this chapter involve alkynes tethered to alkynyl sulfides. Specifically, example **3.021e** has been summarized here (Figure 3-5). A Sonogashira cross coupling leads from propargyl alcohol to **3.013**. Propargylation using propargyl bromide provides the diyne **3.014**. In parallel, the sulfonylation of tert-butyl thiol provides the thiosulfonate **3.015**. The diyne **3.014** is lithiated and trapped with thiosulfonate **3.015** to provide the yne-alkynyl sulfide example **3.021e**.

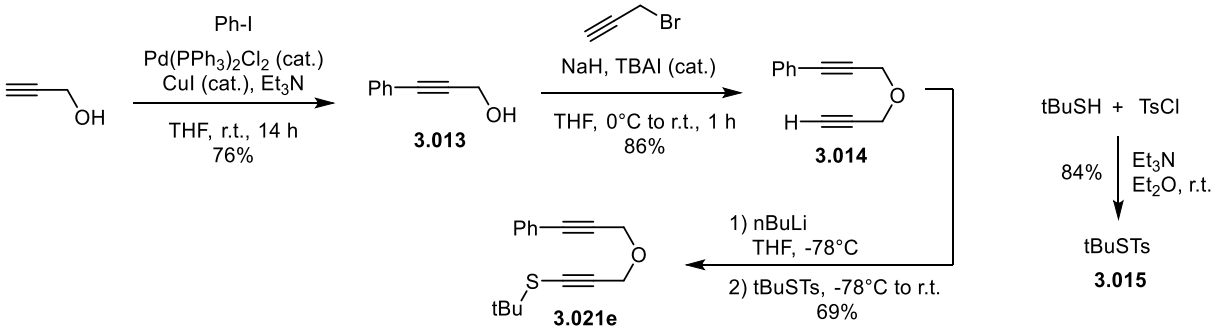

Figure 3-5. Representative procedure for the synthesis of yne-alkynyl sulfides.

Although this sequence of steps demonstrates how this scaffold can be accessed quickly with robust chemistry, a variety of approaches were used to access all derivatives of interest (Figure 3-6).

The most versatile and functional group-tolerant route for generating alkyl- and aryl- alkynyl sulfides was the copper-catalyzed cross-coupling method between thiols and bromoalkynes recently developed by the group of Collins.[7] When low functional group compatibility issues were expected, the formation of lithium acetylides **3.017** followed by trapping with thiosulfonate esters was found to

be a great way to produce alkyl- or aryl- alkynyl sulfides, and in particular, the most efficient route when scaling up. The generation of lithium alkynyl sulfide salts **3.018** was mostly used to access the more exotic class of acyl- alkynyl sulfides.

Derivatizations of the alkyne termini and formation of the linker groups were achieved quite similarly to what was previously described for the yne-ynamide scaffolds (see section 2.4). Electrophilic trapping of lithium acetylides and classical cross-coupling reactions (Sonogashira, Cadiot-Chodkiewicz) proved to be a reliable group of methods in providing various classes of alkyne substitutions. The reactive alkynyl groups were joined together typically via condensation or substitution chemistry.

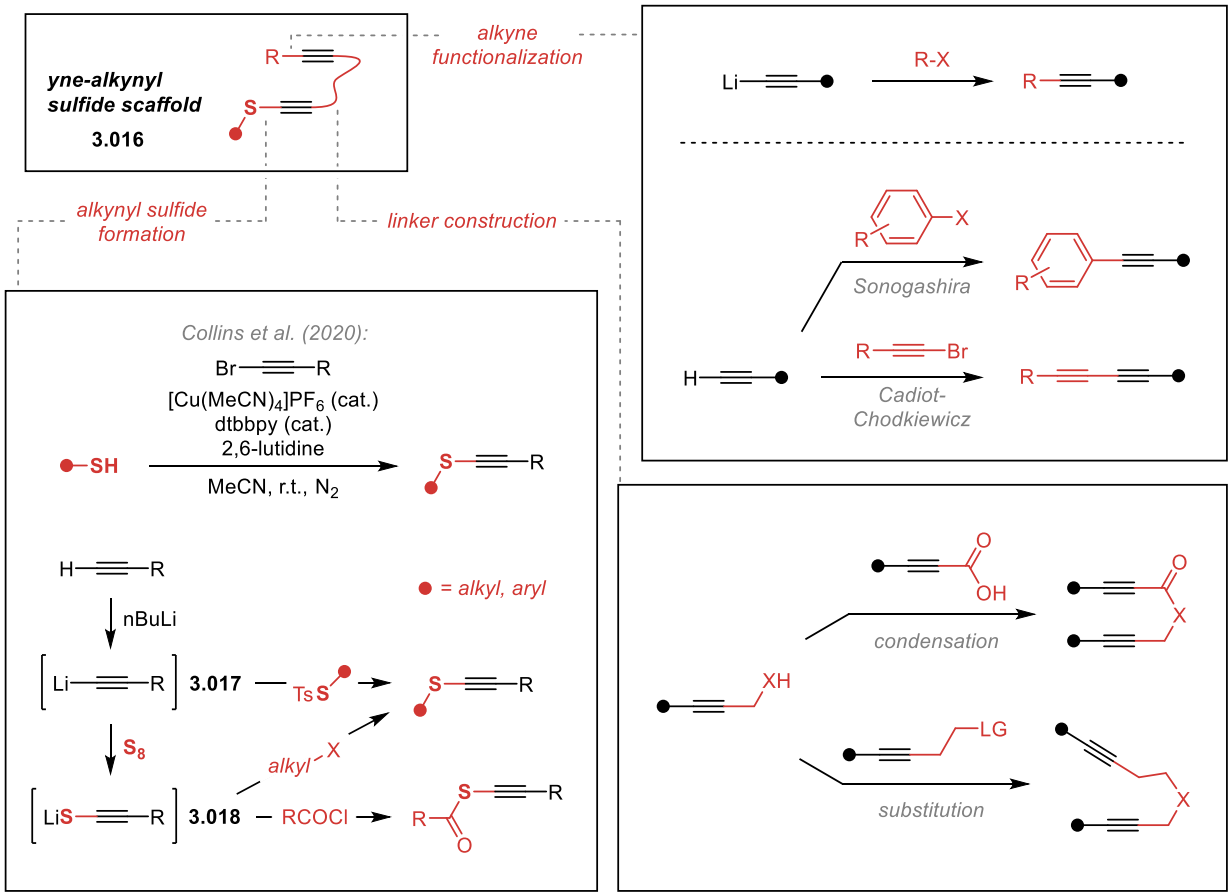

Figure 3-6. Various synthetic strategies employed towards the yne-alkynyl sulfide scaffolds.

3.3. Alkynyl sulfides as viable neutral TACs – Initial hits

Our first attempts to apply alkynyl sulfides as TACs in intramolecular (3+2) cycloadditions involved the aryl alkynyl sulfides derivatives **3.019** and **3.020** (Figure 3-7). Upon submitting these scaffolds to

the conditions previously optimized for the yne-ynamide (3+2) cascade, both substrates were fully consumed within 30 minutes, yet produced quite complex mixtures of species, as observed by TLC and NMR analyses. Cleaner reaction profiles could not be obtained by repeating at lower temperature for longer periods, or by removing the BHT additive.

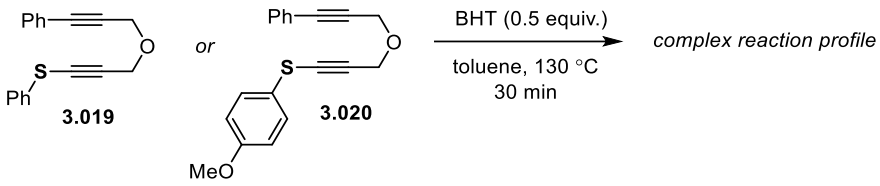

Figure 3-7. Initial investigations using the aryl alkynyl sulfide scaffolds **3.019** and **3.020**.

The failure seen above was initially attributed to the stronger C(sp^2)-S bond in this particular scaffold. Under the assumption that a (3+2) cycloaddition event *does* take place, the difficulty in cleaving this C-S bond may lead to alternative degradation pathways, explaining the observed complex reaction profile.

Success was rather obtained when Alice Pommainville[8] accessed the alkyl alkynyl sulfide scaffold **3.021a**, which upon heating, produced a significant amount of an interesting fused thiophene product **3.022a** (Figure 3-8).

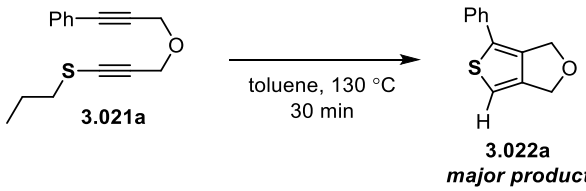

Figure 3-8. First observation of (3+2) reactivity in alkynyl sulfides. *Result in this figure obtained by Alice Pommainville.*

The structure of **3.022a** was confirmed by a series of NMR experiments (see Supporting Information, section 6.3.13) and single crystal X-ray diffraction studies (Figure 3-9). This result suggested that the (3+2) cyclization chemistry previously observed in ynamides may also be possible with alkynyl sulfides.

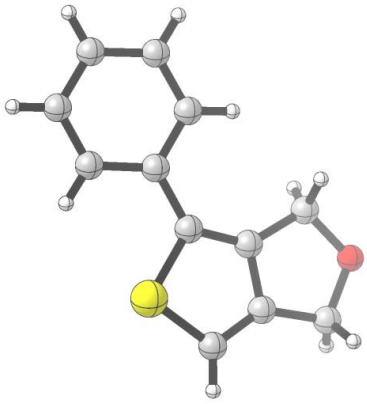

Figure 3-9. SCXRD of **3.022a**. See CCDC deposition # 2149613 for acquisition data. *Result in this figure obtained by Alice Pommainville.*

With these positive results, it was conceived that chemistry closely analogous to that of ynamides, involving a 1,2-migration event of an electron withdrawing group, may be possible as well for alkynyl sulfides. So, the scaffold **3.024** was synthesized through the acylation of a lithium alkynyl sulfide (Figure 3-10). Although analysis of the reaction crude did show the major formation of the desired product **3.024**, degradation of this species was observed when in a $CDCl_3$ solution over the weekend at room temperature. Degradation was also observed when purification by silica gel chromatography was attempted. Heating the crude mixture at 130 °C in toluene for 10 minutes showed consumption of the starting material and trace amounts of promising signals by NMR analysis, but resulted mostly in a complex mixture of unidentified species. The use of the thioester-based scaffold was not further pursued.

Through the same synthetic sequence, the thiocarbonate derived scaffold **3.025a** was obtained and observed to be a stable species, even when subjected to silica gel chromatography.

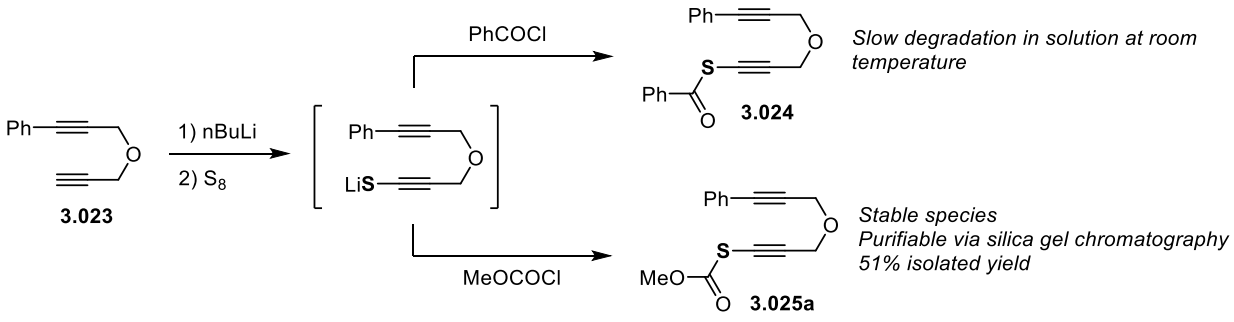

Figure 3-10. Stability limitation for S-acylated yne-alkynyl sulfides.

Gratifyingly, upon heating, **3.025a** and its benzyl analog **3.025b** were observed to cleanly rearrange to the desired 2-ester substituted thiophenes **3.026a** and **3.026b** in high yields (Figure 3-11), as previously seen for yne-ynamides.

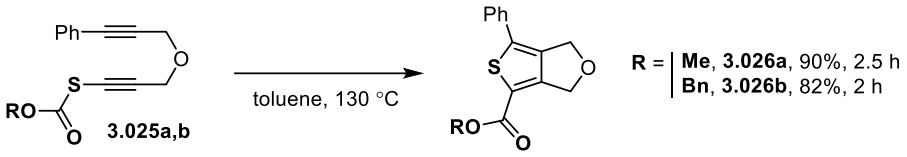

Figure 3-11. Acyl alkynyl sulfides display 1,2-migratory behaviour of the EWG in (3+2) reactions with alkynes.

Our first guiding mechanistic considerations were heavily influenced by that previously proposed for the yne-ynamide (3+2) chemistry (Figure 3-12). The reactivity leading from yne-alkynyl sulfides **3.027** to the two (3+2) products observed **3.029** and **3.030** was proposed to stem from a common thiophenium ylide cycloadduct **3.028**.

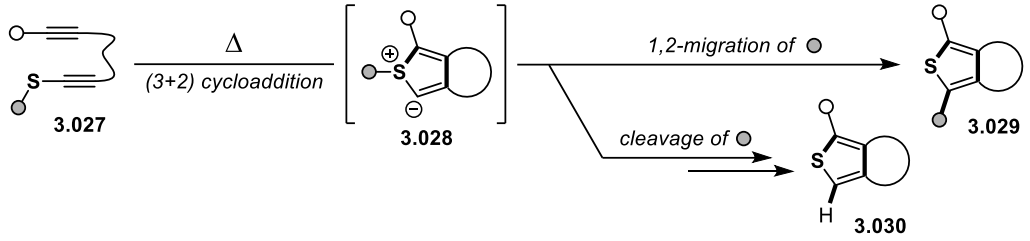

Figure 3-12. Initial guiding mechanistic considerations for the yne-alkynyl sulfides (3+2) cascade.

The proposed steps involved in the cleavage of a pendant group to generate trisubstituted thiophene **3.030** are further discussed in section 3.8.

3.4. Structure optimization for the alkyl alkynyl sulfide-based scaffold

Although the thiocarbonate-derived yne-alkynyl sulfides scaffolds gave clean (3+2) reaction profiles, the alkyl alkynyl sulfides-based scaffolds were selected for further study. Their more varied and higher-yielding synthetic routes proved to be more attractive for the purpose of generating and studying variations on the whole yne-alkynyl sulfide scaffold.

A series of alkyl-substituted alkynyl sulfides **3.021a-f** were synthesized and their reactivity evaluated under similar conditions (Table 3-1).

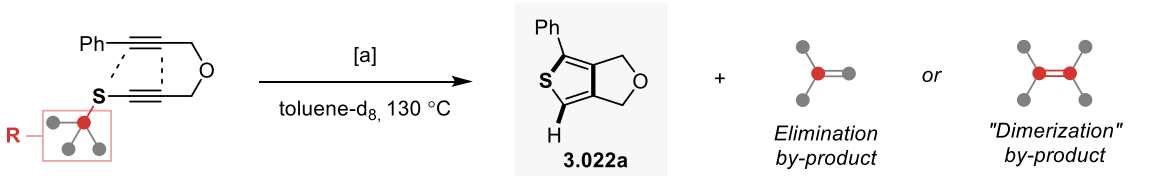

	R	Time (h)	yield (%)[b]	A, yield (%)[b]	B, yield (%)[b]
3.021a	*n*-Pr	1	46	propene, 17	-
3.021b	Me	1	38	-	ethylene, traces
3.021c	*n*-Oct	0.75	40	1-octene, 25	-
3.021d	*i*-Pr	0.75	73	propene, 53	-
3.021e	*t*-Bu	1	91 (85)[c]	isobutene, 60	-
3.021f	Bn	1	90	-	(*Z*)-stilbene, 12

Table 3-1. Exploration and optimization of alkyl alkynyl sulfides in (3+2) cycloadditions with a tethered alkyne. [a] All reactions performed in sealed NMR tubes at the 0.05 mmol scale in toluene-d_8 (0.1 M) with 2.0 µL mesitylene as internal NMR standard. [b] Yields assessed by ^{1}H NMR after the indicated time. [c] Isolated yield. *Results in this table obtained by Alice Pommainville.*

Interestingly, they were all thermally converted into the same trisubstituted thiophene **3.022a**, observed to be the major and sole isolable reaction product (38-91%). Furthermore, by monitoring the reactions of substrates **3.021a-f** by ^{1}H NMR spectroscopy in sealed NMR tubes, appreciable amounts of alkenes derived from elimination of the corresponding alkyl chains could be identified, thus suggesting that the hydrogen atom recovered at position C(5) of the thiophene originated from this side chain.

Although substrates **3.021b** and **3.021f** cannot proceed through an elimination mechanism, these still provided large amounts of the same thiophene **3.022a**, and small amounts of ethylene and *cis*-stilbene by-products, respectively. *Cis*-stilbene was identified during ^{1}H-NMR analysis of the reaction mixture as a clear singlet at 6.43 ppm (in toluene-d_8). Evaluating the presence or absence of *trans*-stilbene (6.93 ppm) was rendered difficult due to overlapping with other signals in the aromatic region.

These observations are further explored in the mechanistic section of this chapter (see Figure 3-27). The *tert*-butyl alkynyl sulfide **3.021e**, in particular, gave an excellent isolated yield of thiophene **3.022a** (85%). In addition, this model transformation could be successfully scaled up to the gram-scale with minimal loss of efficiency, affording 0.85 g (80% yield) of the desired thiophene (Table 3-2). For these reasons, as well as for its convenient generation of traceless isobutene by-product, the

tert-butyl group was employed as the *S*-substituent of choice for the study of other structural parameters influencing the formation of trisubstituted thiophenes.

3.5. Substrate scope

The modification of the alkyne substituent was first studied (Table 3-2). Variations of the aryl group involving either substitution on the phenyl ring (**3.022g**) or replacement with other heteroaromatic cycles (**3.022h** and **3.022i**) were all well tolerated, giving good to excellent yields (61-92%) of trisubstituted thiophenes in short reaction times. We then turned our attention to alkynyl, alkenyl, alkyl, as well as non-substituted alkynyl derivatives. Pleasingly, the use of a conjugated 1,3-diyne rapidly afforded the desired alkynyl thiophene **3.022k** with an excellent yield (90%). Cyclohexenyl derivative **3.022j** could be cleanly obtained as well, albeit with a longer reaction time (4.5 h). These two last examples emphasize the favourable nature of the studied (3+2) process when other thermal cycloaddition events (hexadehydro- and tetrahydro-Diels-Alder reactions)[9] could be possible. Notably, a higher reaction temperature was required for C-sp^3 methyl substituted alkyne **3.021l** which could be converted into thiophene **3.022l** in a moderate 44% yield. A similar reactivity was observed for terminal alkyne **3.021m** (**3.022m**: 43%). The lower yields obtained for thiophenes **3.022l** and **3.022m** can be attributed in part to their low molecular weight and volatility, which made their isolation more challenging on small scale. Acyl substituted alkyne **3.021n** was highly active in the (3+2) process, showing some formation of the desired thiophene **3.022n** even at room temperature, and full consumption after only a few minutes of heating. Both silyl and sulfide-substituted alkynes also cleanly provided hetero-substituted thiophenes **3.022o** and **3.022p**. Overall, this (3+2) process was tolerant of all types of alkynyl groups that were accessed.

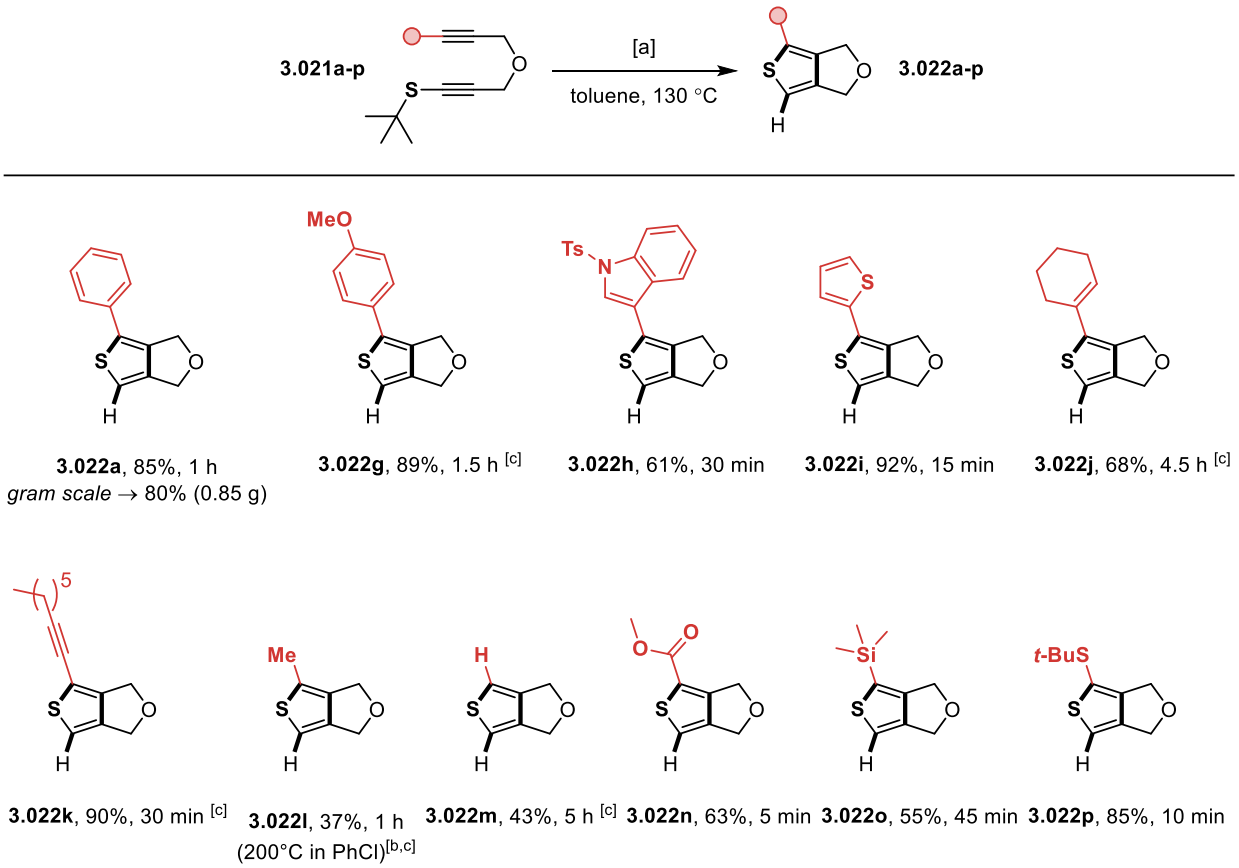

Table 3-2. Reaction scope for the (3+2) cyclization in yne-alkynyl sulfides: alkyne substitutions. [a] Unless otherwise specified, reactions were performed in sealed reaction tubes at the 0.1 mmol scale in toluene (0.1 M) under air. [b] Brought to the indicated temperature using a microwave reactor. [c] Result obtained by Alice Pommainville.

A variety of substrates possessing a three, four and five-membered linker were synthesized, many promoting the yne-alkynyl sulfide (3+2) cycloaddition (Table 3-3). Exchanging the model ether linker by a sulfonamide or a malonate group led to moderate to good yields of the corresponding thiophenes **3.022q** and **3.022s**. Even the simplest all-methylene linker, upon heating to a higher temperature, led to a good yield (69%) of the corresponding thiophene **3.022r**. Inserting an ester functionality in the linker led to the quantitative formation of lactone-fused thiophene **3.022t**. Further substitution/functionalization of the linker was found advantageous, such as can be seen for **3.022u** and spirocyclic fused thiophene **3.022v**, which were obtained in higher yields (91-97%) while running the reaction at a lower temperature. When using higher reaction temperatures (200 °C), substrates with four-membered linkers were also found to efficiently undergo the (3+2) cycloaddition, expanding the access to [3.4.0] bicycles in moderate yields for **3.022w** and **3.022x** (62% and 37%, respectively). An improved yield was obtained when a geometrically constrained linker was

employed (**3.022y,** 75%). Following this success, substrates with a five-membered linker were also synthesized, but their thermal reaction only led to degradation with no observable formation of the desired [3.5.0] bicyclic structures.

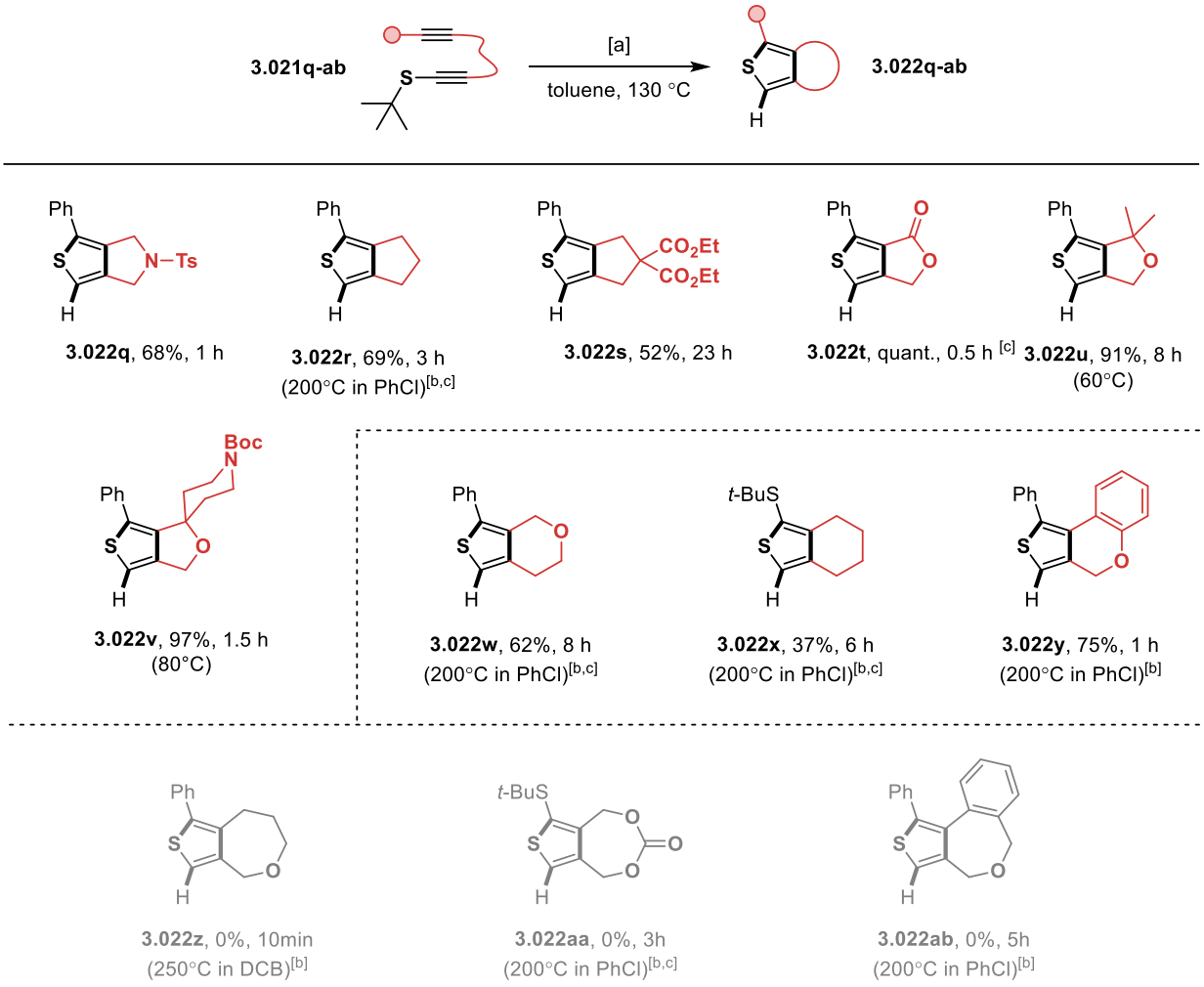

Table 3-3. Reaction scope for the (3+2) cyclization in yne-alkynyl sulfides: linker variations. [a] Unless otherwise specified, reactions were performed in sealed reaction tubes at the 0.1 mmol scale in toluene (0.1M) under air. [b] Brought to the indicated temperature using a microwave reactor. [c] Result obtained by Alice Pommainville.

3.6. Thiophenium ylide intermediate and electrophilic trapping

Hypothesizing the advent of a thiophenium ylide cycloadduct (**3.028**, Figure 3-12), we considered that this intermediate could be trapped in the presence of an appropriate electrophile, prior to the transfer of a hydrogen at position C(5), to provide fully substituted thiophenes. This method would permit access to more complex thiophenes without recourse of the 1,2-migration pathway, and

starting instead from simpler, more accessible *S*-alkyl derivatives. Gratifyingly, interception of the intermediate ylide was indeed observed when using methyl chloroformate (Figure 3-13).

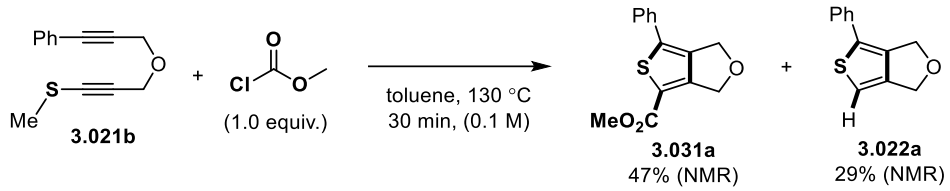

Figure 3-13. Observation of electrophile trapping in the presence of methyl chloroformate. Reaction performed at the 0.06 mmol scale, yields assessed by NMR analysis of the reaction crude, using 1,2-DBE as standard.

A control experiment was performed showing that thiophene **3.022a** could not be converted into **3.031a** in the presence of methyl chloroformate in toluene at 130 °C, thus demonstrating that the electrophilic trapping occurs *independently* of the formation of **3.022a** (Figure 3-14).

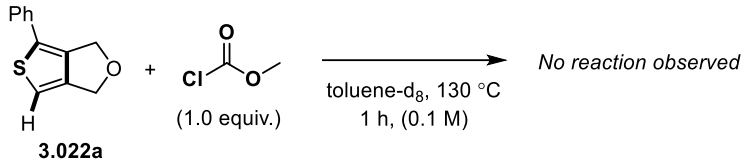

Figure 3-14. Control experiment demonstrating lack of reactivity between **3.022a** and methyl chloroformate. Reaction performed at the 0.06 mmol scale in an NMR tube, following by NMR analysis using mesitylene as internal standard.

A second control experiment was performed to ascertain that the reaction occurred with an *intermediate* of the (3+2) reaction, rather than being derived from a direct reaction between methyl chloroformate and the starting material (Figure 3-15). This was tested by heating **3.032**, bearing an isolated methyl alkynyl sulfide moiety, and methyl chloroformate in toluene-d_8. NMR analysis showed no reaction occurring after 1 hour of heating.

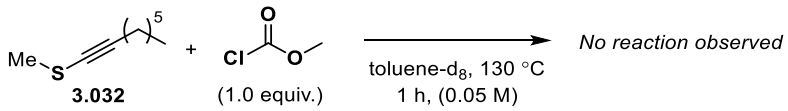

Figure 3-15. Control experiment demonstrating lack of direct reactivity between alkynyl sulfides and methyl chloroformate. Reaction performed at the 0.03 mmol scale in an NMR tube, following by NMR analysis using trimethylphenylsilane as internal standard.

With confirmation that this reactivity is possible, the propensity for a series of alkyl-substituted alkynyl sulfides **3.021a-f** towards electrophilic trapping was evaluated (Table 3-4). Interestingly, the nature of the alkyl substituent was found to be a key factor affecting the amount of thiophene resulting from the trapping event. Notably, while *S*-benzyl and *S*-*tert*-butyl substituted substrates gave the highest yields of simple thiophene **3.022a** in the previous optimization (See Table 3-1), they provided ester-substituted thiophene **3.031a** with the poorest yields. *n*-Propyl substrate **3.021a** was chosen as the most suitable substituent for studying the cyclization / electrophilic trapping sequence, due to a combination of both its ease of synthesis and the highest ratio obtained in favour of the trapping product **3.031a.** As can be reasonably suspected, increasing the amount of methyl chloroformate present also significantly increased the amount of thiophene **3.031a** obtained (up to 85% isolated yield for 10 equivalents of methyl chloroformate used).

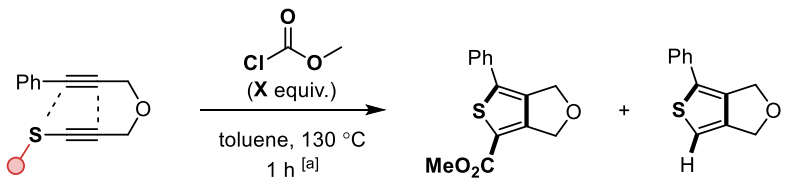

		X	3.031a (%)[b]	3.022a (%)[b]	3.031a:3.022a ratio
3.021b	**Me**	1	59	35	1.7 : 1
3.021a	***n*-Pr**	1	48	20	2.4 : 1
3.021d	***i*-Pr**	1	59	27	2.2 : 1
3.021e	***t*-Bu**	1	4	82	1 : 20
3.021f	**Bn**	1	7	70	1 : 10
3.021a	***n*-Pr**	2	57	16	3.4 : 1
3.021a	***n*-Pr**	4	61	13	4.9 : 1
3.021a	***n*-Pr**	10	91 (85)[c]	8	11 : 1

Table 3-4. Optimization of intermediate trapping by an electrophile in the yne-alkynyl sulfide (3+2) cyclization. [a] All reactions performed in sealed reaction tubes at the 0.05 mmol scale in toluene (0.1 M). [b] Yields assessed by ^{1}H NMR analysis of the concentrated reaction crude with 2.0 µL 1,2-DBE as NMR standard. [c] Isolated yield. *Results in this table obtained by Alice Pommainville.*

Considering that the efficiency of the thiophene functionalization should be directly dependent on the electrophilic strength of the trapping agent, we then investigated the reaction outcomes of different electrophilic species under the same optimized conditions (Table 3-5). Similarly to methyl chloroformate, propargyl chloroformate and pivaloyl chloride were found to be effective

electrophiles affording the acylated derivatives **3.031b** and **3.031d** in moderate yields (62% and 58%, respectively). Trapping with the comparatively weaker electrophilic diethylcarbamoyl chloride was possible as demonstrated by the formation of amide **3.031c**, which was isolated however in a much lower 29% yield. The same trend was subsequently observed, where the yields of desired functionalized thiophenes were affected by competitive trapping by protons to form **3.022a** when poorer electrophiles were used. We found that trapping of both aldehydes and ketones was possible, providing secondary and tertiary alcohols **3.031e** and **3.031f**, respectively. Interestingly, when an *N*-sulfonylimide derivative was used as electrophile, a transfer of the propyl chain from the sulfur to the nitrogen was observed in **3.031g'** alongside the predicted product **3.031g** in a 1:1 ratio and for an overall 46% yield. Analogously, when carbon dioxide (dry ice) was directly added to a reaction mixture containing methyl alkynyl sulfide **3.021b**, the same model product **3.031a** was obtained without need of any dealkylation (25% yield).

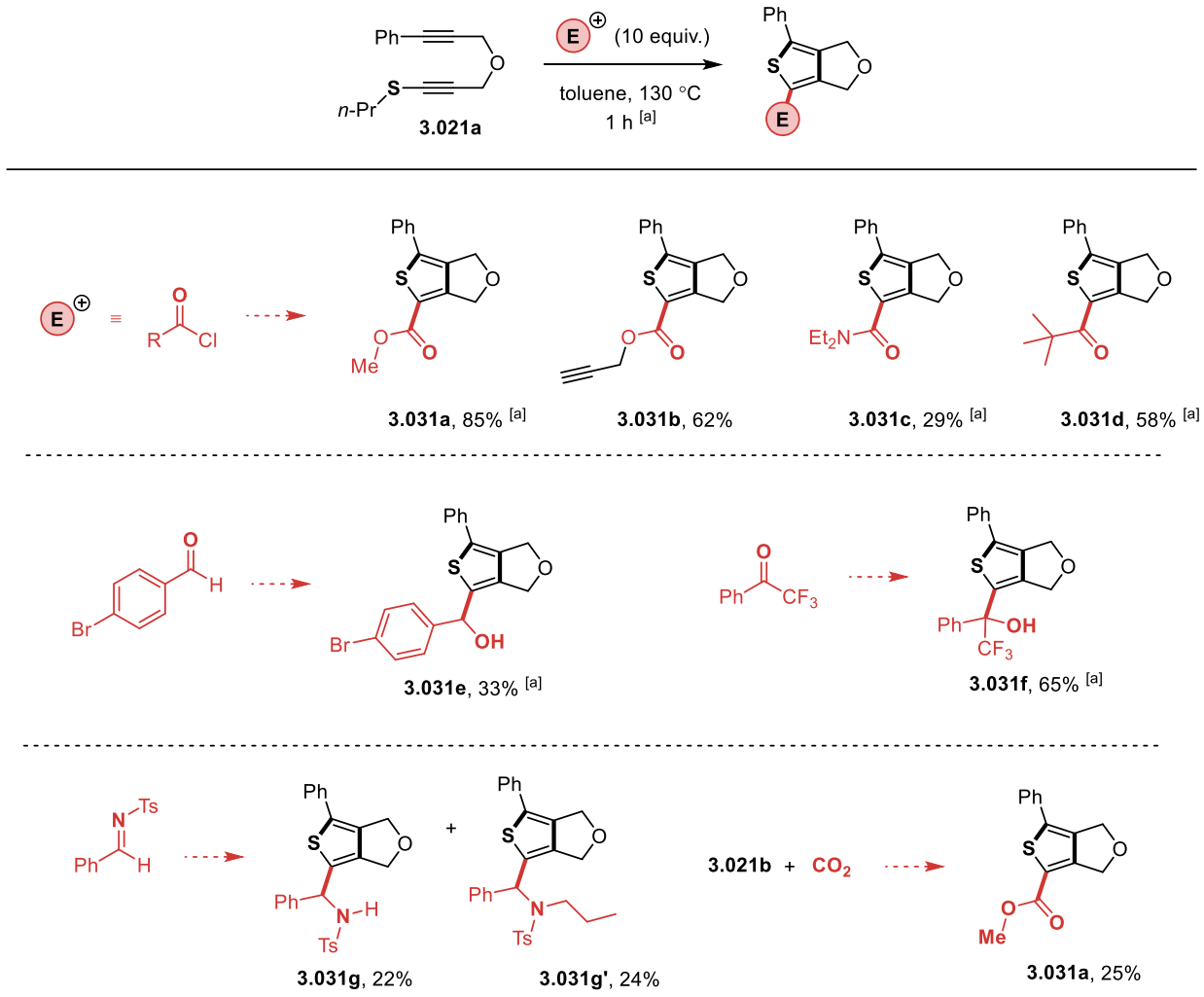

Table 3-5. Scope of successful carbon-based electrophile traps. [a] All reactions were performed in sealed reaction tubes at the 0.1 mmol scale with 10 equivalents of an electrophile in toluene (0.1 M) under air. [a] Entry obtained by Alice Pommainville.

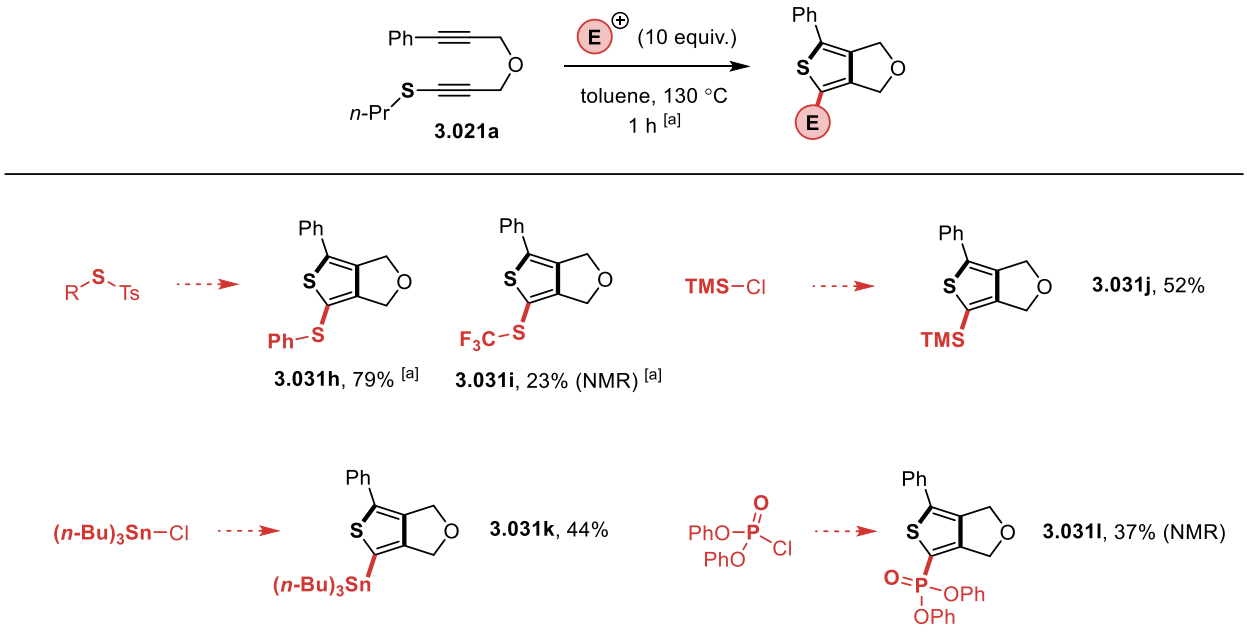

Table 3-6. Scope of successful non-carbon electrophile traps. [a] All reactions were performed in sealed reaction tubes at the 0.1 mmol scale with 10 equivalents of an electrophile in toluene (0.1 M) under air. [a] Entry obtained by Alice Pommainville.

With the aim to further diversify the 5-position of the thiophene, thiolation with electrophilic sulfide sources was carried out, gratifyingly affording **3.031h** (79% yield) and trifluoromethylthio derivative **3.031i** (23% yield) (Table 3-6). Electrophilic trapping of silyl, stannyl, and phosphoryl derivatives were all successful, leading to hetero-substituted thiophenes **3.031j-l** in moderate yields. Exploiting the nucleophilic nature of the proposed thiophenium ylide intermediate allowed for a rapid and efficient synthesis of 5-functionalized thiophenes using an analogous yne-alkynyl sulfide substrate (**3.021a**). The electrophilic trapping approach explored in this scope provides a much more diverse and convergent route to fully substituted fused thiophenes than by accessing more complex substrates, such as those initially studied (**3.025a** and **3.025b**, Figure 3-11).

There are however multiple electrophiles which were not successful partners in this reactivity (Table 3-7). Alkyl halides, carboxylic anhydrides, paraformaldehyde and carbon disulfide were all carbon-based electrophiles which seemed to be unreactive under this set of conditions. Trimethylsilyl triflate was observed to directly decompose the yne-alkynyl sulfide when mixed at room temperature. Borate esters were unreactive under these conditions, having little impact on the formation of **3.022a**. Sulfonyl chlorides, elemental sulfur and alkyl disulfides were all found to produce complex mixtures, with reduced amounts of **3.022a** obtained.

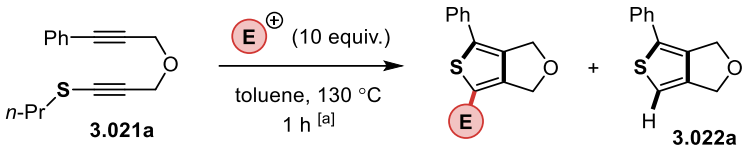

Type	**Electrophile**	X (equiv.)	Observation	**"Trapped"** (NMR %)	**3.022a** (NMR %)
Alkylation	MeI	10	-	< 5	48
	BnBr	10	-	0	50
Silylation	TMSOTf	10	Degraded S.M. at room temperature	0	0
Borylation	$B(OMe)_3$	10	-	0	60
Sulfonylation	TsCl	10	Complex mixture	0	34
Thiolation	S_8	10	Complex mixture	0	5
	MeSSMe [a]	1	Complex mixture	8	26
Acylation	Ac_2O	1	-	0	43
	Paraformaldehyde [a]	10	-	0	29
	CS_2	10	-	0	64

Table 3-7. List of unsuccessful electrophiles and associated observations. [a] Entry completed by Alice Pommainville.

From these lists of attempted electrophiles, it can be observed that the trapping event is generally more successful with hard electrophiles.

3.7. Procedure simplification and synthetic applications

While isolation of the yne-alkynyl sulfide substrates was necessary for their comparative study in the previous scopes, the particularly simple reaction conditions (only solvent and heat) necessary for the (3+2) cyclization renders itself attractive for one-pot procedures involving consecutive synthetic steps (Figure 3-16). It was found that Sonogashira cross-coupling conditions are compatible with the reactivity of these yne-alkynyl sulfides. For example, coupling of 2-iodothiophene and terminal alkyne **3.021m** in dry toluene rapidly afforded yne-alkynyl sulfide substrate **3.021i** at room temperature, which then cyclized upon heating yielding the desired thiophene **3.022i** in 52% overall yield. Alternatively, *in situ* condensation of propargyl amine **3.033** and aldehyde **3.034** followed by (3+2) cycloaddition upon mild heating provided imine derivative **3.036** in 69% yield. Finally, the

alkynyl sulfide itself could be synthesized *in-situ* from a C-S coupling.[7] To avoid using foul-smelling *tert*-butyl thiol as the source of sulfide, *tert*-dodecyl mercaptan was used as a thiol bearing an alternative tertiary alkyl chain. This grapefruit-scented thiol, along with bromoalkyne **3.037**, smoothly afforded alkynyl sulfide **3.038** which underwent cyclization towards thiophene **3.022q** in 59% overall yield.

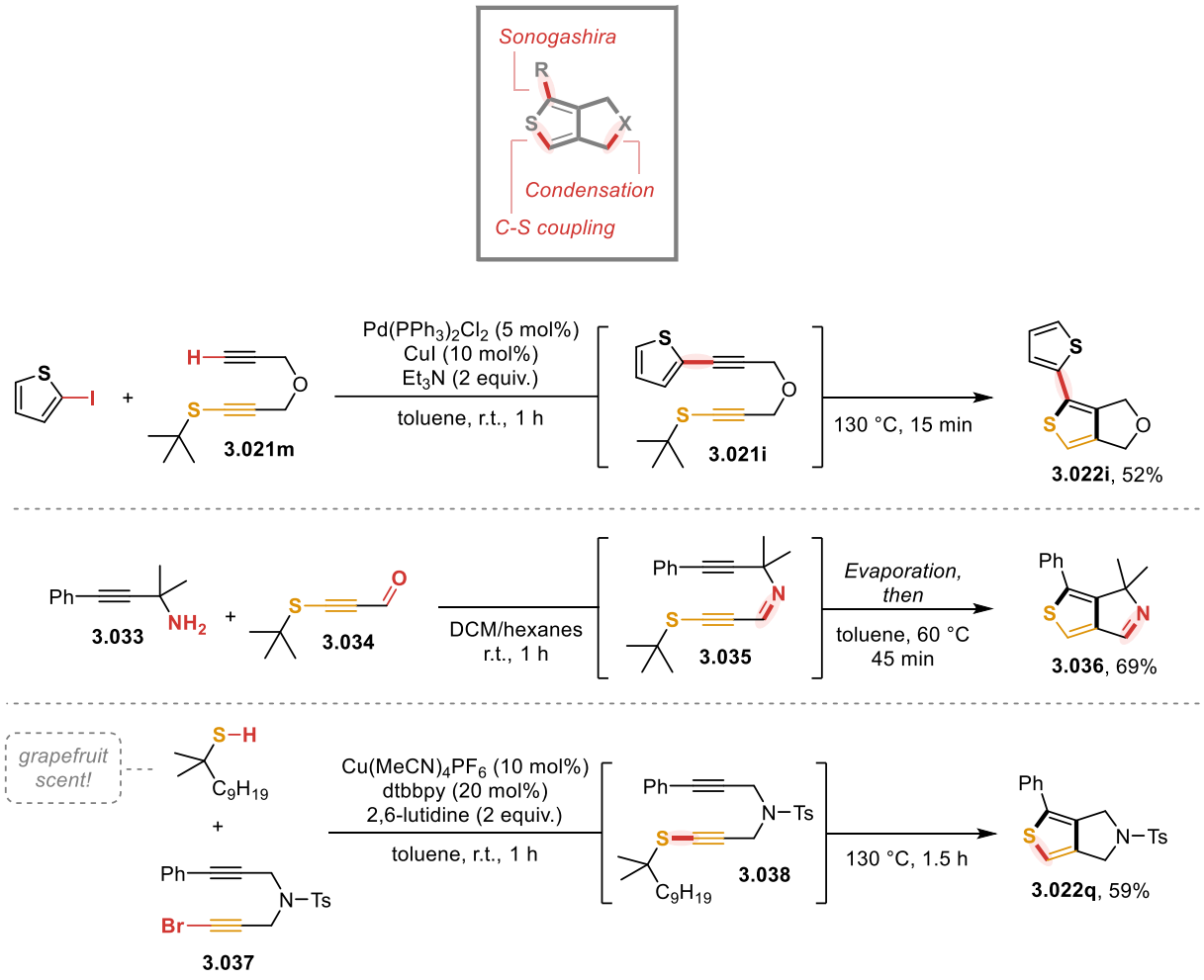

Figure 3-16. Telescoped procedures involving the (3+2) cyclization of yne-alkynyl sulfide scaffolds. *Results in this figure obtained by Alice Pommainville.*

Polythiophenes are an important class of conjugated structures capable of efficient charge transport, and have diverse applications in material science.[10] The synthetic accessibility of a broad scope of yne-tethered alkynyl sulfides and their efficient cyclization into thiophenes makes them great precursors for oligothiophene building blocks. For instance, two terminal yne-alkynyl sulfides units of **3.021m** were easily coupled via Sonogashira reaction to afford oligothiophene precursor

3.039 (Figure 3-17). This precursor smoothly underwent a (3+2) cyclization generating the symmetrical tris-thiophene unit **3.040** in 83% yield. Since the elimination of the *tert*-butyl groups led to the formation of 2,3,4-trisubstituted thiophenes, the C(5) position is free to be brominated afterward, affording building block **3.041**. The findings that the thiophenium ylide intermediate can be trapped by various electrophiles (see Tables 3-5 and 3-6), particularly with tributyltin chloride, can be exploited for the synthesis of oligothiophene building blocks containing contrasting synthetic handles. Precursor **3.042** can be readily synthesized from a sequence of Sonogashira coupling, propargylation and thiolation reactions. Using the previously optimized reaction conditions (see Table 3-4), cyclization of **3.042** in the presence of tributyltin chloride allows for regioselective stannylation upon cyclization yielding the asymmetrical bis-thiophene **3.043** in 58% yield. Exploiting the nucleophilic reactivity of the intermediate ylide allows to access a bis-thiophene containing both bromine and tin as two synthetically useful handles for subsequent functionalization or polymerization.

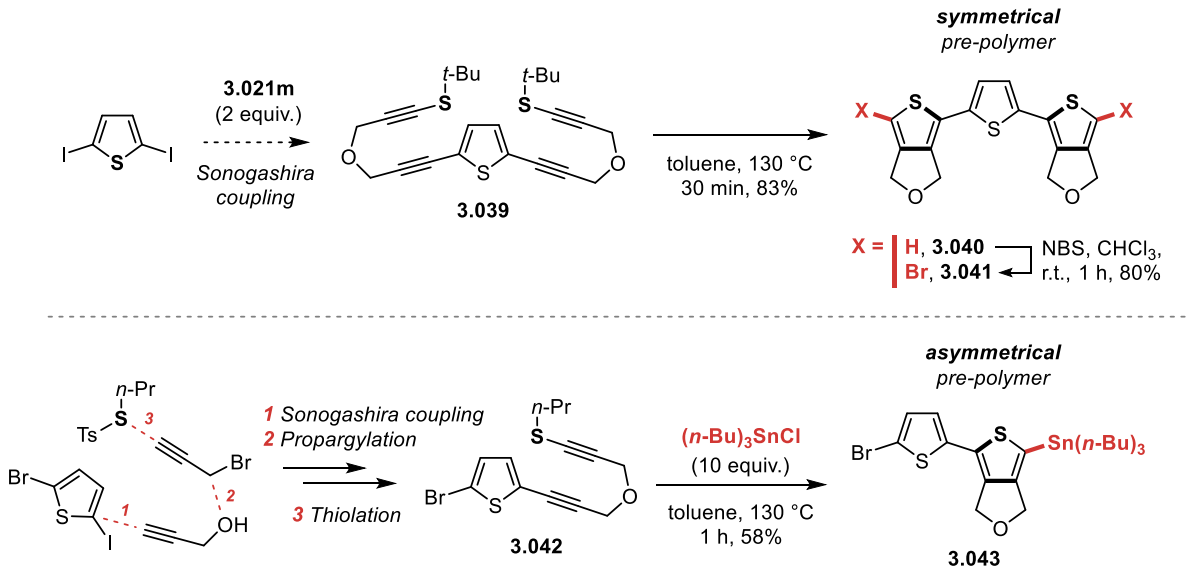

Figure 3-17. Synthetic sequences towards polythiophene building blocks. *Results in this figure obtained by Alice Pommainville.*

Further application of this method involves the core transformation of the obtained fused thiophenes by exploiting the diene character of their oxidized counterpart, thiophene *S,S*-dioxides (Figure 3-18). These are known to undergo Diels-Alder reactions generating substituted benzenes upon extrusion of SO_2.[11-12] Oxidation of model product **3.022a** was achieved using mCPBA and sodium bicarbonate yielding thiophene *S,S*-dioxide **3.044** in 41% yield. Thermally induced (4+2)

cycloaddition of **3.044** in the presence of dimethyl acetylenedicarboxylate or 1,4-naphthoquinone as dienophiles afforded the corresponding penta-substituted benzene derivatives **3.045** and **3.046** in non-optimized 22% and 34% yields, respectively.

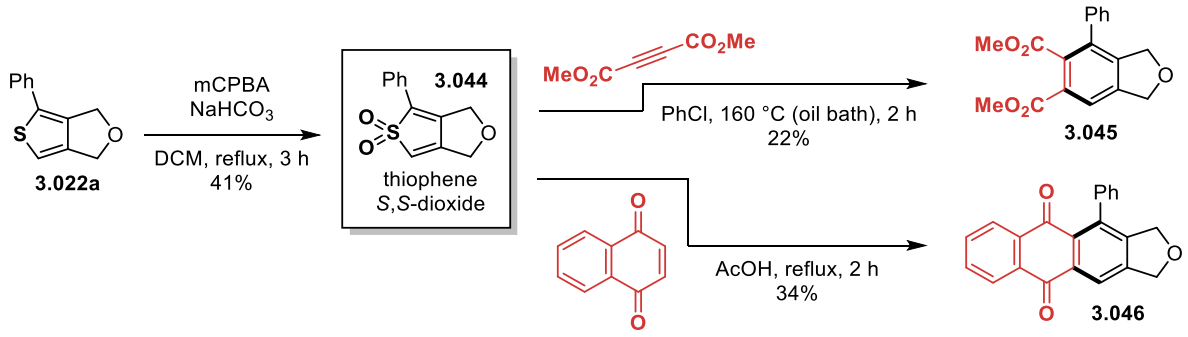

Figure 3-18. Core transformations of the model fused thiophene.

The yne-alkynyl sulfide (3+2) / oxidation / (4+2) sequence provided above (not optimized) serves as a stepwise transition metal-free alternative to a (2+2+2) trimerization. It is however necessary to contextualize this comparison. The diyne **3.023** is a synthetic precursor within our work to the fused thiophene **3.022a**, yet it can be directly subjected to (2+2+2) chemistry with DMAD to provide the fused benzene **3.045** (Figure 3-19). In our hands, using the procedure by Tanaka and coworkers,[13] this provided a 28% isolated yield of **3.045**.

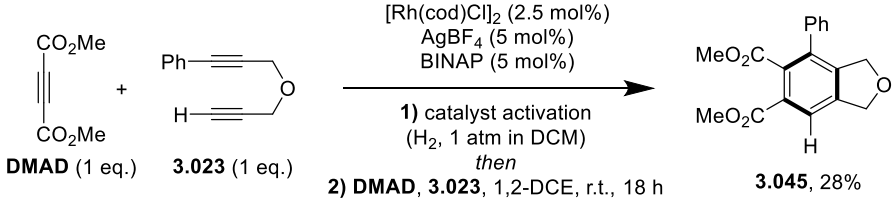

Figure 3-19. Synthesis of **3.045** via a direct (2+2+2) trimerization reaction.

Although arguments based on green chemistry principles could be made on the benefits of avoiding the use of rhodium, these preliminary results do suggest that the direct (2+2+2) route is, at the moment, more efficient, especially when taking in consideration the number of operations involved.

3.8. Refinement of the reaction model with experimental and computational studies

With the consistent obtention of thiophenes when heating these yne-alkynyl sulfide substrates **3.047**, a common endocyclic thiophenium ylide intermediate **3.048** resulting from a (3+2) cycloaddition seemed the most plausible mechanism (Figure 3-20).

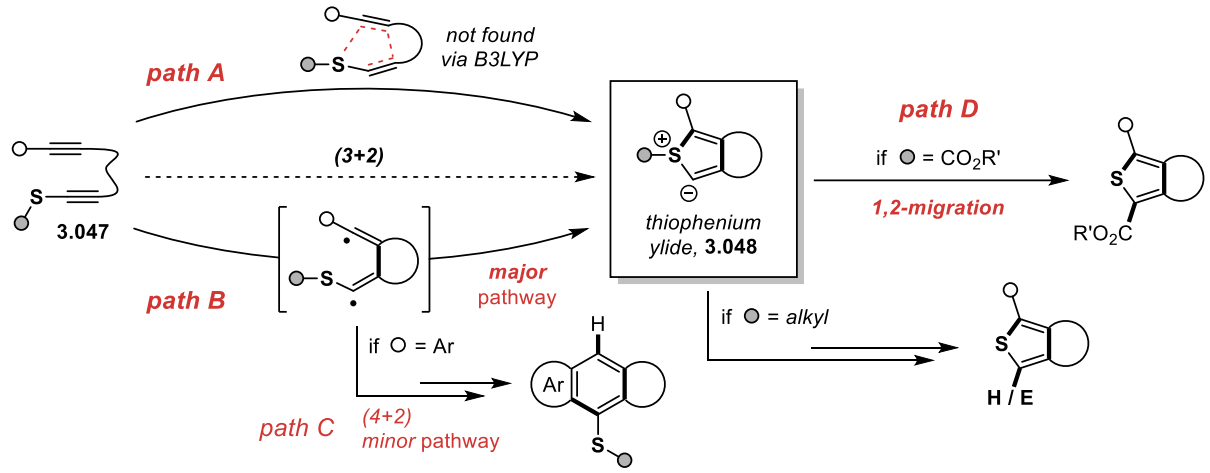

Figure 3-20. Proposed mechanistic outcomes depending on substrate structure.

Although this fleeting species could never be directly observed, two case studies in density functional theory (DFT) calculations (performed at the B3LYP/6-31+G(d) level of theory) confirmed this type of thiophenium ylide is a viable intermediate, with energies of 6.3 kcal/mol (**3.053**, R=*t*-Bu) and 11.4 kcal/mol (**3.053**, R=CO_2Me)(Figure 3-21). The (3+2) cycloaddition leading to the thiophenium ylide intermediate may occur via either a concerted (Path A) or stepwise diradical (Path B) mechanism. Using the B3LYP functional, no stable closed shell transition state for a concerted (3+2) cycloaddition could be located for either case studies. This is in very close agreement with the computational results previously obtained with yne-ynamide scaffold (See section 2.8). A stepwise diradical pathway could however be easily located in both cases, with rate-limiting steps of 24.9 kcal/mol (**3.050**, R=*t*-Bu) and 25.6 kcal/mol (**3.050**, R=CO_2Me).

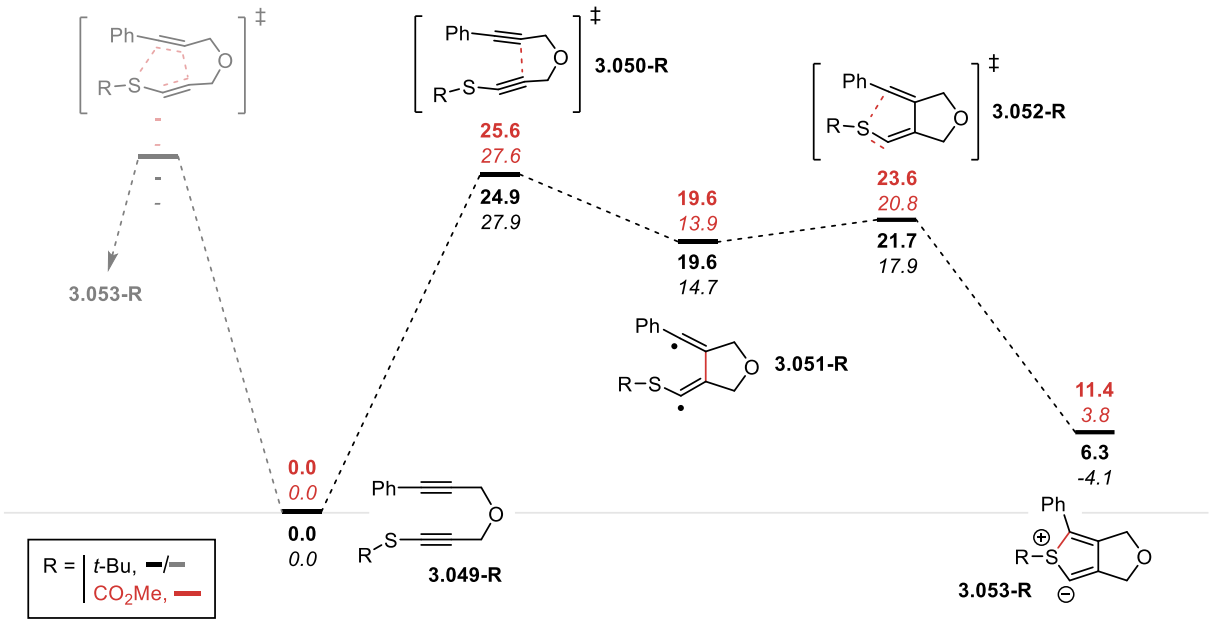

Figure 3-21. DFT studies on the (3+2) cycloaddition step. All stationary points obtained via optimization of the structure at the gas phase using the B3LYP/6-31+G(d) level of theory. Values in bold: Relative Gibbs free energy at the B3LYP/6-31+G(d) level of theory. Values in italics: Relative electronic energy at the B2PLYPD/aug-cc-pVDZ level of theory. The unrestricted functionals were employed for the open-shell surface involving stationary points **3.050**, **3.051** and **3.052**.

Interestingly, the diradical species **3.051** involved in the stepwise (3+2) pathway is in common with the diradical mechanism proposed for the tetradehydro Diels-Alder (TDDA) reaction (Path C).[14] It is worthy to note that very minor amounts of TDDA products were observed in the resulting reaction crudes involving substrates **3.021i** and **3.021y** (Figure 3-22).

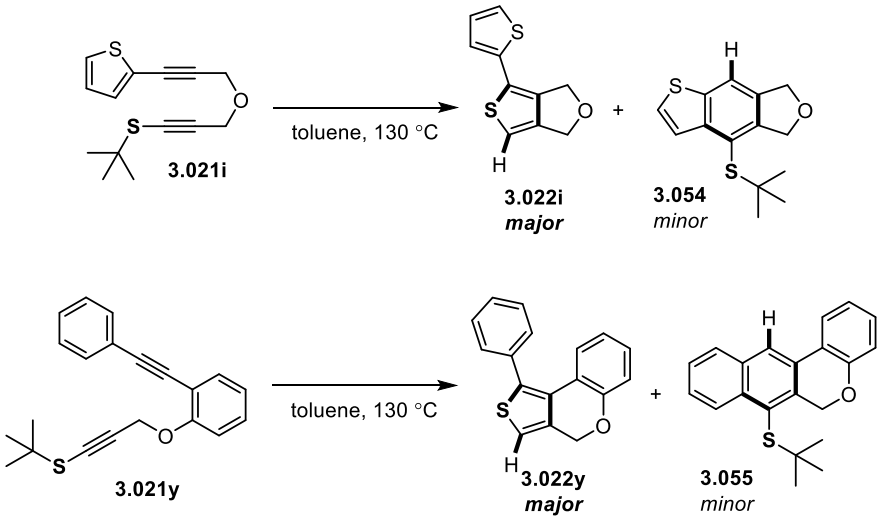

Figure 3-22. Observation of minor TDDA by-products in select cases.

It is not understood yet why a more significant amount of TDDA by-products were observed for these two specific substrates. However, the barrier diverging from the (3+2) mechanism towards a TDDA outcome is quite high at 33.3 kcal/mol for the *tert*-butyl case study (Figure 3-23), which is consistent with the (3+2) cyclization process being exclusively observed for the majority of substrates studied.

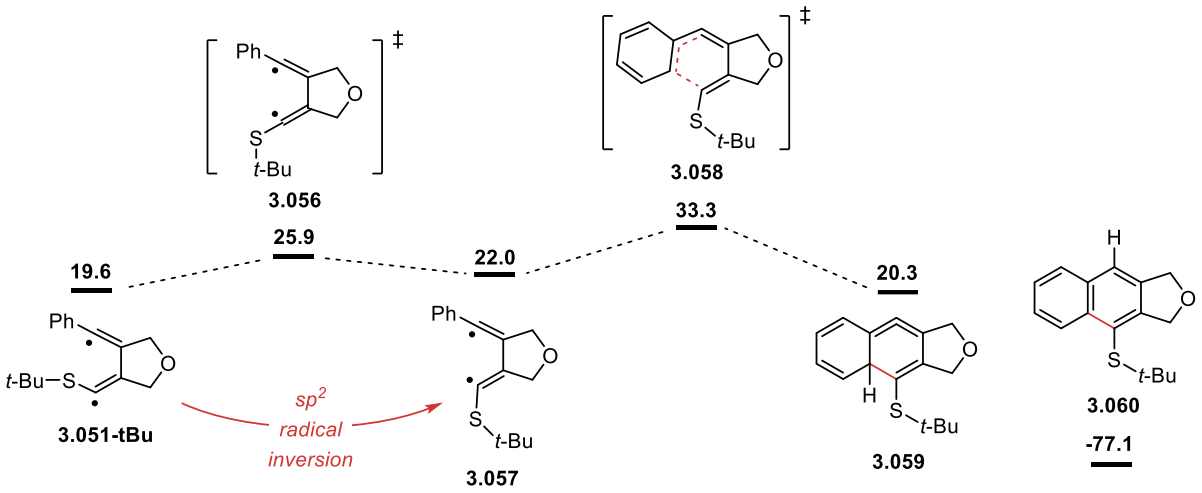

Figure 3-23. Potential energy surface diverting from diradical intermediate **3.051-tBu** towards a (4+2) process. All stationary points obtained via optimization of the structure at the gas phase using the B3LYP/6-31+G(d) level of theory. Values in bold: Relative Gibbs free energy at the B3LYP/6-31+G(d) level of theory. The unrestricted functionals were employed for the open-shell surface involving stationary points **3.056**, **3.057** and **3.058**.

When the alkyne terminus is methyl-substituted, scanning the key C-C bond forming step using both *restricted* and *unrestricted* calculations led to the same closed shell transition state **3.062** (Figure 3-24). IRC calculations from **3.062** with either B3LYP or UB3LYP show slightly different "routes" downhill to the zwitterionic intermediate **3.063**, with UB3LYP displaying a steeper descent to a diradical species before resolving to the same closed shell zwitterion. In this case, the *E*,*Z*-diradical species is <u>not</u> a discrete intermediate, and proceeds with C-S bond formation without any energetic barrier.

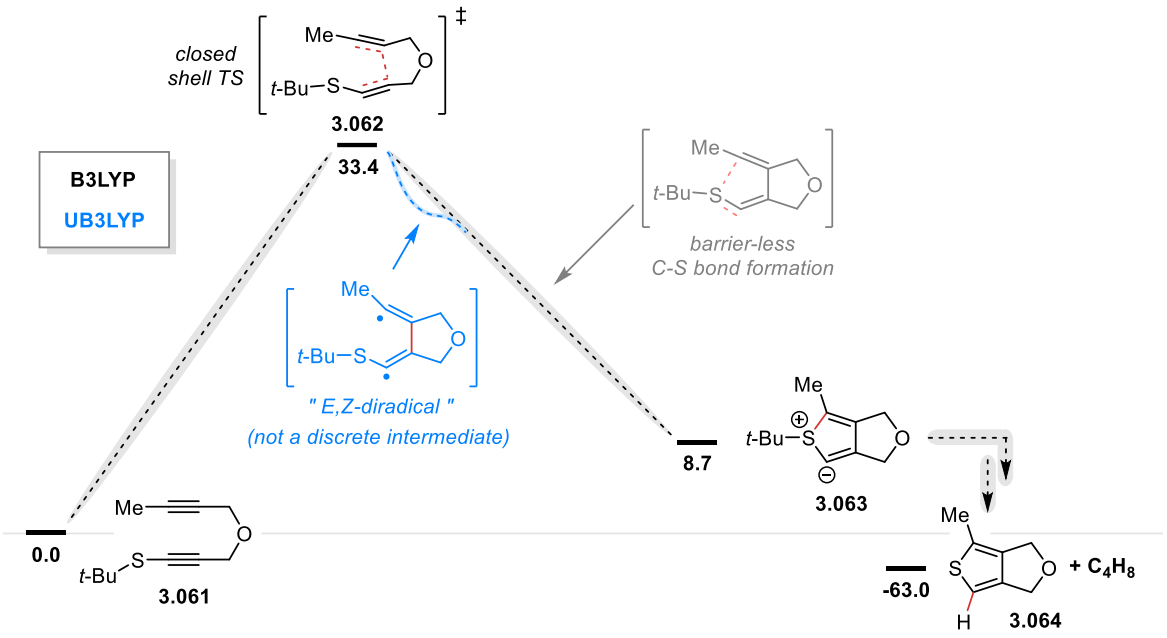

Figure 3-24. Potential energy surface data for the alkyl-substituted alkyne terminus. Gibbs free energies reported. All structures optimized and evaluated at the (U)B3LYP/6-31+G(d) level of theory. When using *unrestricted* UB3LYP, the "guess=(mix,always)" input was included in the calculation to allow for singlet diradicals.

This subtlety can be qualitatively observed upon further analysis of this IRC calculation (Figure 3-25). A slight shouldering in the total energy can be observed post-transition state in the *unrestricted* calculation, showing a slight deviation of the pathway before coming back on the same "path" as the restricted calculation. Matching this deviation, the gradient norm values obtained from these coordinates show a curious "dip" in the *unrestricted* calculation that is not observed in the *restricted* calculation. These "dips" that never quite reach a gradient norm of zero are sometimes called "hidden intermediates".[15] Interestingly, the coordinates involved in this "dip" demonstrate non-zero $\hat{S}^2$ values[2], which indicates spin contamination from higher-order spins states; this is typically observed in calculations involving singlet diradical species.[16]

[2] The $\hat{S}$ operator represents the total angular spin of the species, which should be zero for a singlet system.

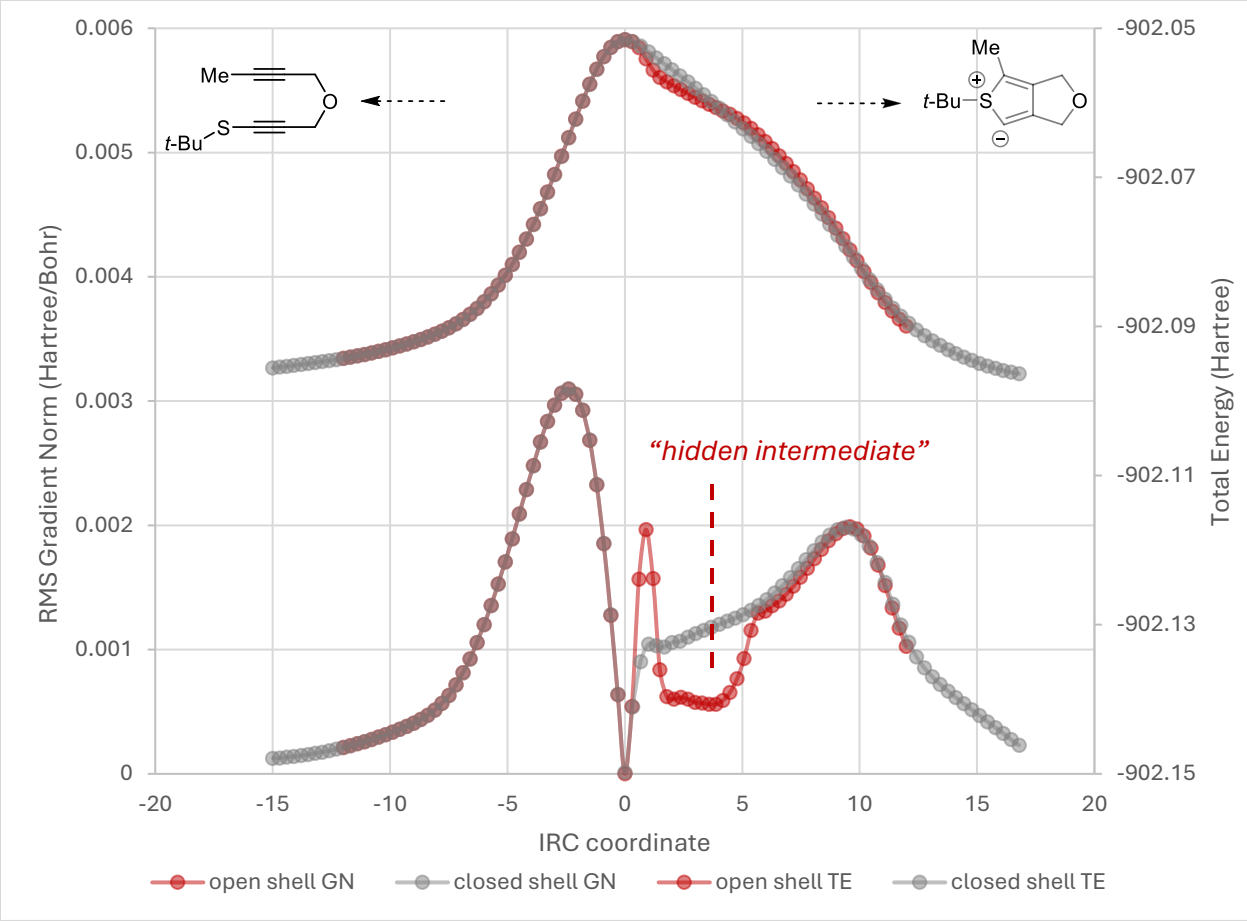

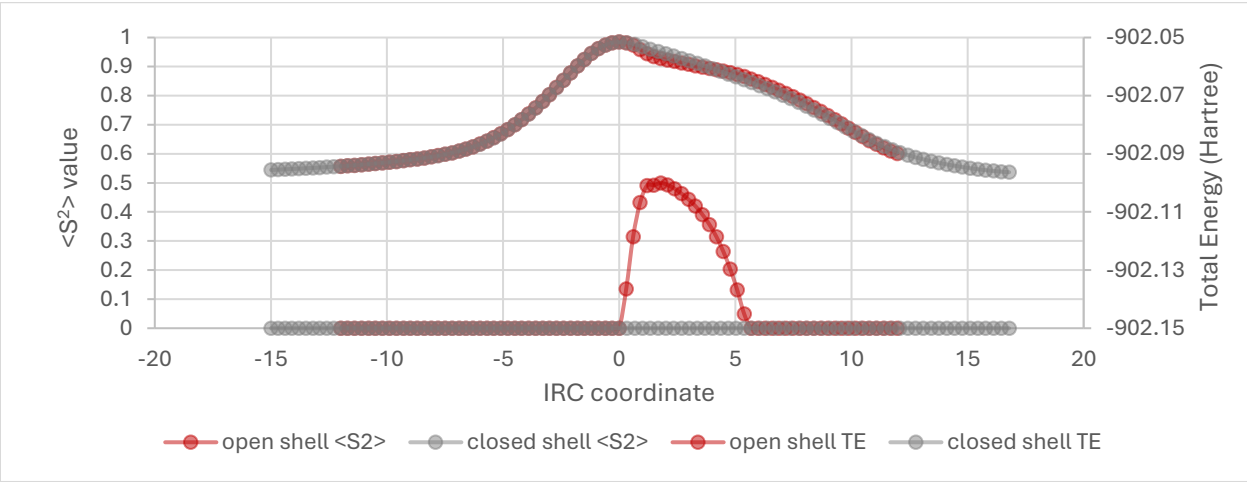

Figure 3-25. Potential energy surface around the transition state 3.062 using either *restricted* or *unrestricted* IRC calculations. [17] IRC calculations were performed using either *restricted* or *unrestricted* B3LYP/6-31+G(d) level of theory. When using unrestricted UB3LYP, the "guess=(mix,always)" input was included in the calculation to allow for singlet diradicals. IRC

coordinate values post-transition state are uniformly scaled (multiplied by a constant) for optimal overlap of the "tail end" of the IRC.

Although discrete diradical minima were not necessarily obtained in all cases, the PES obtained for both the phenyl and methyl-substituted models seem to indicate that there is a significant diradical character in the pathway leading from yne-alkynyl sulfides to thiophenium ylide cycloadducts.

The located rate-limiting TS of 33.4 kcal/mol for the methyl-substituted alkyne is significantly higher than that of the phenyl-substituted alkyne (24.9 kcal/mol), which correlates with the observed slower reaction rate for alkyl substitution at the alkyne terminus.

From the common endocyclic thiophenium ylide, the 1,2-migration outcome (Path D) is theoretically possible for both *S*-alkyl and *S*-ester species. DFT studies show, however, that the barriers for this step, 17.2 kcal/mol (**3.065**, R=CO_2Me) and 27.3 kcal/mol (**3.065**, R=*t*-Bu), largely varies (Figure 3-26). The barrier for the 1,2-migration step being so high for the *S*-alkyl species, this may explain divergence of outcomes from the thiophenium ylide depending on substrate substitution.

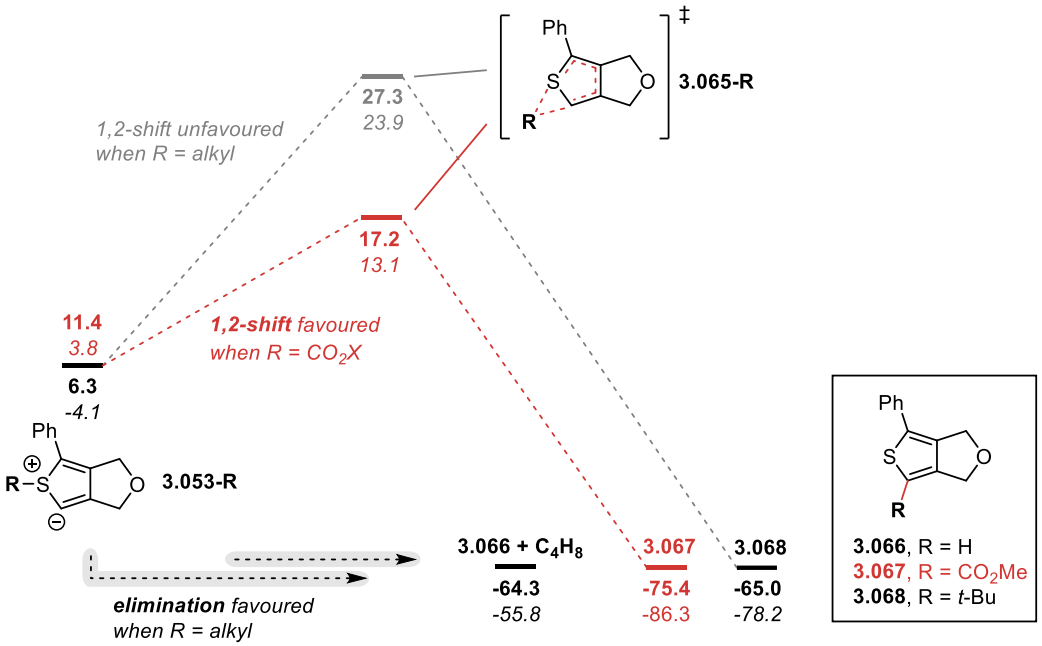

Figure 3-26. DFT studies on the 1,2-migration step. All stationary points obtained via optimization of the structure at the gas phase using the B3LYP/6-31+G(d) level of theory. Values in bold: Relative Gibbs free energy at the B3LYP/6-31+G(d) level of theory. Values in italics: Relative electronic energy at the B2PLYPD/aug-cc-pVDZ level of theory.

While electrophiles can clearly be trapped by the intermediate ylide when present in the reaction medium (Figure 3-27, Path E), it may be what follows protonation of the ylide (Figure 3-27, Path F) which dictates the efficiency of production of the observed thiophene.

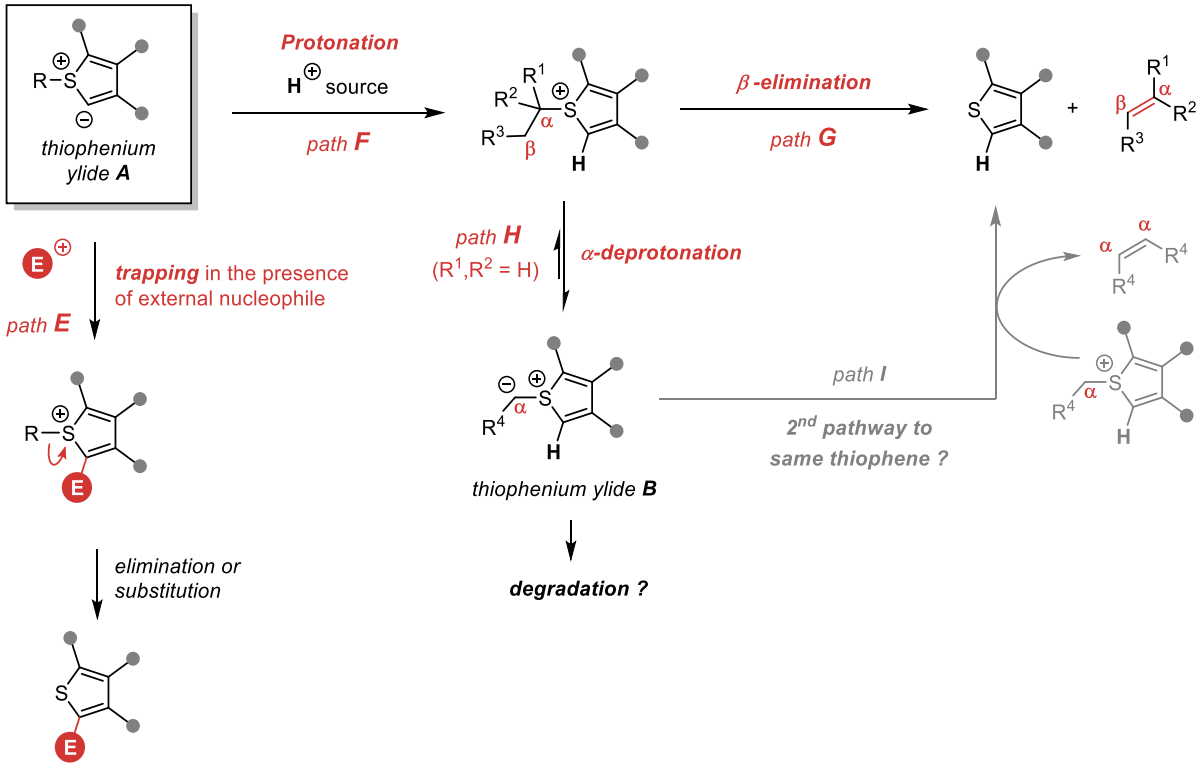

Figure 3-27. Proposed mechanistic outcomes for *S*-alkyl thiophenium ylides.

Despite our effort, no concerted protonation-elimination transition state could be located that would directly link intermediate **3.053** (R=*t*-Bu) to the observed thiophene product **3.066** and isobutene. Although an alternate pathway making use of a reactive thioketene could be theorized, as *tert*-butyl alkynyl sulfides have previously been proposed to fragment to these and isobutene,[17] this is highly unlikely when taking in account the high dependence of reaction rates and yields to the nature of the alkyne and its tether to the alkynyl sulfide. In order to better understand the outcome of *S*-alkyl thiophenium ylides, we consequently shifted our efforts to experimental studies.

First, deuteration studies were performed with *tert*-butyl and *n*-propyl alkynyl sulfides **3.021e** and **3.021a** and in the presence of several deuterated additives (AcOH-d_4, MeOH-d_4 and MeCN-d_3) (Figure 3-28). For both **3.021e** and **3.021a**, the percentage of deuteration observed at position C(5) of the thiophene product **3.022a** is consistent with the acidity of the various additives. It is also in agreement with the amount of external deuterium source employed, substrate **3.021a** leading up to

96% deuteration of the resulting thiophene when MeOH-d_4 was used as a co-solvent. These observations are in line with the intermediacy of an endocyclic thiophenium ylide, which is both nucleophilic and basic at the 5-position of the thiophene.

A control study on the thiophene product (Figure 3-28) also indicates that the deuteration occurs along the reaction pathway, and not in the product.

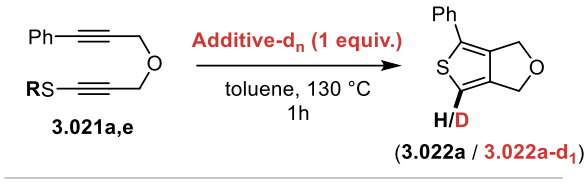

	% Yield (% D)		
R	AcOH-d_4	MeOH-d_4	MeCN-d_3
t-Bu	79 (51)	75 (37)	75 (<5)
n-Pr	85 (79)	35 (23) co-solv: 29 (96)	38 (<5)

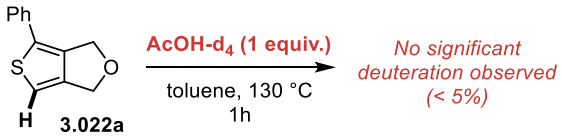

Figure 3-28. Deuteration studies on the (3+2) cyclization of S-alkyl substituted yne-alkynyl sulfides.

Interestingly, the presence of AcOH-d_4 in the case of the *n*-propyl alkynyl sulfide **3.021a** greatly increased the yield of observed thiophene product from ~40% all the way to 85%. Since the (3+2) process occurs *independently* from the presence of AcOH-d_4 additive, this result seems to indicate that the intermediate derived from the *n*-propyl alkynyl sulfide **3.021a** is rather inefficient in producing the desired thiophene, but rendered efficient when protonated.

Along with a weaker C-S bond, the *tert*-butyl-substituted thiophenium ylide differs from the *n*-propyl by the *absence* of α-hydrogens, and so the former only proceeds via an elimination mechanism (Figure 3-27, Path G). In the *n*-propyl case, proton transfer may occur to provide a more stable exocyclic thiophenium ylide (Path H), which may lead to secondary degradation pathways. To test this idea, a probe **3.021ac** was designed where the hypothesized stabilized exocyclic thiophenium ylide **3.071** (Figure 3-29) has been previously shown to undergo ring expansion via a [1,2] alkenyl shift to produce 2*H*-thiopyrans of type **3.070**.[18-20] Indeed, upon heating of the probe with either MeOH or no additive, 2*H*-thiopyran **3.070** was observed as the major product of the reaction. In line with the effect of AcOH-d_4 observed in the study previously described (see Figure 3-28), when the probe **3.021ac** was heated in the presence of a stoichiometric amount of AcOH, only the thiophene **3.022a** was observed, along with a stoichiometric amount of acetate substitution by-product **3.069**. This

interesting set of observations shows yet another controllable outcome of the (3+2) cycloaddition of yne-alkynyl sulfides dictated by both substrate substitution and reaction conditions.

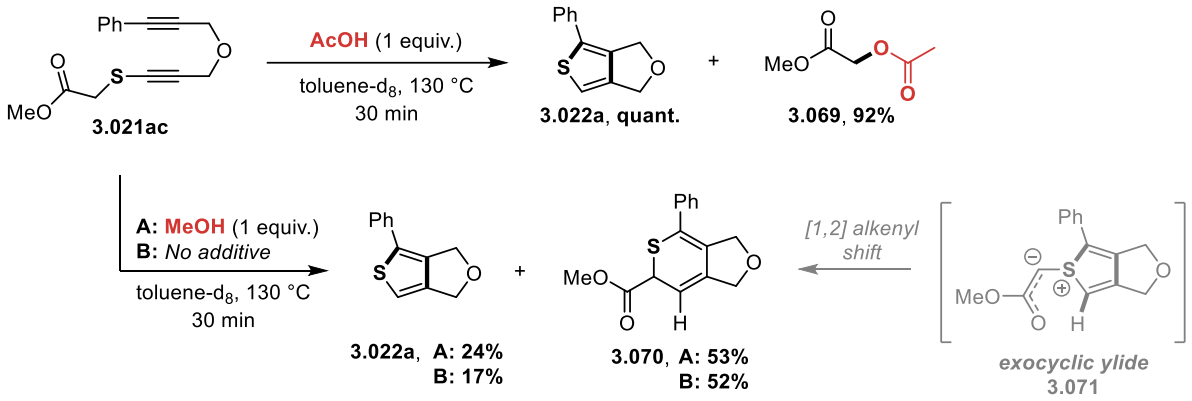

Figure 3-29. Support for the possible intermediacy of an exocyclic thiophenium ylide.

It is important to note, however, that the observation of a significant amount of thiophene **3.022a** upon heating **3.021ac** when no additive was present indicates that elimination of a β-hydrogen is not the only pathway leading to thiophene **3.022a**. The same can be concluded from substrates **3.021b** and **3.021f** (see Table 3-1), which upon heating, produce large amounts of thiophene **3.022a** along with by-products derived from the "dimerization" of the corresponding alkyl groups used. These observations suggest an alternative pathway to **3.022a**, where a protic-mediated sequence of alkylation-elimination between two ylide intermediates provide two units of thiophene **3.022a** along with a symmetrical alkene by-product (Figure 3-27, Path I).

3.9. Limited overlap of chemistry with gold(I) catalysis

Interestingly, the temperature needed for the (3+2) process can be greatly reduced under specific structural requirements (Figure 3-30). The Anderson group reported in 2021 than (3+2) reactivity of yndiamides can be catalyzed by gold(I),[21] this is further discussed in section 5.1.1. The analogous introduction of an amide-substituent directly attached to the alkynyl sulfide in the case of **3.021ad** permits the (3+2) transformation to be catalyzed with a gold(I) complex at room temperature. This feature is, however, limited to thioynamides, and its application to other substrates was not found successful. When subjecting the *S*-propyl derived yne-alkynyl sulfide **3.021a** to the same gold(I) catalytic conditions, no formation of the thiophene **3.022a** is observed. Rather, the diene product **3.073** is observed as the major product. The capability of gold(I) salts to catalyze the reaction of ynamides species via keteniminium species, such as **3.072**, is well documented.[22] This intermediate

3.072 is well-placed to promote a (3+2) cyclization event. Simpler yne-phenyl acetylene scaffolds have previously shown to lead to similar diene products under gold(I) catalysis.[23] These precedents may explain the divergence in chemistry observed here.

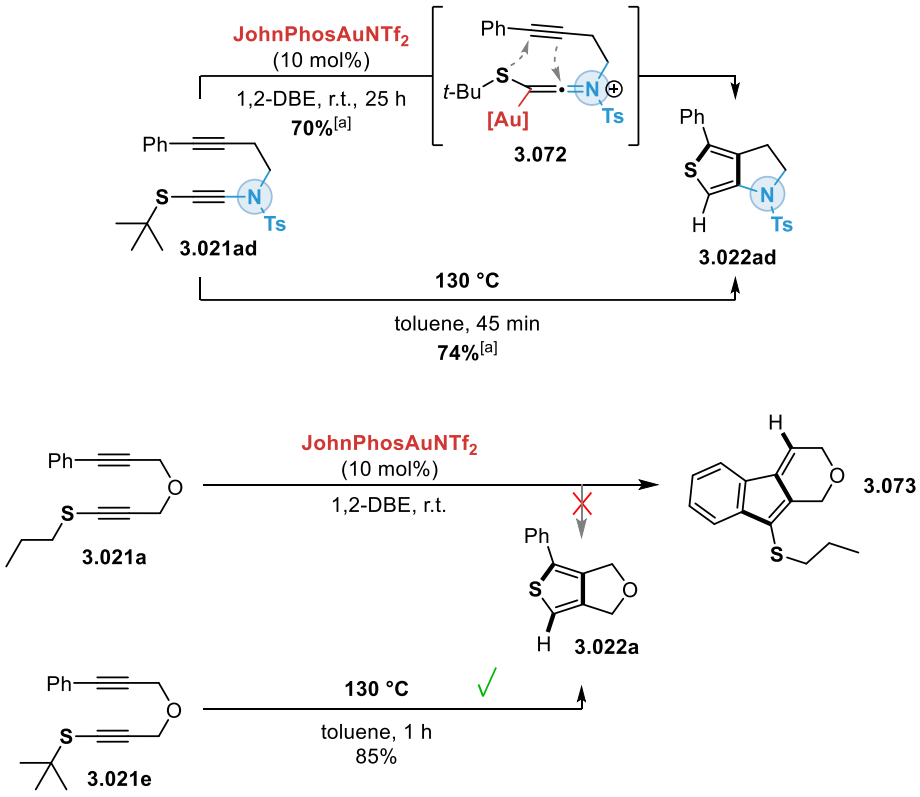

Figure 3-30. Exclusive application of gold(I) catalysis to the case of amido-alkynyl sulfides. [a] Thermal and catalyzed transformations from **3.021ad** to **3.022ad** were performed by Alice Pommainville.

3.10. Conclusion

To summarize, the concept of *neutral* TACs in (3+2) cycloadditions has been successfully applied to the formation of polyfunctionalized thiophenes from easily accessible alkyl and acyl alkynyl sulfides tethered with alkynes. Gratifyingly, alkynyl sulfides were used as representative heteroatom-substituted alkynes to study the outcome of diverse heteroarylium ylide (3+2) cycloadducts stemming from X-alkynyl species. It was found that acyl derivatives lead to 2-acylthiophenes via a 1,2-migration step, and alkyl derivatives lead to trisubstituted thiophenes mainly via a β-elimination mechanism.

The scope of alkynes that may participate as two-atom partners in this (3+2) cycloaddition is quite diverse. Essentially, all variations on the alkyne leading to an isolable yne-alkynyl sulfide substrate were tolerated in the (3+2) process. The scope of linkers capable of promoting the transformation was also quite varied, the best results obtained with 3-atom linkers. The effect of larger linkers on reaction rate could be generally alleviated by increasing the temperature, allowing for the use of 4-atom linkers in this transformation. The simplicity in required conditions (only heating!) for this reliable cyclization method renders it easy to be used in conjunction with multiple other reactions to rapidly build molecular diversity. Finally, *S*-alkyl thiophenium ylide intermediates were successfully intercepted using a wide range of electrophiles, providing a series of uniquely functionalized tetrasubstituted fused thiophenes, and thus highlighting their synthetic potential for the generation of molecular diversity.

The thiophenium ylide intermediates proposed in this chapter may also serve to explain previous curious observations from alkynyl sulfide chemistry. As briefly introduced in Section 1.3.2.1, Markovsky and coworkers reported in 1998 the thermal dimerization of fluoroalkylated alkynyl sulfides **3.074** to form thiophene derivatives **3.079** and **3.081** depending on reaction conditions (Figure 3-31).[3] The authors proposed a heterolytic pathway going through the thiolate anion **3.075**. In light of the results within this chapter, an alternative path involving a (3+2) cycloaddition and the intermediacy of a thiophenium ylide **3.078** can also be envisaged.

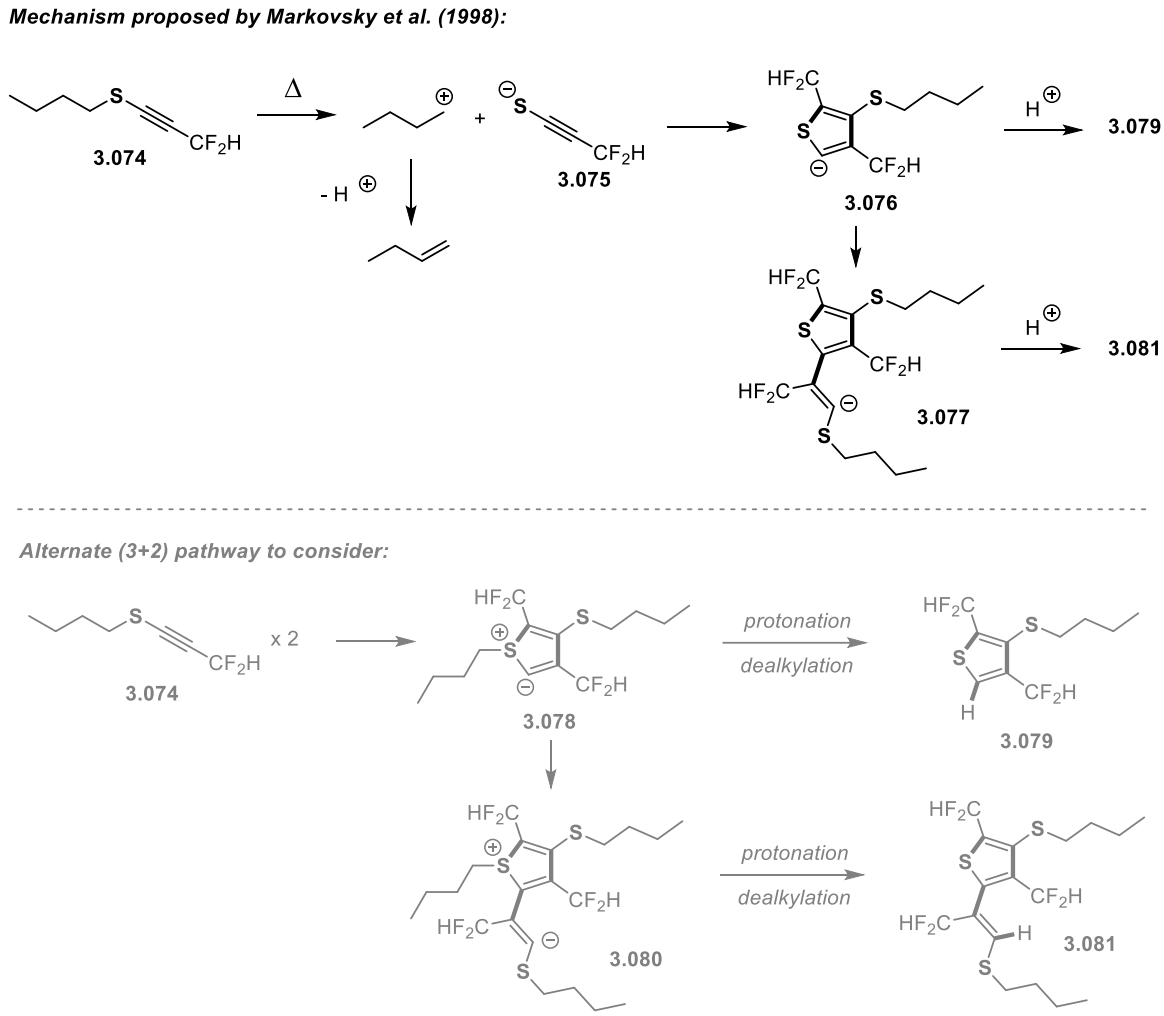

Figure 3-31. Original and alternate mechanisms explaining Markovsky and coworkers' results.

The work in this chapter demonstrates that endocyclic heteroarylium ylides are tangible species that can be taken advantage of to obtain specific heterocyclic structures of interest. The synthetic potential of these underexplored intermediates, which may extend to the realm of redox transformations, has yet to be exploited.

3.11. Chapter references

1. Boonstra, H. J.; Arens, J. F., Chemistry of acetylenic ethers XLII: A simplified method for the preparation of acetylenic thioethers; a number of new reactions of these compounds. *Recl. Trav. Chim. Pays-Bas* **1960,** *79* (8), 866-887.
2. Matsuzawa, T.; Hosoya, T.; Yoshida, S., One-step synthesis of benzo[b]thiophenes by aryne reaction with alkynyl sulfides. *Chem. Sci.* **2020,** *11* (35), 9691-9696.
3. Shermolovich, Y. G.; Timoschenko, V. M.; Musyanovich, R. Y.; Povolotsky, M. I.; Pirozhenko, V. V.; Markovsky, L. N., 1-(alkylthio)-polyfluoroalkynes. Reactions with mercaptans and thermal transformations. *Heteroat. Chem* **1998,** *9* (2), 151-154.
4. Wasserman, H. H.; Fernandez, J. M., Novel reactions of benzyne with acetylenic ethers. *J. Am. Chem. Soc.* **1968,** *90* (19), 5322-5323.
5. Haas, A.; Krächter, H.-U., Darstellung und Reaktionen Trifluormethylchalkogenyl-substituierter Alkine. *Chem. Ber.* **1988,** *121* (10), 1833-1840.
6. Narangoda, C. J.; Lex, T. R.; Moore, M. A.; McMillen, C. D.; Kitaygorodskiy, A.; Jackson, J. E.; Whitehead, D. C., Accessing the Rare Diazacyclobutene Motif. *Org. Lett.* **2018,** *20* (24), 8009-8013.
7. Godin, É.; Santandrea, J.; Caron, A.; Collins, S. K., General Cu-Catalyzed Csp–S Coupling. *Org. Lett.* **2020,** *22* (15), 5905-5909.
8. Pommainville, A. Avenues Towards Fused Pyrroles and Thiophenes by Exploiting the Reactivity of Heteroarylium Cycloadducts. MSc Thesis, University of Ottawa, Ottawa, 2023.
9. Wessig, P.; Müller, G., The Dehydro-Diels–Alder Reaction. *Chem. Rev.* **2008,** *108* (6), 2051-2063.
10. Kaloni, T. P.; Giesbrecht, P. K.; Schreckenbach, G.; Freund, M. S., Polythiophene: From Fundamental Perspectives to Applications. *Chem. Mater.* **2017,** *29* (24), 10248-10283.
11. Bailey, D.; Williams, V. E., An efficient synthesis of substituted anthraquinones and naphthoquinones. *Tetrahedron Lett.* **2004,** *45* (12), 2511-2513.
12. Nakayama, J.; Hasemi, R.; Yoshimura, K.; Sugihara, Y.; Yamaoka, S., Preparation of Congested Thiophenes Carrying Bulky Substituents on the 3- and 4-Positions and Their Conversion to the Benzene Derivatives. *J. Org. Chem.* **1998,** *63* (15), 4912-4924.
13. Tanaka, K.; Sawada, Y.; Aida, Y.; Thammathevo, M.; Tanaka, R.; Sagae, H.; Otake, Y., Rhodium-catalyzed convenient synthesis of functionalized tetrahydronaphthalenes. *Tetrahedron* **2010,** *66* (8), 1563-1569.
14. Rodríguez, D.; Navarro, A.; Castedo, L.; Domínguez, D.; Saá, C., Intramolecular [4 + 2] Cycloaddition Reactions of Diarylacetylenes: Synthesis of Benzo[b]fluorene Derivatives via Cyclic Allenes. *Org. Lett.* **2000,** *2* (11), 1497-1500.
15. Kraka, E.; Cremer, D., Computational Analysis of the Mechanism of Chemical Reactions in Terms of Reaction Phases: Hidden Intermediates and Hidden Transition States. *Acc. Chem. Res.* **2010,** *43* (5), 591-601.
16. Baker, J.; Scheiner, A.; Andzelm, J., Spin contamination in density functional theory. *Chem. Phys. Lett.* **1993,** *216* (3), 380-388.
17. Schaumann, E., The chemistry of thioketens. *Tetrahedron* **1988,** *44* (7), 1827-1871.
18. Bowles, T.; Gillespie, R. J.; Porter, A. E. A.; Rechka, J. A.; Rzepa, H. S., Thermally induced rearrangement of thiopheniobis(alkoxycarbonyl)methanides. *J. Chem. Soc., Perkin Trans. 1* **1988,** (4), 803-807.
19. Storflor, H.; Skramstad, J.; Nordenson, S., Stevens rearrangement of a potentially aromatic thiophenium ylide: formation of 10-methoxycarbonyl-10H-benzo[3,4]cyclopenta[1,2-b]thiopyran-9-one. *J. Chem. Soc., Chem. Commun.* **1984,** (4), 208-209.

20. Tranmer, G. K.; Capretta, A., Intermolecular carbenoid insertions: Reactions of 2-substituted thiophenes with ethyl diazoacetate in the presence of rhodium (II) acetate. *Tetrahedron* **1998,** *54* (51), 15499-15508.
21. Smith, P. J.; Jiang, Y.; Tong, Z.; Pickford, H. D.; Christensen, K. E.; Nugent, J.; Anderson, E. A., Synthesis of Polysubstituted Fused Pyrroles by Gold-Catalyzed Cycloisomerization/1,2-Sulfonyl Migration of Yndiamides. *Org. Lett.* **2021,** *23* (16), 6547-6552.
22. Campeau, D.; León Rayo, D. F.; Mansour, A.; Muratov, K.; Gagosz, F., Gold-Catalyzed Reactions of Specially Activated Alkynes, Allenes, and Alkenes. *Chem. Rev.* **2021,** *121* (14), 8756-8867.
23. Lian, J.-J.; Chien, P.-C.; Lin, Y.-P.; Ting, H.-C.; Liu, R.-S., Gold-Catalyzed Intramolecular [3+2]-Cycloaddition of Arenyne-Yne Functionalities. *J. Am. Chem. Soc.* **2006,** *128* (35), 11372-11373.

4. Chapter 4 – Rate enhancements by coinage metals in the (3+2) reactivity of yne-alkynyl sulfides

Reprinted (adapted) with permission from [Campeau, D.; Pommainville, A.; Gorodnichy, M.; Gagosz, F., Copper and Silver Catalysis in the (3+2) Cycloaddition of Neutral Three-Atom Components with Terminal Alkynes. *J. Am. Chem. Soc.* **2023**, *145* (34), 19018-19029]. Copyright 2023 American Chemical Society.

This report involves results by D. Campeau, A. Pommainville and M. Gorodnichy. Results in this chapter were obtained by D. Campeau unless otherwise noted with "*Results in this figure obtained by …*".

4.1. Catalysis in cycloadditions involving alkynyl sulfides

Scouring the literature for the involvement of alkynyl sulfides in cycloaddition reactions (both thermal or catalyzed) leads to very similar results to that found for ynamides. Research on alkynyl sulfides is generally more sparse than ynamides, and to date, is almost exclusively limited to α,β-based cycloadditions. This reinforces the idea that heteroatom-substituted alkynes traditionally react as simple alkynes.

This idea is reflected in the few instances where alkynyl sulfides have been used as partners in transition metal-catalyzed cycloadditions. For example, Hilt and coworkers demonstrated in 2004 that the (4+2) cycloaddition between alkynyl sulfides **4.002** and dienes **4.001** can be catalyzed by a cobalt complex (Figure 4-1).[1] It is unlikely, however, that ligation to the sulfide moiety is important for this catalysis, as this report is an extension of work previously done on cobalt-catalyzed (4+2) cycloadditions between dienes and simpler alkynes.[2] The authors further mention lower conversions when using alkyl alkynyl sulfides, and requiring higher catalyst loading for alkynyl sulfides than simpler alkynes, attributing it to deleterious complexation to the sulfide moiety.

Hilt et al. (2004):

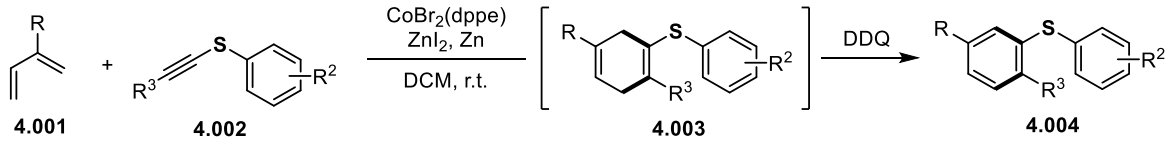

Figure 4-1. The cobalt-catalyzed (4+2) cycloaddition of dienes with alkynyl sulfides.

In 2006, Riddell and Tam reported the ruthenium-catalyzed (2+2) cycloaddition of norbornadiene **4.005** and alkynyl sulfides **4.006** (Figure 4-2).[3] In this case as well ligation of the metal complex to the sulfide moiety is unlikely to be productive towards this chemistry, as the authors observe that alkynyl sulfones proceed in the same chemistry with higher conversion rates, and this chemistry was previously shown to work for simpler alkyne derivatives.[4]

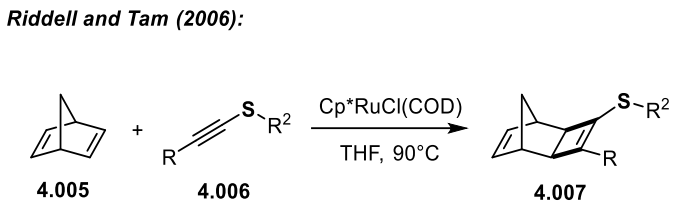

Figure 4-2. The ruthenium-catalyzed (2+2) cycloaddition of norbornadiene with alkynyl sulfides.

There is however a section of cycloaddition reactivity for alkynyl sulfides that makes particular use of the sulfide moiety. In 2014, the group of Jia and Sun demonstrated that the (3+2) cycloaddition between azides **4.008** and alkynyl sulfides **4.009** can be catalyzed by iridium at room temperature (Figure 4-3).[5] This process is completely regioselective when using alkynyl sulfides, yet no catalysis whatsoever is observed with alkynes functionalized only with alkyl or aryl groups. The authors propose that complexation to the sulfide moiety must take place in the catalytic cycle which leads to triazole **4.010**.

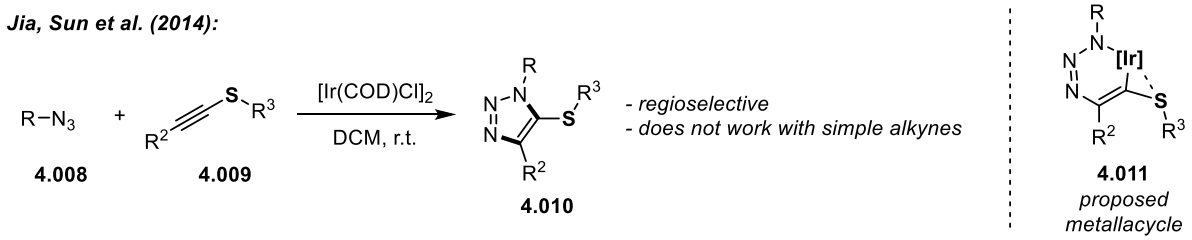

Figure 4-3. Iridium catalysis in the (3+2) cycloaddition between azides and alkynyl sulfides.

Ruthenium[6] and rhodium-catalyzed[7] variants of the same chemistry have since been reported. Despite these few instances, from a general perspective, making use of the complexation capability of the sulfide moiety on alkynyl sulfides in cycloaddition chemistry is not a widespread strategy. It is however likely to be the very thing enabling the chemistry delved in this chapter.

4.2. Failures and surprises while attempting to catalyze neutral (3+2) cycloadditions

While investigating the (3+2) reactivity of the yne-ynamide scaffold, it was noted that terminal alkyne derivative **2.014n** was a particularly sluggish scaffold in this chemistry, providing lower yields and requiring longer reaction times for conversion (see Section 2.5). Hypothesizing that substituting the hydrogen on the terminal alkyne with a copper(I) unit may induce higher (3+2) cyclization rates, the stoichiometric formation of the corresponding copper(I) acetylide was first tested (Figure 4-4). Although large formation of a yellow precipitate indicated the clear formation of the desired copper acetylide, vigorous stirring of the suspensions at room temperature for extended periods of time did not yield any of the desired pyrrole **2.015n**. Worried that the insolubility of the copper acetylide at high concentrations may prevent the desired chemistry from occurring, a few conditions involving catalytic amounts of copper(I) salt and base and mild heating were also tested. Unfortunately, no formation of **2.015n** was observed, providing mostly unreacted starting material.

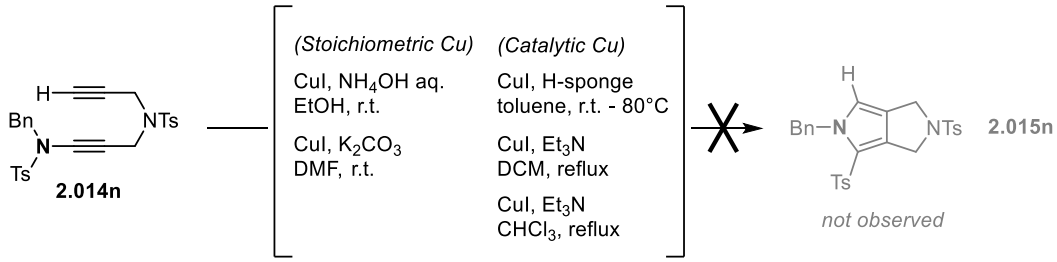

Figure 4-4. No rate enhancements by copper observed for the yne-ynamide scaffold.

With no trace of positive result in catalyzing this (3+2) reactivity through the formation of copper(I) acetylides, this hypothesis was initially put aside.

Later on, in the course of our studies on the thermally promoted (3+2) cycloaddition cascade of yne-alkynyl sulfides, it was observed by Alice Pommainville that the terminal alkyne derivative **4.012a** would produce significant amounts of 3,4-fused thiophene **4.013a** when subjected to conditions promoting a Sonogashira coupling.[8] Further investigations by Mila Gorodnichy unveiled that this cyclization process was catalyzed at room temperature in the presence of a copper salt and a base (Table 4-1) yielding two types of thiophene products having either "lost" or "retained" the R alkyl group initially attached to the S atom (**4.013** or **4.014**, respectively). The same thiophene derivatives could be observed for a few S-(alkyl) substituted substrates (Entries 1-3). A small amount of a dimerized by-product **4.015** was also observed in this set of conditions, this by-product is further discussed in Section 4.8. Notably, while phenyl substitution on the alkyne terminus was previously beneficial to the thermally promoted (3+2) cycloaddition (see Chapter 3), the reverse was observed under catalytic conditions (Entry 4), with substrate **3.021q** remaining unaltered. These observations also

counter the analogous tests previously made on the terminal alkyne-ynamide scaffold **2.014n**, where no catalysis whatsoever had been observed under similar conditions.

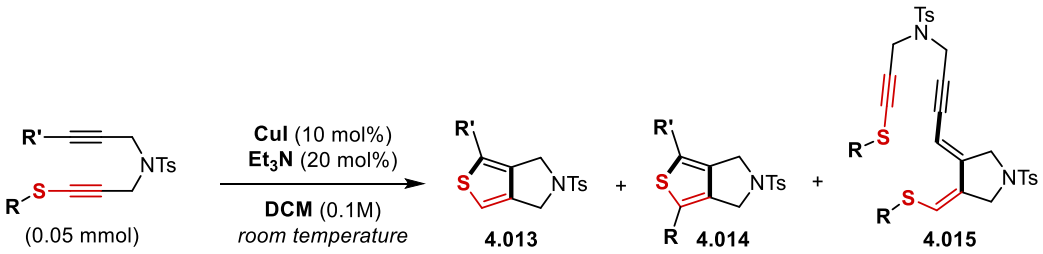

Entry		R	R'	Time	Conv. (%)	Yield (%)	Yield (%)	Yield (%)
1[a]	**4.012a**	*t*-Bu	H	1 h	61 %	22 %	11 %	3 %
2[a]	**4.012b**	Bn	H	1 h	56 %	6 %	4 %	N/A
3[a]	**4.012c**	*n*-Pr	H	1 h	76 %	2 %	0 %	N/A
4	**3.021q**	*t*-Bu	Ph	21 h	0 %	0 %	0 %	0 %

Table 4-1. Initial investigations on yne-alkynyl sulfide substrates. [a] Entries obtained by Mila Gorodnichy and Alice Pommainville.

Two important considerations were drawn from these observations: 1) the need for base in conjunction with a terminal alkyne suggested that the observed catalytic effect likely involved the formation of a copper acetylide; and 2) since sulfides may chelate coinage metals favourably, while amides do not (from the nitrogen atom), chelation from the heteroatom to the metal may play an important role in favouring this reaction pathway (Figure 4-5). These observations are reminiscent of the factors previously established as promoting the azide-alkyne cycloaddition in the CuAAC process (see Section 1.4.1), which may provide clues on the mechanism of the present transformation.

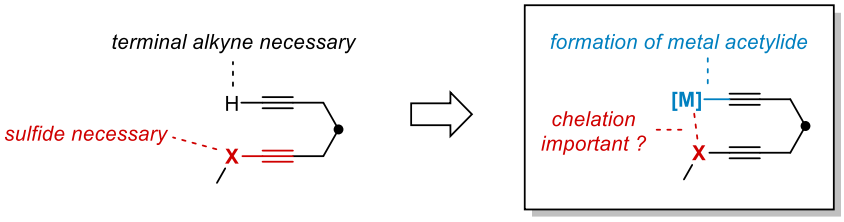

Figure 4-5. Catalytic activity may be explained by a chelating metal acetylide.

Since a drastic reduction in required temperature (from 130 °C to room temperature) was observed, further investigations in this transformation were done, considering that this new set of conditions

could be leveraged to tackle previous limitations observed with the thermal (3+2) cycloaddition process, such as the length of the linker group.

4.3. First evaluation of the reaction parameters and scope of three-atom linkers

The "alkyl migration" event leading to products of type **4.014**, whose formation was not observed under thermal conditions, was found to be strongly dependent on the nature of the alkyl group. The optimization of this process, despite its interest, was not successful to date, and all optimization tests always produced **4.013** in larger amounts. For this reason, focus was put on improving the reaction profile towards the formation of **4.013**. The drastic rate enhancement of this (3+2) process by a copper catalyst was quite reminiscent of the CuAAC process, which has also been shown to proceed via the intermediacy of copper acetylides.[9] On the basis that azide-alkyne couplings have also been successfully catalyzed by other coinage metals,[10] it was considered that the nature of the metal catalyst was a critical factor to be evaluated (Table 4-2, entries 1-4). Along with significant rate enhancements, a great improvement in selectivity towards the desired thiophene **4.013a** was observed when opting for a silver catalyst (entry 2), providing an already excellent set of conditions for this transformation. The reaction could also be promoted by a gold catalyst (entry 3) but was inhibited when the gold species was stabilized by a bulky ligand (entry 4). It is noteworthy that non-strongly ligated gold salts tend to suffer reduction by trialkylamines,[11] which likely explains the poor reaction conversion when Me_2S•AuCl was used as the catalyst. A control experiment showed that only trace amounts of the desired thiophene product were formed in the absence of base (entry 5). However, the use of base as an additive could be avoided by employing a mildly basic acetate counter anion on the metal catalyst (AgOAc, entry 6). The choice of solvent proved to be a crucial element also affecting the rate of the reaction. While exchanging DCM for the protic EtOH increased the selectivity of the reaction towards **4.013a** (entry 7), the use of acetic acid had the largest effect on reaction rate. In this case, a full and selective conversion of the substrate was observed at the first analysis after 5 minutes (entry 8). Wondering if the same effect could be effective under copper catalysis, an analogous set of conditions was developed using copper(I) acetate in acetic acid. An impressive enhancement in reaction rate was similarly observed in this case (entry 9). The rate enhancement effect of acetic acid is further discussed in Section 4.7.

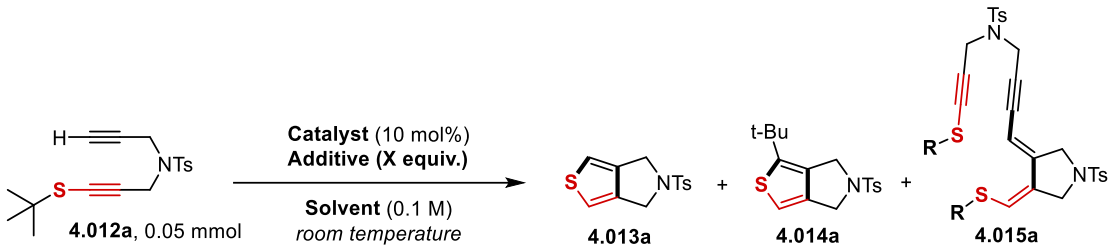

	Entry	Catalyst	Additive (X equiv.)	Solvent	Time	Conv. 4.012a (%)	Yield 4.013a (%)	Yield 4.014a (%)	Yield 4.015a (%)
nature of metal	1	CuI	Et_3N (0.2)	DCM	1 h	61	22	11	3
	2	AgOTf	Et_3N (0.2)	DCM	1 h	>95	>95	2	0
	3	(DMS)AuCl	Et_3N (0.2)	DCM	13 h	47	13	5	0
	4	(IPr)AuNTf$_2$	Et_3N (0.2)	DCM	17 h	11	0	0	0
base	5	AgOTf	-	DCM	1 h	44	1	0	0
	6	AgOAc	-	DCM	4 h	84	61	15	0
solvent	7	AgOAc	-	EtOH	4 h	>95	>95	2	0
	8	AgOAc	-	AcOH	5 min	>95	>95	0	0
Applying the optimized conditions to copper catalysis:									
	9	CuOAc	Na-Asc (1.0)	AcOH	10 min	>95	89	7	3

Table 4-2. Optimization of the catalyzed (3+2) cyclization for model substrate **4.012a**.

The improvement brought by these new sets of conditions is quite striking. What previously yielded poor yields after multiples hours of heating at 130 °C (Table 4-3) can now be achieved quantitatively in minutes at room temperature. These initial results made this catalytic approach promising in terms of functional groups tolerance, and the possibility to limit degradation pathways, all of which could result in a cleaner reaction profile towards the desired 3,4-fused thiophenes **4.013**.

The optimized AgOAc/AcOH system was consequently employed for a series of terminal alkynes and alkynyl sulfides tethered by various 3-atom linkers (Table 4-3). Substrates with tosylamide (**4.012a,d**), carbamate (**4.012e**), ether (**4.012f,g**), and ester (**4.012h**) linkers gave quasi-quantitative yields (>92%) of the desired thiophenes in minutes. Only in the case of the amide linker in **4.012i** was the yield in thiophene slightly lower (81%), a result that may be attributed to the electron-poor nature of this specific alkynyl sulfide. The more complex reaction profile of **4.012i** is further discussed in Section 4.8. In line with the previous uses of a malonate-derived linker in thermal variants of the (3+2) reaction, **4.012j** resulted in a much slower reaction time, but an excellent yield.

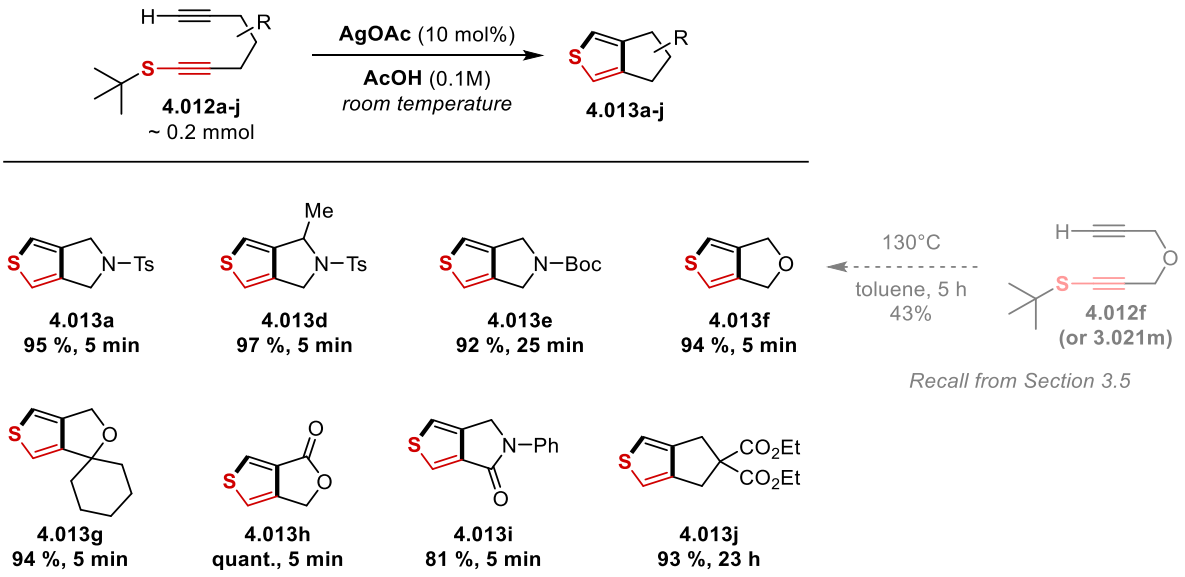

Table 4-3. Scope of the catalyzed (3+2) cyclization for 3-atom linkers. Terminal alkynes are a structural limitation in analogous thermal-promoted (3+2) cycloadditions.

4.4. Applying catalysis to tackle previous limitations with S-(aryl) alkynyl sulfides

While S-(aryl) alkynyl sulfides were not productive partners in the previously studied thermal (3+2) reactions, their behaviour under the new catalytic conditions was still unknown.

Interestingly, Alice Pommainville[8] observed quantitative formation of the thiophenium acetate salt **4.017c-OAc-d$_5$** by NMR analysis when S-(phenyl) alkynyl sulfide derivative **4.016c** was subjected at room temperature to the optimized AgOAc/AcOH catalytic conditions (Figure 4-6). This result seemed to indicate that thiophenium salts are common intermediates in the metal-catalyzed (3+2) of alkynyl sulfides. Heating at 70 °C, the in situ formed thiophenium salt **4.017c-OAc-d$_5$** quantitatively generated the 2-phenyl thiophene **4.018c-d$_1$**.

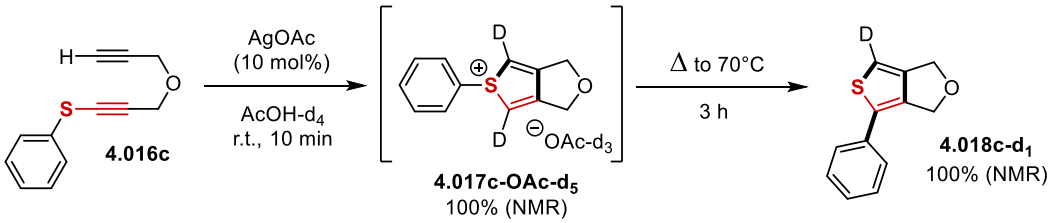

Figure 4-6. Observation of a thiophenium salt intermediate by NMR. *Results in this figure obtained by Alice Pommainville.*

The migratory behaviour of aryl groups in S-aryl benzothiophenium salts **4.019** leading to 2-aryl benzothiophenes **4.020** has been observed in the past by Kitamura and coworkers (Figure 4-7).[12] This

migration was proposed by the authors to proceed through an intramolecular pathway via the intermediate **4.021**.

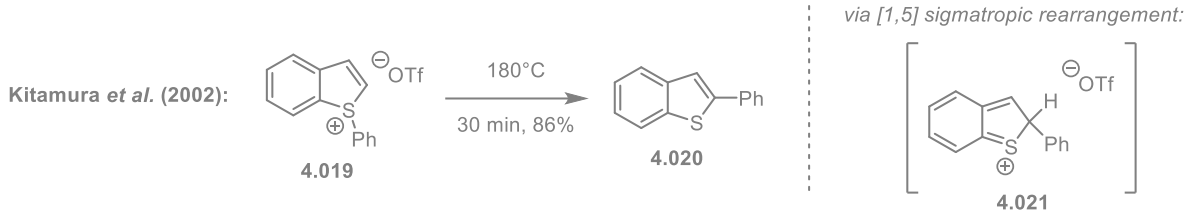

Figure 4-7. Migration of aryl group in S-aryl benzothiophenium salts, as studied by Kitamura *et al*.

The transformation of S-(aryl) thiophenium salts **4.022** to thiophenes **4.024** likely proceeds via a similar 1,5-sigmatropic rearrangement of the aryl group, resulting in its migration from sulfur to the adjacent carbon atom forming **4.023**, with consecutive loss of acetic acid (Figure 4-8). The lower temperature required to observe aryl migration in thiophenium salts is consistent with this mechanism; formation of **4.021** requires breaking the aromaticity in the fused benzo group, the latter lacking in **4.022**.

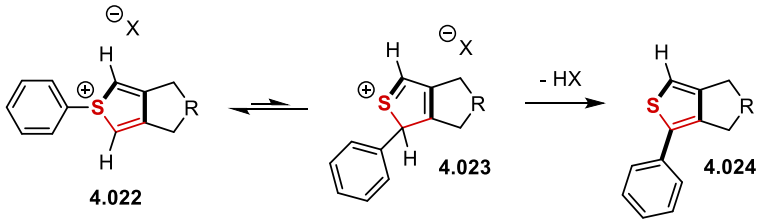

Figure 4-8. Proposed mechanism explaining the 1,2-migration of an aryl group.

While isolating the acetate salt of this thiophenium derivative proved challenging, an alternative procedure to access the triflate salt **4.017c-OTf** was developed by Alice Pommainville (Figure 4-9). Under these new conditions, the salt could be easily obtained with good purity by simple trituration. Crystals of **4.017c-OTf** were then grown and analyzed by SCXRD, confirming the identity of the thiophenium salt. To our knowledge, simple S-(aryl) thiophenium salts such as **4.017c-OTf** have not been previously reported.

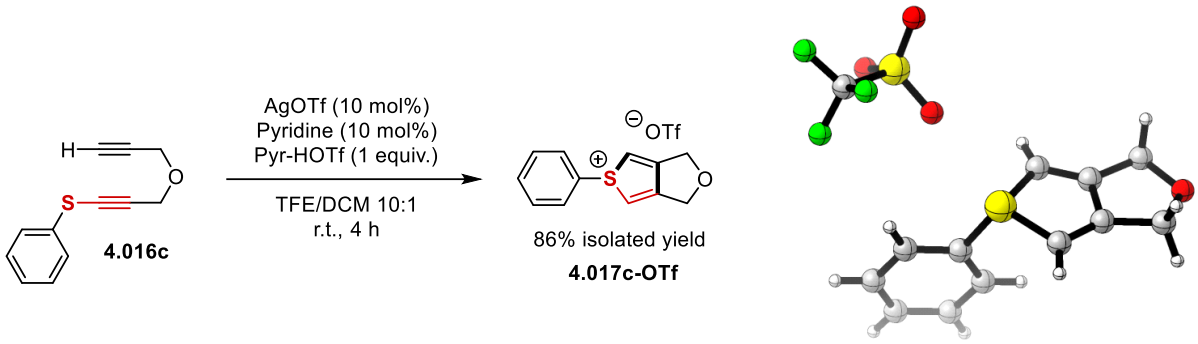

Figure 4-9. Isolation of thiophenium triflate salt and SCXRD structure. See CCDC deposition # 2260026 for acquisition data. *Results in this figure obtained by Alice Pommainville.*

This one-pot metal-catalyzed (3+2) cycloaddition to S-(aryl) thiophenium salts and their rearrangement to the corresponding 2-aryl thiophenes constituted a more efficient and selective pathway to (3+2) cycloaddition products than previously observed under thermal conditions. In fact, the analogous substrate **3.019**, previously mentioned in Section 3.3, had only produced a complex mixture upon heating (Figure 4-10).

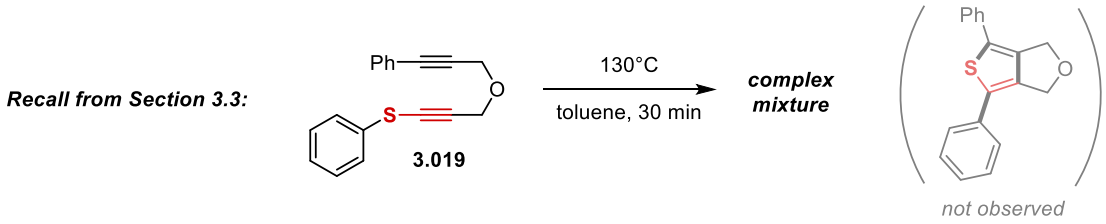

Figure 4-10. Outcome of the thermally promoted (3+2) cycloaddition of yne-alkynyl sulfides.

To address this limitation using these new results, a scope with substrates possessing differently substituted aryl groups was performed by Alice Pommainville and Mila Gorodnichy using this new catalytic cascade (Table 4-4). A range of electron-rich to electron-poor phenyl derivatives were evaluated (**4.016a-g**), all providing excellent yields of 2-aryl substituted fused thiophenes. Even derivative **4.016h** showed good reactivity in generating bis-thiophene **4.018h**, although requiring a long reaction time for completion. In most cases, the catalyzed (3+2) component of the reaction was completed immediately at 70 °C, while the 1,2-migration of the aryl group required several hours of heating.

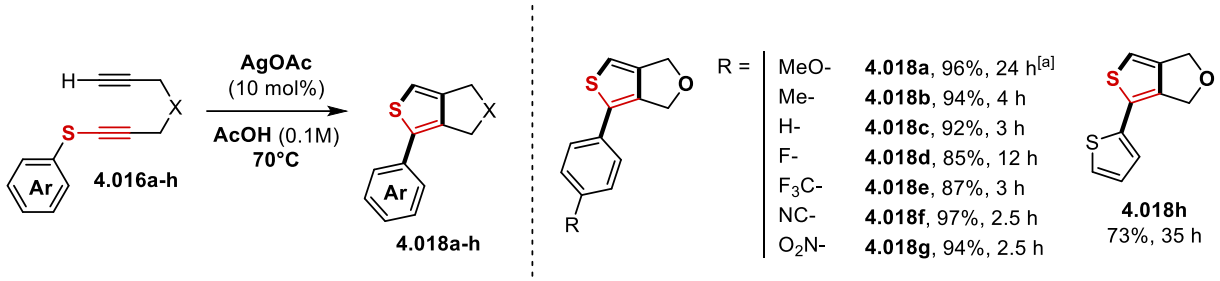

Table 4-4. Scope of the metal-catalyzed (3+2) cyclization involving 1,2-aryl migration. [a] Reaction nearly complete after 6h but left overnight. *Results in this table obtained by Alice Pommainville and Mila Gorodnichy.*

The reactivity of an S-(alkynyl) alkynyl sulfide **4.025** was also evaluated but did not fare well under the AgOAc/AcOH catalytic conditions. The alternative method developed making use of AgOTf/PyrHOTf in TFE/DCM proved to be useful (Figure 4-11). In this case, the alkynyl migration seemed to be quite rapid (no thiophenium intermediate was observed during the reaction) and the 2-alkynyl thiophene **4.026** was directly obtained in a modest but non-optimized 33% yield.

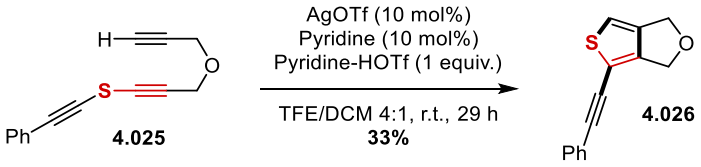

Figure 4-11. (3+2) cyclization with 1,2-migration of an alkynyl group.

This single result obtained with bis-alkynyl thioether **4.025** demonstrates that the cyclization-cascade process could be generally extended to substrates possessing C(sp) hybridized substituents on the S atom.

4.5. Second optimization of the reaction parameters and application to longer linkers

The singular slow kinetics observed for the formation of malonate-derived product **4.013j** (see Table 4-3) foreshadowed an issue that was rapidly discovered for structures with linkers comprising more than 3 atoms. In the representative case of substrate **4.027a**, no conversion could be observed after 22 hours with the AgOAc/AcOH catalytic system at room temperature (Table 4-5, entry 1). This issue could not be solved solely by raising the temperature (entry 2). Under these modified conditions, the formation of a silver mirror was observed during the course of the reaction as an indication of catalyst degradation. The starting material was also fully consumed to produce enol acetate **4.030a** and thioester **4.031a**, both likely occurring from the addition of acetic acid to the alkyne moiety of the alkynyl sulfide. This process was found to be independent of the metal catalyst (entry 3). The catalyst

degradation could be alleviated by the alternate use of copper(I) acetate in combination with sodium ascorbate as a co-catalyst (entry 4). This modification provided a small quantity of the desired thiophene **4.028a**, but starting material degradation by acetic acid remained highly competitive. Swapping acetic acid to mildly acidic trifluoroethanol successfully repressed the formations of **4.030a** and **4.031a** (entry 5) while still promoting the production of the desired thiophene **4.028a**.

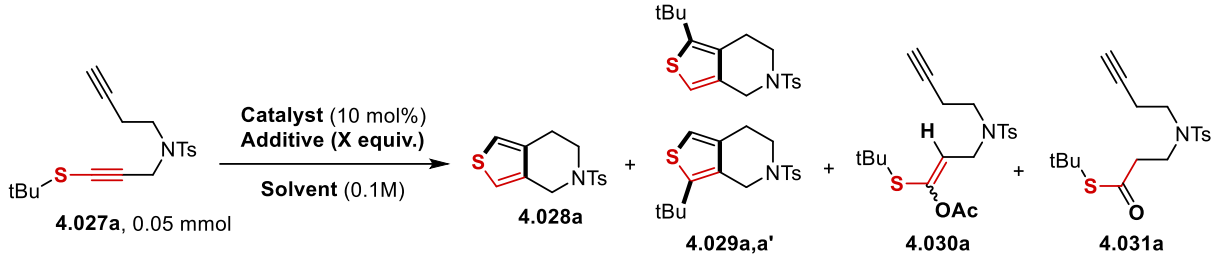

Entry	Catalyst	Additive (X equiv.)	Solvent	Temp.	Time	Conv. 4.027a (%)	4.028a (%)	4.029a,a' (%)	4.030a (%)	4.031a (%)
1	AgOAc	-	AcOH	r.t.	22 h	0	0	0	0	0
2	AgOAc	-	AcOH	80°C	7 h	>95	0	0	74	17
3	-	-	AcOH	100°C	3 h	>95	0	0	87	13
4	CuOAc	Na-Asc (1.0)	AcOH	100°C	3 h	>95	6	1	72	10
5	CuOAc	Na-Asc (1.0)	TFE	80°C	15 min	>95	89	11	0	0

Table 4-5. Optimization for longer linkers: suppressing acetic acid-derived by-products.

A final parameter was left to optimize, which was minimizing the formation of alkyl migration products **4.029a** and **4.029a'**. Although the mechanism of the alkyl group migration event was not studied, the 1:1 mixture of by-products suggested a possible origin from a singular "symmetrical" intermediate (Figure 4-12). Considering the previous isolation of S-aryl thiophenium salts, it is likely that S-alkyl species proceed through the same mechanism. So, a thiophenium species **4.032** may be a common precursor to both by-products **4.029a** and **4.029a'**.

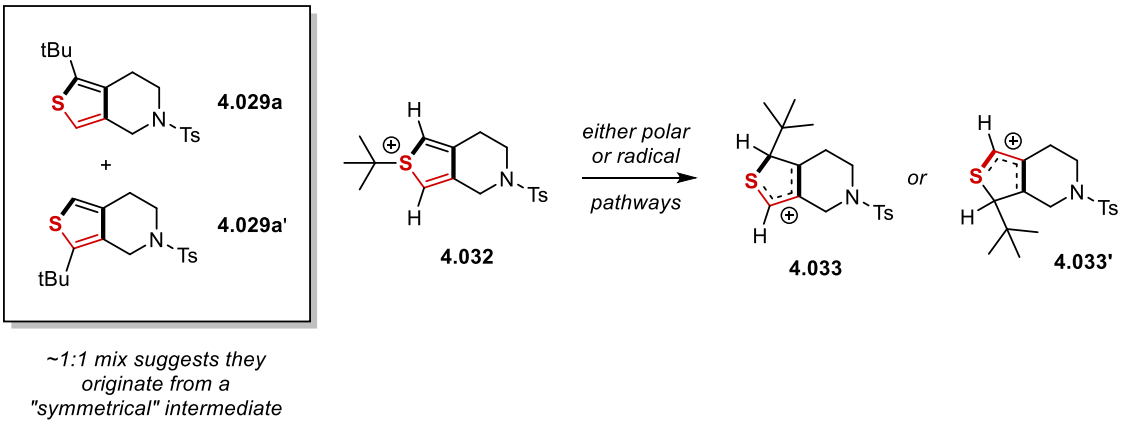

Figure 4-12. Hypothesis on the origin of 1,2-alkyl shift by-products.

Either polar or radical pathways that would lead to 1,2-shift intermediates **4.033** and **4.033'** should see intermediate stabilization by the bulky *tert*-butyl group (i.e. *tert*-butyl radical/cation). It was then anticipated that changing the *tert*-butyl group to a primary alkyl chain could suppress this pathway regardless of its nature. This hypothesis proved to be true when using the *n*-propyl group (Table 4-6, entry 2), for which none of **4.029a** or **4.029a'** were observed. The addition of a sole equivalent of acetic acid helped to increase the yields of **4.028a** obtained (entry 3). It is believed that higher amounts of acetate species in the mixture may help to cleanly dealkylate intermediate thiophenium species (as was observed in the thermal variant of this chemistry, see Section 3.8). The trifluoroethanol solvent proved to be beneficial, as switching to simple ethanol led to lower yields of the desired thiophene (entry 4). Finally, the more expensive copper(I) acetate was replaced by copper(II) acetate to no detriment of the obtained yield (entry 5), compromising instead for a slightly longer induction period to active catalysis.

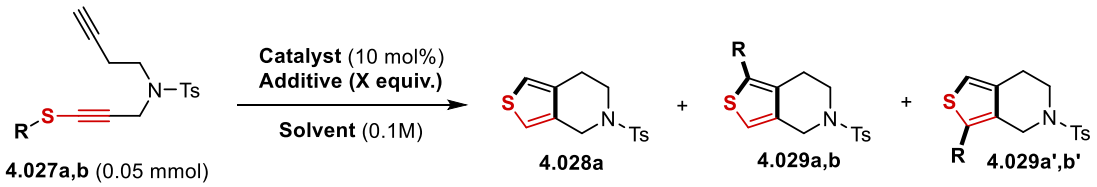

Entry	R	Catalyst	Additive (X equiv.)	Solvent	Temp.	Time	Conv. 4.027 (%)	Yield 4.028 (%)	Yield 4.029+4.029' (%)
1	tBu	CuOAc	Na-Asc (1.0)	TFE	80°C	15 min	>95	89	11
2	nPr	CuOAc	Na-Asc (0.2)	TFE	80°C	30 min	>95	80	0
3	nPr	CuOAc	Na-Asc (1.0) + AcOH (1.0)	TFE	80°C	15 min	>95	>95	0
4	nPr	CuOAc	Na-Asc (1.0) + AcOH (1.0)	EtOH	80°C	15 min	>95	87	0
5	nPr	$Cu(OAc)_2$	Na-Asc (0.2) + AcOH (1.0)	TFE	80°C	30 min	>95	>95	0

Table 4-6. Optimization for longer linkers: suppressing 1,2-alkyl shift by-products.

In the case of 4-atom linkers, it is again a staggering improvement from the thermal conditions. 4-Atom linkers and terminal alkynes both previously proved to be scope-limiting elements in the thermal (3+2) cycloaddition (see Section 3.5). Heating the model yne-alkynyl sulfide **4.027a** at 200 °C in chlorobenzene for 4 hours was not long enough for full conversion (Figure 4-13). A large amount (85%) of unselective degradation of the starting material occurred, and only 9% NMR yield of the desired thiophene was observed.

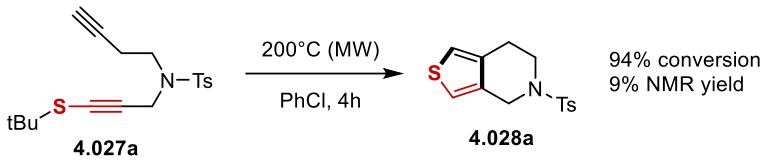

Figure 4-13. Clear limitation for the thermal (3+2) cyclization of yne-alkynyl sulfides.

With the newly optimized copper-catalyzed conditions, full consumption of the starting material took place in only 30 min at 80 °C, and the desired thiophene could be obtained in 93% isolated yield (Table 4-7).

These conditions were further applied to a selection of yne-alkynyl sulfide substrates bearing linkers composed of 4 to 6 atoms. In the case of 4-atom linkers, the substrates tolerated these conditions quite well, showing rapid conversion for *o*-phenylene derivative **4.028c**, and a comparable yield for **4.028d** possessing a free alcohol. Lactone **4.028e** could also be obtained over a longer period of reaction, but in a lesser yield (28%). On the other hand, in the presence of 5-atom linkers, higher temperatures were required, and poor conversions were observed when evaluated with a 10 mol% catalyst loading. At higher catalyst loadings, good results were obtained with **4.028f** bearing a simple 5-atom linker (59%). At this temperature, however, the sensitivity of homopropargyl groups **4.027g** proved to be more significant, and a lower 29% yield of **4.028g** was obtained. While propargyl carboxylates were tolerated for substrates with a smaller linker size (see Table 4-3), their 3,3-sigmatropic rearrangement seemed to be competitive in the case of **4.027h**, leading to a negligible yield of the desired thiophene **4.028h**. Silylated alkynes, which are known to undergo desilylative metalation, were also considered as alternative substrates to terminal alkynes. Trimethylsilyl alkyne **4.027i** was pleasingly observed to convert selectively to its corresponding thiophene **4.028i**. Interestingly, the unreacted substrate remained fully silylated, which seems to indicate that the metalation step is slower than the ensuing cyclization for this class of substrates. A limit in reactivity was reached in the case of 6-atom tethers. The catalyzed (3+2) cycloaddition could also be successfully observed but only with the additional help of geometrical constraint, such as in the case of the *ortho*-phenylene derived linker found in **4.028j**.

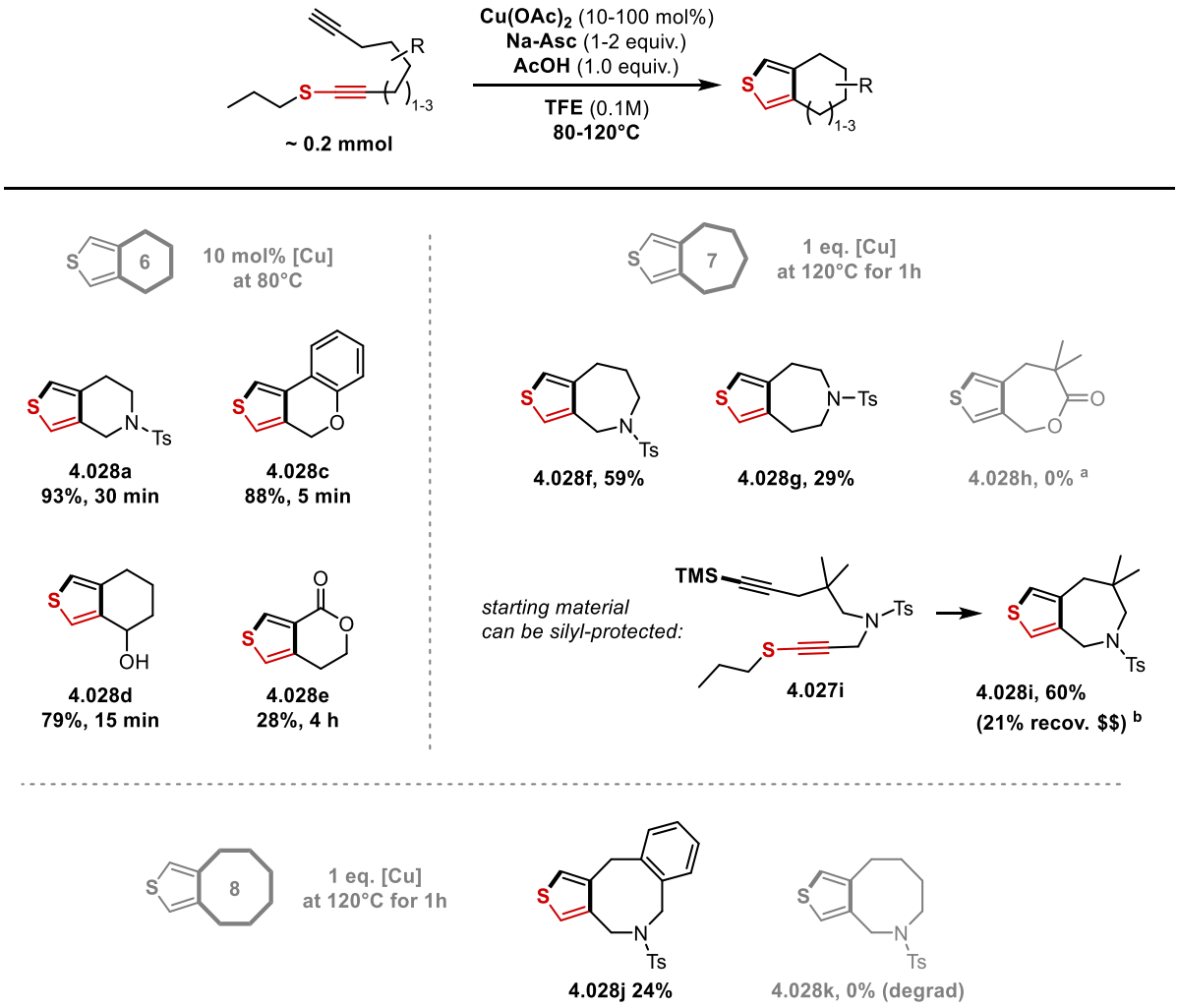

Table 4-7. Scope of the catalyzed (3+2) cyclization for longer linkers. [a]Substrate seems to degrade via a copper-catalyzed [3,3]-sigmatropic rearrangement; [b]2 equivalents of acetic acid were used.

It is important to note that at higher temperature, catalyst degradation in the form of metallic copper can be observed in significant amounts. While this scope selection shows the potential of this catalytic method for the formation of fused thiophenes, further optimization and screening of stabilizing ligands may help in lowering catalyst loadings.

4.6. Scale-up and product derivatizations

Alkynyl sulfides, although seeming as "exotic" functional groups, are quite easily accessed (as previously described in Section 3.2). In particular, *S*-(*n*-octyl) alkynyl sulfide **4.035** was conveniently prepared in two steps and an 82% overall yield from trimethylsilyl acetylene and a thiosulfonate ester using robust and scalable chemistry, without need of any purification by chromatography (Figure 4-14). Lithiation of these terminal alkynyl sulfides using nBuLi proceeds cleanly, and subsequent

trapping with hex-5-ynal provided the yne-alkynyl sulfide **4.027d**. This sequence worked reliably at larger scale, and this substrate could be obtained at the gram-scale with good yields.

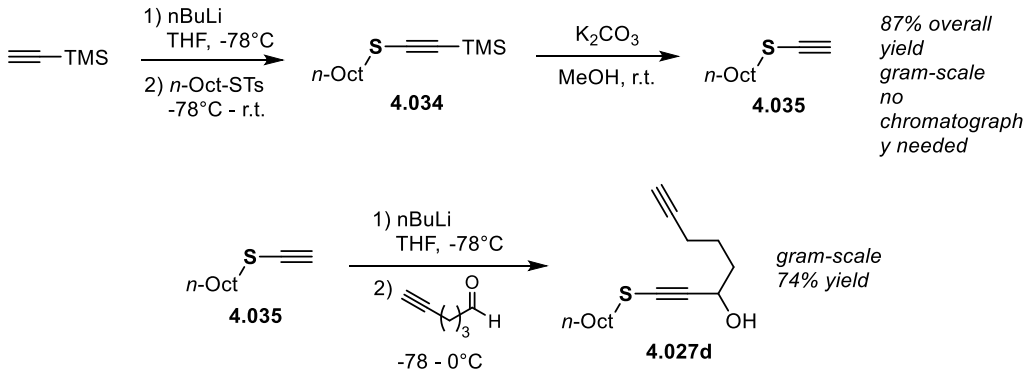

Figure 4-14. Gram-scale synthesis of an yne-alkynyl sulfide substrate.

Increasing the copper-catalyzed (3+2) transformation to gram-scale (Figure 4-15) gave a comparable yield (77%) of **4.028d** as previously obtained at lower scale (79%) (see Table 4-7). At this larger scale, the mixture was purged with N_2 and heated only at 70 °C to avoid a pressure build-up. This longer reaction time made it possible to distinctly observe multiple stages of catalytic activity. At room temperature, a beige suspension is observed, with the dense and insoluble copper salt resting at the bottom of the flask. The mixture slowly turns green upon heating as the $Cu(OAc)_2$ granules begin dissolving. The green hue changes to yellow after a few minutes, indicating the reduction of Cu(II) to Cu(I) by sodium ascorbate. Cu(I) is presumed to be the catalytically active oxidation state. As the reaction proceeds, the reaction mixture gradually takes on a darker brown colour, which may be associated with catalyst degradation.

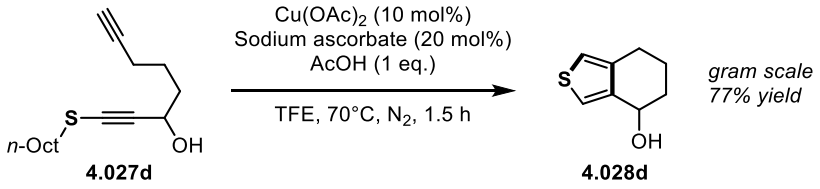

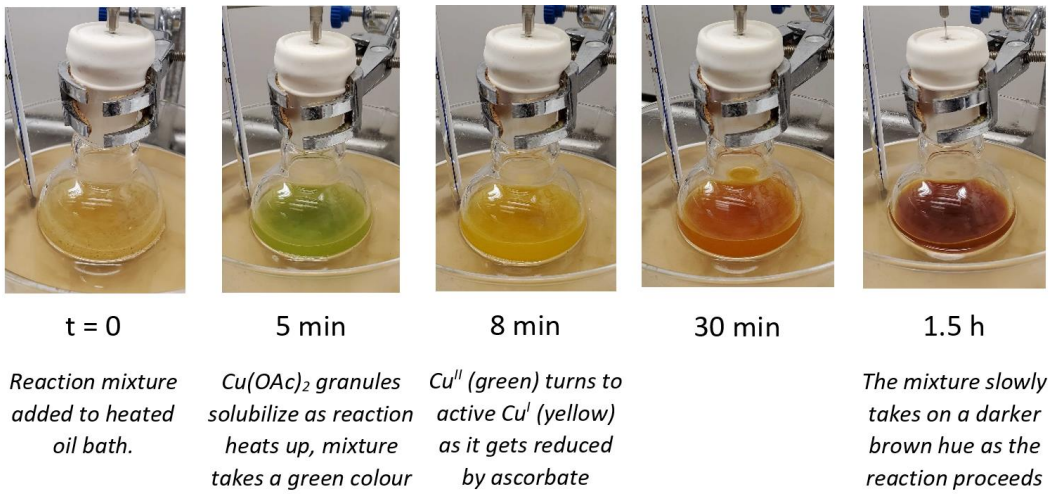

Figure 4-15. Copper-catalyzed (3+2) method at the gram-scale and visual cues during catalysis.

With a larger amount of thiophene **4.028d** in hand, the alcohol group itself was employed as a useful handle towards new fused thiophene cores not yet accessed using the (3+2) chemistry (Figure 4-16). DMP oxidation of **4.028d** cleanly provided the fused ketone **4.037**. The subsequent Schmidt reaction of this ketone led to the ring-expanded lactam **4.038** in very good yield. Consecutive homologation to **4.039** and condensation with hydrazine led to the fused imidazole derivative **4.040** with 84% yield in two steps. It is interesting to note that **4.028d**, **4.037** and **4.040** comprise the fused thiophene core of several medicinally-relevant compounds.[13-16]

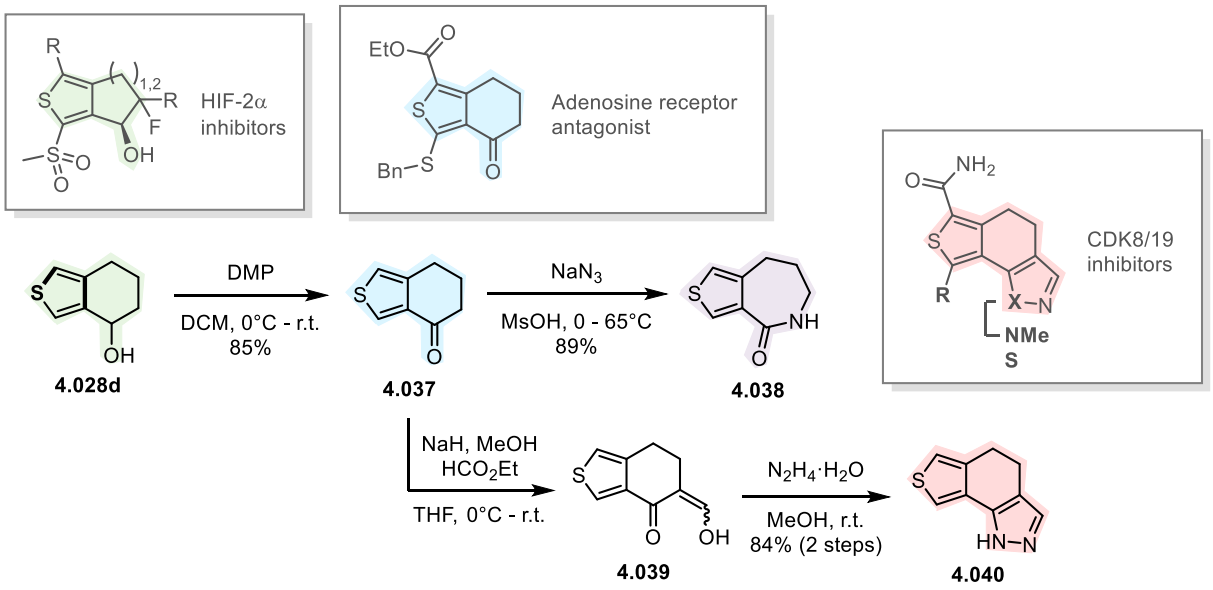

Figure 4-16. Product diversification towards medicinally relevant cores.

When attempting to generate the thieno spirolactone **4.043**, constituting an analogous core to thiophene-based σ_1 receptor ligands,[17-18] some issues arise during substrate synthesis (Figure 4-17). The direct yne-alkynyl sulfide precursor **4.042** could not be accessed by esterification of the alcohol **4.041**. Bulky tertiary alcohols are notoriously sluggish in esterification reactions. Instead, propargylation and submission to silver catalysis provided the simpler ether-fused thiophene **4.013g**. The latter was predictably oxidized at the "benzylic" position using Bobbitt's salt, ultimately providing the desired spirolactone **4.043** through this alternate route.

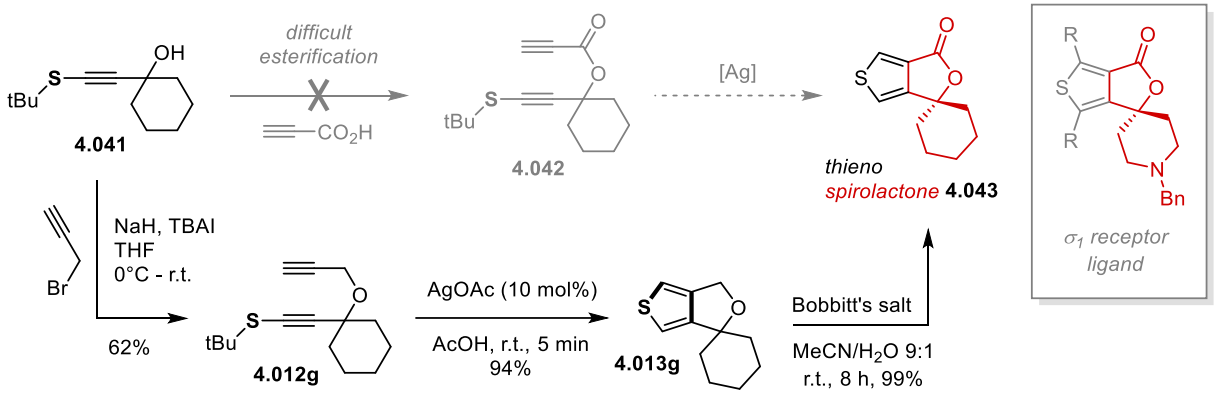

Figure 4-17. Circumventing scope issues with product derivatization.

4.7. Towards an understanding of the reaction mechanism

The remarkable rate increase observed when acetic acid was used as the solvent was quite informative. It suggested a mechanism more complex in nature than the simple formation of a copper acetylide, which is naturally favoured under more basic conditions. In the case of the CuAAC reaction, the rate increase by carboxylic acids has been ascribed to two factors: 1) the displacement of the equilibrium of copper acetylide species towards a catalytically active dinuclear acetylide complex (Figure 4-18-i),[19-22] and 2) the expedited protodemetallation of the resulting organo-copper heterocycle (Figure 4-18-ii).[19-23] Similar effects could be envisaged as well in catalysis involving the yne-alkynyl sulfide scaffold.

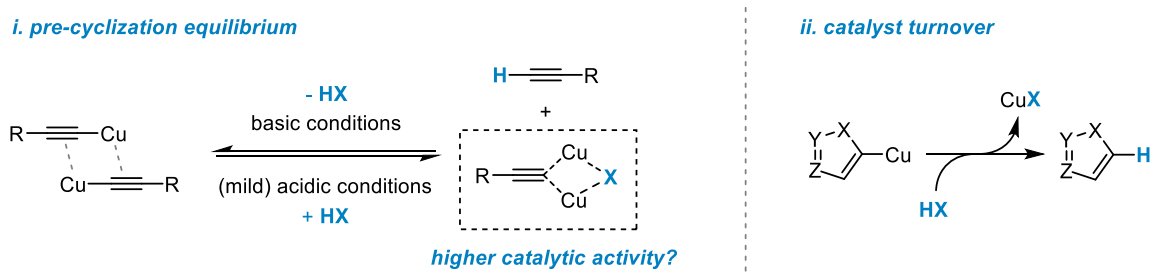

Figure 4-18. Proposed rate-enhancing roles of protic sources in the CuAAC.

The current mechanism generally proposed for CuAAC features a metallacycle of type **4.044** as a key intermediate in the cycloaddition process (Figure 4-19). Notably, the rate-limiting step of the cyclization portion in this mechanism is the formation of the first C-N bond,[24-26] which results in a lone pair of electrons being stabilized on the central nitrogen atom of the azide moiety. Transposition of this mechanism onto the yne-alkynyl sulfide system shows a similar event could occur to form an analogous metallacycle **4.045**. However, such a mechanistic scenario would result in an unstable lone pair of electrons being localized onto the central carbon atom, likely making the initial C-C bond formation less favourable than in the case of CuAAC.

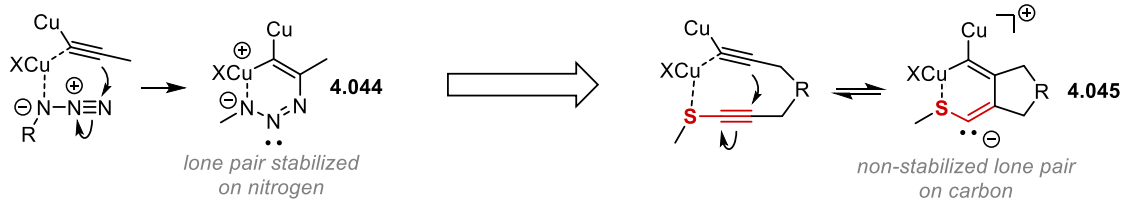

Figure 4-19. Transposition of the CuAAC mechanism onto the yne-alkynyl sulfide scaffold.

Upon scanning short distances between the terminal alkyne and alkynyl sulfide moieties in the bis-copper model **4.046**, a metallacycle **4.047** was observed as a stable minimum on the PES (Figure 4-20). This metallacycle is 2.0 kcal/mol higher in energy than the starting complex. This 6-membered intermediate was consistently observed as a stable minimum on the PES for any copper acetylide derivative later studied.

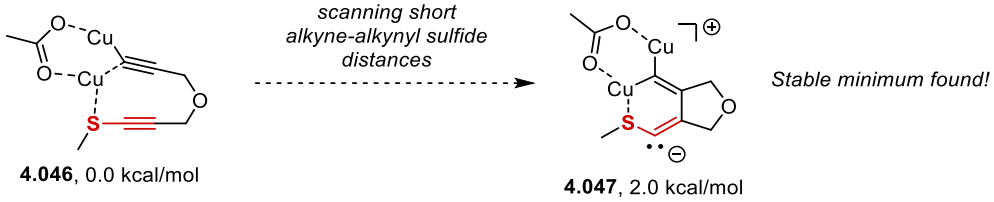

Figure 4-20. Identification of a stable metallacycle on the catalyzed (3+2) potential energy surface. Optimized at the PBE0(GD3-BJ)/def2SVP level of theory with SMD (AcOH) solvation model; free energy calculated with augmented def2TZVP basis set.

The Lewis structure for this metallacycle **4.047** could be reasonably ascertained through NBO analysis (Figure 4-21). Although the bonding surrounding both copper units is complex, a strong bonding between the internal copper unit and adjacent sulfur and carbon atoms convincingly indicates a metallacyclic structure. The development of negative charge on the alpha carbon was

further confirmed from the electrostatic potential (ESP) density map of the metallacycle, suggesting the presence of a lone pair of electrons.

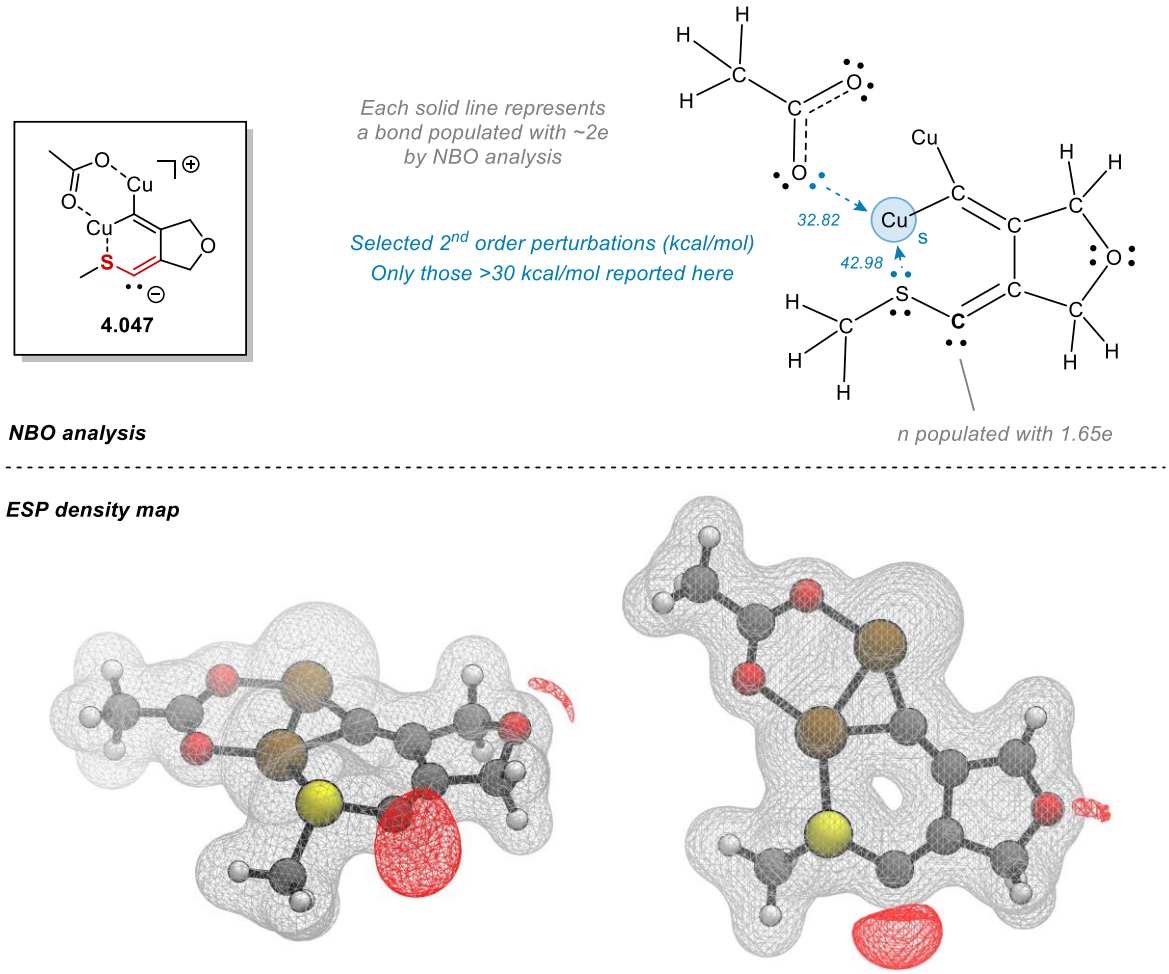

Figure 4-21. Analysis of the metallacycle minimum. Using the NBO7 utility on the same Gaussian16 software (basis set = def2TZVP), bond order analysis was performed on **4.047**, providing the given Lewis structure. Using the SCF method, an electrostatic potential density map was produced to confirm the presence of a lone pair of electrons on the carbon atom. Using the VMD software,[27] the ESP surface (with isovalue = ± 0.08) was plotted on the structure skeleton (top and side views shown).

It can be considered, however, that such an anion would be quite short-lived or nonexistent in a process involving the use of acetic acid as the solvent. It was therefore conjectured that protic sources could participate in stabilizing this charge development both at the transition state and in the cupracyclic intermediate (Figure 4-22). This stabilization could partly explain the rate-increasing effect observed when weak acids are employed.

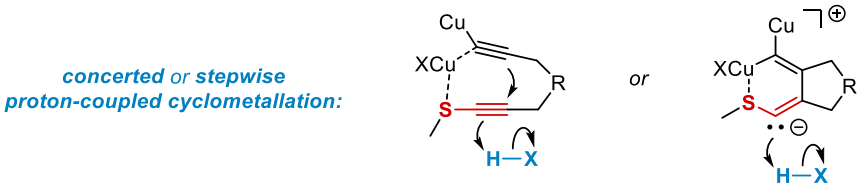

Figure 4-22. A third possible rate-enhancing effect of protic sources in the metal-catalyzed (3+2) cyclization of yne-alkynyl sulfides.

In order to evaluate the involvement of mono- or bis-metallic species in the mechanism and the explicit role of acetic acid in this transformation, five potential cyclization pathways were characterized via DFT studies (Figure 4-23). Calculations were carried out using the Gaussian16 software.[28] Stationary point optimization and frequency calculations were performed using the PBE0/def2SVP level of theory, with empirical dispersion correction (GD3-BJ).[29] This methodology has previously shown reasonable accuracy for comparatively low computation cost in bench-marking studies concerning transition metal-mediated transformations,[30] and has been used in recent mechanistic work involving metal-catalyzed (3+2) cycloadditions.[31] A solvation model using SMD33 (acetic acid) was also applied. Single point energy calculations were finally performed using the same methodology, but with the use of def2TZVP augmented basis set.

To get some insight into the C-C bond formation event and compare the energy demand as a function of metallic nuclearity and acid co-catalysis, the energy of the five pre-cyclization complexes **4.048-A** to **4.048-E** was normalized to 0. The conformational equilibria of substrates and the distribution between various copper complexes (and their possible aggregates) were not examined. The relative stability of the different possible metal acetylides and complexes is likely heavily influenced by the reaction medium and the conditions employed, and there is a high likelihood for error when building the model system. The stabilization imparted by the geminal acetylide complex in the di-copper mechanism was however estimated by comparing the energy of complexes **4.048-B** and **4.048-C**, showing a large gap of 18.7 kcal/mol in favor of the geminal di-Cu complex **4.048-B**.

For the C-C bond formation step, calculated transition state barriers range between 11.4 and 16.1 kcal/mol. Notably, the two lowest barriers (**4.049-B** and **4.049-D**) are those involving a geminal di-copper acetylide complex. It is worth noting that formation of metallacycles **4.050-A** and **4.050-B**, which do not involve any additional stabilization of the charge development on the central carbon atom, were both calculated to be endergonic processes. As hypothesized, transition states which involve concerted protonation of the central carbon atom during the C-C bond formation event

(**4.049-C,D,E**) could be located on the PES. The resulting metallacycles **4.050-C**, **4.050-D** and **4.050-E**, which involve stabilization of the charge, are all favourable exergonic processes.

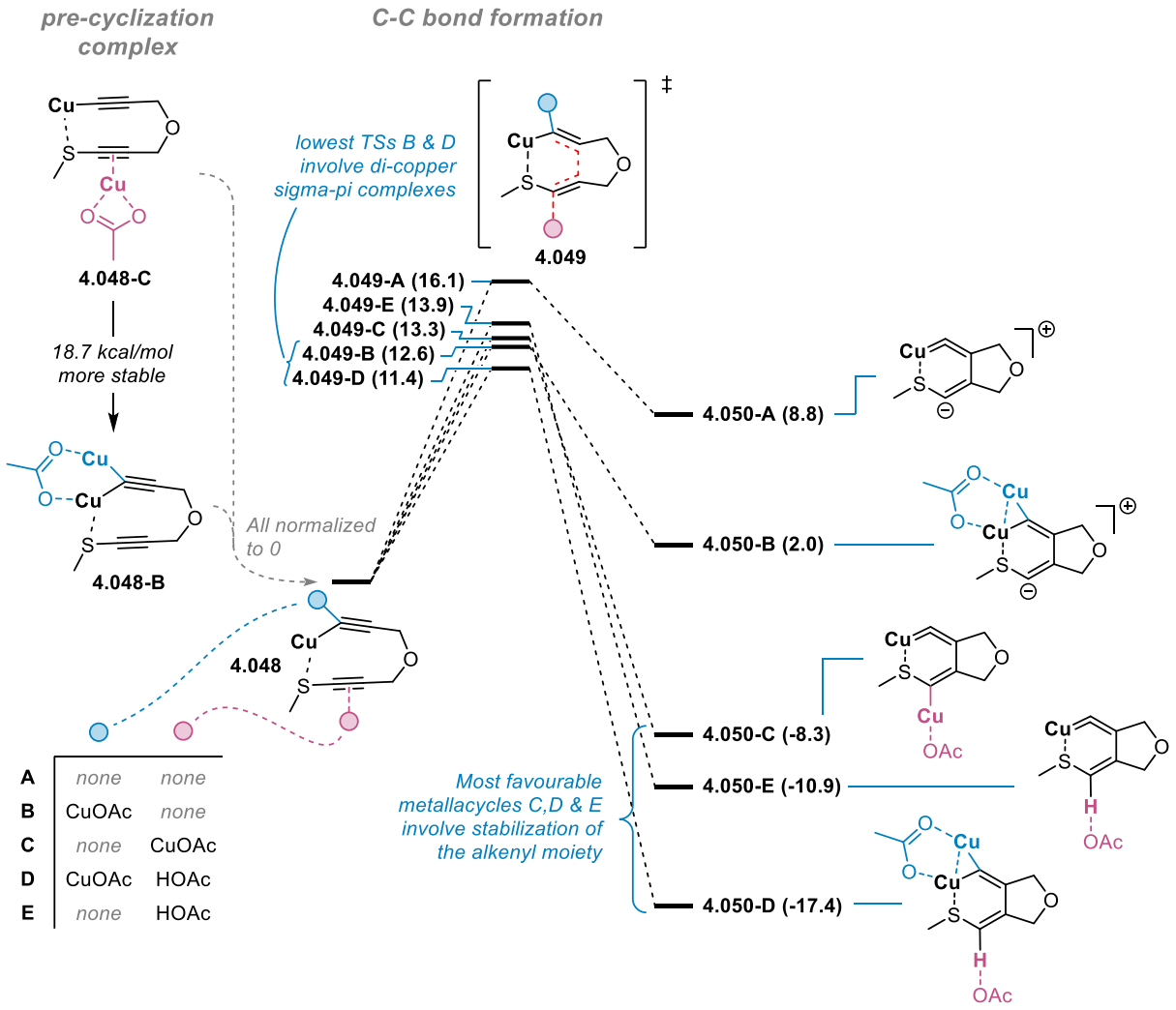

Figure 4-23. DFT studies on the copper-catalyzed stepwise (3+2) cyclization event: C-C bond formation step. Free energies in parentheses reported in kcal/mol.

The subsequent C-S bond formation step was further studied for metallacycle **4.050-D**, being the most exergonic pathway with lowest C-C bond formation barrier. Once the proton is delivered to **4.050-D**, a more stable complex **4.050-D'** can be found, approximately 17 kcal/mol lower, where the acetate species released complexes to the two copper units (Figure 4-24). From this new complex, the C-S bond formation step was found to be facile and unlikely to be turnover-limiting. The transition state **4.051-D** leading from metallacyle **4.050-D'** to thiophenium **4.052-D** was located, showing a low energy barrier of 6.6 kcal/mol. From this thiophenium intermediate, a sequence of de-alkylation from

sulfur and decomplexation/protodemetallation of the copper units would lead to the observed thiophene products.

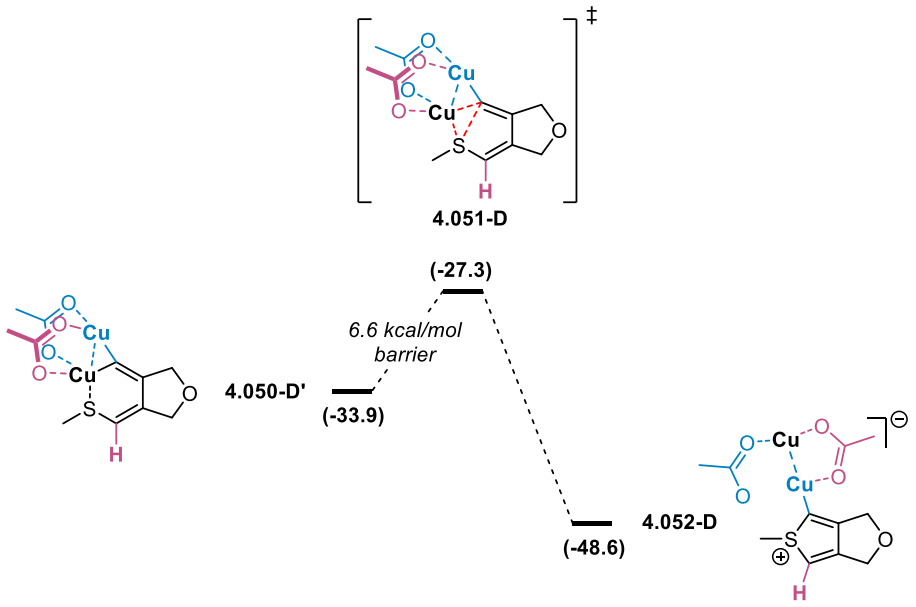

Figure 4-24. DFT studies on the copper-catalyzed stepwise (3+2) cyclization event: C-S bond formation step. Free energies in parentheses reported in kcal/mol.

Supplementary calculations were then performed on pathways A, B and D using AgOAc as the model catalyst (Figure 4-25). These calculations were found to be in qualitative agreement with the outcome of those performed using CuOAc. While the protonation event seemed slightly decoupled from the cyclometallation for the silver pathway using this DFT methodology, it remains that protonation is necessary to render the overall process thermodynamically favourable.

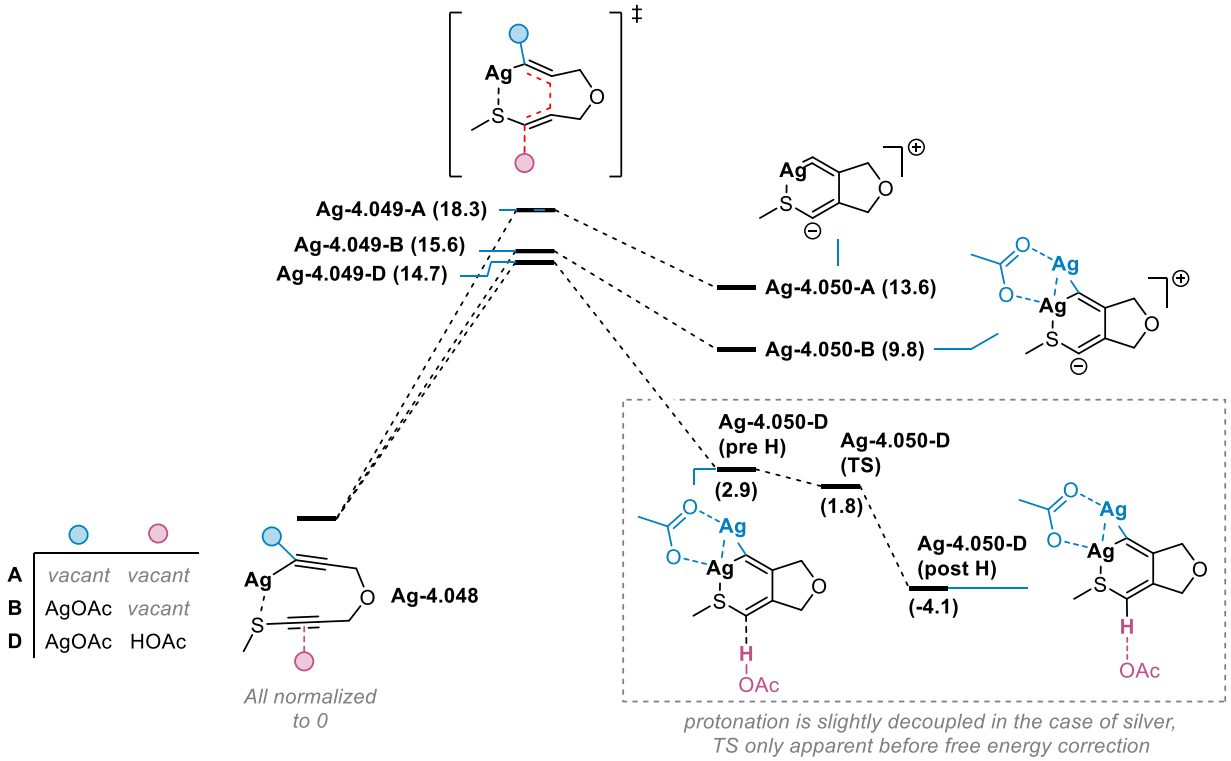

Figure 4-25. DFT studies on selected silver-catalyzed step-wise (3+2) cyclization events. Free energies in parentheses reported in kcal/mol.

The importance of the protonation event for rendering this process exergonic leads one to wonder whether a similar effect may be in effect for the CuAAC reaction, which also benefits from the presence of weak acids.[19-23] This thermodynamic effect for the yne-alkynyl sulfide scaffold is however less likely for the alkyne-azide system since the pK_a of 1,2,3-triazolium salts is around 0-1,[32] which is significantly lower than that of participating carboxylic acids.

Given the efficiency and selectivity of the silver-catalyzed transformation of S-aryl alkynyl sulfides to S-aryl thiophenium salts, the substrate **4.016a** was used in an experiment stoichiometric in catalyst to test our mechanistic hypotheses (Figure 4-26). When this substrate was dissolved in the presence of excess triethylamine and a stoichiometric quantity of silver triflate, a few important observations could be made: 1) the formation of silver acetylide **4.016a-Ag** was immediate and quantitative; 2) no bis-silver thiophenium intermediate of type **4.017a-Ag_2-OTf** could be observed; and 3) the mono-silver thiophenium **4.017a-Ag-OTf** was produced in a quantitative manner over time along with a small amount of fully protonated thiophenium **4.017a-OTf**. The sum of all three species (mass balance) remains constant throughout the experiment, ascertaining that the process observed exclusively involves these three species. With **4.016a-Ag** being clearly converted to **4.017a-Ag-OTf**,

this experiment supports that protonation is a key component in the (3+2) cyclization to thiophenium intermediates.

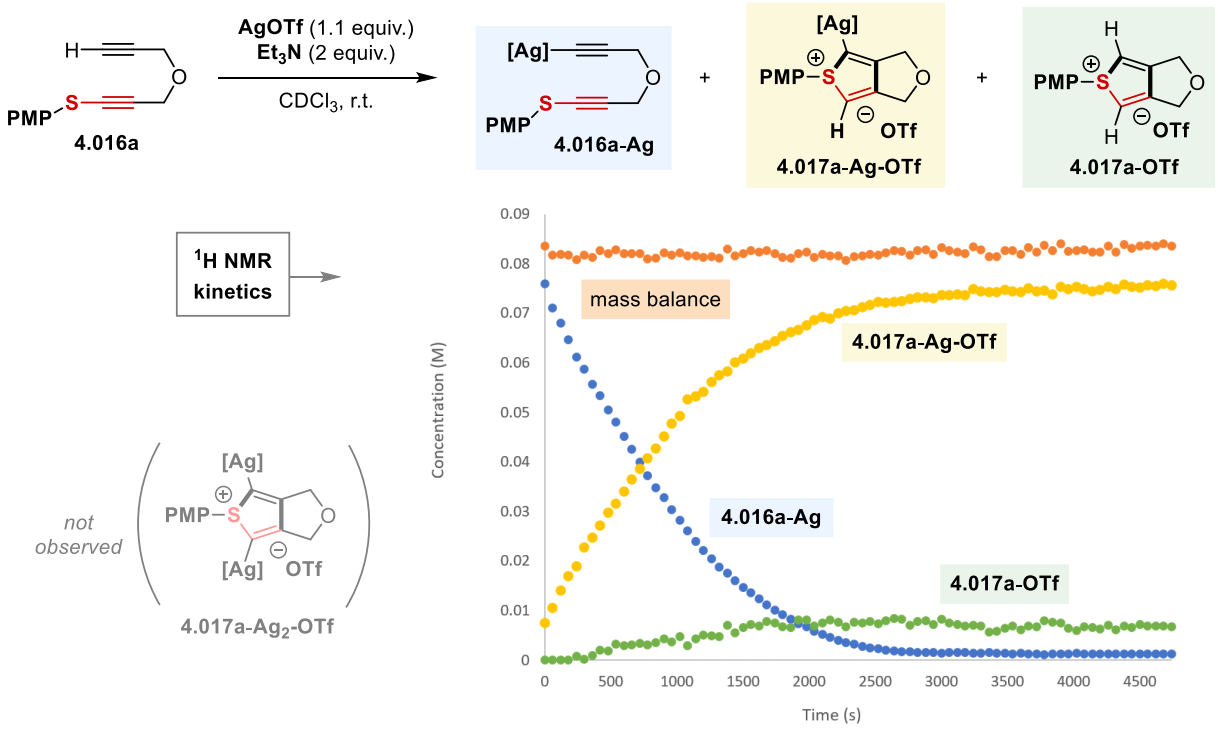

Figure 4-26. NMR kinetic data from an experiment using a stoichiometric amount of catalyst.

The simplest model explaining these observations would involve the direct reaction of silver acetylide **4.016a-Ag** with the triethylammonium salt to form the mono-silver thiophenium salt **4.017a-Ag-OTf**, i.e. the "mononuclear bimolecular model" (Figure 4-27). A slight deviation that may have an important impact on the observed kinetics would rather involve the initial formation of an "active" version of **4.016a-Ag**, which would then react with the triethylammonium salt, i.e. the "mononuclear unimolecular model". An alternative, more complex, mechanism may invoke a second unit of "free" silver triflate, forming a bis-metallated complex **4.053** which would then be susceptible to reaction with triethylammonium triflate, i.e. the "dinuclear model".

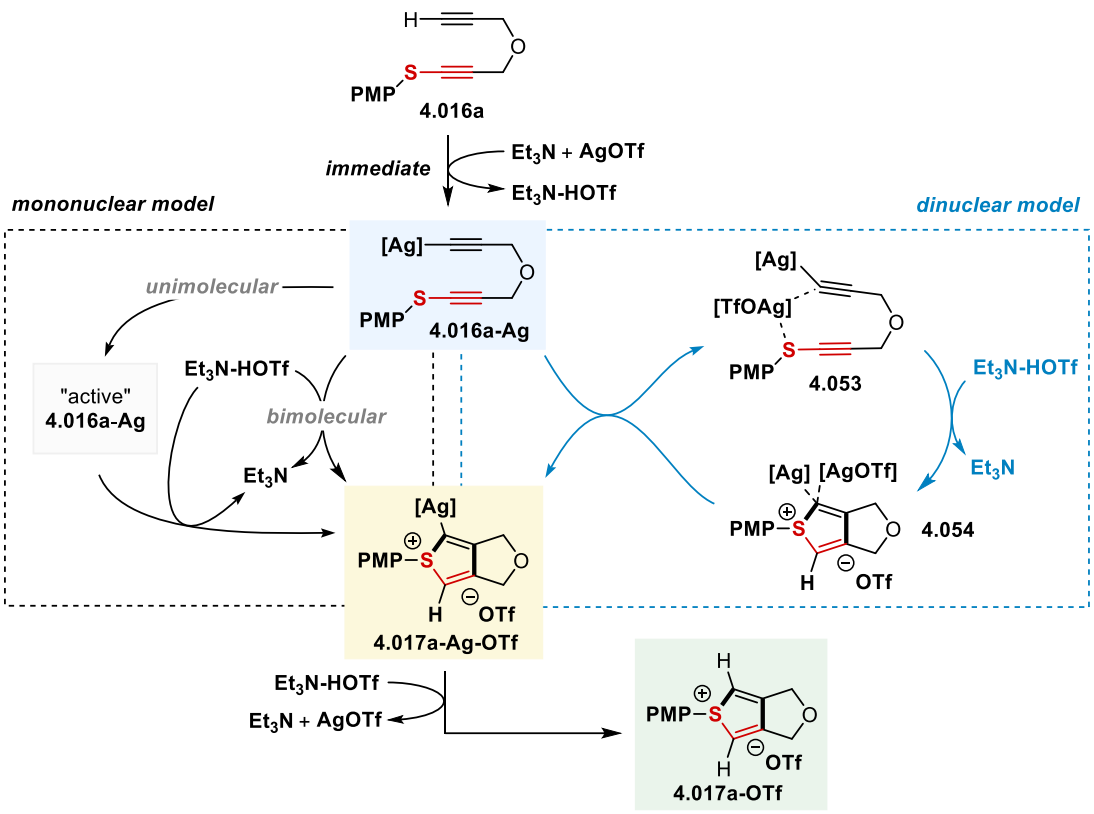

Figure 4-27. Two possible models explaining the stoichiometric catalytic kinetics results.

Kinetic modelling was subsequently performed using the COPASI software[33] to further evaluate the viability of these three pathways (Figure 4-28) (see Supporting Information 6.4.7 for details on the use of COPASI software).

The COPASI (Complex Pathway Simulator) software was developed to solve complex systems of biochemical processes, but can be used to solve for any system of chemical reactions (the use of COPASI herein was inspired by its use in recent work by the Hein group towards solving for pathways in palladium catalysis, see Ref 34). Fundamentally, this software is used by defining a *model*: a set of unique chemical reactions written as balanced equations following given rate laws. The user can define certain input values, such as initial concentration of species and rate constants. In this case, the initial concentrations of observable species **4.016a-Ag**, **4.017a-Ag-OTf** and **4.017a-OTf** are known from the NMR data, and the triethylammonium salt and excess silver catalyst concentrations are calculated based on the stoichiometric formation of the silver acetylide. The rate constants are however unknown. By using the COPASI software, the value of the rate constants can be freely optimized (in this case, using a genetic algorithm) to produce the closest possible concentration plot

to that obtained experimentally. In this way, different models can be evaluated and compared for plausibility in explaining the experimental data.

The best possible fit for the mononuclear bimolecular model is quite poor, which indicates this simple model is clearly not at play. While the bimolecular model displays a sharp inflection, the unimolecular version shows, as expected, a much less pronounced inflection, and is a much better fit to the experimental data. However, there are clear systematic deviations from the experimental data in the mononuclear unimolecular model, which prompts the investigation of other models. The dinuclear model clearly has the best fit with the obtained kinetics data and may therefore be at play.

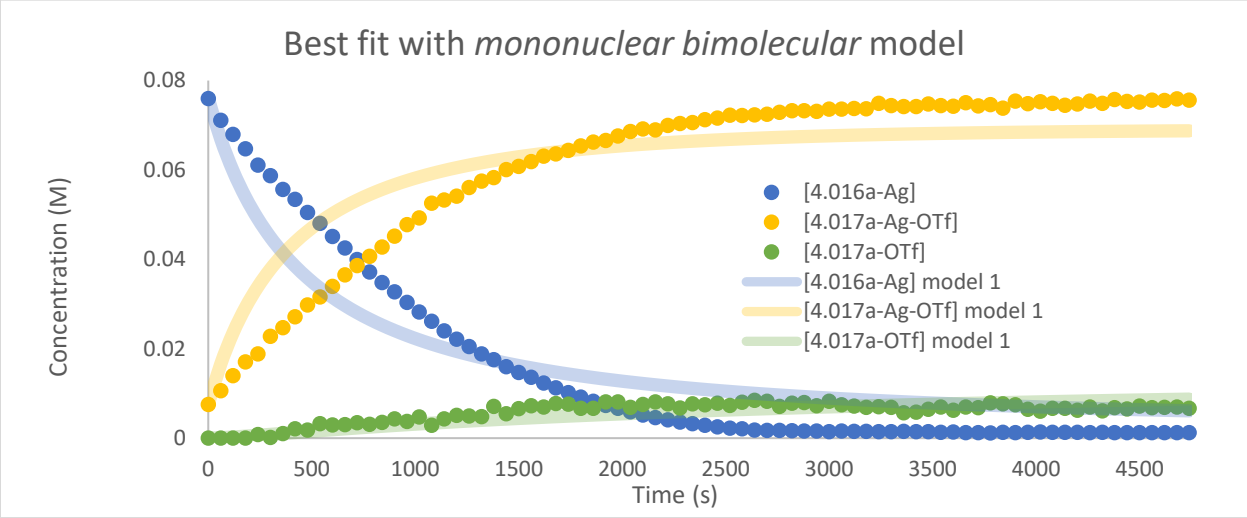

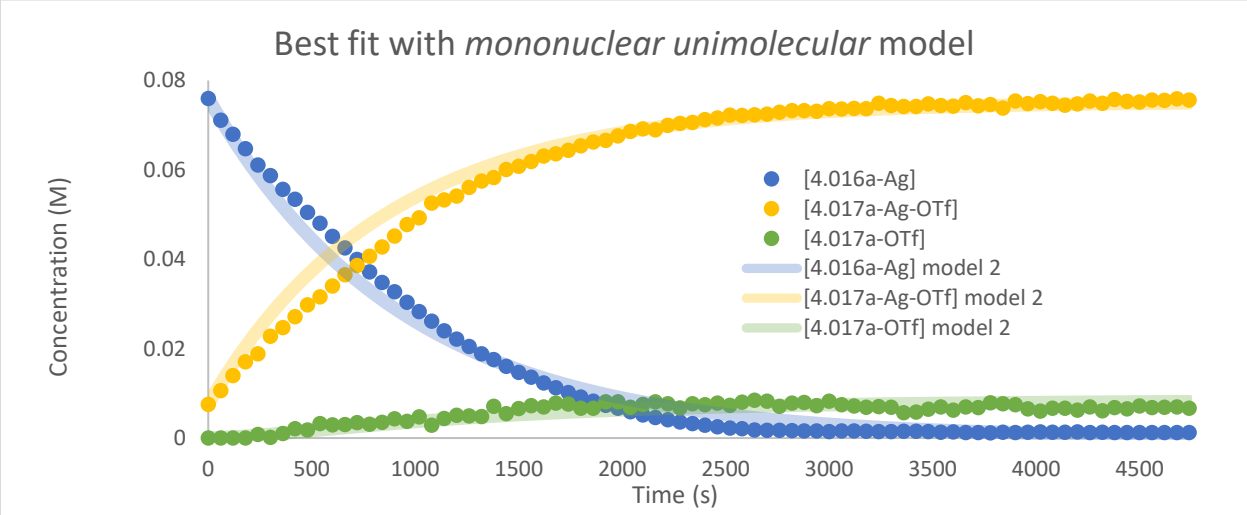

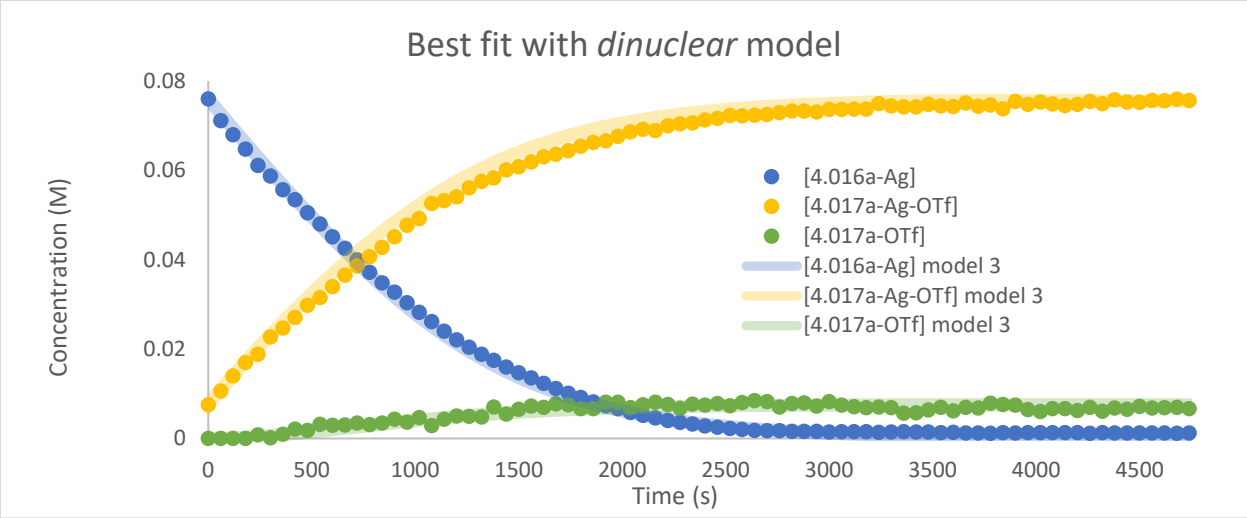

Figure 4-28. Overlap of three kinetic models optimized for best fit with experimental data.

Other factors such as ligation and solvation of silver species by triethylamine may provide a more accurate picture of the medium but could not be determined from the given data. So, these were not included in the models. It is also important to consider that the *mononuclear unimolecular* and *dinuclear* models possess a greater number of steps, and therefore a greater number of rate constants to optimize using this software. It may not be surprising then to observe a closer correlation for these two models with the experimental data (more independent variables = higher attainable R^2).

Nevertheless, it can be concluded that the cyclization process is unlikely described by the *mononuclear bimolecular* model, and that the best current explanation to the observed data involves the *dinuclear* model.

4.8. New links to literature precedents and by-product formation using the proposed mechanistic model

Although initially optimized out of the reaction outcome, the dimer by-product **4.015a** was quite interesting. It was consistently produced as a sole stereoisomer under copper catalysis, and its formation could be promoted when using higher base loadings (Entry 3, Table 4-8).

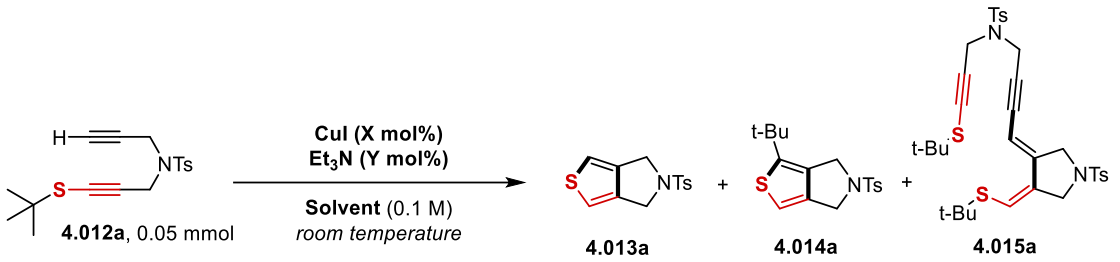

Entry	CuI (X mol%)	Et_3N (Y mol%)	Solvent	Time	Conv. 4.012a (%)	Yield 4.013a (%)	Yield 4.014a (%)	Yield 4.015a (%)
1	10	20	DCM	1 h	61	22	11	3
2	5	5	DCM	1 h	60	22	15	2
3	5	150	DCM	1 h	100	44	11	12

Table 4-8. Effect of base loading on the formation of the dimer by-product.

Its formation may also be explained by a metallacyclic intermediate (Figure 4-29). Under basic conditions, a higher concentration of simple copper acetylides is present, meaning complexes of type **4.055** may be more prevalent. In the absence of "CuX" species where X is weakly coordinating, the second unit of copper acetylide could then act as the "catalyst" to reach metallacycle **4.056**. A transposition of the strongly coordinated acetylide could then "compete" with the alternative transposition of the (poorly nucleophilic) sulfide to give the species **4.058** or **4.058'**. Demetallation of this species would provide the observed dimer **4.059** along with its proposed stereochemistry.

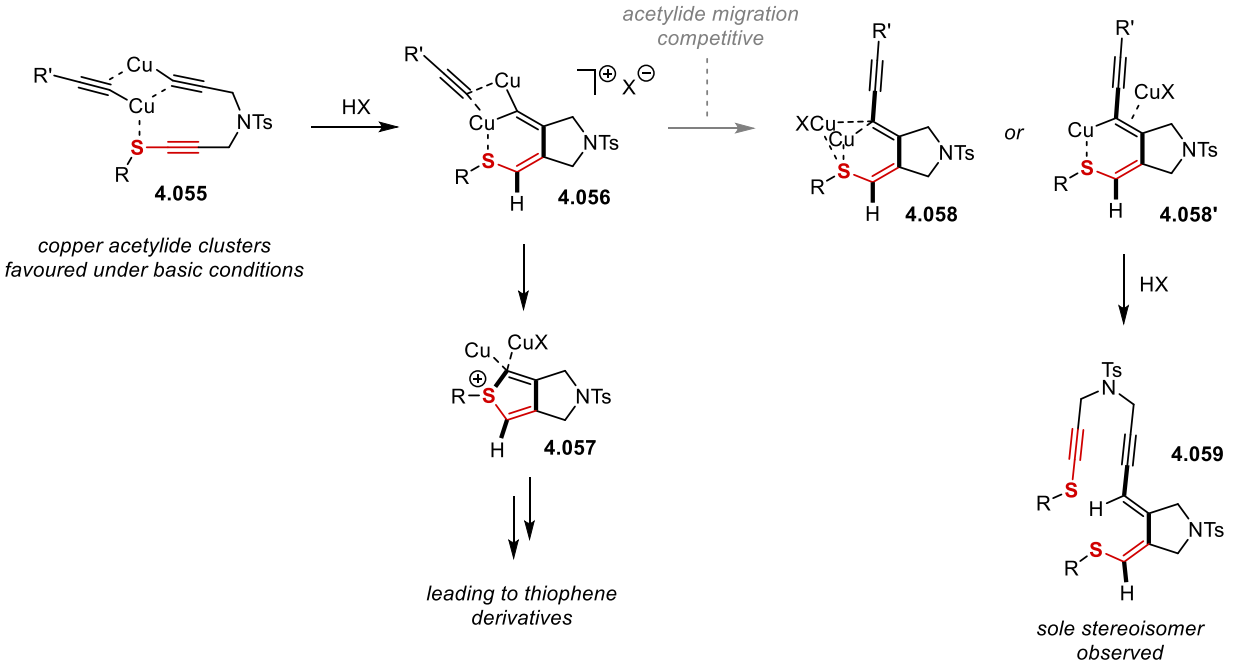

Figure 4-29. Formation of by-product **4.059** as explained by the intermediacy of a metallacycle.

Although a sole stereoisomer of **4.059** was observed, its stereochemistry could not be unambiguously assigned with NMR studies. Its proposed stereochemistry is rather based on related work by Yoshimatsu and coworkers, who observed the same type of adduct from S-aryl yne-alkynyl sulfides of type **4.060** (Figure 4-30).[35] Mixing these substrates with excess exogeneous terminal alkynes **4.061** in the presence of a copper(I) catalyst and a large excess of base, the authors observed diene-ynes **4.062** as the major products. X-Ray diffraction studies on the product confirmed the proposed stereochemistry. Importantly, their use of an asymmetric linker unequivocally maps the addition of the exogeneous alkyne **4.061** to the terminal alkyne position of the yne-alkynyl sulfide **4.060**. This also suggests that these diene-yne species **4.062** do not result from the addition of exogeneous alkynes to thiophenium intermediates).

Additionally, the Yoshimatsu group submitted simple diyne **4.063** to the same conditions and did not observe the formation of any analog of the diene-yne species. This is another indication that a chelation event involving the sulfide moiety is important in this transformation.

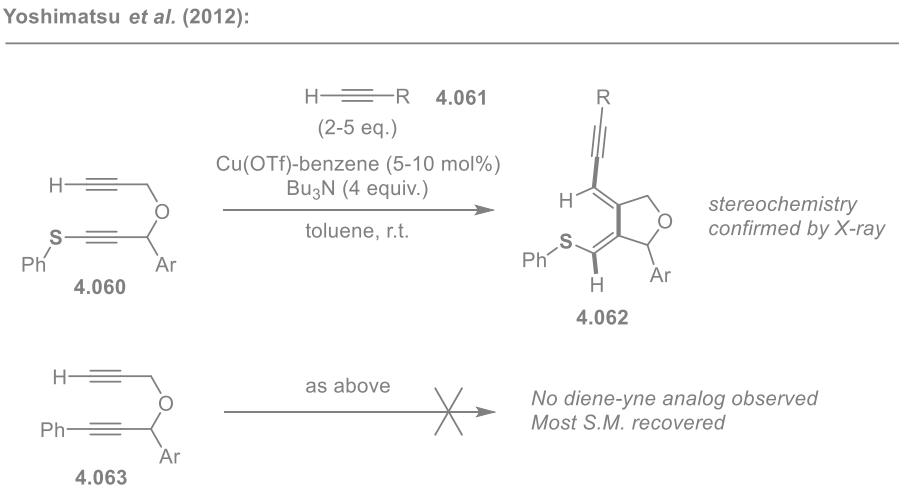

Figure 4-30. Observation of diene-ynes from yne-alkynyl sulfides, as studied by Yoshimatsu *et al*.

Another by-product that could be further explained through these new mechanistic studies, **4.064**, was observed when submitting substrate **4.012i** to the optimized set of conditions making use of AgOAc in AcOH as solvent (Figure 4-31). Interestingly, the alkynyl sulfide in **4.012i** is the most electron-deficient of the series studied here, and this substrate is the only one observed to produce this type of by-product. These two products may be explained by a common thiophenium acetate intermediate **4.065**. An elimination pathway would produce the expected thiophene **4.013i**, as was observed for most substrates. An alternative nucleophilic attack from the acetate counter anion on

the α-carbon of the thiophenium species (now rendered more electrophilic due to the attached carbonyl group) would deliver the ring-opened diene **4.064**.

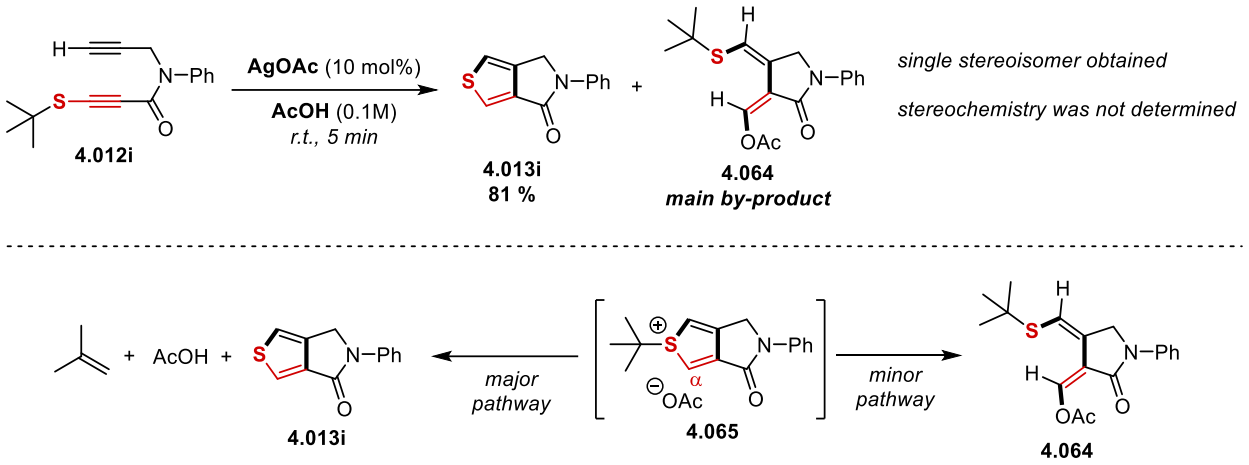

Figure 4-31. Possible explanation of the ring-opened by-product **4.064**.

4.9. Extension of the catalytic (3+2) reactivity to alkynyl selenides

Finally, we were intrigued by the possibility that the reactivity principle developed for alkynyl sulfide derivatives could be expanded to another class of closely related X-alkynyl groups: alkynyl selenides. To this end, substrate **4.065** was prepared and reacted under the previously optimized AgOAc/AcOH catalytic conditions (Figure 4-32).

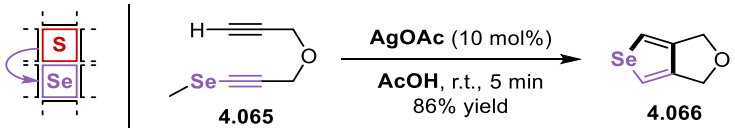

Figure 4-32. Catalytic method applied to alkynyl selenides.

The reaction was found efficient and selective providing selenophene **4.066** in very good yield (86%), without need of purification. 3 or 3,4-substituted selenophenes are of interest in material science, as their incorporation as building blocks in materials can be often beneficial in terms of optoelectronic properties.[36-38]

4.10. Conclusion

With consideration of the reactivity principles at the heart of the CuAAC reaction, several sets of catalytic conditions were successfully developed for the (3+2) cycloaddition between X-alkynes (a

neutral three-atom component) and terminal alkynes, permitting a dramatic decrease in required reaction temperature. This rate enhancement was instrumental in expanding the scope of the reaction and permitting the isolation of key thiophenium intermediates.

From optimization and mechanistic studies, pathways as shown in Figure 4-33 are now proposed as a general mechanistic overview of the reactivity offered by the copper- or silver-catalyzed (3+2) cycloaddition of alkynyl sulfides with terminal alkynes. In the first stage of the catalytic transformation, an equilibrium of metal acetylide species ultimately provides a catalytically active geminal bis-metallic acetylide complex. This complex undergoes a cyclization reaction to produce a fleeting metallacyclic intermediate similar in nature to that proposed for the CuAAC reaction. Due to the "neutral" nature of alkynyl sulfides, this cyclization must be proton-coupled to be thermodynamically favourable. Ring contraction ensues to form key metallated thiophenium intermediates. Turn-over of the catalyst liberates protonated thiophenium salts, some of which can be observed and isolated.

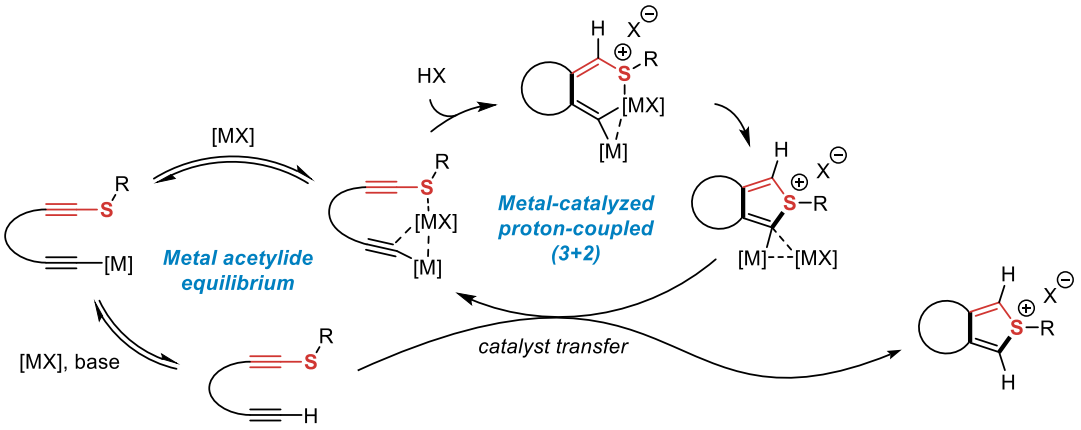

Figure 4-33. Proposed mechanism for the metal-catalyzed (3+2) reactivity of yne-alkynyl sulfides.

Finally, these thiophenium salts decompose following different predictable pathways, depending on structure and reaction conditions (the dealkylation pathways having been previously studied in Section 3.8), to produce various 3,4-fused thiophene products (Figure 4-34).

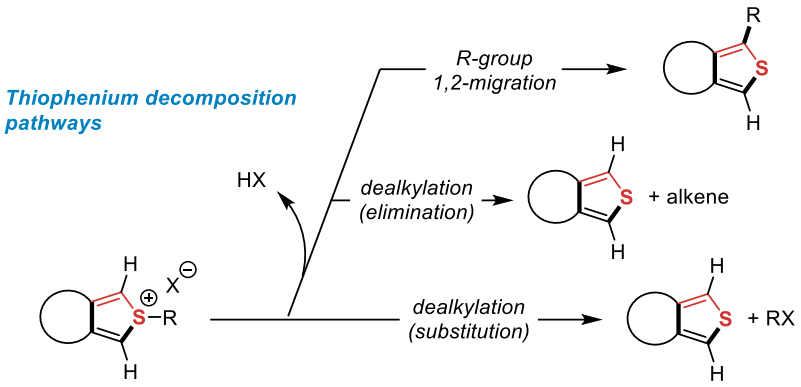

Figure 4-34. Proposed pathways for the evolution of thiophenium salt intermediates.

Fundamentally, this study demonstrates that mechanistic pathways akin to the ones involved in coinage metal-catalyzed 1,3-dipolar cycloadditions are also accessible to neutral three-atom components. Applying this general concept to the (3+2) cycloaddition of neutral three-atom components may unveil yet undiscovered reactivities in cycloaddition chemistry.

4.11. Chapter references

1. Hilt, G.; Lüers, S.; Harms, K., The First Broad Application of Alkynyl Sulfides as Dienophiles in Cobalt(I)-Catalyzed Diels–Alder Reactions. *J. Org. Chem.* **2004,** *69* (3), 624-630.
2. Hilt, G.; du Mesnil, F.-X., An improved cobalt catalyst for homo Diels–Alder reactions of acyclic 1,3-dienes with alkynes. *Tetrahedron Lett.* **2000,** *41* (35), 6757-6761.
3. Riddell, N.; Tam, W., Ruthenium-Catalyzed [2+2] Cycloadditions of Alkynyl Sulfides and Alkynyl Sulfones. *J. Org. Chem.* **2006,** *71* (5), 1934-1937.
4. Mitsudo, T.-a.; Naruse, H.; Kondo, T.; Ozaki, Y.; Watanabe, Y., [2 + 2]Cycloaddition of Norbornenes with Alkynes Catalyzed by Ruthenium Complexes. *Angew. Chem. Int. Ed. Engl.* **1994,** *33* (5), 580-581.
5. Ding, S.; Jia, G.; Sun, J., Iridium-Catalyzed Intermolecular Azide–Alkyne Cycloaddition of Internal Thioalkynes under Mild Conditions. *Angew. Chem. Int. Ed.* **2014,** *53* (7), 1877-1880.
6. Destito, P.; Couceiro, J. R.; Faustino, H.; López, F.; Mascareñas, J. L., Ruthenium-Catalyzed Azide–Thioalkyne Cycloadditions in Aqueous Media: A Mild, Orthogonal, and Biocompatible Chemical Ligation. *Angew. Chem. Int. Ed.* **2017,** *56* (36), 10766-10770.

7. Song, W.; Zheng, N.; Li, M.; He, J.; Li, J.; Dong, K.; Ullah, K.; Zheng, Y., Rhodium(I)-Catalyzed Regioselective Azide-internal Alkynyl Trifluoromethyl Sulfide Cycloaddition and Azide-internal Thioalkyne Cycloaddition under Mild Conditions. *Adv. Synth. Catal.* **2019,** *361* (3), 469-475.
8. Pommainville, A. Avenues Towards Fused Pyrroles and Thiophenes by Exploiting the Reactivity of Heteroarylium Cycloadducts. MSc Thesis, University of Ottawa, Ottawa, 2023.
9. Zhu, L.; Brassard, C. J.; Zhang, X.; Guha, P. M.; Clark, R. J., On the Mechanism of Copper(I)-Catalyzed Azide–Alkyne Cycloaddition. *The Chemical Record* **2016,** *16* (3), 1501-1517.
10. Wang, C.; Ikhlef, D.; Kahlal, S.; Saillard, J.-Y.; Astruc, D., Metal-catalyzed azide-alkyne "click" reactions: Mechanistic overview and recent trends. *Coord. Chem. Rev.* **2016,** *316*, 1-20.
11. Newman, J. D. S.; Blanchard, G. J., Formation of Gold Nanoparticles Using Amine Reducing Agents. *Langmuir* **2006,** *22* (13), 5882-5887.
12. Kitamura, T.; Zhang, B.-X.; Fujiwara, Y., Novel phenyl migration of 1-phenylbenzo[b]thiophenium triflates in the thermolysis. *Tetrahedron Lett.* **2002,** *43* (12), 2239-2241.
13. Leiendecker, M.; Buchstaller, H.-P.; Fuchss, T. Condensed thiophene derivatives as hypoxia inducible factor (HIF) inhibitors and their preparation. WO2021105069, 2021.
14. Okaniwa, M.; Banno, H.; Hirayama, T.; Cary, D. R.; Ono, K.; Iwamura, N. Preparation of fused heterocyclic compounds as cyclin-dependent protein kinase inhibitors for prophylactic and therapeutic treatment of cancer. WO2015159937, 2015.
15. Ono, K.; Banno, H.; Okaniwa, M.; Hirayama, T.; Iwamura, N.; Hikichi, Y.; Murai, S.; Hasegawa, M.; Hasegawa, Y.; Yonemori, K.; Hata, A.; Aoyama, K.; Cary, D. R., Design and synthesis of selective CDK8/19 dual inhibitors: Discovery of 4,5-dihydrothieno[3',4':3,4]benzo[1,2-d]isothiazole derivatives. *Biorg. Med. Chem.* **2017,** *25* (8), 2336-2350.
16. van Rhee, A. M.; Siddiqi, S. M.; Melman, N.; Shi, D.; Padgett, W. L.; Daly, J. W.; Jacobson, K. A., Tetrahydrobenzothiophenone Derivatives as a Novel Class of Adenosine Receptor Antagonists. *J. Med. Chem.* **1996,** *39* (2), 398-406.
17. Meyer, C.; Neue, B.; Schepmann, D.; Yanagisawa, S.; Yamaguchi, J.; Würthwein, E.-U.; Itami, K.; Wünsch, B., Improvement of σ1 receptor affinity by late-stage C–H-bond arylation of spirocyclic lactones. *Biorg. Med. Chem.* **2013,** *21* (7), 1844-1856.
18. Meyer, C.; Schepmann, D.; Yanagisawa, S.; Yamaguchi, J.; Itami, K.; Wünsch, B., Late-Stage C–H Bond Arylation of Spirocyclic σ1 Ligands for Analysis of Complementary σ1 Receptor Surface. *Eur. J. Org. Chem.* **2012,** *2012* (30), 5972-5979.
19. Özen, C.; Tüzün, N. Ş., Mechanism of CuAAC reaction: In acetic acid and aprotic conditions. *J. Mol. Catal. A: Chem.* **2017,** *426*, 150-157.
20. Shao, C.; Cheng, G.; Su, D.; Xu, J.; Wang, X.; Hu, Y., Copper(I) Acetate: A Structurally Simple but Highly Efficient Dinuclear Catalyst for Copper-Catalyzed Azide-Alkyne Cycloaddition. *Adv. Synth. Catal.* **2010,** *352* (10), 1587-1592.
21. Shao, C.; Wang, X.; Xu, J.; Zhao, J.; Zhang, Q.; Hu, Y., Carboxylic Acid-Promoted Copper(I)-Catalyzed Azide−Alkyne Cycloaddition. *J. Org. Chem.* **2010,** *75* (20), 7002-7005.
22. Shao, C.; Wang, X.; Zhang, Q.; Luo, S.; Zhao, J.; Hu, Y., Acid–Base Jointly Promoted Copper(I)-Catalyzed Azide–Alkyne Cycloaddition. *J. Org. Chem.* **2011,** *76* (16), 6832-6836.
23. Nolte, C.; Mayer, P.; Straub, B. F., Isolation of a Copper(I) Triazolide: A "Click" Intermediate. *Angew. Chem. Int. Ed.* **2007,** *46* (12), 2101-2103.
24. Ben El Ayouchia, H.; Bahsis, L.; Anane, H.; Domingo, L. R.; Stiriba, S.-E., Understanding the mechanism and regioselectivity of the copper(i) catalyzed [3 + 2] cycloaddition reaction between azide and alkyne: a systematic DFT study. *RSC Advances* **2018,** *8* (14), 7670-7678.
25. Calvo-Losada, S.; Pino-González, M. S.; Quirante, J. J., Rationalizing the Catalytic Activity of Copper in the Cycloaddition of Azide and Alkynes (CuAAC) with the Topology of ∇2ρ(r) and ∇∇2ρ(r). *The Journal of Physical Chemistry B* **2015,** *119* (4), 1243-1258.

26. Özkılıç, Y.; Tüzün, N. Ş., A DFT Study on the Binuclear CuAAC Reaction: Mechanism in Light of New Experiments. *Organometallics* **2016,** *35* (16), 2589-2599.
27. Humphrey, W.; Dalke, A.; Schulten, K., VMD: Visual molecular dynamics. *J. Mol. Graph.* **1996,** *14* (1), 33-38.
28. Frisch, M. J.; Trucks, G. W.; Schlegel, H. B.; Scuseria, G. E.; Robb, M. A.; Cheeseman, J. R.; Scalmani, G.; Barone, V.; Petersson, G. A.; Nakatsuji, H.; Li, X.; Caricato, M.; Marenich, A. V.; Bloino, J.; Janesko, B. G.; Gomperts, R.; Mennucci, B.; Hratchian, H. P.; Ortiz, J. V.; Izmaylov, A. F.; Sonnenberg, J. L.; Williams; Ding, F.; Lipparini, F.; Egidi, F.; Goings, J.; Peng, B.; Petrone, A.; Henderson, T.; Ranasinghe, D.; Zakrzewski, V. G.; Gao, J.; Rega, N.; Zheng, G.; Liang, W.; Hada, M.; Ehara, M.; Toyota, K.; Fukuda, R.; Hasegawa, J.; Ishida, M.; Nakajima, T.; Honda, Y.; Kitao, O.; Nakai, H.; Vreven, T.; Throssell, K.; Montgomery Jr., J. A.; Peralta, J. E.; Ogliaro, F.; Bearpark, M. J.; Heyd, J. J.; Brothers, E. N.; Kudin, K. N.; Staroverov, V. N.; Keith, T. A.; Kobayashi, R.; Normand, J.; Raghavachari, K.; Rendell, A. P.; Burant, J. C.; Iyengar, S. S.; Tomasi, J.; Cossi, M.; Millam, J. M.; Klene, M.; Adamo, C.; Cammi, R.; Ochterski, J. W.; Martin, R. L.; Morokuma, K.; Farkas, O.; Foresman, J. B.; Fox, D. J. *Gaussian 16 Rev. C.01*, Wallingford, CT, 2016.
29. Grimme, S.; Ehrlich, S.; Goerigk, L., Effect of the damping function in dispersion corrected density functional theory. *J. Comput. Chem.* **2011,** *32* (7), 1456-1465.
30. Iron, M. A.; Janes, T., Evaluating Transition Metal Barrier Heights with the Latest Density Functional Theory Exchange–Correlation Functionals: The MOBH35 Benchmark Database. *J. Phys. Chem. A* **2019,** *123* (17), 3761-3781.
31. Héron, J.; Balcells, D., Concerted Cycloaddition Mechanism in the CuAAC Reaction Catalyzed by 1,8-Naphthyridine Dicopper Complexes. *ACS Catalysis* **2022,** *12* (8), 4744-4753.
32. Abboud, J.-Luis M.; Foces-Foces, C.; Notario, R.; Trifonov, Rostislav E.; Volovodenko, Anna P.; Ostrovskii, Vladimir A.; Alkorta, I.; Elguero, J., Basicity of N-H- and N-Methyl-1,2,3-triazoles in the Gas Phase, in Solution, and in the Solid State − An Experimental and Theoretical Study. *Eur. J. Org. Chem.* **2001,** *2001* (16), 3013-3024.
33. Hoops, S.; Sahle, S.; Gauges, R.; Lee, C.; Pahle, J.; Simus, N.; Singhal, M.; Xu, L.; Mendes, P.; Kummer, U., COPASI—a COmplex PAthway SImulator. *Bioinformatics* **2006,** *22* (24), 3067-3074.
34. Deem, M.C.; Derasp, J.S.; Malig, T.C.; Legard, K.; Berlinguette, C.P.; Hein, J.E., Ring walking as a regioselectivity control element in Pd-catalyzed C-N cross-coupling. *Nat. Commun.* **2022**, *13*, 2869.
35. Yoshimatsu, M.; Sasaki, H.; Sugimoto, Y.; Nagase, Y.; Tanabe, G.; Muraoka, O., Copper-Catalyzed Complete Regio- and Stereoselective Cyclization of 1-Aryl-3-sulfanyl-4-oxahepta-1,6-diynes Triggered by Alkynylation. *Org. Lett.* **2012,** *14* (12), 3190-3193.
36. Hollinger, J.; Gao, D.; Seferos, D. S., Selenophene Electronics. *Isr. J. Chem.* **2014,** *54* (5-6), 440-453.
37. Marsh, A. V.; Heeney, M., Conjugated polymers based on selenophene building blocks. *Polym. J.* **2023,** *55* (4), 375-385.
38. Otsubo, T.; Takimiya, K., Selenophenes as Hetero-Analogues of Thiophene-Based Materials. In *Handbook of Thiophene-Based Materials*, 2009; pp 321-340.

5. Chapter 5 – Recent developments and concluding remarks

5.1. Recent developments on the (3+2) reactivity of heteroatom-substituted alkynes

In the course of the work described in this thesis, a few new contributions to the use of heteroatom-substituted alkynes as three-atom components in cycloaddition reactions have been reported and are worthy of discussion.

5.1.1. The Anderson group's study on yndiamides

Shortly after our study on the (3+2) reactivity of yne-ynamides was published,[1] the Anderson group reported that the same transformation could also be observed in yne-yndiamides **5.001** (Figure 5-1).[2] In their work, the authors found that the (3+2) process can be catalyzed by a gold(I) complex, and showed that it can also be thermally-promoted by heating in toluene, using BHT as an additive to improve yields.

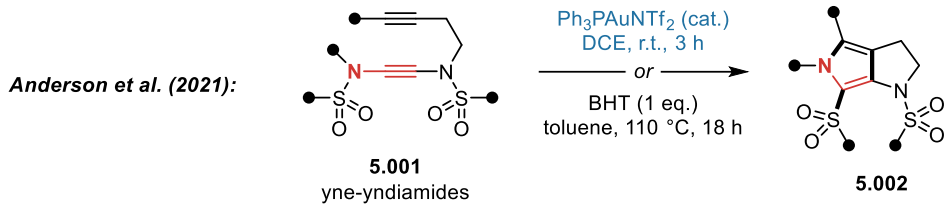

Figure 5-1. The (3+2) reactivity of yne-yndiamides as reported by Anderson and coworkers.

The success of the yndiamides in the gold-catalyzed variant of this reaction can be directly linked to the proposed mechanism (Figure 5-2). The authors propose that the inner amide moiety shares electron density to form the gold-activated keteniminium species **5.005**. A nucleophilic attack by the alkyne moiety, followed by trapping of the proposed alkenyl cation **5.006** by the second amide group generates the formal (3+2) cycloadduct **5.007**. 1,2-Sulfonyl shift and liberation of the gold catalyst would then provide the observed fused pyrrole **5.009**.

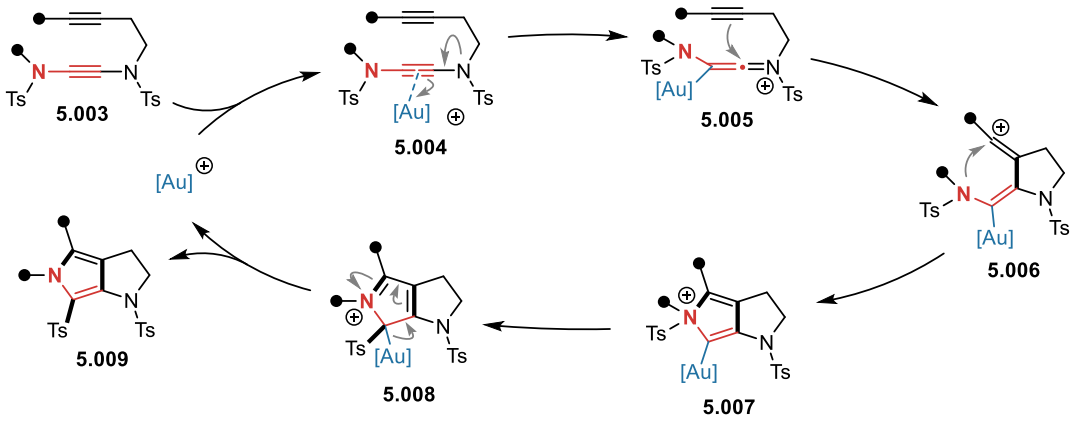

Figure 5-2. Mechanism proposed by Anderson and coworkers for the gold-catalyzed (3+2) reaction.

The mechanism the authors propose for the reaction under thermal conditions is the same as provided in this thesis and will therefore not be discussed here.

The derivatives investigated, involving the groups attached to the tethered alkyne and amide moieties, seem to be generally active under both catalytic and thermal conditions (Figure 5-3). The yields are however lower for the gold-catalyzed variant in most examples, and in some cases only decomposition is observed. This is unsurprising considering that the electron rich yndiamides would be rapidly activated by the electrophilic gold catalyst, and oligomerization of this unit is a very probable side reaction.

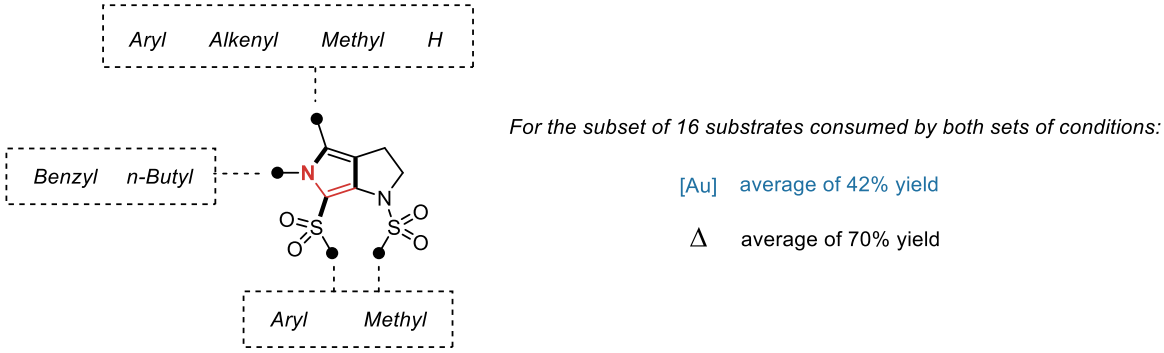

Figure 5-3. Differing average yields for the gold-catalyzed and thermal (3+2) reactions.

Particularly relevant information can be found in their supporting information document, where the authors also briefly investigate yne-ynamide scaffolds (Figure 5-4). Interestingly, they note that the gold-catalyzed conditions permit to access the tris-methylene linker-derived pyrrole **5.011**, and that no reaction is observed using thermal conditions at 110 °C. This is in line with our own observations that all-carbon linkers are particularly poor at promoting this reactivity under thermal conditions (see

malonate linker in Section 2.5), yet it is interesting that the gold catalysis is successful for this unique linker. The ether-derived pyrrole **5.012**, however, could only be obtained through thermal activation, and decomposition was observed under gold catalytic conditions.

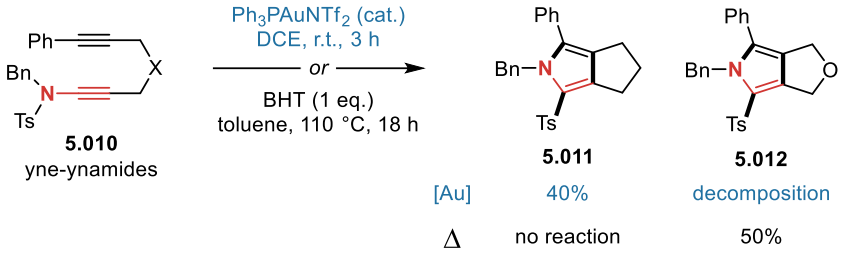

Figure 5-4. Limitations in gold catalysis for the yne-ynamide scaffold.

This last result is in line with our own initial investigations on the yne-ynamide scaffold (which was in fact originally synthesized for the purpose of investigating gold(I) chemistry!), where submission of our model yne-ynamide **2.014a** to similar conditions with JohnPhosAuNTf$_2$ led to non-selective degradation of the starting material.

The work by Anderson and coworkers inspired us to investigate analogous chemistry in similar scaffolds involving a thioynamide group, wondering if the same catalytic process could also promote the formation of thiophenes. This was successful and is briefly discussed in Section 3.9.

5.1.2. Takasu and Takikawa group's study on intramolecular benzyne-ynamide reactivity

As part of their research program on the intramolecular reactivity of benzyne species, the group of Takasu and Takikawa recently reported in 2023 that scaffolds of the **5.013** type produce indole derivatives **5.014** upon activation of the pendant benzyne precursors (Figure 5-5).[3]

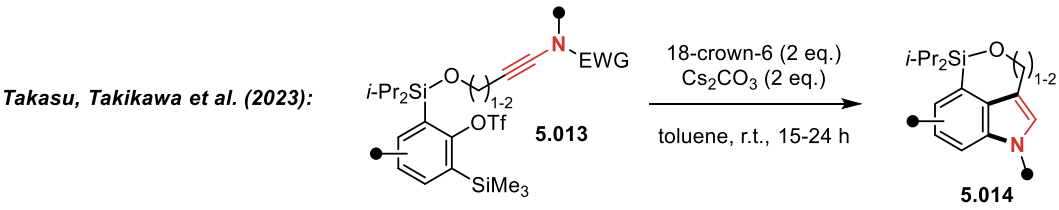

Figure 5-5. The intramolecular benzyne-ynamide (3+2) reactivity observed by Takasu, Takikawa and coworkers.

The authors propose that the intermediate benzyne **5.016** reacts in a (3+2) cycloaddition fashion with the tethered ynamide to form an indolium ylide **5.018** (Figure 5-6). This ylide is then susceptible to protonation and cleavage of the EWG to produce the observed indole **5.019**. This outcome is different

to our own studies on the yne-ynamide scaffolds, where only products with 1,2-migration of the EWG were observed. In their case, either Boc or tosyl groups are observed to be cleaved off. Two factors may explain this. First, a significant amount of protic sources and water are likely present when working with 18-crown-6 and Cs_2CO_3, so protonation of the intermediate ylide may occur more readily under this set of conditions. Second, a 1,2-sigmatropic rearrangement in the indolium ylide would require to *dearomatize* the benzo group, surely increasing the barrier for this pathway. Combined, these two factors may make the protonation/cleavage of EWG pathway much more favourable in their case. Interestingly, in their DFT studies, the authors located a diradical intermediate **5.017** when investigating the open shell PES. This mechanism has a strong analogy with the yne-ynamide (3+2) mechanism proposed in this thesis (see Section 2.8).

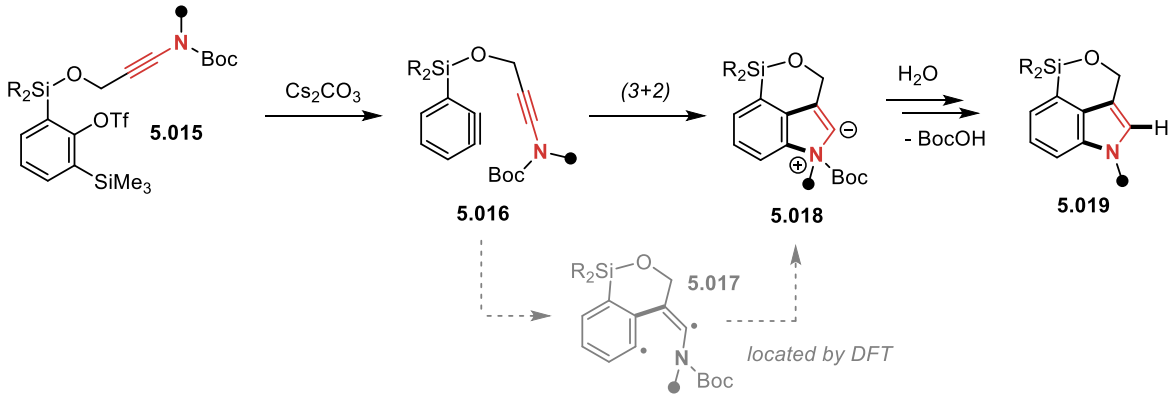

Figure 5-6. Proposed mechanism by Takasu, Takikawa and coworkers for the intramolecular benzyne-ynamide (3+2) reactivity.

This chemistry extends on the initial studies in 1968 by Wasserman and coworkers on the reactivity between ynol (thio)ethers and benzyne (see Section 1.3.2.1), showing that the same (3+2) reactivity is also possible in ynamides. In closer spirit to those initial studies, Takasu, Takikawa and coworkers also show that alkynyl sulfide and ynol ether derivatives of the same scaffold lead to fused benzothiophenes and benzofurans **5.021** (Figure 5-7).

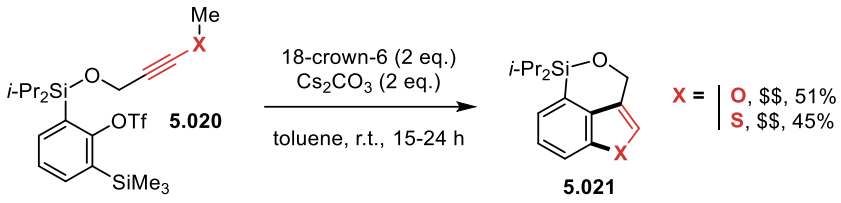

Figure 5-7. Extension of chemistry to alkynyl sulfides and thioethers.

A particularly interesting ynamine derivative **5.022** studied by the authors displays an alternate outcome to this (3+2) reactivity leading to fused quinoline **5.025** instead (Figure 5-8). The authors propose that breakage of a C-N bond in the indolium ylide **5.023** provides the vinylidene species **5.024**, which can then undergo C-H insertion to provide the observed product **5.025**. Equilibrium towards the carbene **5.024** is likely favoured in this scaffold due to reintroduction of aromaticity to the indole group.

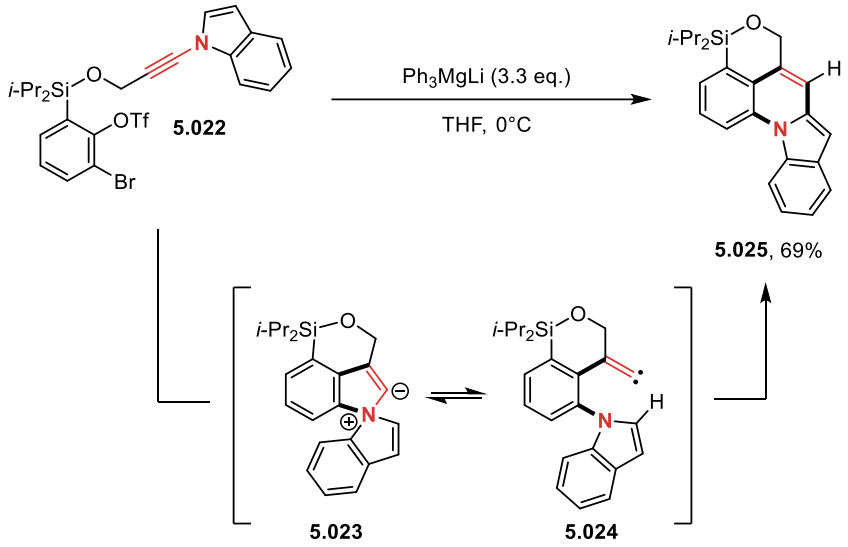

Figure 5-8. A new reaction outcome for indole-derived ynamines.

Unexpectedly, the authors observed the major formation of 2-phenyl indole product **5.026** when using a different benzyne-forming strategy, alongside a small amount of the 2-sulfonyl indole **5.027** (Figure 5-9). By using the probe **5.028**, known to produce vinylidene intermediates of type **5.029** under the same reaction conditions, the authors were able to verify that the same type of 2-phenyl indole product **5.030** could be produced from analogous vinylidene intermediate. For this reason, the authors propose attack of the nucleophilic phenyl group onto the carbene, and an unusual substitution directly on nitrogen.

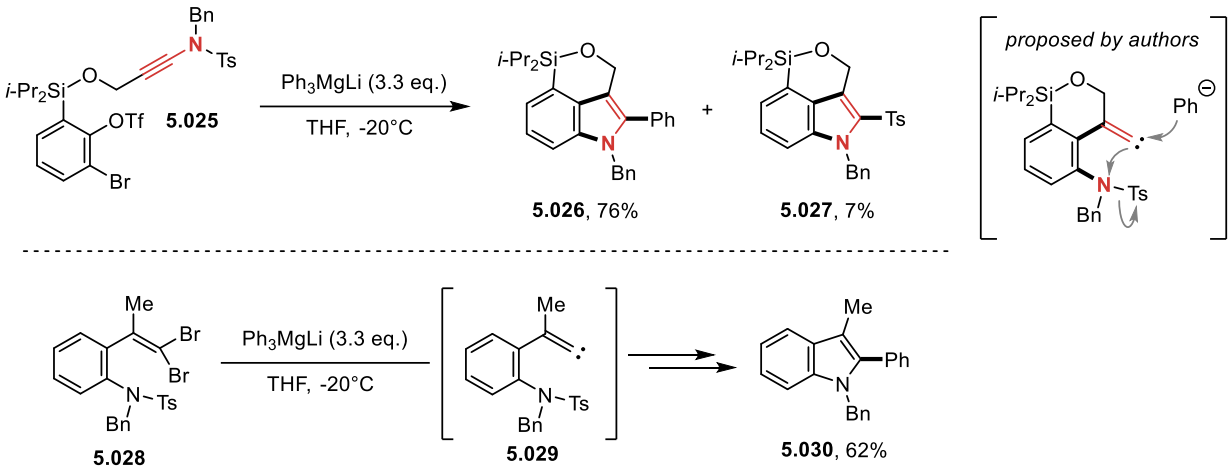

Figure 5-9. Functionalized indoles produced with a different benzyne precursor strategy.

It could be conceived however that *ipso*-substitution by a nucleophilic phenyl species to displace the sulfone group in **5.027** may be a more reasonable pathway; this was not verified by the authors.

5.2. Thermal (3+2) reactivity within the context of diyne-initiated diradical reactions

Upon first locating a favourable diradical pathway during our DFT studies, it was immediately apparent that there was a strong link between the (3+2) chemistry described herein, and the tetra- and hexadehydro Diels-Alder reactions (TDDA and HDDA).

The tetradehydro Diels-Alder reaction involving tethered diynes has been thoroughly explored in recent times by the group of Wessig, and the same group have written a review on the subject.[4] The group of Hoye has a longstanding research program on the HDDA reaction, and have also reviewed this topic.[5]

It is generally proposed, for both TDDA and HDDA, that tethered di-yne species of type **5.031**, upon heating, generate diradical species **5.032** (Figure 5-10). In the case of TDDA, a conjugated alkene group mediates the ring closure to form a strained 6-membered cyclic allene **5.033**. For HDDA, a conjugated alkyne plays a similar role to provide instead a benzyne species **5.034**. From the work done in this thesis, we can now supplement this reaction paradigm with the case of conjugated heteroatoms, which mediate the ring closure to form heteroarylium ylides **5.035**.

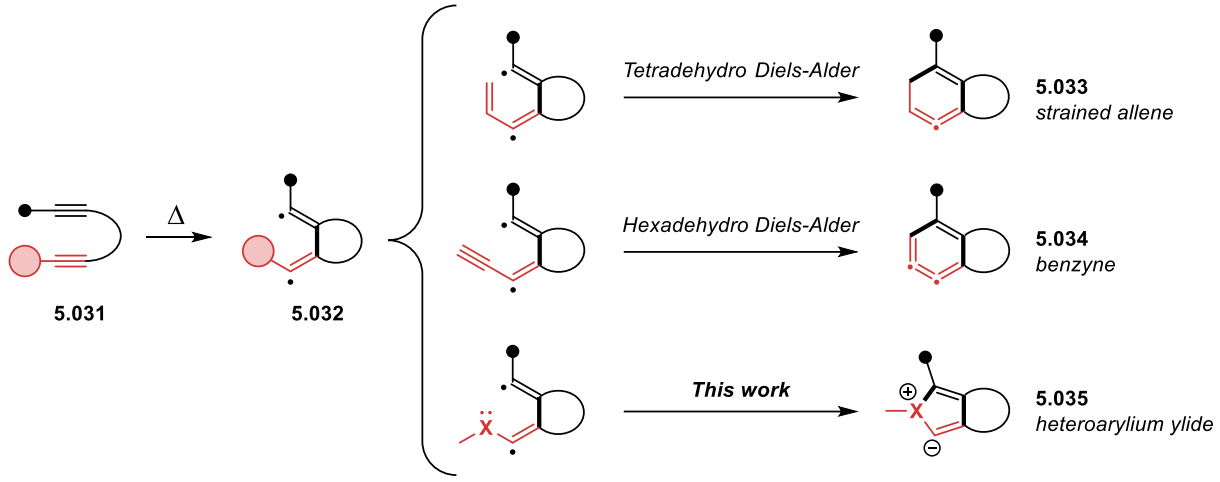

Figure 5-10. Possible outcomes of di-yne-based diradical intermediates.

The rate limiting step in the TDDA, HDDA, and (3+2) variants is the formation of diradical species **5.032**. It is unsurprising then that limitations on the linker structure observed for the intramolecular TDDA and HDDA reactions (3-4 atom linkers only) and the high temperatures required (typically >100 °C) are both very similar to that observed in the thermal (3+2) reactivity described in this thesis.

It is interesting to note that the scaffolds **5.036** and **5.039** studied in this thesis, which could possibly lead to TDDA and HDDA products **5.038** and **5.041**, provided only pyrroles **5.037** and **5.040** as major products (Figure 5-11). This seems to indicate that the diradical ring closure occurs more rapidly through a (3+2) process than the alternative TDDA and HDDA routes.

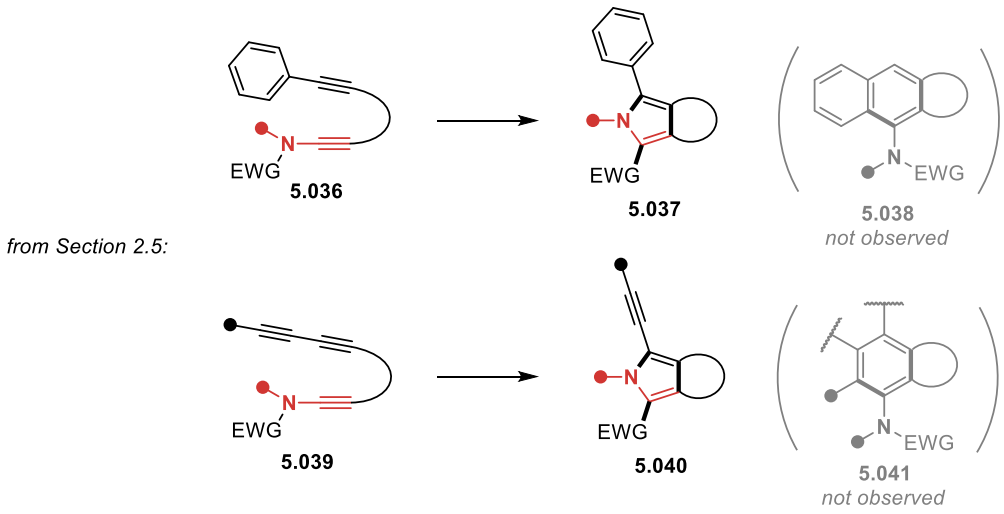

Figure 5-11. (3+2) outcome seemingly faster than TDDA and HDDA.

Although rates of competitive TDDA and HDDA reactions have never been systematically studied to the best of my knowledge, enyne-diyne scaffolds of the type **5.042** typically provide TDDA products as the observed outcome. In a particularly telling example, Domínguez, Saá and coworkers demonstrated in 2000 that the highly constrained scaffold **5.042** provided a 98% yield of the TDDA product **5.043** (Figure 5-12).[6] This leaves little doubt that the TDDA outcome is more favourable than the HDDA.

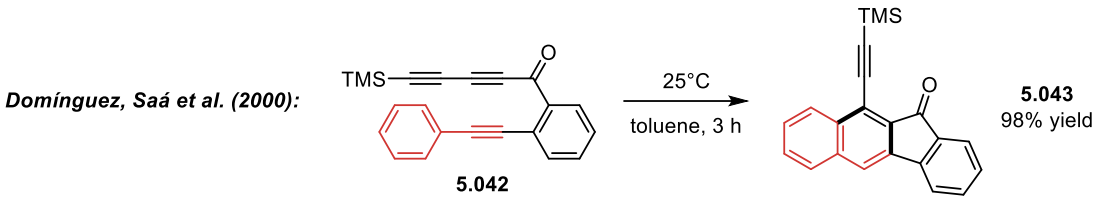

Figure 5-12. TDDA outcome favoured in studies by Domínguez, Saá and coworkers.

Given the results in this thesis and information taken from literature, the rates of diradical ring closure in (3+2), TDDA, and HDDA processes can be ranked in decreasing order (Figure 5-13).

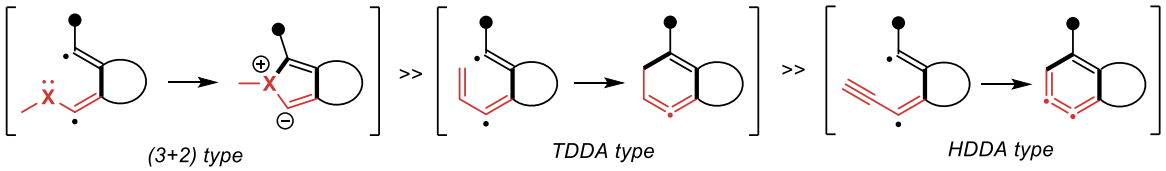

Figure 5-13. Relative rates of diradical ring closure processes based on empirical evidence.

5.3. Possible future directions

The most obvious shortfall of the chemistry described in this thesis is its intramolecular nature. These new unique strategies towards pyrroles and thiophenes would be rendered much more valuable if they were applicable towards structures that are not necessarily fused. So, an important avenue for future studies would be the development of methodologies enabling the *intermolecular* (3+2) reactivity between heteroatom-substituted alkynes and alkynes.

At first glance, the similarity between limitations within this (3+2) chemistry and that of TDDA and HDDA reactions would suggest that the *intermolecular* reaction would be extremely difficult to access. In fact, our own tests on the matter only led to failure, even when heating the appropriate reagents together *neat* at high temperatures.

There are however some unknowns in the structural parameters affecting the rate of the (3+2) chemistry observed (Figure 5-14). From this thesis, the effects of substitution on the terminal alkyne

position and nature of the linker structure on the rate of the reaction are well understood. On the other hand, the effect of substitution and nature of the amide or sulfide group on the rate of (3+2) reactivity has not been studied. The nature of the group directly attached on the linker end of both alkynyl species has also not been systematically studied, yet is likely to have a strong impact on the rate of the reaction.

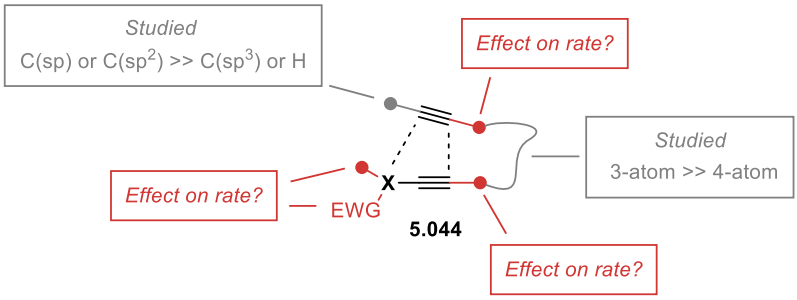

Figure 5-14. Unknown structural parameters affecting the rate of (3+2) reactivity.

By identifying new alkyne and heteroatom-substituted alkyne derivatives that have higher reactivity in the intramolecular version of the (3+2) reaction, a better "starting point" might be envisaged for testing the intermolecular version.

It is clear however that, even if possible, thermal intermolecular reactivity will only be obtained under specific structural requirements. This approach would have its own scope limitations.

Some alternative strategies may permit to obtain formal variants of an intermolecular (3+2) reactivity (Figure 5-15). For example, certain functional group pairings could be used to maintain a temporary covalent bond during a (3+2) event, and be subsequently cleaved. This would provide a "formal" intermolecular process expanding the scope to non-fused heterocycles. This strategy has been used by the Hoye group towards HDDA reactions with "traceless" sulfide-based linker groups.[7] Yamamoto and coworkers used a boron tether strategy to link alkyne groups in a metal-catalyzed (2+2+2) alkyne trimerization reaction.[8] The use of silicon-based tethers could also be envisaged.[9]

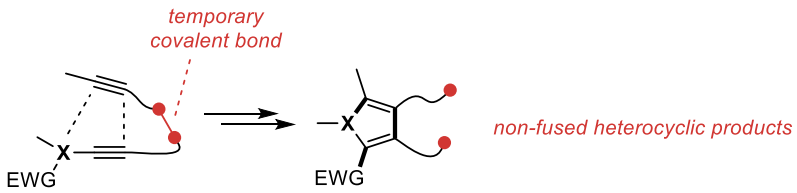

Figure 5-15. The temporary tether strategy for formal intermolecular (3+2) cyclizations.

For this strategy as well, the need to use very specific tethers will also present its own scope limitations. Further chemical transformations would be needed to diversify the 3 and 4 positions of the resulting heterocycles.

Access to an intermolecular (3+2) cyclization may perhaps be achieved with further improvements on the catalytic conditions developed in Chapter 4.

As discussed along with the scope of catalyzed (3+2) reactions involving longer linker structures (see Section 4.5), a significant amount of catalyst degradation in the form of metallic copper could be observed at higher temperatures. The classical approach to reducing metal catalyst degradation is the use of tightly bound ligands. It could be hypothesized then that intermolecular reactivity may be achieved at *higher temperatures*, should the active catalyst persist with use of the proper ligand.

There are subtleties that may render this strategy more difficult, however. Bulky (and thermally stabilizing) ligands, such as IPr, were found to drastically reduce the rate of catalysis observed. In order to get a hit on intermolecular reactivity, the use of high-throughput experimentation may enable the evaluation of large libraries of ligands known to form stable complexes with copper(I).

At the moment, however, the steric and electronic requirements around copper that permit complexation to the alkynyl sulfide are not well understood. In order to include some logic in the choice of ligands investigated, a more organometallic approach may be employed. Synthesis of ligated and well-defined mono- and dinuclear copper acetylides, and analysis of the species obtained in the presence of alkynyl sulfides may permit to gain a better understanding of the interactions involved between these two units (Figure 5-16).

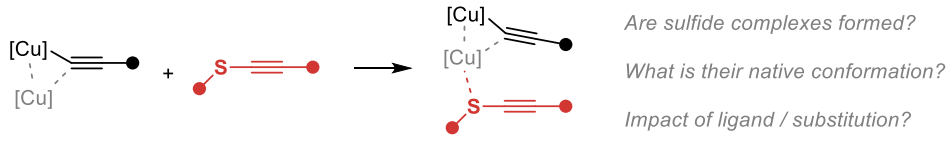

Figure 5-16. Studying the interaction between alkynyl sulfides and metal acetylides.

5.4. Concluding remarks

In this thesis, it was shown that heteroatom-substituted alkynes can participate in (3+2) cycloadditions with tethered alkynes **5.045** to form zwitterionic cycloadducts **5.046** (Figure 5-17). Although the overall cycloaddition is reminiscent of 1,3-dipolar cycloadditions, its kinetic parameters are more closely tied to cycloaddition reactions of poly-ynes, such as TDDA and HDDA.

This proposed ylide evolves into a variety of products **5.048**, **5.049**, **5.051** or **5.052** depending strongly on the substrate structure and reaction conditions. Thiophenium salt intermediates **5.050** can be accessed under milder conditions using copper or silver catalysis.

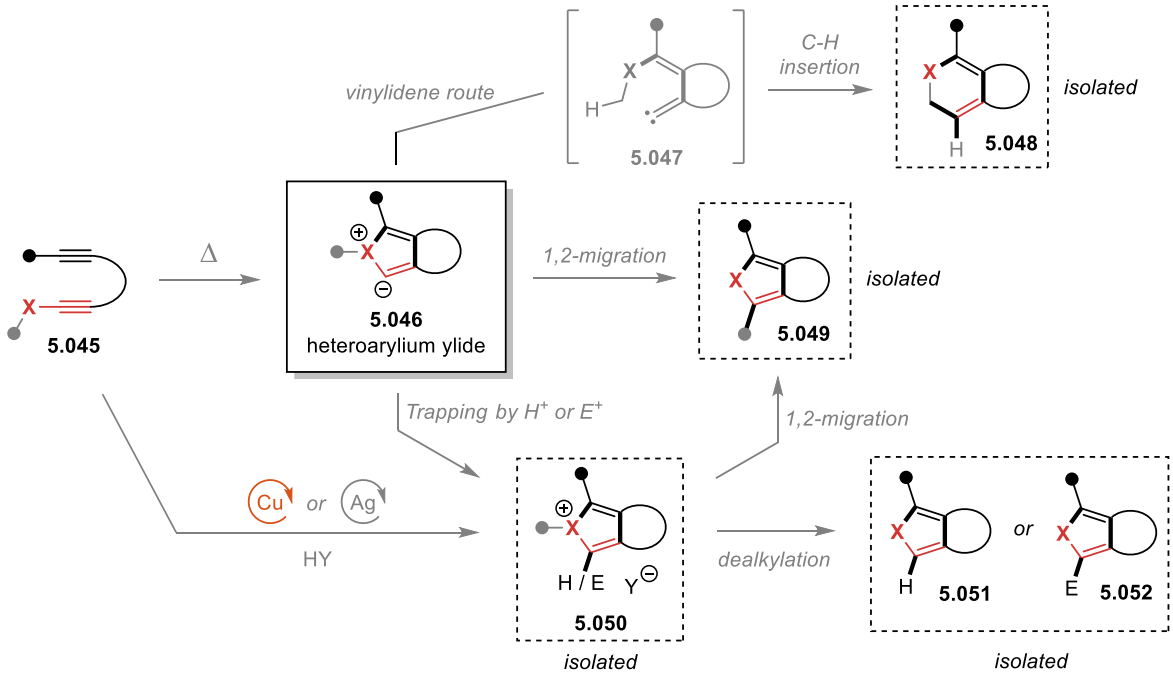

Figure 5-17. Overview of discovered routes in the (3+2) reactivity of scaffold **5.045**.

It is surprising that all the chemistry described in this thesis derives from a single observation of a curious by-product during the synthesis of an ynamide derivative. Along the way, it seemed to be happenstance that other completely unexplored modes of reactivity were identified as well. In hindsight, this is surely associated with the more obscure nature of the species investigated. To this day, ynamides and alkynyl sulfides are comparatively little studied building blocks. Despite their ease of synthesis and stability, only a handful of ynamides can be bought (at high prices!) and no alkynyl sulfide is commercially available. Recent advances in the synthesis of these two classes of building blocks have greatly enabled the work described in this thesis, as the majority of the scaffolds studied were synthesized from complex ynamide and alkynyl sulfide derivatives possessing functional groups as diversifiable synthetic handles. It is gratifying to know that new reactivity patterns in organic chemistry can still be learned from such exotic building blocks.

5.5. Chapter references

1. Campeau, D.; Pommainville, A.; Gagosz, F., Ynamides as Three-Atom Components in Cycloadditions: An Unexplored Chemical Reaction Space. *J. Am. Chem. Soc.* **2021,** *143* (25), 9601-9611.
2. Smith, P. J.; Jiang, Y.; Tong, Z.; Pickford, H. D.; Christensen, K. E.; Nugent, J.; Anderson, E. A., Synthesis of Polysubstituted Fused Pyrroles by Gold-Catalyzed Cycloisomerization/1,2-Sulfonyl Migration of Yndiamides. *Org. Lett.* **2021,** *23* (16), 6547-6552.
3. Tawatari, T.; Kato, R.; Kudo, R.; Takasu, K.; Takikawa, H., Intramolecular Ynamide–Benzyne (3+2) Cycloadditions. *Angew. Chem. Int. Ed.* **2023,** *62* (19), e202300907.
4. Wessig, P.; Müller, G., The Dehydro-Diels–Alder Reaction. *Chem. Rev.* **2008,** *108* (6), 2051-2063.
5. Fluegel, L. L.; Hoye, T. R., Hexadehydro-Diels–Alder Reaction: Benzyne Generation via Cycloisomerization of Tethered Triynes. *Chem. Rev.* **2021,** *121* (4), 2413-2444.
6. Rodríguez, D.; Navarro, A.; Castedo, L.; Domínguez, D.; Saá, C., Intramolecular [4 + 2] Cycloaddition Reactions of Diarylacetylenes: Synthesis of Benzo[b]fluorene Derivatives via Cyclic Allenes. *Org. Lett.* **2000,** *2* (11), 1497-1500.
7. Smela, M. P.; Hoye, T. R., A Traceless Tether Strategy for Achieving Formal Intermolecular Hexadehydro-Diels–Alder Reactions. *Org. Lett.* **2018,** *20* (17), 5502-5505.
8. Yamamoto, Y.; Ishii, J.-i.; Nishiyama, H.; Itoh, K., Ru(II)-Catalyzed Chemo- and Regioselective Cyclotrimerization of Three Unsymmetrical Alkynes through Boron Temporary Tether. One-Pot Four-Component Coupling via Cyclotrimerization/Suzuki−Miyaura Coupling. *J. Am. Chem. Soc.* **2004,** *126* (12), 3712-3713.
9. Bols, M.; Skrydstrup, T., Silicon-Tethered Reactions. *Chem. Rev.* **1995,** *95* (5), 1253-1277.

6. Supporting information

6.1. General information

On reagents, solvents, and materials:

Commercially available reagents were purchased from Sigma-Aldrich, Alfa-Aesar, Oakwood Chemicals, TCI America, Fluorochem Chemical or Combi-Blocks suppliers and were used as delivered without further purification unless otherwise noted. Reactions carried out under inert atmosphere were performed under nitrogen gas. Thin layer chromatography was performed on TLC Silicagel 60 F254 plates. Flash column chromatography was carried out on silica gel using a forced flow of eluents.

On collection of NMR & MS data:

NMR spectra were recorded at room temperature in the given deuterated solvent on a Bruker Avance II 400, Bruker Avance II 300, Bruker Avance 300, Bruker Avance III 500, or Bruker Avance III 600 instrument operating at the indicated frequency. Chemical shifts (δ) are given in parts per million (ppm) using $CHCl_3$ and $CDCl_3$ solvent peaks as the reference for ^{1}H-NMR and ^{13}C-NMR spectra, respectively. Signal multiplicities are depicted using the following abbreviations: s = singlet, d = doublet, t = triplet, q = quartet, p = pentuplet, sex = sextuplet, sept = septuplet, m = multiplet, dd = doublet of doublet, dt = doublet of triplet, tt = triplet of triplet, dq = doublet of quartet, ddd = doublet of doublet of doublet, ddt = doublet of doublet of triplet, bs = broad singlet.

^{77}Se spectra were collected with ^{1}H decoupling, and the IUPAC recommendation of an internal TMS standard signal in the ^{1}H NMR spectrum for chemical shift referencing in the selenium spectrum was used.

High-resolution mass spectrometry by electron impact (HRMS-EI) was performed on a JEOL JMCGCmate II mass spectrometer, and high-resolution mass spectrometry by electrospray ionization (HRMS-ESI) was performed on a Micromass Q-TOF II Mass Spectrometer. Low resolution mass spectra were obtained on an Advion ExpressIon CMS spectrometer using an APCI or ESI probe, as indicated. Molecular ion and/or fragment signals were given in mass per charge number (m/z).

Routine building blocks in this Supporting Information document have been characterized by ^{1}H and ^{13}C NMR, while all investigated (3+2) cyclization substrates and heterocyclic products have been characterized by ^{1}H NMR, ^{13}C NMR & HRMS.

Due to the often fragmenting nature of the poly-yne substrates leading to low molecular ion [M]+ intensities, either of the consistently observed [M-H]+ or [M-alkyl group]+ fragments were used as characteristic HRMS-EI signals for these substrates when the molecular ion could not be adequately obtained.

6.2. Supporting information for Chapter 2

The synthesis of selected scope examples is detailed herein. For synthetic details on all the examples discussed in Chapter 2, please refer to the original publication:

> [Campeau, D.; Pommainville, A.; Gagosz, F., Ynamides as Three-Atom Components in Cycloadditions: An Unexplored Chemical Reaction Space. *J. Am. Chem. Soc.* **2021**, *143* (25), 9601-9611].

6.2.1. Preparation of yne-ynamides

*Standard procedure **SP1**:*

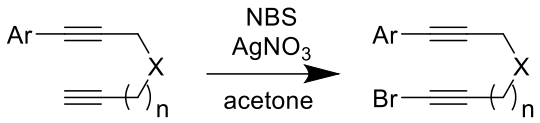

In a round bottom flask, di-ynes were dissolved in acetone (0.3 M). To flask was added *N*-bromosuccinimide (1.1 eq) and silver nitrate (0.1 eq). The reaction mixture was stirred at room temperature for 15 minutes, or until consumption of the di-yne by TLC analysis. The mixture was then filtered through celite using EtOAc as the eluent. The filtrate was then concentrated under reduced pressure to give a crude. The crude was purified by silica gel chromatography using indicated eluent system to yield the desired pure bromoalkyne.

2.012

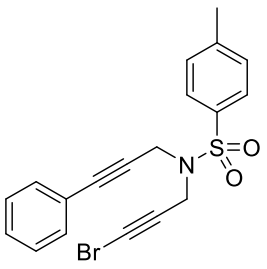

Using standard procedure ***SP1*** with 7.18 mmol of 4-methyl-*N*-(3-phenylprop-2-yn-1-yl)-*N*-(prop-2-yn-1-yl)benzenesulfonamide[3]. Reaction time = 20 min. Solvent system = Hexanes/EtOAc 7:3. Produced 1.53 g (53% yield) as a white solid.

[3] Prepared as previously reported by: Strom, K.R.; Impastato, A.C.; Moy, K.J.; Landreth, A.J.; Snyder, J.K. *Org. Lett.* **2015**, 17 (*9*), 2126 – 2129.

^{1}H NMR (400 MHz, $CDCl_3$) δ 7.75 (d, *J* = 8.3 Hz, 2H), 7.35 – 7.23 (m, 5H), 7.23 – 7.18 (m, 2H), 4.36 (s, 2H), 4.23 (s, 2H), 2.37 (s, 3H).

^{13}C NMR (101 MHz, $CDCl_3$) δ 144.1, 135.3, 131.8, 129.7, 128.7, 128.3, 128.1, 122.2, 86.1, 81.5, 73.0, 45.6, 37.9, 37.7, 21.6.

SI-2.003

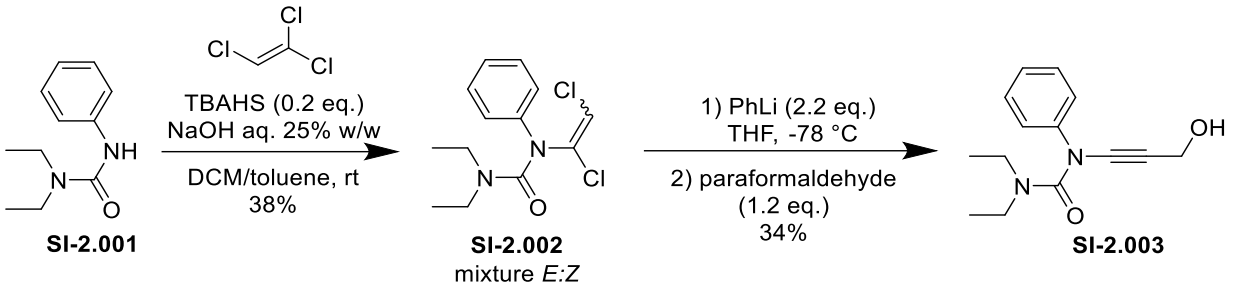

SI-2.001 **SI-2.002** mixture *E:Z* **SI-2.003**

To a mixture of urea **SI-2.001** (195 mg, 1.01 mmol, 1.00 eq) and tetrabutylammonium hydrogensulfate (68 mg, 0.20 mmol, 0.20 eq) in DCM (2.5 mL) and toluene (3 mL) was added 25% w/w aq. NaOH solution (3 mL). The mixture was stirred vigorously at room temperature for 15 min. Trichloroethylene (0.27 mL, 3.0 mmol, 3.0 eq) was added via syringe pump over 30 min. The reaction mixture was then stirred overnight to completion. The aqueous layer was extracted three times with Et_2O, and the combined organic fractions were washed once with brine, and then dried using $MgSO_4$. The organic phase was then concentrated under reduced pressure to produce a crude. The crude was then purified via flash chromatography, using hexanes/Et_2O 4:1, to yield 110 mg (38% yield) of dichloroenamide **SI-2.002** as a beige solid. The product is a 1:1.6 mixture of stereoisomers. **^{1}H NMR** (300 MHz, $CDCl_3$) δ 7.46 – 7.27 (m, $2H_A$ & $2H_B$), 7.25 – 7.15 (m, $1H_A$ & $1H_B$), 7.15 – 7.05 (m, $2H_A$ & $2H_B$), 6.32 (s, $1H_A$), 6.22 (s, $1H_B$), 3.31 (q, *J* = 7.1 Hz, $4H_B$), 3.28 (q, *J* = 7.2 Hz, $4H_A$), 1.08 (t, *J* = 7.2 Hz, $6H_A$), 1.05 (t, *J* = 7.2 Hz, $6H_B$).

In a flame-dried round bottom flask under N_2 atmosphere was cooled a stirred solution of dichloroenamide **SI-2.002** (105 mg, 0.366 mmol, 1.00 eq) in dry THF (3.7 mL, 0.1 M) to -78 °C. PhLi (0.42 mL, 1.9 M in dibutyl ether, 0.805 mmol, 2.20 eq) was added dropwise over 10 min. The solution was then stirred at -78 °C for 1 h. Paraformaldehyde (13.2 mg, 0.439 mmol, 1.20 eq) was added at -78 °C, and the reaction mixture was stirred and slowly warmed to room temperature, until the end of the reaction as determined by TLC analysis. The mixture was then quenched with water, and

extracted with EtOAc. The organic phase was dried using $MgSO_4$, filtered, and concentrated under reduced pressure to produce a crude. The crude was then purified via flash chromatography, using a 7:3 → 3:2 gradient of hexanes/EtOAc, to yield 30.4 mg (34% yield) of ynamide **SI-2.003** as a yellow oil. **^{1}H NMR** (400 MHz, $CDCl_3$) δ 7.37 – 7.29 (m, 2H), 7.28 – 7.22 (m, 2H), 7.13 (tt, *J* = 7.0, 1.2 Hz, 1H), 4.49 (d, *J* = 6.0 Hz, 2H), 3.44 (q, *J* = 7.1 Hz, 4H), 1.81 (t, *J* = 5.9 Hz, 1H), 1.21 (t, *J* = 7.1 Hz, 6H). **^{13}C NMR** (101 MHz, $CDCl_3$) δ 156.7, 141.5, 129.2, 124.8, 120.8, 81.5, 69.6, 51.6, 42.7, 13.3.

*Standard procedure **SP2a** – Hsung's method*[4]

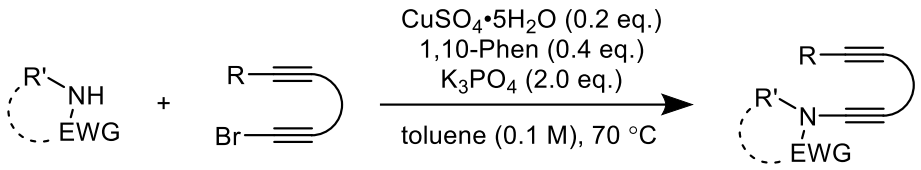

In a flame-dried round bottom flask was added the sulfonamide (0.500 mmol, 1.00 eq), bromoalkyne (0.650 mmol, 1.30 eq), $CuSO_4$-$5H_2O$ (0.1 mmol, 0.2 eq), 1,10-phenanthroline (0.2 mmol, 0.4 eq) and K_3PO_4 (1.0 mmol, 2.0 eq). Three cycles of vacuum/purging with N_2 were done to render the flask inert. Dry toluene (5.0 mL, 0.1 M) was added via syringe. The reaction mixture was stirred at 70 °C until full consumption of the substrate by TLC analysis. The mixture was then filtered through celite using EtOAc as the eluent. The filtrate was then concentrated under reduced pressure to produce a crude. The crude was then purified via flash chromatography, using the indicated solvent system, to yield the pure ynamide.

*Standard procedure **SP2b** – Substitution reaction*

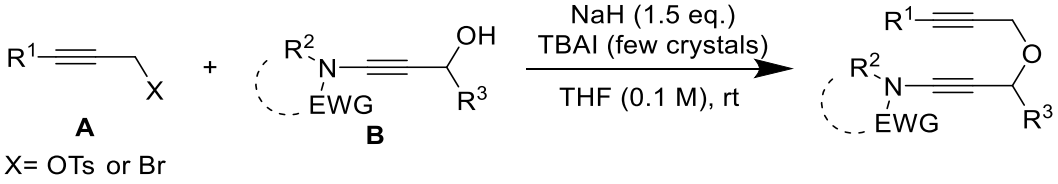

In a flame-dried round bottom flask under N_2 atmosphere was added a solution of propargyl bromide **A** (0.100 mmol, 1.00 eq), ynamide **B** (0.100 mmol, 1.00 eq) and a few crystals of tetrabutylammonium iodide in dry THF (1.0 mL, 0.1 M). To the stirred solution at room temperature was quickly added NaH

[4] Procedure based on: Hsung, R.P. *et al. Organic Letters.* **2004**, 6 (*7*), 1151–1154.

(60% w/w, 0.150 mmol, 1.50 eq). The reaction mixture was stirred until full consumption of the substrate was observed by TLC analysis. The mixture was diluted with EtOAc, and washed three times with water, then once with brine. The organic phase was dried using $MgSO_4$, and then concentrated under reduced pressure to produce a crude. The crude was then purified via flash chromatography, using the indicated solvent system, to yield the pure ynamide.

*Standard procedure **SP2c** – Stahl's method*[5]

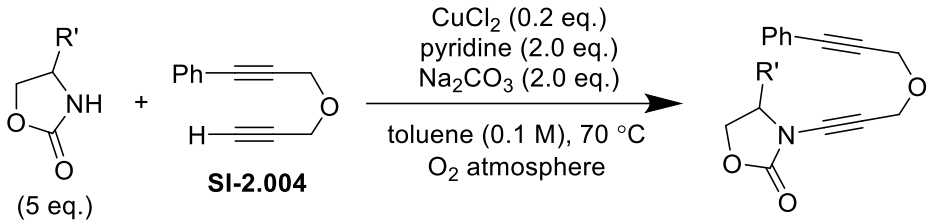

In a flame-dried round bottom flask was added $CuCl_2$ (0.0400 mmol, 0.20 eq), the oxazolidinone (1.00 mmol, 5.00 eq) and Na_2CO_3 (0.400 mmol, 2.00 eq). Three cycles of vacuum/purging with O_2 were done and an O_2 balloon was added. A solution of pyridine (0.400 mmol, 2.00 eq) in half the dry toluene (5.0 mL) was added via syringe. The reaction mixture was stirred and heated to 70 °C. A solution of the diyne **SI-2.004**[6] (0.200 mmol, 1.00 eq) in half the dry toluene (5.0 mL) was added via syringe pump over 4 h. The reaction mixture was directly loaded onto a flash chromatography column for purification, using the indicated solvent system, to yield the isolated ynamide.

2.014a

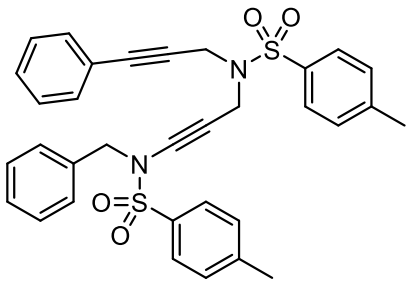

Using standard procedure ***SP2a*** with 1.94 mmol of *N*-benzyl-4-methylbenzenesulfonamide and bromoalkyne **2.012**. Reaction time = 2 h. Solvent system = Hexanes/EtOAc gradient of 4:1 → 7:3. Produced 543 mg (48% yield) of a white solid.

^{1}H NMR (400 MHz, $CDCl_3$) δ 7.73 – 7.65 (m, 4H), 7.34 – 7.20 (m, 10H), 7.20 – 7.14 (m, 4H), 4.39 (s, 2H), 4.23 (s, 2H), 4.04 (s, 2H), 2.41 (s, 3H), 2.33 (s, 3H).

[5] Procedure based on: Hamada, T.; Ye, X.; Stahl, S.S. *J. Am. Chem. Soc.* **2008**, 130 (*3*), 833–835.
[6] Prepared as described in literature: Chang, H.-T.; Jeganmohan, M.; Cheng, C.-H. *Org. Lett.* **2007**, 9 (*3*), 505 – 508.

^{13}C NMR (101 MHz, $CDCl_3$) δ 144.8, 143.8, 135.1, 134.6, 134.2, 131.6, 129.8, 129.6, 128.7, 128.6, 128.5, 128.4, 128.2, 127.8, 127.6, 122.2, 85.8, 81.4, 79.1, 64.6, 55.3, 37.0, 36.7, 21.6, 21.5.

HRMS-ESI : Calculated for $C_{33}H_{30}N_2O_4S_2$ [M+Na]$^+$: 605.1539; found: 605.1547.

2.014ah

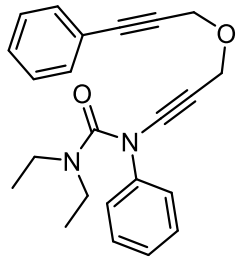

Using standard procedure ***SP2b*** with 0.123 mmol of **SI-2.004** and (3-bromoprop-1-yn-1-yl)benzene. Reaction time = 0.75 h. Solvent system = Hexanes/EtOAc 4:1. Produced 24.2 mg (55% yield) of a pale yellow oil.

^{1}H NMR (400 MHz, $CDCl_3$) δ 7.48 – 7.41 (m, 2H), 7.39 – 7.24 (m, 7H), 7.17 – 7.09 (m, 1H), 4.57 (s, 2H), 4.50 (s, 2H), 3.48 (q, *J* = 7.1 Hz, 4H), 1.23 (t, *J* = 7.1 Hz, 6H).

^{13}C NMR (101 MHz, $CDCl_3$) δ 156.6, 141.4, 131.9, 129.1, 128.7, 128.4, 124.8, 122.6, 120.8, 86.8, 84.6, 82.4, 66.8, 57.5, 56.9, 42.7, 13.4.

HRMS-ESI : Calculated for $C_{23}H_{24}N_2O_2$ [M+Na]$^+$: 383.1730; found: 383.1758.

2.014ai

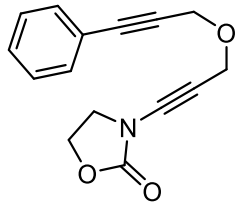

Using standard procedure ***SP2c*** with 1.00 mmol of oxazolidin-2-one. Reaction time = 4 h. Solvent system = Hexanes/EtOAc 3:2. Produced 12.0 mg (23% yield) of a beige oil.

^{1}H NMR (400 MHz, $CDCl_3$) δ 7.49 – 7.40 (m, 2H), 7.37 – 7.27 (m, 3H), 4.47 (s, 2H), 4.46 (s, 2H), 4.46 – 4.41 (m, 2H), 3.99 – 3.86 (m, 2H).

^{13}C NMR (101 MHz, $CDCl_3$) δ 156.2, 131.9, 128.7, 128.4, 122.5, 86.9, 84.4, 76.8, 67.5, 63.2, 57.5, 57.2, 46.8.

HRMS-ESI : Calculated for $C_{15}H_{13}NO_3$ [M+Na]$^+$: 278.0788; found: 278.0813.

6.2.2. (3+2) Thermal rearrangement to pyrroles

*Standard procedure **SP3** – General procedure for rearrangement*

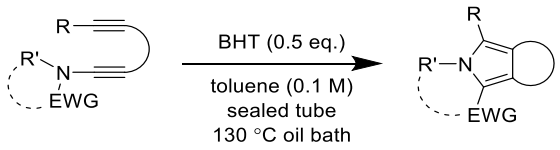

In a sealed vial or sealed NMR tube was added the ynamide (0.0500 mmol, 1.00 eq), BHT (0.0250 mmol, 0.500 eq) and dry toluene (0.5 mL, 0.1 M)[7]. The tube was shaken vigorously before placing in an oil bath pre-heated to 130 °C. The reaction was followed by TLC or ^{1}H NMR analysis until full consumption of the substrate. The reaction mixture was then concentrated under reduced pressure to produce a crude mixture. The crude mixture was then purified via flash chromatography, using the indicated solvent system, to yield the pure pyrrole.

2.015a

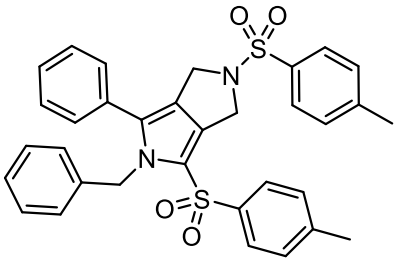

Using standard procedure ***SP3*** with 0.0360 mmol of ynamide **2.014a**. Reaction time = 1.5 h. Solvent system = Hexanes/EtOAc 7:3. Produced 18.9 mg (90% yield) of a white solid.

^{1}H NMR (400 MHz, $CDCl_3$) δ 7.80 (d, *J* = 8.2 Hz, 2H), 7.39 – 7.32 (m, 4H), 7.32 – 7.27 (m, 3H), 7.12 – 7.07 (m, 2H), 7.04 (t, *J* = 7.3 Hz, 1H), 7.00 – 6.92 (m, 4H), 6.45 (d, *J* = 7.6 Hz, 2H), 5.36 (s, 2H), 4.79 (t, *J* = 1.2 Hz, 2H), 4.44 (t, *J* = 1.2 Hz, 2H), 2.45 (s, 3H), 2.30 (s, 3H).

^{13}C NMR (101 MHz, $CDCl_3$) δ 143.8 (x2), 138.5, 137.2, 134.3, 132.8, 132.1, 130.0, 129.9, 129.6, 129.1, 129.0, 129.0, 128.4, 127.8, 127.1, 126.8, 125.5, 122.7, 121.2, 50.1, 48.9, 48.7, 21.7, 21.6.

HRMS-EI : Calculated for $C_{33}H_{30}N_2O_4S_2$ $[M]^+$: 582.1647; found: 582.1648.

2.015ah

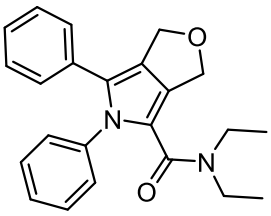

Using standard procedure ***SP3*** with 0.0338 mmol of ynamide **2.014ah**. Reaction time = 4.5 h. Solvent system = Hexanes/EtOAc gradient of 3:2 → 1:1. Produced 8.9 mg (64% yield) of a brown oil.

[7] For reactions followed by ^{1}H NMR, toluene-d_8 was instead used as solvent, and 3.5μL of mesitylene or 2.0μL 1,2-dichloroethane was added as internal standard.

^{1}H NMR (400 MHz, $CDCl_3$) δ 7.34 – 7.27 (m, 3H), 7.24 – 7.09 (m, 5H), 6.98 – 6.91 (m, 2H), 5.03 (t, *J* = 1.4 Hz, 2H), 4.97 (t, *J* = 1.4 Hz, 2H), 3.28 (q, *J* = 7.1 Hz, 4H), 0.95 (t, *J* = 7.1 Hz, 6H).

^{13}C NMR (101 MHz, $CDCl_3$) δ 163.5, 138.9, 131.9, 129.0, 128.4, 128.1, 127.8 (x3), 127.5, 126.6, 125.0, 119.9, 68.2, 67.7, 53.6, 13.4.

HRMS-EI : Calculated for $C_{23}H_{24}N_2O_2$ $[M]^+$: 360.1832; found: 360.1863.

2.015ai

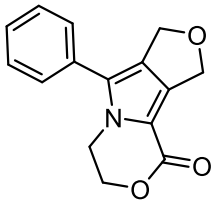

Using standard procedure ***SP3*** with 0.0470 mmol of ynamide **2.014ai**. Reaction time = 2.5 h. Solvent system = Hexanes/EtOAc 1:1. Produced 8.7 mg (72% yield) of a white solid.

^{1}H NMR (400 MHz, $CDCl_3$) δ 7.48 (tt, *J* = 8.1, 1.5 Hz, 2H), 7.43 – 7.37 (m, 1H), 7.37 – 7.30 (m, 2H), 5.14 (t, *J* = 1.8 Hz, 2H), 4.98 (t, *J* = 1.8 Hz, 2H), 4.65 – 4.53 (m, 2H), 4.33 – 4.20 (m, 2H).

^{13}C NMR (101 MHz, $CDCl_3$) δ 158.9, 137.2, 130.1, 129.3, 128.7, 128.7, 128.2, 128.0, 110.5, 68.8, 68.1, 66.5, 42.8.

HRMS-EI : Calculated for $C_{15}H_{13}NO_3$ $[M]^+$: 255.0890; found: 255.0904.

6.2.3. Scaled-up synthesis of pyrrole 2.015a

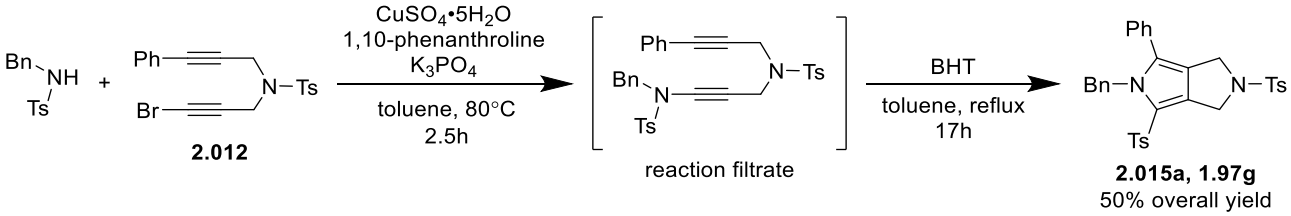

In a flame-dried round bottom flask was added *N*-benzyl-4-methylbenzenesulfonamide (1.75 g, 6.71 mmol, 1.00 eq), bromoalkyne **2.012** (2.70 g, 6.71 mmol, 1.00 eq), $CuSO_4$-$5H_2O$ (335 mg, 1.34 mmol, 0.200 eq), 1,10-phenanthroline (483 mg, 2.68 mmol, 0.400 eq) and K_3PO_4 (2.84 g, 13.4 mmol, 2.00 eq). Toluene (50 mL, 0.1 M) was added and the reaction mixture was stirred at 80 °C for 2.5 h. The mixture was then filtered through a

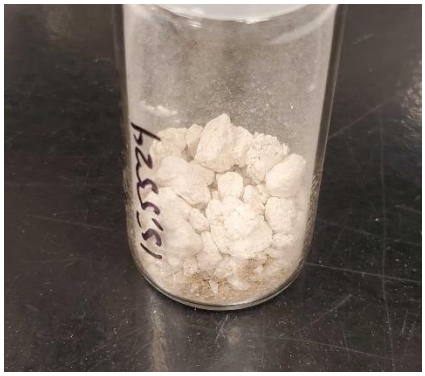

short pad of silica and eluted with a small quantity of EtOAc. BHT (1.48 g, 6.71 mmol, 1.00 eq) was added to the filtrate, which was then directly brought to reflux for 17 h (overnight). Once the reaction done, the mixture was cooled to room temperature to induce precipitation of the product, then to 0 °C before directly filtering it off to give 1.97 g of pure **2.015a** as a brittle white solid.

6.2.4. One-pot condensation / (3+2) rearrangement

*Standard procedures **SP4a** & **SP4b**: Preparation of amidopropynals*

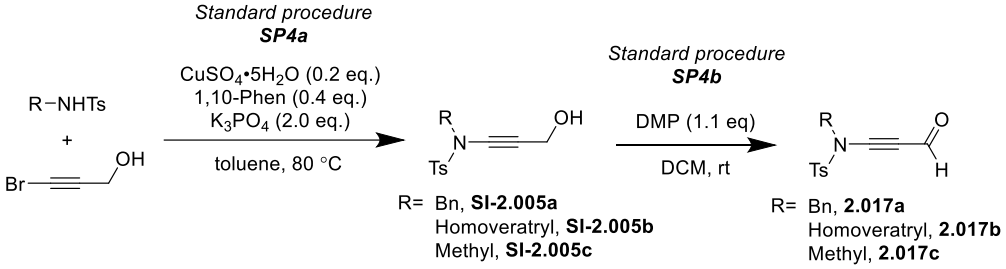

SP4a. In a flame-dried round bottom flask was added a sulfonamide (3.00 mmol, 1.00 eq), $CuSO_4$-$5H_2O$ (0.60 mmol, 0.20 eq), 1,10-phenanthroline (1.2 mmol, 0.40 eq) and K_3PO_4 (6.00 mmol, 2.00 eq). Three cycles of vacuum/purging with N_2 were done to render the flask inert. A solution of 3-bromoprop-2-yn-1-ol (3.0 mmol, 1.0 eq) in toluene (10 mL, 0.3 M) was added via syringe. The reaction mixture was stirred at 80 °C until full consumption of the sulfonamide by TLC analysis. The mixture was then filtered through celite using EtOAc as the eluent. The filtrate was then concentrated under reduced pressure to produce a crude. The crude was then purified via flash chromatography, using the indicated solvent system, to yield the corresponding 1-amidoprop-1-yn-3-ols **SI-2.005a-c**.

SP4b. To a solution of 1-amidoprop-1-yn-3-ol **SI-2.005a-c** (1.00 mmol, 1.00 eq) in DCM (10 mL, 0.1 M) in a round bottom flask was added $NaHCO_3$ (2.00 mmol, 2.00 eq), then Dess-Martin periodinane (1.10 mmol, 1.10 eq). The reaction mixture was stirred at room temperature for 5 minutes, then filtered through a short pad of silica gel, using DCM as the eluent. The filtrate was then concentrated under reduced pressure to produce a corresponding amidopropynal **2.017a-c.**

SI-2.005c

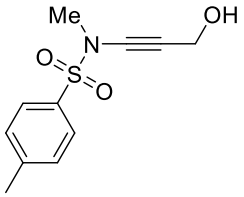

Using standard ***SP4a*** with 3.30 mmol of *N*-methyl-*p*-toluenesulfonamide. Reaction time = 1 h. Solvent system = Hexanes/EtOAc 3:2. Produced 350 mg (44% yield) of a beige solid.

^{1}H NMR (400 MHz, $CDCl_3$) δ 7.79 (d, *J* = 8.3 Hz, 2H), 7.36 (d, *J* = 8.0 Hz, 2H), 4.37 (d, *J* = 6.1 Hz, 2H), 3.07 (s, 3H), 2.46 (s, 3H), 1.65 (t, *J* = 6.1 Hz, 1H).

^{13}C NMR (101 MHz, $CDCl_3$) δ 145.0, 133.5, 130.0, 127.9, 80.9, 68.2, 51.3, 39.2, 21.8.

2.017c

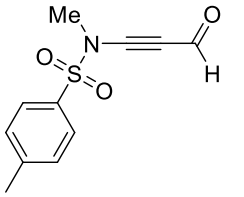

Using standard procedure ***SP4b*** with 0.811 mmol of 1-amidoprop-1-yn-3-ol **SI-2.005c**. Produced 154 mg (80% yield) of a yellow oil.

^{1}H NMR (400 MHz, $CDCl_3$) δ 9.24 (s, 1H), 7.82 (d, *J* = 8.4 Hz, 2H), 7.41 (d, *J* = 8.1 Hz, 2H), 3.21 (s, 3H), 2.48 (s, 3H).

^{13}C NMR (101 MHz, $CDCl_3$) δ 174.9, 146.2, 133.2, 130.4, 128.0, 94.6, 76.9, 39.1, 21.9.

MS-APCI (*m/z*) : 155.6 (55%, $[Ts]^+$), 238.3 (33%, $[M+H]^+$), 255.3 (17%), 308.0 (16%), 372.9 (16%), 392.1 (19%), 405.0 (100%), 447.1 (24%), 475.1 (28%, $[2M+H]^+$).

*Standard procedure **SP5**: One-pot condensation / (3+2) rearrangement*

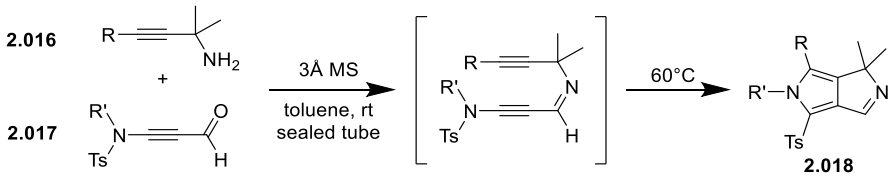

In a reaction vial under vacuum was flame-dried molecular sieves (3Å). To the room temperature-cooled flask was added a solution of the amidopropynal **2.017a-c** (0.100 mmol, 1.00 eq) and propargylamine **2.016a-b** (0.100 mmol, 1.00 eq) in toluene (1.00 mL, 0.1 M). The tube was lightly shaken, and the condensation was followed by TLC. Once the condensation step completed, the tube was heated to 60 °C until full consumption of the condensate. The reaction mixture was then concentrated under reduced pressure to produce a crude mixture. The crude mixture was then purified via flash chromatography, using the indicated solvent system, to yield the pure pyrrole.

1,1,5-trimethyl-6-phenyl-4-tosyl-1,5-dihydropyrrolo[3,4-*c*]pyrrole (**2.018ac**)

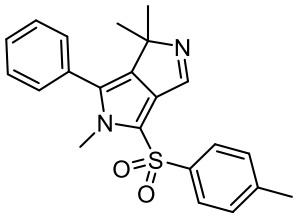

Using standard procedure ***SP5*** with 0.100 mmol of 2-methyl-4-phenylbut-3-yn-2-amine[8] and 0.100 mmol of amidopropynal **2.017a**. Condensation time = rt for 1 h, rearrangement time = 60 °C for 1 h. Solvent system = Hexanes/EtOAc gradient of 1:1 to 2:3. Produced 9.9 mg (26% yield) of a white solid.

^{1}H NMR (400 MHz, $CDCl_3$) δ 8.25 (s, 1H), 7.87 (d, *J* = 8.3 Hz, 2H), 7.50 – 7.40 (m, 3H), 7.36 (d, *J* = 8.0 Hz, 2H), 7.31 – 7.24 (m, 2H), 3.56 (s, 3H), 2.44 (s, 3H), 1.33 (s, 6H).

^{13}C NMR (101 MHz, $CDCl_3$) δ 153.4, 144.6, 142.4, 138.8, 135.4, 131.5, 130.3, 130.2, 130.1, 129.2, 128.8, 127.8, 117.8, 72.4, 33.3, 25.8, 21.8.

HRMS-EI : Calculated for $C_{22}H_{22}N_2O_2S$ [M]$^+$: 378.1397; found: 378.1404.

6.2.5. Derivatization products

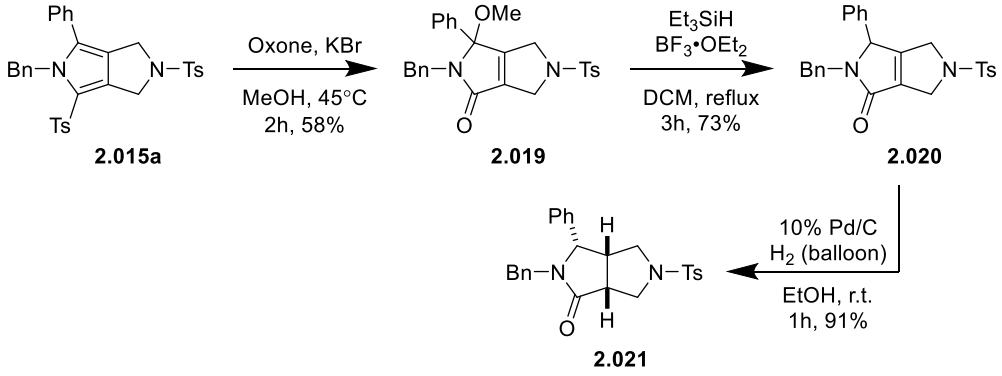

2.019

[8] Prepared as previously reported in literature: Ying, J.; Le,Z.; Wu, W.F. *Organic Letters* 2020, 22 (*1*), 194–198.

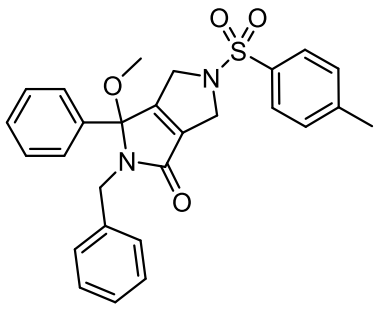

To a suspension of finely grounded[9] pyrrole **2.015a** (280 mg, 0.480 mmol, 1.00 eq) and KBr (28.6 mg, 0.240 mmol, 0.500 eq) in MeOH (10 mL) was added Oxone® (443 mg, 1.44 mmol, 3.00 eq). The suspension was heated to 45 °C and stirred for 2 h. The reaction mixture was quenched with a saturated aqueous solution of $Na_2S_2O_5$, and then extracted three times with EtOAc. The combined organic phases were then washed once with H_2O, dried using $MgSO_4$, filtered, and concentrated under reduced pressure to produce a crude. The crude was then recrystallized from MeOH to yield 132 mg (58% yield) of 5-methoxypyrrolone **2.019** as white crystals.

^{1}H NMR (400 MHz, $CDCl_3$) δ 7.65 (d, *J* = 8.3 Hz, 2H), 7.34 – 7.23 (m, 5H), 7.20 – 7.11 (m, 7H), 4.49 (d, *J* = 14.8 Hz, 1H), 4.46 – 4.34 (m, 2H), 4.16 (ddd, *J* = 16.0, 5.5, 3.8 Hz, 1H), 3.90 (ddd, *J* = 16.0, 5.7, 3.6 Hz, 1H), 3.79 (d, *J* = 14.8 Hz, 1H), 2.68 (s, 3H), 2.42 (s, 3H).

^{13}C NMR (101 MHz, $CDCl_3$) δ 164.7, 158.5, 144.1, 139.4, 137.2, 135.1, 133.9, 130.1, 129.4, 129.2, 129.0, 128.2, 127.5, 127.4, 125.9, 93.9, 51.1, 51.0, 50.3, 43.6, 21.7.

HRMS-ESI : Calculated for $C_{27}H_{26}N_2O_4S[M+Na]^+$: 497.1505; found: 497.1535.

2.020

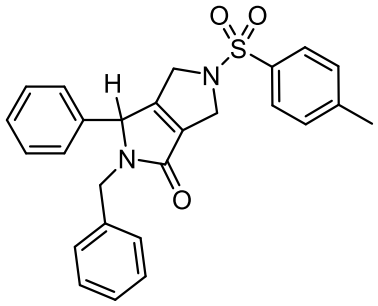

In a flame-dried round bottom flask equipped with a reflux condenser under N_2 atmosphere was added a solution of 5-methoxypyrrolone **2.019** (47.2 mg, 0.0995 mmol, 1.00 eq) in dry DCM (1.0 mL) via syringe. Et_3SiH (79.5 µL, 0.498 mmol, 5.00 eq) and $BF_3 \cdot OEt_2$ (0.120 mL, 0.995 mmol, 10.0 eq) were sequentially added dropwise. The reaction mixture was heated to reflux and stirred for 3 h. The reaction mixture was quenched with a saturated aqueous solution of $NaHCO_3$, and then extracted three times with DCM. The combined organic phases were then washed with H_2O and brine, dried using $MgSO_4$, filtered, and concentrated under reduced pressure to produce a crude. The crude was then purified via flash chromatography (hexanes/EtOAc 7:3) to yield 32.3 mg (73% yield) of pyrrolone **2.020** as a white solid.

[9] Due to its poor solubility in MeOH, grounding the pyrrole to a fine powder is necessary for its timely consumption in this reaction.

^{1}H NMR (400 MHz, $CDCl_3$) δ 7.66 (d, *J* = 8.2 Hz, 2H), 7.39 – 7.22 (m, 8H), 7.08 (m, 2H), 6.91 (m, 2H), 5.09 (d, *J* = 15.0 Hz, 1H), 4.75 (s, 1H), 4.44 (dddd, *J* = 13.9, 5.7, 2.9, 1.6 Hz, 1H), 4.40 – 4.29 (m, 1H), 4.18 (dddd, *J* = 15.4, 5.6, 3.5, 1.1 Hz, 1H), 4.01 (ddd, *J* = 15.6, 5.7, 2.9 Hz, 1H), 3.53 (d, *J* = 15.0 Hz, 1H), 2.45 (s, 3H).

^{13}C NMR (101 MHz, $CDCl_3$) δ 165.3, 158.7, 144.0, 137.2, 136.7, 134.2, 133.2, 130.1, 129.6, 129.4, 128.9, 128.5, 127.8, 127.5, 127.4, 62.0, 51.6, 50.3, 44.2, 21.7.

HRMS-ESI : Calculated for $C_{26}H_{24}N_2O_3S$ [M+Na]$^+$: 467.1400; found: 467.1420.

2.021

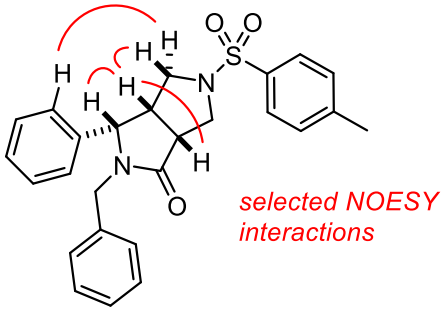

In a dry round bottom flask was added 10% Pd/C (10.0 mg). The flask was vacuum/backfilled once with N_2 gas, then three times with H_2 gas, and a H_2 balloon was attached. A solution of pyrrolone **2.020** (27.3 mg, 0.0614 mmol) in EtOH (1.0 mL) was added to the flask via syringe. The suspension was stirred at room temperature for 1h. The reaction mixture was then filtered through celite, eluted with DCM, and evaporated under reduced pressure to directly produce 25.0 mg (91% yield) of pyrrolidinone **2.021** as a white solid without need for further purification.

^{1}H NMR (400 MHz, $CDCl_3$) δ 7.58 (d, *J* = 8.3 Hz, 2H), 7.46 – 7.38 (m, 3H), 7.30 (d, *J* = 8.0 Hz, 2H), 7.25 – 7.21 (m, 3H), 7.15 – 7.07 (m, 2H), 7.02 – 6.94 (m, 2H), 5.14 (d, *J* = 14.4 Hz, 1H), 4.58 (d, *J* = 8.6 Hz, 1H), 3.82 (dd, *J* = 9.8, 2.1 Hz, 1H), 3.54 (d, *J* = 14.4 Hz, 1H), 3.16 (ddd, *J* = 9.8, 8.4, 2.2 Hz, 1H), 3.03 (dd, *J* = 9.8, 8.4 Hz, 1H), 2.98 (apparent qd, *J* = 8.7, 3.5 Hz, 1H), 2.83 (dd, *J* = 10.5, 3.5 Hz, 1H), 2.53 (dd, *J* = 10.5, 8.1 Hz, 1H), 2.43 (s, 3H).

^{13}C NMR (101 MHz, $CDCl_3$) δ 174.5, 144.0, 135.7, 135.3, 131.8, 129.8, 129.2, 129.0, 128.8, 128.7, 128.3, 128.1, 127.9, 63.0, 50.9, 50.3, 46.6, 45.4, 39.3, 21.7.

HRMS-EI : Calculated for $C_{26}H_{26}N_2O_3S$ [M]$^+$: 446.1664; found: 446.1666.

6.2.6. Mechanistic Studies

General information for mechanistic studies

Toluene stock was dried with 4Å MS. Thin layer chromatography was performed on TLC Silicagel 60 F254 plates. NMR spectra were recorded at room temperature (unless otherwise noted) in the given deuterated solvent on a Bruker Avance II 300 operating at 300 MHz. Low resolution mass spectra were obtained on an Advion ExpressIon CMS spectrometer using an APCI probe at 350 °C.

Hammett Plot

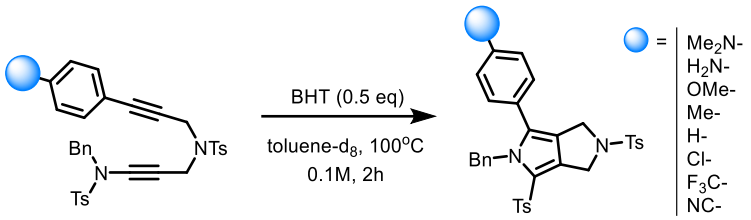

			Slope Data				
Substrate	**R-**	**σ**[10]	**k (s^{-1})**	**(± SE) (s^{-1})**	**R^2**	**ln(k/k_H)**	**(± SE)**
2.014a	Me_2N-	-0.83	1.219E-04	(± 4.37E-07)	0.9985	0.7774	(± 6.83E-03)
2.014c	H_2N-	-0.66	8.220E-05	(± 3.82E-07)	0.9975	0.3835	(± 7.44E-03)
2.014d	MeO-	-0.27	6.088E-05	(± 1.80E-07)	0.9990	0.0833	(± 6.52E-03)
2.014e	Me-	-0.17	6.109E-05	(± 2.56E-07)	0.9979	0.0867	(± 7.17E-03)
2.014a	H-	0	5.602E-05	(± 3.26E-07)	0.9960	0	-
2.014f	Cl-	0.23	6.102E-05	(± 2.65E-07)	0.9978	0.0856	(± 7.26E-03)
2.014g	F_3C-	0.54	1.254E-04	(± 4.24E-07)	0.9987	0.8056	(± 6.73E-03)
2.014h	NC-	0.66	2.912E-04	(± 6.99E-07)	0.9993	1.6483	(± 6.29E-03)

Table SI-6.2-1. Processed kinetic data for Hammett analysis. Reaction repeated with each indicated substrate in toluene-d_8 (0.1 M) with 0.5 eq BHT at the 0.05 mmol scale. 2.0 µL of 1,2-DBE was added as internal NMR standard. Reactions were done in sealed NMR tubes and heated to 100.0 °C in a Bruker Avance II 300 instrument. ^{1}H NMR spectra were collected every 60 seconds for 2 h, giving a stack of 120 spectra. Data was processed as indicated in Figure SI-1.

[10] σ parameters obtained from: Hansch, C.; Leo, A.; Taft, R.W. *Chem. Rev.* **1991**, 91 (*2*), 165–195.

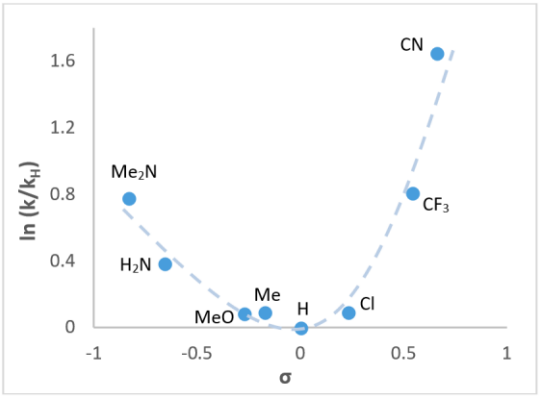

Figure SI-6.2-3. Hammett plot. Plotted data from Table SI-6.2-1.

Kinetic analyses on 9al and 10al

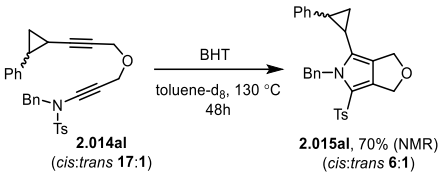

Time (h)	(*cis*)-2.014al (%)	(*trans*)-2.014al (%)	(*cis*)-2.015al (%)	(*trans*)-2.015al (%)
0	100.0	5.9	0	0
2.25	87.4	4.8	16.2	0.8
6.25	60.4	2.9	40.1	2.4
60	-	-	60.0	10.7

Table SI-6.2-2. Kinetic data for reaction of substrate 2.014al. Reaction completed with **2.014al** (29.9 mg, 0.0637 mmol) and BHT (7.0 mg, 0.0318 mmol) in toluene-d_8 (0.64 mL). 2.0 µL of 1,2-DBE was added as internal NMR standard. Reaction was completed in a sealed NMR tube and heated in an oil bath set to 130 °C. The reaction was followed by ^{1}H NMR at given time intervals until completion. Data above is represented using relative percentage (%).

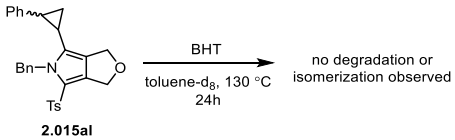

Time (h)	(*cis*)-2.015al (%)	(*trans*)-2.015al (%)
0	100.00	17.2
24	99.60	19.0

Table SI-6.2-3. Kinetic data for heating of pyrrole 10al. Mixture prepared with **2.015al** (15.0 mg, 0.0319 mmol) and BHT (7.0 mg, 0.0318 mmol) in toluene-d_8 (0.60 mL). 2.0 µL of 1,2-DBE was added as internal NMR standard. Reaction was completed in a sealed NMR

tube and heated in an oil bath set to 130 °C. The reaction mixture was analyzed by ^{1}H NMR after 24 h. Data above is represented using relative percentage (%).

Effects of TEMPO and O_2

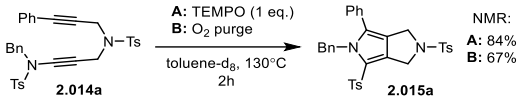

Table SI-6.2-4. Kinetic data for special additives. Two sealed NMR tubes were prepared each with **2.014a** (30.9 mg, 0.0530 mmol) in toluene-d_8 (0.53 mL). 3.5 µL of mesitylene was added as internal NMR standard for each tube.

	10a (NMR %)	
Time (h)	**A**	**B**
0	0	0
2	84	67

Tube A: 8.3 mg (0.0530 mmol) of TEMPO was added, the tube was then sealed and shaken.

Tube B: O_2 gas was bubbled through the solution for 2 minutes before sealing the tube.

The sealed NMR tubes were heated in an oil bath set to 130 °C. The reaction mixture was analyzed by ^{1}H NMR before heating (0 h) and after heating (2 h).

6.2.7. DFT studies

Potential energy surfaces data

General methodology for calculation of potential energy surfaces:

Using the Gaussian16 software,[11] structural optimization and vibrational frequency calculations for minima and maxima (transition states) were carried out at the B3LYP/6-31G(d) [12] and/or the M06-2X/6-31+G(d) [13] levels of theory. Vibrational frequency calculations were performed at the gas phase, 1 atm, and 298.15 K. Normal modes of vibration were analyzed to assure either 0 (minima) or 1 (maxima) imaginary frequencies were obtained. Intrinsic reaction coordinate (IRC)

[11] Frisch, M. J. *et al.* Gaussian 16 Rev. C.01, Wallingford, CT, **2016**.
[12] (a) Becke, A. D. *J. Chem. Phys.* **1993**, *98*, 5648–5652; (b) Lee, C.; Yang, W.; Parr, R. G. *Phys. Rev. B: Condens. Matter Mater. Phys.* **1988**, *37*, 785–789; (c) Miehlich, B.; Savin, A.; Stoll, H.; Preuss, H. *Chem. Phys. Lett.* **1989**, *157*, 200–206.
[13] Y. Zhao & D.G. Truhlar, *Theor. Chem. Acc.* **2006**, *120*, 215–241.

calculations were performed on each transition state structure to assign connectivity (dotted lines) to the indicated minima.

When using *unrestricted* functionals, the "guess=(mix,always)" input line was included to allow the construction of wavefunctions for singlet diradicals.

Methodology for conformational search within the flexible minima **2.032-Ph** and **2.032-Me**:

Using the Spartan software,[14] an array of 34 possible conformers was produced for **2.032-Me**, and 42 possible conformers for **2.032-Ph**. In each case, the five most stable conformers were reoptimized and evaluated at the M06-2X/6-31+G(d) level of theory. The conformer with the lowest electronic energy was selected as **2.032-Me** or **2.032-Ph**.

RB3LYP or UB3LYP	**Structure**	**EE (Hartrees)**	**Thermal Free Energy Correction (Hartrees)**	**EE + Thermal Free Energy Correction (Hartrees)**	**ΔG (kcal/mol)**	**Imaginary frequencies**	**$\langle S^2 \rangle$**

[14] Except for molecular mechanics and semi-empirical models, the calculation methods used in Spartan Student have been documented in: Y. Shao *et al. Phys. Chem. Chem. Phys.* **2006**, *8*, 3172.

RB3LYP	**2.032-Ph**	-1220.910638	0.213381	-1220.697257	0.0	0	-
	2.033-Ph	Only TS found for **TS-I-Ph** using *restricted* B3LYP had a RHF -> UHF wavefunction instability![15]					
	2.034-Ph	-1220.903099	0.222652	-1220.680447	10.5	0	-
	2.047-Ph	-1220.901010	0.221962	-1220.679048	11.4	1	-
	2.048-Ph	-1221.036179	0.223331	-1220.812848	-72.5	0	-
UB3LYP	**2.035-Ph**	-1220.869694	0.212153	-1220.657541	24.9	1	0.1340
	2.036-Ph	-1220.881489	0.214165	-1220.667324	18.8	0	0.8459
	2.037-Ph	-1220.878841	0.217968	-1220.660873	22.8	1	0.2774
RB3LYP	**2.032-Me**	-1029.170943	0.161744	-1029.009200	0.0	0	-
	2.033-Me	-1029.121171	0.168011	-1028.953160	35.2	1	-
	2.034-Me	-1029.164583	0.174220	-1028.990363	11.8	0	-
UB3LYP	**2.038-Me**	-1029.119781	0.164682	-1028.955099	33.9	1	0.2611
	2.039-Me	-1029.129354	0.166719	-1028.962635	29.2	0	0.9218
	2.040-Me	-1029.127664	0.166886	-1028.960777	30.4	1	0.7833
	2.041-Me	-1029.130850	0.166372	-1028.964477	28.1	0	0.8404
	2.042-Me	-1029.130218	0.168731	-1028.961486	29.9	1	0.5478

Table SI-6.2-5. Potential energy surface data using the B3LYP functional. All structures optimized and evaluated at the B3LYP/6-31G(d) level of theory. When using *unrestricted* UB3LYP, the "guess=(mix,always)" input was included in the calculation to allow for singlet diradicals.

[15] After an exhaustive effort (various scanning methods and directions) to locate **TS-I-Ph** using the *restricted* B3LYP method (using either 6-31G(d), 6-31G(2d,p) or 6-31+G(d) basis sets), the only structure optimized with a single imaginary frequency is the one with coordinates reported in section 6.7.2 below. However, it possesses the same geometry as the one obtained using the *unrestricted*

Structure	EE (Hartrees)	Thermal Free Energy Correction (Hartrees)	EE + Thermal Free Energy Correction (Hartrees)	ΔG (kcal/mol)	Imaginary frequencies
M06-2.032-Ph	-1028.890892	0.169564	-1220.341331	0.0	0
M06-2.033-Ph	-1220.512265	0.219211	-1220.293054	30.3	1
M06-2.034-Ph	-1220.563234	0.227220	-1220.336014	3.3	0
M06-2.047-Ph	-1220.555139	0.225947	-1220.329193	7.6	1
M06-2.048-Ph	-1220.687662	0.227535	-1220.460127	-74.5	0
M06-2.032-Me	-1028.890892	0.169564	-1028.721327	0.0	0
M06-2.033-Me	-1028.837930	0.171892	-1028.666038	34.7	1
M06-2.034-Me	-1028.894850	0.178014	-1028.716836	2.8	0

Table SI-6.2-6. Potential energy surface data using the M06-2X functional. All structures optimized and evaluated at the M06-2X/6-31+G(d) level of theory.

Restricted or Unrestricted	**Structure**	**Electronic energy, in Hartrees (ΔE, in kcal/mol)**					
		B3LYP/6-31G(d)		**B3LYP-d3/6-311++G(d,p)**		**B2PLYPD/*aug*-cc-pVDZ**	
Restricted	**2.032-Ph**	-1220.910638	(0.0)	-1221.201743	(0.0)	-1219.146545	(0.0)
	2.033-Ph	-1220.903099	(4.7)	-1221.195366	(4.0)	-1219.143735	(1.8)
	2.047-Ph	-1220.901010	(6.0)	-1221.193256	(5.3)	-1219.136749	(6.1)
	2.048-Ph	-1221.036179	(-78.8)	-1221.317873	(-72.9)	-1219.272789	(-79.2)
Unrestricted	**2.035-Ph**	-1220.869694	(25.7)	-1221.156304	(28.5)	-1219.098758	(30.0)
	2.036-Ph	-1220.881489	(18.3)	-1221.168580	(20.8)	-1219.123292	(14.6)

	2.037-Ph	-1220.878841	(20.0)	-1221.169607	(20.2)	-1219.111871	(21.8)
Restricted	**2.032-Me**	-1029.170943	(0.0)	-1029.407277	(0.0)	-1027.792407	(0.0)
	2.033-Me	-1029.121171	(31.2)	-1029.359919	(29.7)	-1027.729484	(39.5)
	2.034-Me	-1029.164583	(4.0)	-1029.402982	(2.7)	-1027.791694	(0.4)
Unrestricted	**2.038-Me**	-1029.119781	(32.1)	-1029.356081	(32.1)	-1027.738336	(33.9)
	2.039-Me	-1029.129354	(26.1)	-1029.363667	(27.4)	-1027.760486	(20.0)
	2.040-Me	-1029.127664	(27.2)	-1029.362618	(28.0)	-1027.755189	(23.4)
	2.041-Me	-1029.130850	(25.5)	-1029.364682	(26.7)	-1027.760213	(20.2)
	2.042-Me	-1029.130218	(25.6)	-1029.366155	(25.8)	-1027.754022	(24.1)

Table SI-6.2-7. Single point energy benchmarking for B3LYP-optimized geometries. All structures optimized at the B3LYP/6-31G(d) level of theory. Single point energy calculations were then performed using the indicated levels of theory. When using *unrestricted* functionals (i.e. UB3LYP or UB2PLYPD), the "guess=(mix,always)" input was included in the calculation to allow for singlet diradicals. In particular, the inclusion of dispersion correction and a higher basis set in B3LYP-d3/6-311++G(d,p) did not drastically affect the PES, and the same could be observed when using B2PLYPD/*aug*-cc-pVDZ. Apart from **2.033-Me**, all calculated electronic energies are in general agreement across the three computed levels of theory.

6.2.8. Cartesian coordinates for reported minima/maxima

2.032-Ph

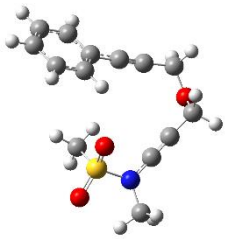

Atom type	X	Y	Z
C	1.47275200	3.17782600	0.71048800
C	1.95167400	1.83461200	0.39259200
C	2.39716400	0.73959900	0.12218900
N	2.86557600	-0.47632600	-0.22187100
S	1.77597200	-1.81336800	-0.03924500
O	2.56403500	-3.00459700	-0.36024700
O	1.05863900	-1.70959700	1.23298000
C	0.61796700	-1.46940200	-1.37377400
H	-0.19152200	-2.19714400	-1.28820500
H	0.22821300	-0.45762200	-1.24776000
H	1.14664700	-1.57631700	-2.32169600
C	4.31689700	-0.73518500	-0.19049300
H	4.80654500	0.02484400	-0.80422000
H	4.71023900	-0.69091200	0.83105300
H	4.50174400	-1.72321600	-0.61106900
O	0.77016800	3.80689200	-0.36710300
C	-0.64092700	3.86771200	-0.20241700
C	-1.33285300	2.57280000	-0.15526300
C	-1.94683500	1.52977300	-0.06484500
C	-2.68325000	0.30788100	0.03934500
C	-2.20908000	-0.74704500	0.84366200
C	-2.93208800	-1.93479600	0.93648300
C	-4.13459100	-2.08678500	0.24173300
C	-4.61304200	-1.04325400	-0.55485300
C	-3.89489100	0.14518700	-0.66039300
H	-4.26192700	0.95712000	-1.28090800
H	-5.54787700	-1.15615000	-1.09733600
H	-4.69653500	-3.01354000	0.32026500
H	-2.55188800	-2.74219800	1.55619100
H	-1.27064400	-0.63671200	1.37697400
H	-0.89145500	4.43818100	0.70835800
H	-0.99922700	4.45177300	-1.05727800
H	0.84745200	3.16001200	1.61476100
H	2.33953300	3.81493300	0.93012600

2.033-Ph

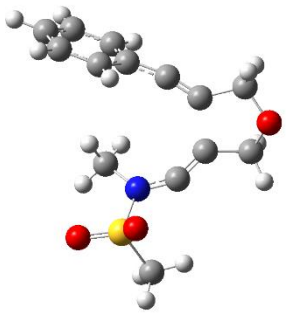

Possesses RHF -> UHF wavefunction instability

i.e. Not a real TS in RB3LYP !

Atom type	X	Y	Z
C	-0.80046100	3.59076500	0.54359300
C	-0.86308100	2.09995600	0.22496700
C	-1.79107700	1.25038300	0.17316500
C	-2.60299700	0.10964300	0.12162400
C	-3.42341300	-0.15785000	-1.00665700
C	-4.22794200	-1.28886100	-1.04379900
C	-4.25478700	-2.17849300	0.03727700
C	-3.45465300	-1.93140000	1.15688900
C	-2.63100100	-0.81146300	1.20300100
H	-2.00703800	-0.62010300	2.07062500
H	-3.46754800	-2.62071000	1.99691600
H	-4.89292400	-3.05692000	0.00526400
H	-4.84723300	-1.47777400	-1.91673900
H	-3.41485100	0.53997000	-1.83868300
N	1.42929900	-0.59331800	-0.47576700
C	1.45461500	0.73415700	-0.37669400
C	0.81310200	1.83673700	-0.29463400
C	1.17245900	3.27012200	-0.57910600
O	0.52391500	4.05630100	0.40723800
H	0.85033200	3.56862900	-1.59174500
H	2.24692800	3.43667000	-0.48528500
C	0.30870200	-1.37573300	-1.04446900
H	-0.36039000	-1.73807800	-0.25692800
H	-0.24718100	-0.70557600	-1.70131300
H	0.70256600	-2.22192900	-1.60832400
S	2.75156300	-1.47240600	0.24160000
O	2.51896700	-2.87485100	-0.10754900
O	2.90584600	-1.05082200	1.63103000
C	4.15746100	-0.84184900	-0.69572300
H	5.05386200	-1.26429200	-0.23676100
H	4.06227400	-1.16584000	-1.73314600
H	4.15878200	0.24628300	-0.61761600
H	-1.47468600	4.11462400	-0.15220300
H	-1.12439500	3.79505900	1.56834200

2.034-Ph

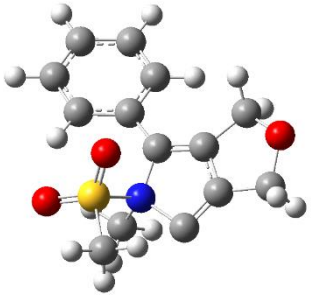

Atom type	X	Y	Z
C	-0.36937600	2.99998100	-0.46212000
C	-0.53075100	1.59212200	0.02336900
C	0.20943300	0.47439200	0.22234600
C	1.65172000	0.25062200	0.10173600
C	2.50444900	1.37669400	0.11435800
C	3.88193800	1.24136300	-0.01968700
C	4.45740500	-0.02443800	-0.15448500
C	3.63170300	-1.14763500	-0.15609900
C	2.24819800	-1.01842000	-0.03406000
H	1.63942800	-1.91379300	-0.06699900
H	4.06134300	-2.14008800	-0.26296400
H	5.53381500	-0.13146600	-0.25438600
H	4.50929200	2.12873900	-0.00669500
H	2.08373300	2.36728100	0.25297600
N	-0.77732400	-0.51649400	0.75370600
C	-2.23140100	0.17206200	0.88829000
C	-1.91212500	1.39760800	0.39713000
C	-2.63362400	2.69347200	0.13502100
O	-1.70617500	3.47701600	-0.64326000
H	-2.88769200	3.22252900	1.06748400
H	-3.54966700	2.58470500	-0.45464100
C	-0.39815200	-1.09197900	2.07297500
H	0.55941200	-1.60774200	2.00447700
H	-0.33604100	-0.25307000	2.76945700
H	-1.18306200	-1.77151900	2.40235800
S	-1.12855500	-1.90801100	-0.49990500
O	-0.31193900	-3.04245400	-0.05423800
O	-0.94180200	-1.29450800	-1.80784900
C	-2.85815100	-2.37394200	-0.26955600
H	-2.95888400	-3.28887000	-0.86348500
H	-3.04293400	-2.56194700	0.78622800
H	-3.48913400	-1.56381600	-0.62362000
H	0.16739700	3.62052600	0.27713100
H	0.16289200	3.08033700	-1.41730500

2.047-Ph

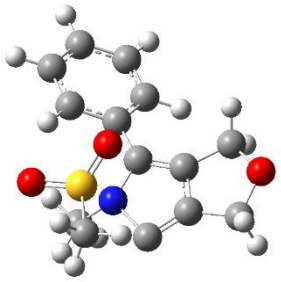

Atom type	X	Y	Z
C	-0.26558900	2.95087900	-0.50936000
C	-0.42882800	1.58499500	0.07499600
C	0.30864400	0.46131800	0.33975600
C	1.73367300	0.18463100	0.13511800
C	2.65046300	1.25268100	0.20255800
C	4.01055800	1.04547000	-0.00939900
C	4.49334600	-0.23617500	-0.28298600
C	3.59781200	-1.30417500	-0.34868300
C	2.23290600	-1.10119700	-0.14886000
H	1.55504000	-1.94341200	-0.24037000
H	3.95860800	-2.30499900	-0.57028000
H	5.55520100	-0.39928500	-0.44457500
H	4.69618600	1.88665100	0.04941700
H	2.29301200	2.24968000	0.44355200
N	-0.63978300	-0.45640100	0.91320900
C	-2.05825500	0.21012200	1.07960100
C	-1.79141700	1.40950700	0.47480100
C	-2.53866300	2.66646100	0.11998500
O	-1.59956300	3.45520400	-0.64148600
H	-2.86166300	3.22668400	1.01090200
H	-3.41982700	2.49755000	-0.50982600
C	-0.23014600	-1.22603700	2.10435100
H	0.67294400	-1.80078700	1.90350100
H	-0.05213200	-0.50487100	2.90716300
H	-1.04913400	-1.88278700	2.39382100
S	-1.35966800	-1.74765600	-0.49611600
O	-0.66422600	-2.99172100	-0.13067900
O	-1.08363800	-1.05735700	-1.75445100
C	-3.13710500	-2.09529300	-0.36513600
H	-3.30656200	-2.95380200	-1.02493300
H	-3.36239900	-2.32979800	0.67297300
H	-3.67419600	-1.20531500	-0.68340200
H	0.32977000	3.60833100	0.14686600
H	0.21333900	2.94532800	-1.49693500

2.048-Ph

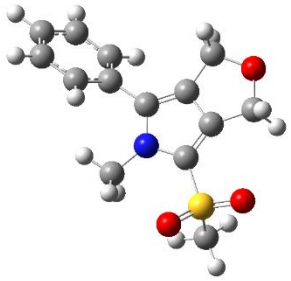

Atom type	X	Y	Z
C	0.62784800	2.84280400	-0.19040900
C	0.29966700	1.38589100	-0.03389200
C	0.88985600	0.13171800	0.01649300
C	2.32375600	-0.21180800	0.01833100
C	3.18513400	0.41992000	0.93100800
C	4.55349200	0.15350700	0.92036200
C	5.08529000	-0.75357100	0.00174400
C	4.24101400	-1.38389000	-0.91451200
C	2.87356500	-1.11123600	-0.91252300
H	2.22940700	-1.57482000	-1.65466400
H	4.64902100	-2.07915100	-1.64314000
H	6.15121400	-0.96374400	-0.00407200
H	5.20383300	0.65007100	1.63539200
H	2.77079700	1.11403800	1.65684600
N	-0.13946600	-0.80298300	0.01939400
C	-1.35693200	-0.12477600	-0.03521400
C	-1.09127500	1.22898400	-0.07632900
C	-1.73882400	2.56556200	-0.25753200
O	-0.65002400	3.49803400	-0.11147700
H	-2.50036400	2.80388500	0.49365700
H	-2.20606000	2.66225800	-1.24799900
C	0.00438900	-2.23077100	0.29908400
H	-0.60476000	-2.80651600	-0.39839400
H	1.05195200	-2.50745400	0.19649900
H	-0.31266100	-2.45740400	1.32433100
S	-2.95583500	-0.86535900	-0.11308700
O	-2.87416400	-2.13343800	-0.85814500
O	-3.86788900	0.20792600	-0.53733400
C	-3.38838000	-1.27728000	1.59619700
H	-4.39246400	-1.70850300	1.56511900
H	-2.67895900	-2.00803400	1.99002700
H	-3.38468100	-0.36303100	2.19240100
H	1.26575400	3.25379300	0.60215500
H	1.11260600	3.06073700	-1.15572100

2.035-Ph

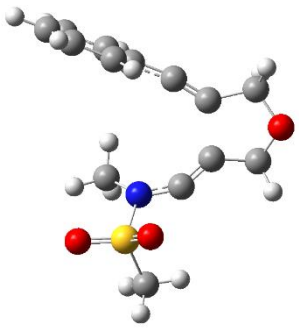

Atom type	X	Y	Z
C	-0.87166700	3.64662200	0.29635000
C	-0.90199600	2.13537800	0.13153600
C	-1.79603400	1.25256500	0.13534000
C	0.86776700	1.86357100	-0.22476200
C	1.27611500	3.29985200	-0.40884200
O	0.45913600	4.09376800	0.43043600
H	1.16057800	3.60292500	-1.46446900
H	2.31404900	3.45753200	-0.10895400
C	1.46986100	0.74785400	-0.31776600
N	1.39259300	-0.58688400	-0.43930100
C	0.62313700	-1.22010100	-1.52865100
H	0.66041800	-2.30039100	-1.39080000
H	-0.41283300	-0.88424300	-1.46082200
H	1.03474100	-0.95412400	-2.50991100
S	2.65577300	-1.50319100	0.33329900
O	2.35459400	-2.90962700	0.06436800
O	2.79080100	-0.98675700	1.68965700
C	4.13653500	-1.03698500	-0.59130900
H	4.98434600	-1.51827200	-0.09892200
H	4.03927700	-1.39157500	-1.61917300
H	4.23393700	0.04919900	-0.55240600
H	-1.35020600	4.10075000	-0.58762400
H	-1.41787500	3.95846300	1.19025300
C	-2.59219800	0.09776200	0.11581500
C	-3.22212600	-0.33169000	-1.08231400
C	-2.80211100	-0.66519200	1.29504600
C	-4.01404000	-1.47452400	-1.09448300
H	-3.08272300	0.25185200	-1.98764300
C	-3.60283100	-1.79888600	1.26766500
H	-2.32159900	-0.34973600	2.21576300
C	-4.21171700	-2.21263200	0.07653300
H	-4.48585000	-1.78977000	-2.02150600
H	-3.75059400	-2.37156400	2.17933500
H	-4.83461500	-3.10243400	0.06257400

2.036-Ph

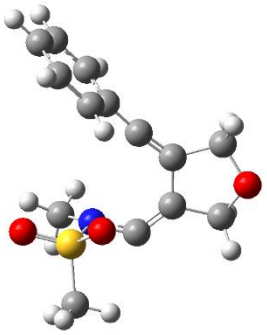

Atom type	X	Y	Z
C	-0.42179000	3.43265400	-0.44152400
C	-0.27046500	1.95975100	-0.02513400
C	0.81997000	1.25761000	0.00359000
C	-1.68074500	1.52991800	0.32148300
C	-2.54238400	2.76533600	0.13980100
O	-1.79991900	3.62395700	-0.71783400
H	-2.73028200	3.25113100	1.11335300
H	-3.50468700	2.55609000	-0.33410800
C	-2.06614300	0.31792500	0.67263200
N	-1.27967000	-0.79784000	0.85981700
C	-0.98561200	-1.24707800	2.23045100
H	-0.23317300	-2.03389300	2.18752100
H	-0.58824400	-0.38906800	2.77706700
H	-1.88269800	-1.61594500	2.74444900
S	-1.34734300	-2.00650100	-0.38245600
O	-0.51953000	-3.11845100	0.08733400
O	-1.08413900	-1.33305800	-1.65070200
C	-3.07541700	-2.53558500	-0.38708600
H	-3.18328600	-3.25653300	-1.20045000
H	-3.30583100	-3.00448000	0.57149000
H	-3.70175300	-1.65893900	-0.55895300
H	-0.08855100	4.08698900	0.38167900
H	0.14673300	3.68110100	-1.34109300
C	2.05042100	0.62577800	-0.03107100
C	2.97299000	0.73856200	1.05384600
C	2.43211600	-0.16653800	-1.15781100
C	4.20435400	0.10423000	0.99965600
H	2.69633500	1.33550000	1.91781300
C	3.66887600	-0.79040500	-1.18867000
H	1.72506200	-0.28686500	-1.97185600
C	4.56495200	-0.66100700	-0.11784800
H	4.89522200	0.20499800	1.83284000
H	3.94079400	-1.39228500	-2.05174300
H	5.53150300	-1.15540200	-0.15172200

2.037-Ph

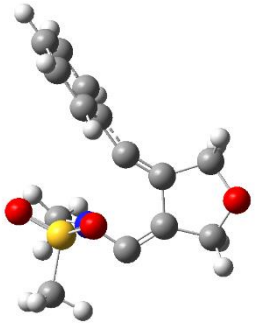

Atom type	X	Y	Z
C	-0.89043800	3.18124000	-0.45371900
C	-0.67850800	1.72941100	-0.03315000
C	0.39017400	0.99844300	0.04293500
C	-2.07494600	1.22776500	0.28352900
C	-3.00903500	2.38884700	0.04734100
O	-2.27187900	3.30460500	-0.76446300
H	-3.30291800	2.86371600	0.99916100
H	-3.91752400	2.11073200	-0.49387200
C	-2.23762300	-0.03161200	0.65259900
N	-1.06139500	-0.76684700	0.78878800
C	-0.60488100	-1.07925000	2.15817900
H	0.39620900	-1.50649200	2.10967900
H	-0.58497700	-0.13698500	2.70901400
H	-1.28677500	-1.77338200	2.66393900
S	-0.88739500	-2.08982800	-0.36601600
O	0.28739300	-2.85129000	0.06326600
O	-0.97082800	-1.50332500	-1.70005100
C	-2.36943100	-3.08839400	-0.09827000
H	-2.34470400	-3.88272100	-0.84769300
H	-2.33850500	-3.51051900	0.90781900
H	-3.23805000	-2.44252400	-0.22922100
H	-0.60778800	3.85188600	0.37541300
H	-0.31511600	3.45949300	-1.34063000
C	1.76854000	0.70754800	-0.01375600
C	2.63678300	1.08690100	1.04275200
C	2.31597200	0.00954700	-1.12147100
C	3.99435400	0.79710400	0.97860700
H	2.22657400	1.61782000	1.89688000
C	3.67524000	-0.26989300	-1.17197700
H	1.65121600	-0.30903600	-1.91763300
C	4.52069600	0.12054600	-0.12693200
H	4.64812200	1.10113400	1.79184700
H	4.08096800	-0.80204500	-2.02801800
H	5.58249700	-0.10504500	-0.17195800

2.032-Me

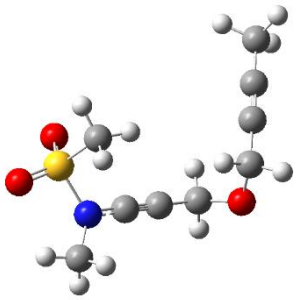

Atom type	X	Y	Z
C	1.76333600	-1.68959200	-0.93255700
C	0.37064800	-1.35416600	-0.62875400
C	-0.79314400	-1.06940000	-0.43302800
N	-2.08721700	-0.78114400	-0.20404900
S	-2.53895600	0.88026300	-0.11156200
O	-1.87709700	1.57523300	-1.20890300
O	-3.99257100	0.88567900	0.05003300
C	-1.78247500	1.43626200	1.43033900
H	-1.98190200	2.50672500	1.51702500
H	-2.23575800	0.89434800	2.26237200
H	-0.70796600	1.25274400	1.37471500
C	-3.00919000	-1.83264400	0.25749900
H	-2.95453500	-2.66971600	-0.44297100
H	-2.74394900	-2.18235200	1.26221200
H	-4.02077200	-1.42804100	0.25773900
O	2.55746500	-2.03580100	0.20178000
C	2.76393500	-0.96531400	1.11800200
C	3.54122600	0.15289200	0.56634900
C	4.17169500	1.07197400	0.09497200
H	1.79485300	-0.59708300	1.49096800
H	3.29296000	-1.41629000	1.96445200
H	1.80710600	-2.57063000	-1.58171400
H	2.22322200	-0.85150600	-1.47776300
C	4.94087500	2.18234400	-0.46067800
H	4.29325300	2.90189200	-0.97580900
H	5.47784700	2.72252200	0.32849100
H	5.68564000	1.82617000	-1.18251900

2.033-Me

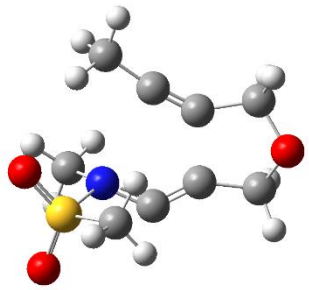

Atom type	X	Y	Z
C	-3.35755400	0.51882200	-0.34913600
C	-1.89607600	0.80409300	-0.09744600
C	-1.04128200	1.71403100	-0.11916500
N	0.76896200	-0.12710100	0.75604500
C	-0.20960900	-1.08926500	0.70907400
C	-1.44075600	-0.93021300	0.43914300
C	-2.77022100	-1.59830800	0.36374900
O	-3.56795600	-0.86807000	-0.55747700
H	-3.24506900	-1.62041400	1.35993000
H	-2.69426200	-2.62470500	-0.00547200
C	1.18921200	0.34681700	2.09294700
H	1.85374800	1.20259600	1.96091200
H	0.28658500	0.65658400	2.62187900
H	1.70051000	-0.43944100	2.65869800
S	2.14058100	-0.35237000	-0.31789100
O	2.98010400	-1.47018900	0.11969900
O	2.72454200	0.98715400	-0.45745100
C	1.29973900	-0.80164100	-1.84376100
H	2.07891500	-0.81126900	-2.60938700
H	0.85418500	-1.78916800	-1.72812100
H	0.53998900	-0.05079800	-2.06314900
H	-3.94094000	0.87466000	0.51730500
H	-3.71652700	1.03316300	-1.24431100
C	-0.19626800	2.90320300	-0.18360000
H	0.02670700	3.28194200	0.82213900
H	0.76349800	2.70226000	-0.67276700
H	-0.69601100	3.71581400	-0.73271400

2.034-Me

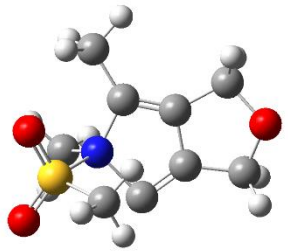

Atom type	X	Y	Z
C	-2.96157200	0.79984100	-0.55095500
C	-1.56093900	0.54833700	-0.07954800
C	-0.37115900	1.16941300	-0.01823200
C	-1.50978400	-0.78056100	0.50950000
C	-2.89193000	-1.36763100	0.38296200
O	-3.57768200	-0.49328300	-0.54001400
H	-3.42294300	-1.38909000	1.34802100
H	-2.91875600	-2.37668200	-0.04113000
C	-0.31144500	-1.17444300	1.01357400
N	0.51439700	0.17988900	0.68953700
C	1.04852300	0.70562000	1.98376500
H	0.18056900	0.97328500	2.58867700
H	1.61340100	-0.08626500	2.47010200
H	1.67580100	1.58244800	1.80363000
S	1.98215400	-0.36875100	-0.33309000
O	2.88202500	-1.05469200	0.58524600
O	2.43797800	0.80946800	-1.07354100
C	1.22746400	-1.53354500	-1.47666900
H	2.02332600	-1.79228600	-2.18009900
H	0.87987500	-2.38752100	-0.89901600
H	0.40521100	-1.03241700	-1.98890900
H	-3.48730700	1.49537100	0.12594900
H	-3.03398700	1.20215200	-1.56788100
C	0.05773700	2.55968200	-0.36147500
H	0.37163300	3.12706400	0.52599300
H	0.88898000	2.58035800	-1.07128200
H	-0.79098500	3.09216500	-0.80243400

2.038-Me

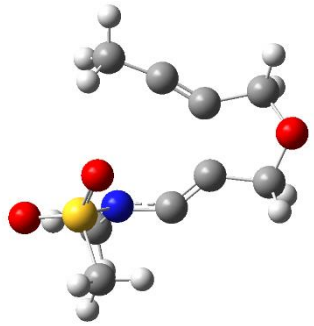

Atom type	X	Y	Z
C	-3.58676700	0.21380100	0.03579400
C	-2.17145100	0.74379700	0.10907200
C	-1.59026300	1.85348900	0.09356600
C	-1.33673900	-0.87892800	0.19742200
C	-2.48591700	-1.79996900	-0.13084200
O	-3.57329000	-1.03844500	-0.62129300
H	-2.77383200	-2.34661800	0.78323000
H	-2.22412900	-2.53059300	-0.90136200
C	-0.11748100	-1.05935000	0.51879700
N	0.99586100	-0.32554700	0.85267400
C	1.59348800	-0.56717400	2.17885000
H	2.40019400	0.14796400	2.33531500
H	0.81030000	-0.40485500	2.92290200
H	1.97471500	-1.59177700	2.28138200
S	2.08381300	0.05193000	-0.43545100
O	3.23734200	0.70412000	0.18825800
O	1.30569600	0.71439800	-1.47953600
C	2.60403000	-1.55473600	-1.07969800
H	3.23719500	-1.36040800	-1.94796500
H	3.16698300	-2.08155700	-0.30676800
H	1.71173700	-2.11309900	-1.36767300
H	-3.99613400	0.11796200	1.05662500
H	-4.23319200	0.87764800	-0.54188800
C	-0.70274000	3.00579500	0.05505300
H	-0.30605600	3.24545900	1.04953900
H	0.14517300	2.80558100	-0.61229400
H	-1.21994100	3.90132200	-0.32006200

2.039-Me

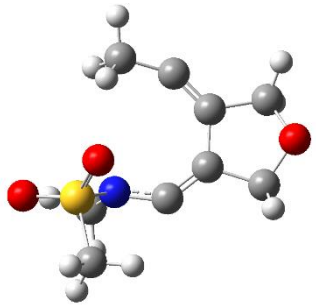

Atom type	X	Y	Z
C	-3.65295900	0.23043800	0.00328900
C	-2.17580700	0.64373700	0.03874300
C	-1.73339000	1.87000300	-0.07145300
C	-1.43845300	-0.67507200	0.15037100
C	-2.50729800	-1.75125700	-0.02820500
O	-3.66202400	-1.08948600	-0.52001200
H	-2.71640800	-2.23709900	0.94025900
H	-2.22057700	-2.52427000	-0.74686600
C	-0.16723700	-0.92948000	0.39748400
N	0.90650100	-0.14166600	0.75111200
C	1.25576500	-0.04041700	2.18002500
H	2.05715600	0.68898500	2.29502600
H	0.36496100	0.30414900	2.71011300
H	1.56886200	-1.00623200	2.59712500
S	2.20066600	-0.04659300	-0.39382400
O	3.27183300	0.70668900	0.26176800
O	1.61138700	0.39999700	-1.65415400
C	2.74448100	-1.75544400	-0.61294400
H	3.51437100	-1.74494700	-1.38754900
H	3.15646100	-2.11978900	0.33010200
H	1.88581700	-2.35106700	-0.92631800
H	-4.08398500	0.25201500	1.01963300
H	-4.25920600	0.86247900	-0.64907900
C	-0.60577200	2.79546900	-0.22812700
H	-0.14171400	3.03437900	0.73834200
H	0.16615700	2.36735200	-0.88190500
H	-0.93360900	3.74574500	-0.67139800

2.040-Me

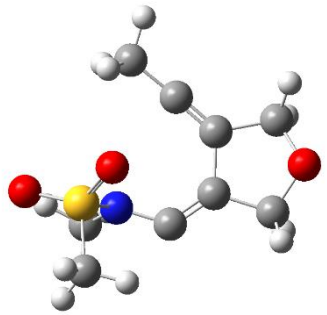

Atom type	X	Y	Z
C	-3.47408200	0.36093600	-0.12784900
C	-1.96841200	0.61333100	0.07205800
C	-1.34077100	1.74278000	0.05288600
C	-1.40148500	-0.79863900	0.25442400
C	-2.57054600	-1.74345800	0.03647900
O	-3.59051900	-0.97464500	-0.58793800
H	-2.91987100	-2.14458700	1.00347800
H	-2.32925300	-2.58525000	-0.61832700
C	-0.16173900	-1.11533100	0.56249900
N	0.89597500	-0.26211400	0.82161800
C	1.41997900	-0.21851900	2.19852900
H	2.16105400	0.57705300	2.26997500
H	0.57803800	0.00082000	2.85902500
H	1.86876200	-1.17383500	2.50037400
S	2.04245100	-0.03736500	-0.45705300
O	3.12209500	0.77930700	0.10371600
O	1.29449500	0.39619500	-1.63421900
C	2.68145900	-1.69482300	-0.78795900
H	3.36347700	-1.60828700	-1.63658400
H	3.21417200	-2.05323000	0.09500300
H	1.83842700	-2.34358500	-1.03042200
H	-4.00653900	0.49749800	0.82934000
H	-3.91928600	1.02019900	-0.87666600
C	-0.57382200	2.97211800	-0.04056700
H	-0.12557000	3.24515200	0.92420500
H	0.24221300	2.85612000	-0.76685800
H	-1.18871000	3.82734300	-0.36649600

2.041-Me

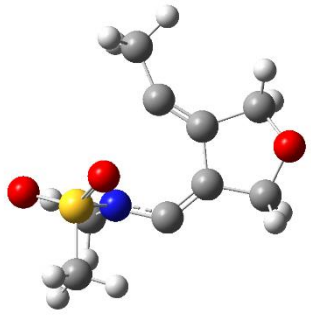

Atom type	X	Y	Z
C	-3.40275900	0.12215200	-0.21397100
C	-1.92313100	0.43826300	0.05021900
C	-1.31733500	1.59783400	0.04601800
C	-1.30239400	-0.90567900	0.30176900
C	-2.41420500	-1.92485800	0.15328000
O	-3.45051100	-1.25461900	-0.55802300
H	-2.77151800	-2.25713500	1.14346700
H	-2.12047900	-2.80751300	-0.42126900
C	-0.02781800	-1.10899800	0.58911000
N	0.92828600	-0.13924200	0.77145300
C	1.31777900	0.23696800	2.14109500
H	1.95699000	1.11823200	2.09547000
H	0.40223000	0.47437400	2.68676000
H	1.84204400	-0.57846900	2.65601500
S	2.13097100	0.01706700	-0.47269100
O	3.01552300	1.10286100	-0.04524600
O	1.42880300	0.05070100	-1.74982300
C	3.04666000	-1.53812200	-0.38223000
H	3.79029400	-1.51539700	-1.18199600
H	3.53685900	-1.60856400	0.59074100
H	2.34235300	-2.35812200	-0.53078700
H	-4.00066600	0.32236300	0.69192200
H	-3.82404700	0.69509600	-1.04505000
C	-1.49199800	3.03698900	-0.17993400
H	-1.29052800	3.61615400	0.73095300
H	-0.80049800	3.39886900	-0.95165300
H	-2.51589400	3.28291000	-0.50909300

2.042-Me

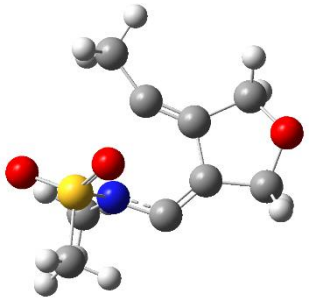

Atom type	X	Y	Z
C	-3.28336800	0.44314500	-0.25581100
C	-1.78590500	0.52639100	0.04726400
C	-0.96122000	1.53187200	0.07647800
C	-1.39202000	-0.91171800	0.31903400
C	-2.63926700	-1.74332300	0.13874500
O	-3.54584300	-0.91388400	-0.58681100
H	-3.06719100	-2.02742700	1.11558500
H	-2.47319400	-2.65476800	-0.44230300
C	-0.14632900	-1.21662200	0.63633400
N	0.77855600	-0.19976000	0.76739100
C	1.22194400	0.17005600	2.12506000
H	1.82774100	1.07387700	2.06635900
H	0.32396200	0.36167800	2.71547600
H	1.79503400	-0.63728000	2.59786500
S	1.99376700	-0.09498300	-0.49022500
O	2.83657700	1.05057500	-0.13897600
O	1.30039800	-0.17499100	-1.76958400
C	2.95300500	-1.61106100	-0.27717500
H	3.69618000	-1.62809700	-1.07752800
H	3.44429500	-1.59263700	0.69746800
H	2.26893000	-2.45683500	-0.36027500
H	-3.86385600	0.75237100	0.63031900
H	-3.58535600	1.06281600	-1.10505700
C	-0.71725200	2.96235100	-0.12159000
H	-0.42424200	3.45800800	0.81341700
H	0.09354900	3.12543600	-0.84273000
H	-1.61259100	3.48075400	-0.50381000

M06-2.032-Ph

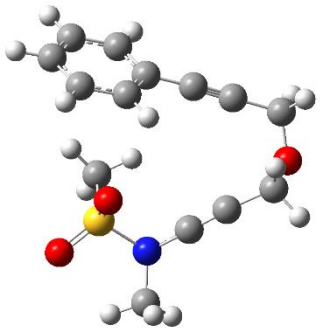

Atom type	X	Y	Z
C	2.50659800	2.48264000	0.68422600
C	2.33485000	1.07116400	0.32095000
C	2.27044600	-0.10397500	0.03919400
N	2.18652500	-1.40520000	-0.32043300
S	0.68137500	-2.16646500	-0.04186300
O	0.88637600	-3.55705600	-0.41583700
O	0.18801600	-1.82942500	1.28307000
C	-0.31851700	-1.34802700	-1.26714400
H	-1.35877600	-1.61960600	-1.06900300
H	-0.18239000	-0.26950300	-1.16205200
H	0.01126800	-1.69850200	-2.24526200
C	3.39993200	-2.23433400	-0.22640300
H	4.18975400	-1.71416100	-0.77002300
H	3.70065500	-2.38221800	0.81535700
H	3.19716000	-3.19595600	-0.69613200
O	2.16620200	3.38431200	-0.35668200
C	0.87793600	3.95259400	-0.23639800
C	-0.21066300	2.96530000	-0.16499700
C	-1.10321000	2.15578200	-0.04837300
C	-2.12090300	1.15125500	0.08012200
C	-2.06783000	0.24229200	1.14572400
C	-3.00381600	-0.78439200	1.23239400
C	-4.00504800	-0.90389200	0.26882100
C	-4.06775700	0.00620700	-0.78894700
C	-3.13018400	1.02920500	-0.88748200
H	-3.16275300	1.73292800	-1.71381000
H	-4.84629700	-0.08515200	-1.54058700
H	-4.73300700	-1.70692100	0.33778100
H	-2.93510900	-1.50038100	2.04545600
H	-1.26693500	0.31794300	1.87383300
H	0.83331700	4.59370000	0.65737900
H	0.75330300	4.58997300	-1.11495300
H	1.93167600	2.71223600	1.59196600
H	3.56470100	2.65188900	0.90835600

M06-2.033-Ph

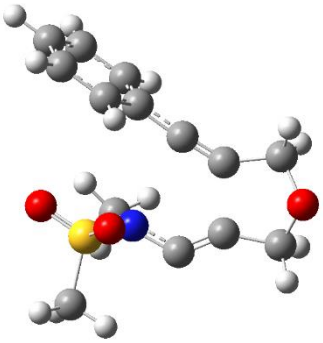

Atom type	X	Y	Z
C	2.55415900	-2.55417200	-0.43404000
C	1.44513700	-1.57720200	-0.13022500
C	0.20103500	-1.46786100	-0.11066100
C	-1.21857500	-1.44291300	-0.11077900
C	-1.94016700	-1.92553100	0.99909700
C	-3.33013300	-1.89595700	0.99676700
C	-4.02077600	-1.39291100	-0.10618900
C	-3.31212200	-0.91694100	-1.21145900
C	-1.92451700	-0.93641700	-1.22044400
H	-1.36616400	-0.53923200	-2.06273400
H	-3.84622000	-0.51478600	-2.06703300
H	-5.10632700	-1.36873700	-0.10364100
H	-3.87691100	-2.26951200	1.85778700
H	-1.39680600	-2.32411200	1.85148500
C	2.51436900	-0.16508200	0.34106800
C	3.86648100	-0.78160600	0.20204800
O	3.74685500	-1.85238100	-0.70887400
H	4.21749900	-1.14598300	1.18015700
H	4.59160300	-0.07337200	-0.20145300
C	1.86171100	0.88017300	0.63195800
N	0.50962200	1.03886500	0.75052700
C	-0.10851200	0.89731800	2.07469000
H	-1.18129400	0.75310100	1.94075500
H	0.33047400	0.00965700	2.53425500
H	0.08165600	1.77152600	2.70898600
S	-0.23342100	2.12141100	-0.33906100
O	-1.63971600	2.13466400	0.02877700
O	0.19756400	1.74897200	-1.67194400
C	0.48476100	3.70875200	0.05506800
H	0.02451800	4.43378000	-0.61910700
H	0.25142600	3.94832300	1.09385300
H	1.56078200	3.64617200	-0.11086200
H	2.69015600	-3.21414400	0.43648700
H	2.31826300	-3.15524000	-1.31271500

M06-2.034-Ph

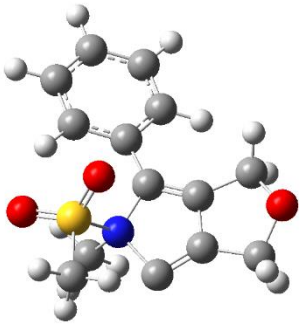

Atom type	X	Y	Z
C	-0.45989700	2.98455200	-0.44257000
C	-0.58481400	1.56558200	0.01732100
C	0.16646600	0.46763000	0.21213100
C	1.61616700	0.28246700	0.10110900
C	2.42052700	1.43690900	0.13363600
C	3.80095400	1.35476700	0.00490500
C	4.41958100	0.11301400	-0.14190300
C	3.63718200	-1.03787700	-0.16038600
C	2.25034500	-0.96006800	-0.04583100
H	1.67491600	-1.87745500	-0.08676200
H	4.10324900	-2.01199900	-0.27553100
H	5.49895500	0.04542700	-0.23724200
H	4.39613100	2.26280200	0.03188000
H	1.95876100	2.40865500	0.28140000
N	-0.79620500	-0.55444900	0.72151300
C	-2.25247400	0.09626900	0.84780700
C	-1.96748900	1.33194200	0.37811600
C	-2.70657300	2.61969700	0.13608500
O	-1.80448300	3.39851200	-0.66399900
H	-2.92413300	3.14892500	1.07443000
H	-3.63258400	2.50503300	-0.43084700
C	-0.40295000	-1.09023000	2.05247900
H	0.57917000	-1.55956000	1.99114700
H	-0.39210400	-0.23559700	2.73144200
H	-1.15605500	-1.80677500	2.37866800
S	-1.02781600	-1.92788400	-0.48405700
O	-0.19704800	-3.01576100	0.01022700
O	-0.79436100	-1.32921200	-1.77875800
C	-2.72809200	-2.44005500	-0.32086200
H	-2.75530700	-3.38547900	-0.87111000
H	-2.95983000	-2.57886200	0.73377700
H	-3.36716800	-1.67598800	-0.75521400
H	0.00993600	3.61098000	0.33282300
H	0.09809200	3.10126800	-1.37651500

M06-2.047-Ph

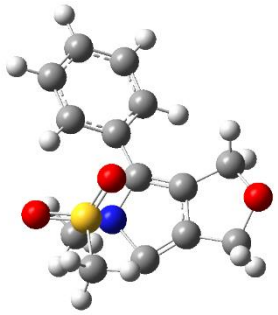

Atom type	X	Y	Z
C	-0.37865400	2.90375800	-0.48419500
C	-0.46682800	1.54417200	0.12619800
C	0.31227200	0.46077300	0.40614700
C	1.73631900	0.21852400	0.16143200
C	2.63123600	1.29403600	0.26060800
C	3.98645200	1.11561600	0.00278800
C	4.47190200	-0.14345100	-0.34916800
C	3.58977000	-1.21807000	-0.44987000
C	2.23048900	-1.04198100	-0.20468200
H	1.55152500	-1.88239400	-0.32381200
H	3.95706800	-2.19922000	-0.73581700
H	5.53010400	-0.28503000	-0.54689000
H	4.66547300	1.95913500	0.08539100
H	2.25959700	2.27155300	0.55834000
N	-0.58266900	-0.49475200	0.96146900
C	-2.00328800	0.07852300	1.12017200
C	-1.81845900	1.28895500	0.50582500
C	-2.63327000	2.49159500	0.12247800
O	-1.73883000	3.29957600	-0.65915100
H	-2.97241000	3.05770500	0.99983200
H	-3.50016500	2.25964700	-0.50272000
C	-0.12937200	-1.31576600	2.09561800
H	0.78518300	-1.84910500	1.84004800
H	0.03802400	-0.63244800	2.93199300
H	-0.92274700	-2.01588400	2.35188500
S	-1.32365500	-1.67566000	-0.47876700
O	-0.67776100	-2.93052300	-0.10658800
O	-0.93970600	-0.95691100	-1.67867300
C	-3.08906200	-2.01057500	-0.52573300
H	-3.19717200	-2.81489000	-1.26088200
H	-3.39526900	-2.31853000	0.47154200
H	-3.58661400	-1.09161900	-0.82671000
H	0.13984800	3.61347200	0.17750300
H	0.11807000	2.90763200	-1.46012000

M06-2.048-Ph

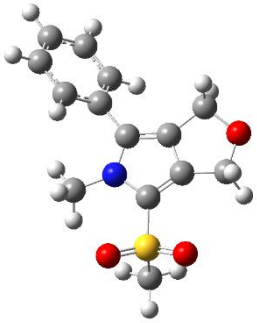

Atom type	X	Y	Z
C	0.59966600	2.84889400	-0.21290900
C	0.28672300	1.38974000	-0.04883600
C	0.87829000	0.14032300	0.02116400
C	2.31032300	-0.20184400	0.02964000
C	3.17779400	0.50333200	0.87328200
C	4.54458000	0.23758000	0.86398700
C	5.06166900	-0.74013100	0.01514200
C	4.20625300	-1.44383300	-0.83209700
C	2.84062600	-1.17285600	-0.83049400
H	2.18216400	-1.69943300	-1.51668400
H	4.60451000	-2.19690900	-1.50556600
H	6.12705200	-0.94976000	0.01005100
H	5.20536700	0.79009600	1.52532100
H	2.76965000	1.25338300	1.54579300
N	-0.13716500	-0.79392700	0.03933400
C	-1.34780700	-0.13013200	-0.04781000
C	-1.10000500	1.22147100	-0.09962000
C	-1.75800800	2.55066900	-0.29429900
O	-0.68163500	3.48104700	-0.11311400
H	-2.53592800	2.78205500	0.43835600
H	-2.18657300	2.64521800	-1.29978700
C	0.02648300	-2.23389700	0.21357200
H	-0.12388500	-2.75927200	-0.73186800
H	1.02834800	-2.42266000	0.59799200
H	-0.70580300	-2.60759500	0.93063800
S	-2.92366000	-0.88783800	-0.09205300
O	-2.79684800	-2.21283100	-0.69940500
O	-3.83183800	0.11719700	-0.63939900
C	-3.38836600	-1.12884800	1.61974700
H	-4.37719100	-1.59363600	1.60616300
H	-2.66381700	-1.78750500	2.10171000
H	-3.42408300	-0.15376800	2.10741700
H	1.23755800	3.27015700	0.56986500
H	1.05460000	3.06642300	-1.18936900

M06-2.032-Me

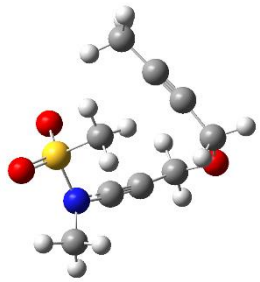

Atom type	X	Y	Z
C	2.37234200	-1.57157000	-0.96048400
C	0.92739800	-1.51702500	-0.71305700
C	-0.26074300	-1.36721300	-0.54133800
N	-1.57620300	-1.12524700	-0.34231000
S	-1.97856200	0.50487800	-0.06398700
O	-1.34020000	1.28725000	-1.10410400
O	-3.41775300	0.51881000	0.13171200
C	-1.17926200	0.89352400	1.48406400
H	-1.44939800	1.92409100	1.72450100
H	-1.55363900	0.21307800	2.25111200
H	-0.09921500	0.80367800	1.34168800
C	-2.39519700	-2.16612100	0.29612000
H	-2.25673200	-3.08605900	-0.27333900
H	-2.09321200	-2.33363300	1.33677700
H	-3.43928300	-1.85997700	0.24935800
O	3.17880400	-1.51347400	0.20443000
C	2.80783700	-0.52907300	1.15327000
C	2.47547000	0.78078700	0.56922600
C	2.10291200	1.81145700	0.05726400
H	1.94057700	-0.88395900	1.72996200
H	3.65845200	-0.44926400	1.83415400
H	2.64600400	-2.50610000	-1.45558800
H	2.62528300	-0.73799800	-1.62927600
C	1.62406800	3.04453200	-0.56942300
H	0.63109400	2.88251300	-1.00065300
H	1.56131900	3.85220300	0.16604500
H	2.30340600	3.36363800	-1.36494800

M06-2.033-Me

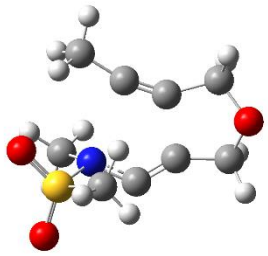

Atom type	X	Y	Z
C	-3.26198900	0.63915100	-0.36369800
C	-1.78941300	0.81979600	-0.10978900
C	-0.83124700	1.61999700	-0.11704400
C	-1.46819600	-0.92370500	0.45978000
C	-2.84018300	-1.49741300	0.37284300
O	-3.55461800	-0.72757100	-0.57264100
H	-3.33325800	-1.45164700	1.35613700
H	-2.82749400	-2.53161400	0.02496000
C	-0.24678800	-1.10439600	0.74445100
N	0.71643500	-0.12808200	0.73958200
C	1.13363900	0.40557400	2.05073700
H	0.22684900	0.73769400	2.55893700
H	1.64080500	-0.36015900	2.64519300
H	1.80024900	1.25292800	1.87909600
S	2.06204600	-0.39481400	-0.31083200
O	2.86507900	-1.51530800	0.14757400
O	2.67919800	0.91744000	-0.45634200
C	1.22192100	-0.83458000	-1.81628300
H	1.99717800	-0.83965200	-2.58543200
H	0.78012400	-1.82330200	-1.69636300
H	0.46102300	-0.07934300	-2.02108300
H	-3.81971200	1.01829800	0.50657500
H	-3.58125500	1.17673500	-1.25749300
C	0.05721600	2.78166100	-0.20471700
H	0.43537400	3.05699300	0.78604600
H	0.92639200	2.57647200	-0.83619500
H	-0.48107800	3.64720300	-0.61055100

M06-2.034-Me

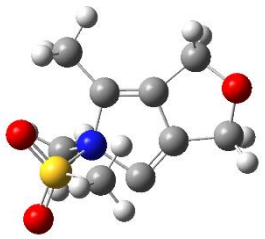

Atom type	X	Y	Z
C	-2.93511400	0.82130600	-0.52981000
C	-1.53385300	0.55756600	-0.07066500
C	-0.33705000	1.15215600	-0.01025800
C	-1.49651200	-0.77308400	0.51829500
C	-2.88752400	-1.33466800	0.39929900
O	-3.53605600	-0.47143800	-0.54981200
H	-3.42502000	-1.30232700	1.35732300
H	-2.93309600	-2.35056000	0.00156300
C	-0.30105600	-1.16914000	1.01475700
N	0.53223100	0.14739600	0.68387100
C	1.09392200	0.67947600	1.96089100
H	0.23918300	1.00215900	2.55757000
H	1.62302800	-0.12935400	2.46060000
H	1.76147700	1.51857800	1.74889800
S	1.93844300	-0.38542400	-0.33867000
O	2.81294200	-1.13350600	0.53501300
O	2.42282900	0.81382300	-1.00093600
C	1.14759000	-1.44400400	-1.52818100
H	1.89589400	-1.58500800	-2.31186700
H	0.88137300	-2.37341400	-1.02876300
H	0.26885500	-0.92578200	-1.91714100
H	-3.45914900	1.48227000	0.17791900
H	-3.01432100	1.24698500	-1.53351900
C	0.11335800	2.53759200	-0.33806700
H	0.48526700	3.06265300	0.55036300
H	0.90404700	2.55759400	-1.09045800
H	-0.74852800	3.09700500	-0.71254300

6.2.9. NMR Spectra

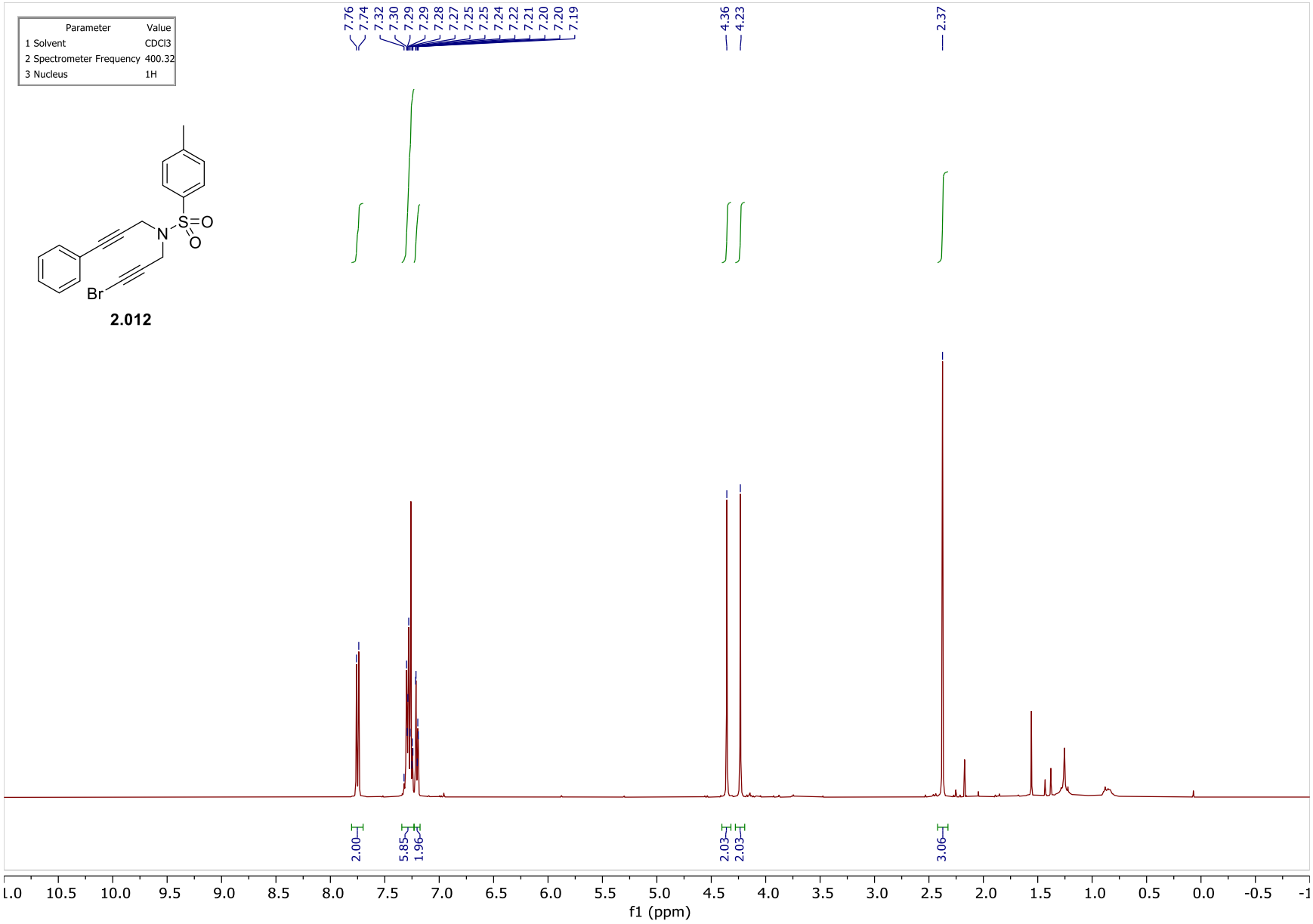
Parameter Value
1 Solvent CDCl3
2 Spectrometer Frequency 400.32
3 Nucleus 1H
7.76
7.74
7.32
7.30
7.29
7.29
7.28
7.27
7.25
7.25
7.24
7.22
7.21
7.20
7.20
7.19
4.36
4.23
2.37
2.012
2.00
5.85
1.96
2.03
2.03
3.06
f1 (ppm)

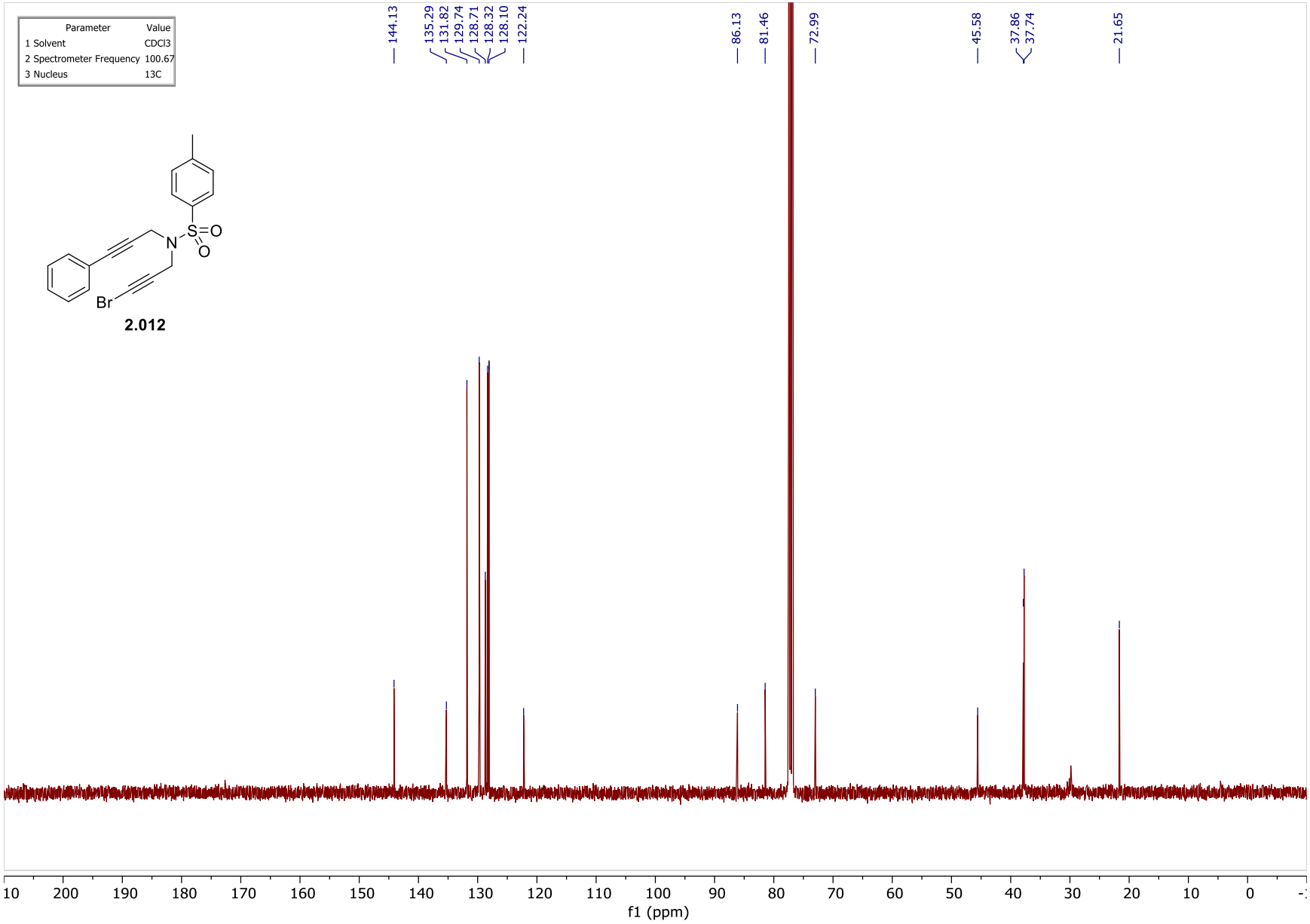
Parameter Value
1 Solvent CDCl3
2 Spectrometer Frequency 100.67
3 Nucleus 13C
144.13
135.29
131.82
129.74
128.71
128.32
128.10
122.24
86.13
81.46
72.99
45.58
37.86
37.74
21.65
S=O
O
N
Br
2.012
f1 (ppm)

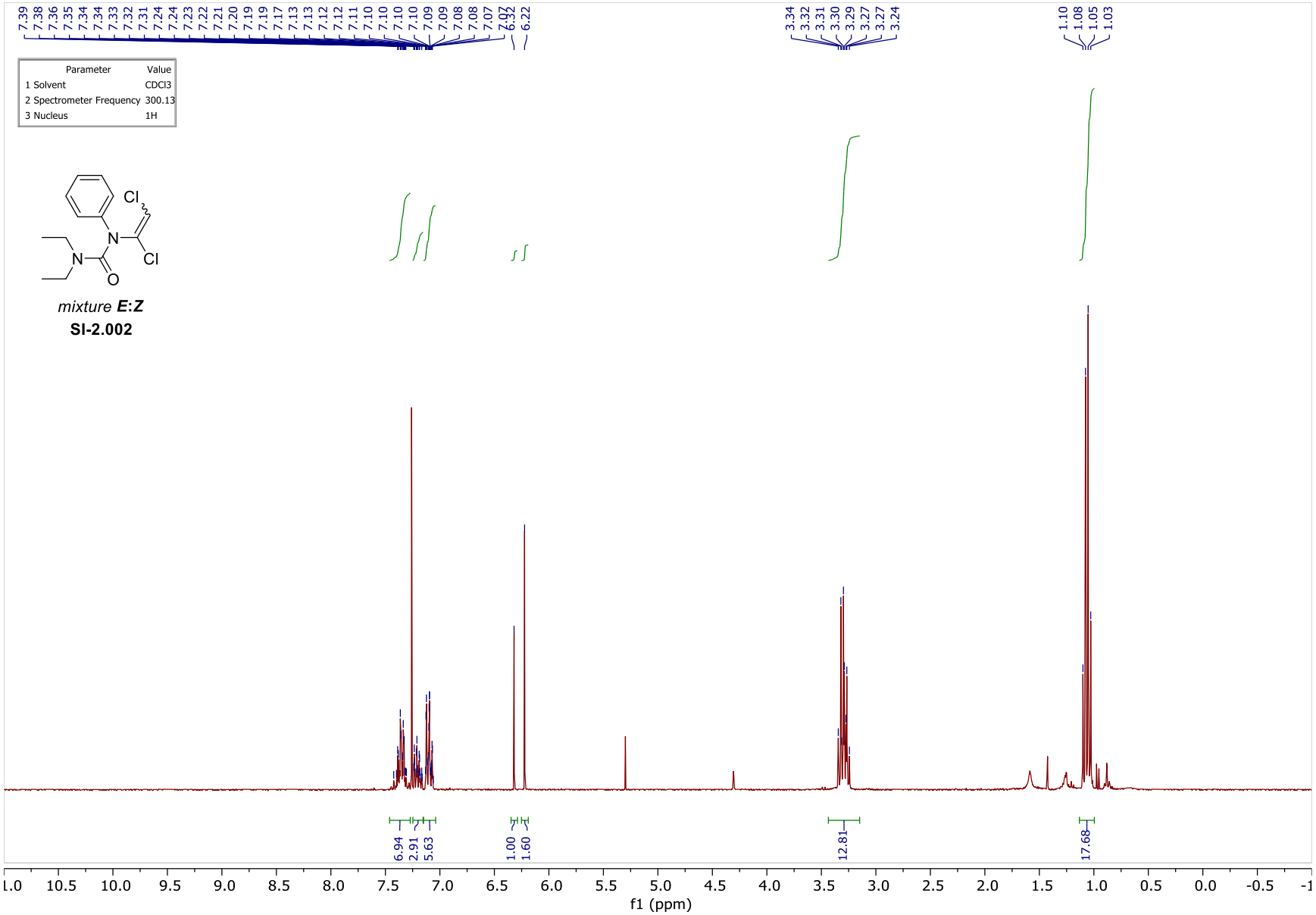
7.39 7.38 7.36 7.35 7.34 7.34 7.33 7.32 7.31 7.24 7.24 7.23 7.22 7.21 7.20 7.19 7.19 7.17 7.13 7.13 7.12 7.12 7.11 7.10 7.10 7.10 7.10 7.09 7.09 7.08 7.08 7.07 7.07 6.32 6.22
3.34 3.32 3.31 3.30 3.29 3.27 3.27 3.24
1.10 1.08 1.05 1.03
Parameter Value
1 Solvent CDCl3
2 Spectrometer Frequency 300.13
3 Nucleus 1H
Cl
N
N
Cl
O
mixture E:Z
SI-2.002
6.94 2.91 5.63 1.00 1.60 12.81 17.68
f1 (ppm)

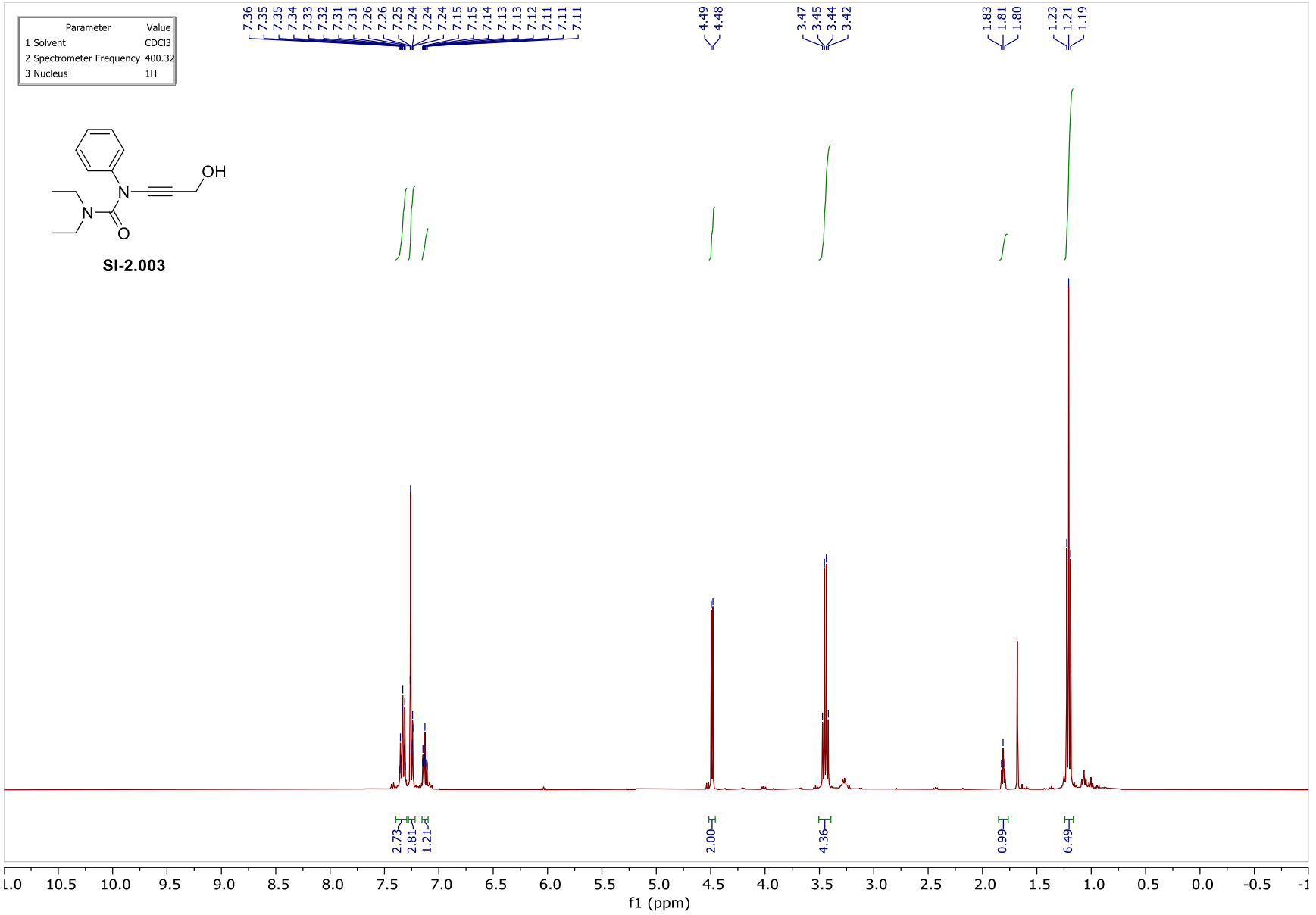
Parameter Value
1 Solvent CDCl3
2 Spectrometer Frequency 400.32
3 Nucleus 1H
OH
N
N
O
SI-2.003
7.36 7.35 7.35 7.34 7.33 7.32 7.31 7.31 7.26 7.26 7.25 7.24 7.24 7.24 7.15 7.15 7.14 7.13 7.13 7.12 7.11 7.11 7.11
4.49 4.48
3.47 3.45 3.44 3.42
1.83 1.81 1.80
1.23 1.21 1.19
2.73 2.81 1.21 2.00 4.36 0.99 6.49
f1 (ppm)

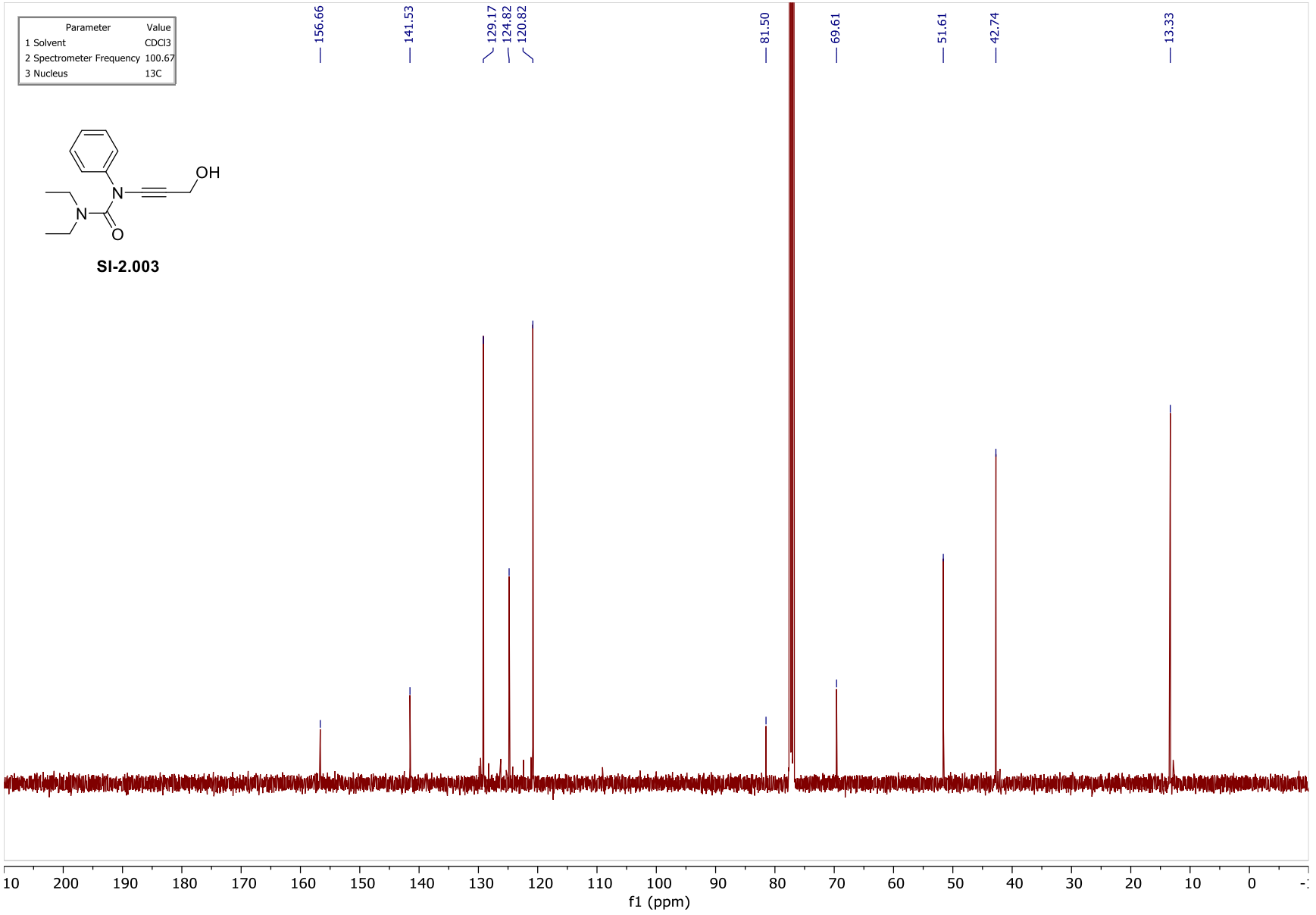
Parameter Value
1 Solvent CDCl3
2 Spectrometer Frequency 100.67
3 Nucleus 13C
156.66
141.53
129.17
124.82
120.82
81.50
69.61
51.61
42.74
13.33
OH
N
N
O
SI-2.003
10 200 190 180 170 160 150 140 130 120 110 100 90 80 70 60 50 40 30 20 10 0
f1 (ppm)

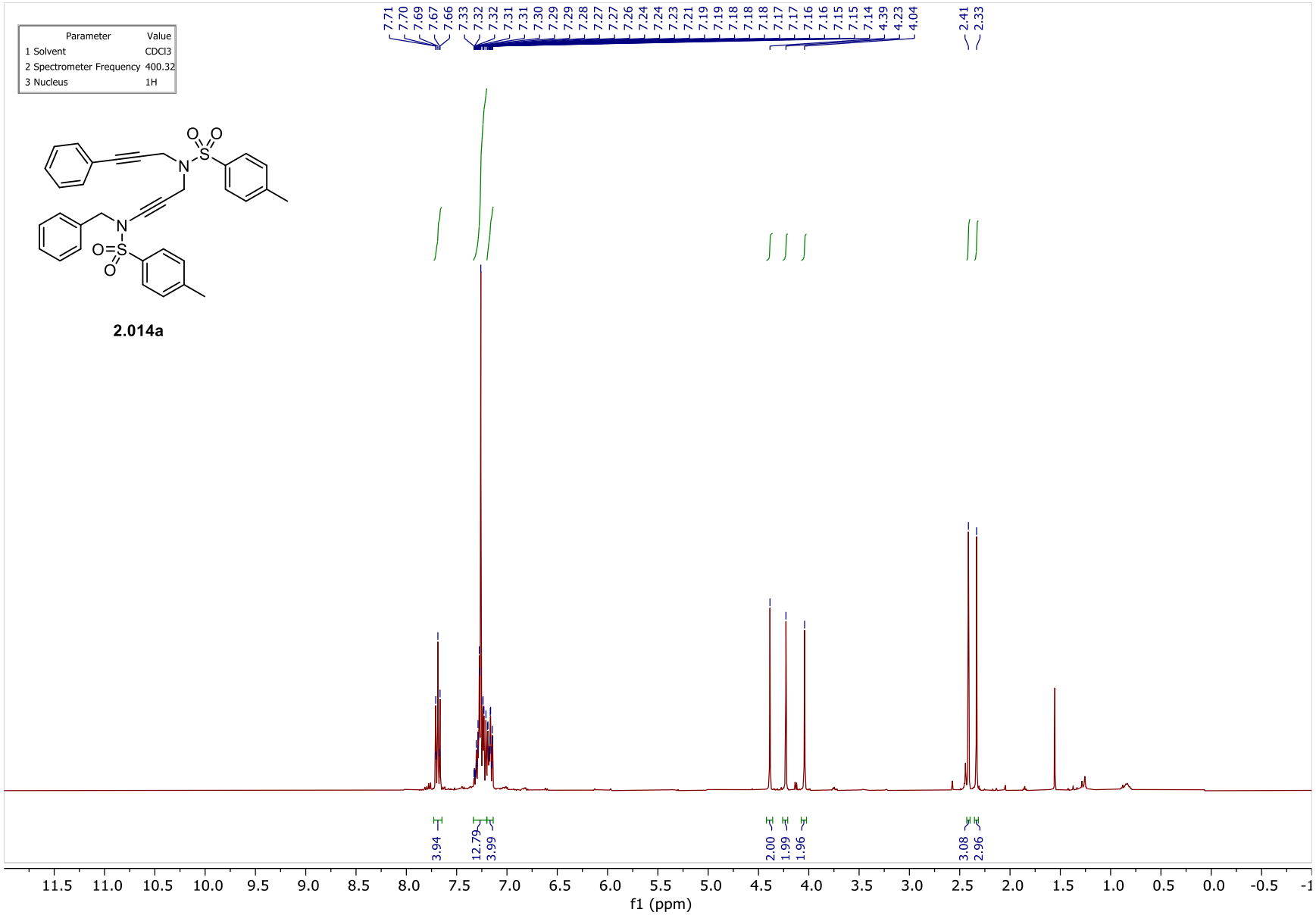
Parameter Value
1 Solvent CDCl3
2 Spectrometer Frequency 400.32
3 Nucleus 1H
2.014a
7.71 7.70 7.69 7.67 7.66 7.33 7.32 7.32 7.31 7.31 7.30 7.29 7.29 7.28 7.27 7.27 7.26 7.24 7.24 7.23 7.21 7.19 7.19 7.18 7.18 7.18 7.17 7.17 7.16 7.16 7.15 7.15 7.14 4.39 4.23 4.04 2.41 2.33
3.94 12.79 3.99 2.00 1.99 1.96 3.08 2.96
11.5 11.0 10.5 10.0 9.5 9.0 8.5 8.0 7.5 7.0 6.5 6.0 5.5 5.0 4.5 4.0 3.5 3.0 2.5 2.0 1.5 1.0 0.5 0.0 -0.5 -1
f1 (ppm)

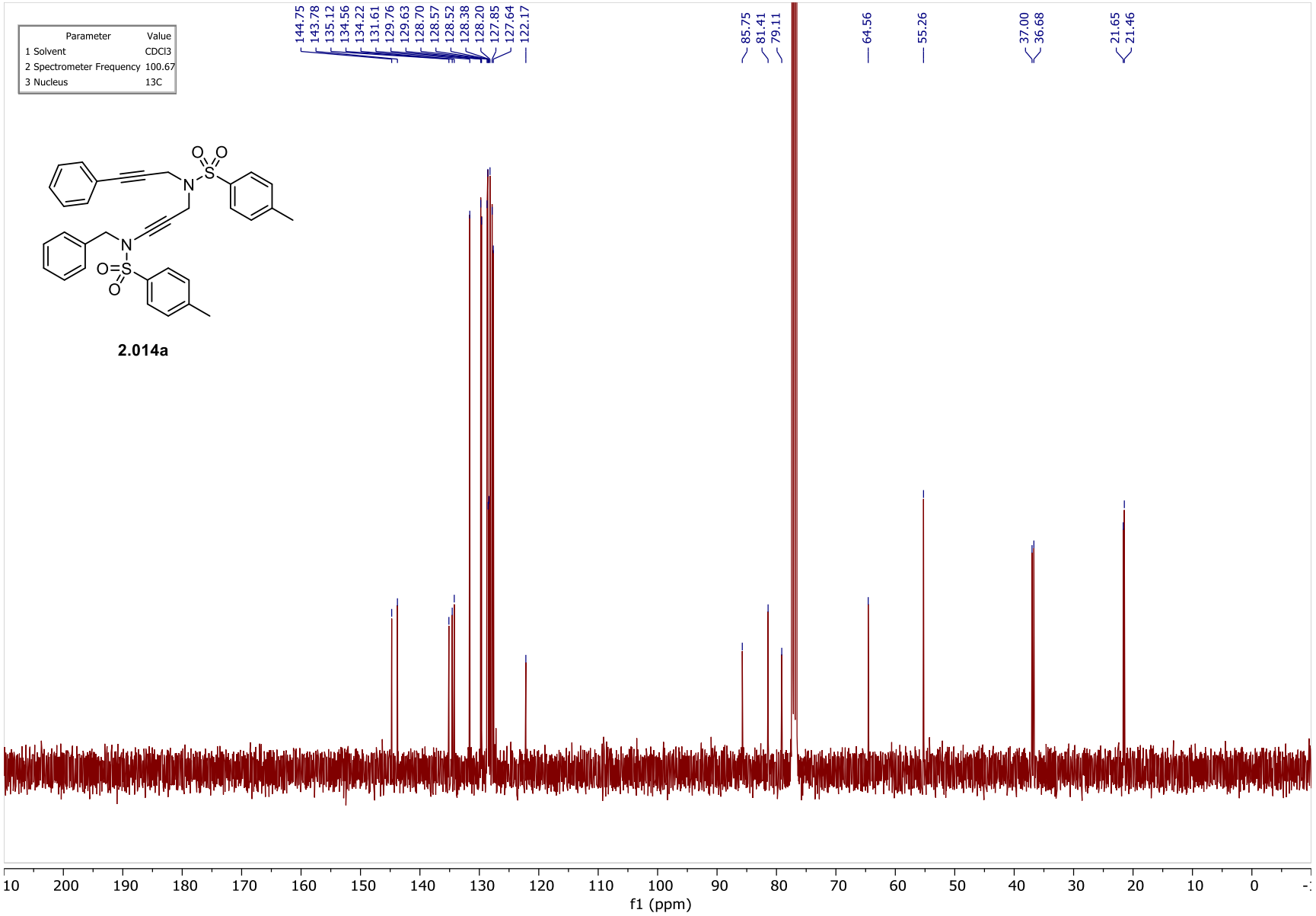
Parameter Value
1 Solvent CDCl3
2 Spectrometer Frequency 100.67
3 Nucleus 13C
144.75
143.78
135.12
134.56
134.22
131.61
129.76
129.63
128.70
128.57
128.52
128.38
128.20
127.85
127.64
122.17
85.75
81.41
79.11
64.56
55.26
37.00
36.68
21.65
21.46
2.014a
f1 (ppm)

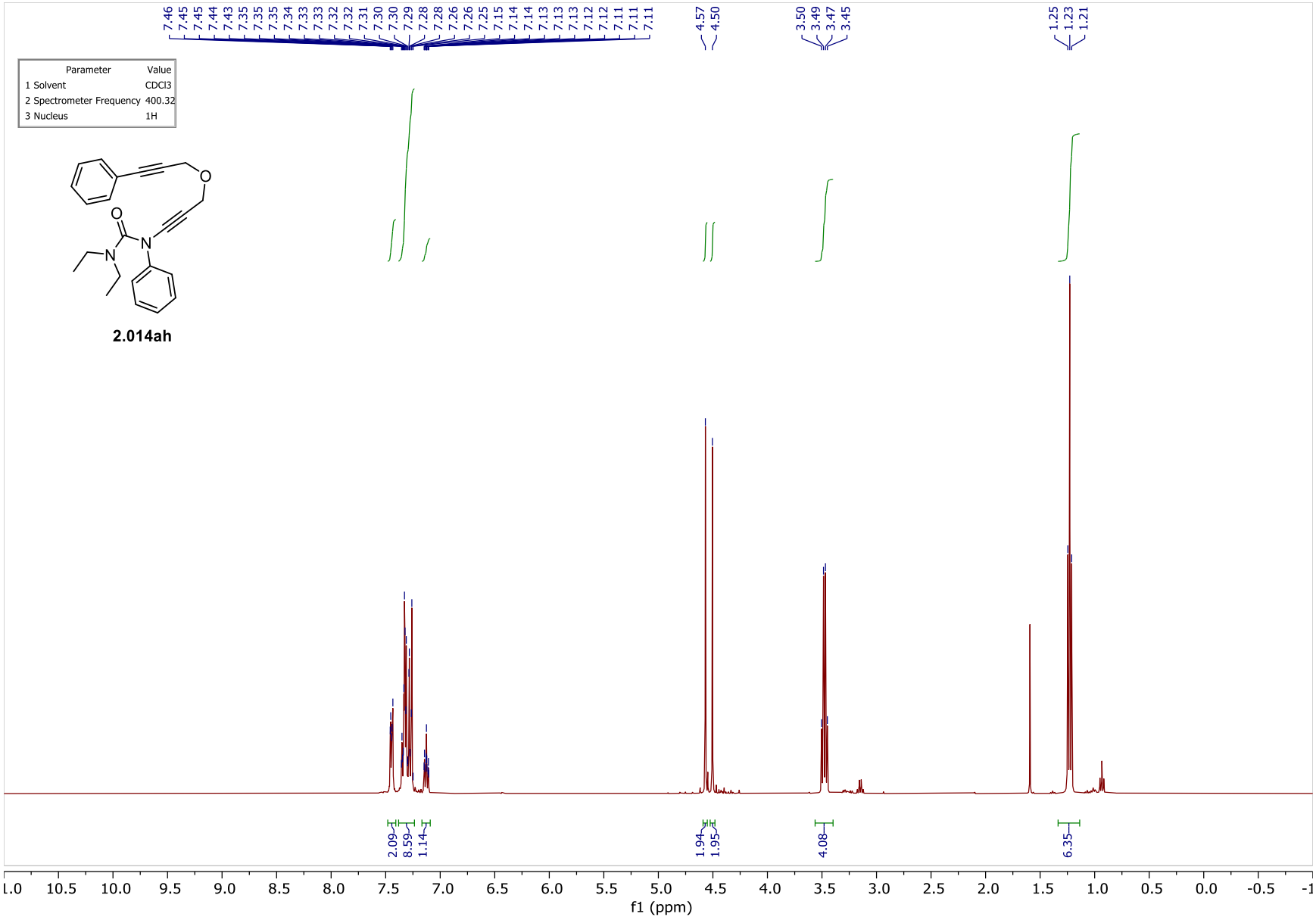
Parameter Value
1 Solvent CDCl3
2 Spectrometer Frequency 400.32
3 Nucleus 1H
2.014ah
f1 (ppm)

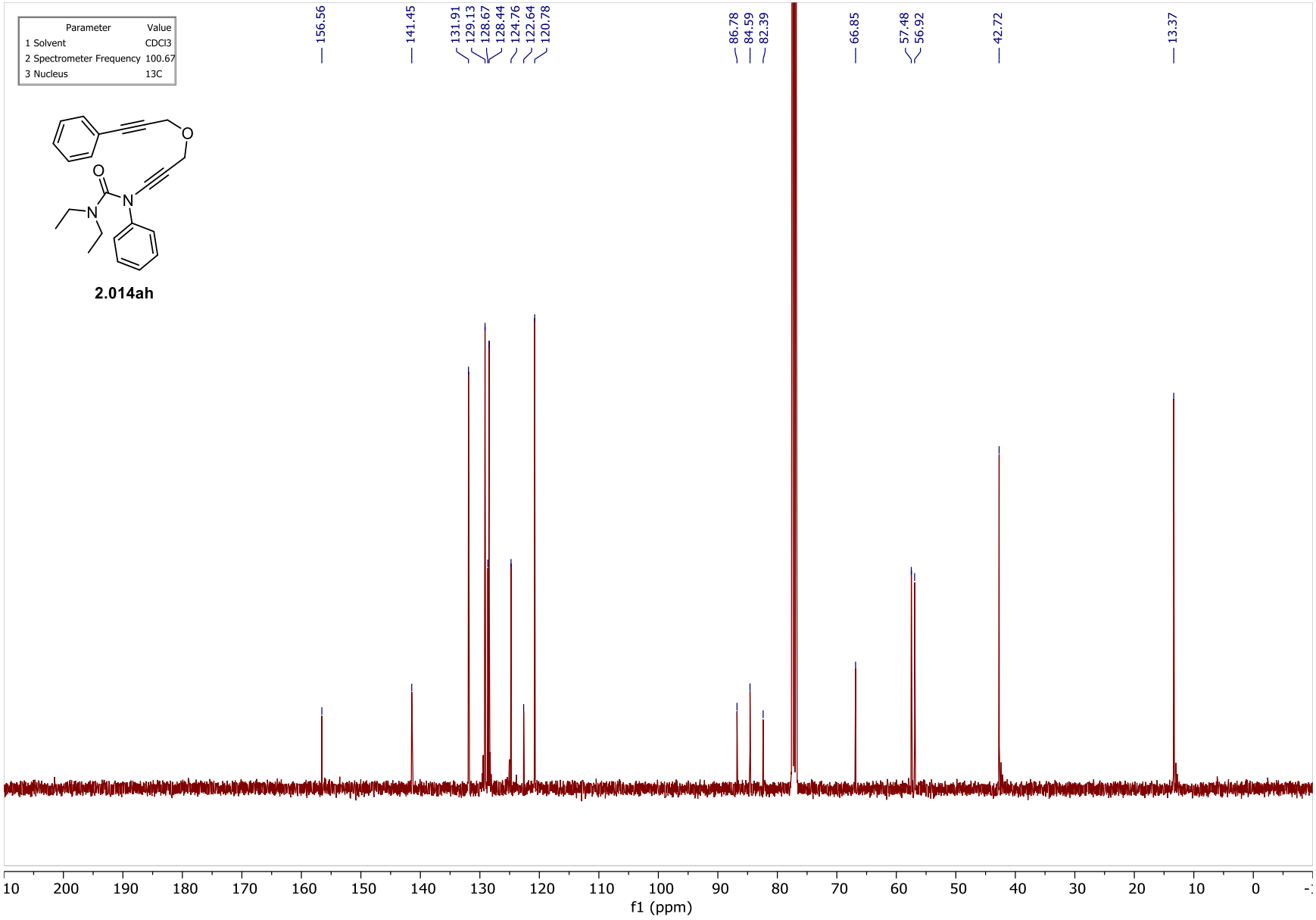
Parameter Value
1 Solvent CDCl3
2 Spectrometer Frequency 100.67
3 Nucleus 13C
156.56
141.45
131.91
129.13
128.67
128.44
124.76
122.64
120.78
86.78
84.59
82.39
66.85
57.48
56.92
42.72
13.37
O
O
N
N
2.014ah
10 200 190 180 170 160 150 140 130 120 110 100 90 80 70 60 50 40 30 20 10 0
f1 (ppm)

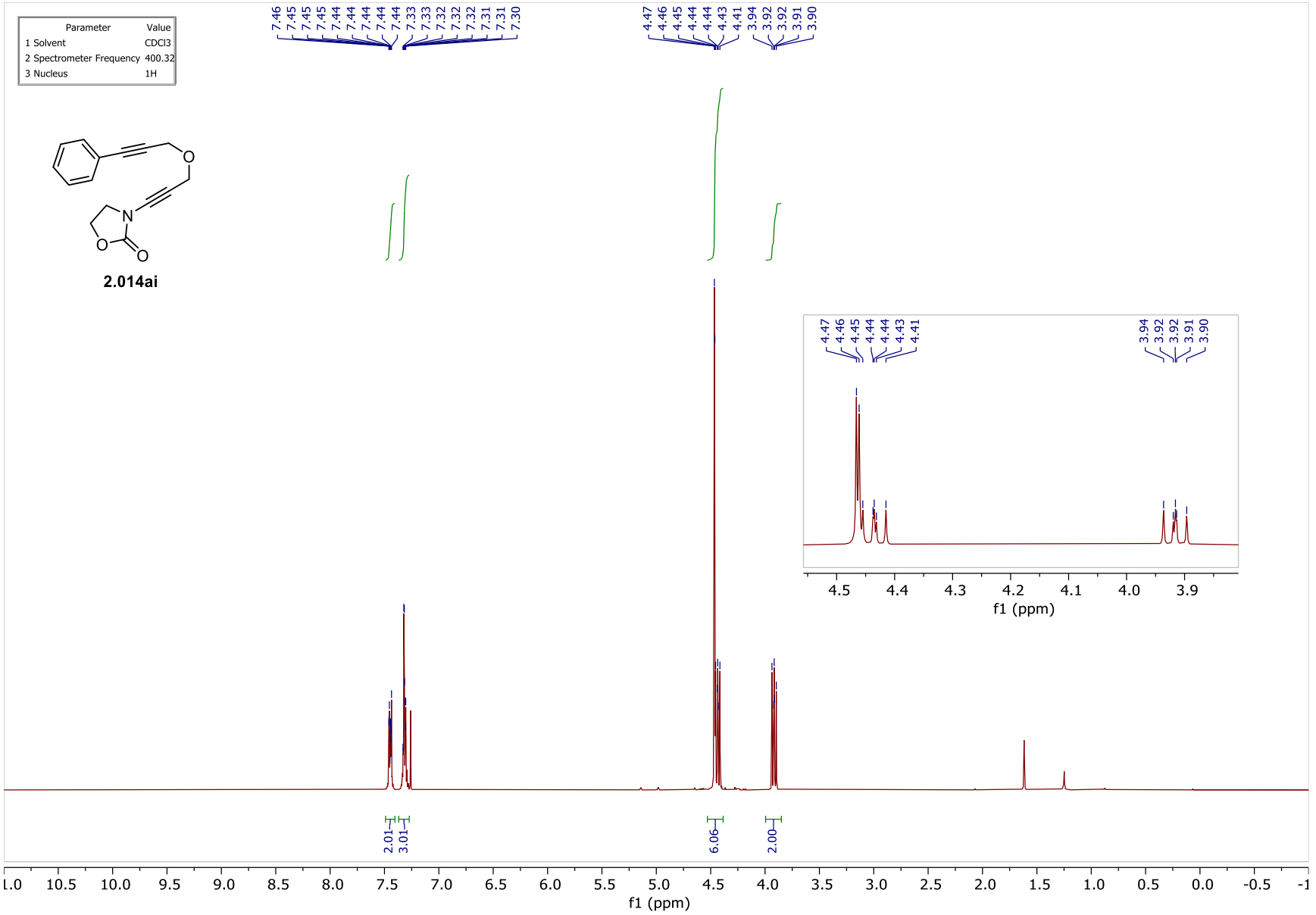
Parameter Value
1 Solvent CDCl3
2 Spectrometer Frequency 400.32
3 Nucleus 1H
2.014ai
7.46 7.45 7.45 7.45 7.44 7.44 7.44 7.44 7.44 7.33 7.33 7.32 7.32 7.32 7.31 7.31 7.30
4.47 4.46 4.45 4.44 4.44 4.43 4.41 3.94 3.92 3.92 3.91 3.90
2.01 3.01 6.06 2.00
f1 (ppm)

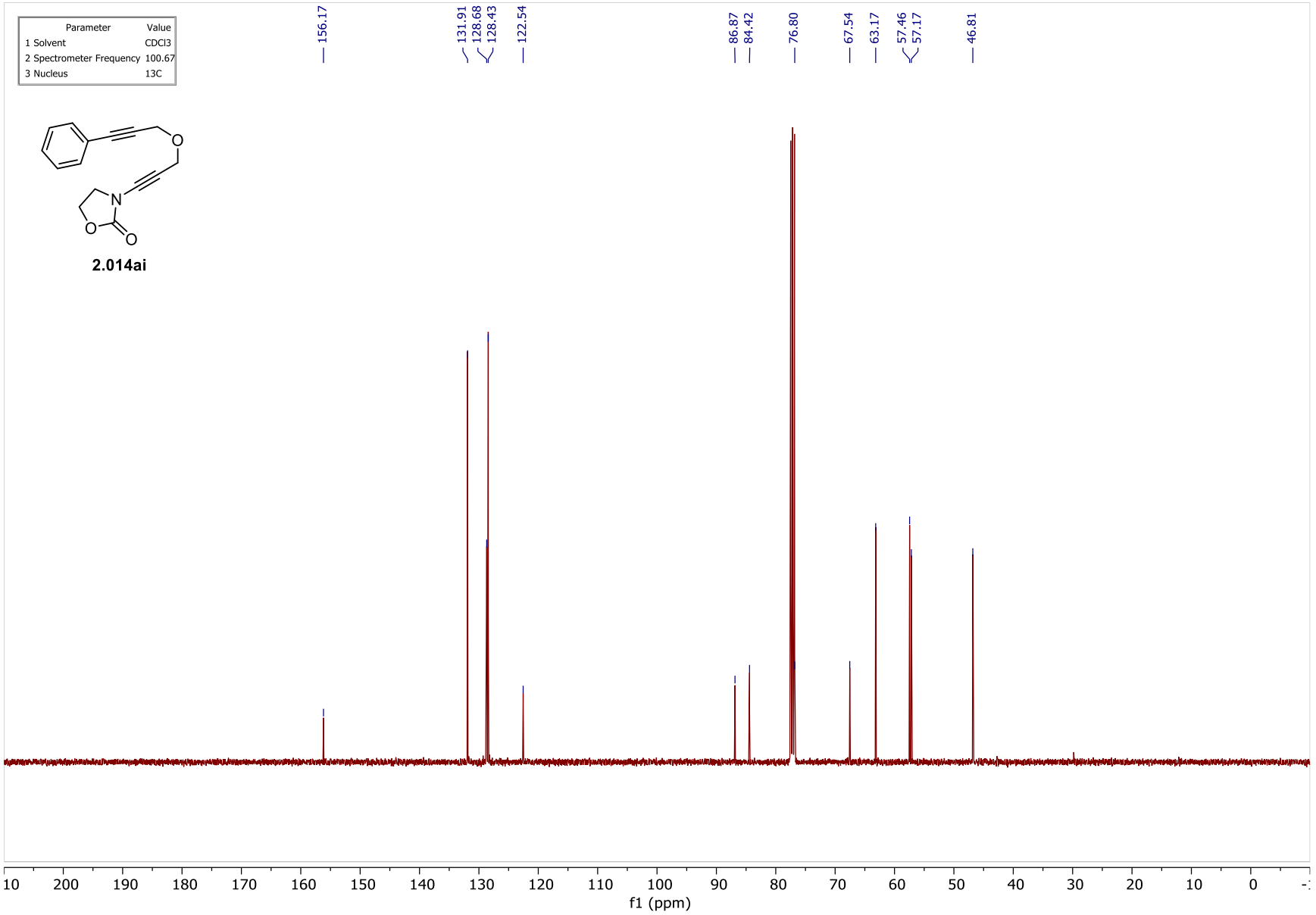
Parameter Value
1 Solvent CDCl3
2 Spectrometer Frequency 100.67
3 Nucleus 13C
156.17
131.91
128.68
128.43
122.54
86.87
84.42
76.80
67.54
63.17
57.46
57.17
46.81
O
N
O
O
2.014ai
f1 (ppm)

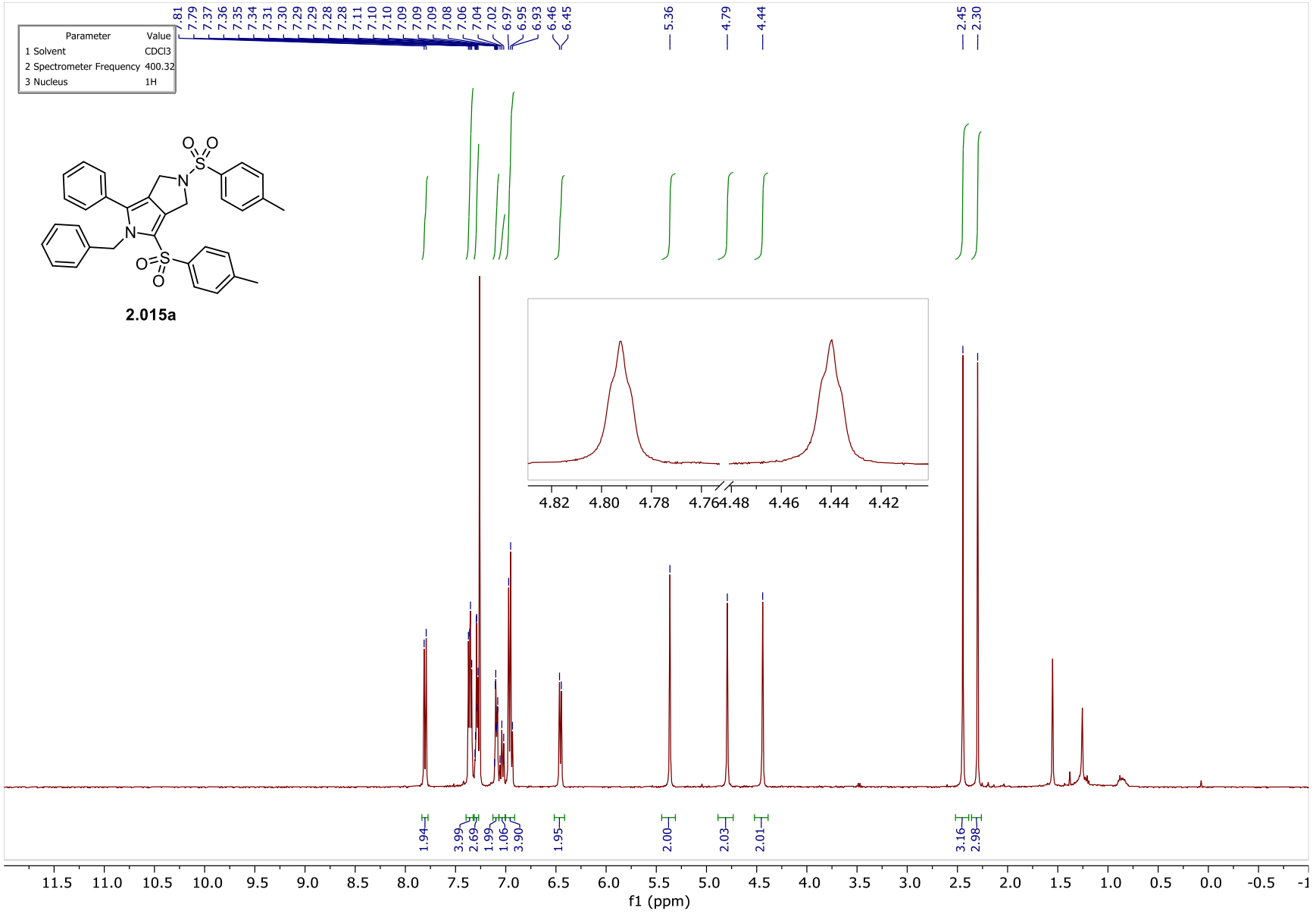
Parameter Value
1 Solvent CDCl3
2 Spectrometer Frequency 400.32
3 Nucleus 1H
2.015a
7.81 7.79 7.37 7.36 7.35 7.34 7.31 7.30 7.29 7.29 7.28 7.28 7.11 7.10 7.10 7.09 7.09 7.09 7.08 7.06 7.04 7.02 6.97 6.95 6.93 6.46 6.45
5.36
4.79
4.44
2.45
2.30
4.82 4.80 4.78 4.76 4.48 4.46 4.44 4.42
1.94 3.99 2.69 1.99 1.06 3.90 1.95 2.00 2.03 2.01 3.16 2.98
11.5 11.0 10.5 10.0 9.5 9.0 8.5 8.0 7.5 7.0 6.5 6.0 5.5 5.0 4.5 4.0 3.5 3.0 2.5 2.0 1.5 1.0 0.5 0.0 -0.5 -1
f1 (ppm)

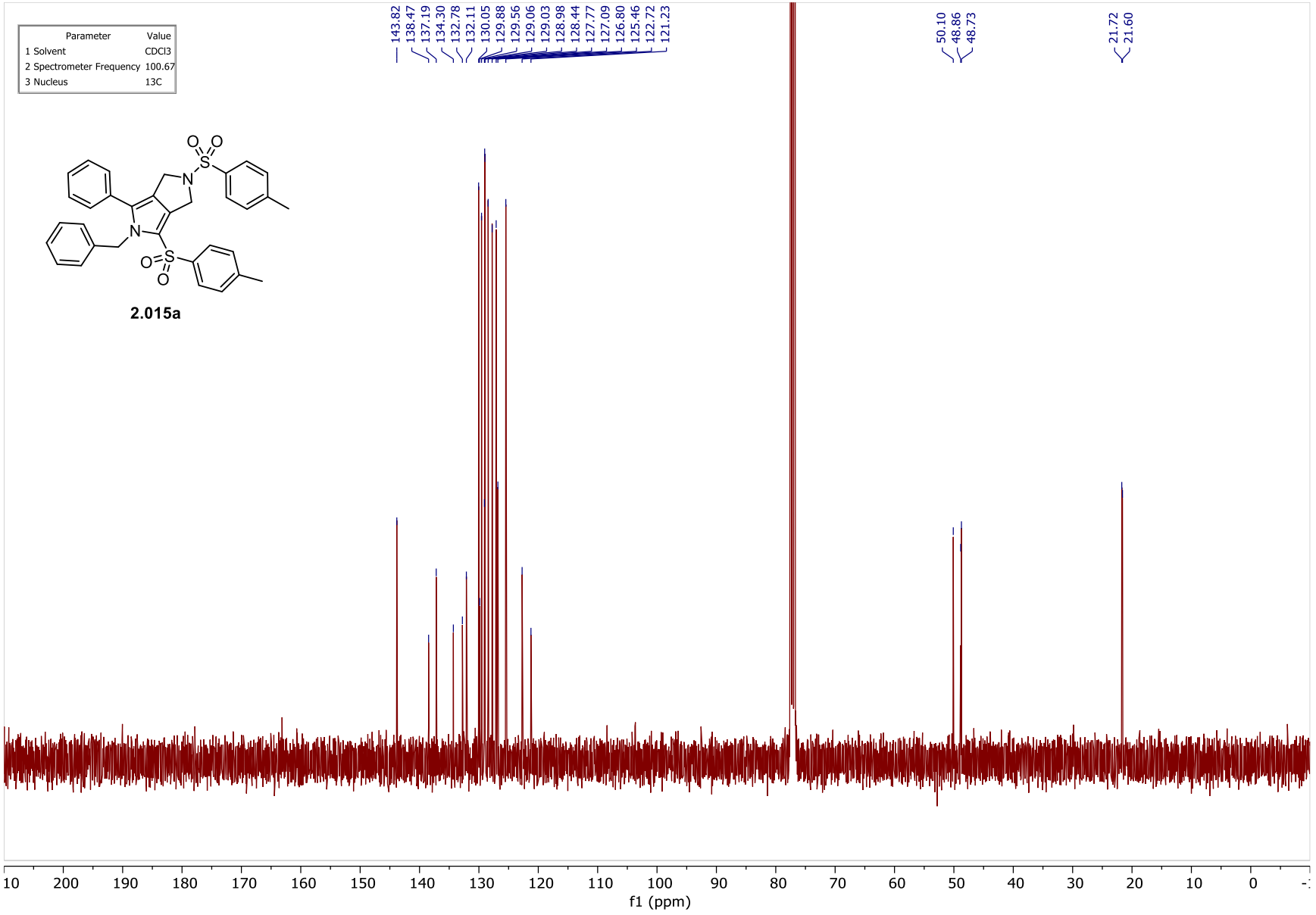
Parameter Value
1 Solvent CDCl3
2 Spectrometer Frequency 100.67
3 Nucleus 13C
143.82
138.47
137.19
134.30
132.78
132.11
130.05
129.88
129.56
129.06
129.03
128.98
128.44
127.77
127.09
126.80
125.46
122.72
121.23
50.10
48.86
48.73
21.72
21.60
2.015a
f1 (ppm)

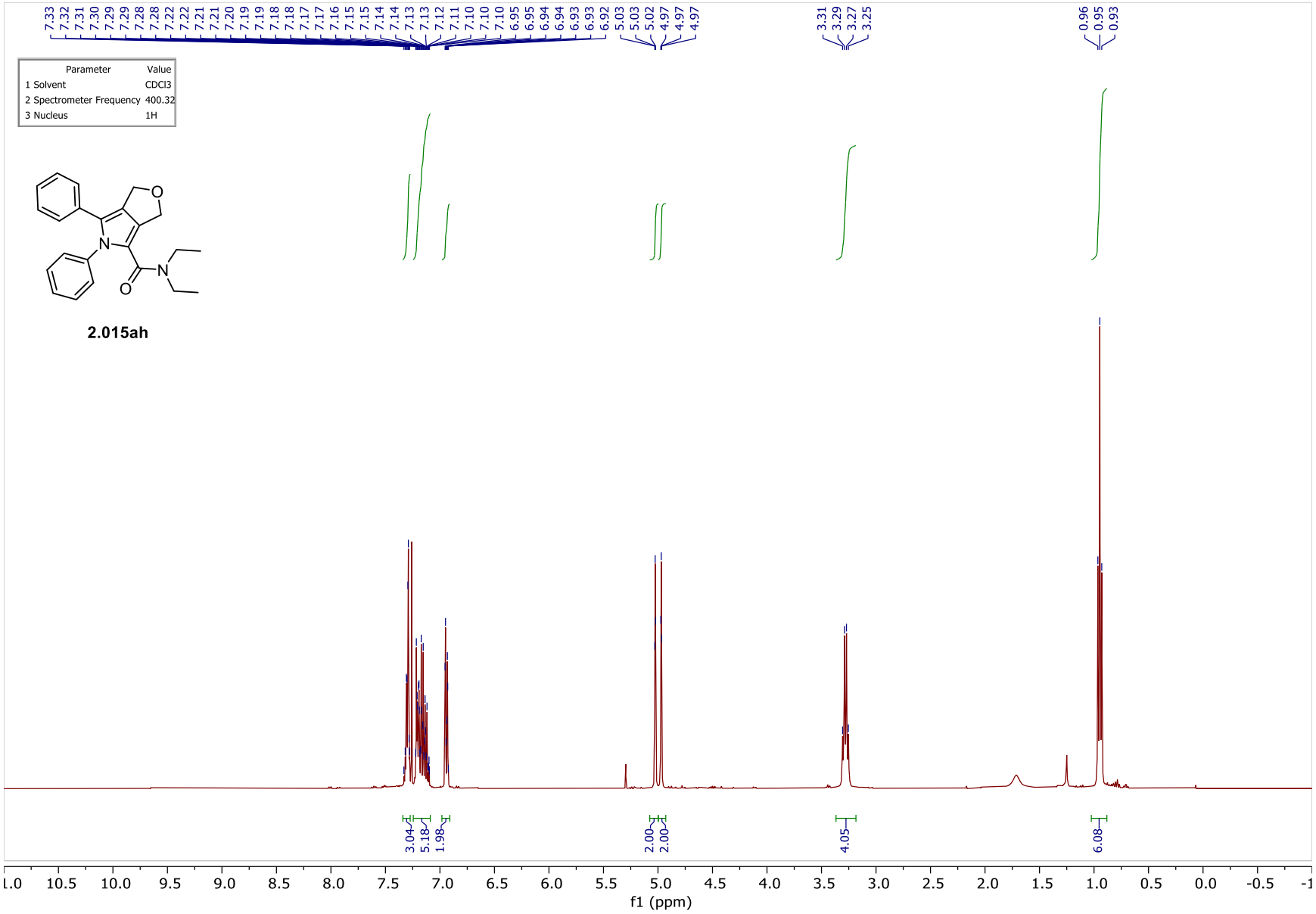
7.33 7.32 7.31 7.30 7.29 7.29 7.28 7.28 7.22 7.22 7.21 7.21 7.20 7.19 7.19 7.18 7.18 7.17 7.17 7.16 7.15 7.15 7.14 7.14 7.13 7.13 7.12 7.11 7.10 7.10 7.10 6.95 6.95 6.94 6.94 6.93 6.93 6.92 5.03 5.03 5.02 4.97 4.97 4.97
3.31 3.29 3.27 3.25
0.96 0.95 0.93
Parameter Value
1 Solvent CDCl3
2 Spectrometer Frequency 400.32
3 Nucleus 1H
O
N
N
O
2.015ah
3.04 5.18 1.98 2.00 2.00 4.05 6.08
1.0 10.5 10.0 9.5 9.0 8.5 8.0 7.5 7.0 6.5 6.0 5.5 5.0 4.5 4.0 3.5 3.0 2.5 2.0 1.5 1.0 0.5 0.0 -0.5 -1
f1 (ppm)

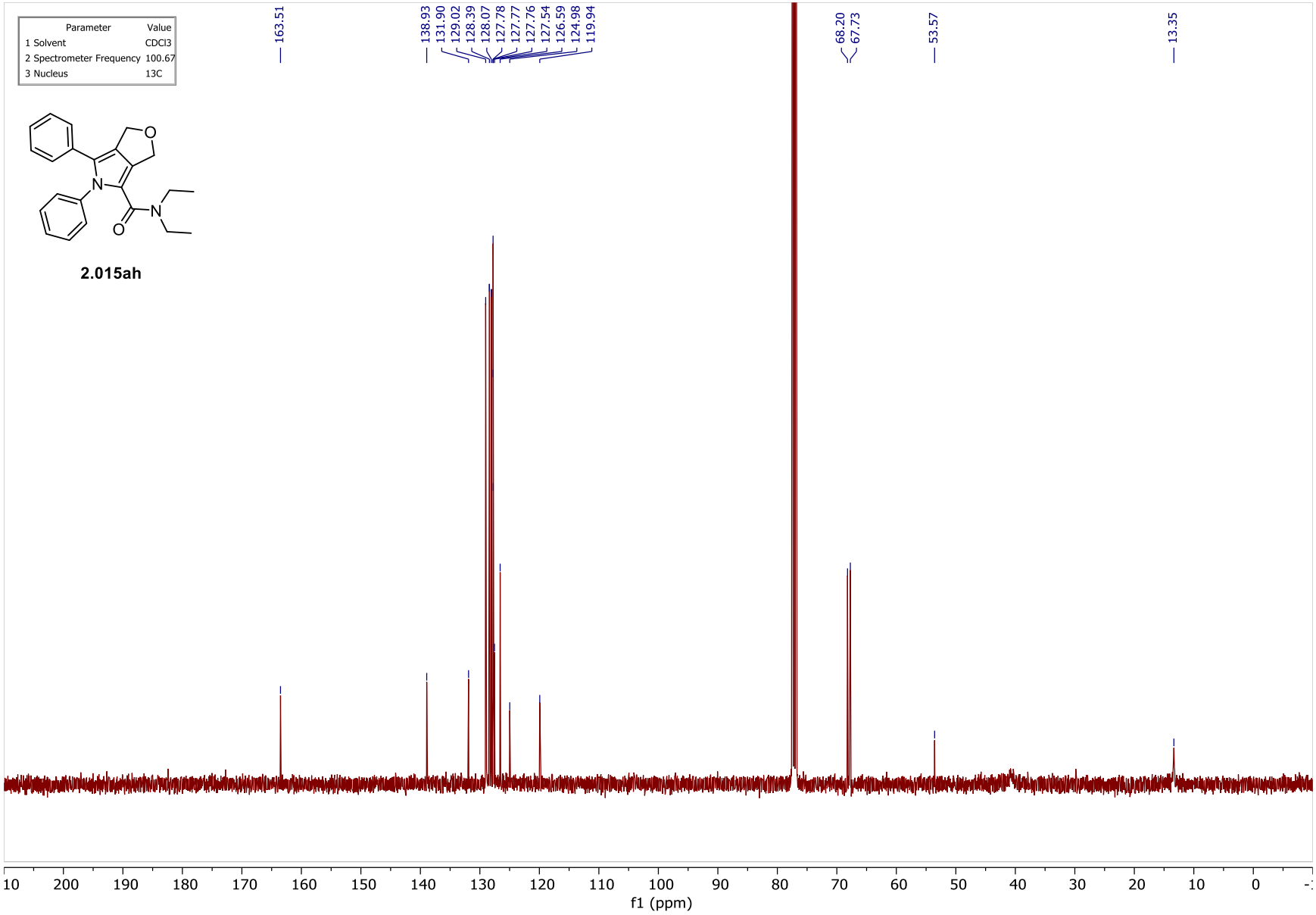
Parameter Value
1 Solvent CDCl3
2 Spectrometer Frequency 100.67
3 Nucleus 13C
163.51
138.93
131.90
129.02
128.39
128.07
127.78
127.77
127.76
127.54
126.59
124.98
119.94
68.20
67.73
53.57
13.35
O
N
N
O
2.015ah
10 200 190 180 170 160 150 140 130 120 110 100 90 80 70 60 50 40 30 20 10 0
f1 (ppm)

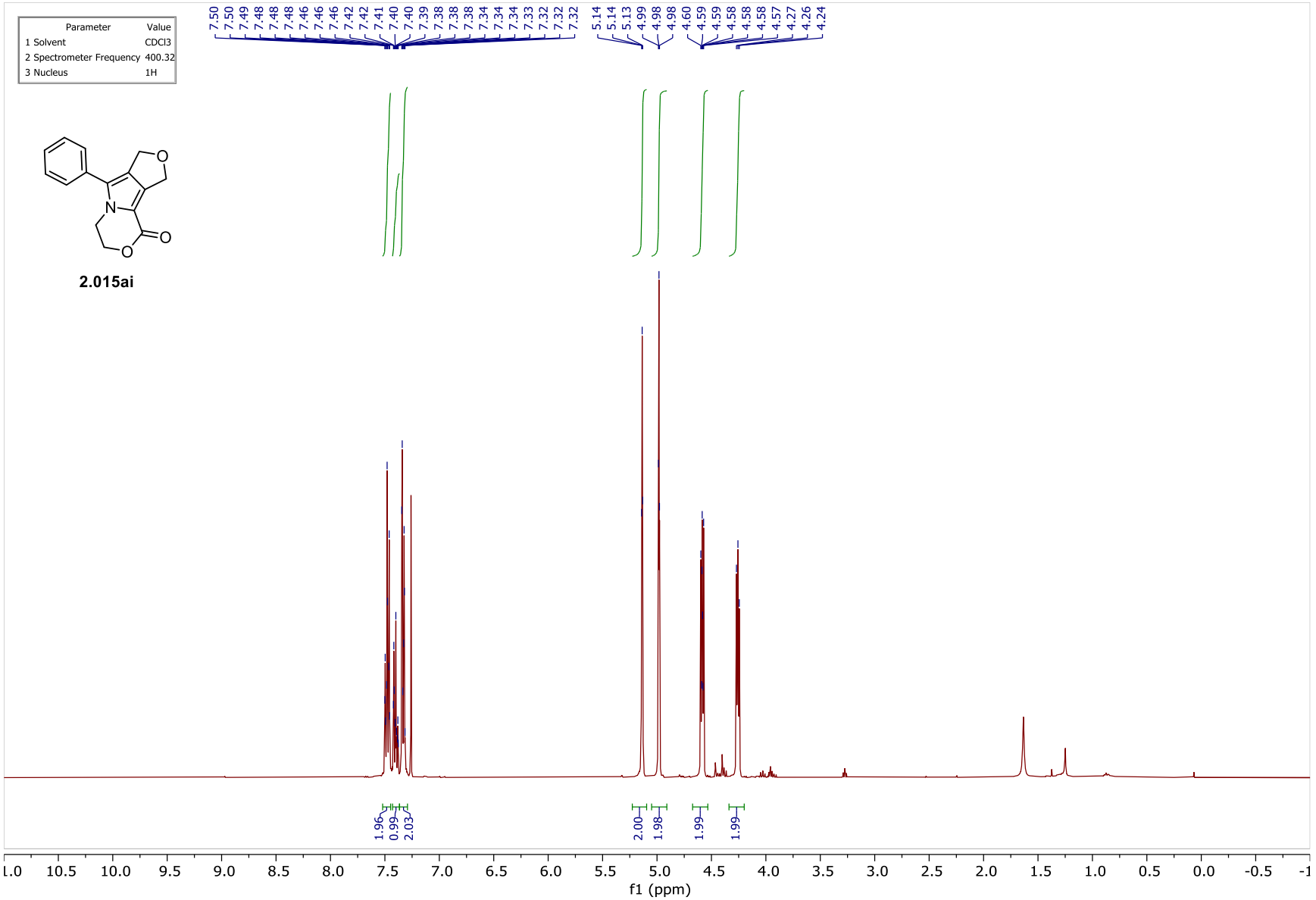
Parameter Value
1 Solvent CDCl3
2 Spectrometer Frequency 400.32
3 Nucleus 1H
2.015ai
7.50 7.50 7.49 7.48 7.48 7.48 7.46 7.46 7.46 7.42 7.42 7.41 7.40 7.40 7.39 7.38 7.38 7.38 7.34 7.34 7.34 7.33 7.32 7.32 7.32
5.14 5.14 5.13 4.99 4.98 4.98 4.60 4.59 4.59 4.58 4.58 4.58 4.57 4.27 4.26 4.24
1.96 0.99 2.03 2.00 1.98 1.99 1.99
f1 (ppm)

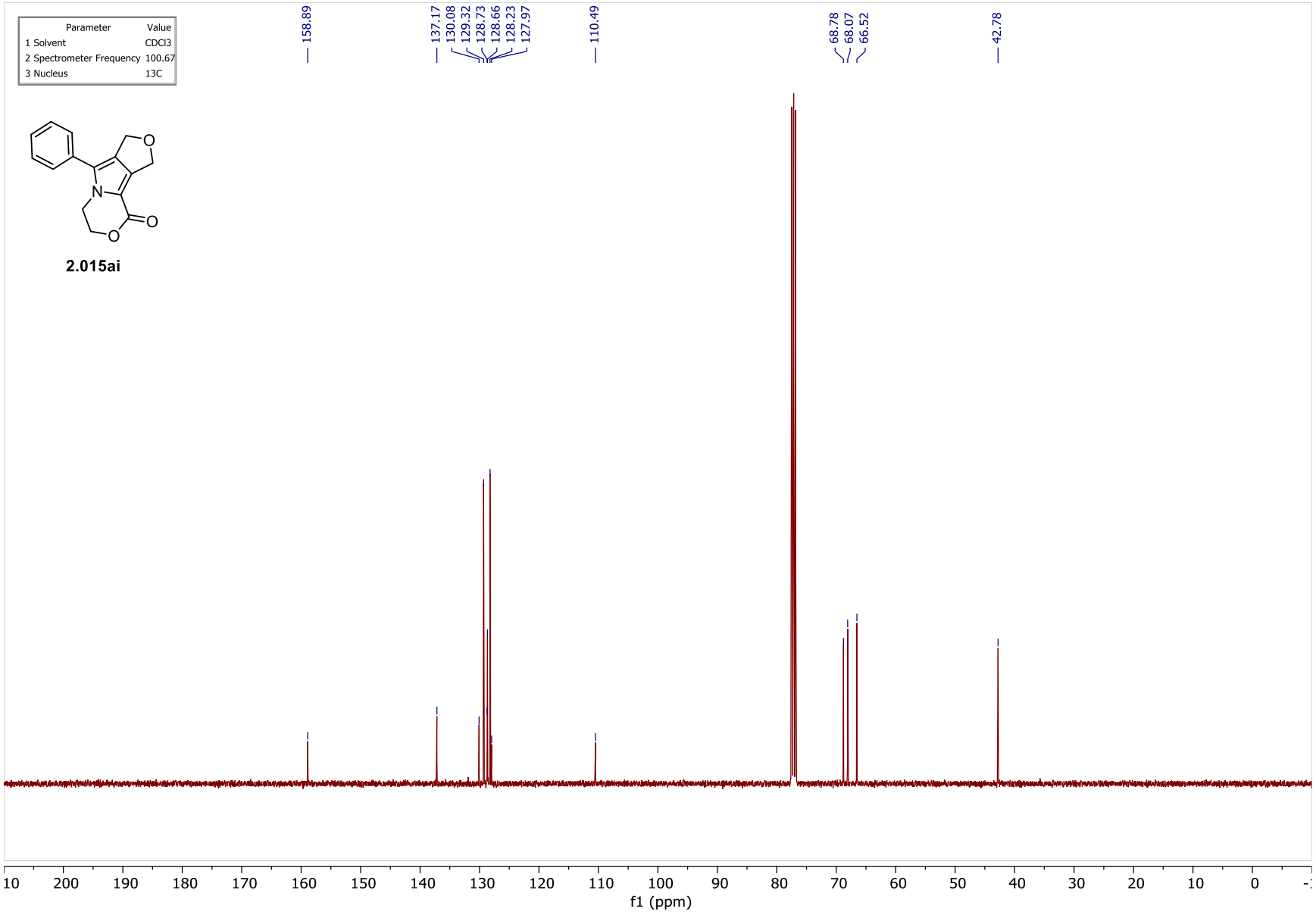
Parameter Value
1 Solvent CDCl3
2 Spectrometer Frequency 100.67
3 Nucleus 13C
158.89
137.17
130.08
129.32
128.73
128.66
128.23
127.97
110.49
68.78
68.07
66.52
42.78
O
N
O
O
2.015ai
10 200 190 180 170 160 150 140 130 120 110 100 90 80 70 60 50 40 30 20 10 0
f1 (ppm)

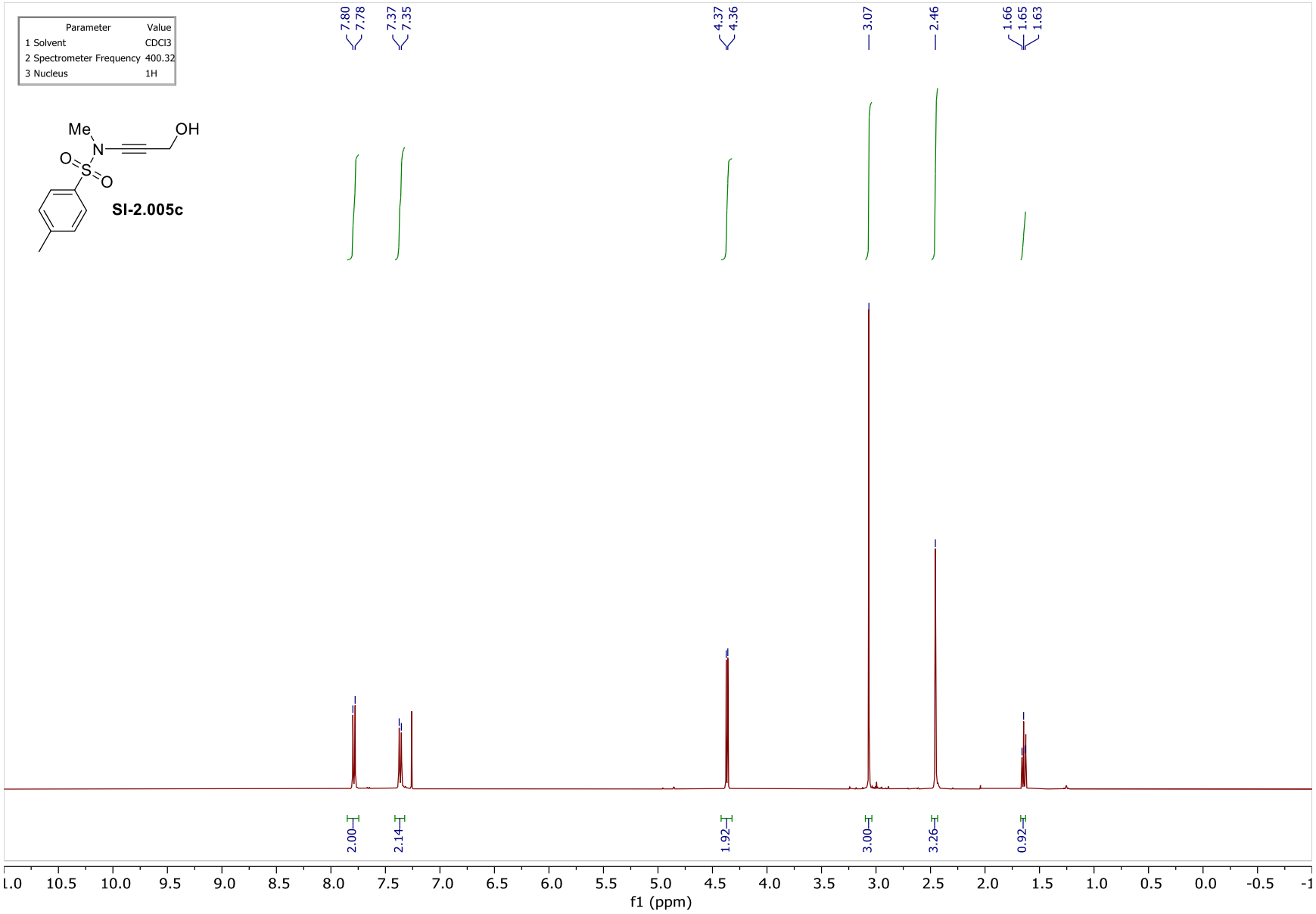
Parameter Value
1 Solvent CDCl3
2 Spectrometer Frequency 400.32
3 Nucleus 1H
Me
N
OH
O
S
O
SI-2.005c
7.80
7.78
7.37
7.35
4.37
4.36
3.07
2.46
1.66
1.65
1.63
2.00
2.14
1.92
3.00
3.26
0.92
f1 (ppm)

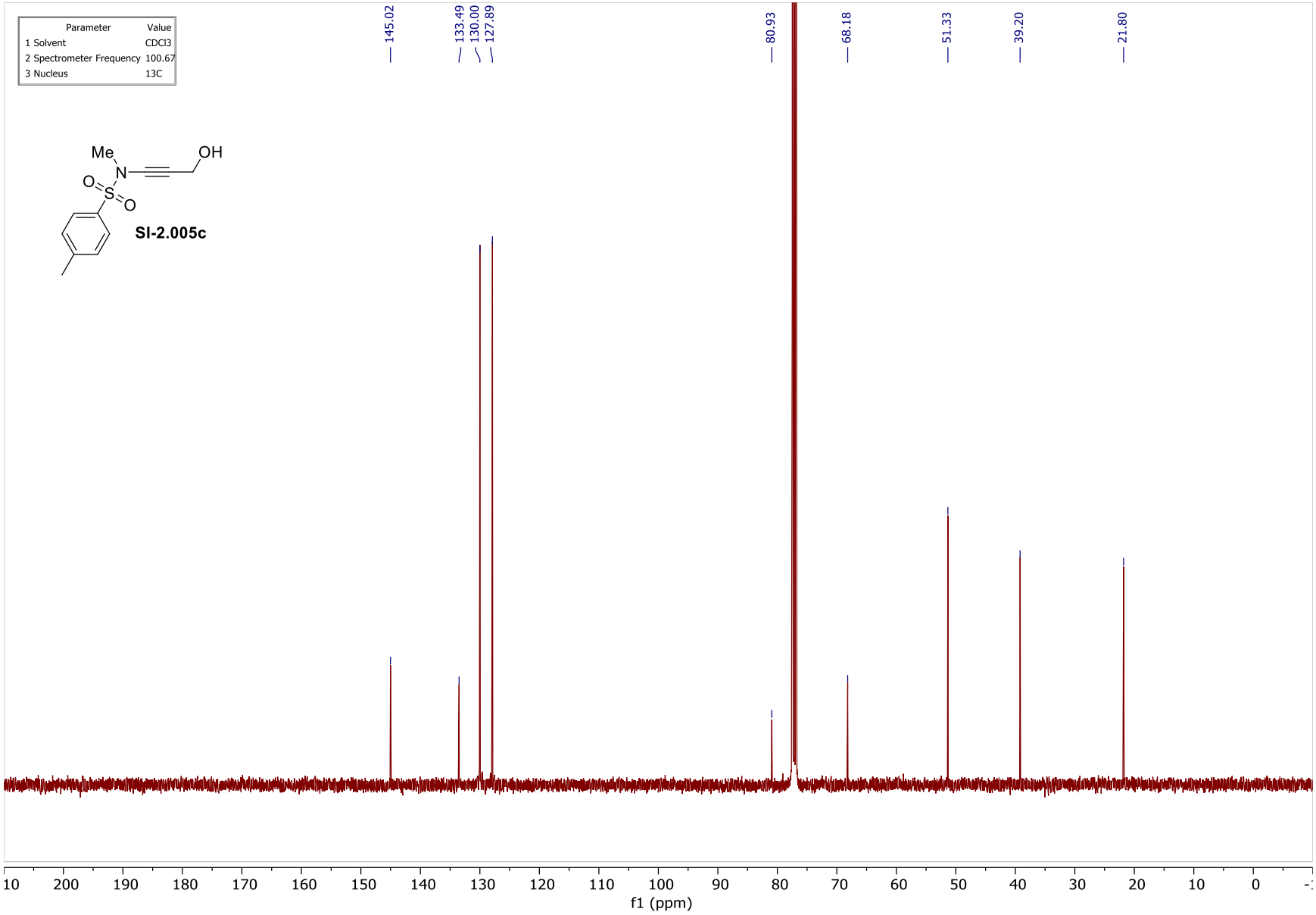
Parameter Value
1 Solvent CDCl3
2 Spectrometer Frequency 100.67
3 Nucleus 13C
145.02
133.49
130.00
127.89
80.93
68.18
51.33
39.20
21.80
Me
N
OH
O
S
O
SI-2.005c
f1 (ppm)

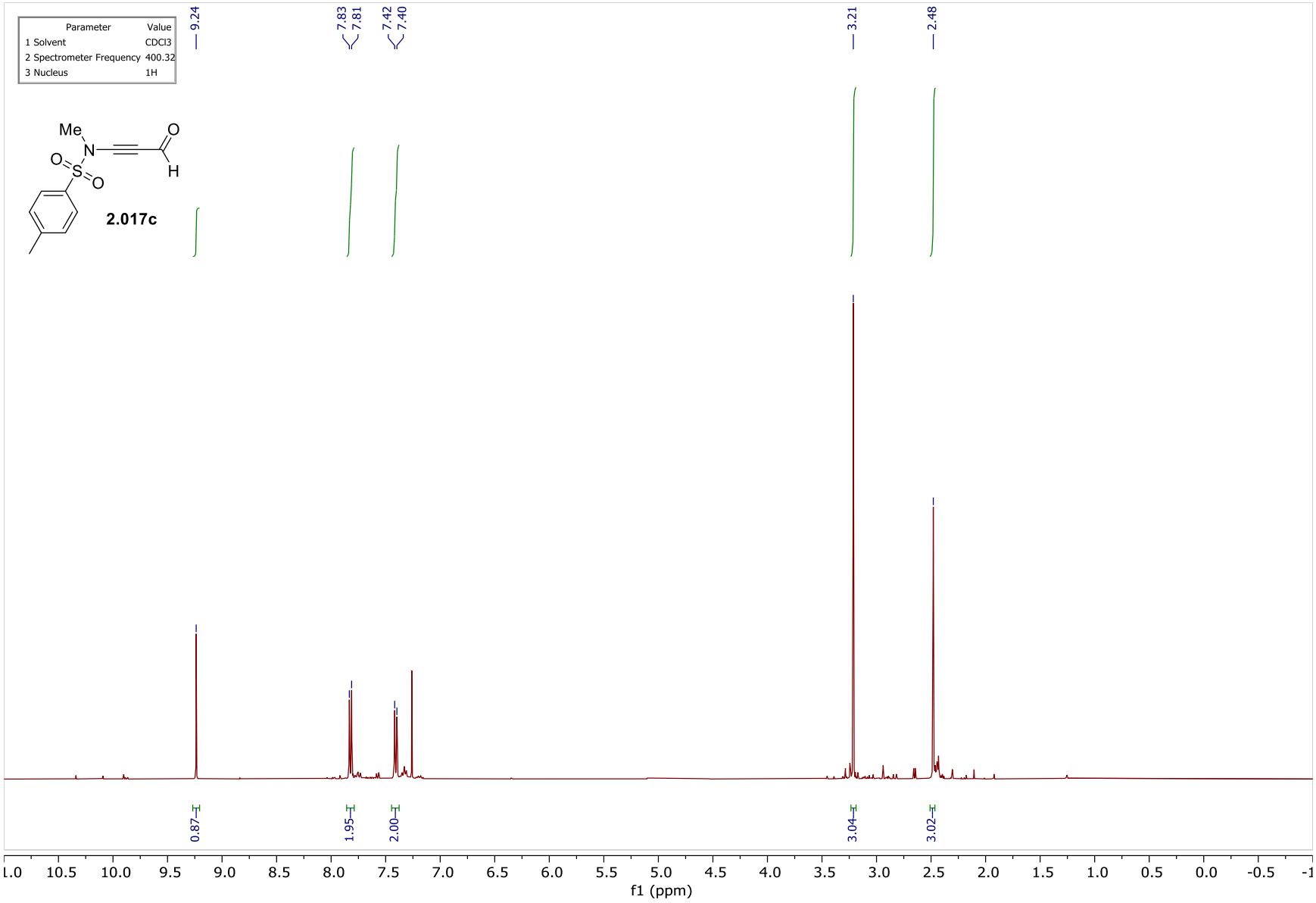
Parameter Value
1 Solvent CDCl3
2 Spectrometer Frequency 400.32
3 Nucleus 1H
Me
N
O
S
O
O
H
2.017c
9.24
7.83
7.81
7.42
7.40
3.21
2.48
0.87
1.95
2.00
3.04
3.02
f1 (ppm)

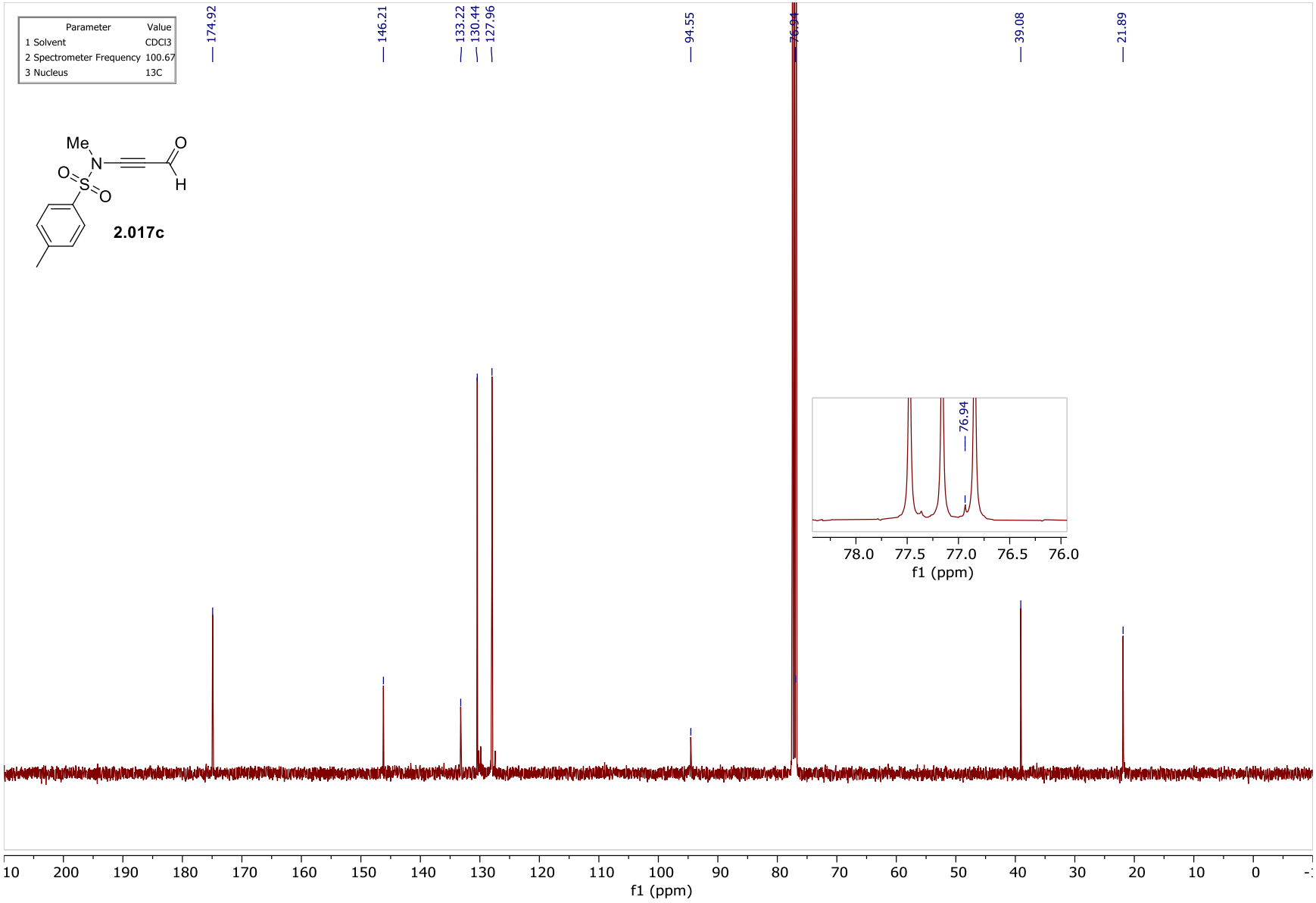
Parameter Value
1 Solvent CDCl3
2 Spectrometer Frequency 100.67
3 Nucleus 13C
174.92
146.21
133.22
130.44
127.96
94.55
76.94
39.08
21.89
Me
N
O
S
O
O
O
H
2.017c
76.94
78.0
77.5
77.0
76.5
76.0
f1 (ppm)
10
200
190
180
170
160
150
140
130
120
110
100
90
80
70
60
50
40
30
20
10
0
f1 (ppm)

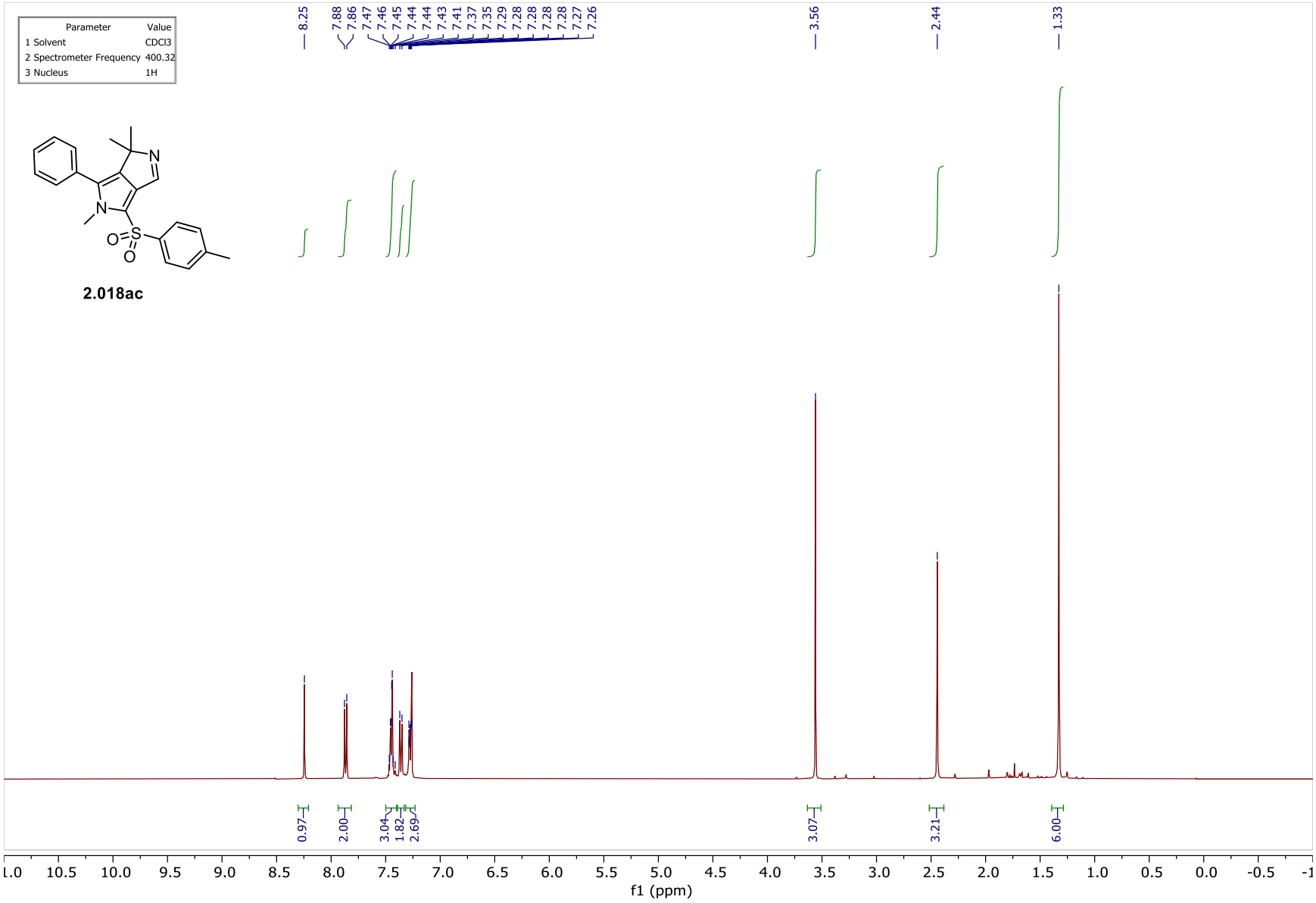
Parameter Value
1 Solvent CDCl3
2 Spectrometer Frequency 400.32
3 Nucleus 1H
2.018ac
8.25
7.88
7.86
7.47
7.46
7.45
7.44
7.44
7.43
7.41
7.37
7.35
7.29
7.28
7.28
7.28
7.27
7.26
3.56
2.44
1.33
0.97
2.00
3.04
1.82
2.69
3.07
3.21
6.00
f1 (ppm)

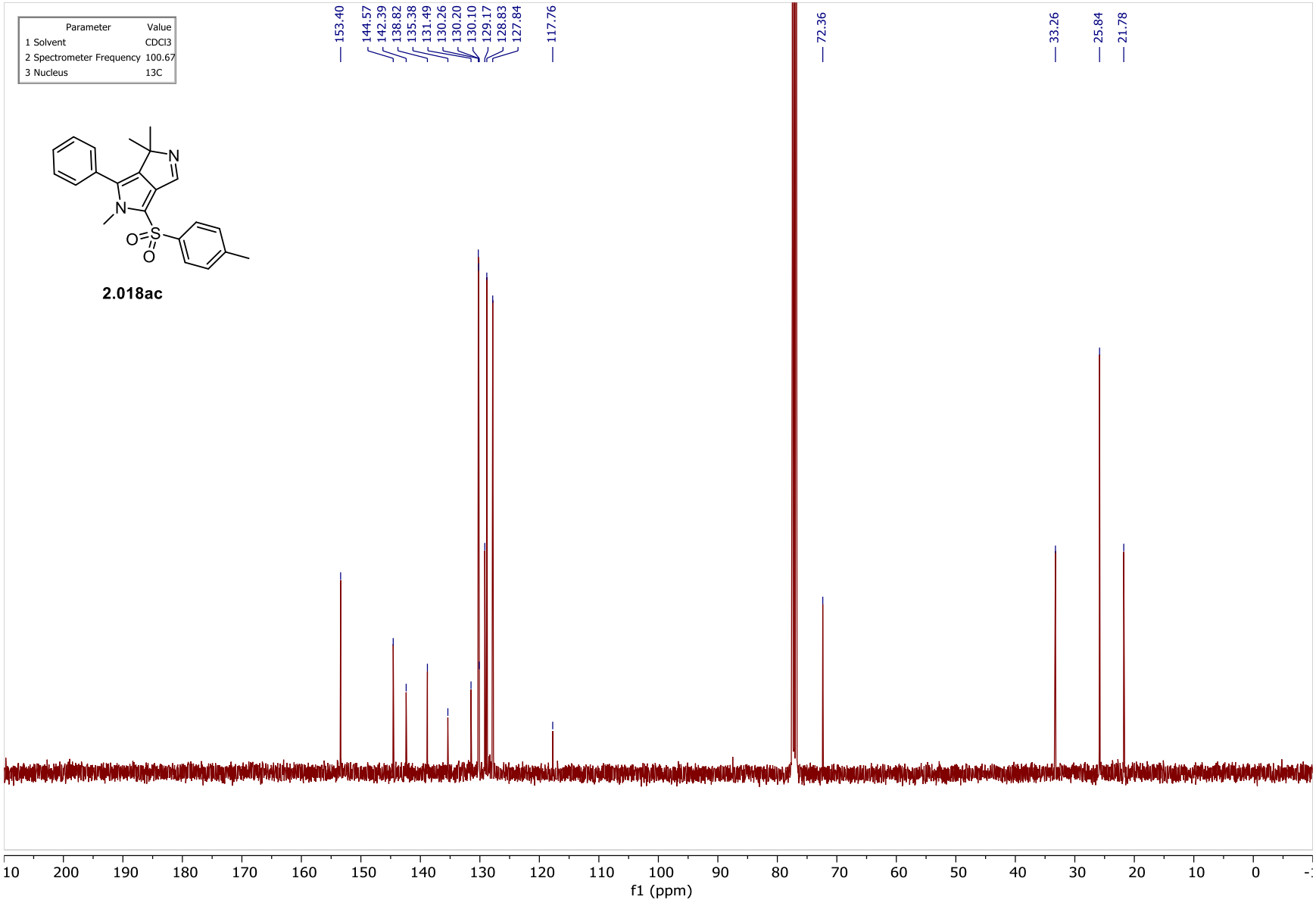
Parameter Value
1 Solvent CDCl3
2 Spectrometer Frequency 100.67
3 Nucleus 13C
153.40
144.57
142.39
138.82
135.38
131.49
130.26
130.20
130.10
129.17
128.83
127.84
117.76
72.36
33.26
25.84
21.78
2.018ac
f1 (ppm)

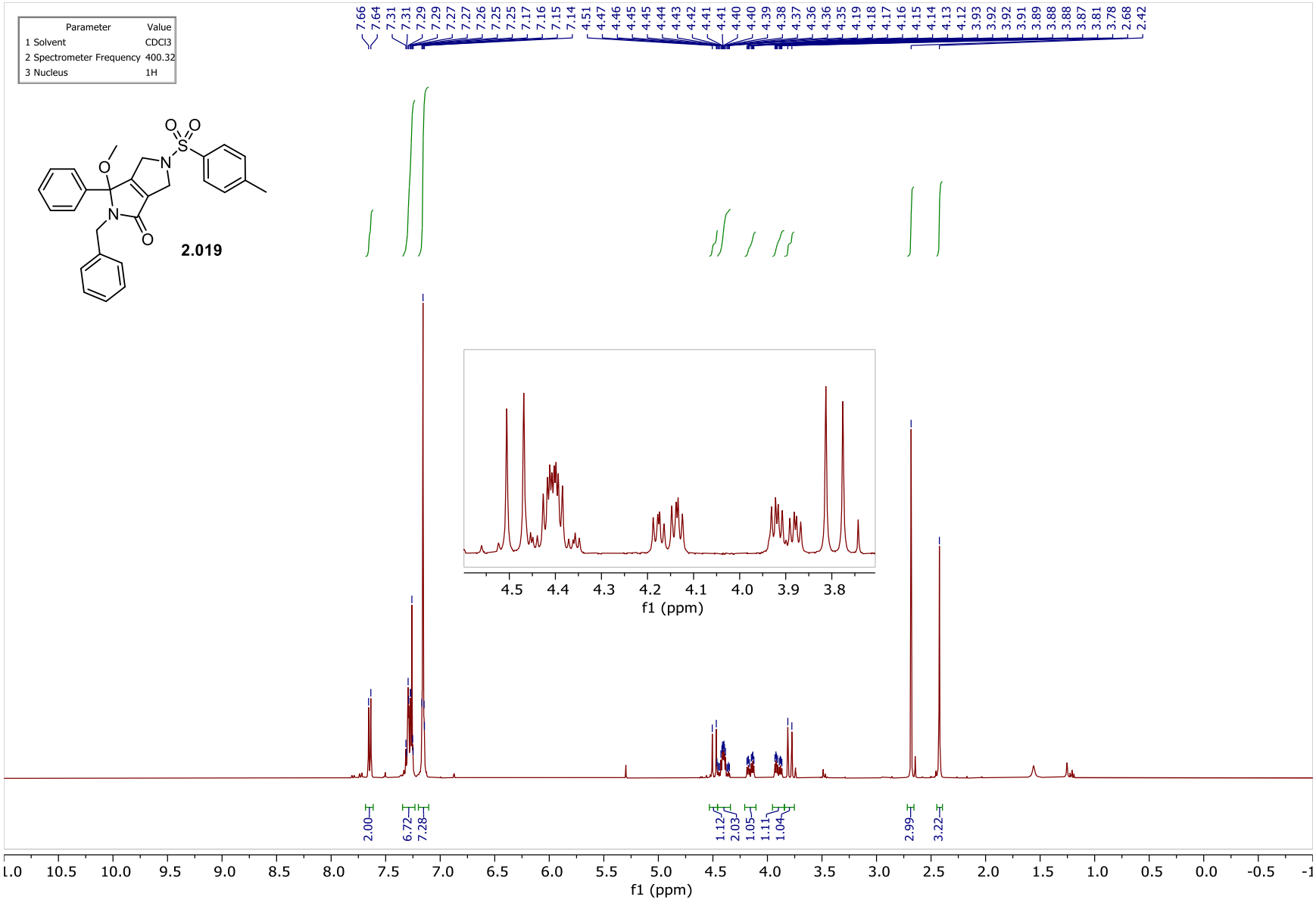
Parameter Value
1 Solvent CDCl3
2 Spectrometer Frequency 400.32
3 Nucleus 1H
2.019
f1 (ppm)

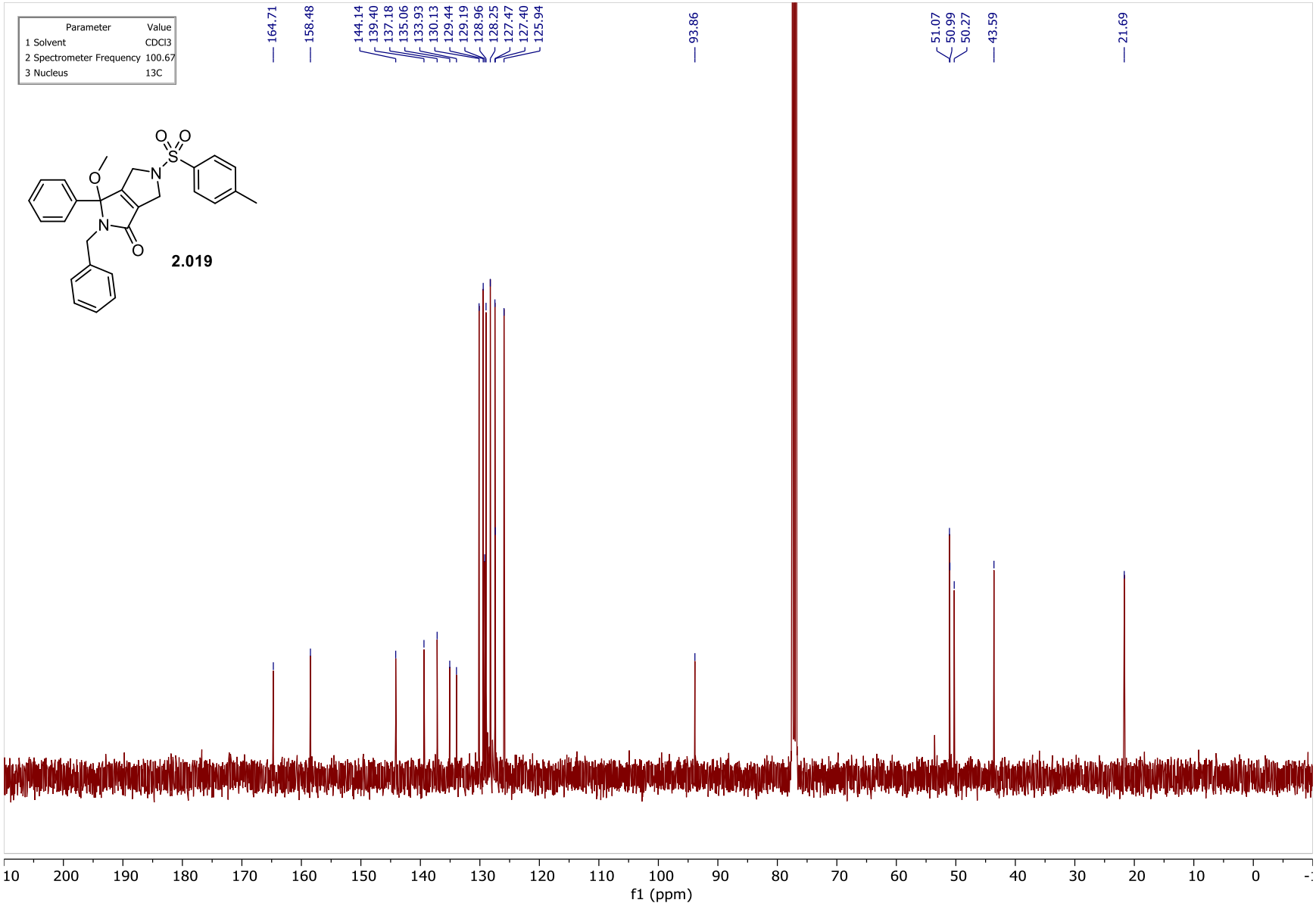
Parameter Value
1 Solvent CDCl3
2 Spectrometer Frequency 100.67
3 Nucleus 13C
164.71
158.48
144.14
139.40
137.18
135.06
133.93
130.13
129.44
129.19
128.96
128.25
127.47
127.40
125.94
93.86
51.07
50.99
50.27
43.59
21.69
2.019
f1 (ppm)

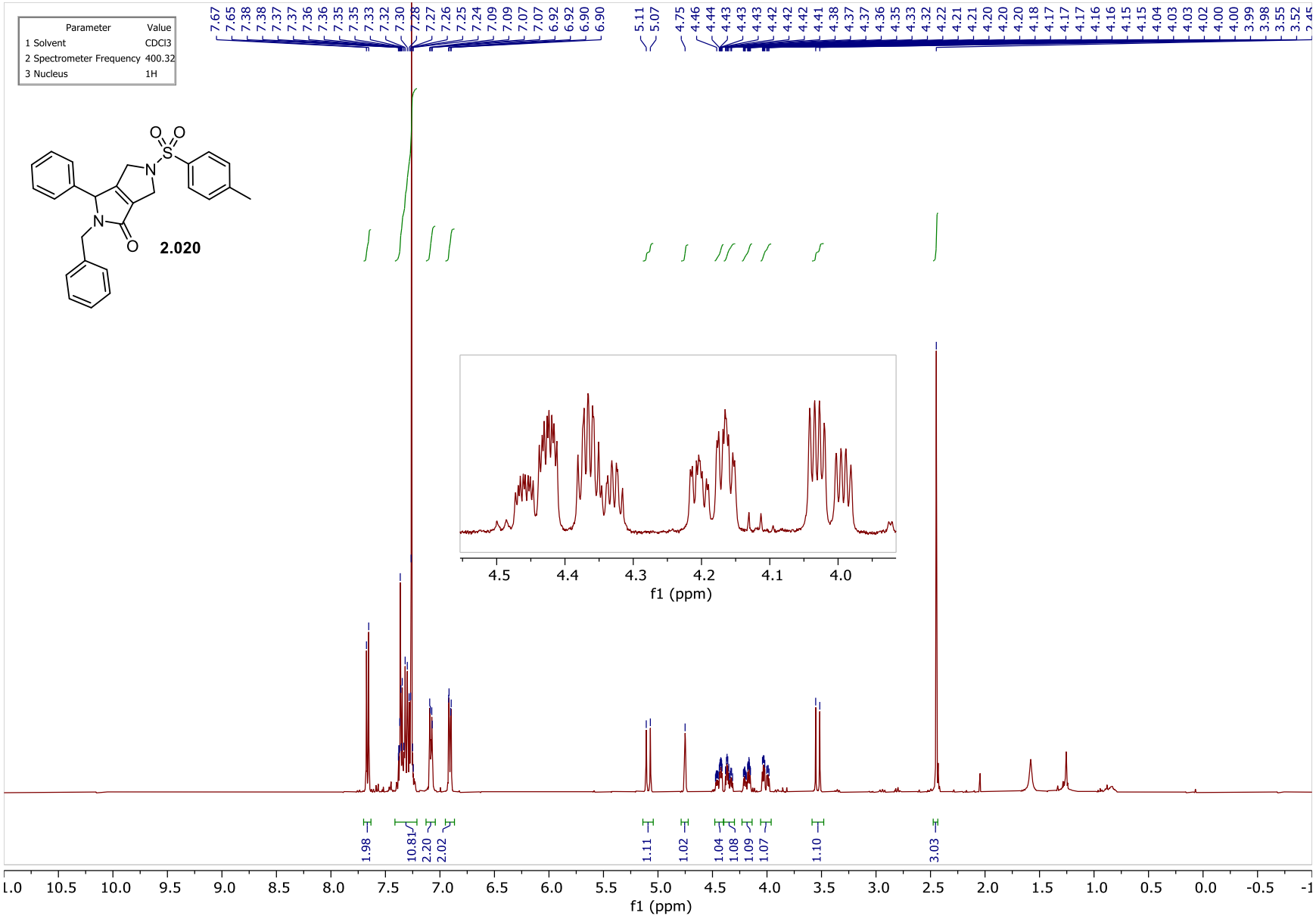
Parameter Value
1 Solvent CDCl3
2 Spectrometer Frequency 400.32
3 Nucleus 1H
2.020
f1 (ppm)
f1 (ppm)

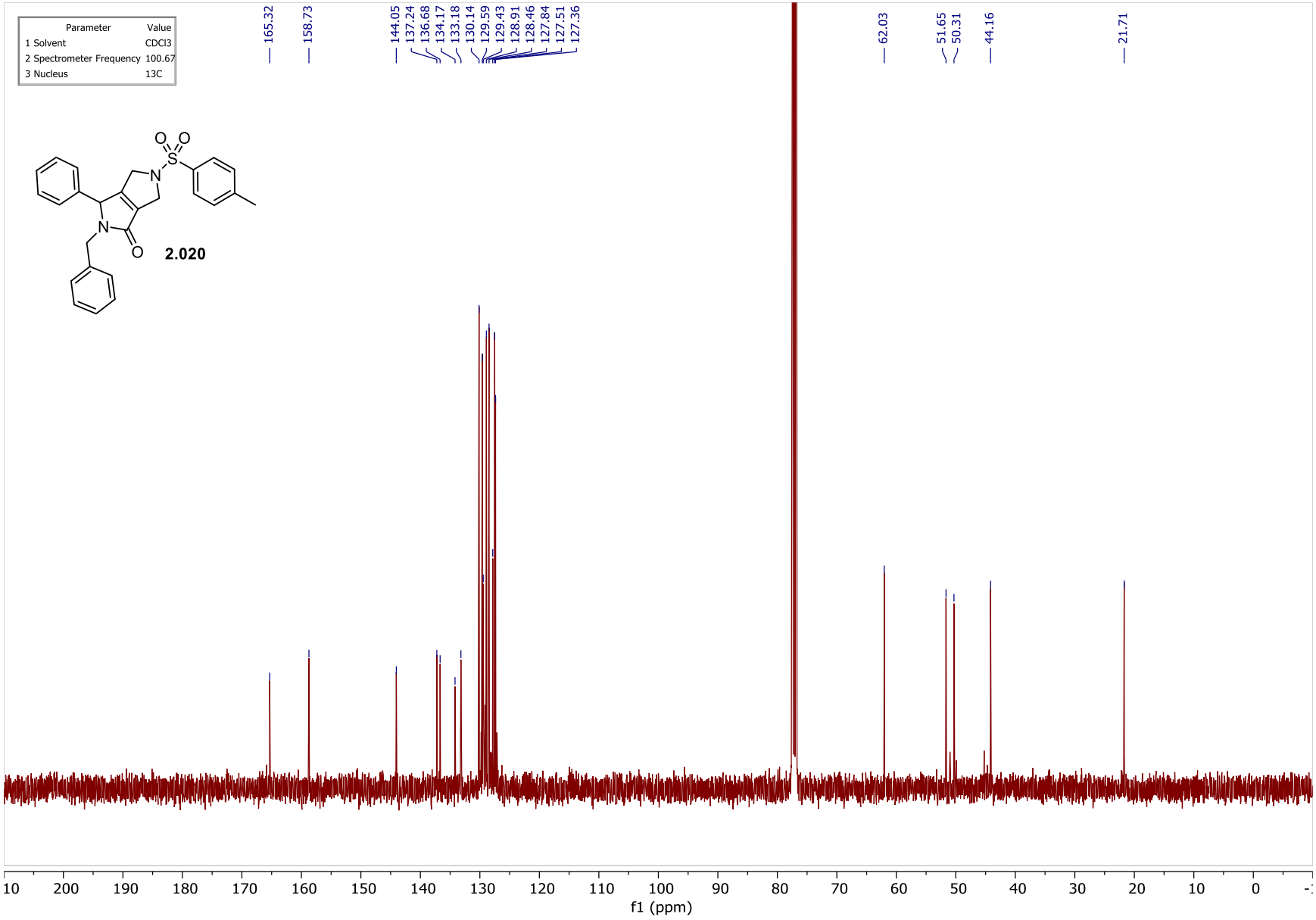
Parameter Value
1 Solvent CDCl3
2 Spectrometer Frequency 100.67
3 Nucleus 13C
165.32
158.73
144.05
137.24
136.68
134.17
133.18
130.14
129.59
129.43
128.91
128.46
127.84
127.51
127.36
62.03
51.65
50.31
44.16
21.71
2.020
f1 (ppm)

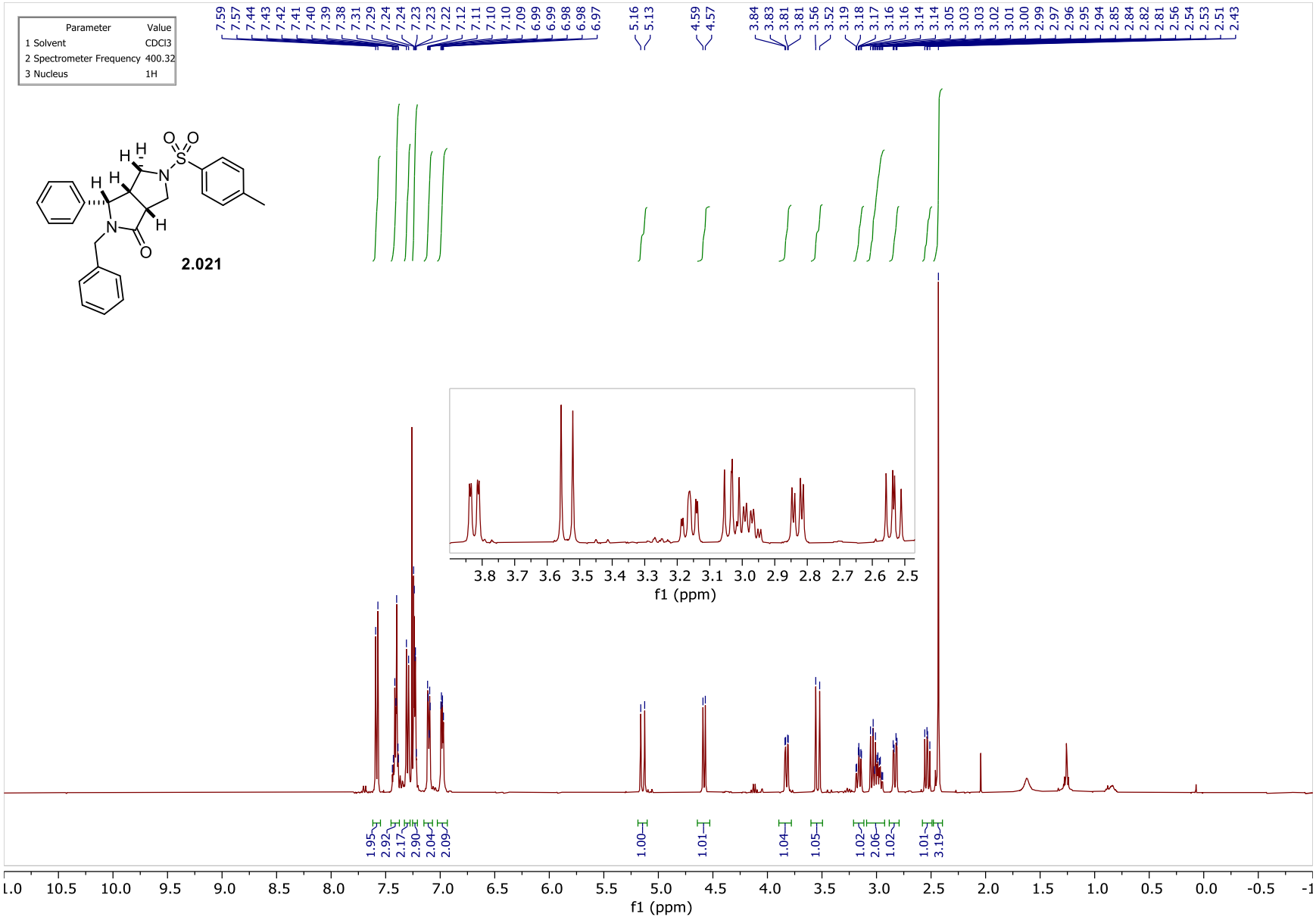
Parameter Value
1 Solvent CDCl3
2 Spectrometer Frequency 400.32
3 Nucleus 1H
2.021
f1 (ppm)
f1 (ppm)

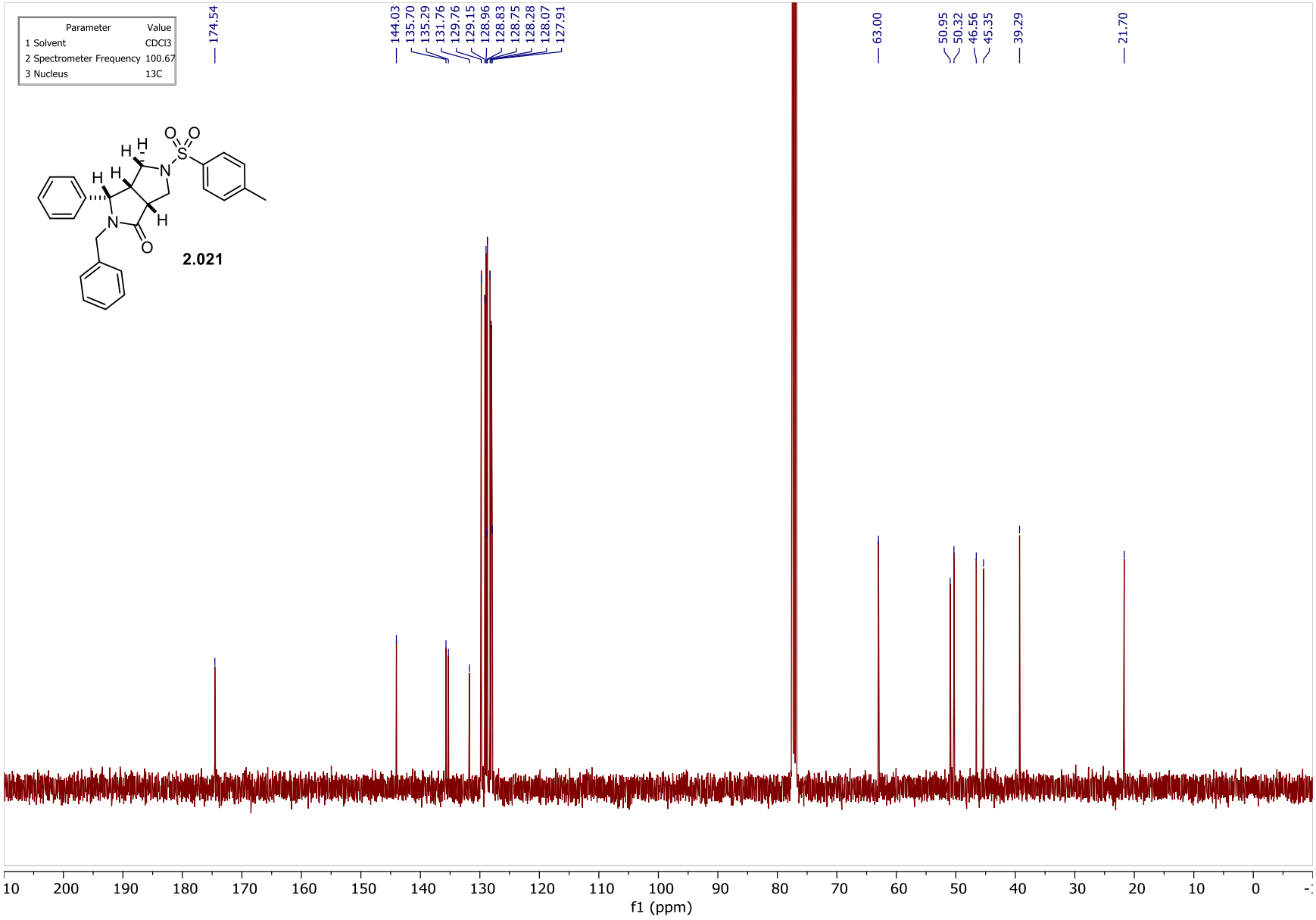
Parameter Value
1 Solvent CDCl3
2 Spectrometer Frequency 100.67
3 Nucleus 13C
174.54
144.03
135.70
135.29
131.76
129.76
129.15
128.96
128.83
128.75
128.28
128.07
127.91
63.00
50.95
50.32
46.56
45.35
39.29
21.70
2.021
f1 (ppm)

NOESY:

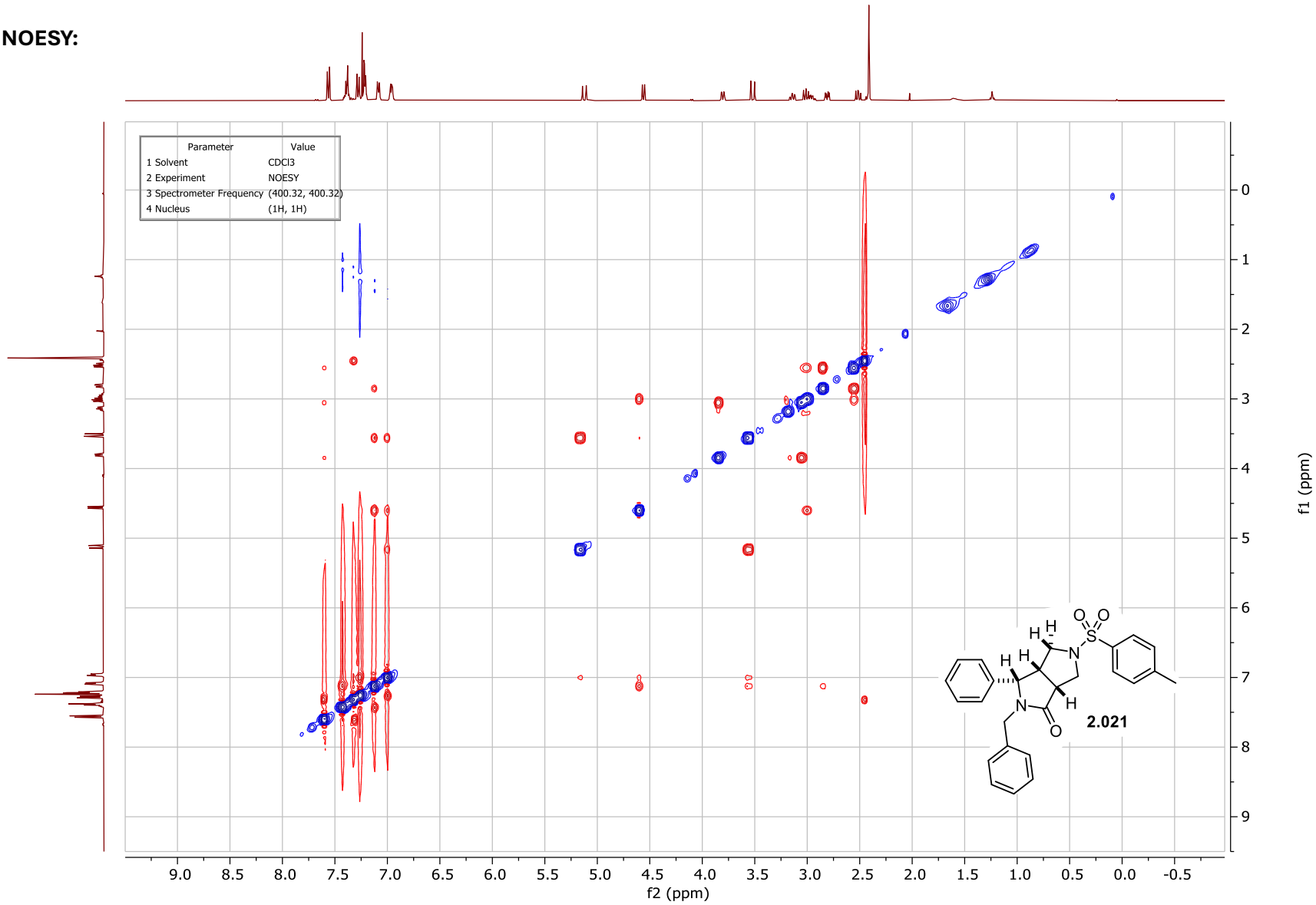
Parameter Value
1 Solvent CDCl3
2 Experiment NOESY
3 Spectrometer Frequency (400.32, 400.32)
4 Nucleus (1H, 1H)
2.021
f2 (ppm)
f1 (ppm)

6.2.10. Additional NMR Spectra for compound 2.015a

COSY:

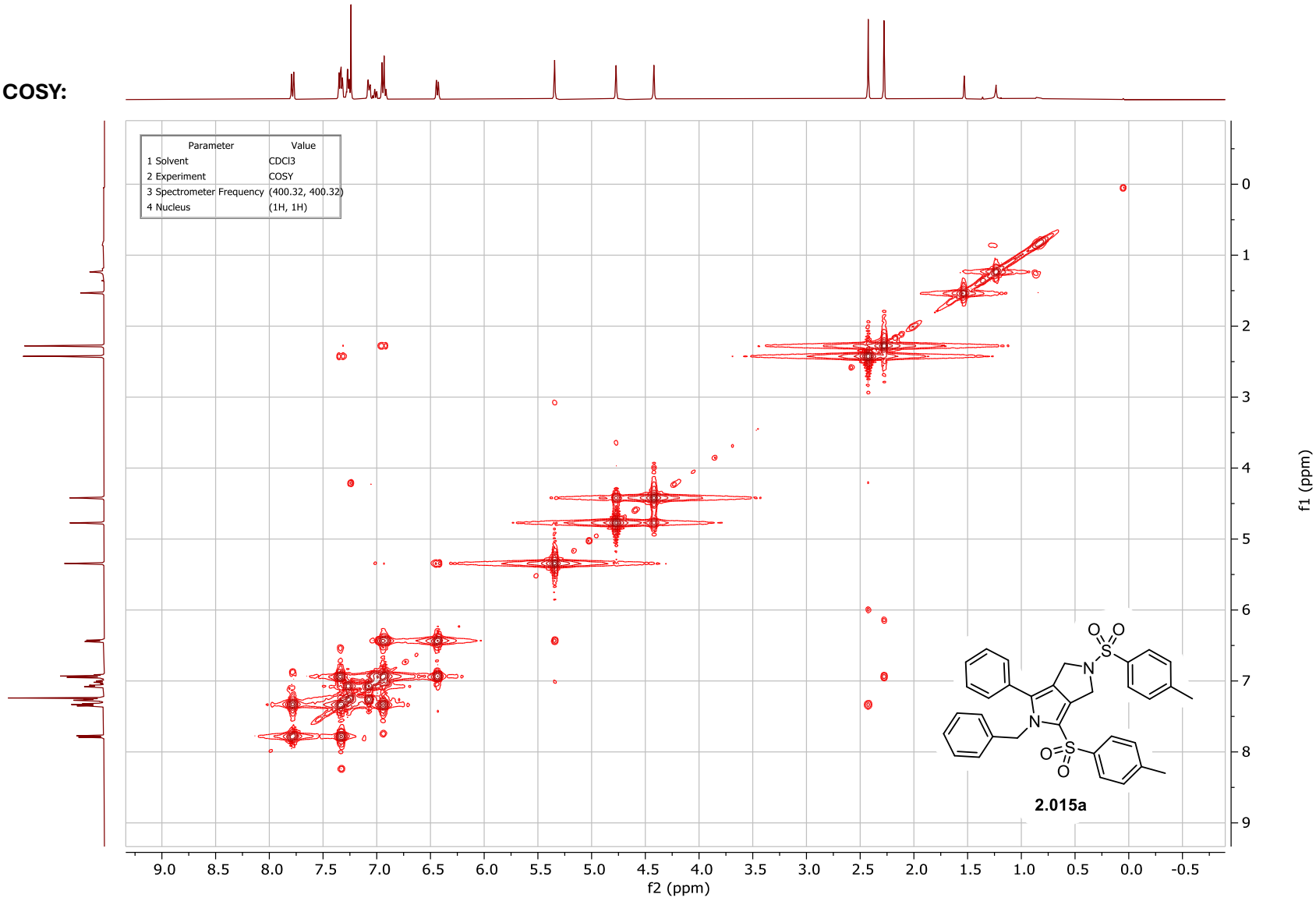

HSQC:

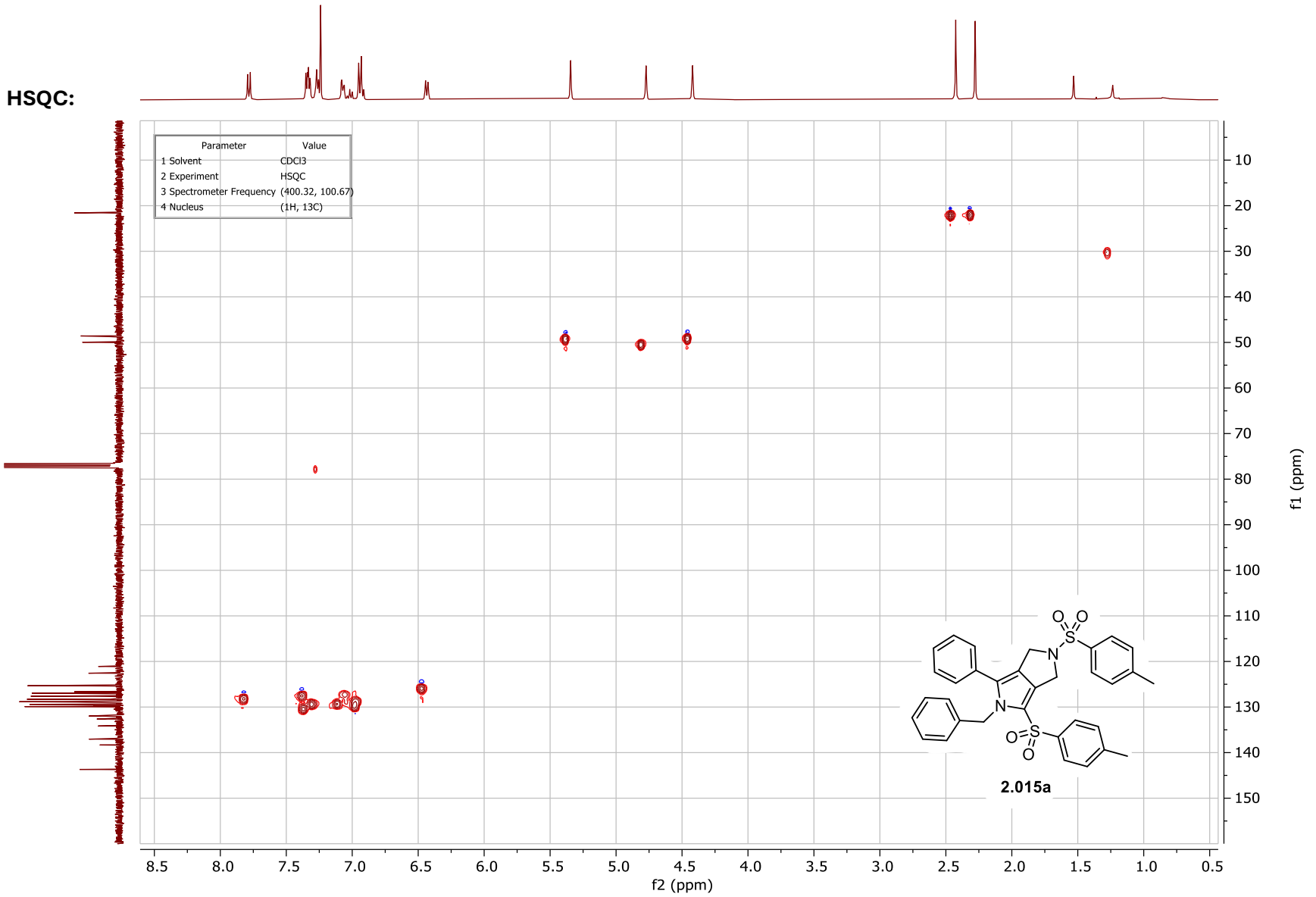
Parameter Value
1 Solvent CDCl3
2 Experiment HSQC
3 Spectrometer Frequency (400.32, 100.67)
4 Nucleus (1H, 13C)
f2 (ppm)
f1 (ppm)
2.015a

HMBC:

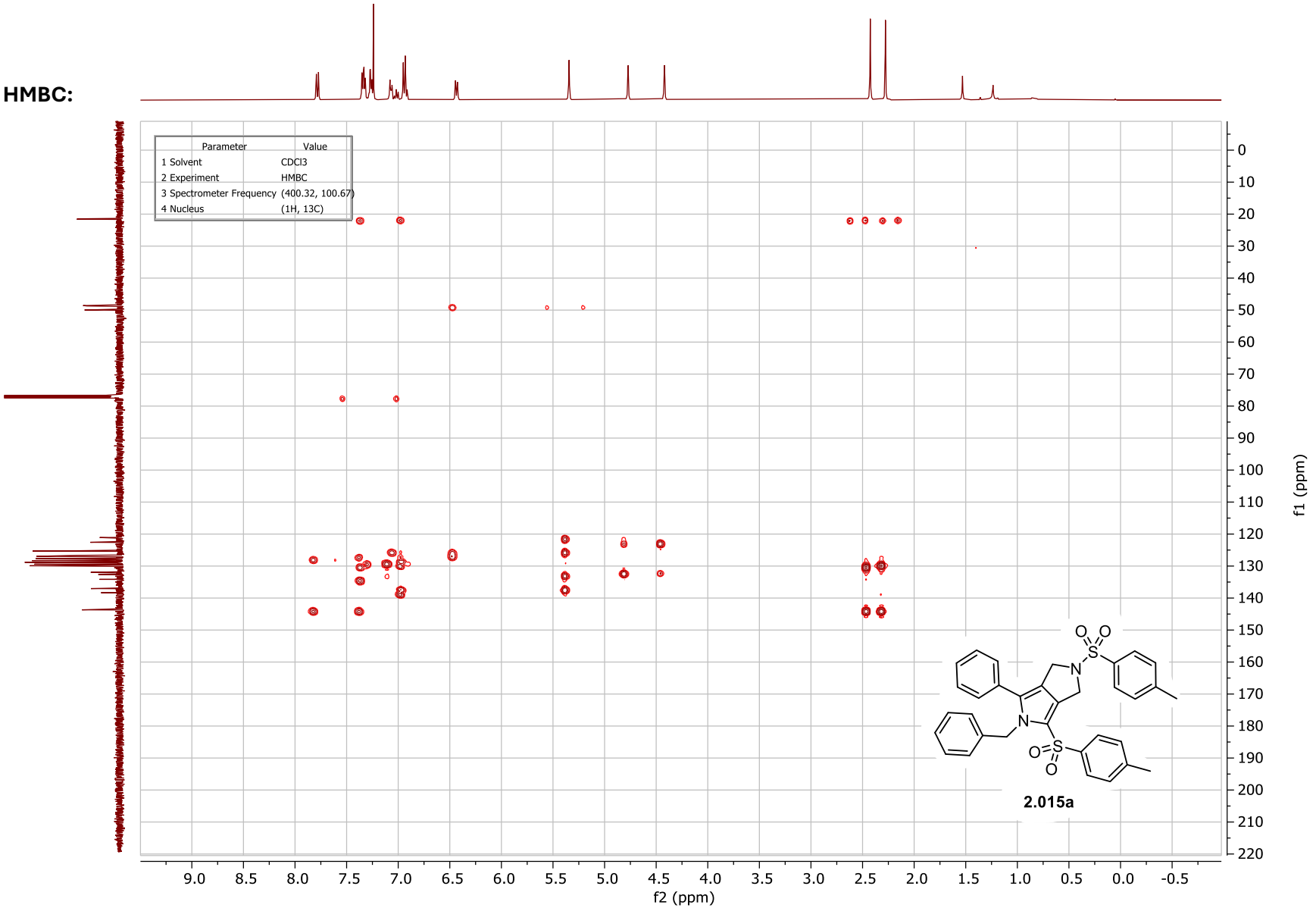
Parameter Value
1 Solvent CDCl3
2 Experiment HMBC
3 Spectrometer Frequency (400.32, 100.67)
4 Nucleus (1H, 13C)
f2 (ppm)
f1 (ppm)
2.015a

NOESY:

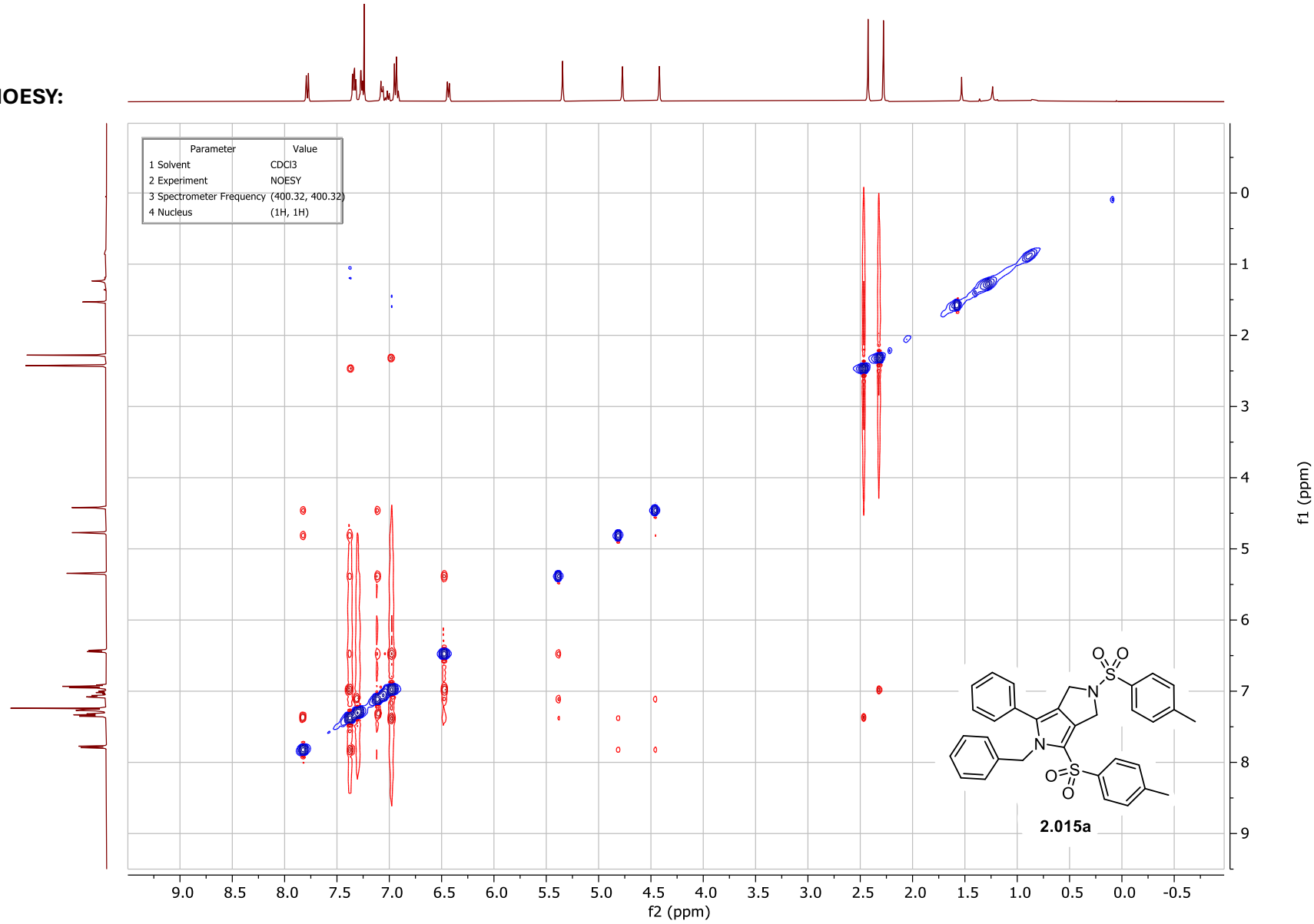
Parameter Value
1 Solvent CDCl3
2 Experiment NOESY
3 Spectrometer Frequency (400.32, 400.32)
4 Nucleus (1H, 1H)
f2 (ppm)
f1 (ppm)
2.015a

6.2.11. X-Ray crystallography data

ORTEP drawing of S0152_FP (**2.015a**+DMSO):

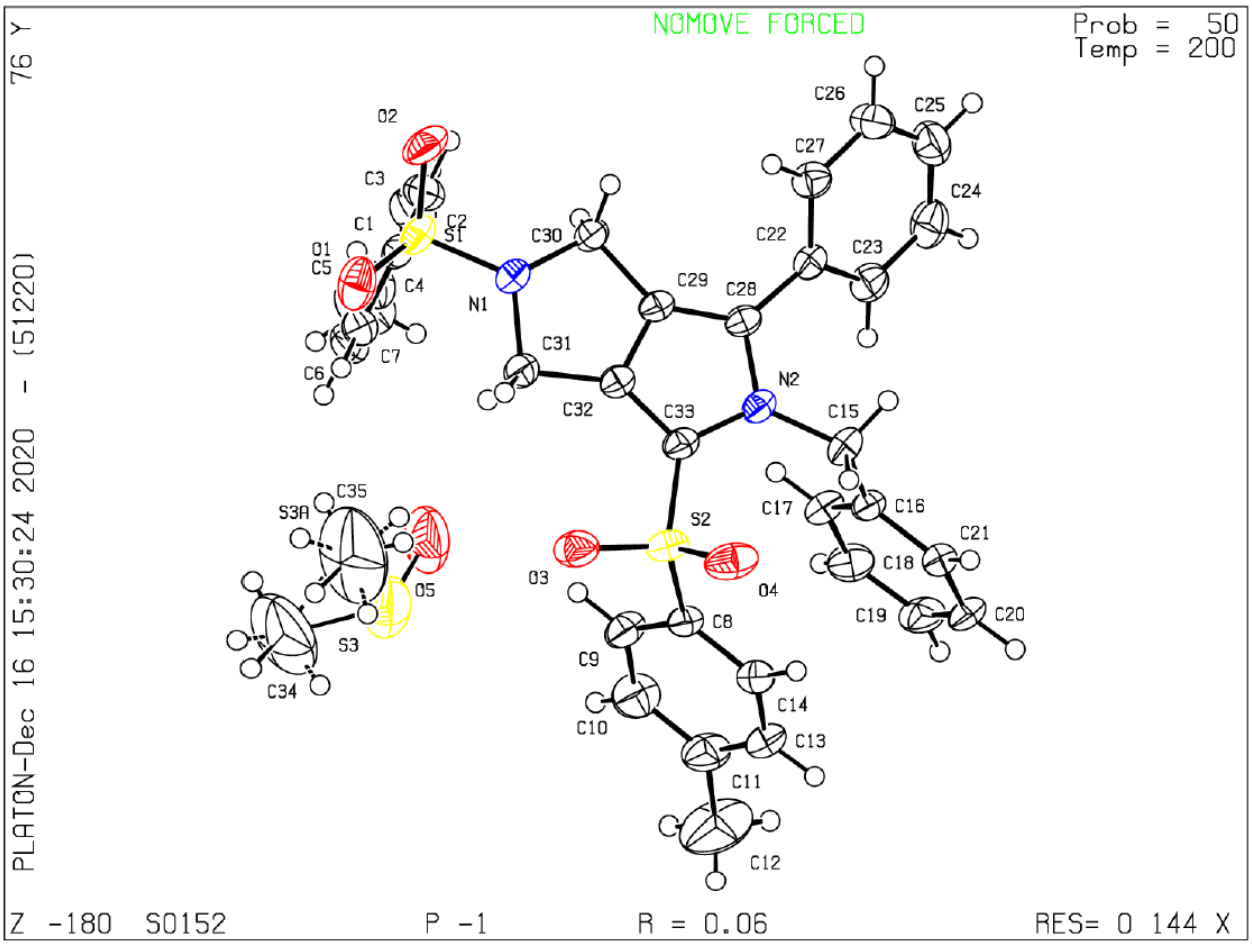

White crystals of **2.015a**+DMSO were obtained via slow diffusion of a layer of DMSO over a solution of **2.015a** in DCM.

6.3. Supporting information for Chapter 3

The synthesis of selected scope examples is detailed herein. For synthetic details on all the examples discussed in Chapter 3, please refer to the original publication:

[Pommainville, A.; Campeau, D.; Gagosz, F., The Synthetic Potential of Thiophenium Ylide Cycloadducts. *Angew. Chem. Int. Ed.* **2022**, *61* (32), e202205963].

6.3.1. Main scope of the (3+2) reaction

Synthesis of yne-alkynyl sulfide substrates

Preparation of unreported di-yne precursors

SI-3.001

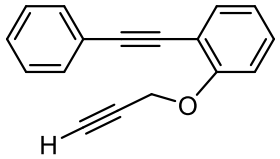

Using standard procedure ***SP2b*** with 0.695 mmol of 2-(phenylethynyl)phenol[16] and propargyl bromide. Solvent system = Hexanes/Et_2O 24:1. Produced 137 mg (85% yield) of a pale yellow oil.

^{1}H NMR (400 MHz, $CDCl_3$) δ 7.59 – 7.54 (m, 2H), 7.52 (dd, *J* = 7.6, 1.7 Hz, 1H), 7.39 – 7.29 (m, 4H), 7.08 (dd, *J* = 8.4, 0.8 Hz, 1H), 7.01 (td, *J* = 7.5, 1.0 Hz, 1H), 4.83 (d, *J* = 2.4 Hz, 2H), 2.54 (t, *J* = 2.4 Hz, 1H).

^{13}C NMR (101 MHz, $CDCl_3$) δ 158.1, 133.8, 131.8, 129.6, 128.4, 128.3, 123.6, 121.8, 113.6, 113.4, 93.9, 85.5, 78.6, 76.0, 56.8.

*Standard procedure **SP6a**: Nucleophilic attack onto electrophilic sulfur species*

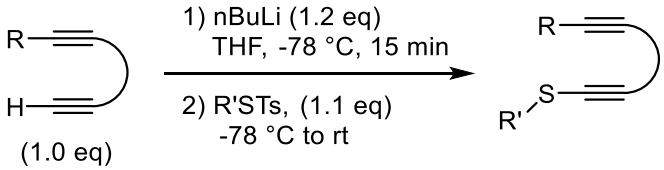

In a flame-dried round bottom flask under N_2 atmosphere was added the alkyne (1.00 mmol, 1.0 equiv.) and dry THF (10 mL, 0.1 M) via syringe. The solution was cooled to -78 °C. To the stirred solution was added nBuLi (0.48 mL, 2.5 M in hexanes, 1.20 mmol, 1.2 equiv.) dropwise. The solution

[16] Prepared as previously reported in literature: Kimura, M.; Ezoe, A.; Mori, M.; Tamaru, Y. *Journal of the American Chemical Society*, **2005**, 127 *(1)*, 201 – 209.

was then stirred at -78 °C for another 15 min. The alkyl thiosulfonate (1.10 mmol, 1.1 equiv.) was added at once and the reaction mixture was slowly warmed to room temperature. Upon reaction completion (30 min to 1h, followed by TLC), the mixture was quenched with NH_4Cl aq. solution. The reaction mixture was then extracted with Et_2O, washed once with water, then brine. The organic phase was dried over $MgSO_4$, filtered, and concentrated under reduced pressure to produce a crude. The crude was then purified by silica gel chromatography using the indicated eluent system to yield the desired alkynyl sulfide.

*Standard procedure **SP6b**: Electrophilic trapping of lithium alkynyl thiolate*

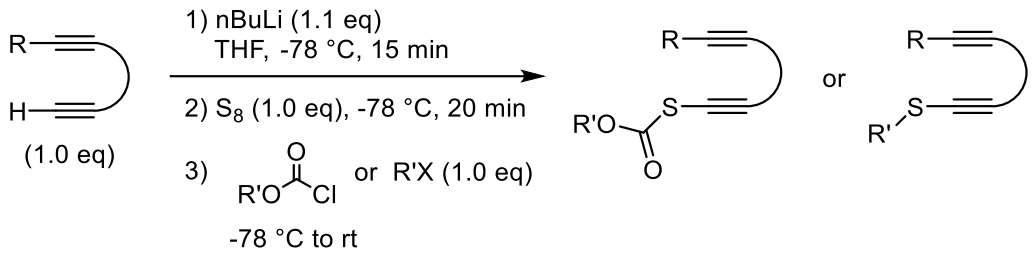

In a flame-dried round bottom flask under N_2 atmosphere was added the alkyne (1.00 mmol, 1.0 equiv.) and dry THF (10 mL, 0.1 M) via syringe. The solution was cooled to -78 °C. To the stirred solution was added nBuLi (0.44 mL, 2.5 M in hexanes, 1.10 mmol, 1.1 equiv.) dropwise. The solution was then stirred at -78 °C for 15 min. Sublimation-grade sulfur (32.0 mg, 1.00 mmol, 1.0 equiv.) was added at once and the reaction mixture was stirred at -78 °C for another 20 min, developing a bright orange colour. The chloroformate or alkyl halide (1.00 mmol, 1.0 equiv.) was then added at once, and the reaction mixture is warmed to room temperature. After 30 min, the mixture was quenched with NH_4Cl aq. solution. The reaction mixture was then extracted with Et_2O, washed once with water, then brine. The organic phase was dried over $MgSO_4$, filtered, and concentrated under reduced pressure to produce a crude. The crude was then purified by silica gel chromatography using the indicated eluent system to yield the desired alkynyl sulfide.

3.025a

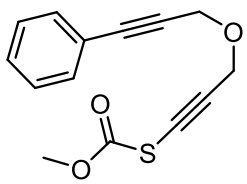

Using standard procedure ***SP6b*** with 0.452 mmol of (3-(prop-2-ynyloxy)prop-1-ynyl)benzene[17] and methyl chloroformate. Solvent system = Hexanes/Et_2O 95:5. Produced 60.0 mg (91% yield) of a pale yellow oil.

^{1}H NMR (400 MHz, $CDCl_3$) δ 7.50 – 7.41 (m, 2H), 7.38 – 7.27 (m, 3H), 4.51 (s, 2H), 4.50 (s, 2H), 3.91 (s, 3H).[18]

^{13}C NMR (101 MHz, $CDCl_3$) δ 167.0, 132.0, 128.7, 128.4, 122.6, 97.5, 87.1, 84.2, 69.1, 57.6 (x2), 56.0.

HRMS-EI : Calculated for $C_{14}H_{12}O_3S$ [M]$^+$: 260.0507; found: 260.0509.

3.021e

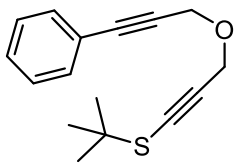

Using standard procedure ***SP6a*** with 0.774 mmol of (3-(prop-2-ynyloxy)prop-1-ynyl)benzene[19] and *S*-*tert*-butyl *p*-tolylthiosulfonate[20]. Solvent system = Hexanes/Et_2O 95:5. Produced 116 mg (69% yield) of a pale yellow oil.

^{1}H NMR (400MHz, $CDCl_3$) δ 7.49 – 7.41 (m, 2H), 7.36 – 7.28 (m, 3H), 4.50 (s, 2H), 4.49 (s, 2H), 1.43 (s, 9H).

^{13}C NMR (101 MHz, $CDCl_3$) δ 132.0, 128.7, 128.4, 122.7, 92.8, 86.8, 84.5, 77.6, 57.9, 57.1, 48.0, 30.4.

HRMS-EI : Calculated for $C_{15}H_{15}OS$ [M-CH_3]$^+$: 243.0844; found: 243.0839.

3.021y

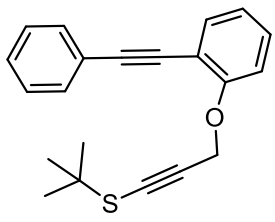

Using standard procedure ***SP6a*** with 0.330 mmol of alkyne **SI-3.001** and *S*-*tert*-butyl *p*-tolylthiosulfonate[21]. Solvent system = Hexanes/Et_2O 99:1. Produced 37.0 mg (35% yield) of a colourless oil.

[17] Prepared as previously reported in: *Org. Lett.* **2007**, *9*, 505-508.
[18] Inseparable by-product observed in 1H NMR spectrum, internal NMR standard shows the purified sample is ~90%w/w desired product.
[19] Prepared as previously reported in: *Org. Lett.* **2007**, *9*, 505-508.
[20] Prepared as described in : *Phosphorus Sulfur Silicon Relat. Elem.* **2015**, *190*, 1934-1941.
[21] Prepared as described in : *Phosphorus Sulfur Silicon Relat. Elem.* **2015**, *190*, 1934-1941.

^{1}H NMR (400 MHz, $CDCl_3$) δ 7.59 – 7.53 (m, 2H), 7.51 (dd, *J* = 7.6, 1.6 Hz, 1H), 7.39 – 7.27 (m, 4H), 7.07 (dd, *J* = 8.4, 0.8 Hz, 1H), 6.98 (td, *J* = 7.5, 1.0 Hz, 1H), 4.98 (s, 2H), 1.38 (s, 9H).

^{13}C NMR (101 MHz, $CDCl_3$) δ 158.3, 133.8, 131.8, 129.6, 128.4, 128.3, 123.7, 121.5, 113.6 (x2), 93.8, 92.3, 85.8, 78.6, 58.0, 48.3, 30.4.

HRMS-EI : Calculated for $C_{21}H_{20}OS$ $[M]^+$: 320.1235; found: 320.1239.

6.3.2. (3+2) Thermal rearrangements to thiophenes

*Standard procedure **SP7a**:*

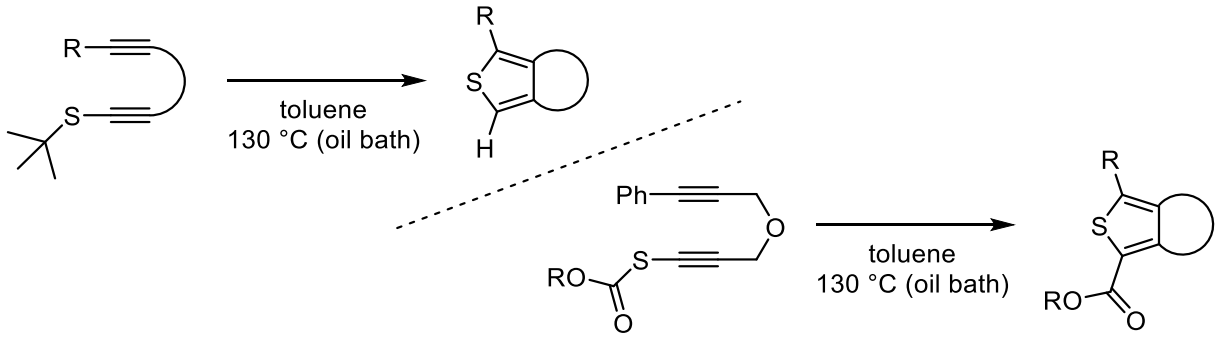

In a sealed reaction vial was added the yne-alkynyl sulfide substrate (0.100 mmol, 1.0 equiv.) and dry toluene (1.0 mL, 0.1 M). The solution was heated in an oil bath at 130 °C for the indicated time. Upon completion (determined by TLC), the mixture was evaporated under reduced pressure to produce a crude. The crude was then purified by silica gel chromatography using the indicated eluent system to yield the desired thiophene.

*Standard procedure **SP7b**:*

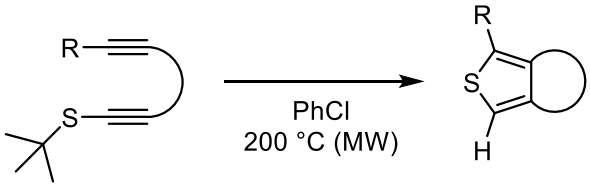

In a microwave vial was added the yne-alkynyl sulfide substrate (0.100 mmol, 1.0 equiv.) and chlorobenzene (1.0 mL, 0.1 M). The solution was heated to 200 °C in an Anton Paar Monowave 400 microwave reactor for the indicated time. Upon completion (determined by TLC), the mixture was

evaporated under reduced pressure to produce a crude. The crude was then purified by silica gel chromatography using the indicated eluent system to yield the desired thiophene.

Characterization of (3+2) rearrangement products

3.026a/3.031a

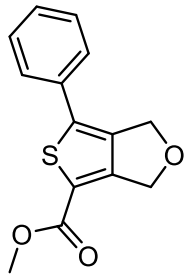

Using standard procedure ***SP7a*** with 0.0519 mmol of substrate **3.025a**. Reaction time = 2.5 h. Solvent system = Hexanes/Et_2O 4:1. Produced 12.1 mg (90% yield) of a white solid.

^{1}H NMR (400 MHz, $CDCl_3$) δ 7.46 – 7.30 (m, 5H), 5.06 (t, *J* = 1.1 Hz, 2H), 5.04 (t, *J* = 1.1 Hz, 2H), 3.87 (s, 3H).

^{13}C NMR (101 MHz, $CDCl_3$) δ 162.4, 153.6, 141.7, 138.7, 132.8, 129.4, 128.8, 126.5, 119.0, 69.6, 69.2, 52.4.

HRMS-EI : Calculated for $C_{14}H_{12}O_3S$ [M]$^+$: 260.0507; found: 260.0514.

3.022a

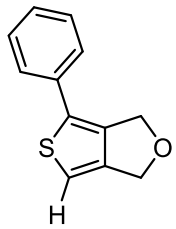

Using standard procedure ***SP7a*** with 0.100 mmol of substrate **3.021e**. Reaction time = 1 h. Solvent system = Hexanes/Et_2O 9:1. Produced 17.2 mg (85% yield) of a white solid.

^{1}H NMR (400MHz, $CDCl_3$) δ 7.41 – 7.35 (m, 4H), 7.31 – 7.23 (m, 1H), 6.79 (t, *J* = 1.3 Hz, 1H), 5.05 (s, 2H), 4.85 (q, *J* = 1.1 Hz, 2H).

^{13}C NMR (101 MHz, $CDCl_3$) δ 146.7, 141.2, 133.8, 132.2, 129.2, 127.4, 126.0, 111.6, 69.1, 68.1.

HRMS-EI : Calculated for $C_{12}H_{10}OS$ [M]$^+$: 202.0452; found: 202.0442.

Supplementary ^{1}H, ^{13}C, COSY, HSQC, HMBC and NOESY data for **10c** in C_6D_6 provided in section 6.3.14.

3.022y

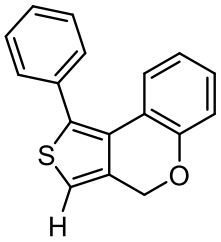

Using standard procedure ***SP7b*** with 0.0877 mmol of substrate **3.021y**. Reaction time = 1 h. Solvent system = Hexanes/toluene 9:1. Produced 17.4 mg (75% yield) of a white solid.[22]

^{1}H NMR (400 MHz, $CDCl_3$) δ 7.56 – 7.48 (m, 2H), 7.48 – 7.36 (m, 3H), 7.21 (dd, *J* = 7.8, 1.5 Hz, 1H), 7.13 (ddd, *J* = 8.2, 7.3, 1.6 Hz, 1H), 7.05 (t, *J* = 1.1 Hz, 1H), 7.03 (dd, *J* = 8.1, 1.1 Hz, 1H), 6.75 (ddd, *J* = 7.8, 7.3, 1.3 Hz, 1H), 5.10 (d, *J* = 1.1 Hz, 2H).

^{13}C NMR (101 MHz, $CDCl_3$) δ 154.4, 137.6, 136.0, 134.5, 129.7, 128.9, 128.6, 128.5, 127.2, 125.5, 122.0, 121.8, 118.0, 117.1, 67.0.

HRMS-EI : Calculated for $C_{17}H_{12}OS$ $[M]^+$: 264.0609; found: 264.0604.

5.5.1. Electrophilic trapping of thiophenium ylide intermediate

*Standard procedure **SP8**: Electrophilic trapping*

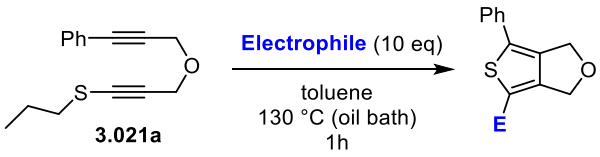

In a sealed reaction vial was added substrate **3.021a** (24.4 mg, 0.100 mmol, 1.0 equiv.), the electrophile (1.00 mmol, 10.0 equiv.) and dry toluene (1.0 mL, 0.1 M). The solution was heated in an oil bath at 130 °C for 1 h. The mixture was evaporated under reduced pressure to produce a crude. The crude was then purified by silica gel chromatography using the indicated eluent system to yield the desired thiophene.

3.026a/3.031a

[22] A small amount of (4+2) naphthalene product was observed in the crude reaction mixture, most of which could be separated during purification with flash chromatography.

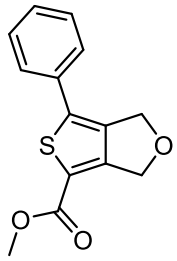

Using standard procedure ***SP8*** with 0.100 mmol of substrate **3.021a** and methyl chloroformate. Solvent system = Hexanes/EtOAc gradient of 9:1 → 17:3. Produced 20.8 mg (85% yield) of a yellow solid.

OR

In a 15mL pressure vessel, using standard procedure 4 with 0.148 mmol of substrate **3.021b** and 2 small scoops (approx. 1.7g) of powdered dry ice. Solvent system = Hexanes/Et_2O 4:1. Produced 9.7 mg (25% yield) of a white solid.

3.026a/3.031a was previously characterized in section 6.3.2.

3.031k

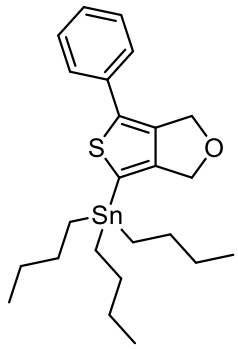

Using a slightly modified version of standard procedure ***SP8*** with 0.0986 mmol of substrate **3.021a** and tributyltin chloride. Crude concentrate was first filtered through silica pad with hexanes/Et_3N 97:3 eluent to remove the majority of excess Bu_3SnCl before proceeding with flash chromatography. Solvent system = Hexanes/Et_2O 49:1. Produced 21.2 mg (44% yield) of a colourless oil.

^{1}H NMR (400 MHz, $CDCl_3$) δ 7.42 – 7.31 (m, 4H), 7.23 (m, 1H), 5.08 (t, *J* = 1.0 Hz, 2H), 4.81 (m, 2H), 1.69 – 1.46 (m, 6H), 1.41 – 1.29 (m, 6H), 1.21 – 1.01 (m, 6H), 0.91 (t, *J* = 7.3 Hz, 9H).

^{13}C NMR (101 MHz, $CDCl_3$) δ 155.4, 141.8, 138.1, 134.0, 129.1, 127.0, 125.9, 123.4, 69.2, 69.0, 29.1, 27.4, 13.8, 10.9.

HRMS-EI : Calculated for $C_{24}H_{36}OSSn$ $[M]^+$: 488.1504; found: 488.1501.

6.3.3. Gram-scale production of model thiophene 3.022a

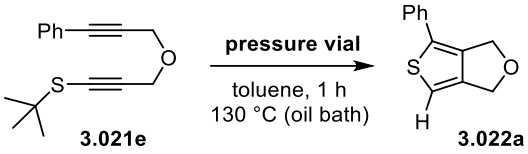

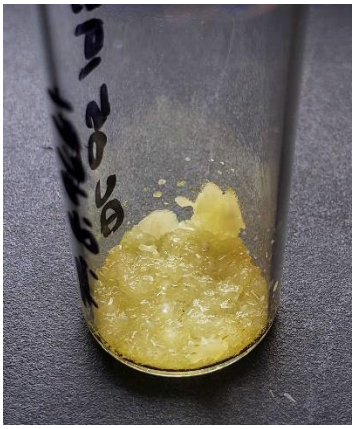

In a sealed 48 mL pressure vial was added the yne-alkynyl sulfide substrate **3.021e** (1.44 g, 5.25 mmol) and dry toluene (10.5 mL, 0.5 M). The solution was stirred in an oil bath at 130 °C for 1 h. The mixture was evaporated under reduced pressure to produce a crude. The crude was then purified as previously described for the smaller scale reaction in section 6.3.2 to produce 851 mg of **3.022a** as a pale yellow solid.

6.3.4. Two-step procedures

Sonogashira reaction & (3+2)

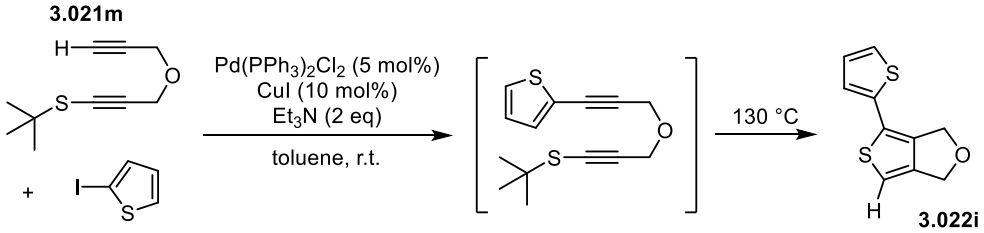

In a flame-dried reaction vial was added yne-alkynyl sulfide **3.021m** (18.2 mg, 0.100 mmol, 1.0 equiv.), 2-iodothiophene (11.6 µL, 0.105 mmol, 1.05 equiv.), triethylamine (27.9 µL, 0.200 mmol, 2.0 equiv.) and dry toluene (1 mL, 0.1 M). The stirred solution was purged with N_2 gas over one minute. To the stirred solution was added at once both $Pd(PPh_3)_2Cl_2$ (3.5 mg, 0.005 mmol, 0.05 equiv.) and copper(I) iodide (1.9 mg, 0.01 mmol, 0.1 equiv.). The stirred reaction mixture was purged with further N_2 gas over another minute and then stirred at room temperature for 1 hour (until completion of the Sonogashira coupling, followed by TLC) then at 130 °C for 15 minutes. The resulting mixture was then filtered through a short pad of celite using DCM as the eluent, then evaporated under reduced pressure to produce a crude. The crude was then purified by silica gel chromatography using hexanes/Et_2O 95:5 as the eluent system to yield 10.8 mg (52% yield) of the desired product **3.022i** as a white solid.

Condensation & (3+2)

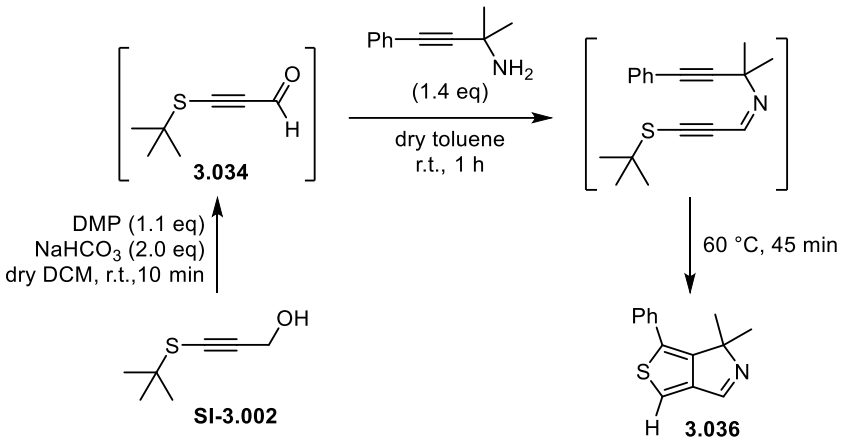

In a reaction vial was added a solution of alcohol **SI-3.002** (22.6 mg, 0.157 mmol, 1.0 equiv.) in dry DCM (0.5 mL, 0.3 M). $NaHCO_3$ (26.4 mg, 0.314 mmol, 2.0 equiv.) is then added, followed by Dess-Martin periodinane (73.4 mg, 0.173 mmol, 1.1 equiv.). The reaction mixture was stirred at room temperature for 10 minutes, then filtered through a short pad of silica gel using hexanes/DCM 1:1 (around 2 mL) as the eluent to afford a solution of aldehyde **3.034**.[23] 2-methyl-4-phenylbut-3-yn-2-amine[24] (29.9 mg, 0.188 mmol, 1.4 equiv.) was added to the filtrate and the mixture is stirred at room temperature for 1 hour to obtain the imine condensate intermediate. Dry toluene (2 mL, 0.08 M) was then added to the mixture, and the hexanes and DCM are evaporated under reduced pressure at 40 °C. The resulting solution is stirred at 60 °C for 45 minutes in a reaction vial, then the mixture is concentrated under reduced pressure to produce a crude mixture. The crude mixture was then purified via flash chromatography using hexanes/acetone 3:1 as the eluent system to yield 24.6 mg (69% yield) of the desired product **3.036** as a pale yellow solid.

3.036

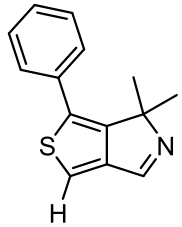

^{1}H NMR (500MHz, $CDCl_3$) δ 8.05 (s, 1H), 7.54 (dd, *J* = 8.2, 1.3 Hz, 2H), 7.45 – 7.34 (m, 3H), 7.12 (s, 1H), 1.49 (s, 6H).

^{13}C NMR (126 MHz, $CDCl_3$) δ 154.4, 153.9, 148.8, 133.5, 133.3, 129.0, 128.7, 128.1, 114.1, 71.0, 25.9.

HRMS-EI : Calculated for $C_{14}H_{13}NS$ [M]$^+$: 227.0769; found: 227.0776.

[23] The aldehyde is used in solution as it degrades upon concentration.
[24] Prepared as previously reported by: Ying, J.; Le, Z.; Wu, X.-F. *Organic Letters* **2020,** 22 *(1)*, 194-198.

C-S coupling & (3+2)

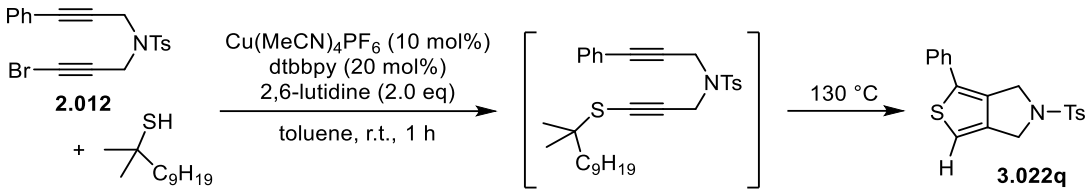

Derived from the coupling method developed by Collins *et al.*[25]:

In a flame-dried reaction vial was added 4,4'-di-tert-butyl-2,2'-bipyridine (2.7 mg, 0.01 mmol, 0.2 equiv.) and bromoalkyne **2.012** (20.1 mg, 0.05 mmol, 1.0 equiv.). Three vacuum/N_2 purge cycles were performed to refill the flask with N_2 atmosphere. *Tert*-dodecyl thiol (13.0 μL, 0.055 mmol, 1.1 equiv.), 2.6-lutidine (11.6 μL, 0.1 mmol, 2.0 equiv.) and dry toluene (0.5 mL, 0.1M) were all added to the vial via syringe. The solution was degassed with N_2 for 2 minutes, then $Cu(MeCN)_4PF_6$ (1.9 mg, 0.003 mmol, 0.1 equiv.) was added quickly. The reaction vial was sealed then stirred at room temperature for one hour (until completion of the C-S coupling, followed by TLC) then at 130 °C for 1.5 hours. The resulting mixture was concentrated under reduced pressure then purified by silica gel chromatography using a gradient of hexanes/EtOAc 19:1 → 9:1 as the eluent system to yield 8.6 mg (48% yield) of the desired product **3.022q** as a yellow solid.

6.3.5. Gold(I)-catalyzed (3+2)

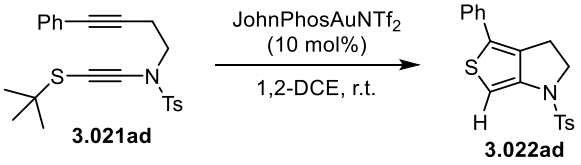

To a small reaction vial was added the yne-alkynyl sulfide substrate **3.021ad** (20.6 mg, 0.0500 mmol, 1.0 equiv.) in 1,2-DCE (0.5 mL, 0.1 M). $JohnPhosAuNTf_2$ (3.9 mg, 0.005 mmol, 10 mol%) was then added and the mixture was stirred at room temperature for 25 hours. Volatiles were then evaporated under reduced pressure to yield a crude mixture. The crude was purified by silica gel chromatography

[25] Godin, É.; Santandrea, J.; Caron, A.; Collins, S.K. *Org. Lett.* **2020**, 22 *(15)*, 5905–5909.

using hexanes:EtOAc gradient 9:1 → 8:2 as the eluent system to yield 12.4 mg (70% yield) of **3.022ad** as a yellow solid.

3.022ad

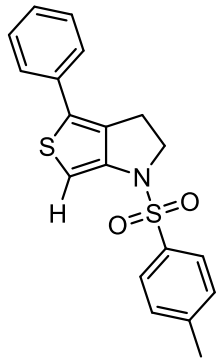

^{1}H NMR (400MHz, $CDCl_3$) δ 7.76 (d, *J* = 8.3 Hz, 2H), 7.43 – 7.21 (m, 7H), 6.77 (s, 1H), 4.16 (t, *J* = 7.8 Hz, 2H), 2.97 (t, *J* = 7.8 Hz, 2H), 2.40 (s, 3H).

^{13}C NMR (101 MHz, $CDCl_3$) δ 144.5, 144.1, 133.9, 133.7, 133.4, 132.6, 129.9, 129.0, 127.7, 127.6, 126.0, 100.8, 55.7, 25.8, 21.7.

HRMS-EI : Calculated for $C_{19}H_{17}NO_2S_2$ $[M]^+$: 355.0701; found: 355.0676.

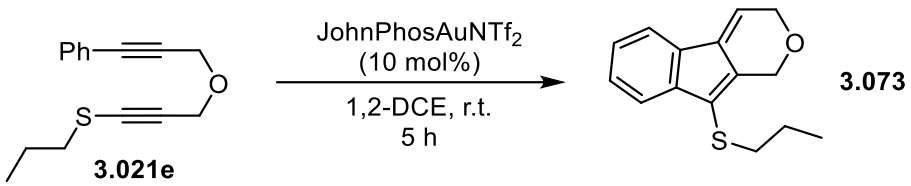

3.021e **3.073**

Reaction performed in a qualitative manner. A small amount of substrate **3.021e** was dissolved in ~1 mL of 1,2-DCE. The tip of a spatula of JohnPhosAuNTf2 was added and the solution was stirred at room temperature. The reaction was followed by TLC until approximately 50% conversion of the starting material was observed (about 5 hours).

The mixture was directly concentrated and analyzed by ^{1}H NMR in $CDCl_3$. The crude mixture contained the starting material and the TDDA product **3.073** as the two major species.

A rapid purification by silica gel chromatography (hexanes/Et_2O 95:5) provided a sample of pure **3.073** for analysis:

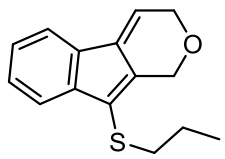

^{1}H NMR (300 MHz, $CDCl_3$) δ 7.54 (d, J = 7.3 Hz, 1H), 7.43 (d, J = 7.5 Hz, 1H), 7.32 (td, J = 7.5, 1.1 Hz, 1H), 7.20 (td, J = 7.4, 1.1 Hz, 1H), 6.79 (t, J = 3.5 Hz, 1H), 4.84 (s, 2H), 4.49 (d, J = 3.5 Hz, 2H), 2.85 – 2.74 (m, 2H), 1.66 – 1.52 (m, 2H), 0.98 (t, J = 7.3 Hz, 3H).

6.3.6. Synthesis of functionalized oligothiophenes

Synthesis of tris-thiophenes

3.039

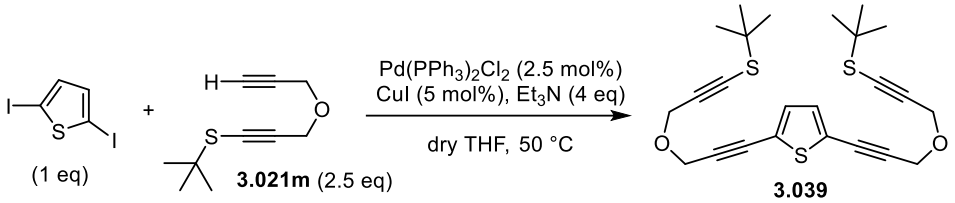

In a flame-dried round bottom flask under N_2 atmosphere was added yne-alkynyl sulfide **3.021m** (1.406 mmol, 2.5 equiv.), 2,5-diiodothiophene (0.562 mmol, 1.0 equiv.), triethylamine (0.31 mL, 2.248 mmol, 4.0 equiv.) and dry THF (6.0 mL, 0.1M). The stirred solution was purged with N_2 gas over 5 min. To the stirred solution was added at once both $Pd(PPh_3)_2Cl_2$ (9.9 mg, 0.0141 mmol, 0.025 equiv.) and copper(I) iodide (5.4 mg, 0.0281 mmol, 0.05 equiv.). The stirred reaction mixture was purged with further N_2 gas over another 5 min, and then stirred at 50 °C for 2 hours until completion. Et_2O and 2.5% HCl aq. solution were then added to the reaction mixture. The organic phase was washed three times with 2.5% HCl aq. solution and once with brine. The organic phase was dried with $MgSO_4$, filtered, and concentrated under reduced pressure to produce a crude. The crude was then purified by silica gel chromatography using Hexanes/Et_2O 95:5 as the eluent system to yield 89 mg (36% yield) of the desired bis alkynyl sulfide **3.039** as a yellow oil.[26]

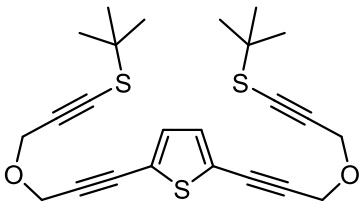

^{1}H NMR (400MHz, $CDCl_3$) δ 7.06 (s, 2H), 4.49 (s, 4H), 4.46 (s, 4H), 1.43 (s, 18H).

^{13}C NMR (101 MHz, $CDCl_3$) δ 132.4, 124.1, 92.6, 89.6, 79.4, 77.9, 58.1, 57.0, 48.1, 30.4.

3.040

[26] Despite testing a variety of conditions and temperatures, **3.039** seems to fragment too readily during MS analysis. Characteristic molecular peaks could not be obtained with either of EI, APCI or ESI.

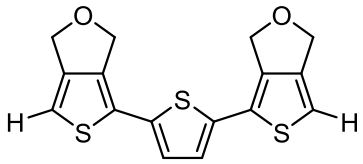

Using standard procedure ***SP7a*** with 0.177 mmol of substrate **3.039**. Reaction time = 0.5 h. Solvent system = EtOAc. Produced 48.9 mg (83% yield) of a white solid.

^{1}H NMR (400MHz, $CDCl_3$) δ 6.92 (s, 2H), 6.72 (s, 2H), 4.96 (s, 4H), 4.84 (s, 4H).

^{13}C NMR (101 MHz, $CDCl_3$) δ 146.4, 141.8, 135.8, 125.1, 124.7, 111.4, 68.7, 68.3.

HRMS-EI : Calculated for $C_{16}H_{12}O_2S_3$ $[M]^+$: 331.9999; found: 331.9992.

3.041

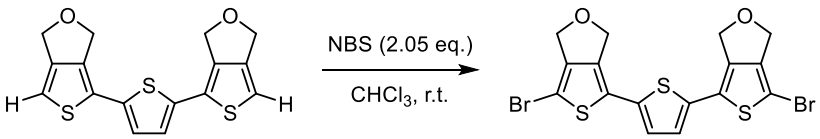

3.040 **3.041**

In a small reaction vial was added a solution of **3.040** (16.8 mg, 0.0505 mmol, 1.0 equiv.) in $CHCl_3$ (0.1 M) then *N*-bromosuccinimide (18.4 mg, 0.104 mmol, 2.05 equiv.) was added in small portions. The mixture was stirred at room temperature for one hour before it was quenched with H_2O, and extracted with chloroform. The collected organic phases were then washed with brine. The organic phase was dried with $MgSO_4$, filtered, and concentrated under reduced pressure to produce a crude. The crude was then purified by silica gel chromatography (dry load) using Hexanes:EtOAc 8:2 as the eluent system to yield 19.9 mg (80% yield) of the desired product **3.041** as a yellow solid.

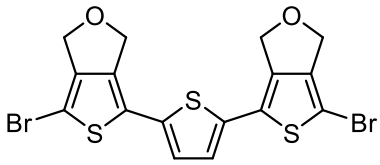

^{1}H NMR (500MHz, $CDCl_3$) δ 6.85 (s, 2H), 4.96 (s, 4H), 4.74 (s, 4H).

^{13}C NMR (126 MHz, $CDCl_3$) δ 146.8, 141.6, 135.2, 126.1, 124.9, 98.6, 69.6, 68.6.

HRMS-EI : Calculated for $C_{16}H_{10}Br_2O_2S_3$ $[M]^+$: 487.8210; found: 487.8218.

<u>Synthesis of bis-thiophene 3.043</u>

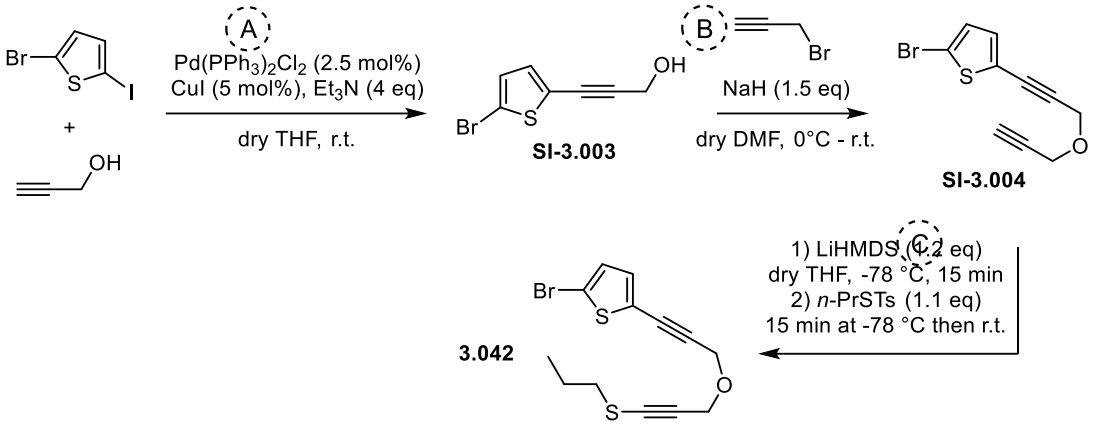

A In a flame-dried round bottom flask under N_2 atmosphere was added propargyl alcohol (1.05 mmol, 1.05 equiv.), 2-bromo-5-iodothiophene (1.00 mmol, 1.00 equiv.), triethylamine (0.28 mL, 2.00 mmol, 2.0 equiv.) and dry THF (10 mL, 0.1 M). The stirred solution was purged with N_2 gas over about 5 min. To the stirred solution was added at once both $Pd(PPh_3)_2Cl_2$ (9.9 mg, 0.0141 mmol, 0.025 equiv.) and copper(I) iodide (5.4 mg, 0.0281 mmol, 0.05 equiv.). The stirred reaction mixture was purged with further N_2 gas over another 5 min, and then stirred at room temperature overnight (16 hours). Et_2O and 2.5% HCl aq. solution were then added to the reaction mixture. The organic phase was washed three times with 2.5% HCl aq. solution and once with brine. The organic phase was dried with $MgSO_4$, filtered, and concentrated under reduced pressure to produce a crude. The crude was then purified by silica gel chromatography using hexanes/EtOAc 70:30 as the eluent system to yield 193 mg (89% yield) of the desired propargyl alcohol **SI-3.003** as a brown solid.

SI-3.003

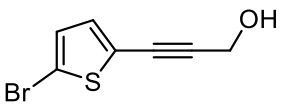

^{1}H NMR (400MHz, $CDCl_3$) δ 6.96 (d, *J* = 3.9 Hz, 1H), 6.92 (d, *J* = 3.9 Hz, 1H), 4.49 (s, 2H), 1.68 (s, 1H).

^{13}C NMR (101 MHz, $CDCl_3$) δ 132.9, 130.1, 124.3, 113.5, 92.3, 78.3, 51.8.

B In a round bottom flask was cooled to 0 °C a solution of alcohol **SI-3.003** (181 mg, 0.832 mmol, 1.0 equiv.) in dry DMF (1.7 mL, 0.5 M). To the cooled solution was added NaH (40 mg, 60% w/w, 0.998 equiv.). When most of the evolution of H_2 gas had passed, propargyl bromide (0.14 mL, 80% w/w solution in toluene, 1.249 mmol, 1.5 equiv.) was added then the solution was brought to room temperature and stirred for 1 h. The mixture was quenched with NH_4Cl sat. aq. solution and diluted with Et_2O. The organic phase was washed once with water, then with brine. The organic phase was

dried using $MgSO_4$, and then concentrated under reduced pressure to produce a crude. The crude was then purified via flash chromatography using hexanes/Et_2O 98:2 as the eluent system to yield 97 mg (46% yield) of the desired alkyne **SI-3.004** as a pale yellow liquid.

SI-3.004

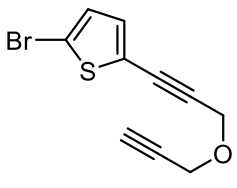

^{1}H NMR (400MHz, $CDCl_3$) δ 6.98 (d, *J* = 3.8 Hz, 1H), 6.93 (d, *J* = 3.9 Hz, 1H), 4.48 (s, 2H), 4.29 (d, *J* = 2.4 Hz, 2H), 2.48 (t, *J* = 2.4 Hz, 1H).

^{13}C NMR (101 MHz, $CDCl_3$) δ 133.2, 130.1, 124.2, 113.6, 89.4, 79.3, 78.9, 75.4, 57.4, 56.9.

C In a flame-dried round bottom flask N_2 atmosphere was added the alkyne **SI-3.004** (0.392 mmol, 1.0 equiv.) and dry THF (3 mL, 0.13 M) via syringe. The solution was cooled to -78 °C. To the stirred solution was added LiHMDS (0.47 mL, 0.1 M in THF, 0.470 mmol, 1.2 equiv.) dropwise over 5 minutes. The solution was then stirred at -78 °C for another 15 min. A prepared solution of *S*-*n*-propyl *p*-tolylsulfonate (0.431 mmol, 1.1 equiv.) in dry THF (1 mL) was then added dropwise to the reaction mixture via syringe, then the solution was stirred for an additional 15 min at -78 °C before slowly warming to room temperature. The solution was stirred at room temperature for 45 minutes before it was quenched with NH_4Cl aq. solution. The reaction mixture was then extracted with Et_2O, washed once with water, then brine. The organic phase was dried over $MgSO_4$, filtered, and concentrated under reduced pressure to produce a crude. The crude was then purified by silica gel chromatography using hexanes/Et_2O 95:5 as the eluent system to yield 113 mg (84% yield) of the desired alkynyl sulfide **3.042** as a dark yellow oil.

3.042

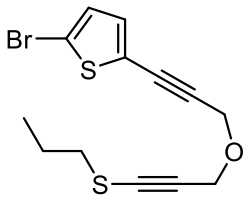

^{1}H NMR (400MHz, $CDCl_3$) δ 6.97 (d, *J* = 3.9 Hz, 1H), 6.92 (d, *J* = 3.9 Hz, 1H), 4.46 (s, 2H), 4.38 (s, 2H), 2.70 (dd, *J* = 7.4, 6.9 Hz, 2H), 1.77 (h, *J* = 7.3 Hz, 2H), 1.02 (t, *J* = 7.3 Hz, 3H).

^{13}C NMR (101 MHz, $CDCl_3$) δ 133.1, 130.1, 124.2, 113.6, 89.7, 89.2, 79.1, 78.5, 58.0, 57.2, 37.6, 22.8, 13.0.

HRMS-EI : Calculated for $C_{13}H_{13}OS_2$ $[M]^+$: 327.9591; found: 327.9586.

3.043

Using a slightly modified version of standard procedure ***SP8*** with 0.075 mmol of substrate **3.042** and tributyltin chloride. Crude concentrate was first filtered through silica pad with hexanes/Et_3N 97:3 eluent to remove the majority of excess (*n*-Bu)$_3$SnCl before proceeding with flash chromatography. Solvent system = Hexanes/Et_2O 98:2. Produced 25.0 mg (58% yield) of a pale yellow oil.

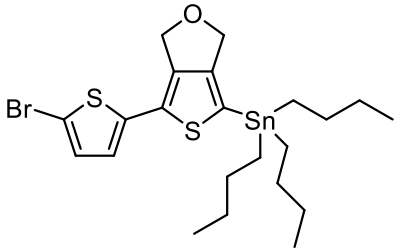

^{1}H NMR (400MHz, $CDCl_3$) δ 6.96 (d, *J* = 3.8 Hz, 1H), 6.77 (d, *J* = 3.9 Hz, 1H), 4.93 (t, *J* = 1.1 Hz, 2H), 4.80 – 4.76 (m, 2H), 1.67 – 1.44 (m, 6H), 1.34 (hex, *J* = 7.3 Hz, 6H), 1.21 – 0.99 (m, 6H), 0.91 (t, *J* = 7.3 Hz, 9H).

^{13}C NMR (101 MHz, $CDCl_3$) δ 154.9, 142.4, 138.4, 130.8, 130.3, 123.9, 123.6, 111.2, 69.1, 68.6, 29.1, 27.4, 13.8, 10.9.

HRMS-EI : Calculated for $C_{22}H_{33}BrOS_2Sn$ [M]$^+$: 578.1058; found: 578.0154.[27]

6.3.7. Conversion of model thiophene to benzene-derived products

<u>Synthesis of thiophene S,S-dioxide</u>

3.044

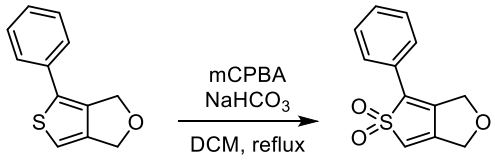

3.022a **3.044**

To a stirred suspension of thiophene **3.022a** (423 mg, 2.09 mmol, 1.0 equiv.) and $NaHCO_3$ (439 mg, 5.23 mmol, 2.5 equiv.) in DCM (42 mL, 0.05 M) was added mCPBA (1.29 g, 5.23 mmol, 2.5 equiv.). The mixture was heated and stirred at reflux for 3 h. Showing completion by TLC analysis, the mixture was cooled to rt, and filtered through celite. The reaction mixture was washed once with $Na_2S_2O_5$ sat. aq. solution, once with $NaHCO_3$ sat. aq. solution, and once with brine. The organic phase was then dried over $MgSO_4$, filtered, and concentrated under reduced pressure to produce a crude. The crude was

[27] [M]$^+$ reported for the abundant ^{81}Br / ^{120}Sn isotopologue.

then purified by silica gel chromatography using Hexanes/EtOAc 3:2 as the eluent system to yield 201 mg (41% yield) of the desired thiophene dioxide **3.044** as a white solid.

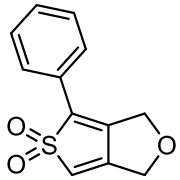

^{1}H NMR (400 MHz, $CDCl_3$) δ 7.60 – 7.55 (m, 2H), 7.53 – 7.41 (m, 3H), 6.49 (tt, *J* = 2.4, 0.8 Hz, 1H), 4.97 (s, 2H), 4.79 (d, *J* = 2.3 Hz, 2H).

^{13}C NMR (101 MHz, $CDCl_3$) δ 146.7, 135.7, 132.3, 130.3, 129.6, 127.6, 126.8, 117.7, 68.1, 67.4.

HRMS-EI : Calculated for $C_{12}H_{10}O_3S$ $[M]^+$: 234.0351; found: 234.0373.

(4+2) cycloadditions of thiophene S,S-dioxide

3.045

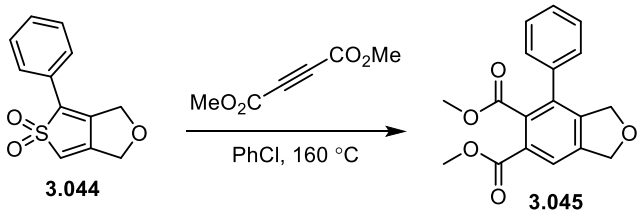

In a sealed reaction vial was added thiophene dioxide **3.044** (24.4 mg, 0.104 mmol, 1.0 equiv.), dimethyl acetylenedicarboxylate (15.3 µL, 0.125 mmol, 1.2 equiv.) and chlorobenzene (1.0 mL, 0.1 M). The solution was heated in an oil bath at 160 °C for 2 h. Showing completion by TLC analysis, the mixture was evaporated under reduced pressure to produce a crude. The crude was then purified by silica gel chromatography using a gradient of Hexanes/EtOAc 17:3 → 13:7 as the eluent system to yield 7.0 mg (22% yield) of the desired benzene derivative **3.045** as a white solid.

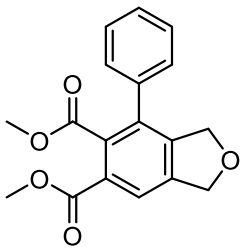

^{1}H NMR (400 MHz, $CDCl_3$) δ 7.88 (s, 1H), 7.44 – 7.34 (m, 3H), 7.29 – 7.23 (m, 2H), 5.24 – 5.19 (m, 2H), 4.94 (t, *J* = 2.0 Hz, 2H), 3.91 (s, 3H), 3.60 (s, 3H).

^{13}C NMR (101 MHz, $CDCl_3$) δ 168.9, 166.1, 143.7, 140.6, 136.6, 135.0, 134.6, 128.6, 128.4 (x2), 128.1, 121.8, 73.9, 73.5, 52.8, 52.4.

MS-ESI+ : 375.9 ($[M+CH_3CN+Na]^+$, 35%), 359.9 (21%), 280.9 ($[M-CH_3OH+H]^+$, 100%).

3.046

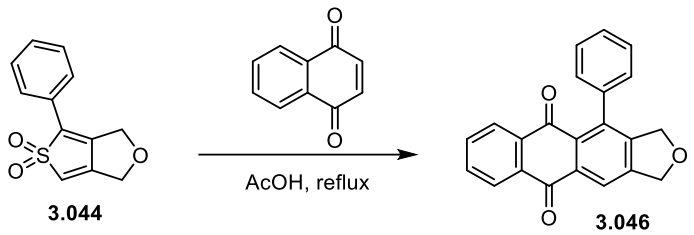

3.044 **3.046**

In a round bottom flask was added thiophene dioxide **3.044** (25.0 mg, 0.107 mmol, 1.0 equiv.), 1,4-naphthoquinone (169 mg, 1.07 mmol, 10.0 equiv.) and glacial acetic acid (5.0 mL, 0.02 M). The solution was heated and stirred at reflux for 2 h. Showing completion by TLC analysis, the mixture was poured over 25 mL H_2O, and extracted using DCM. The organic phase was then washed three times with H_2O and once with brine. The organic phase was dried over $MgSO_4$, filtered, and concentrated under reduced pressure to produce a crude. The crude was then purified by silica gel chromatography using a gradient of Hexanes/Et_2O 17:3 → 3:1 as the eluent system to yield 11.7 mg (34% yield) of the desired quinone derivative **3.046** as an orange solid.

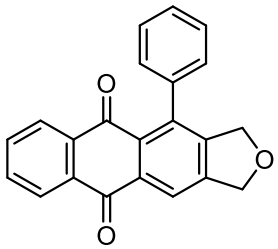

^{1}H NMR (400 MHz, $CDCl_3$) δ 8.32 – 8.25 (m, 2H), 8.14 – 8.07 (m, 1H), 7.80 – 7.69 (m, 2H), 7.53 – 7.41 (m, 3H), 7.24 – 7.17 (m, 2H), 5.30 (td, *J* = 2.0, 1.0 Hz, 2H), 4.86 (t, *J* = 2.0 Hz, 2H).

^{13}C NMR (101 MHz, $CDCl_3$) δ 183.4, 183.3, 146.9, 144.9, 139.7, 138.2, 135.2, 134.5, 134.4, 133.9, 132.9, 130.4, 128.8, 127.6 (x2), 126.9, 120.0, 74.3, 73.7.[28]

HRMS-EI : Calculated for $C_{22}H_{14}O_3$ $[M]^+$: 326.0943; found: 326.0969.

<u>Alternative route to fused benzene 3.045</u>

Based on Tanaka *et al.*'s procedure[29] on the diyne-alkyne (2+2+2), with available reagents, the following was obtained:

[28] Missing 13C NMR signal. There are probably two peaks located under the same signal at 126.9 ppm due to its notably high intensity.
[29] K. Tanaka *et al. Tetrahedron* **2010**, *66*, 1563–1569.

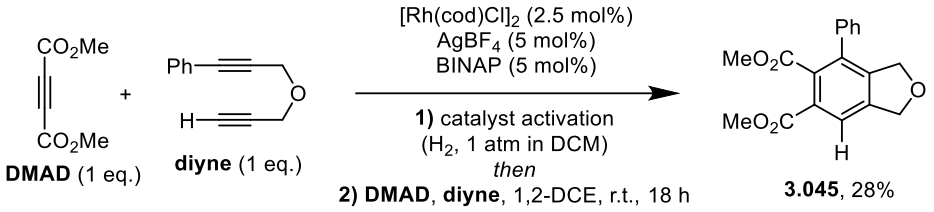

Catalyst activation: In a Schlenk flask was added $[Rh(cod)Cl]_2$ (3.7 mg, 0.0075 mmol, 2.5 mol%), $AgBF_4$ (2.9 mg, 0.015 mmol, 5 mol%) and 2,2'-bis(diphenylphosphino)-1,1'-binaphthyl (9.3 mg, 0.015 mmol, 5 mol%). The flask was evacuated under high vacuum and backfilled with nitrogen gas three times. DCM (3 mL) was added via syringe, and the mixture was stirred at room temperature for 5 minutes. H_2 gas was bubbled through the solution for 30 seconds and an H_2 balloon was installed on the system, after which the mixture was stirred for an additional 30 minutes. The mixture was then evaporated to dryness under high vacuum and backfilled once with nitrogen gas.

Yne-diyne trimerization: To the above obtained activated catalyst solid mass was added some 1,2-DCE (1 mL). A solution of dimethyl acetylenedicarboxylate (37 µL, 0.300 mmol, 1.0 eq.) and (3-(prop-2-ynyloxy)prop-1-ynyl)benzene[30] (51.1 mg, 0.300 mmol, 1.0 eq.) in 1,2-DCE (2mL) were added at once to the flask, and the reaction mixture was stirred at room temperature overnight (18 h). The mixture was finally concentrated under reduced pressure to provide a reaction crude. The crude was then purified by silica gel chromatography using Hexanes/EtOAc 4:1 as the eluent system to yield 26.3 mg (28% yield) of **3.045** as a white solid.

6.3.8. Mechanistic studies – Experimental studies

Deuteration studies

Unless otherwise noted, for each experiment, in a reaction tube was added the indicated substrate (0.100 mmol, 1.0 equiv.), the indicated additive (0.100 mmol, 1.0 equiv.) and dry toluene (1 mL, 0.1 M). The reaction mixture was heated in an oil bath at 130 °C for 1 h. The mixture was then concentrated under reduced pressure, transferred to an NMR tube along with $CDCl_3$, and supplemented with 2.0 µL of 1,2-dibromoethane to be used as an internal NMR standard upon ^1H NMR analysis.

[30] Prepared as previously reported in: *Org. Lett.* **2007**, *9*, 505-508.

The ratio of ^{1}H NMR signal integration between the thiophene α-hydrogen and either of the CH_2 groups in a pure sample of **3.022a** is 0.92 : 2.00. Obtained ratios in each experiment are set against this 0.92:2.00 ratio in order to determine the percentage of deuteration.

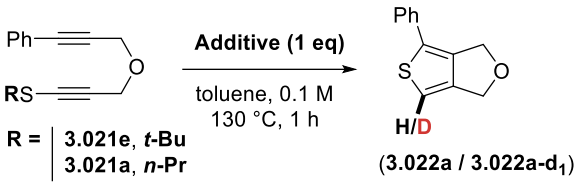

Entry	Substrate	Additive	NMR Yield (%)	Deuteration (%)
1	**3.021e**, R = *t*-Bu	AcOH-d_4	79	51
2		MeOH-d_4	75	37
3		MeCN-d_3	75	< 5
4	**3.021a**, R = *n*-Pr	AcOH-d_4	85	79
5		MeOH-d_4	35	23
6 [a]		MeOH-d_4 (as co-solvent)	29	96
7		MeCN-d_3	38	< 5

Table SI-6.3-1. Effect of deuterated species with different acidities. [a] the reaction was conducted in a mixture of 0.5 mL MeOH-d_4 + 0.5 mL dry toluene instead.

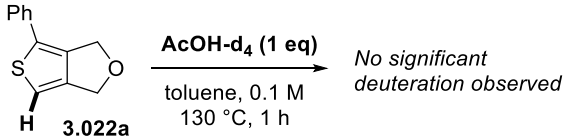

Figure SI-6.3-1. Control experiment with deuterated acetic acid. After subjecting pure thiophene **3.022a** under the same reaction conditions for the same time interval, no significant amount of deuteration (< 5 %) could be detected by ^{1}H NMR analysis.

Study of probe 3.021ac

For each experiment, in a sealed NMR tube was added the indicated substrate (0.0500 mmol, 1.0 equiv.), the indicated additive (0.0500 mmol, 1.0 equiv.) and toluene-d_8 (0.5 mL, 0.1 M). The solution

was analyzed by ^{1}H NMR experiment before and after heating in an oil bath at 130 °C for 30 min. All NMR spectra were recorded at room temperature using a Bruker Avance II 300 spectrometer.

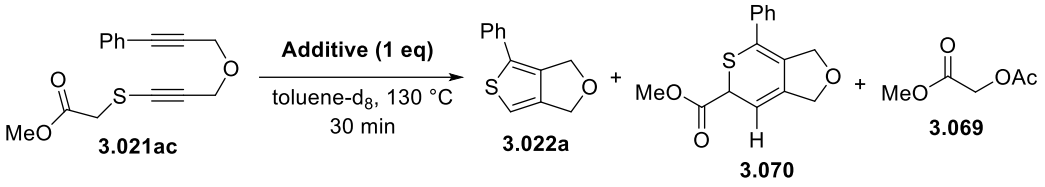

Entry	Additive	NMR Yield of 3.022a (%)	NMR Yield of 3.070 (%)	NMR Yield of 3.071 (%)
1	AcOH-d_4	Quantitative	0	92
2	MeOH-d_4	24	53	-
3	None	17	52	-

Table SI-6.3-2. Effect of additive on reaction outcome of probe 3.021ac.

Thiopyran **3.070** was isolated from entry 3 via silica gel chromatography, using hexanes/Et_2O 13:7 as the eluent system, in 7.5 mg (55% isolated yield) as a pale brown oil.

3.070

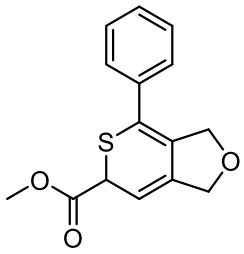

^{1}H NMR (400MHz, $CDCl_3$) δ 7.44 – 7.27 (m, 5H), 5.48 (dt, *J* = 6.2, 1.9 Hz, 1H), 4.67 (d, *J* = 12.7 Hz, 1H), 4.61 (d, *J* = 12.7 Hz, 1H), 4.61 – 4.58 (m, 2H), 4.50 (dt, *J* = 6.2, 1.5 Hz, 1H), 3.78 (s, 3H).

^{13}C NMR (101 MHz, $CDCl_3$) δ 170.9, 140.8, 136.8, 128.7, 128.6, 127.9, 127.4, 124.8, 103.0, 71.6, 71.6, 53.0, 42.8.

HRMS-EI : Calculated for $C_{15}H_{14}O_3S[M]^+$: 274.0664; found: 274.0664.

Supplementary COSY, HSQC, HMBC and NOESY data for **3.070** provided in Section 6.3.14

6.3.9. Mechanistic studies - DFT studies

Potential energy surfaces data

General methodology for calculation of potential energy surfaces:

Using the Gaussian16 software,[31] structural optimization and vibrational frequency calculations for minima and maxima along the potential energy surface were carried out at the (U)B3LYP/6-31+G(d) level of theory.[32] Vibrational frequency calculations were performed at the gas phase, 1 atm, and 298.15 K. Normal modes of vibration were analyzed to assure either 0 (minima) or 1 (maxima) imaginary frequencies were obtained. Intrinsic reaction coordinate (IRC) calculations were performed on each transition state structure to assign connectivity (dotted lines) to the indicated minima.

When using *unrestricted* functionals, the "guess=(mix,always)" input line was included to allow the construction of wavefunctions for singlet diradicals.

Benchmarking/Validation of method:

Single point energy calculations were performed for reported stationary points **3.049–3.062** at the (U)B2PLYPD/*aug*-cc-pVDZ level of theory, a method used in the past which correlates well with higher-level computations regarding the formation of diradicals from multiples alkynes and cycloaddition reactions.[33]

Conformational search for the flexible minima I-tBu and I-CO_2Me:

Using the Spartan software,[34] a conformer distribution calculation using the MMFF method was completed for both **3.049-tBu** and **3.049-CO_2Me**. In each case, the conformer with the lowest electronic energy was selected as the input geometry for optimization at the B3LYP/6-31+G(d) level of theory using Gaussian16.

Table SI-6.3-3. Potential energy surface data for the general (3+2) pathway. All structures optimized and evaluated at the (U)B3LYP/6-31+G(d) level of theory. When using *unrestricted* UB3LYP, the "guess=(mix,always)" input was included in the calculation to allow for singlet diradicals.

[31] Frisch, M. J. *et al.* Gaussian 16 Rev. C.01, Wallingford, CT, **2016**.

[32] (a) Becke, A. D. *J. Chem. Phys.* **1993**, *98*, 5648–5652; (b) Lee, C.; Yang, W.; Parr, R. G. *Phys. Rev. B: Condens. Matter Mater. Phys.* **1988**, *37*, 785–789; (c) Miehlich, B.; Savin, A.; Stoll, H.; Preuss, H. *Chem. Phys. Lett.* **1989**, *157*, 200–206.

[33] See: (a) Haberhauer, G.; Gleiter, R. *J. Am. Chem. Soc.* **2013**, *135*, 8022-8030; (b) Haberhauer, G.; Gleiter, R.; Woitschetzki, S. *J. Org. Chem.* **2015**, *80*, 12321-12332.

[34] Except for molecular mechanics and semi-empirical models, the calculation methods used in Spartan Student have been documented in: Y. Shao *et al. Phys. Chem. Chem. Phys.* **2006**, *8*, 3172.

RB3LYP* or *UB3LYP	**Structure**	**EE (Hartrees)**	**Thermal Free Energy Correction (Hartrees)**	**EE + Thermal Free Energy Correction (Hartrees)**	**ΔG (kcal/mol)**	**Negative frequencies**	**⟨S²⟩**
RB3LYP	**3.049-tBu**	-1093.844956	0.242403	-1093.602553	0.0	0	-
	3.053-tBu	-1093.844885	0.252446	-1093.592440	6.3	0	-
	3.065-tBu	-1093.808552	0.249460	-1093.559092	27.3	1	-
	3.066	-936.701590	0.149797	-936.551793	-	0	-
	C_4H_8	-157.234104	0.080806	-157.153298	-	0	-
	3.066 + C_4H_8	-1093.935694	-	-1093.705091	-64.3	-	-
	3.068	-1093.961553	0.255358	-1093.706196	-65.0	0	-
UB3LYP	**3.050-tBu**	-1093.806939	0.244026	-1093.562913	24.9	1	0.1091
	3.051-tBu	-1093.817015	0.245656	-1093.571359	19.6	0	0.8195
	3.052-tBu	-1093.816014	0.248122	-1093.567892	21.7	1	0.4825
UB3LYP	**3.056-tBu**	-1093.806524	0.245172	-1093.561352	25.9	1	0.9071

	3.057-tBu	-1093.812317	0.244896	-1093.567421	22.0	0	0.9994
	3.058-tBu	-1093.799650	0.250138	-1093.549512	33.3	1	0.2598
RB3LYP	**3.059-tBu**	-1093.823040	0.252779	-1093.570261	20.3	0	-
	3.060-tBu	-1093.982332	0.256896	-1093.725436	-77.1	0	-
RB3LYP	**3.049-CO_2Me**	-1164.460393	0.173623	-1164.286769	0.0	0	-
	3.053-CO_2Me	-1164.449850	0.181308	-1164.268542	11.4	0	-
	3.065-CO_2Me	-1164.441414	0.182101	-1164.259313	17.2	1	-
	3.067	-1164.592845	0.185956	-1164.406889	-75.4	0	-
UB3LYP	**3.050-CO_2Me**	-1164.420522	0.174556	-1164.245966	25.6	1	0.1733
	3.051-CO_2Me	-1164.430897	0.175436	-1164.255461	19.6	0	0.8685
	3.052-CO_2Me	-1164.427771	0.178532	-1164.249239	23.6	1	0.3548

Table SI-6.3-4. Single point energy benchmarking. All structures optimized at the B3LYP/6-31+G(d) level of theory. Single point energy calculations were then performed on these geometries at the (U)B2PLYPD/*aug*-cc-pVDZ level of theory. When using *unrestricted* functionals (i.e. UB3LYP or UB2PLYPD), the "guess=(mix,always)" input was included in the calculation to allow for singlet diradicals. Notably, the PES remains qualitatively the same when comparing the obtained electronic energies for B2PLYPD/*aug*-cc-pVDZ and B3LYP/6-31+G(d).

Restricted or Unrestricted	**Structure**	**Electronic energy, in Hartrees (ΔE, in kcal/mol)**			
		B3LYP/6-31+G(d)		**B2PLYPD/*aug*-cc-pVDZ**	
Restricted	**3.049-tBu**	-1093.844956	(0.0)	-1092.200150	(0.0)
	3.053-tBu	-1093.844885	(0.0)	-1092.206607	(-4.1)
	3.065-tBu	-1093.808552	(22.8)	-1092.162072	(23.9)
	3.066	-936.70159	-	-935.426100	-
	C_4H_8	-157.234104	-	-156.862981	-
	3.066 + C_4H_8	-1093.935694	(-56.9)	-1092.289081	(-55.8)
	3.068	-1093.961553	(-73.2)	-1092.324745	(-78.2)
Unrestricted	**3.050-tBu**	-1093.806939	(23.9)	-1092.155759	(27.9)
	3.051-tBu	-1093.817015	(17.5)	-1092.176717	(14.7)
	3.052-tBu	-1093.816014	(18.2)	-1092.171583	(17.9)
Restricted	**3.049-CO_2Me**	-1164.460393	(0.0)	-1162.792919	(0.0)
	3.053-CO_2Me	-1164.449850	(6.6)	-1162.786879	(3.8)
	3.065-CO_2Me	-1164.441414	(11.9)	-1162.772075	(13.1)
	3.067	-1164.592845	(-83.1)	-1162.930498	(-86.3)
Unrestricted	**3.050-CO_2Me**	-1164.420522	(25.0)	-1162.748970	(27.6)
	3.051-CO_2Me	-1164.430897	(18.5)	-1162.770747	(13.9)
	3.052-CO_2Me	-1164.427771	(20.5)	-1162.759817	(20.8)

6.3.10. Cartesian coordinates for reported minima/maxima

3.049-tBu

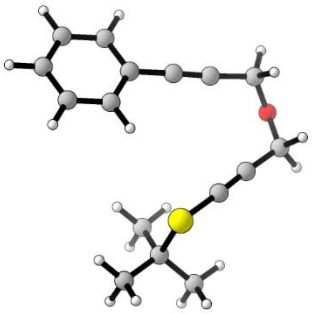

Atom type	X	Y	Z
C	2.12866100	1.26797800	-0.01551000
C	1.54123700	2.33066400	-0.01478300
C	0.90019000	3.65061700	-0.01053600
C	-1.49800100	3.37114300	-0.14408000
C	-1.68119400	1.94928100	-0.43838400
C	-1.89463100	0.77792000	-0.69733200
S	-2.11143800	-0.83656800	-1.13760200
C	-2.90852500	-1.60171800	0.40382100
C	-1.95782900	-1.46452900	1.59740100
C	-3.10563600	-3.07490800	0.01808700
C	-4.25260500	-0.91924900	0.67842400
C	2.79750600	0.00331500	-0.02836300
C	4.11660500	-2.48053400	-0.06403500
C	4.07368700	-0.13858100	0.55258400
C	2.19120900	-1.11991100	-0.62689900
C	2.84908000	-2.34959400	-0.64087700
C	4.72536800	-1.37133900	0.53199000
O	-0.36261200	3.70737900	0.65441600
H	0.79424500	4.02161900	-1.04284100
H	1.53759400	4.35973100	0.52940900
H	-1.46573700	3.93659600	-1.09030700
H	-2.35433300	3.74320300	0.42938500
H	-1.00127500	-1.96181700	1.40606900
H	-1.75674100	-0.41341800	1.82818100
H	-2.41437100	-1.92563900	2.48376700
H	-2.15108200	-3.56514200	-0.20504400
H	-3.76302000	-3.18081000	-0.85260200
H	-3.56930200	-3.60868300	0.85699000
H	-4.93399200	-1.02178500	-0.17289000
H	-4.12023000	0.14730800	0.88793200
H	-4.72569800	-1.38027500	1.55600700
H	4.62667600	-3.44033700	-0.07881400
H	4.54376800	0.72389200	1.01627100
H	1.20541600	-1.01693500	-1.07087000
H	2.37124000	-3.20817800	-1.10611800
H	5.71002000	-1.46661200	0.98272100

3.050-tBu

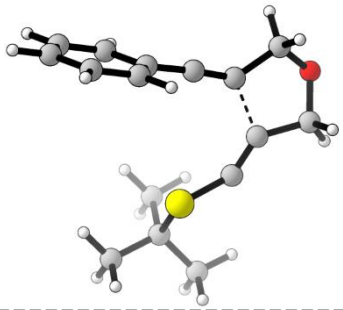

Atom type	X	Y	Z
C	1.53567400	1.13193700	0.11013700
C	0.66444000	2.03700100	0.13265600
C	0.67401500	3.53395100	0.39875500
H	1.21613600	3.77185200	1.31674400
H	1.16306700	4.03758100	-0.45118200
O	-0.65072500	4.00447200	0.55222700
C	-1.47387500	3.30715700	-0.36928500
H	-1.32181400	3.69841000	-1.38991000
H	-2.51296000	3.46872900	-0.07665500
C	-1.10900000	1.85051300	-0.30568400
C	-1.69934700	0.74216400	-0.52035600
S	-1.45638300	-0.88523100	-0.84351300
C	-2.80015300	-1.76332000	0.16045000
C	2.44178100	0.05864800	0.06186800
C	2.72942700	-0.70587000	1.22352500
C	3.12421600	-0.26515300	-1.14046600
C	3.64859400	-1.74807100	1.17472600
H	2.21638400	-0.46659700	2.15050900
C	4.03558400	-1.31533200	-1.17597200
H	2.91788800	0.31479100	-2.03536700
C	4.30481400	-2.06342500	-0.02265000
H	3.85522700	-2.32258400	2.07441800
H	4.54271800	-1.55285200	-2.10789500
H	5.01977900	-2.88112000	-0.05556000
C	-2.63004100	-1.42771200	1.64562600
H	-2.73628100	-0.35244200	1.82316600
H	-3.40027700	-1.94797900	2.23103700
H	-1.64796300	-1.74152800	2.01544500
C	-2.55259500	-3.25562200	-0.10296100
H	-3.29693800	-3.84865200	0.44298000
H	-2.64476500	-3.49823100	-1.16798400
H	-1.55839300	-3.56672800	0.23775400
C	-4.17895100	-1.33318900	-0.35359200
H	-4.30308400	-1.57462200	-1.41481800
H	-4.96188600	-1.85648900	0.21194400
H	-4.32640000	-0.25569400	-0.22688600

3.051-tBu

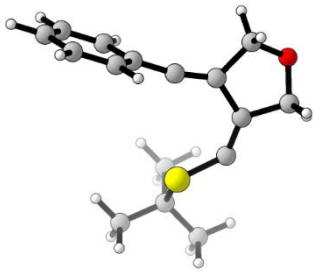

Atom type	X	Y	Z
C	1.25057600	0.83014100	-0.00835400
C	0.42325000	1.83194400	0.01836100
C	0.78469500	3.29652900	0.33753300
H	1.44032800	3.39664500	1.20530200
H	1.26835100	3.75785600	-0.53927200
O	-0.44431700	3.94351100	0.62947400
C	-1.44619900	3.34372100	-0.19026800
H	-1.44308600	3.80492100	-1.19258800
H	-2.41875300	3.51269300	0.27637400
C	-1.06786200	1.87221000	-0.26997100
C	-1.88376900	0.85897000	-0.51082600
S	-1.59136400	-0.75248500	-0.92444500
C	-2.78734300	-1.73654100	0.16179700
C	2.32251900	-0.04939400	0.00653100
C	2.68011000	-0.75824100	1.19603500
C	3.10062300	-0.28833700	-1.16939800
C	3.75541300	-1.63567300	1.20109800
H	2.09651000	-0.59476600	2.09737800
C	4.16609300	-1.17737200	-1.14464500
H	2.84052500	0.23570500	-2.08448800
C	4.50577800	-1.85675200	0.03563700
H	4.01419800	-2.15850100	2.11873500
H	4.74347500	-1.34452200	-2.05072600
H	5.34297000	-2.54914500	0.04690000
C	-2.50847400	-1.43152900	1.63738700
H	-1.48199300	-1.69668300	1.91234300
H	-2.66059400	-0.36985800	1.85782300
H	-3.19433900	-2.01283700	2.26849000
C	-2.48360000	-3.20536100	-0.16724300
H	-3.14773300	-3.85279600	0.41908000
H	-2.65127800	-3.42400200	-1.22817100
H	-1.44943800	-3.46987300	0.08090700
C	-4.22840800	-1.37405400	-0.21858300
H	-4.42908800	-1.58813700	-1.27393900
H	-4.92695000	-1.96395600	0.39030000
H	-4.42715900	-0.31266700	-0.03967900

3.052-tBu

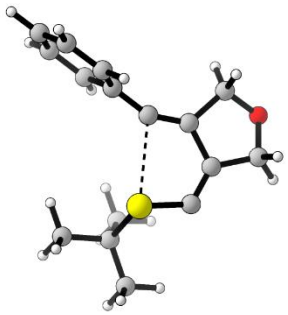

Atom type	X	Y	Z
C	0.82862500	0.70134600	-0.04753900
C	0.06251300	1.75243800	0.01072200
C	0.44874600	3.19362400	0.37242100
H	1.10982100	3.25785200	1.23968300
H	0.93667900	3.67439900	-0.49165900
O	-0.76907200	3.85285800	0.69258500
C	-1.79868200	3.29101700	-0.12585000
H	-1.82346000	3.79808700	-1.10512800
H	-2.75688000	3.44312800	0.37601600
C	-1.42987200	1.83010300	-0.27495900
C	-2.17978200	0.77485400	-0.56408500
S	-1.47902400	-0.70848200	-0.96149300
C	-2.29977100	-1.98120100	0.17088900
C	2.07140600	0.03838700	-0.02156900
C	2.53084300	-0.60564400	1.16013500
C	2.89156400	-0.03191700	-1.18136300
C	3.75733500	-1.26120000	1.18063100
H	1.91132600	-0.57044400	2.05192100
C	4.10967600	-0.70205100	-1.14943700
H	2.54976900	0.44447900	-2.09584400
C	4.55325500	-1.31844300	0.02857600
H	4.09585400	-1.73598600	2.09834100
H	4.72224700	-0.74255100	-2.04680400
H	5.50703600	-1.83870600	0.04794500
C	-2.17320800	-1.53407300	1.63041700
H	-1.12417500	-1.43713600	1.92855800
H	-2.66757400	-0.57124300	1.79378600
H	-2.64944600	-2.27881100	2.28233200
C	-1.52618800	-3.28327900	-0.08304400
H	-1.95912100	-4.08542600	0.52794300
H	-1.58727600	-3.59097200	-1.13335000
H	-0.46897600	-3.18560500	0.18772100
C	-3.77156500	-2.12474900	-0.24063700
H	-3.86716400	-2.43368000	-1.28721000
H	-4.25089400	-2.88852800	0.38694400
H	-4.31019800	-1.18129600	-0.10984700

3.053-tBu

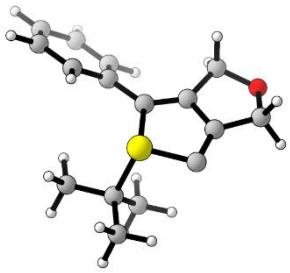

Atom type	X	Y	Z
C	-0.09466800	-0.43271200	-0.26201600
C	0.82591200	-1.42055300	-0.12919900
C	0.80695400	-2.88941600	0.19431100
H	0.22658200	-3.15975100	1.08129200
H	0.41967400	-3.47110600	-0.66004400
O	2.17715000	-3.22109500	0.45713100
C	3.04961700	-2.28496700	-0.21307700
H	3.38178300	-2.70923400	-1.17331600
H	3.92615000	-2.13478100	0.42396100
C	2.21136800	-1.04355200	-0.40609800
C	2.53865000	0.23934600	-0.74462200
S	0.89789800	0.97423600	-0.88686300
C	0.86683500	2.35603000	0.42721600
C	-1.55815600	-0.44182500	-0.16613800
C	-2.19635200	-1.13525300	0.88240900
C	-2.36704400	0.22238800	-1.10981800
C	-3.58799200	-1.17204500	0.97489600
H	-1.59405900	-1.63410000	1.63660100
C	-3.75832800	0.18986200	-1.01041100
H	-1.89970600	0.75223300	-1.93582300
C	-4.37745300	-0.50885800	0.03038900
H	-4.05601000	-1.71328900	1.79345400
H	-4.36043200	0.70565600	-1.75432400
H	-5.46122700	-0.53535800	0.10520100
C	1.26339300	1.78636200	1.79002600
H	2.26160700	1.34169600	1.75759900
H	1.27104400	2.60459500	2.52185300
H	0.55134100	1.03053400	2.13543500
C	1.89196500	3.38362900	-0.07488000
H	1.61499300	3.78618600	-1.05577800
H	1.91819300	4.21861600	0.63706800
H	2.89114300	2.94674700	-0.14581800
C	-0.54549500	2.95097100	0.44621000
H	-0.84656800	3.31840300	-0.54092500
H	-1.29328700	2.23333700	0.79447700
H	-0.55003000	3.80415100	1.13665700

3.065-tBu

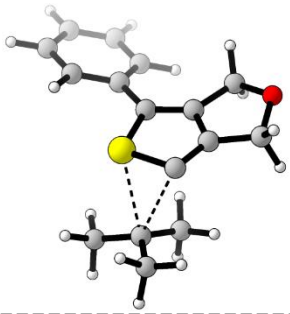

Atom type	X	Y	Z
C	0.51700800	0.22491900	-0.39303300
C	-0.16815800	1.41682000	-0.15428100
C	0.18240200	2.78611500	0.35395900
H	0.38970200	2.78554500	1.43778400
H	1.04477500	3.23803400	-0.15264100
O	-0.97635700	3.58958300	0.08395100
C	-2.11828000	2.75981200	-0.22964000
H	-2.63770400	3.21156700	-1.08111400
H	-2.80813800	2.75259300	0.63074700
C	-1.53434800	1.40107400	-0.52640100
C	-2.05694500	0.25779900	-1.11934200
S	-0.65218600	-0.85407600	-1.12146300
C	-2.42471100	-1.71763400	0.58980600
C	1.92554900	-0.11308200	-0.16159900
C	2.69106500	0.58259500	0.79725000
C	2.56270800	-1.14154100	-0.88699600
C	4.03253700	0.26710300	1.01608200
H	2.22905700	1.36708400	1.38910500
C	3.90091500	-1.46018800	-0.66151200
H	2.00586300	-1.68245800	-1.64764500
C	4.64680000	-0.75719200	0.29031400
H	4.59716500	0.82156000	1.76180000
H	4.36628300	-2.25452400	-1.24004600
H	5.69154800	-1.00263300	0.46141000
C	-2.31266500	-0.74530400	1.71887300
H	-1.29946200	-0.32888400	1.79294000
H	-3.02963700	0.07226800	1.63895700
H	-2.49074500	-1.29564200	2.65928500
C	-1.62757600	-2.98835400	0.76583900
H	-2.17546800	-3.60525200	1.49999600
H	-1.55369100	-3.56918300	-0.15673100
H	-0.62585000	-2.80774000	1.16216100
C	-3.74837200	-1.90636500	-0.08911000
H	-3.63625000	-2.32615200	-1.09240400
H	-4.31344500	-2.64638700	0.51056900
H	-4.31573500	-0.98072200	-0.16364100

3.066

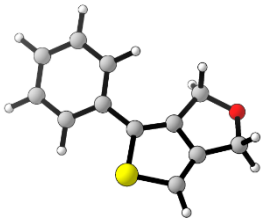

Atom type	X	Y	Z
C	0.09403200	0.43232200	-0.06808200
C	1.19993200	-0.38301200	-0.00631800
C	1.48759000	-1.85431700	0.13243200
H	0.94305000	-2.34389300	0.94764700
H	1.28774100	-2.40887200	-0.79907200
O	2.89302300	-1.91822900	0.43848700
C	3.55529400	-0.69801800	0.05463900
H	4.07632600	-0.83951200	-0.90562300
H	4.30124400	-0.46867600	0.82293600
C	2.44215500	0.30889900	-0.04727800
C	2.31095200	1.66314800	-0.15088100
S	0.62854000	2.10834300	-0.20209200
C	-1.33269400	0.08551800	-0.03109100
C	-1.76786500	-1.18444600	-0.45819200
C	-2.30200500	0.99601000	0.43307400
C	-3.11818400	-1.53208200	-0.41387900
H	-1.04774900	-1.89702500	-0.84906600
C	-3.65240600	0.64969600	0.46764900
H	-1.99365400	1.97645000	0.78651800
C	-4.06866900	-0.61722100	0.04778900
H	-3.42839000	-2.51791900	-0.75115300
H	-4.38041200	1.36973600	0.83270000
H	-5.12076400	-0.88758400	0.07911100
H	3.07298800	2.43063900	-0.19760600

C_4H_8

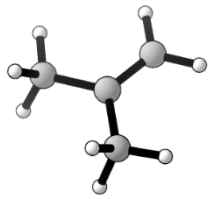

Atom type	X	Y	Z
C	0.00001800	0.12298700	0.00001200
C	1.27832200	-0.68037000	-0.00000300
H	2.16455400	-0.03750600	0.00010300
H	1.33053600	-1.33568600	0.88101800
H	1.33060900	-1.33555000	-0.88111500
C	-0.00022700	1.46300800	-0.00000100
H	-0.92585400	2.03447400	0.00000200
H	0.92520800	2.03480200	-0.00001000
C	-1.27814200	-0.68071900	0.00000000
H	-2.16449400	-0.03803800	-0.00022000
H	-1.33005900	-1.33609700	-0.88098600
H	-1.33032300	-1.33583200	0.88116700

3.068

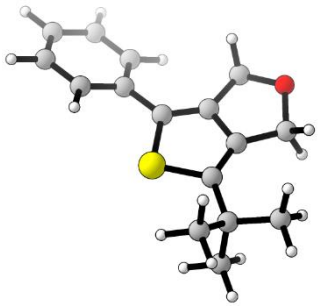

Atom type	X	Y	Z
C	0.82587600	-0.03003000	0.01998200
C	0.11980900	1.14584200	-0.02879900
C	0.44411700	2.61294200	-0.09374900
H	0.81086700	3.00287200	0.87034800
H	1.17127600	2.87876900	-0.86957600
O	-0.80563400	3.24134300	-0.42324700
C	-1.90940000	2.36956500	-0.12002800
H	-2.65099000	2.49910400	-0.91296100
H	-2.36856200	2.66959500	0.83613900
C	-1.29708200	0.98982100	-0.05034100
C	-1.72745500	-0.31263200	-0.00583200
S	-0.31656400	-1.36863600	0.05763200
C	-3.12743900	-0.91253800	0.07230000
C	2.27602200	-0.26001100	0.02205700
C	3.15647700	0.73300500	0.49596200
C	2.83296300	-1.46516000	-0.44979600
C	4.53695000	0.53191000	0.48797300
H	2.75765200	1.66071300	0.89490000
C	4.21269400	-1.66748100	-0.44849500
H	2.18051600	-2.24345500	-0.83675100
C	5.07406000	-0.66938500	0.01681600
H	5.19357200	1.31400900	0.86103100
H	4.61607600	-2.60585000	-0.82085300
H	6.14940600	-0.82642900	0.01359400
C	-4.18118900	0.11967400	-0.37825700
H	-4.19815800	0.99853700	0.27538800
H	-4.00260900	0.45311500	-1.40670700
H	-5.17863600	-0.33407700	-0.34054300
C	-3.42902300	-1.32781300	1.53480800
H	-4.43992200	-1.74876300	1.60993400
H	-2.71886700	-2.08323100	1.88888800
H	-3.36654900	-0.46536700	2.20840800
C	-3.24224000	-2.15542100	-0.84052900
H	-2.55298900	-2.95138300	-0.53589600
H	-4.25919600	-2.56333700	-0.79201500
H	-3.02364000	-1.90113300	-1.88389700

3.056-tBu

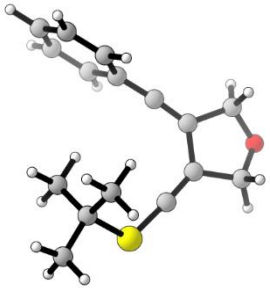

Atom type	X	Y	Z
C	-0.96408500	1.39273900	0.08763600
C	0.15990700	2.04507900	0.10432900
C	0.28612500	3.56084100	0.35203700
H	-0.45688200	4.14694000	-0.19288100
H	0.19354900	3.76877900	1.43104300
O	1.57388300	3.92515000	-0.11724000
C	2.44432200	2.83413200	0.15244200
H	2.80320900	2.88038000	1.19477300
H	3.29741500	2.89960200	-0.52559400
C	1.59970700	1.56956000	-0.07105300
C	2.09512000	0.39053000	-0.35505100
S	2.62165400	-1.11684000	-0.74025000
C	1.52118600	-2.42717600	0.16551500
C	-2.10708500	0.62243700	0.02179900
C	-2.77436700	0.39171300	-1.22634700
C	-2.68213600	0.03765300	1.19789000
C	-3.92985300	-0.37373000	-1.28107000
H	-2.35671200	0.82788400	-2.12913900
C	-3.83501200	-0.72909000	1.11728100
H	-2.19807300	0.20719100	2.15546900
C	-4.47090800	-0.94307200	-0.11675700
H	-4.41859400	-0.53473800	-2.23903000
H	-4.25149000	-1.16438600	2.02263600
H	-5.37596300	-1.54174600	-0.16968900
C	1.32121100	-2.00165500	1.61923200
H	0.79734700	-1.04275000	1.68666100
H	0.71428300	-2.75493300	2.13997000
H	2.27768400	-1.91005900	2.14544100
C	2.34831500	-3.71293000	0.05926800
H	1.78777500	-4.54228000	0.51016700
H	2.55164000	-3.97944700	-0.98488700
H	3.30509200	-3.62392700	0.58557700
C	0.19370800	-2.55392200	-0.58448900
H	-0.37091700	-1.61755900	-0.56636000
H	0.35120300	-2.84158900	-1.62976400
H	-0.42502500	-3.32777800	-0.10845900

3.057-tBu

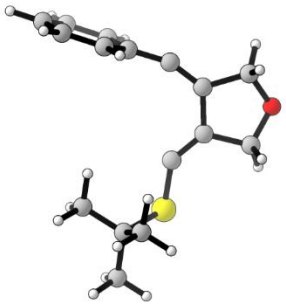

Atom type	X	Y	Z
C	-1.89040400	1.19118100	0.19614100
C	-0.85752400	1.99544300	0.17058100
C	-0.88897200	3.50418000	0.43825100
H	-1.72745900	4.01393500	-0.04126200
H	-0.92134300	3.69932300	1.52318500
O	0.31855700	4.01036300	-0.12174200
C	1.32018700	3.01154600	0.03108400
H	1.80451800	3.09593300	1.01885500
H	2.07226400	3.16225400	-0.74716300
C	0.58469300	1.67094800	-0.08937500
C	1.12825300	0.48681500	-0.33128800
S	2.60257800	-0.11019100	-0.90981800
C	2.91818900	-1.64009900	0.16185000
C	-2.62395900	0.01661100	0.08255000
C	-3.16611700	-0.39551600	-1.17442000
C	-2.89965900	-0.79586100	1.22599900
C	-3.92368800	-1.55466100	-1.27234300
H	-2.96991500	0.21271200	-2.05251600
C	-3.65658800	-1.95334400	1.10617000
H	-2.50345700	-0.49234300	2.19075000
C	-4.17603300	-2.34230600	-0.13842700
H	-4.32208900	-1.85371600	-2.23880600
H	-3.84929300	-2.56103500	1.98703400
H	-4.77159300	-3.24717700	-0.22319200
C	2.98470800	-1.22779700	1.63604000
H	2.03740500	-0.78906600	1.96674600
H	3.18491800	-2.11164200	2.25670700
H	3.78350700	-0.49889700	1.81169700
C	4.27272000	-2.17248600	-0.32649100
H	4.53138200	-3.07707100	0.23804700
H	4.24238800	-2.43708000	-1.38971300
H	5.07408200	-1.44022200	-0.17507600
C	1.80254600	-2.66360800	-0.08074900
H	0.82627300	-2.25855900	0.20353200
H	1.75662300	-2.96157800	-1.13371400
H	1.99199400	-3.56189000	0.52246200

3.058-tBu

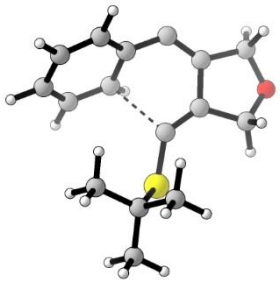

Atom type	X	Y	Z
C	2.57167900	1.06545600	0.26695700
C	2.59270800	-0.25088900	0.12987100
C	3.72179300	-1.26453200	0.16909000
H	4.51278500	-1.06672000	-0.56078600
H	4.17191400	-1.30899600	1.17291700
O	3.12428300	-2.52283500	-0.16387400
C	1.74260000	-2.47999400	0.17515200
H	1.58923000	-2.75907200	1.23148300
H	1.20822900	-3.18707100	-0.46419700
C	1.32000700	-1.03353400	-0.04505400
C	0.12456300	-0.56973400	-0.37098400
S	-1.28822500	-1.29964800	-0.98598800
C	-2.62437100	-1.03368300	0.33201500
C	1.45456700	1.88337500	0.07741000
C	0.60980500	1.60806900	-1.05621200
C	1.02885600	2.86849600	1.01571700
C	-0.52616400	2.42786500	-1.29620100
H	1.01907200	1.04505800	-1.88797600
C	-0.12159600	3.59709000	0.79420800
H	1.64238800	3.04719000	1.89437100
C	-0.89293300	3.39313700	-0.38143300
H	-1.09410400	2.29606500	-2.21354500
H	-0.43094100	4.35276500	1.51214400
H	-1.76405700	4.01761100	-0.56407500
C	-2.91571200	0.45766900	0.51772800
H	-2.03025200	0.99554200	0.86689200
H	-3.25153000	0.91903000	-0.41624600
H	-3.71003500	0.58203600	1.26674000
C	-2.16711100	-1.67227400	1.64816100
H	-2.95479200	-1.55786800	2.40517600
H	-1.96457800	-2.74186400	1.52545100
H	-1.26131400	-1.18866500	2.02876900
C	-3.84693000	-1.76675800	-0.24064200
H	-3.64668400	-2.83343800	-0.39327500
H	-4.68315600	-1.67879800	0.46434800
H	-4.16541100	-1.33431200	-1.19609400

3.059-tBu

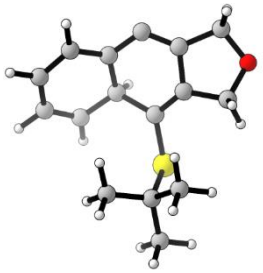

Atom type	X	Y	Z
C	2.78382400	0.45804900	0.22368800
C	2.43388800	-0.82836300	0.15502800
C	3.18016000	-2.13730400	0.09035000
H	3.91639900	-2.18691900	-0.72024200
H	3.69802700	-2.34023500	1.04061700
O	2.18218300	-3.14024700	-0.15544100
C	0.88167500	-2.63922200	0.19570300
H	0.64527400	-2.90129900	1.24013100
H	0.14805000	-3.11093100	-0.46261600
C	0.99047600	-1.14741000	0.01912700
C	0.13845500	-0.23133900	-0.48617400
S	-1.47547700	-0.68078700	-1.10726400
C	-2.66473400	-0.54120900	0.36286200
C	1.89592300	1.48477200	0.04263700
C	0.74373600	1.18647800	-0.89831300
C	1.87087900	2.66841900	0.84770200
C	-0.21643300	2.32624000	-1.06674400
H	1.11289500	0.95470600	-1.91505100
C	0.88712700	3.60367800	0.69304600
H	2.66589600	2.80249800	1.57665600
C	-0.13873700	3.44665600	-0.31562800
H	-0.95416500	2.24171700	-1.85910800
H	0.88177800	4.49621800	1.31374100
H	-0.84071200	4.26146400	-0.47710100
C	-2.70375400	0.88548200	0.91961000
H	-1.72880900	1.19146600	1.31179400
H	-3.00637500	1.60595600	0.15384800
H	-3.42838500	0.93599400	1.74439200
C	-2.27510300	-1.53758600	1.46062500
H	-3.00956900	-1.49177000	2.27656400
H	-2.25261600	-2.56379900	1.07934400
H	-1.29377300	-1.30078700	1.88448300
C	-4.02213500	-0.92006700	-0.25075700
H	-4.00816800	-1.93379500	-0.66682600
H	-4.79452000	-0.88542200	0.52832900
H	-4.31253200	-0.22412100	-1.04577800

3.060-tBu

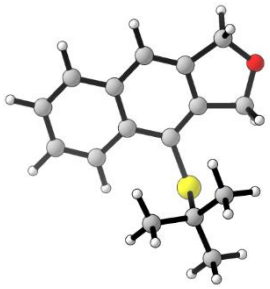

Atom type	X	Y	Z
C	1.63294800	-1.80735900	0.21906700
C	1.68540100	-3.30858200	0.36078400
H	2.57052200	-3.76563600	-0.09552000
H	1.64397500	-3.61944500	1.41865100
O	0.53021300	-3.78114900	-0.34113600
C	-0.44144800	-2.72876100	-0.44171700
H	-1.21529900	-2.85612400	0.32999600
H	-0.92255600	-2.79961800	-1.42172100
C	0.34322300	-1.45167700	-0.24794500
C	-0.01442200	-0.13468300	-0.46556500
S	-1.65188200	0.23828700	-1.11265700
C	-2.73983300	0.61250200	0.39308200
C	2.28677700	0.51602300	0.21237700
C	3.27010700	1.52411800	0.41242600
C	0.75610600	2.26114300	-0.57478400
C	3.00496400	2.84555100	0.12764400
H	4.24668800	1.22738000	0.78915400
C	1.73603300	3.21243500	-0.38065300
H	-0.20897800	2.54816700	-0.97666200
H	3.76857200	3.60342700	0.28229700
H	1.53303900	4.25223300	-0.62443000
C	0.98433000	0.88970600	-0.27561400
C	2.58506400	-0.85269100	0.46566000
H	3.57579600	-1.11844700	0.82983600
C	-2.26445800	1.87236700	1.12691300
H	-1.25634000	1.74879700	1.53467000
H	-2.26337600	2.74471200	0.46550000
H	-2.94183700	2.08377400	1.96608400
C	-2.78106700	-0.58164700	1.35345300
H	-3.44945600	-0.35325100	2.19514800
H	-3.15796200	-1.48085100	0.85563300
H	-1.79046200	-0.79874300	1.76718400
C	-4.12653900	0.84709200	-0.22840200
H	-4.48472700	-0.04141800	-0.76033500
H	-4.84684000	1.08002800	0.56641500
H	-4.11547900	1.68840300	-0.93065200

3.049-CO_2Me

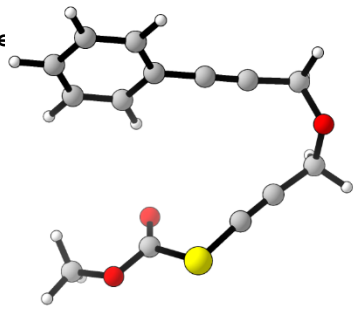

Atom type	X	Y	Z
C	2.23302800	0.70868000	0.18373900
C	2.11524600	1.91093400	0.30649700
C	2.03836400	3.36358300	0.49119800
H	1.99457300	3.59850500	1.56750900
H	2.93959700	3.83589300	0.08658800
O	0.95924800	4.01476700	-0.18130200
C	-0.33114800	3.82668000	0.39443900
H	-0.89648700	4.72817400	0.13040500
H	-0.25825800	3.79361900	1.49311100
C	-1.06737500	2.65231600	-0.08000200
C	-1.75181600	1.71817500	-0.44820000
S	-2.72147000	0.51264700	-1.12036500
C	2.35668800	-0.71020400	0.05178200
C	3.37441100	-1.26901100	-0.74715500
C	1.46788600	-1.56918600	0.72945500
C	3.50120200	-2.65292900	-0.86117400
H	4.05863400	-0.60892500	-1.27242500
C	1.60286800	-2.95220600	0.60904900
H	0.67352900	-1.14325600	1.33473000
C	2.61778500	-3.49911700	-0.18294500
H	4.29077400	-3.07181000	-1.47986700
H	0.91486300	-3.60577200	1.13978000
H	2.72005000	-4.57774200	-0.27154900
C	-2.61223800	-0.78163200	0.15082200
O	-1.98779700	-0.73827100	1.17950700
O	-3.37178700	-1.80047700	-0.28105400
C	-3.43222500	-2.95447600	0.58731200
H	-4.09931200	-3.65255000	0.08239800
H	-2.43560500	-3.38653400	0.70555900
H	-3.83219600	-2.66974800	1.56346900

3.050-CO_2Me

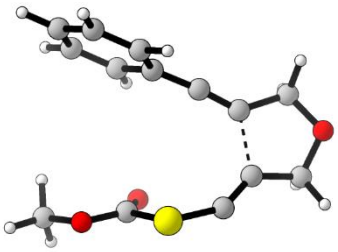

Atom type	X	Y	Z
C	-0.50224600	-1.53007300	-0.11655200
C	-1.72815200	-1.26606900	-0.19360900
C	-2.96372500	-2.00906700	-0.67055200
H	-2.94997600	-2.04184700	-1.77227300
H	-2.99198300	-3.02861000	-0.28031900
O	-4.12531800	-1.34536600	-0.21224500
C	-3.90303500	0.04993600	-0.30587300
H	-4.66489900	0.55113100	0.29339500
H	-3.98382000	0.38728700	-1.35289000
C	-2.51830900	0.34259700	0.21155400
C	-1.94418600	1.34229100	0.74351800
S	-0.52348500	2.01788800	1.34159500
C	0.88757800	-1.70313200	-0.01215500
C	1.47530700	-2.21729300	1.17397100
C	1.73622100	-1.40382700	-1.11140000
C	2.84956800	-2.41374700	1.25261000
H	0.83565200	-2.44980000	2.02033600
C	3.10946000	-1.60540900	-1.01651100
H	1.29586800	-1.00989600	-2.02237500
C	3.67529200	-2.10962600	0.16192400
H	3.28329000	-2.80571200	2.16913900
H	3.74523900	-1.37329300	-1.86760100
H	4.74840700	-2.26741600	0.22887200
C	0.47335800	2.24477800	-0.16986700
O	0.15542700	1.96315200	-1.29646800
O	1.62813400	2.80936900	0.21826000
C	2.57801200	3.08789100	-0.83564200
H	3.42805600	3.54964600	-0.33398800
H	2.87473600	2.15813300	-1.32650900
H	2.13838600	3.77142700	-1.56617300

3.051-CO_2Me

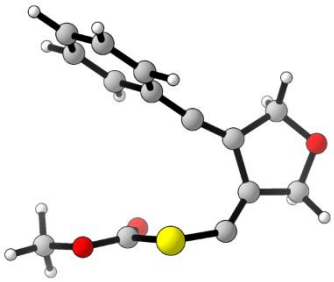

Atom type	X	Y	Z
C	-0.07126500	-1.27438300	-0.00691100
C	-1.36055000	-1.35138300	-0.14835900
C	-2.14131600	-2.53669600	-0.74896800
H	-2.05474900	-2.51633200	-1.84754900
H	-1.80198100	-3.50571600	-0.37684200
O	-3.49056900	-2.35216200	-0.34891300
C	-3.73623400	-0.94930100	-0.30214200
H	-4.57660000	-0.76913600	0.37077000
H	-3.98656200	-0.56670800	-1.30551300
C	-2.43332200	-0.33003600	0.18445000
C	-2.29780100	0.84230100	0.77180500
S	-0.97256200	1.71203900	1.38860200
C	1.30875400	-1.38599400	0.01820300
C	1.99248200	-1.88884900	1.16942800
C	2.09706300	-0.99174200	-1.10927400
C	3.37582000	-1.99574100	1.17748200
H	1.41002900	-2.18418000	2.03708900
C	3.47985200	-1.10524400	-1.07700500
H	1.59295500	-0.60383200	-1.98965400
C	4.13191600	-1.60646400	0.06056100
H	3.87630400	-2.38368100	2.06123400
H	4.06101800	-0.80474600	-1.94552700
H	5.21480300	-1.69270700	0.07653600
C	-0.25191800	2.43999700	-0.12223500
O	-0.61959900	2.25753900	-1.25436900
O	0.76735600	3.22015200	0.26974700
C	1.49555000	3.88222700	-0.78967600
H	2.26554400	4.46270400	-0.28225100
H	1.94336300	3.14145000	-1.45645600
H	0.82518800	4.53386700	-1.35534100

3.052-CO_2Me

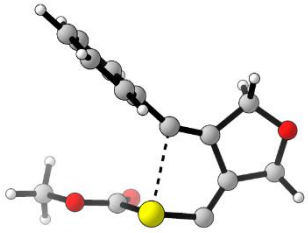

Atom type	X	Y	Z
C	-0.06628900	-0.84360700	0.16730400
C	-1.29746300	-1.17671900	-0.10037200
C	-1.84123100	-2.43339700	-0.78377600
H	-1.69756000	-2.35208200	-1.87365400
H	-1.37351900	-3.35427200	-0.42744300
O	-3.22565700	-2.48461500	-0.46191600
C	-3.70762300	-1.14325300	-0.33976700
H	-4.57212900	-1.15100500	0.32743400
H	-4.01648800	-0.75417400	-1.32383900
C	-2.53914900	-0.35037700	0.20413800
C	-2.47581500	0.81612200	0.82803200
S	-0.95820400	1.36781800	1.34167000
C	1.32731500	-1.08734600	0.09742800
C	2.04371200	-1.57158100	1.22224900
C	2.04753400	-0.83143700	-1.09908300
C	3.41206300	-1.80860700	1.14125500
H	1.50681200	-1.75578900	2.14832900
C	3.41689800	-1.07199600	-1.16638300
H	1.51168500	-0.45319200	-1.96535900
C	4.10700800	-1.56050300	-0.04990100
H	3.94316100	-2.18711000	2.01093500
H	3.95052200	-0.88031100	-2.09404900
H	5.17638900	-1.74493600	-0.10663200
C	-0.37529800	2.35360000	-0.09645700
O	-0.94525600	2.48780800	-1.14587200
O	0.80008700	2.89106200	0.25535000
C	1.45135100	3.69640400	-0.75556200
H	2.37756800	4.03481300	-0.29237600
H	1.65740900	3.09126500	-1.64149200
H	0.81594400	4.54383500	-1.02371700

3.053-CO_2Me

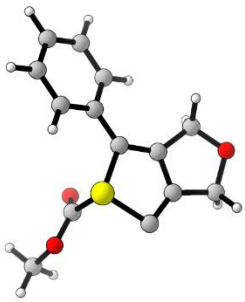

Atom type	X	Y	Z
C	-0.31793600	-0.40515300	-0.31275200
C	0.25950000	-1.60654200	-0.04645700
C	-0.21242600	-2.92998600	0.48668100
H	-0.36725300	-2.88191400	1.57855200
H	-1.13603100	-3.29407500	0.02329800
O	0.84049100	-3.84771900	0.17272100
C	2.08843900	-3.13265400	0.05030700
H	2.68888000	-3.64392500	-0.70595800
H	2.62847300	-3.15611600	1.00973600
C	1.68439100	-1.72503100	-0.33288900
C	2.42522100	-0.69226300	-0.83040600
S	1.00706500	0.56964100	-1.05550900
C	-1.68963000	0.08288100	-0.17550300
C	-2.18066900	1.14827200	-0.95648200
C	-2.56537500	-0.51440100	0.75474800
C	-3.49553900	1.59190000	-0.81911000
H	-1.53368900	1.62337200	-1.68960400
C	-3.88117000	-0.07230300	0.88463800
H	-2.20680100	-1.31302500	1.39682300
C	-4.35530000	0.98264400	0.09906600
H	-3.84999200	2.41301700	-1.43693900
H	-4.53505700	-0.54793400	1.61119900
H	-5.38010000	1.32811000	0.20453800
C	1.50738900	1.68062800	0.34867900
O	1.09127700	1.59276200	1.46900800
O	2.37961000	2.54803400	-0.14511200
C	3.00265200	3.43662200	0.81994600
H	3.67342800	4.05995900	0.23075600
H	2.23873400	4.03826400	1.31708900
H	3.55804900	2.84772000	1.55292800

3.065-CO_2Me

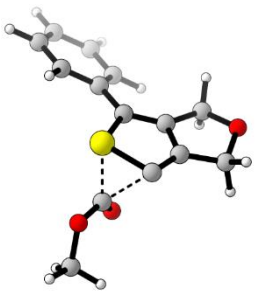

Atom type	X	Y	Z
C	0.49396300	0.21934700	-0.39261200
C	-0.11203300	1.43853800	-0.17483900
C	0.30923900	2.77342500	0.37587900
H	0.45855400	2.72465800	1.46782500
H	1.22014000	3.17791600	-0.07959700
O	-0.77923000	3.65119500	0.06263900
C	-1.98776200	2.88511100	-0.12224200
H	-2.57781500	3.37683100	-0.90003800
H	-2.57270500	2.86999500	0.81143900
C	-1.50065100	1.50607100	-0.49680200
C	-2.16296600	0.41013400	-1.01204800
S	-0.74127100	-0.81666100	-1.10040400
C	1.87249400	-0.22293600	-0.15063800
C	2.43190500	-1.31032200	-0.85112100
C	2.67800300	0.43663900	0.79923600
C	3.74326900	-1.71878600	-0.61319100
H	1.84050300	-1.83161300	-1.59941000
C	3.99165300	0.02905000	1.03151700
H	2.26856500	1.25819300	1.37833800
C	4.53255700	-1.05006100	0.32739900
H	4.15147100	-2.55816400	-1.17021200
H	4.59039200	0.55265600	1.77241300
H	5.55566900	-1.36727000	0.51008000
C	-1.99504500	-1.20973900	0.39475800
O	-1.79822600	-0.86925800	1.52562000
O	-2.76574500	-2.18626800	-0.06990700
C	-3.71209300	-2.73445900	0.88277000
H	-4.20960900	-3.54236100	0.34767600
H	-3.18508700	-3.11015200	1.76273000
H	-4.42934000	-1.96154700	1.16999600

3.067

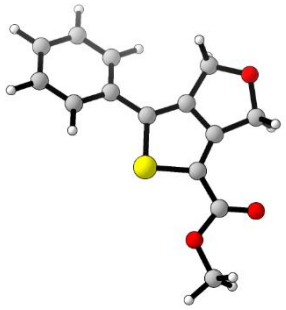

Atom type	X	Y	Z
C	0.82741000	-0.02894100	0.02851600
C	0.22632500	1.21332300	-0.01354900
C	0.65248400	2.65659100	-0.09225200
H	1.07374900	3.01905600	0.85959700
H	1.37536400	2.86609400	-0.88927900
O	-0.55905000	3.37194900	-0.38722400
C	-1.72237400	2.56729800	-0.10074700
H	-2.44979800	2.71280800	-0.90454400
H	-2.18689800	2.88758500	0.84383700
C	-1.18552000	1.17027700	-0.01521200
C	-1.70468700	-0.10114700	0.03991300
S	-0.40660700	-1.27900800	0.09270900
C	2.25546900	-0.37124600	0.02207400
C	2.71266500	-1.61260600	-0.46192600
C	3.20916200	0.54881200	0.49998900
C	4.07218400	-1.92146200	-0.46601600
H	2.00056300	-2.33306100	-0.85554600
C	4.56920900	0.23959000	0.48915900
H	2.88354400	1.50214300	0.90471500
C	5.00814200	-0.99662700	0.00681800
H	4.40153800	-2.88423200	-0.84805700
H	5.28624900	0.96414900	0.86644100
H	6.06786500	-1.23707200	-0.00035600
C	-3.12617100	-0.44822400	0.04754800
O	-4.02564800	0.37648600	0.02591700
O	-3.33347600	-1.78548000	0.08221400
C	-4.70872300	-2.20917900	0.09514200
H	-4.67310600	-3.29838300	0.12700300
H	-5.22044400	-1.81250900	0.97607400
H	-5.22098000	-1.86482900	-0.80721300

6.3.11. X-Ray Data

CCDC deposition number: 2149613

ORTEP drawing of K0878_FP (**3.022a**):

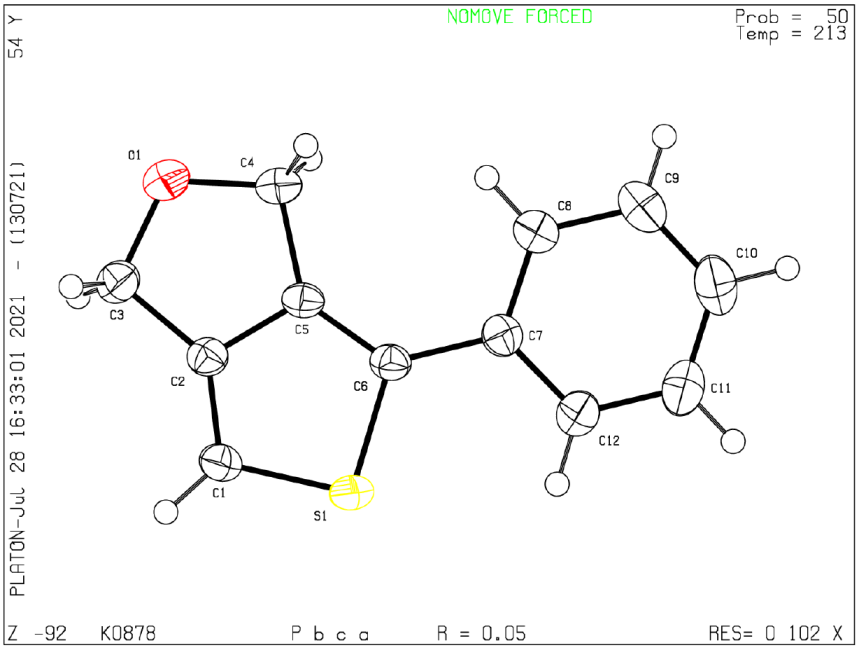

Crystals obtained by slow evaporation (over about 1 week) of a DCM solution of **3.022a**.

6.3.12. NMR Spectra

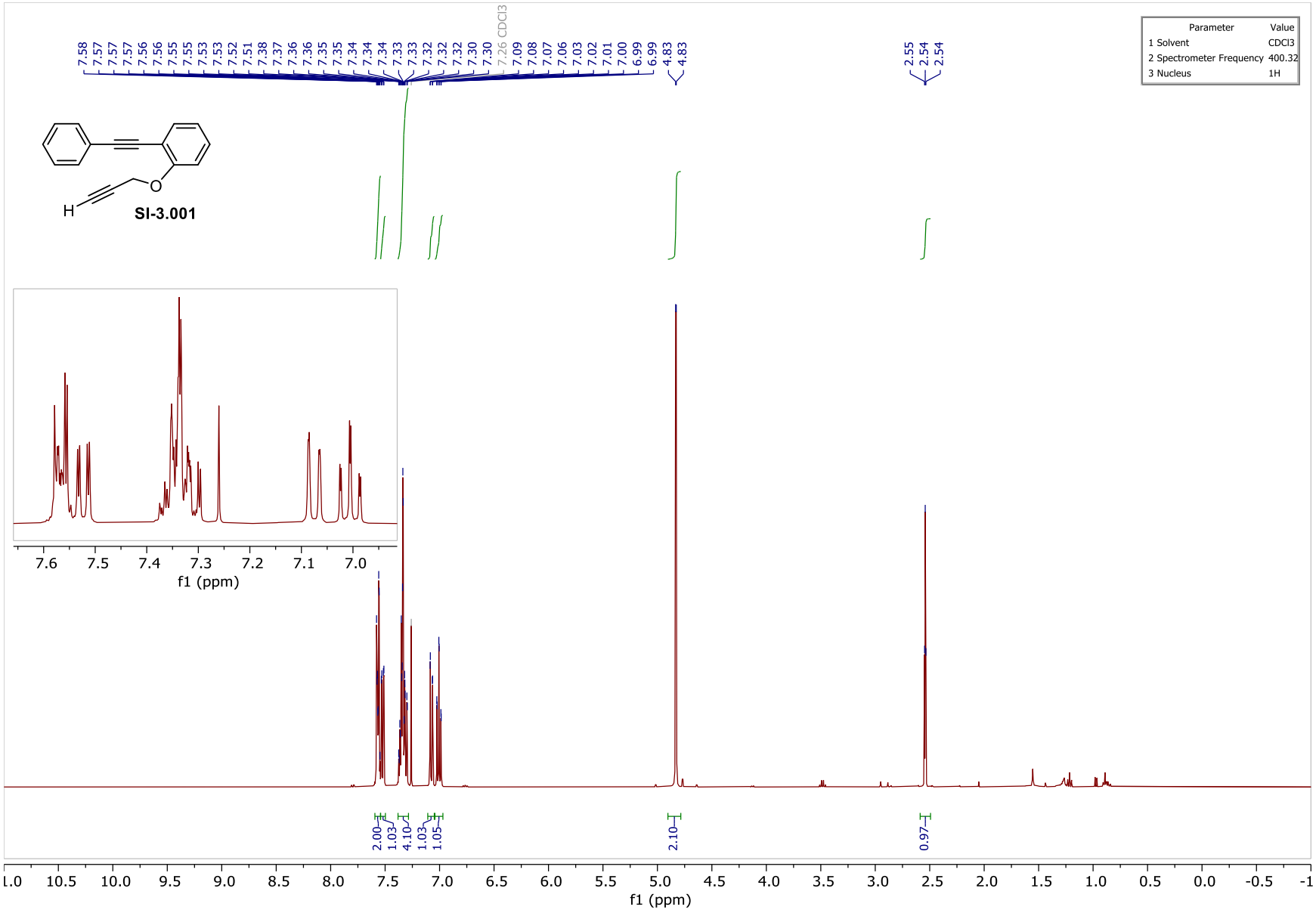
Parameter Value
1 Solvent CDCl3
2 Spectrometer Frequency 400.32
3 Nucleus 1H
SI-3.001
f1 (ppm)

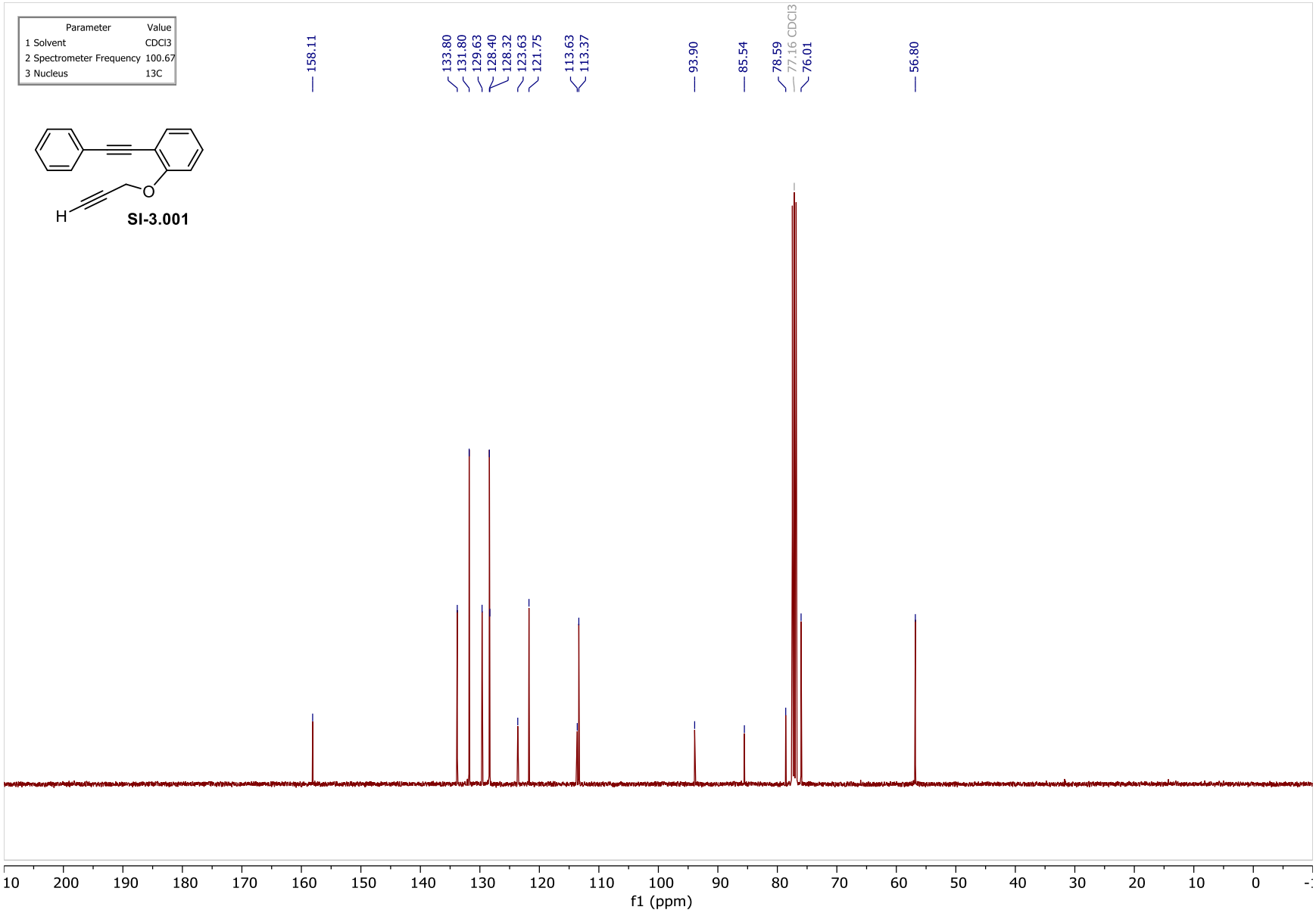
Parameter Value
1 Solvent CDCl3
2 Spectrometer Frequency 100.67
3 Nucleus 13C
158.11
133.80
131.80
129.63
128.40
128.32
123.63
121.75
113.63
113.37
93.90
85.54
78.59
77.16 CDCl3
76.01
56.80
O
H
SI-3.001
f1 (ppm)

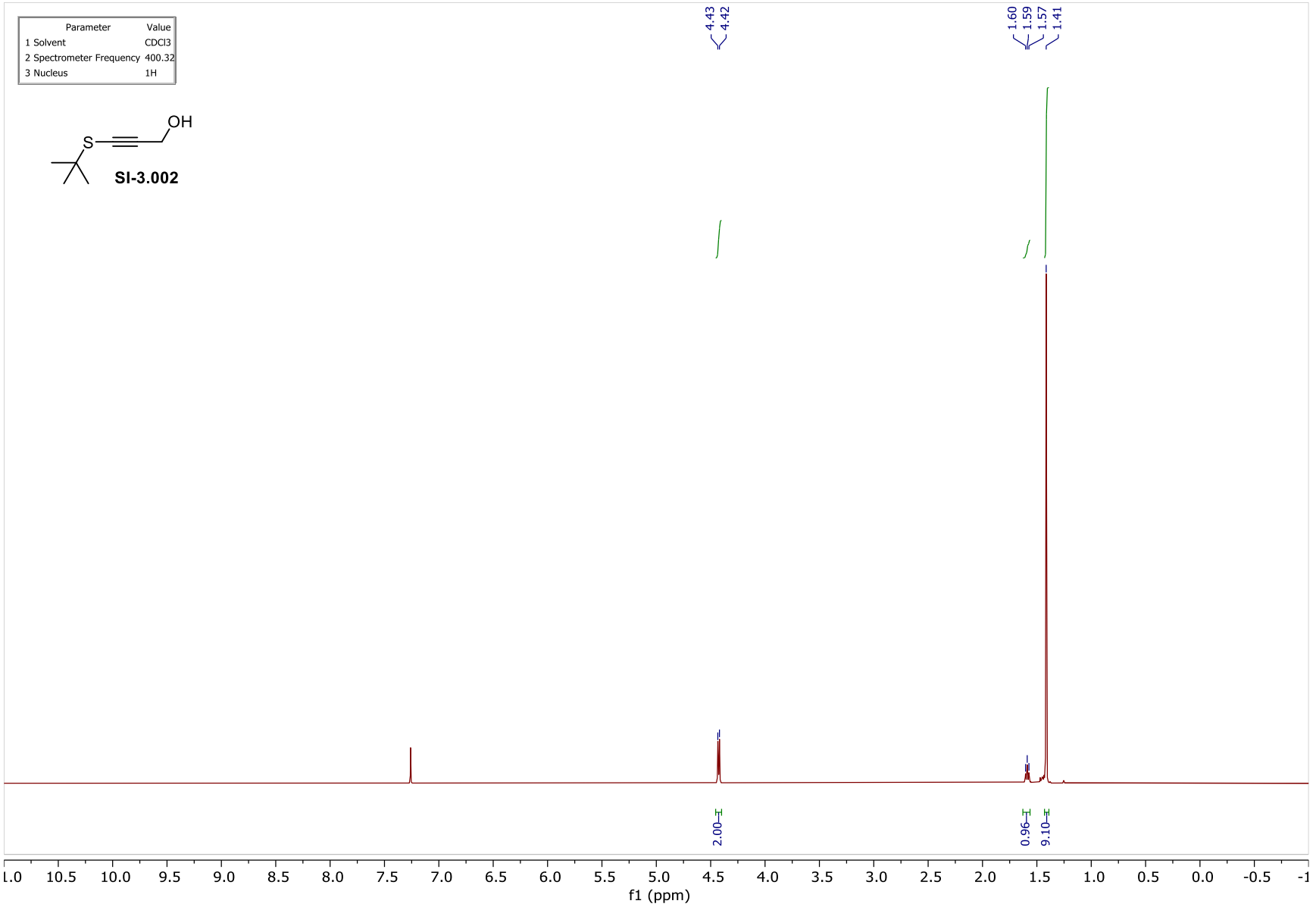
Parameter Value
1 Solvent CDCl3
2 Spectrometer Frequency 400.32
3 Nucleus 1H
OH
S
SI-3.002
4.43
4.42
1.60
1.59
1.57
1.41
2.00
0.96
9.10
f1 (ppm)

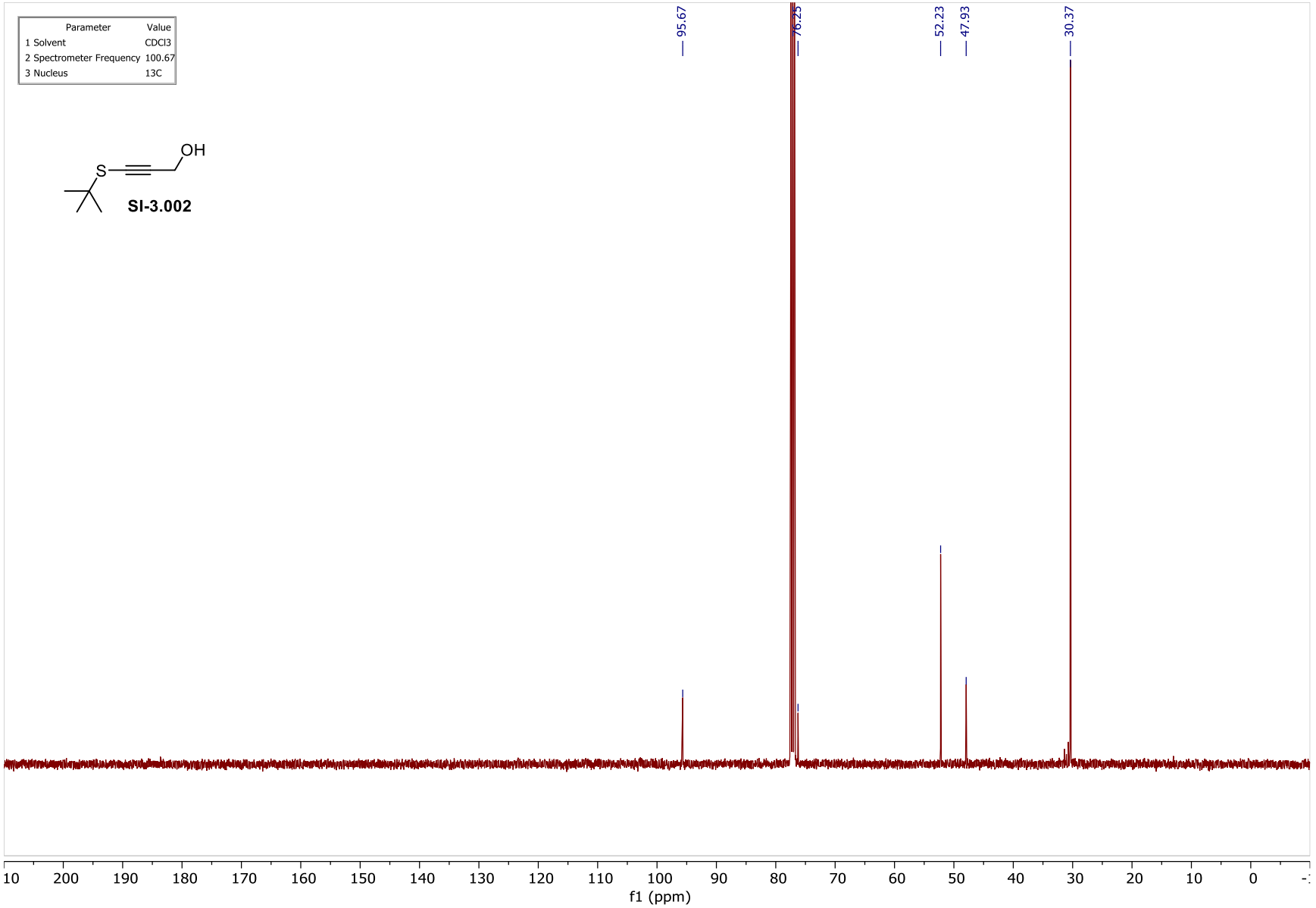
Parameter Value
1 Solvent CDCl3
2 Spectrometer Frequency 100.67
3 Nucleus 13C
OH
S
SI-3.002
95.67
76.25
52.23
47.93
30.37
f1 (ppm)

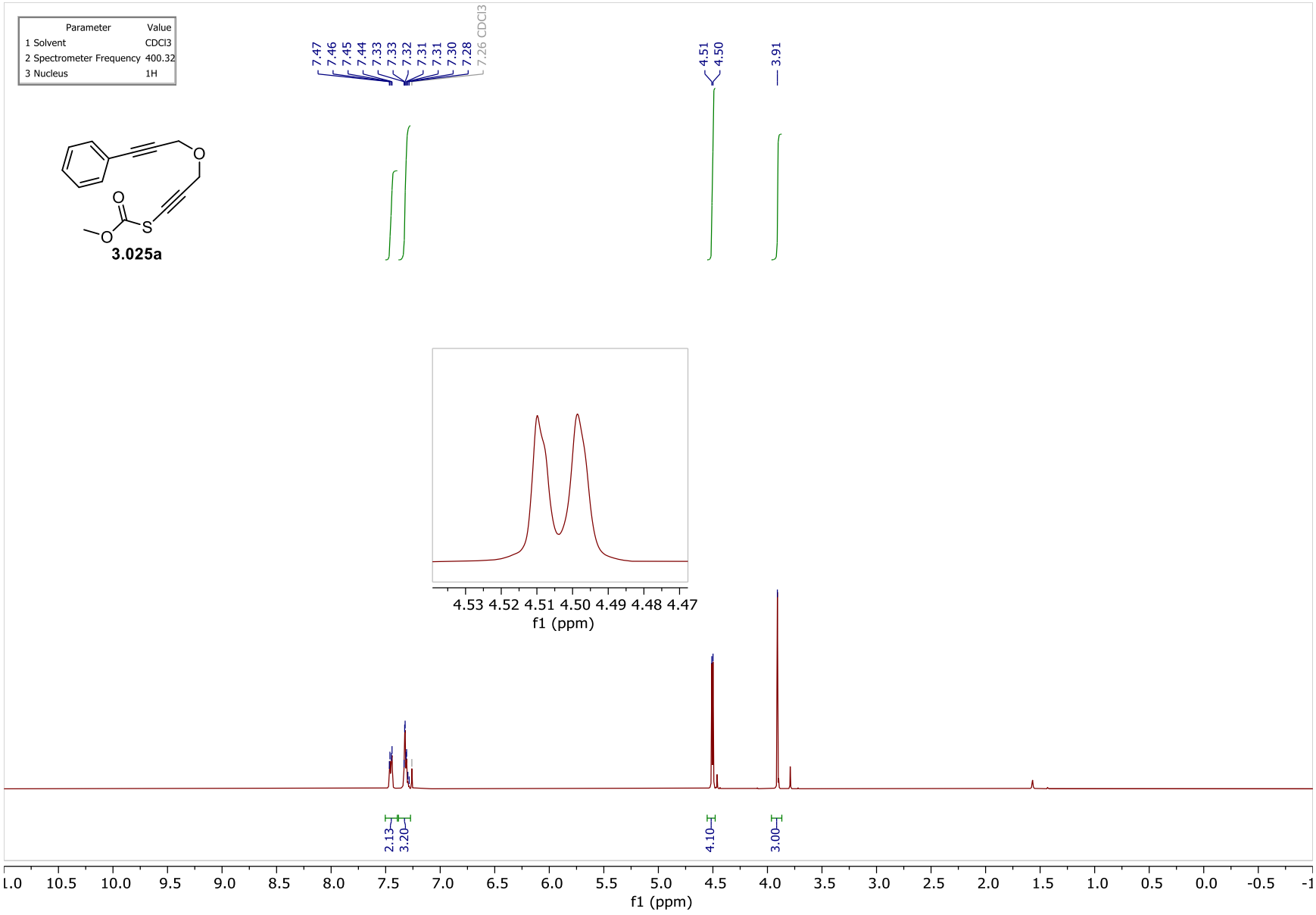
Parameter Value
1 Solvent CDCl3
2 Spectrometer Frequency 400.32
3 Nucleus 1H
7.47
7.46
7.45
7.44
7.33
7.33
7.32
7.31
7.31
7.30
7.28
7.26 CDCl3
4.51
4.50
3.91
O
O
S
O
3.025a
4.53 4.52 4.51 4.50 4.49 4.48 4.47
f1 (ppm)
2.13
3.20
4.10
3.00
f1 (ppm)

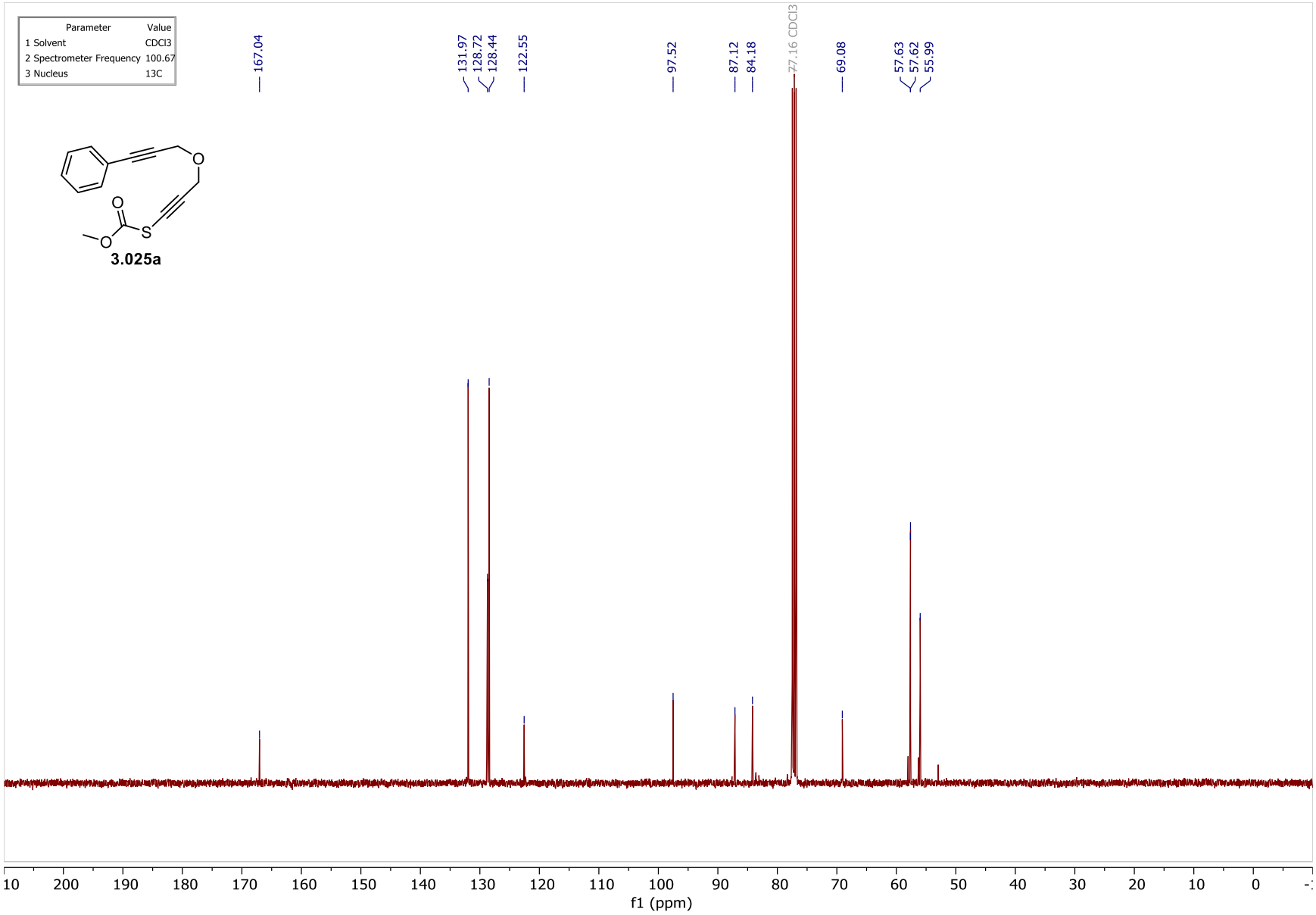
Parameter Value
1 Solvent CDCl3
2 Spectrometer Frequency 100.67
3 Nucleus 13C
167.04
131.97
128.72
128.44
122.55
97.52
87.12
84.18
77.16 CDCl3
69.08
57.63
57.62
55.99
O
O
S
O
3.025a
f1 (ppm)

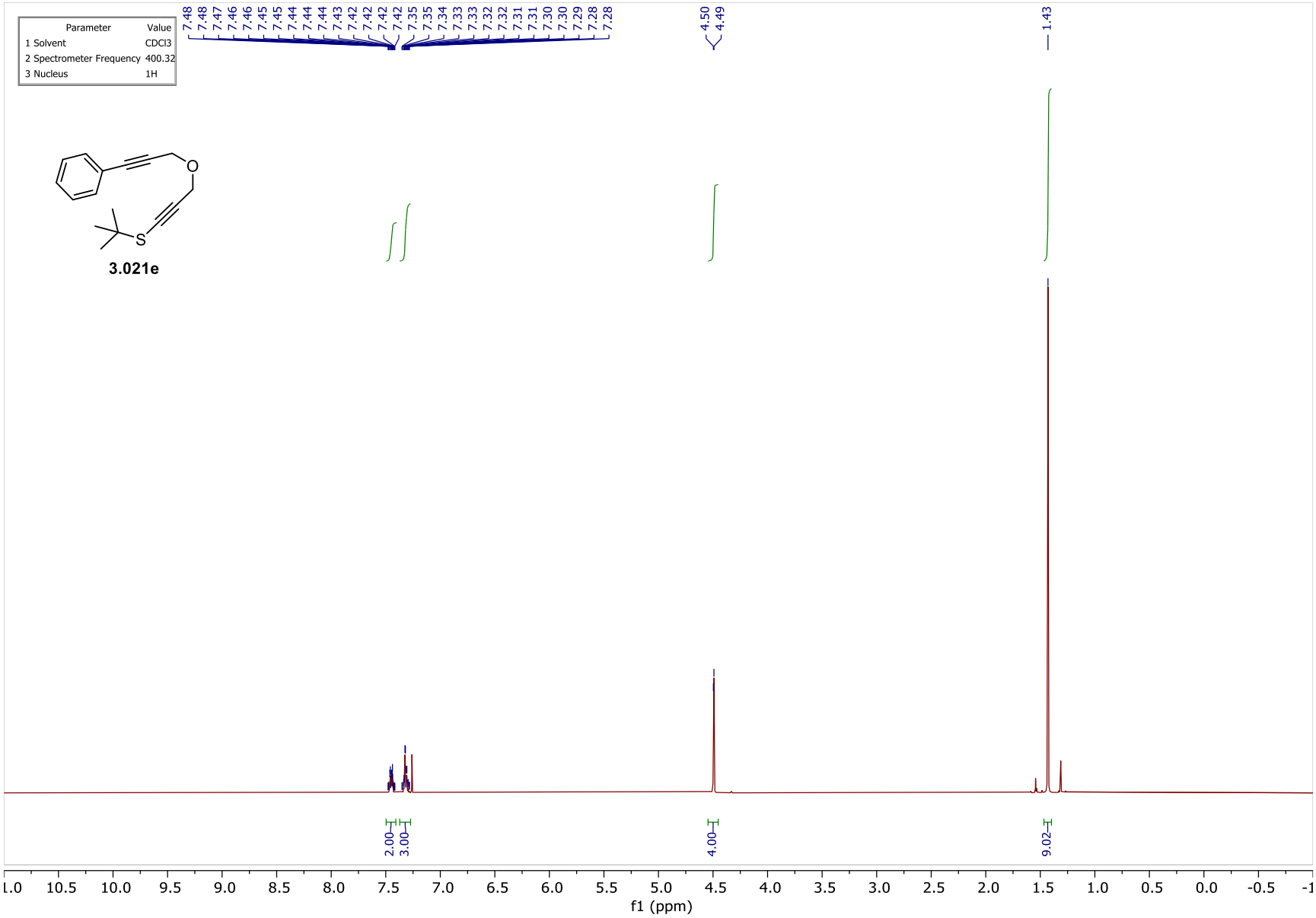
Parameter Value
1 Solvent CDCl3
2 Spectrometer Frequency 400.32
3 Nucleus 1H
7.48 7.48 7.47 7.46 7.46 7.45 7.45 7.44 7.44 7.44 7.43 7.42 7.42 7.42 7.42 7.35 7.35 7.34 7.33 7.33 7.32 7.32 7.31 7.31 7.30 7.30 7.29 7.28 7.28
4.50 4.49
1.43
O
S
3.021e
2.00
3.00
4.00
9.02
f1 (ppm)

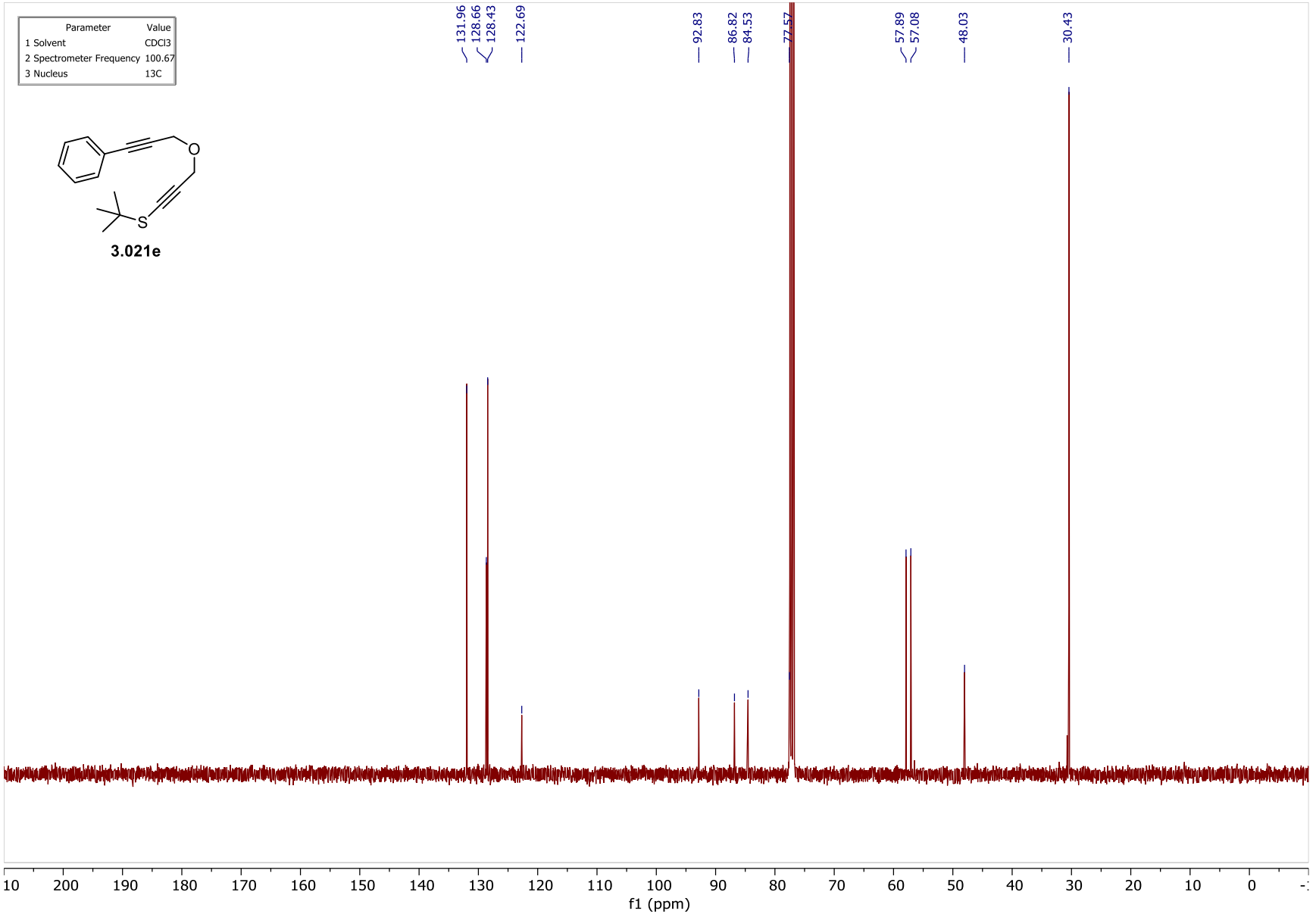
Parameter Value
1 Solvent CDCl3
2 Spectrometer Frequency 100.67
3 Nucleus 13C
O
S
3.021e
131.96
128.66
128.43
122.69
92.83
86.82
84.53
77.57
57.89
57.08
48.03
30.43
f1 (ppm)

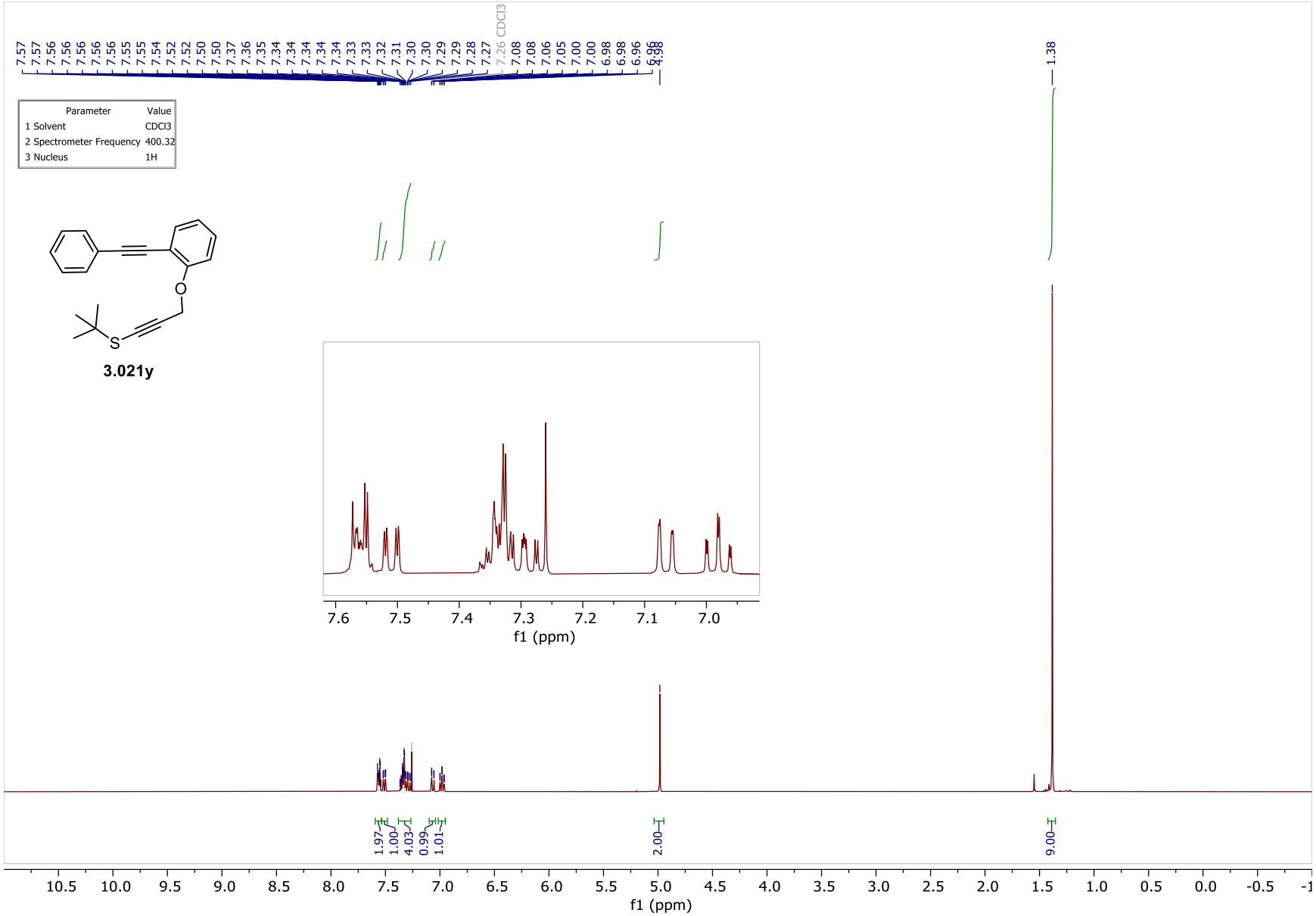
7.57 7.57 7.56 7.56 7.56 7.56 7.55 7.55 7.54 7.52 7.52 7.50 7.50 7.37 7.36 7.35 7.34 7.34 7.34 7.34 7.33 7.33 7.32 7.31 7.30 7.30 7.29 7.29 7.28 7.27 7.26 CDCl3 7.08 7.08 7.06 7.05 7.00 7.00 6.98 6.98 6.96 6.96 4.98
1.38
Parameter Value
1 Solvent CDCl3
2 Spectrometer Frequency 400.32
3 Nucleus 1H
O
S
3.021y
7.6 7.5 7.4 7.3 7.2 7.1 7.0
f1 (ppm)
1.97 1.00 4.03 0.99 1.01 2.00 9.00
10.5 10.0 9.5 9.0 8.5 8.0 7.5 7.0 6.5 6.0 5.5 5.0 4.5 4.0 3.5 3.0 2.5 2.0 1.5 1.0 0.5 0.0 -0.5 -1
f1 (ppm)

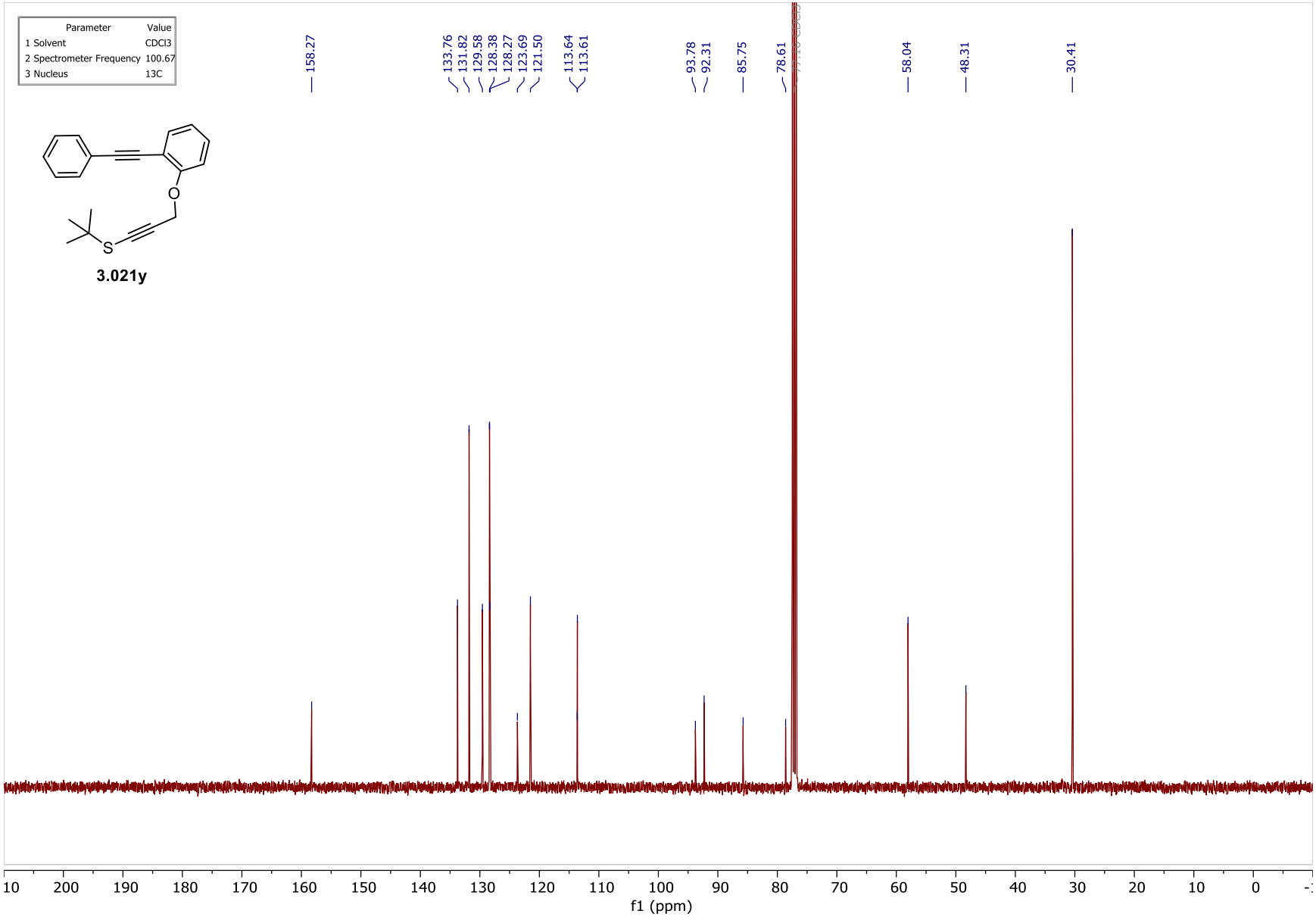
Parameter Value
1 Solvent CDCl3
2 Spectrometer Frequency 100.67
3 Nucleus 13C
158.27
133.76
131.82
129.58
128.38
128.27
123.69
121.50
113.64
113.61
93.78
92.31
85.75
78.61
58.04
48.31
30.41
O
S
3.021y
f1 (ppm)

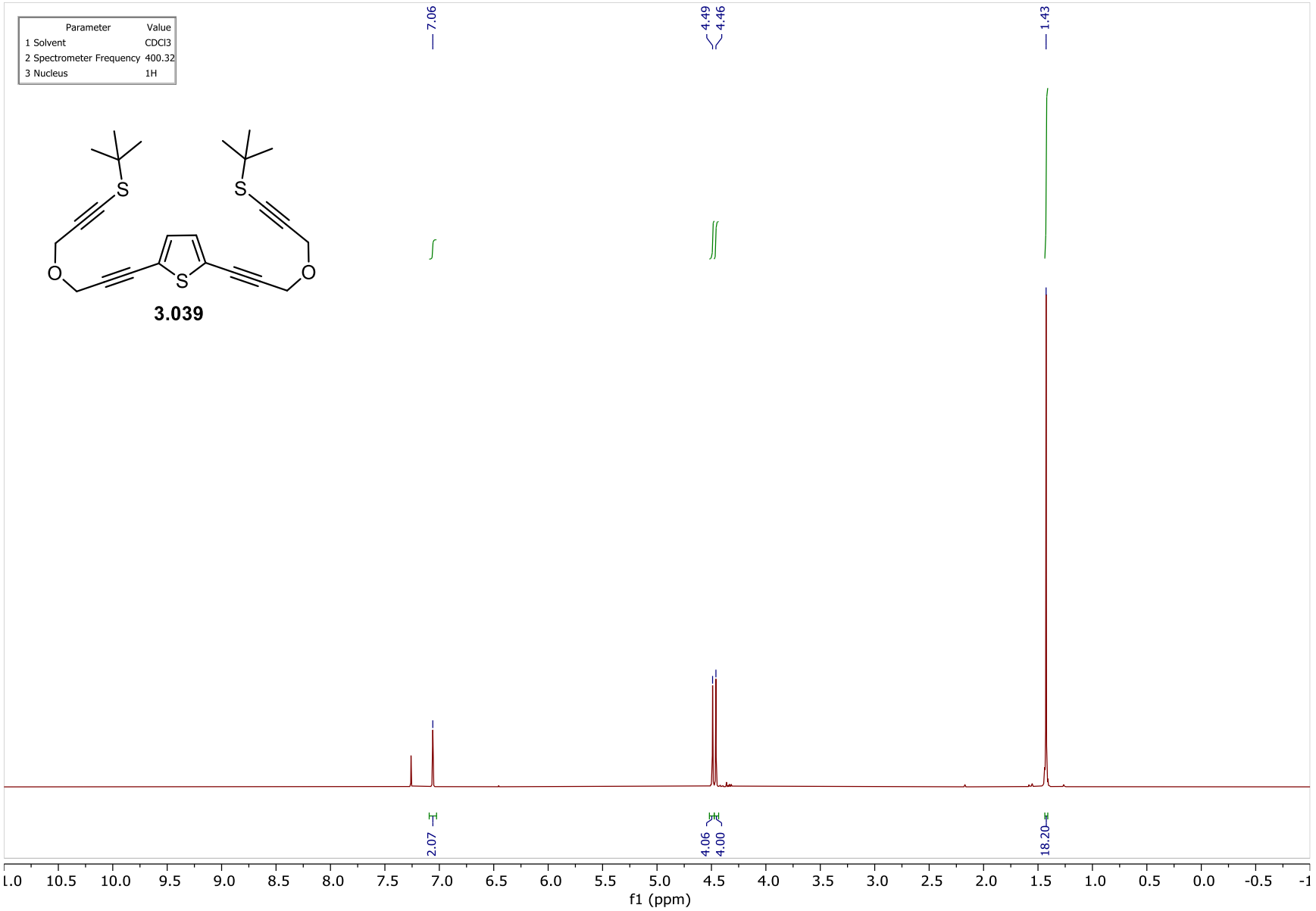
Parameter Value
1 Solvent CDCl3
2 Spectrometer Frequency 400.32
3 Nucleus 1H
7.06
4.49
4.46
1.43
S
S
O
S
O
3.039
2.07
4.06
4.00
18.20
f1 (ppm)

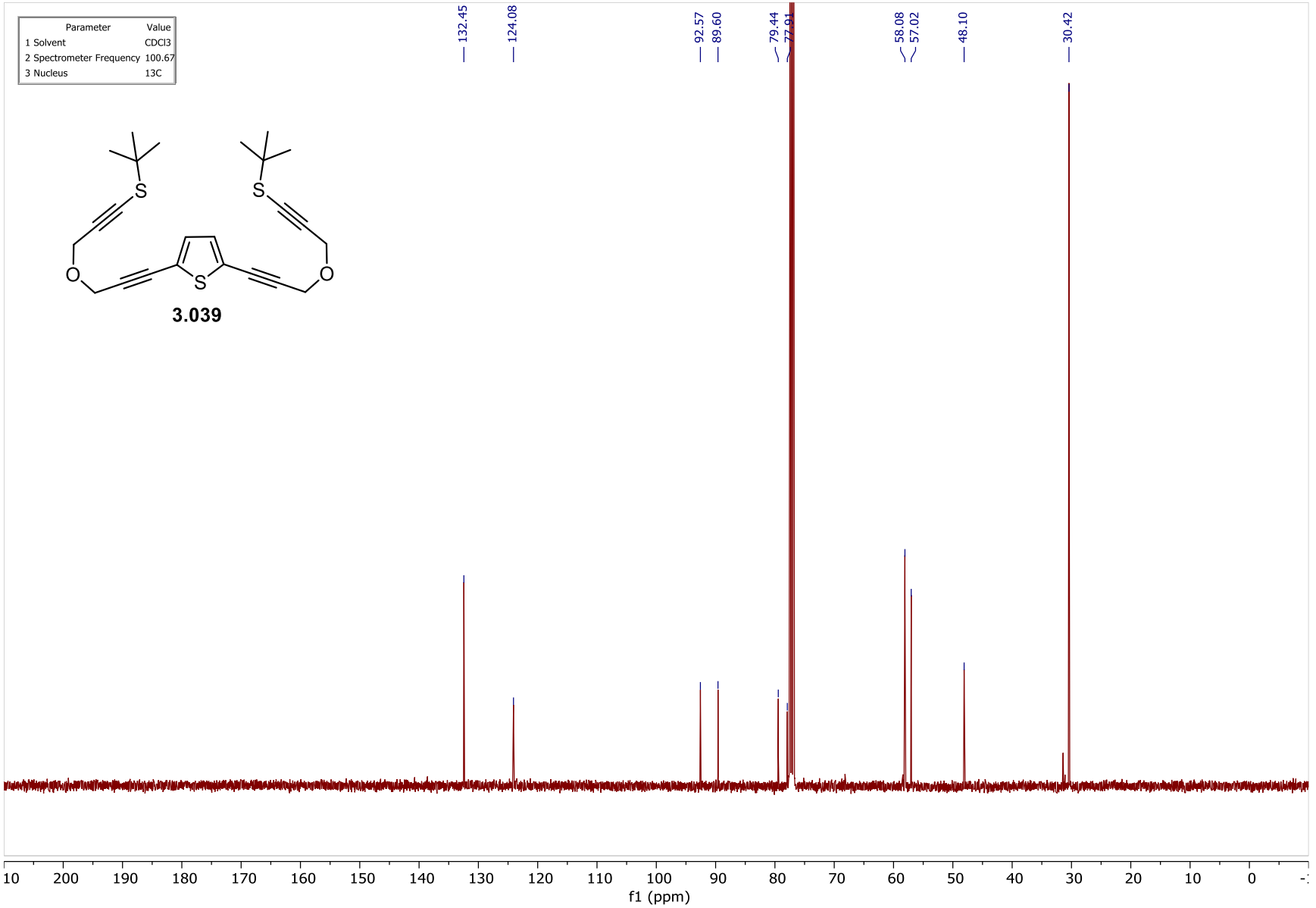
Parameter Value
1 Solvent CDCl3
2 Spectrometer Frequency 100.67
3 Nucleus 13C
S
S
O
S
O
3.039
132.45
124.08
92.57
89.60
79.44
77.91
58.08
57.02
48.10
30.42
10 200 190 180 170 160 150 140 130 120 110 100 90 80 70 60 50 40 30 20 10 0
f1 (ppm)

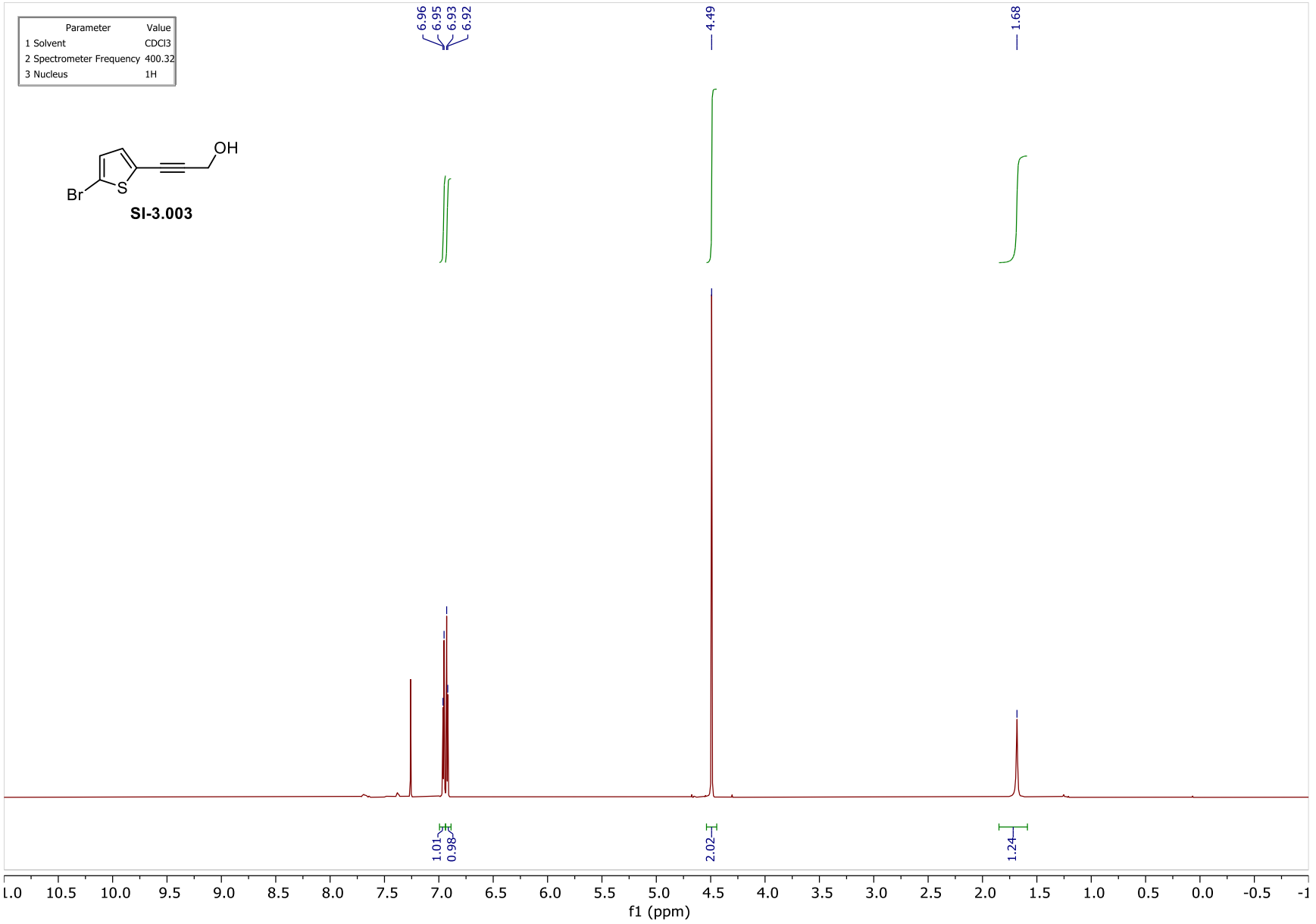
Parameter Value
1 Solvent CDCl3
2 Spectrometer Frequency 400.32
3 Nucleus 1H
6.96
6.95
6.93
6.92
4.49
1.68
OH
Br
S
SI-3.003
1.01
0.98
2.02
1.24
f1 (ppm)

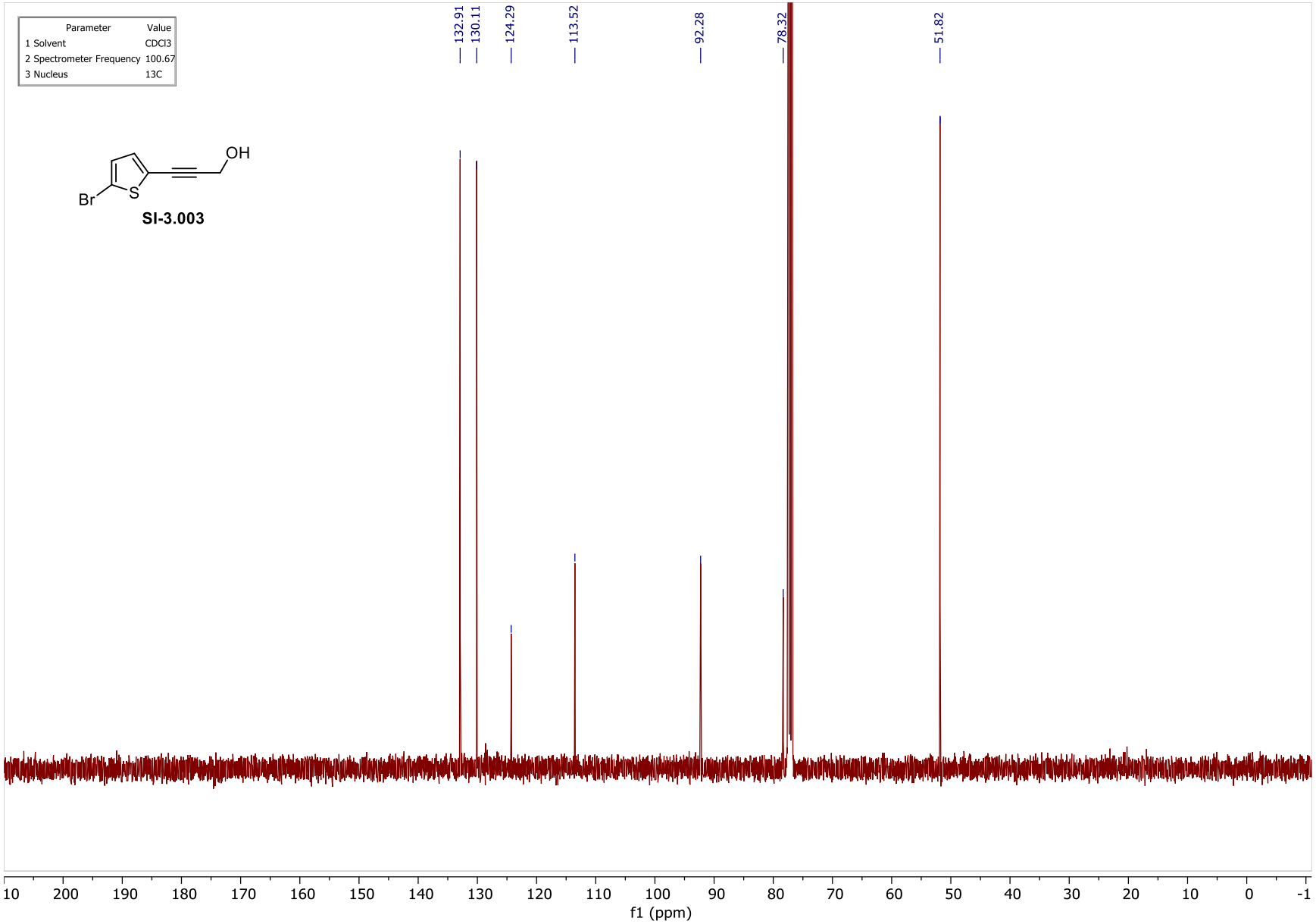
Parameter Value
1 Solvent CDCl3
2 Spectrometer Frequency 100.67
3 Nucleus 13C
132.91
130.11
124.29
113.52
92.28
78.32
51.82
OH
Br
S
SI-3.003
10 200 190 180 170 160 150 140 130 120 110 100 90 80 70 60 50 40 30 20 10 0 -1
f1 (ppm)

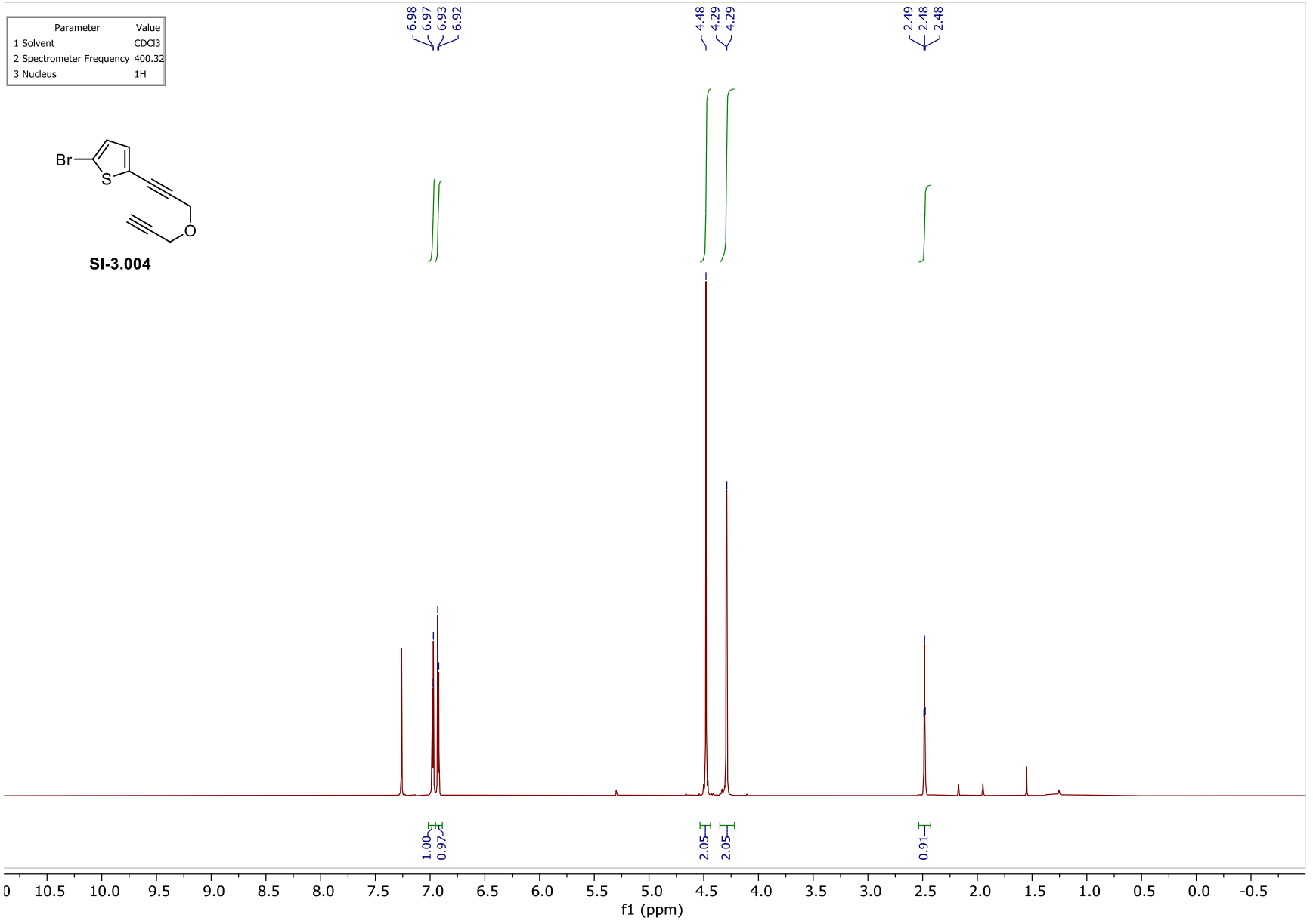
Parameter Value
1 Solvent CDCl3
2 Spectrometer Frequency 400.32
3 Nucleus 1H
Br
S
O
SI-3.004
6.98
6.97
6.93
6.92
4.48
4.29
4.29
2.49
2.48
2.48
1.00
0.97
2.05
2.05
0.91
f1 (ppm)

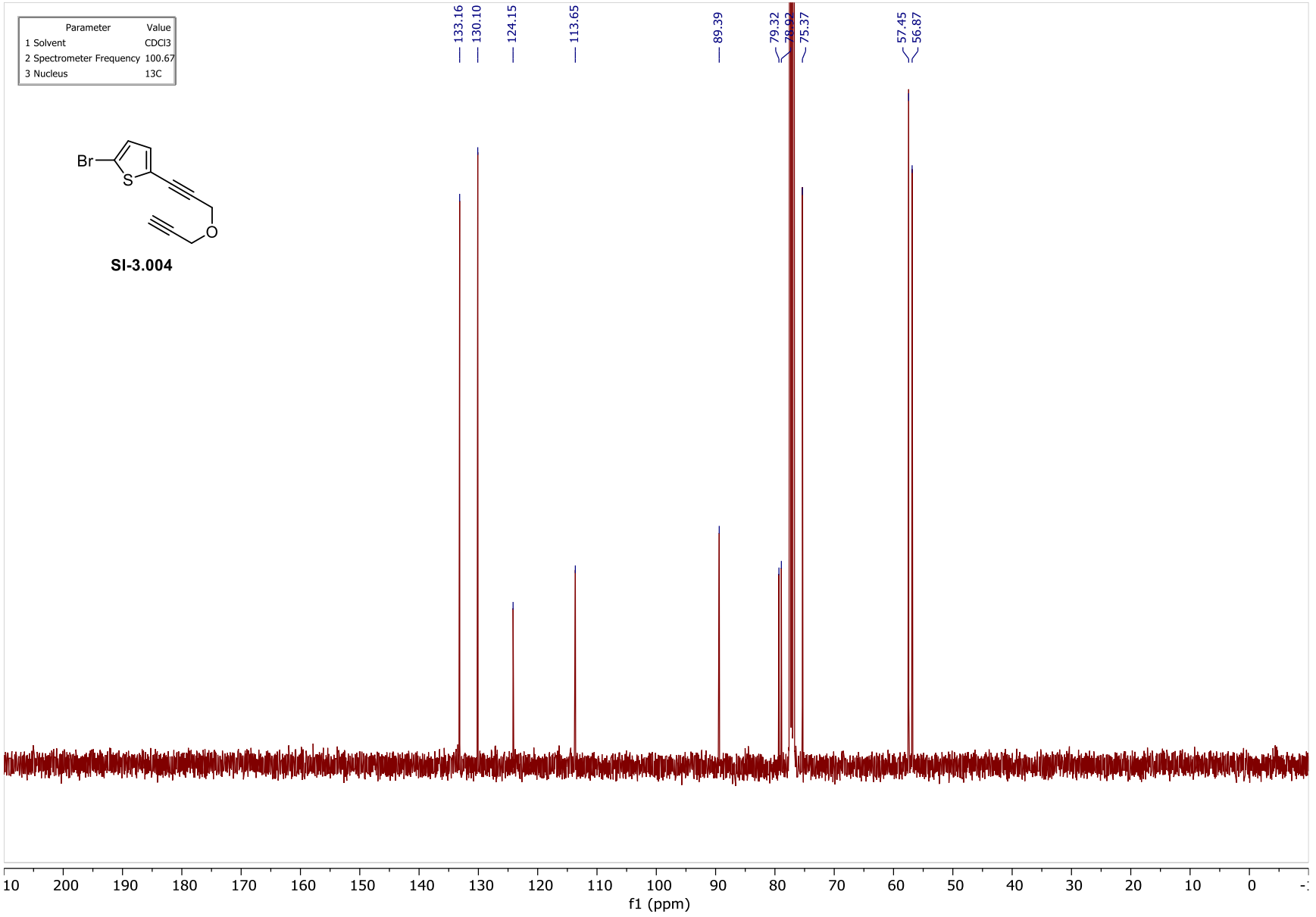
Parameter Value
1 Solvent CDCl3
2 Spectrometer Frequency 100.67
3 Nucleus 13C
Br
S
O
SI-3.004
133.16
130.10
124.15
113.65
89.39
79.32
78.93
75.37
57.45
56.87
f1 (ppm)

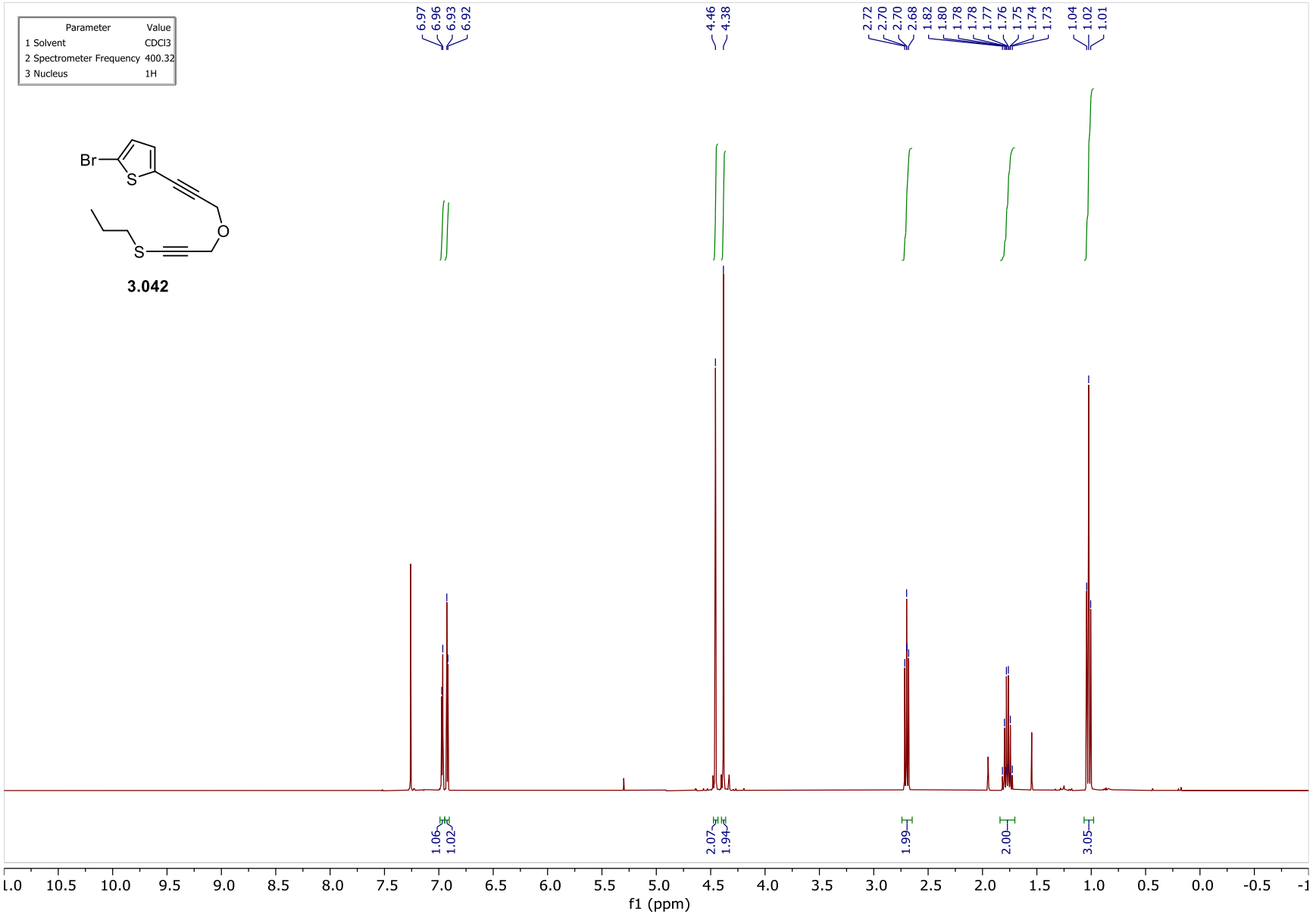
Parameter Value
1 Solvent CDCl3
2 Spectrometer Frequency 400.32
3 Nucleus 1H
Br
S
O
S
3.042
6.97
6.96
6.93
6.92
4.46
4.38
2.72
2.70
2.70
2.68
1.82
1.80
1.78
1.78
1.77
1.76
1.75
1.74
1.73
1.04
1.02
1.01
1.06
1.02
2.07
1.94
1.99
2.00
3.05
f1 (ppm)

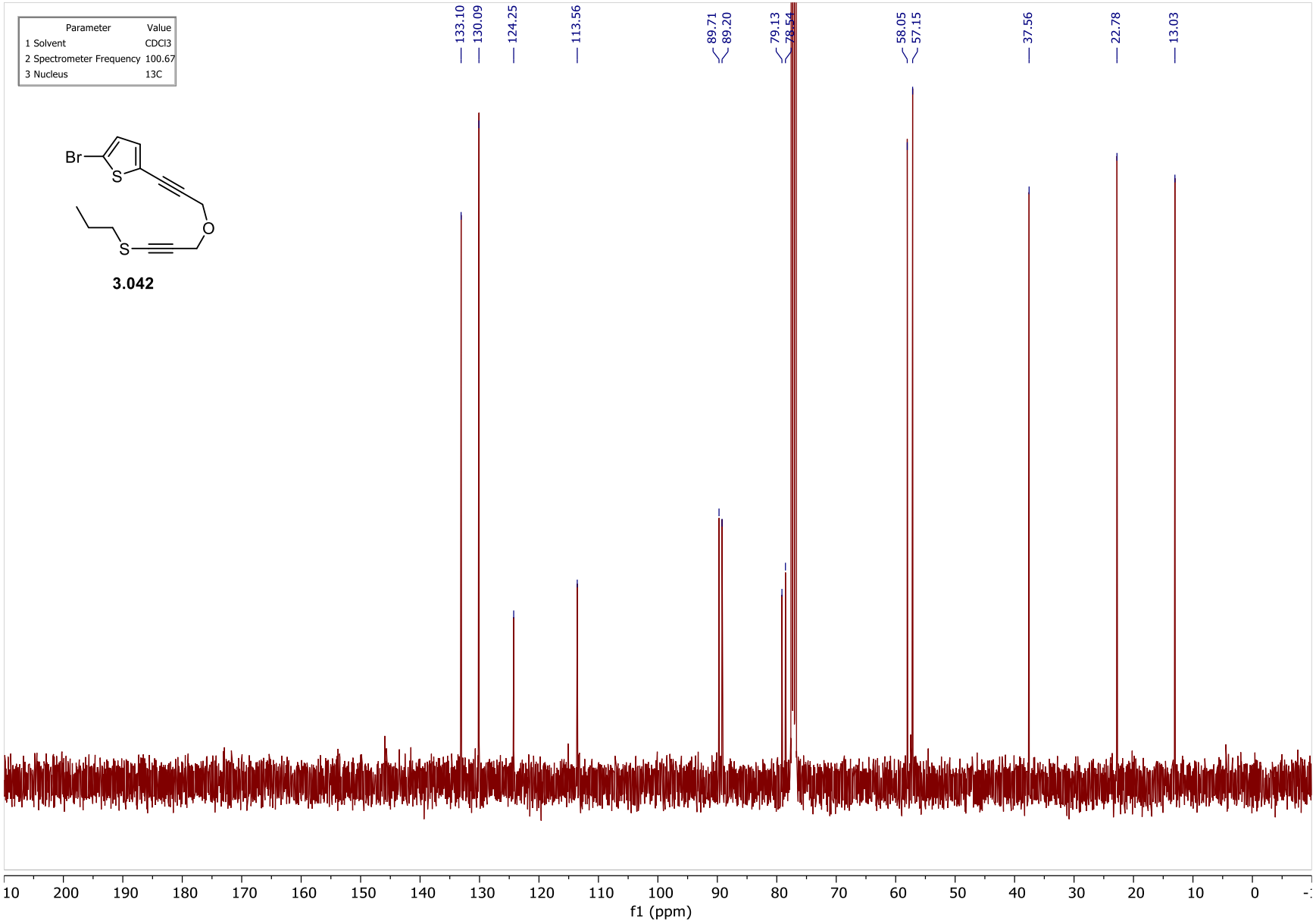
Parameter Value
1 Solvent CDCl3
2 Spectrometer Frequency 100.67
3 Nucleus 13C
Br
S
O
S
3.042
133.10
130.09
124.25
113.56
89.71
89.20
79.13
78.54
58.05
57.15
37.56
22.78
13.03
f1 (ppm)

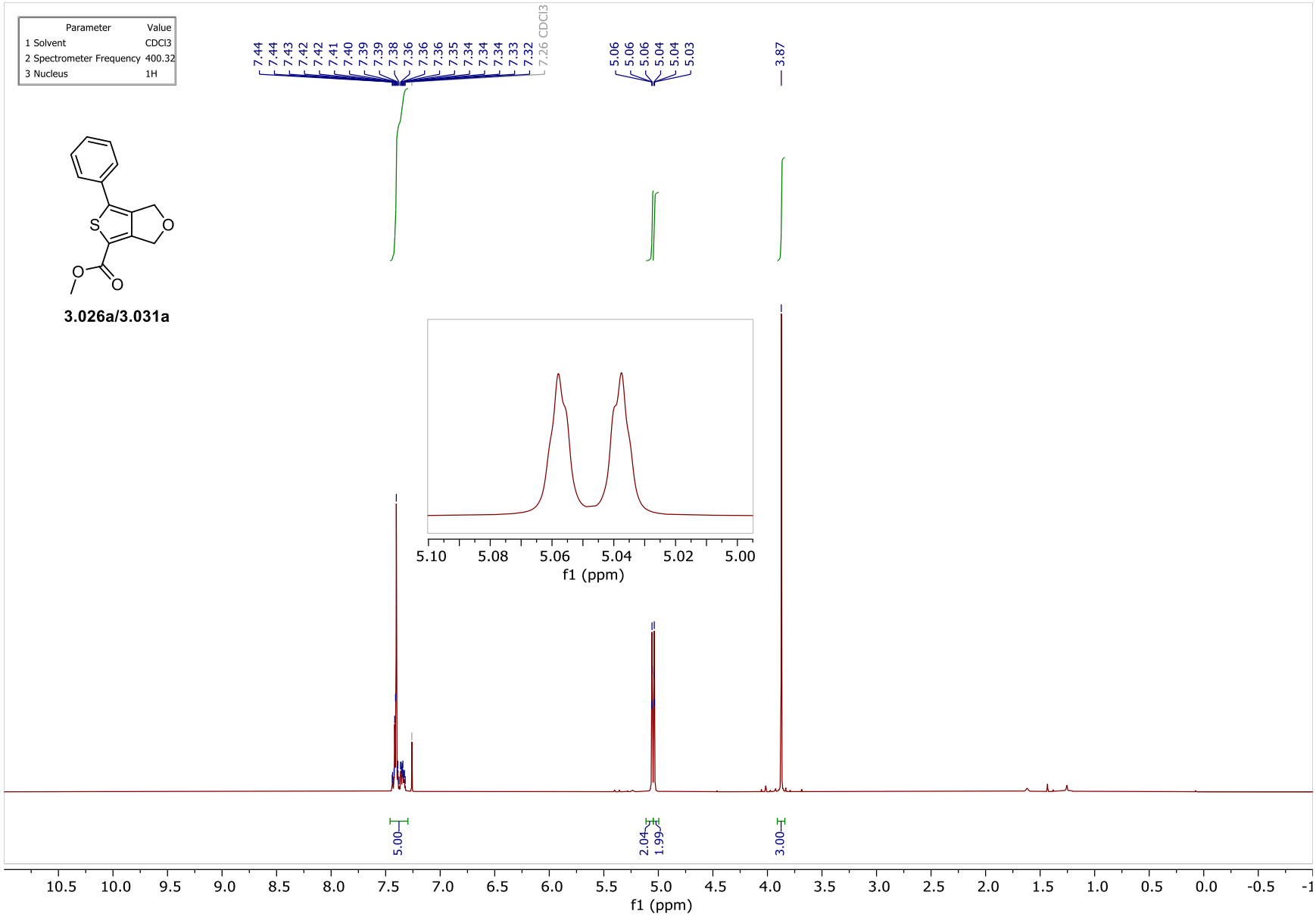
Parameter Value
1 Solvent CDCl3
2 Spectrometer Frequency 400.32
3 Nucleus 1H
3.026a/3.031a
7.44 7.44 7.43 7.42 7.42 7.41 7.40 7.39 7.39 7.38 7.36 7.36 7.36 7.35 7.34 7.34 7.34 7.33 7.32
7.26 CDCl3
5.06 5.06 5.06 5.04 5.04 5.03
3.87
5.10 5.08 5.06 5.04 5.02 5.00
f1 (ppm)
5.00
2.04
1.99
3.00
10.5 10.0 9.5 9.0 8.5 8.0 7.5 7.0 6.5 6.0 5.5 5.0 4.5 4.0 3.5 3.0 2.5 2.0 1.5 1.0 0.5 0.0 -0.5 -1
f1 (ppm)

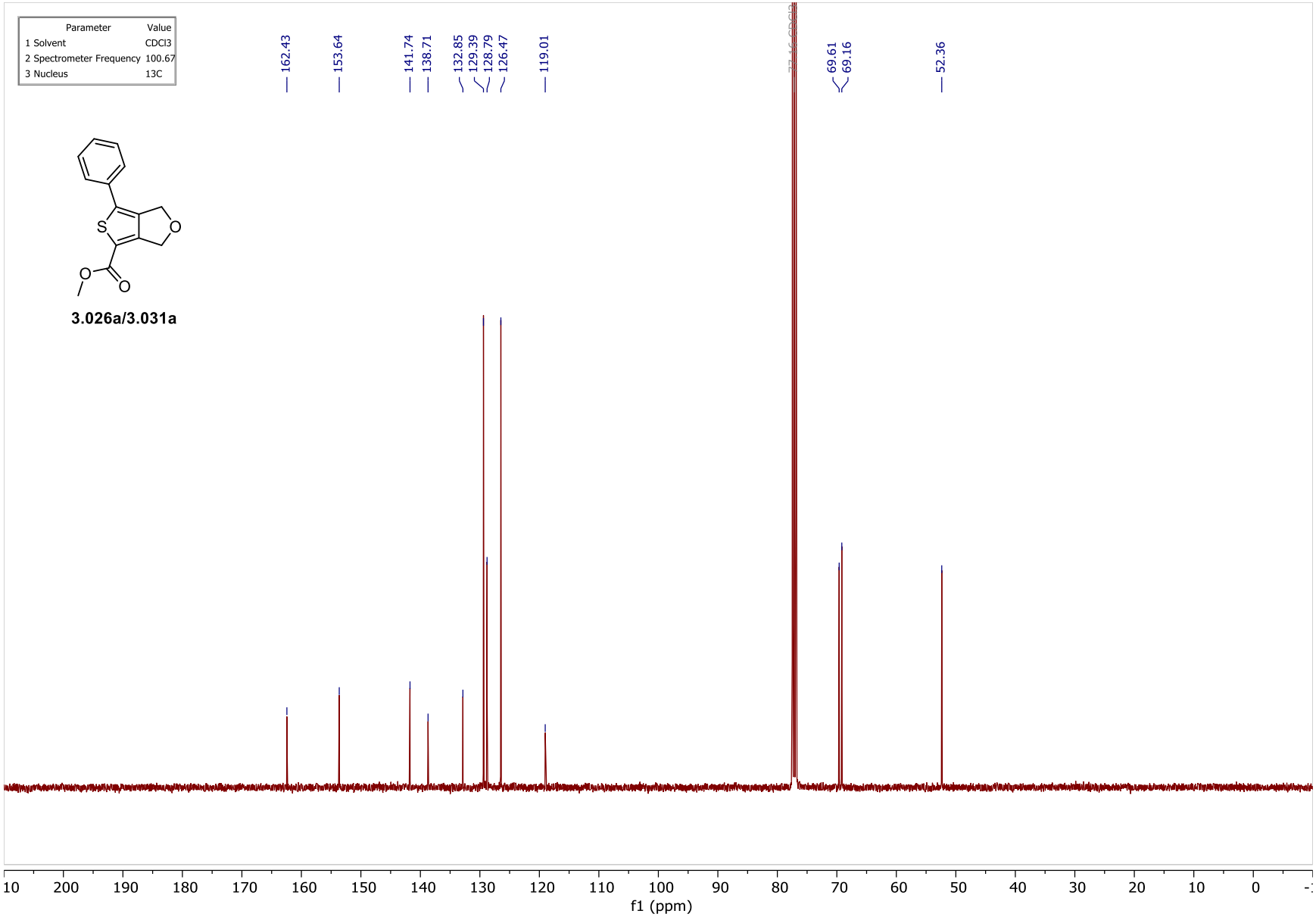
Parameter Value
1 Solvent CDCl3
2 Spectrometer Frequency 100.67
3 Nucleus 13C
162.43
153.64
141.74
138.71
132.85
129.39
128.79
126.47
119.01
69.61
69.16
52.36
S
O
O
O
3.026a/3.031a
f1 (ppm)

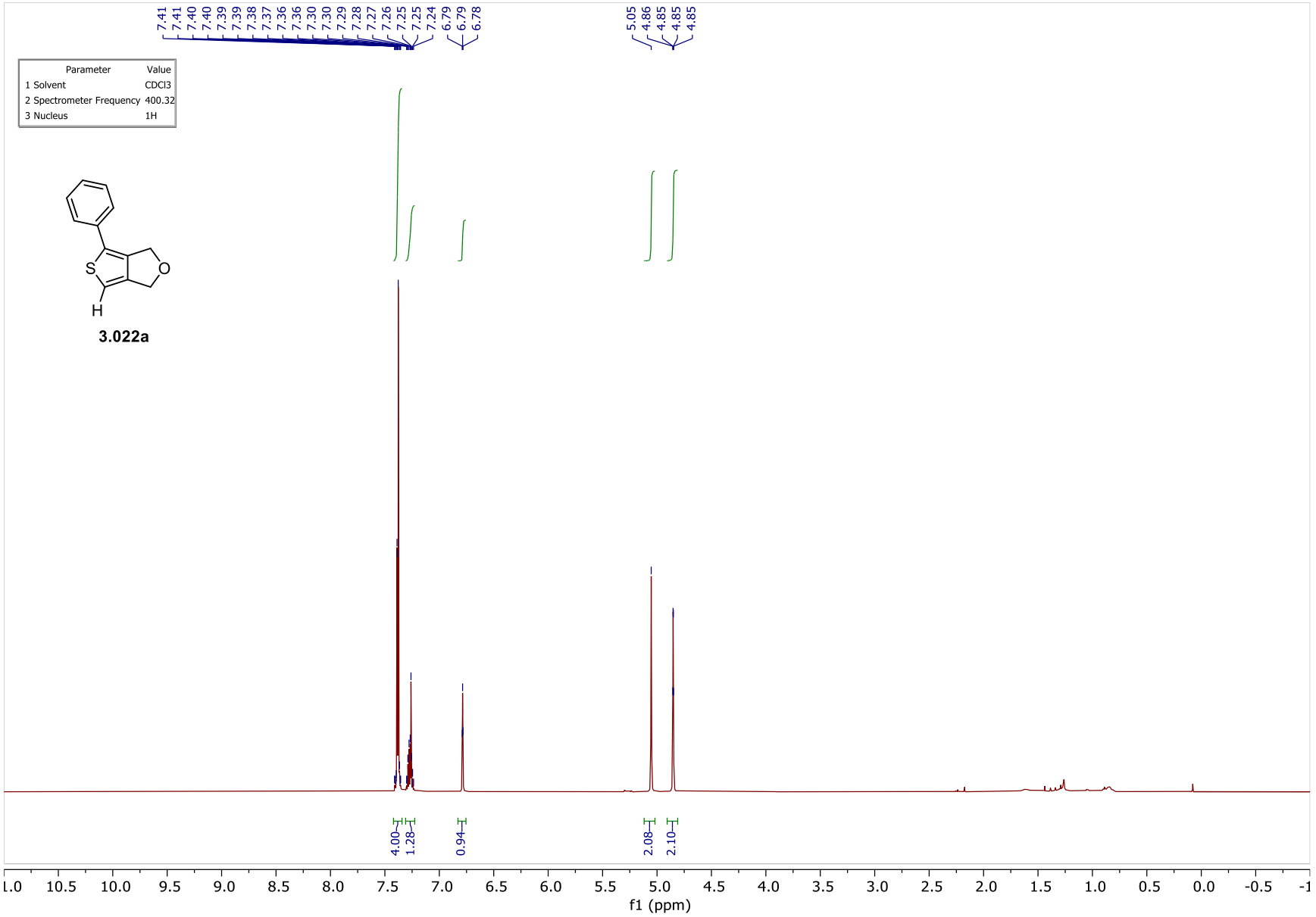
7.41
7.41
7.40
7.40
7.39
7.39
7.38
7.37
7.36
7.36
7.30
7.30
7.29
7.28
7.27
7.26
7.25
7.25
7.24
6.79
6.79
6.78
5.05
4.86
4.85
4.85
4.85
Parameter Value
1 Solvent CDCl3
2 Spectrometer Frequency 400.32
3 Nucleus 1H
S
O
H
3.022a
4.00
1.28
0.94
2.08
2.10
f1 (ppm)

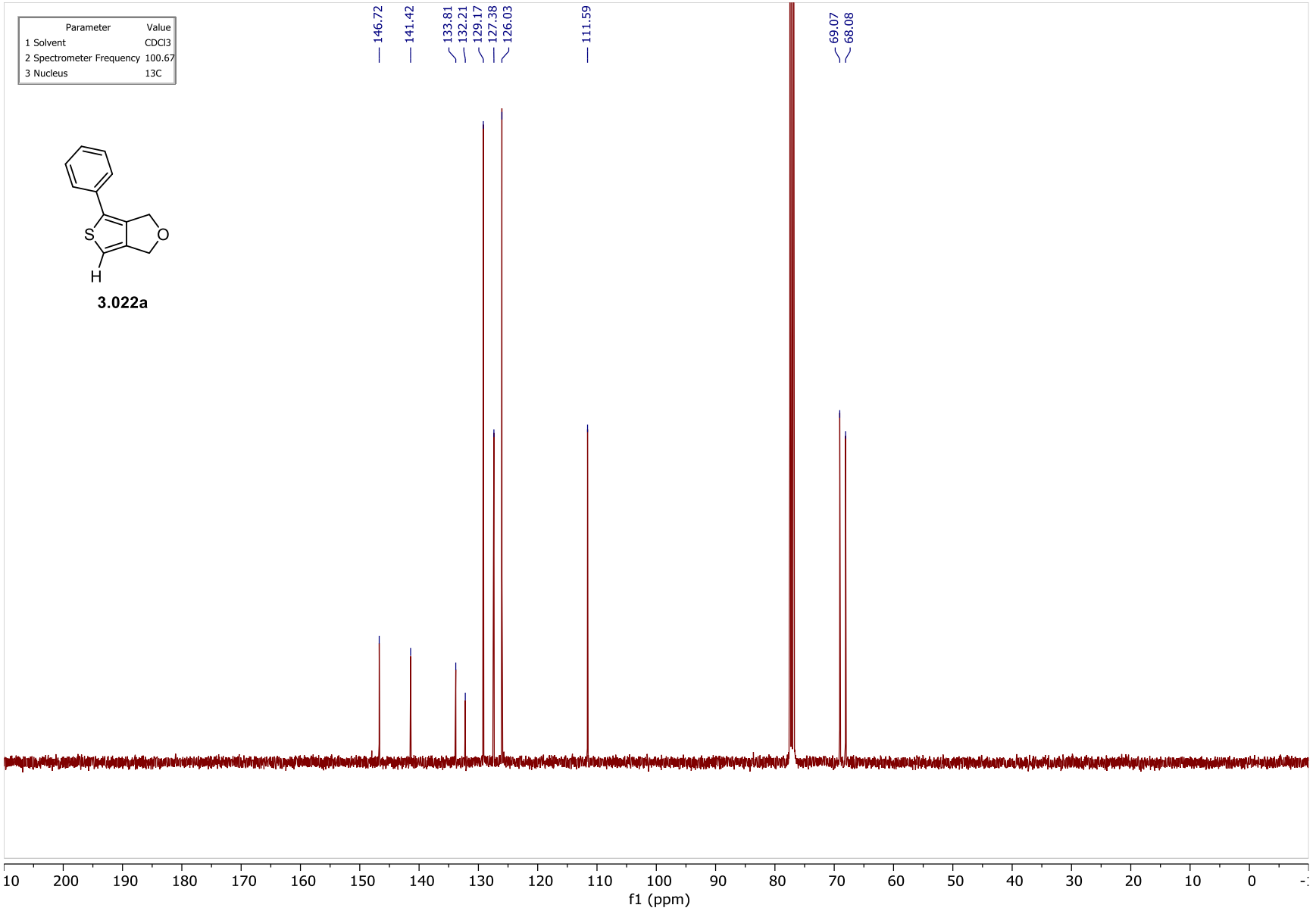
Parameter Value
1 Solvent CDCl3
2 Spectrometer Frequency 100.67
3 Nucleus 13C
146.72
141.42
133.81
132.21
129.17
127.38
126.03
111.59
69.07
68.08
S
O
H
3.022a
10 200 190 180 170 160 150 140 130 120 110 100 90 80 70 60 50 40 30 20 10 0
f1 (ppm)

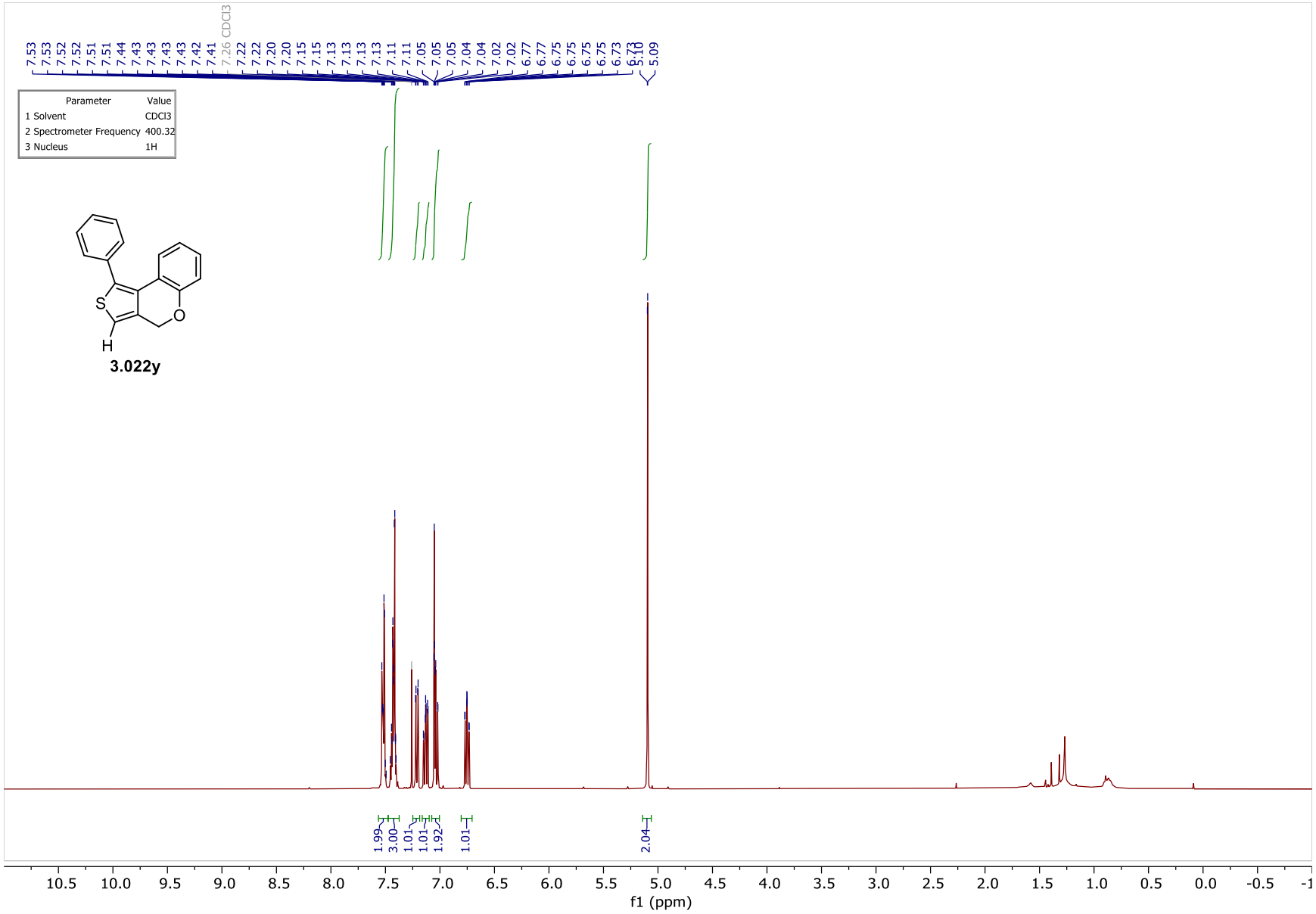
7.53 7.53 7.52 7.52 7.51 7.51 7.44 7.43 7.43 7.43 7.43 7.42 7.41 7.26 CDCl3 7.22 7.22 7.20 7.20 7.15 7.15 7.13 7.13 7.13 7.13 7.11 7.11 7.05 7.05 7.05 7.04 7.04 7.02 7.02 6.77 6.77 6.75 6.75 6.75 6.75 6.73 6.73 5.10 5.09
Parameter Value
1 Solvent CDCl3
2 Spectrometer Frequency 400.32
3 Nucleus 1H
S
O
H
3.022y
1.99 3.00 1.01 1.01 1.92 1.01 2.04
10.5 10.0 9.5 9.0 8.5 8.0 7.5 7.0 6.5 6.0 5.5 5.0 4.5 4.0 3.5 3.0 2.5 2.0 1.5 1.0 0.5 0.0 -0.5 -1
f1 (ppm)

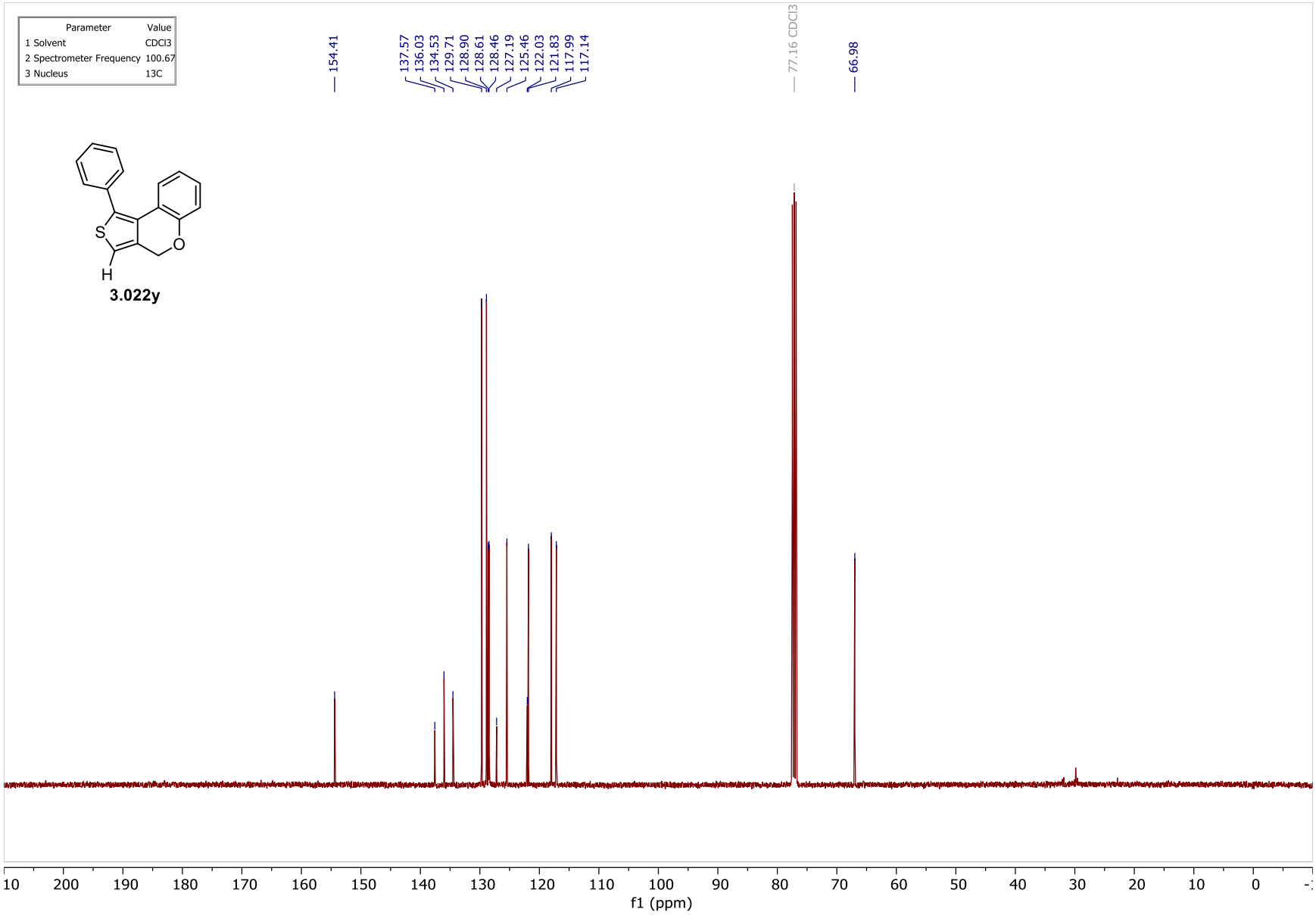
Parameter Value
1 Solvent CDCl3
2 Spectrometer Frequency 100.67
3 Nucleus 13C
154.41
137.57
136.03
134.53
129.71
128.90
128.61
128.46
127.19
125.46
122.03
121.83
117.99
117.14
77.16 CDCl3
66.98
S
O
H
3.022y
f1 (ppm)

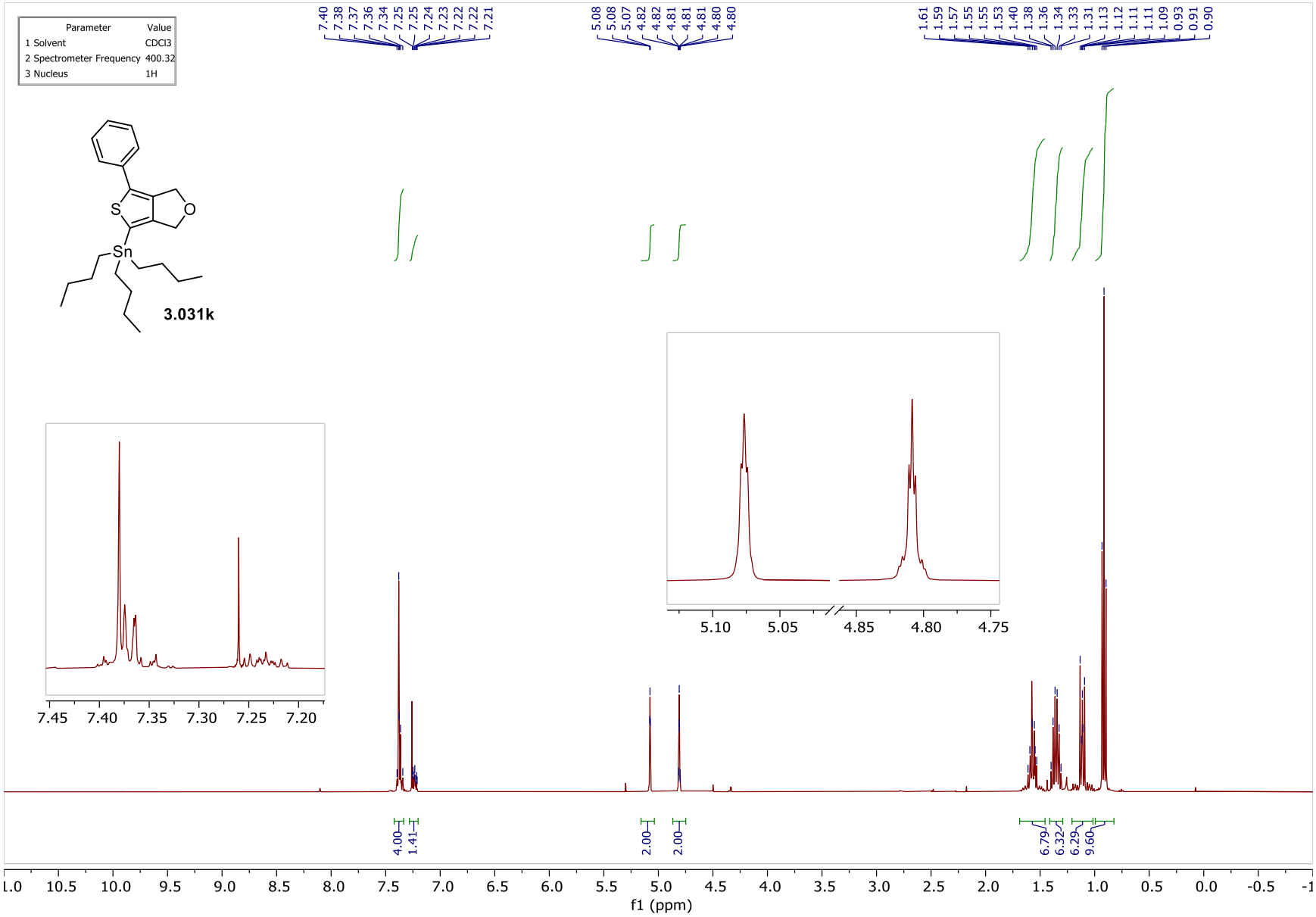
Parameter Value
1 Solvent CDCl3
2 Spectrometer Frequency 400.32
3 Nucleus 1H
3.031k
7.40 7.38 7.37 7.36 7.34 7.25 7.25 7.24 7.23 7.22 7.22 7.21
5.08 5.08 5.07 4.82 4.82 4.81 4.81 4.81 4.80 4.80
1.61 1.59 1.57 1.55 1.55 1.53 1.40 1.38 1.36 1.34 1.33 1.31 1.13 1.12 1.11 1.11 1.09 0.93 0.91 0.90
7.45 7.40 7.35 7.30 7.25 7.20
5.10 5.05 4.85 4.80 4.75
4.00 1.41 2.00 2.00 6.79 6.32 6.29 9.60
f1 (ppm)

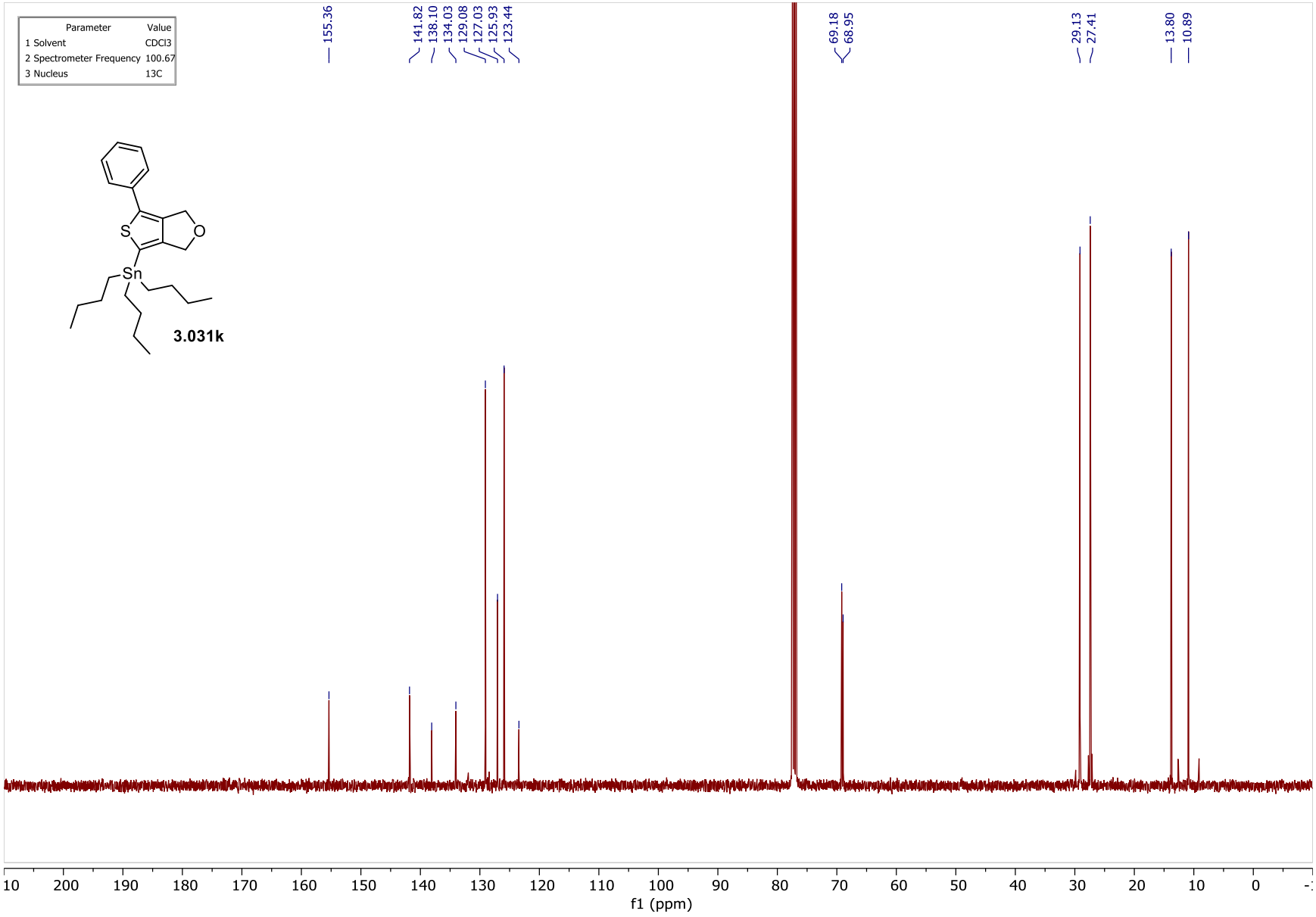
Parameter Value
1 Solvent CDCl3
2 Spectrometer Frequency 100.67
3 Nucleus 13C
155.36
141.82
138.10
134.03
129.08
127.03
125.93
123.44
69.18
68.95
29.13
27.41
13.80
10.89
S
O
Sn
3.031k
f1 (ppm)

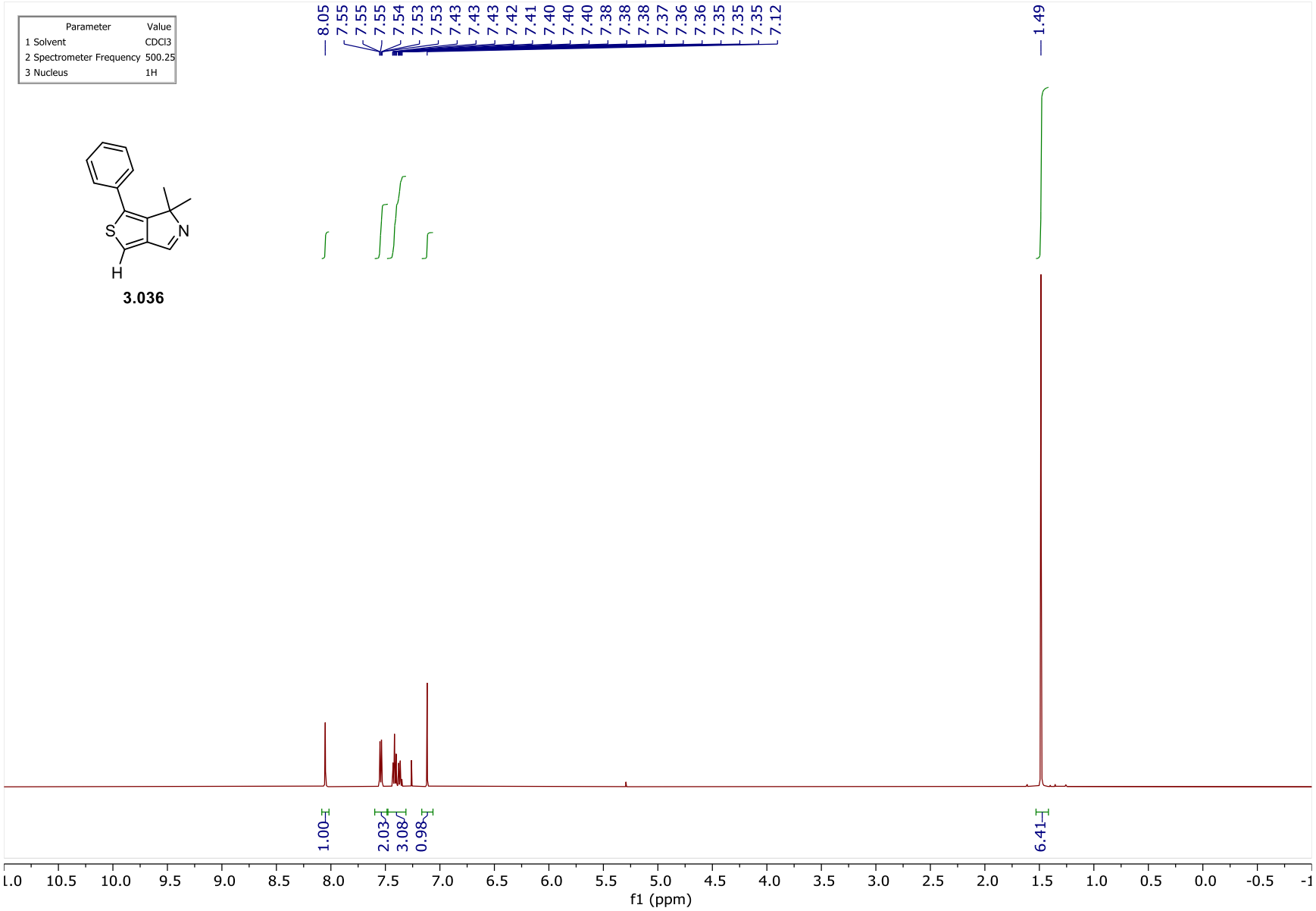
Parameter Value
1 Solvent CDCl3
2 Spectrometer Frequency 500.25
3 Nucleus 1H
8.05
7.55
7.55
7.55
7.54
7.53
7.53
7.43
7.43
7.43
7.42
7.41
7.40
7.40
7.40
7.38
7.38
7.38
7.37
7.36
7.36
7.35
7.35
7.35
7.12
1.49
S
N
H
3.036
1.00
2.03
3.08
0.98
6.41
f1 (ppm)

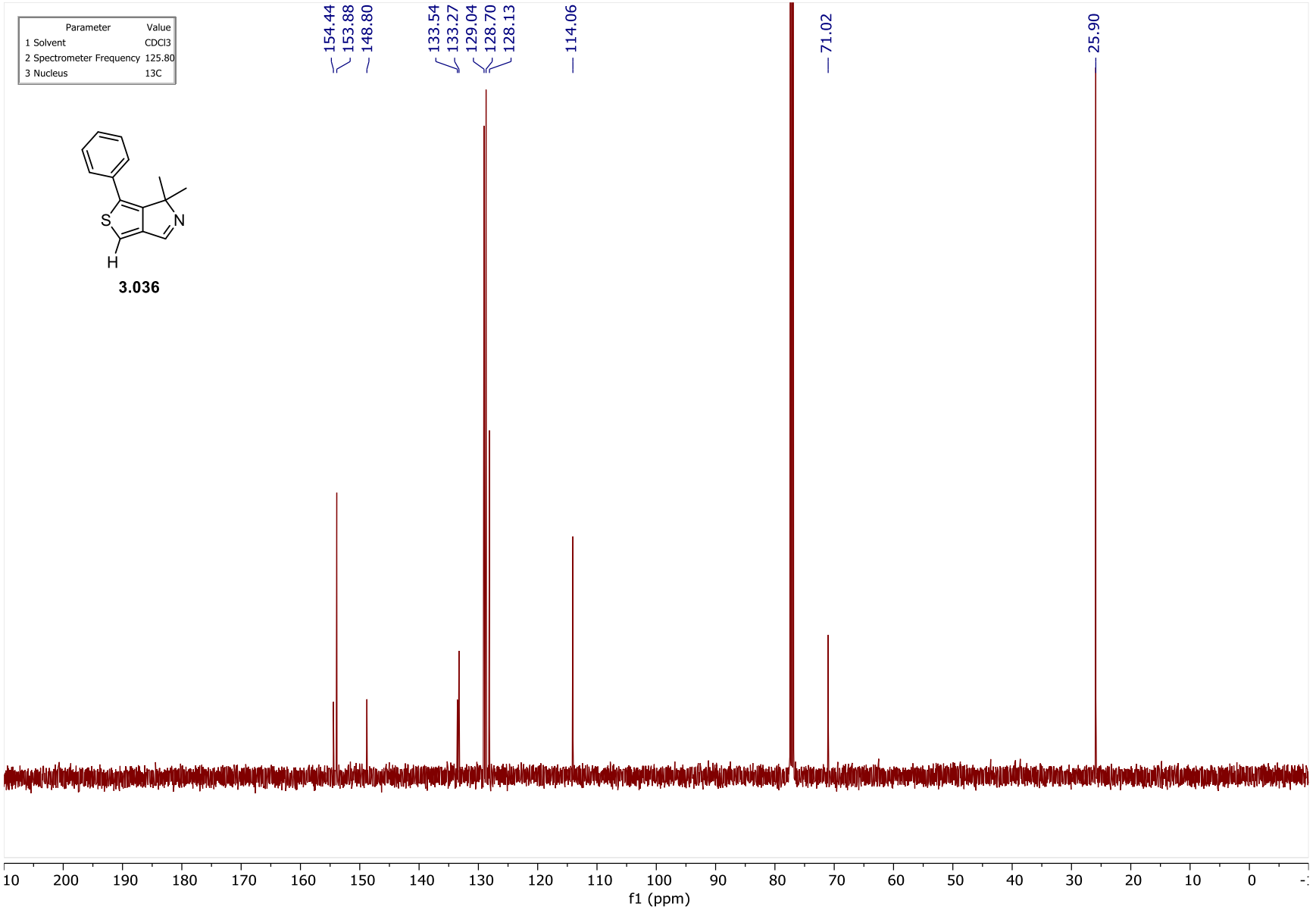
Parameter Value
1 Solvent CDCl3
2 Spectrometer Frequency 125.80
3 Nucleus 13C
154.44
153.88
148.80
133.54
133.27
129.04
128.70
128.13
114.06
71.02
25.90
S
N
H
3.036
10 200 190 180 170 160 150 140 130 120 110 100 90 80 70 60 50 40 30 20 10 0
f1 (ppm)

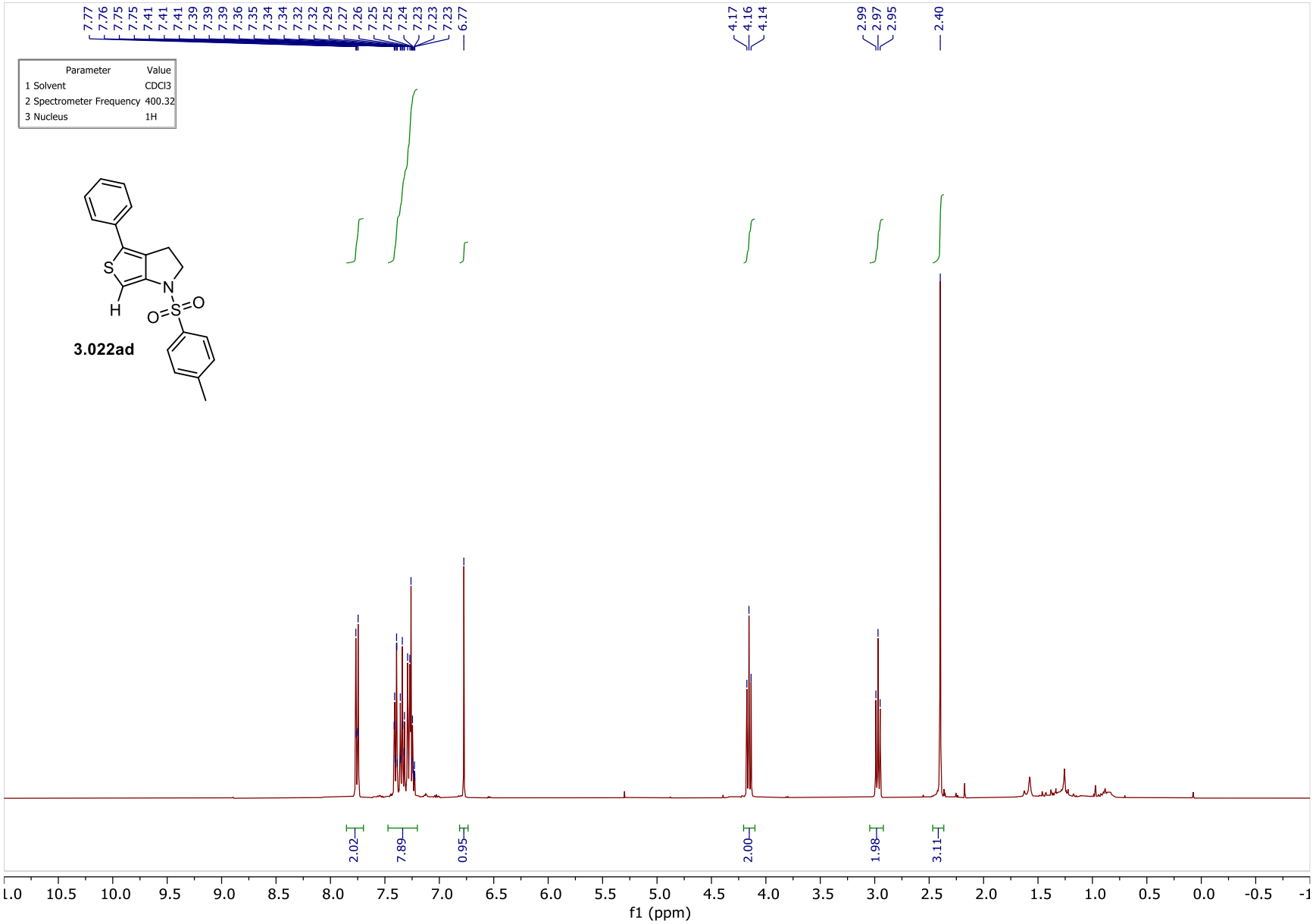
7.77
7.76
7.75
7.75
7.41
7.41
7.41
7.39
7.39
7.39
7.36
7.35
7.34
7.34
7.32
7.32
7.29
7.27
7.26
7.25
7.25
7.24
7.23
7.23
7.23
6.77
4.17
4.16
4.14
2.99
2.97
2.95
2.40
Parameter Value
1 Solvent CDCl3
2 Spectrometer Frequency 400.32
3 Nucleus 1H
S
N
H
O=S=O
3.022ad
2.02
7.89
0.95
2.00
1.98
3.11
f1 (ppm)

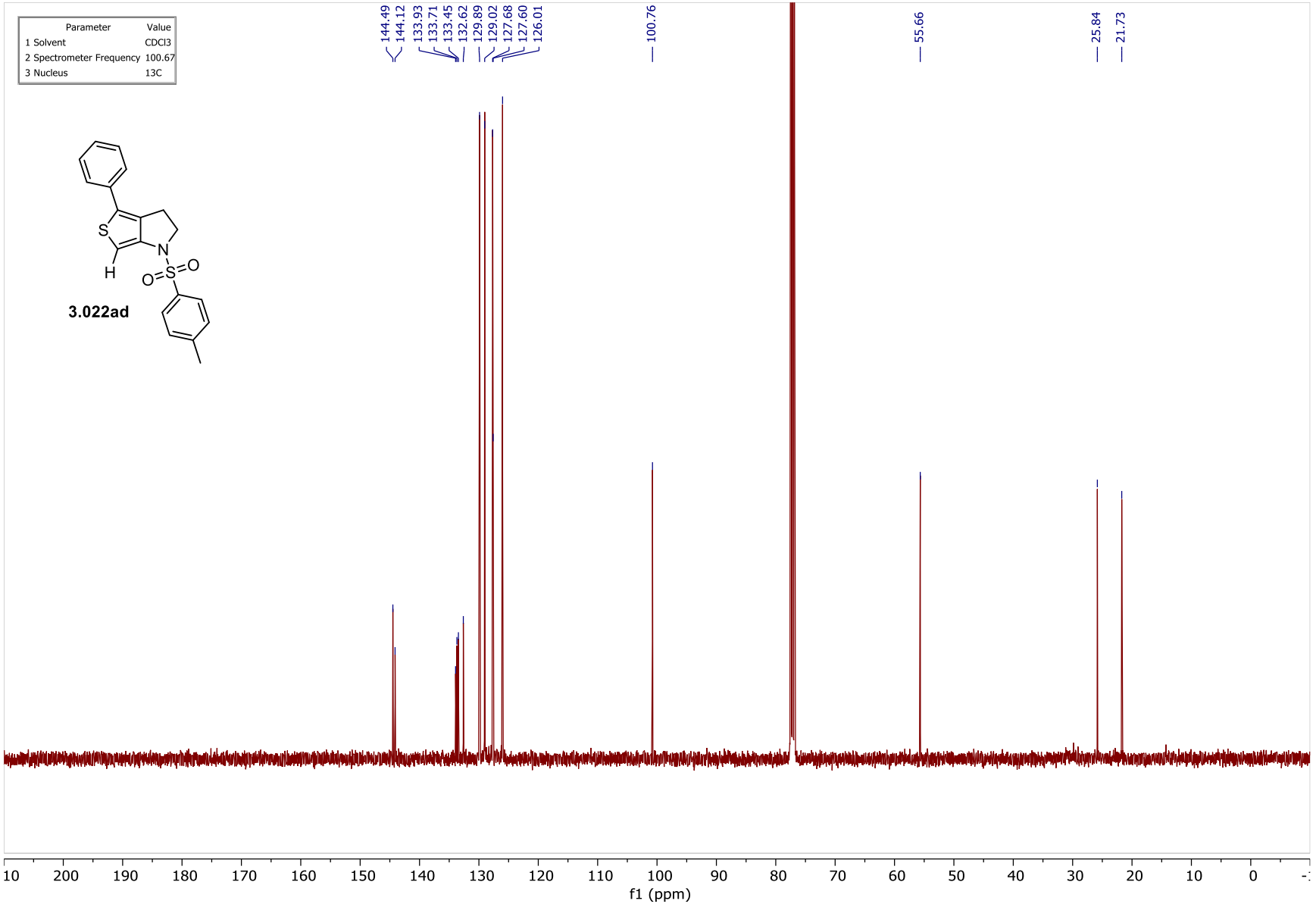
Parameter Value
1 Solvent CDCl3
2 Spectrometer Frequency 100.67
3 Nucleus 13C
144.49
144.12
133.93
133.71
133.45
132.62
129.89
129.02
127.68
127.60
126.01
100.76
55.66
25.84
21.73
3.022ad
f1 (ppm)

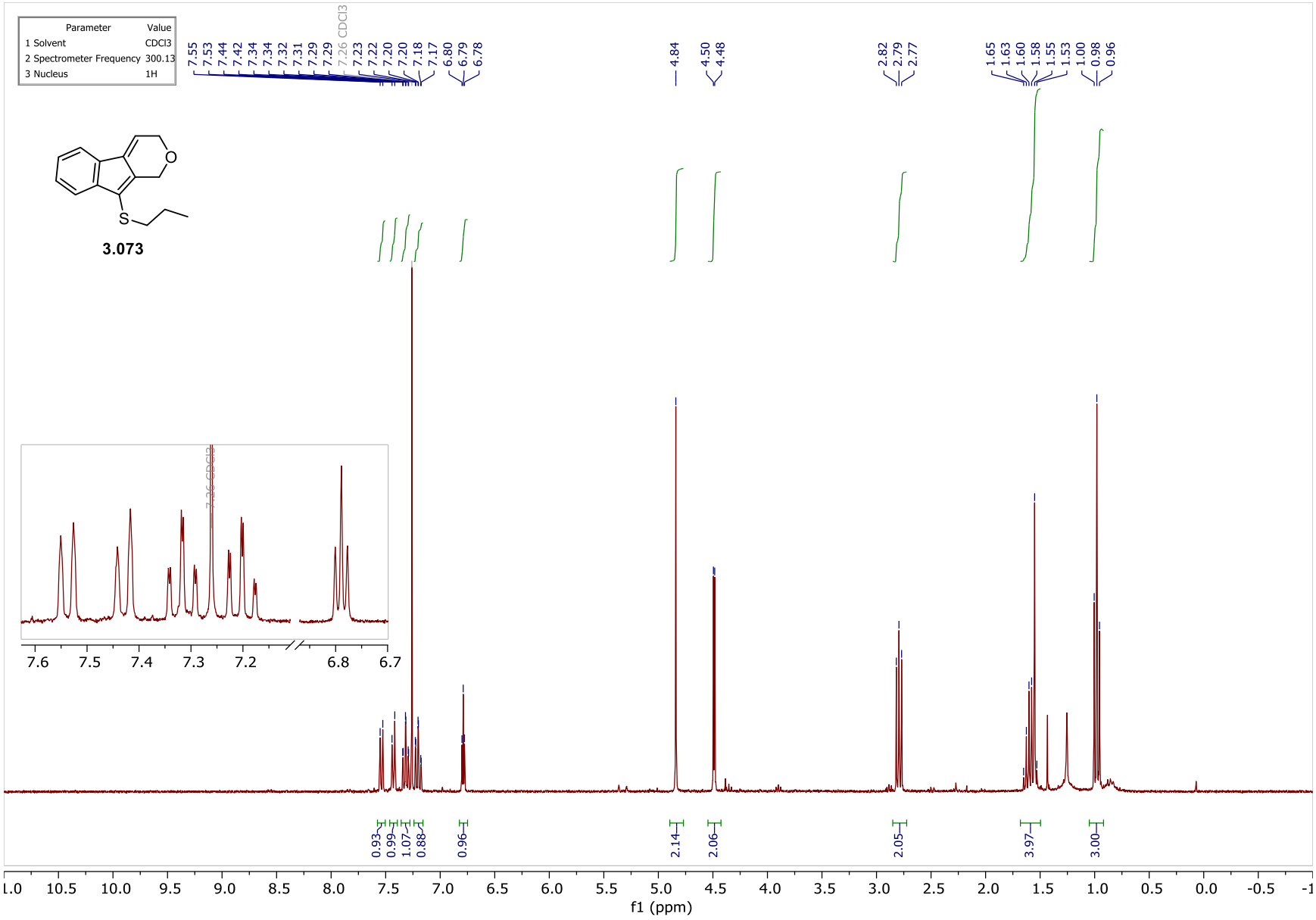
Parameter Value
1 Solvent CDCl3
2 Spectrometer Frequency 300.13
3 Nucleus 1H
7.55 7.53 7.44 7.42 7.34 7.34 7.32 7.31 7.29 7.29 7.26 CDCl3 7.23 7.22 7.20 7.20 7.18 7.17 6.80 6.79 6.78
4.84 4.50 4.48
2.82 2.79 2.77
1.65 1.63 1.60 1.58 1.55 1.53 1.00 0.98 0.96
O
S
3.073
7.26 CDCl3
7.6 7.5 7.4 7.3 7.2 6.8 6.7
0.93 0.99 1.07 0.88 0.96 2.14 2.06 2.05 3.97 3.00
1.0 10.5 10.0 9.5 9.0 8.5 8.0 7.5 7.0 6.5 6.0 5.5 5.0 4.5 4.0 3.5 3.0 2.5 2.0 1.5 1.0 0.5 0.0 -0.5 -1
f1 (ppm)

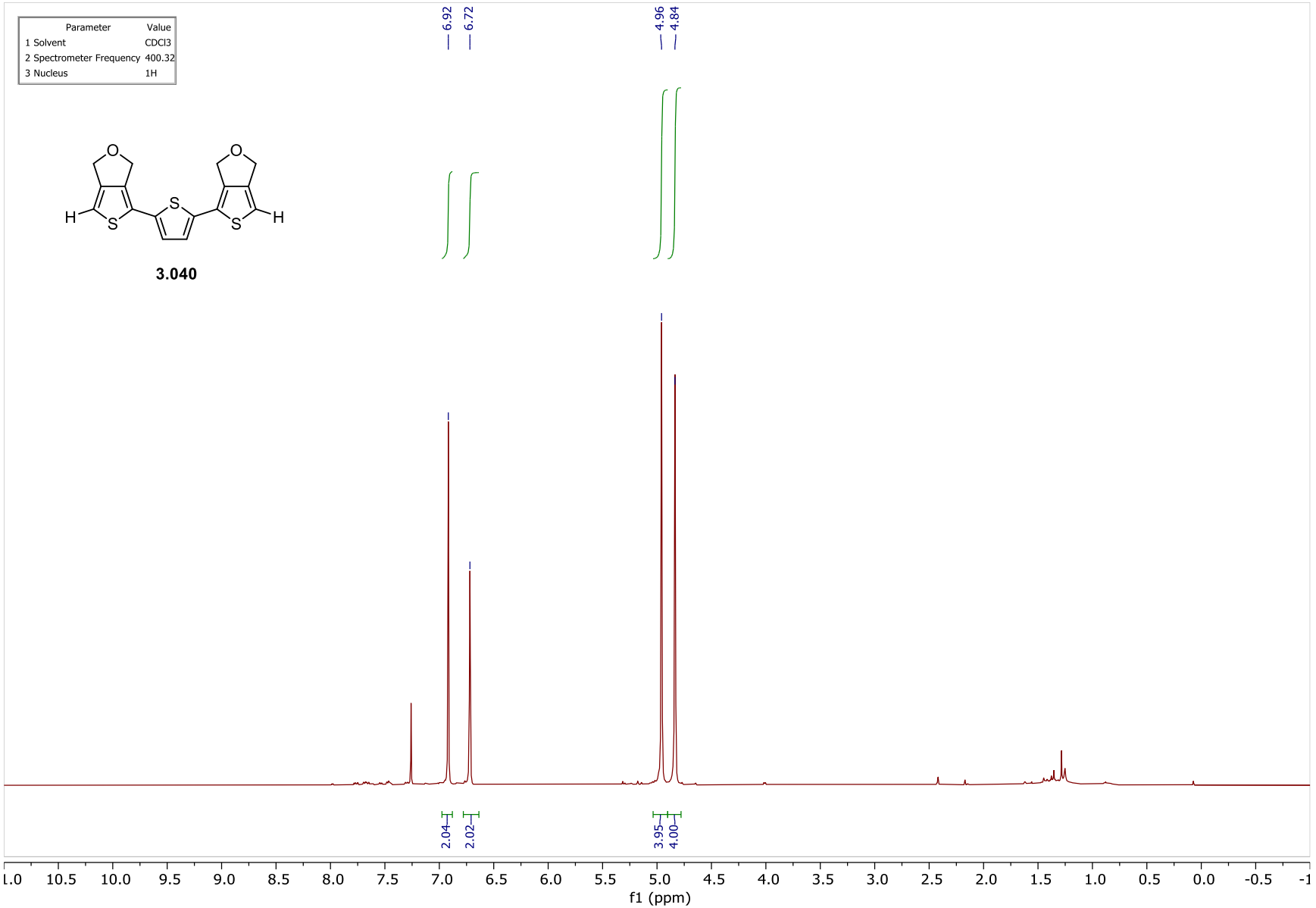
Parameter Value
1 Solvent CDCl3
2 Spectrometer Frequency 400.32
3 Nucleus 1H
6.92
6.72
4.96
4.84
3.040
2.04
2.02
3.95
4.00
f1 (ppm)

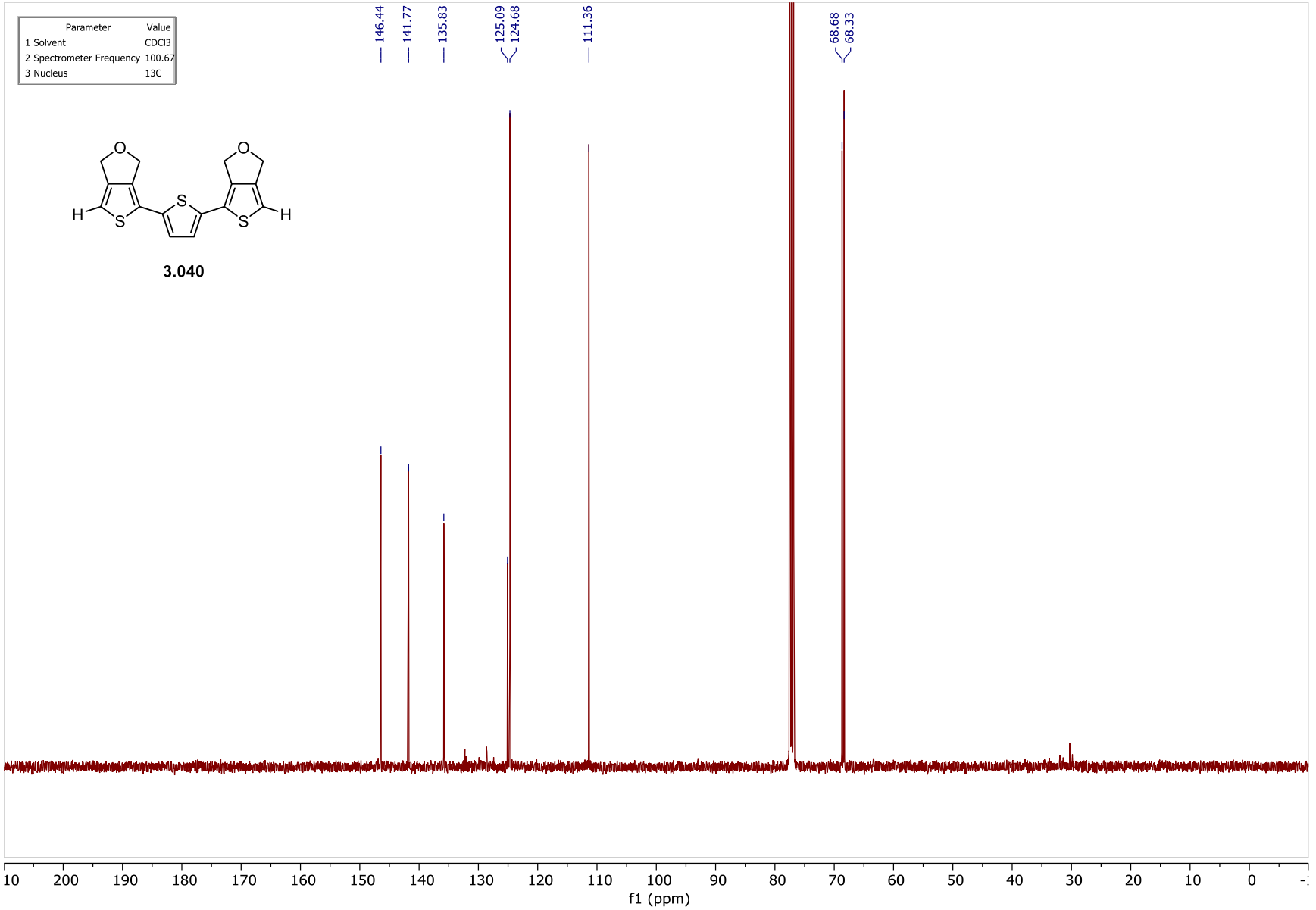
Parameter Value
1 Solvent CDCl3
2 Spectrometer Frequency 100.67
3 Nucleus 13C
146.44
141.77
135.83
125.09
124.68
111.36
68.68
68.33
O
O
S
H
S
S
H
3.040
10 200 190 180 170 160 150 140 130 120 110 100 90 80 70 60 50 40 30 20 10 0
f1 (ppm)

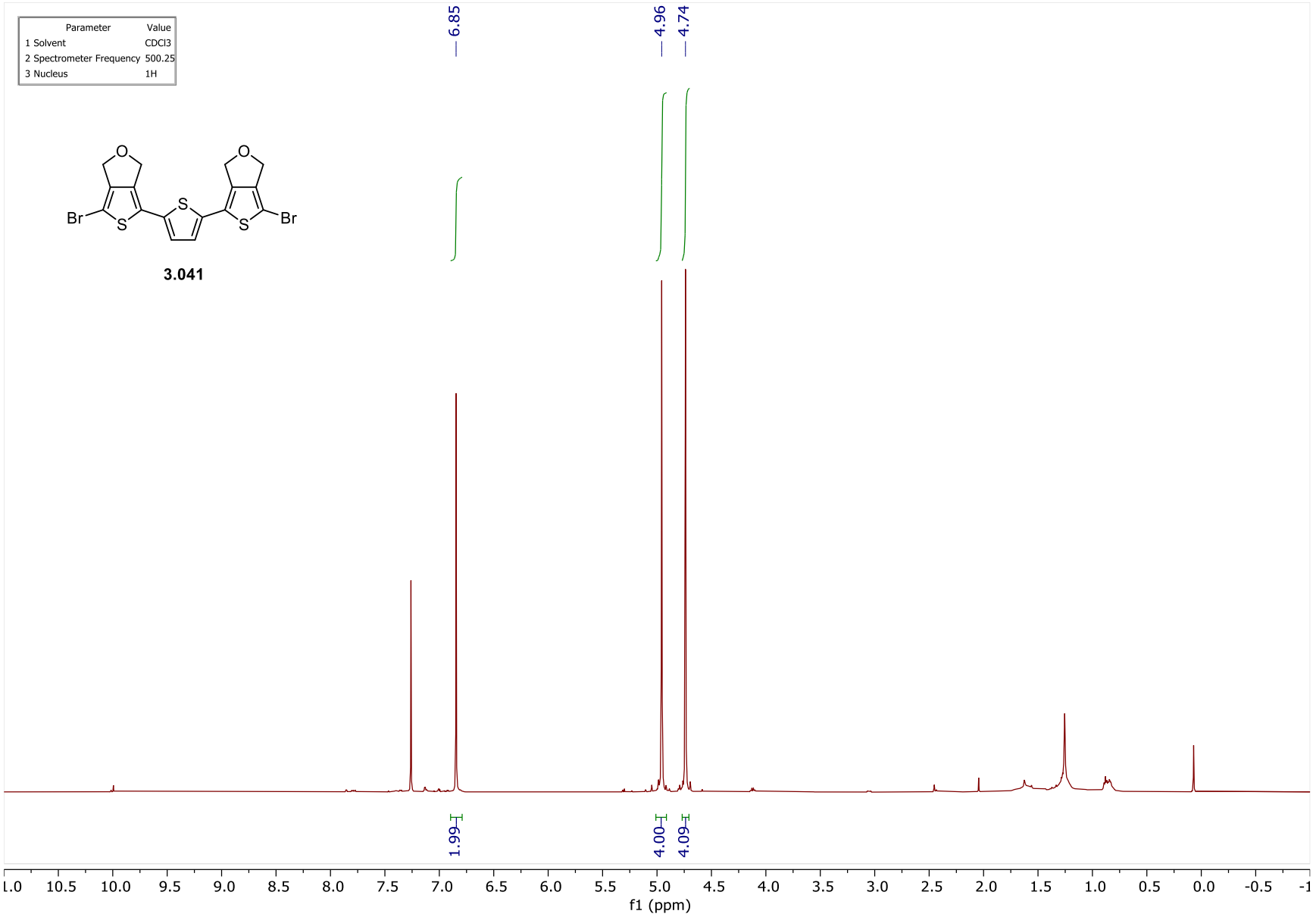
Parameter Value
1 Solvent CDCl3
2 Spectrometer Frequency 500.25
3 Nucleus 1H
6.85
4.96
4.74
Br
Br
S
O
3.041
1.99
4.00
4.09
f1 (ppm)

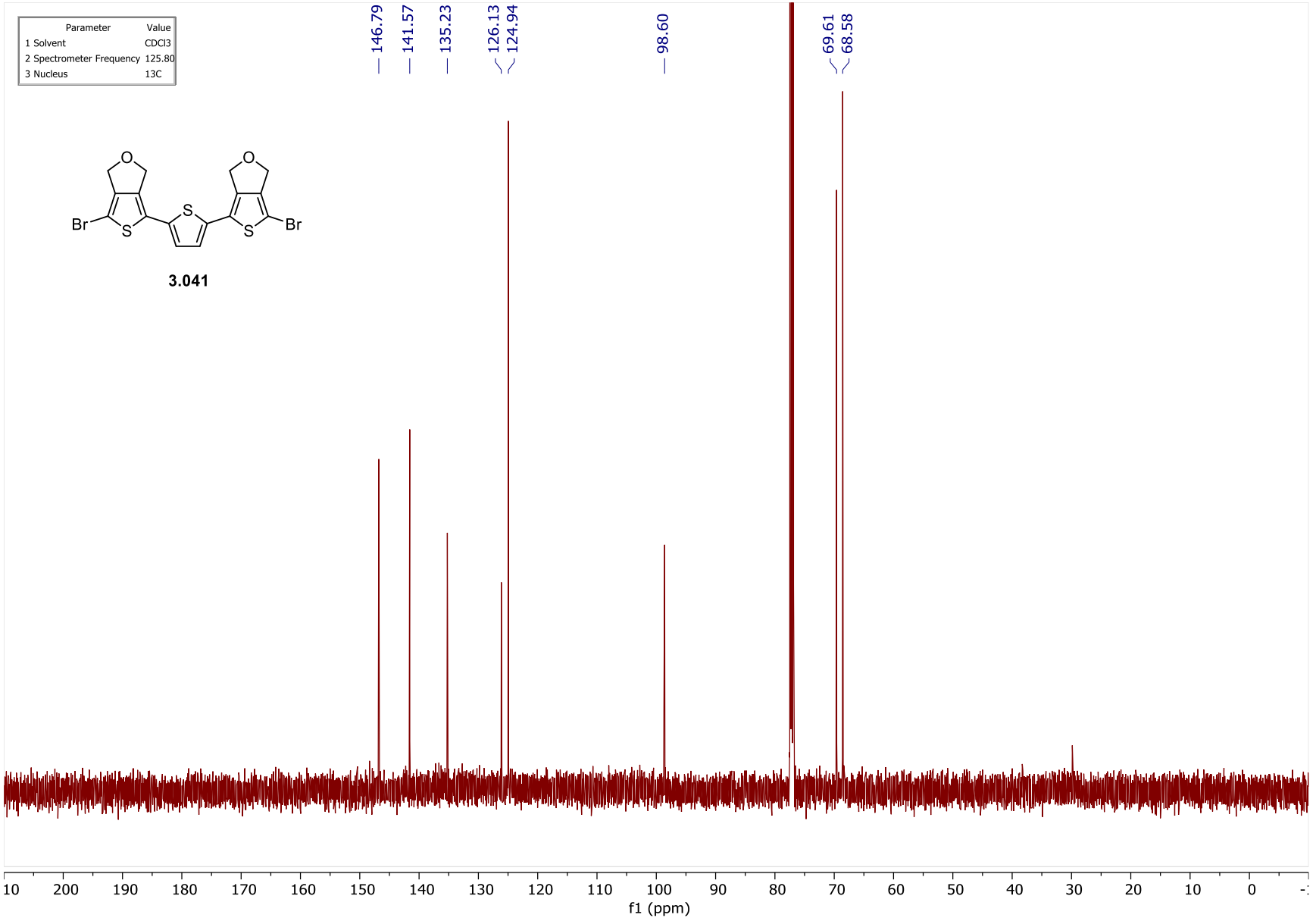
Parameter Value
1 Solvent CDCl3
2 Spectrometer Frequency 125.80
3 Nucleus 13C
146.79
141.57
135.23
126.13
124.94
98.60
69.61
68.58
Br
Br
O
O
S
S
S
3.041
f1 (ppm)

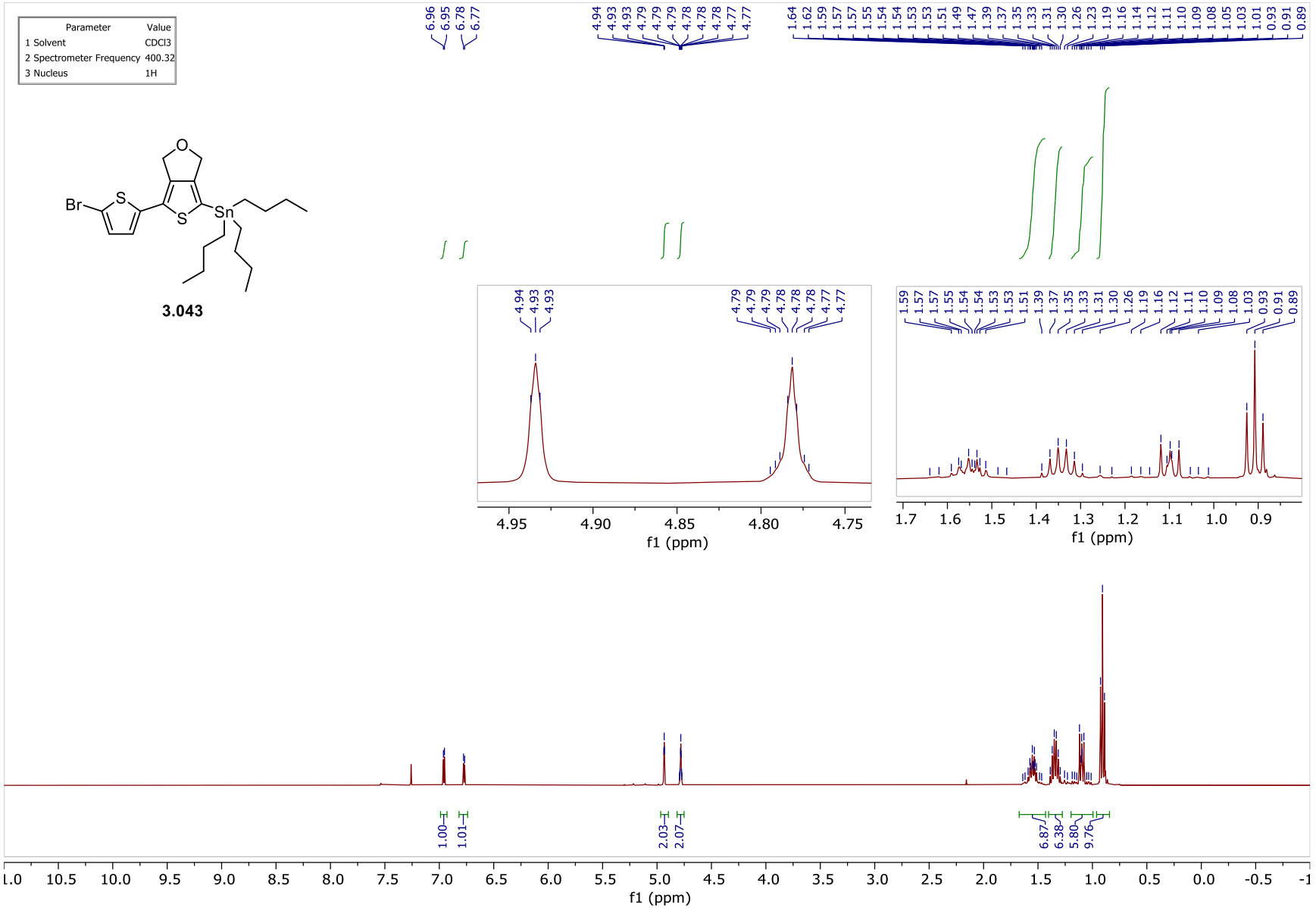
Parameter Value
1 Solvent CDCl3
2 Spectrometer Frequency 400.32
3 Nucleus 1H
Br
S
S
O
Sn
3.043
f1 (ppm)

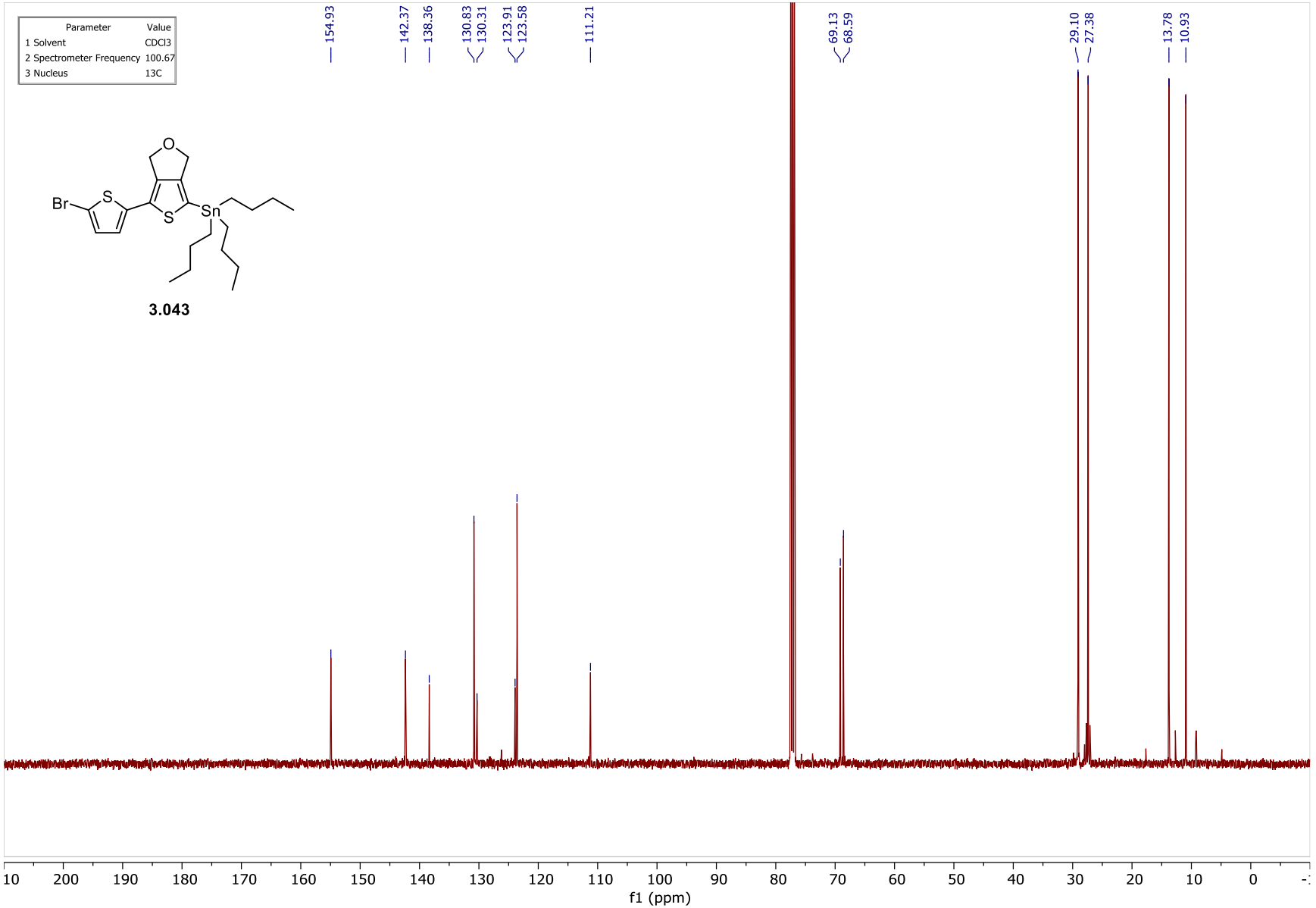
Parameter Value
1 Solvent CDCl3
2 Spectrometer Frequency 100.67
3 Nucleus 13C
154.93
142.37
138.36
130.83
130.31
123.91
123.58
111.21
69.13
68.59
29.10
27.38
13.78
10.93
Br
S
S
O
Sn
3.043
f1 (ppm)

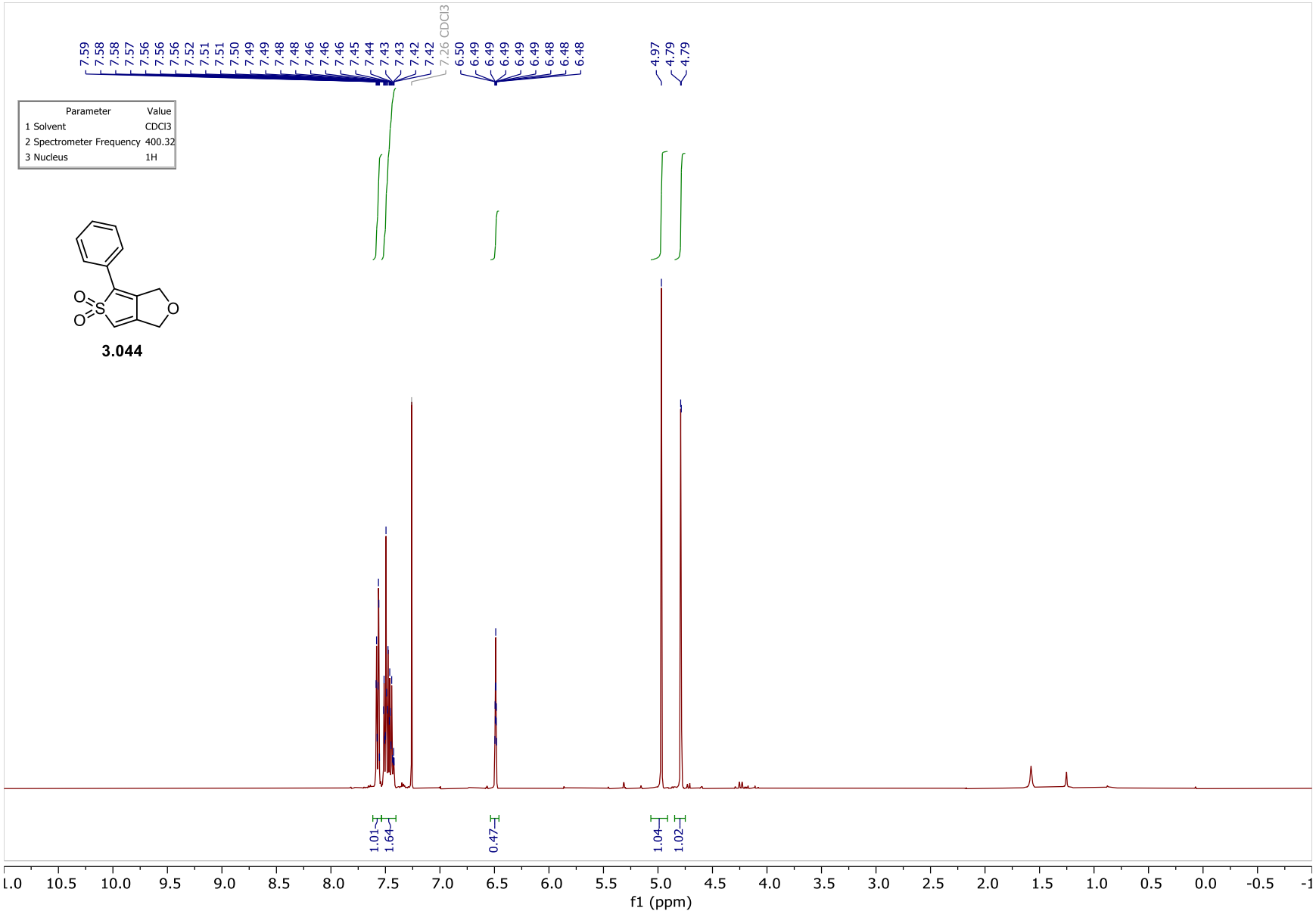
7.59
7.58
7.58
7.57
7.56
7.56
7.56
7.52
7.51
7.51
7.50
7.49
7.49
7.48
7.48
7.46
7.46
7.46
7.45
7.44
7.43
7.43
7.42
7.42
7.26 CDCl3
6.50
6.49
6.49
6.49
6.49
6.49
6.48
6.48
6.48
4.97
4.79
4.79
Parameter Value
1 Solvent CDCl3
2 Spectrometer Frequency 400.32
3 Nucleus 1H
O
O
S
O
3.044
1.01
1.64
0.47
1.04
1.02
f1 (ppm)

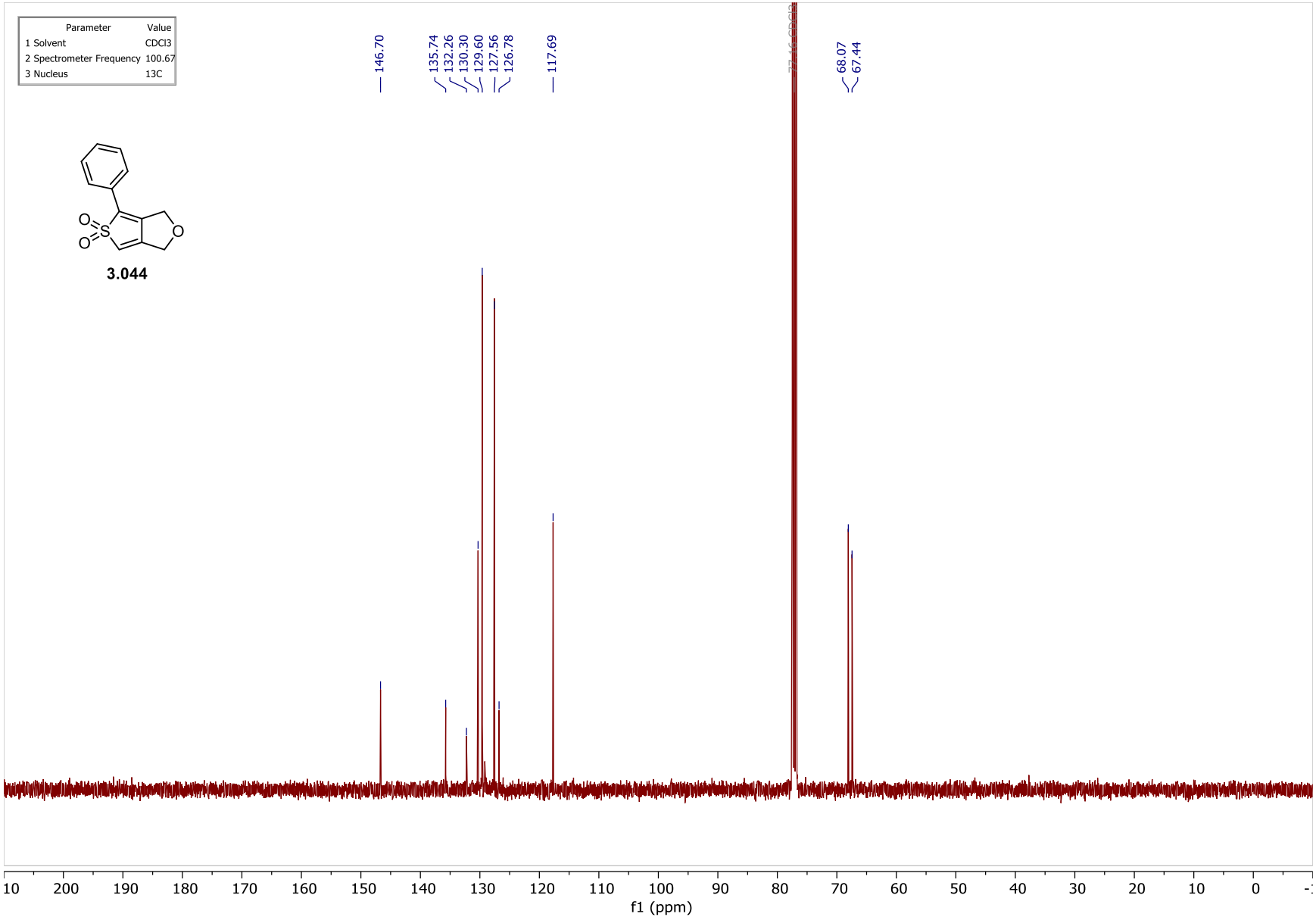
Parameter Value
1 Solvent CDCl3
2 Spectrometer Frequency 100.67
3 Nucleus 13C
146.70
135.74
132.26
130.30
129.60
127.56
126.78
117.69
77.16
68.07
67.44
O
S
O
O
3.044
10 200 190 180 170 160 150 140 130 120 110 100 90 80 70 60 50 40 30 20 10 0
f1 (ppm)

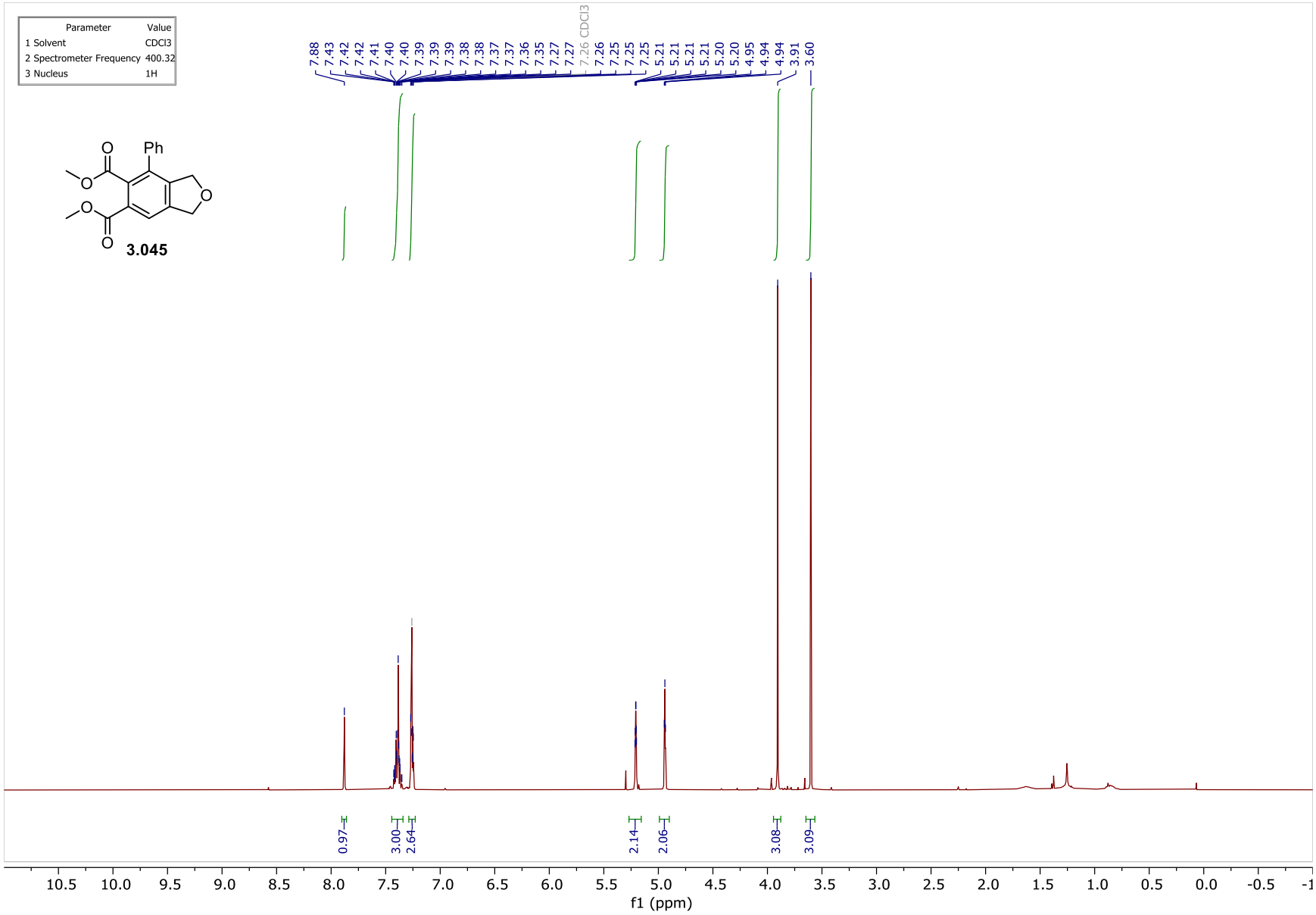
Parameter Value
1 Solvent CDCl3
2 Spectrometer Frequency 400.32
3 Nucleus 1H
Ph
O
O
O
O
O
3.045
7.88 7.43 7.42 7.42 7.41 7.40 7.40 7.39 7.39 7.38 7.38 7.37 7.37 7.36 7.35 7.27 7.27 7.26 CDCl3 7.26 7.25 7.25 5.21 5.21 5.21 5.21 5.20 5.20 4.95 4.94 4.94 3.91 3.60
0.97 3.00 2.64 2.14 2.06 3.08 3.09
10.5 10.0 9.5 9.0 8.5 8.0 7.5 7.0 6.5 6.0 5.5 5.0 4.5 4.0 3.5 3.0 2.5 2.0 1.5 1.0 0.5 0.0 -0.5 -1
f1 (ppm)

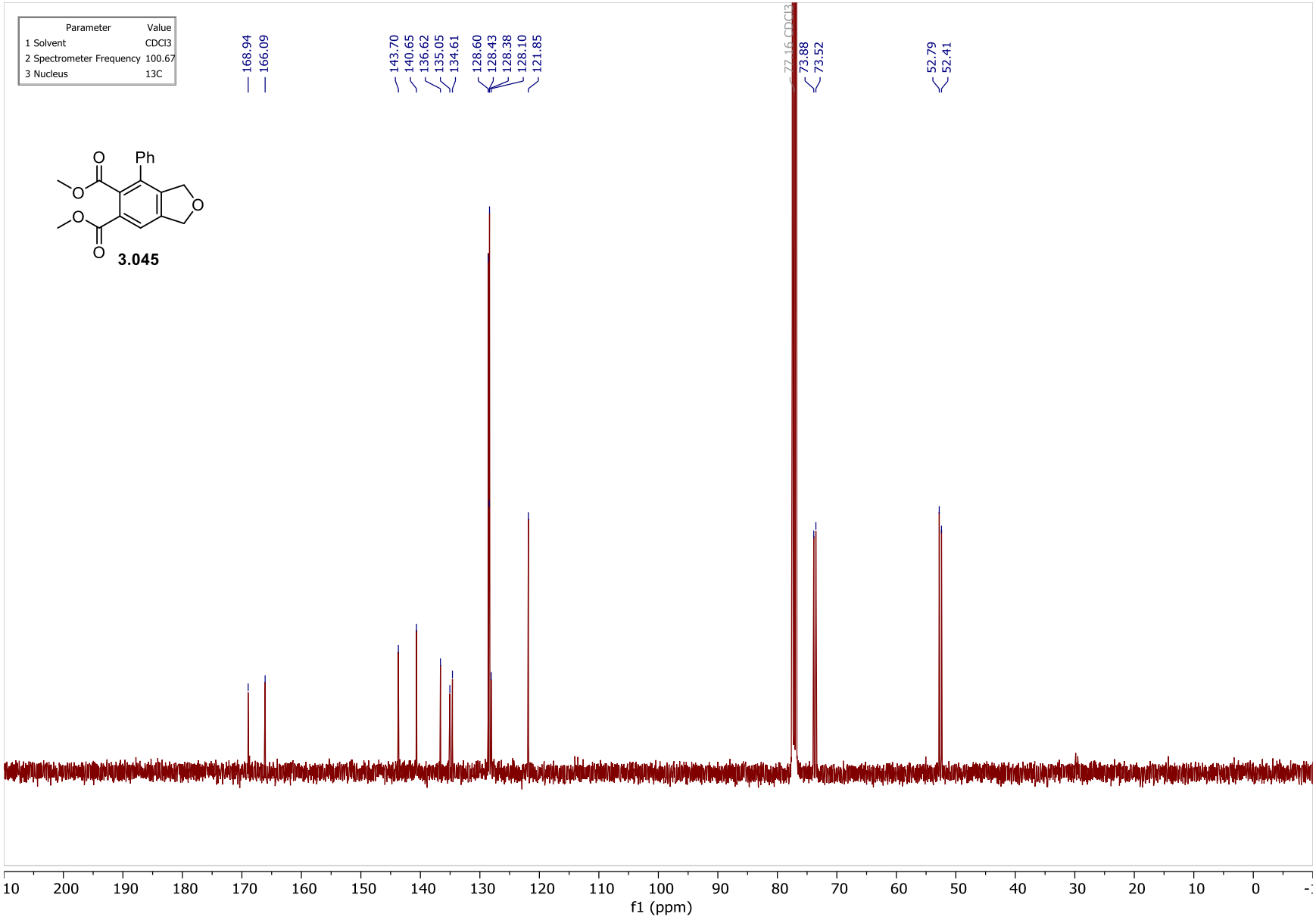
Parameter Value
1 Solvent CDCl3
2 Spectrometer Frequency 100.67
3 Nucleus 13C
168.94
166.09
143.70
140.65
136.62
135.05
134.61
128.60
128.43
128.38
128.10
121.85
77.16 CDCl3
73.88
73.52
52.79
52.41
Ph
O
O
O
O
O
3.045
10 200 190 180 170 160 150 140 130 120 110 100 90 80 70 60 50 40 30 20 10 0
f1 (ppm)

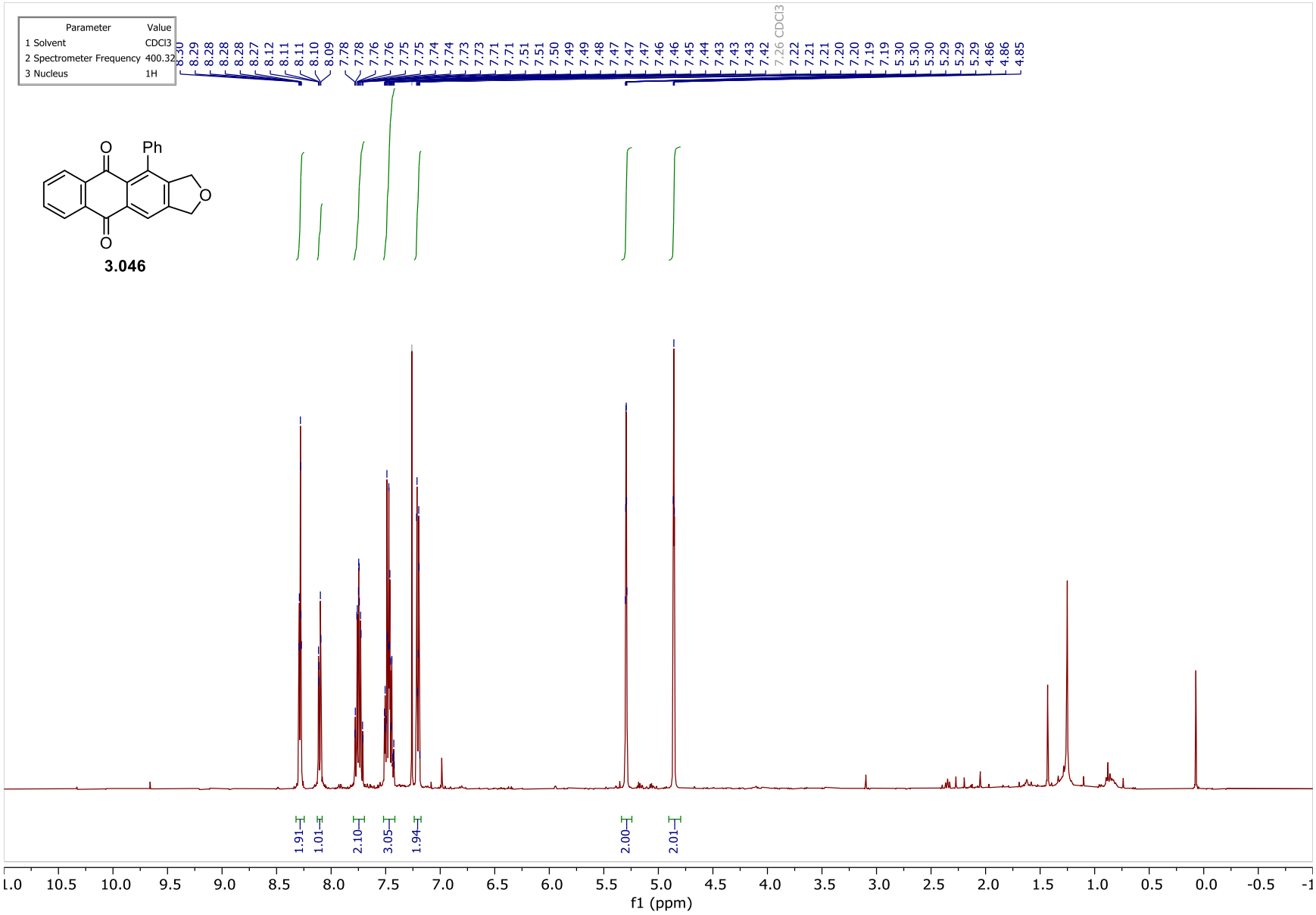
Parameter Value
1 Solvent CDCl3
2 Spectrometer Frequency 400.32
3 Nucleus 1H
O
Ph
O
O
3.046
CDCl3
1.91
1.01
2.10
3.05
1.94
2.00
2.01
f1 (ppm)

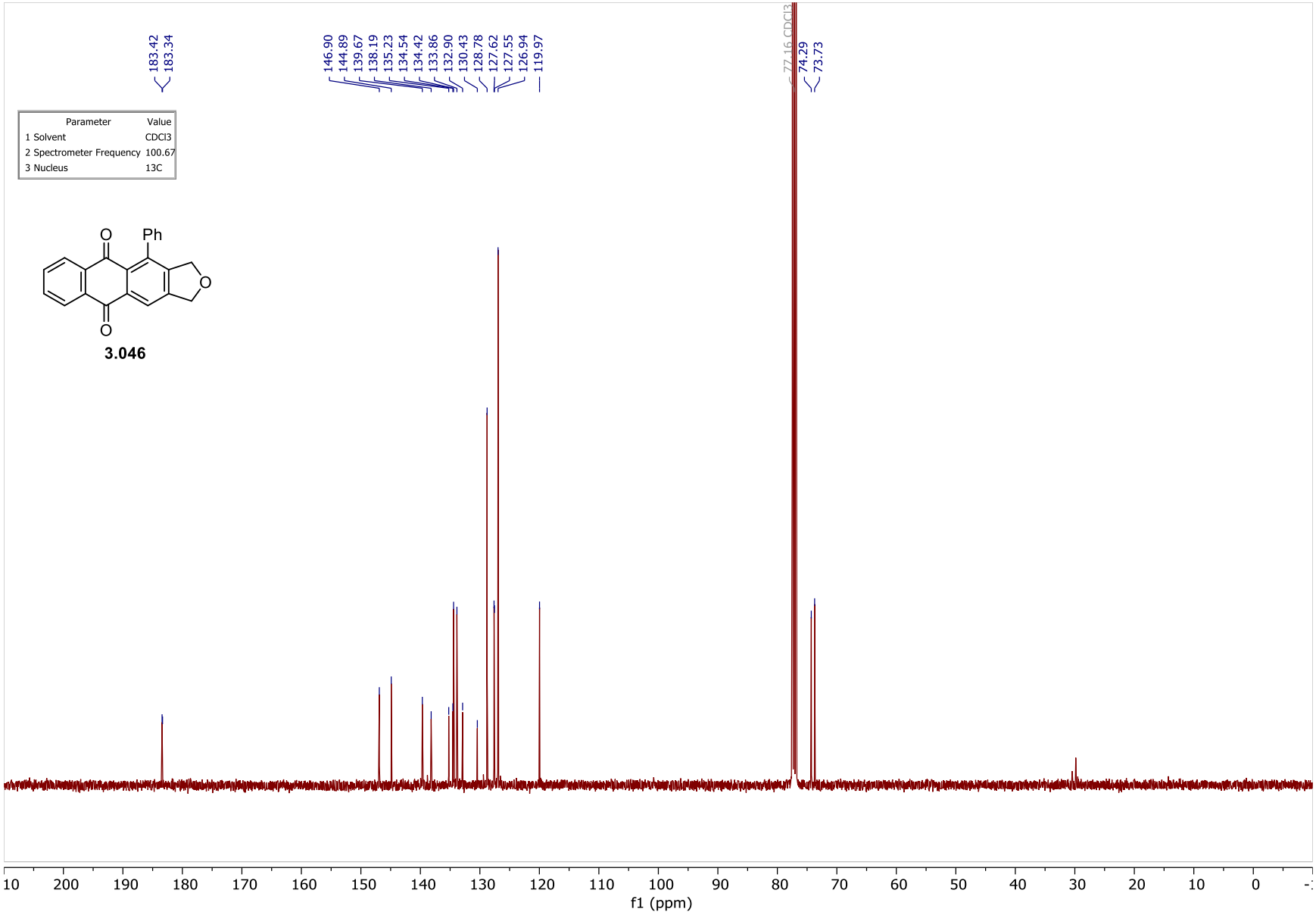
183.42
183.34
146.90
144.89
139.67
138.19
135.23
134.54
134.42
133.86
132.90
130.43
128.78
127.62
127.55
126.94
119.97
77.16 CDCl3
74.29
73.73
Parameter Value
1 Solvent CDCl3
2 Spectrometer Frequency 100.67
3 Nucleus 13C
O
Ph
O
O
3.046
f1 (ppm)

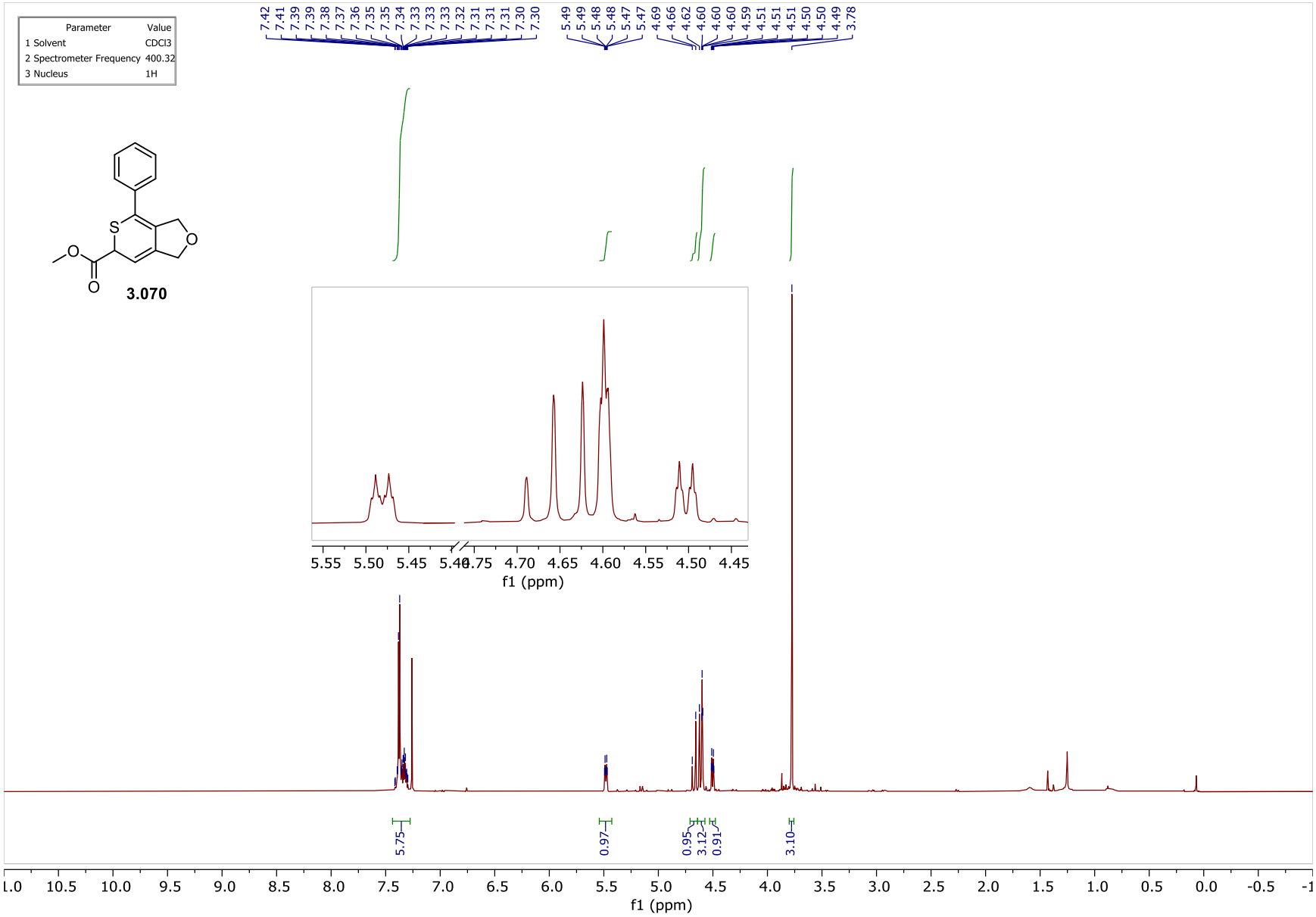
Parameter Value
1 Solvent CDCl3
2 Spectrometer Frequency 400.32
3 Nucleus 1H
3.070
7.42 7.41 7.39 7.39 7.38 7.37 7.36 7.35 7.35 7.34 7.33 7.33 7.33 7.32 7.31 7.31 7.31 7.30 7.30
5.49 5.49 5.48 5.48 5.47 5.47
4.69 4.66 4.62 4.60 4.60 4.60 4.59 4.51 4.51 4.51 4.50 4.50 4.49 3.78
5.75 0.97 0.95 3.12 0.91 3.10
f1 (ppm)

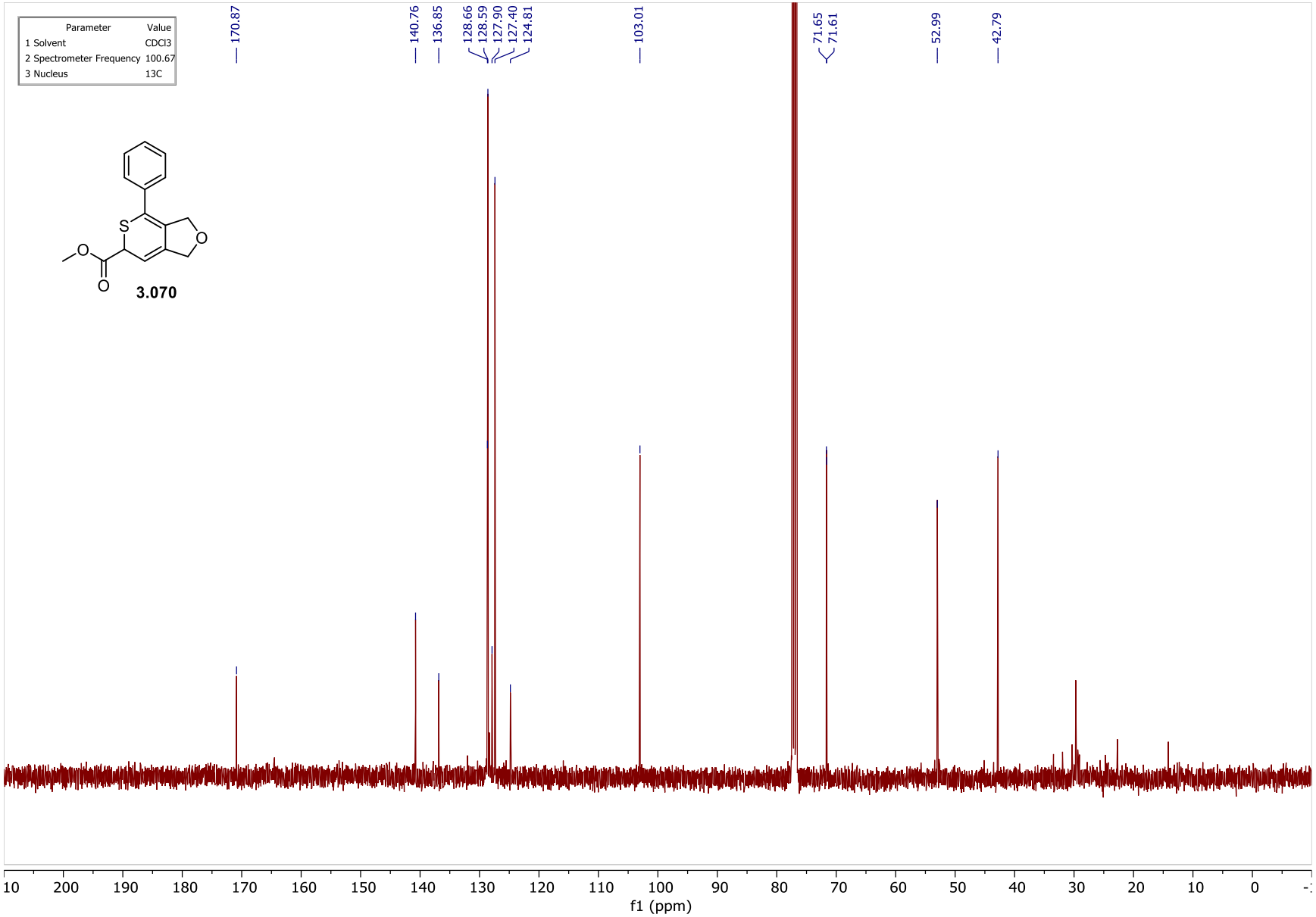
Parameter Value
1 Solvent CDCl3
2 Spectrometer Frequency 100.67
3 Nucleus 13C
170.87
140.76
136.85
128.66
128.59
127.90
127.40
124.81
103.01
71.65
71.61
52.99
42.79
S
O
O
O
3.070
f1 (ppm)

6.3.13. Supplementary NMR spectra for 3.022a & 3.070

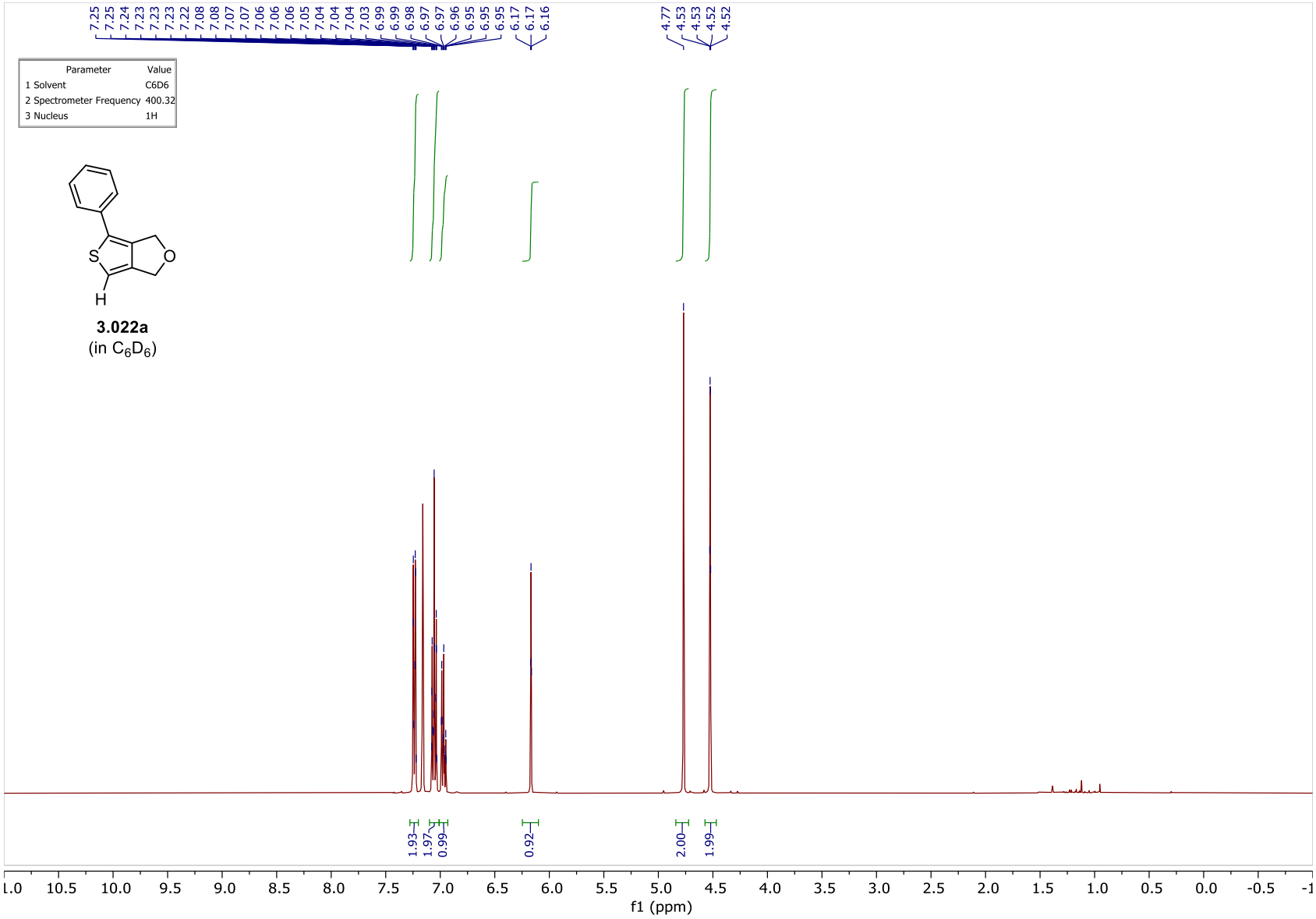

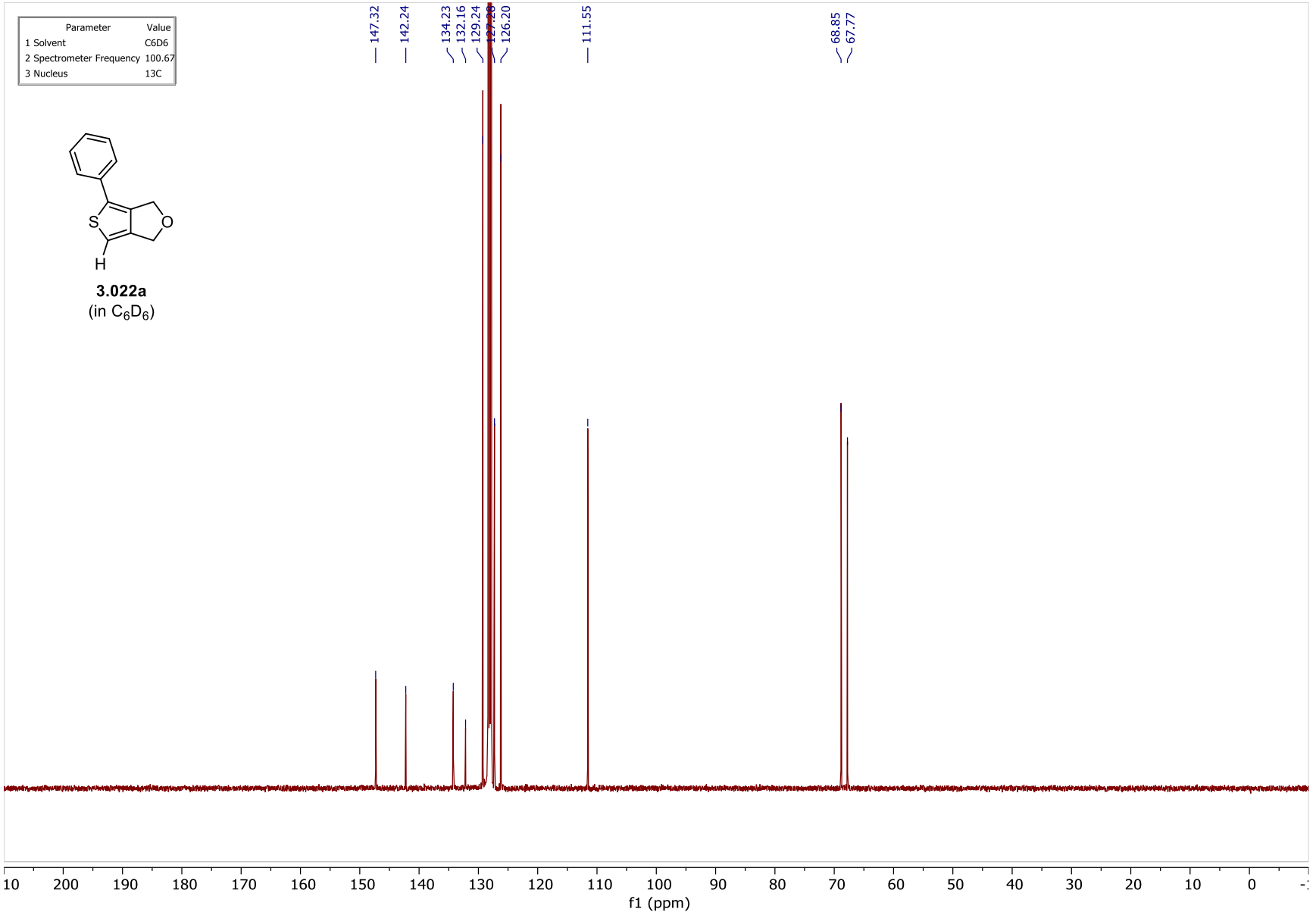
Parameter Value
1 Solvent C6D6
2 Spectrometer Frequency 100.67
3 Nucleus 13C
147.32
142.24
134.23
132.16
129.24
127.26
126.20
111.55
68.85
67.77
S
O
H
3.022a
(in C6D6)
f1 (ppm)

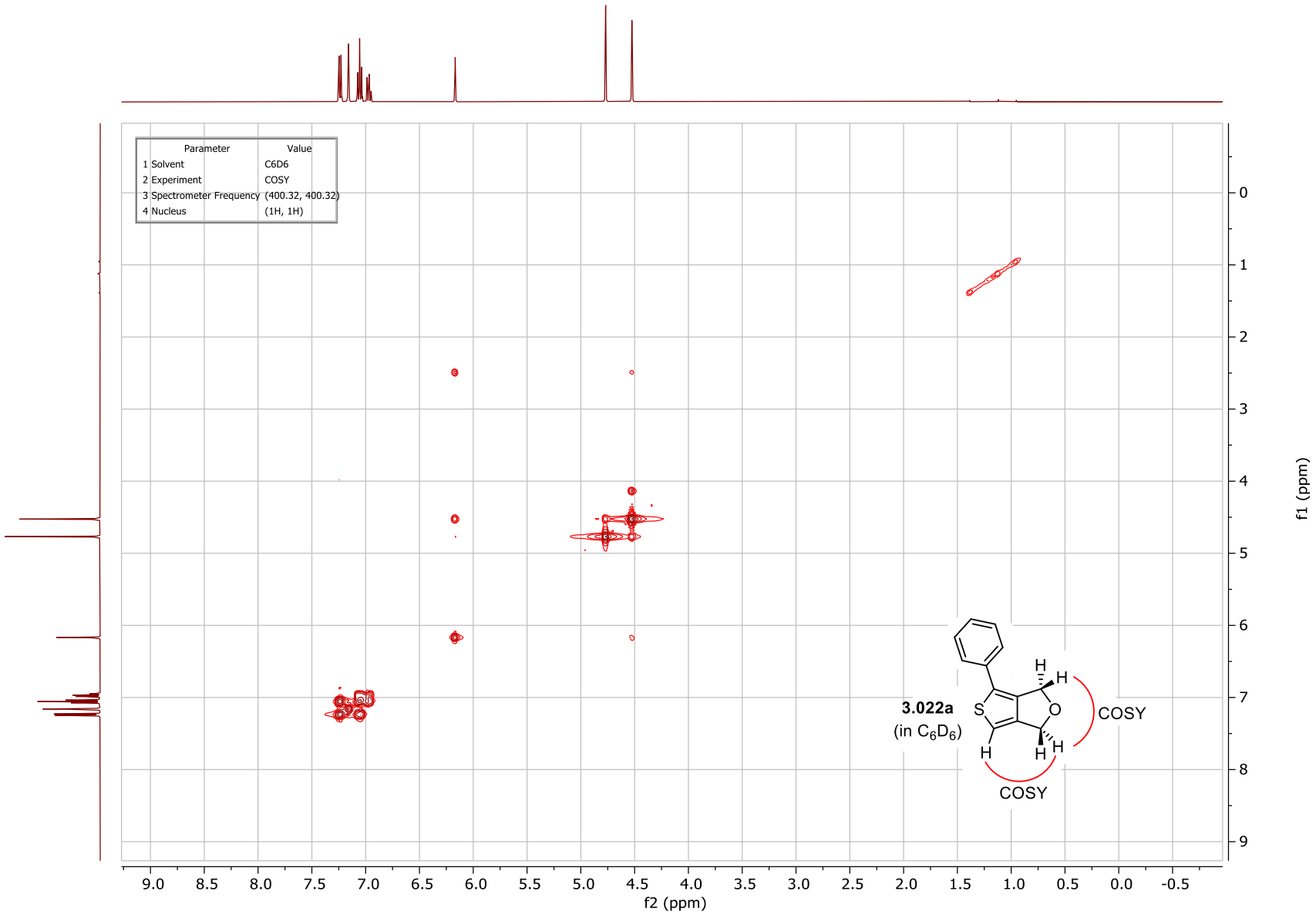
Parameter Value
1 Solvent C6D6
2 Experiment COSY
3 Spectrometer Frequency (400.32, 400.32)
4 Nucleus (1H, 1H)
3.022a
(in C6D6)
COSY
COSY
f2 (ppm)
f1 (ppm)

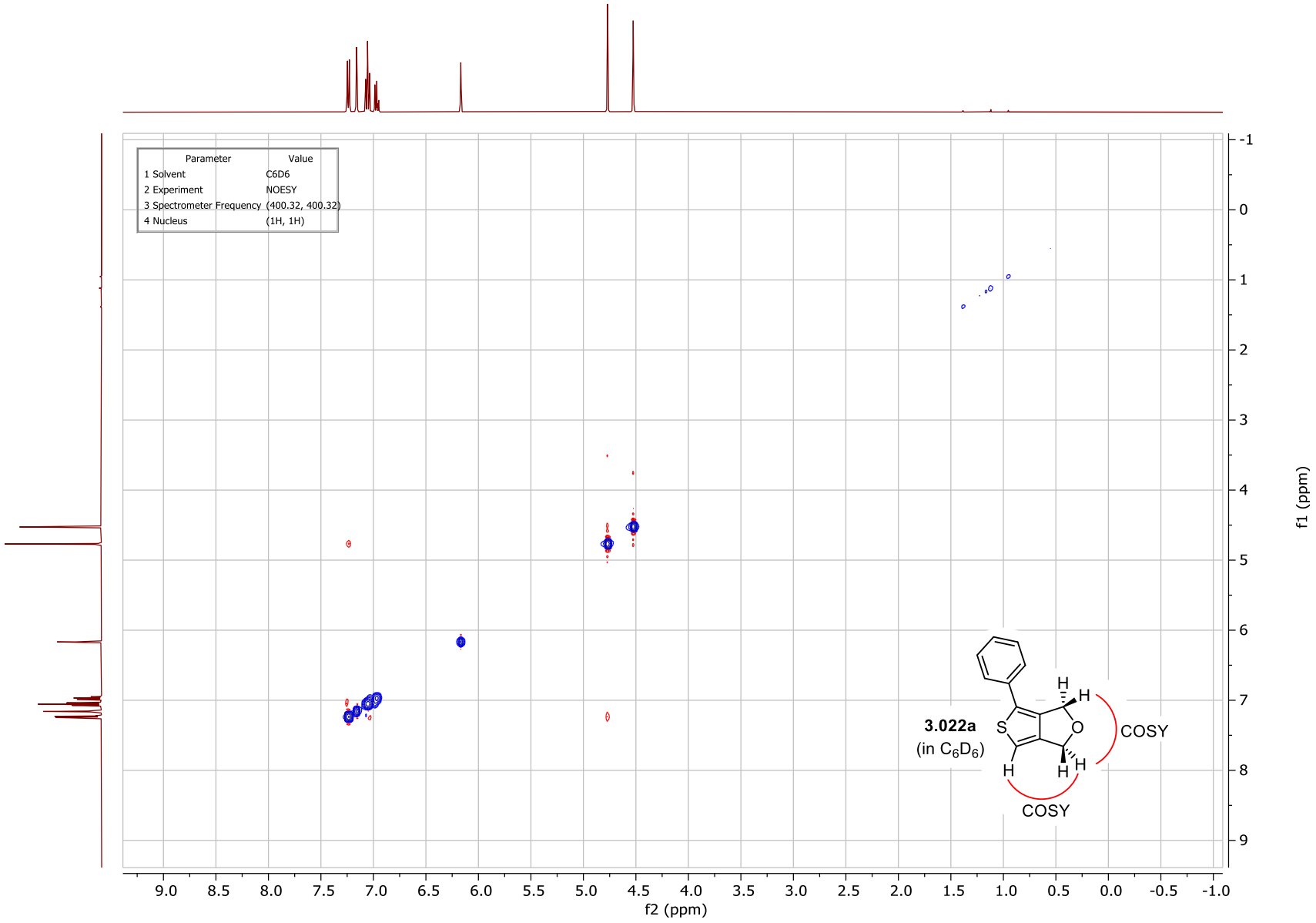
Parameter Value
1 Solvent C6D6
2 Experiment NOESY
3 Spectrometer Frequency (400.32, 400.32)
4 Nucleus (1H, 1H)
3.022a
(in C6D6)
COSY
COSY
f2 (ppm)
f1 (ppm)

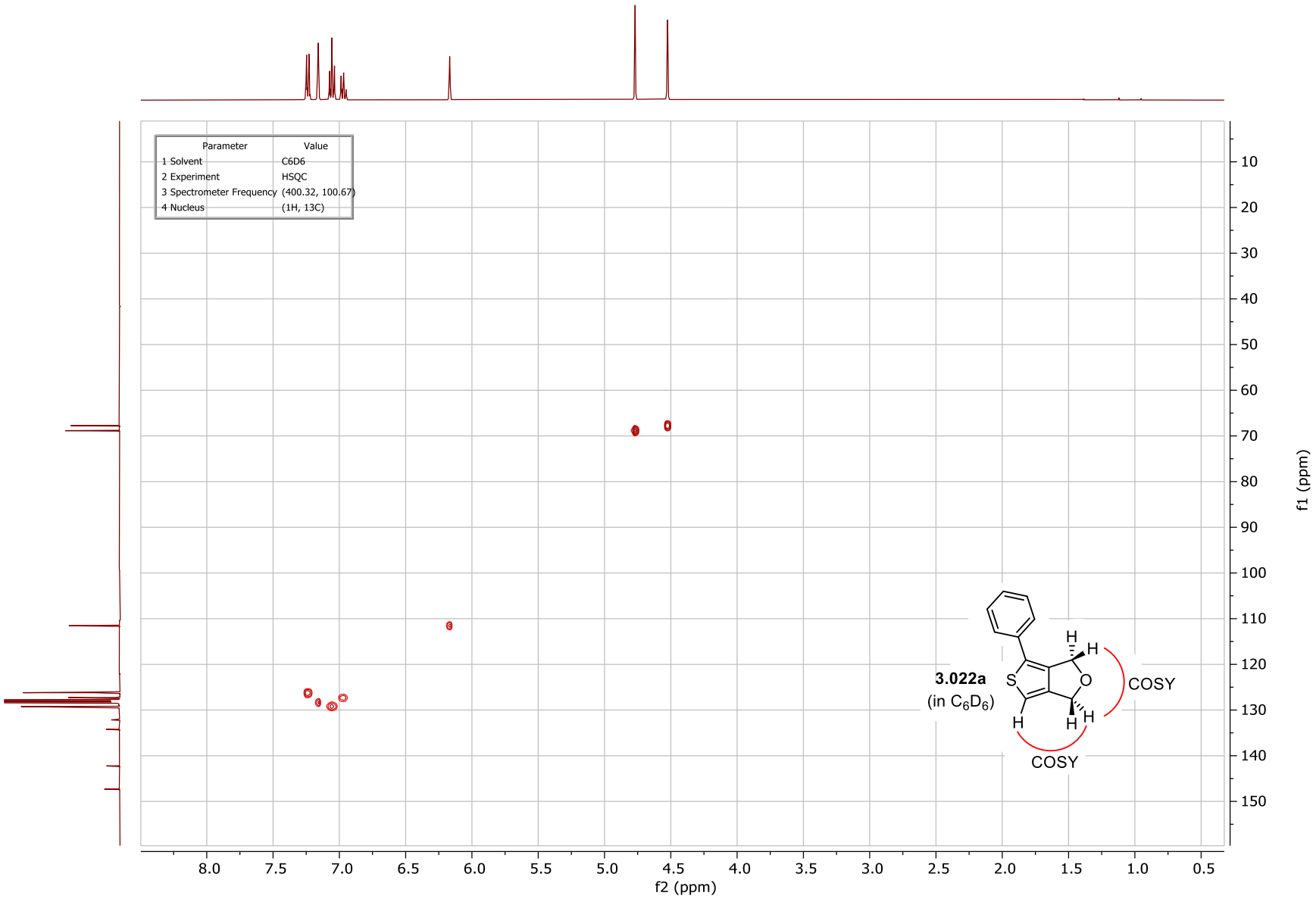
Parameter Value
1 Solvent C6D6
2 Experiment HSQC
3 Spectrometer Frequency (400.32, 100.67)
4 Nucleus (1H, 13C)
f2 (ppm)
f1 (ppm)
3.022a
(in C6D6)
COSY
COSY

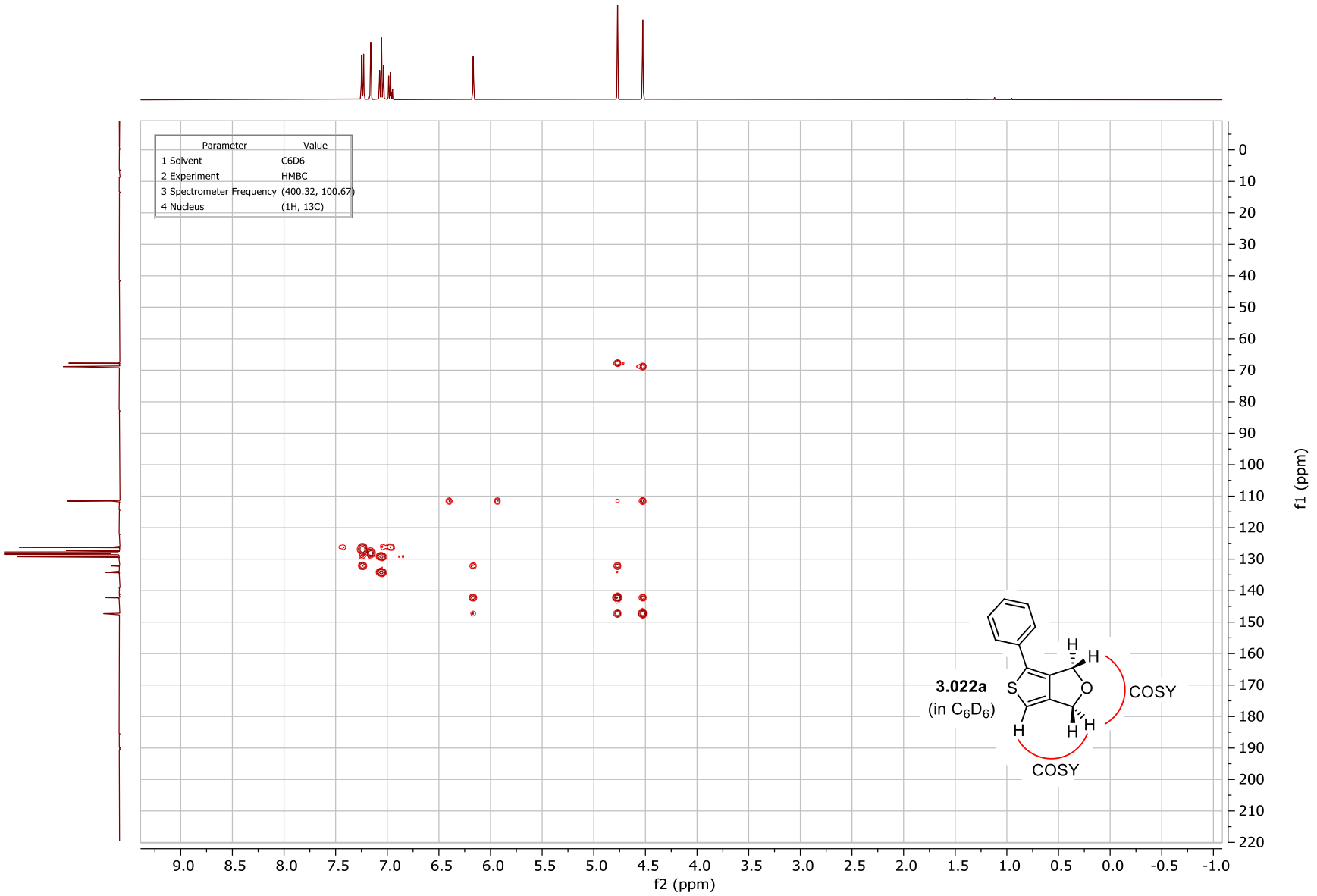
Parameter Value
1 Solvent C6D6
2 Experiment HMBC
3 Spectrometer Frequency (400.32, 100.67)
4 Nucleus (1H, 13C)
f2 (ppm)
f1 (ppm)
3.022a
(in C6D6)
COSY
COSY

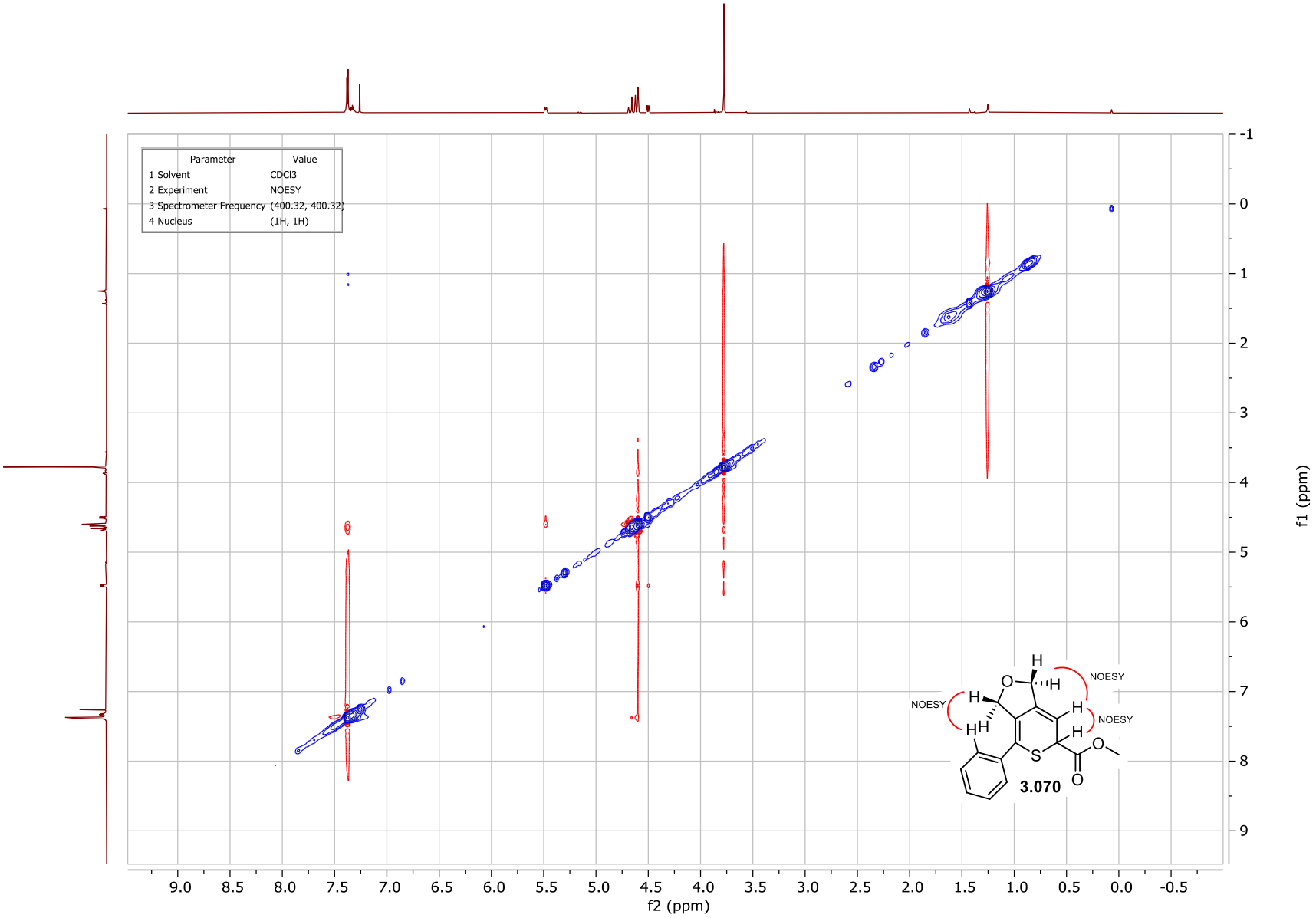
Parameter Value
1 Solvent CDCl3
2 Experiment NOESY
3 Spectrometer Frequency (400.32, 400.32)
4 Nucleus (1H, 1H)
f2 (ppm)
f1 (ppm)
NOESY
NOESY
NOESY
3.070

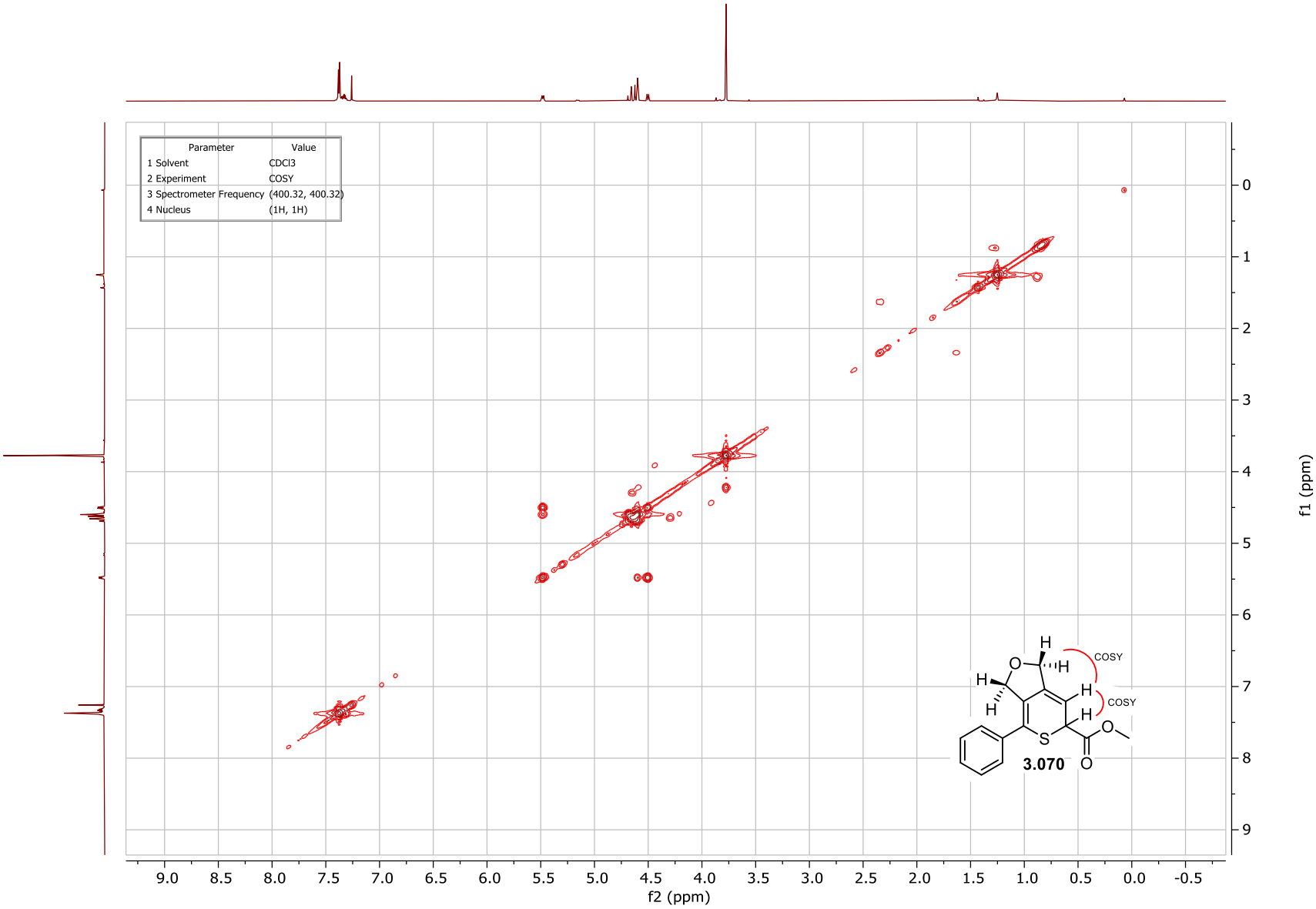
Parameter Value
1 Solvent CDCl3
2 Experiment COSY
3 Spectrometer Frequency (400.32, 400.32)
4 Nucleus (1H, 1H)
f2 (ppm)
f1 (ppm)
COSY
COSY
3.070

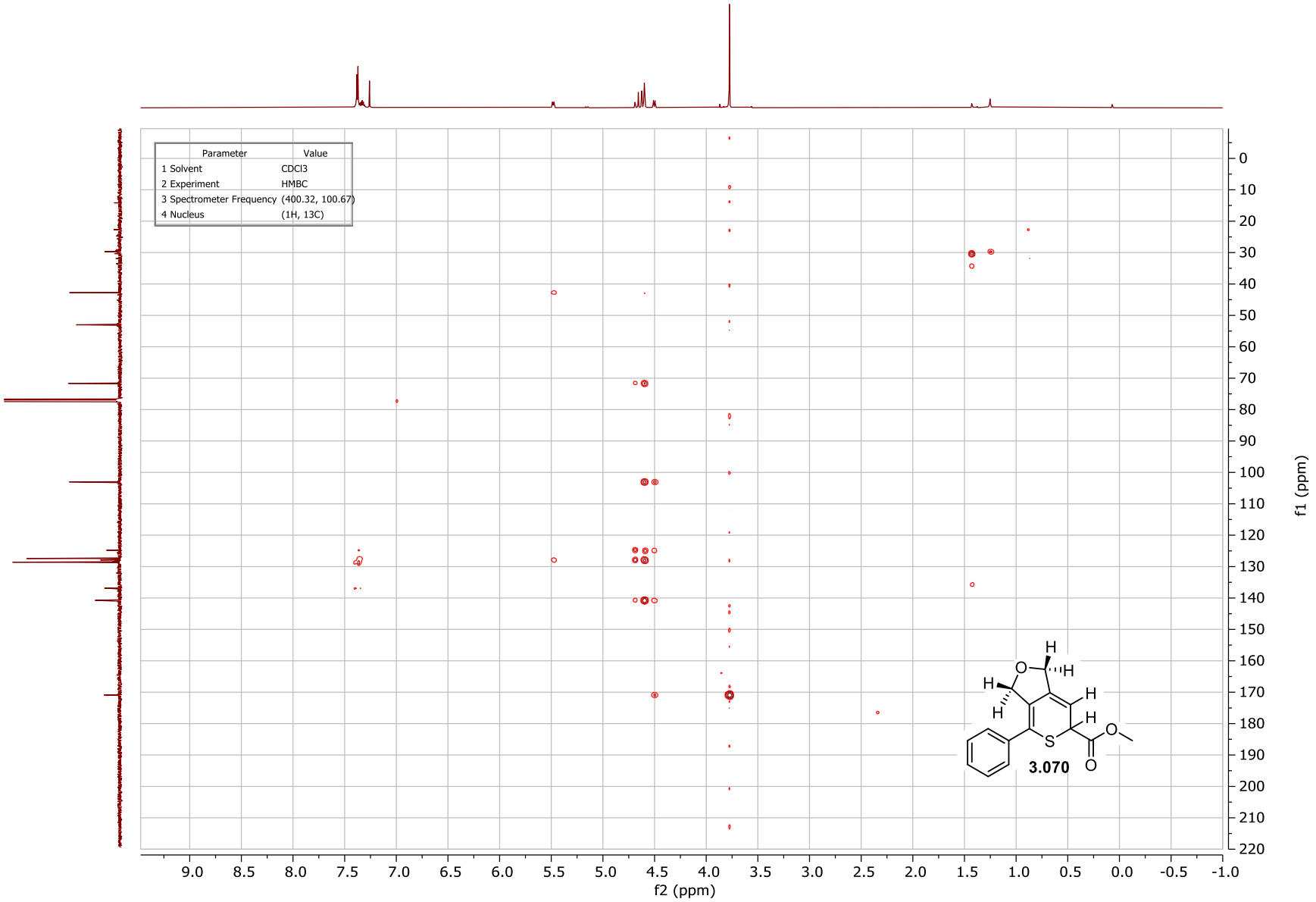
Parameter Value
1 Solvent CDCl3
2 Experiment HMBC
3 Spectrometer Frequency (400.32, 100.67)
4 Nucleus (1H, 13C)
3.070
f2 (ppm)
f1 (ppm)

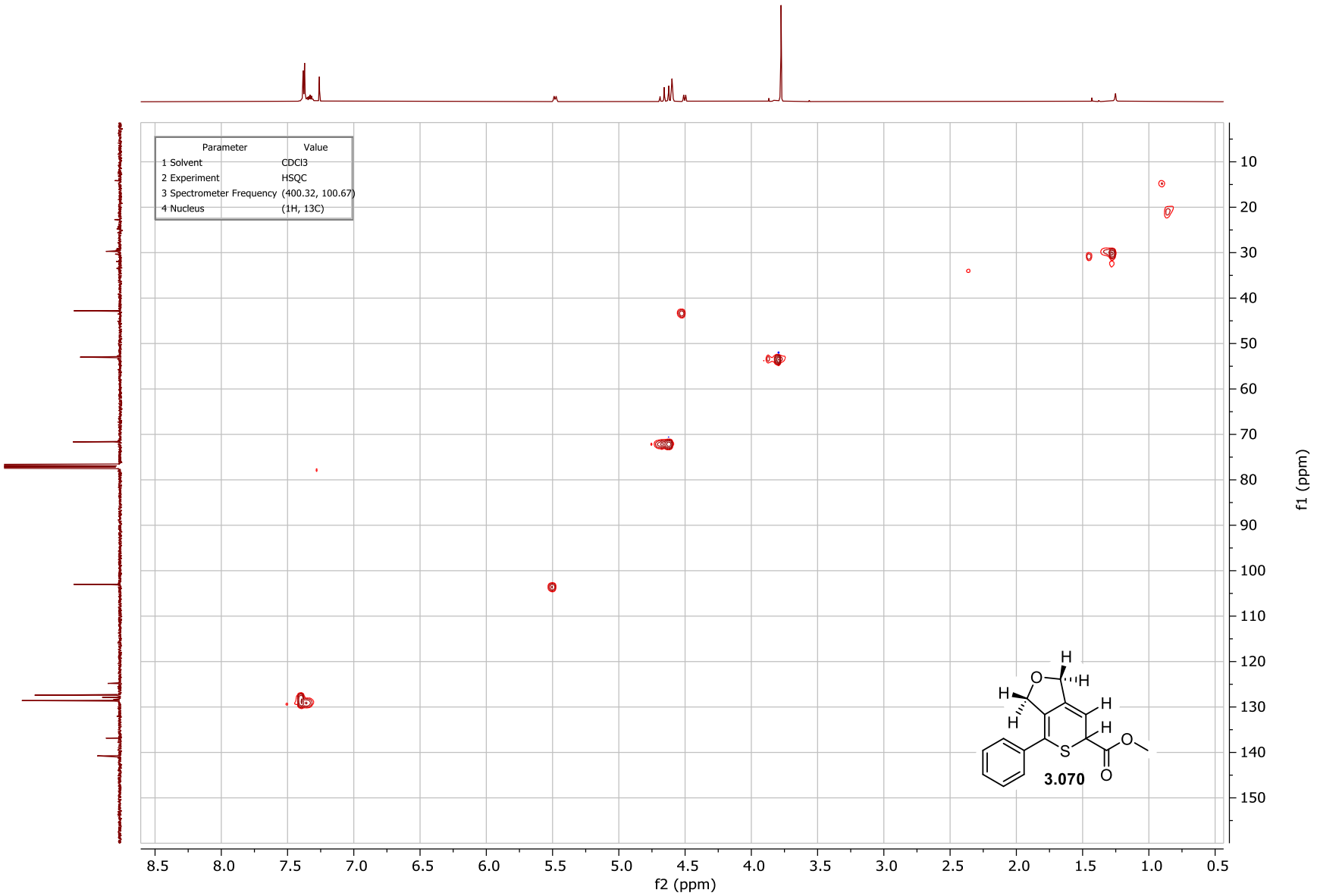
Parameter Value
1 Solvent CDCl3
2 Experiment HSQC
3 Spectrometer Frequency (400.32, 100.67)
4 Nucleus (1H, 13C)
f2 (ppm)
f1 (ppm)
3.070

6.4. Supporting information for Chapter 4

The synthesis of selected scope examples is detailed herein. For synthetic details on all the examples discussed in Chapter 4, please refer to the original publication:

[Campeau, D.; Pommainville, A.; Gorodnichy, M.; Gagosz, F., Copper and Silver Catalysis in the (3+2) Cycloaddition of Neutral Three-Atom Components with Terminal Alkynes. *J. Am. Chem. Soc.* **2023**, *145* (34), 19018-19029].

6.4.1. Reaction parameters in the S-alkyl (3+2) cyclization

Isolated by-products related to the cyclization of substrate (6a)

In the course of the optimization studies for the conversion of **4.012a** to **4.013a**, several by-products were consistently observed. Specifically, by-products **4.014a** and **4.015a**:

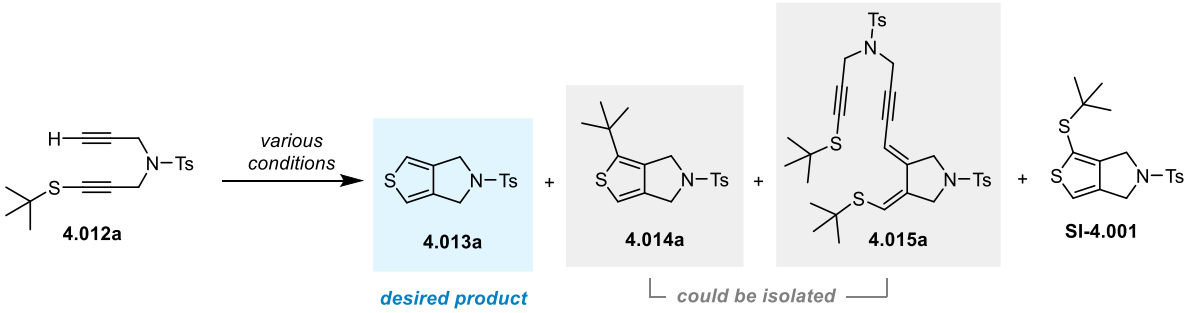

Analytical samples of by-products **4.014a** and **4.015a** were obtained via preparative TLC treatment of crude reaction mixtures from the optimization experiments. Although containing minor impurities, these samples were analyzed by ^{1}H NMR and MS experiments to confirm the proposed structures. (**SI-4.001**) was not obtained in large enough quantity for isolation, but is assumed to be the given structure based on the NMR spectrum and MS analyses of the crude material obtained.

4.014a

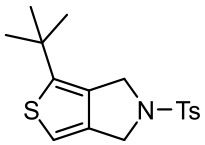

^{1}H NMR (300 MHz, $CDCl_3$) δ 7.79 – 7.70 (m, 2H), 7.34 – 7.30 (m, 2H), 6.96 (s, 1H), 4.43 – 4.40 (d, 2H), 4.38 (s, 2H), 2.42 (s, 3H), 1.30 (s, 9H).

MS-APCI : 131.9 (26%), 142.9 (28%), 144.8 (30%), 152.9 (97%), 179.9 ([M+H-TsH]$^+$, 83%), 195.9 (23%), 198.9 (25%), 200.9 (65%), 221.0 (29%), 221.9 (23%), 257.0 (52%), 279.9 (22%), 307.0 (35%), 336.1 ([M+H]$^+$, 100%), 377.1 ([M+H+CH_3CN]$^+$, 47%).

4.015a

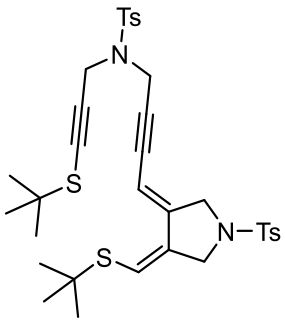

^{1}H NMR (300 MHz, $CDCl_3$) δ 7.74 – 7.67 (m, 4H), 7.33 (d, *J* = 8.2 Hz, 2H), 7.30 (d, *J* = 8.4 Hz, 2H), 6.39 (s, 1H), 5.70 (p, *J* = 2.2 Hz, 1H), 4.35 (d, *J* = 2.2 Hz, 2H), 4.29 (s, 2H), 4.00 (d, *J* = 1.8 Hz, 2H), 3.96 (d, *J* = 2.5 Hz, 2H), 2.43 (s, 3H), 2.40 (s, 3H), 1.37 (s, 9H), 1.33 (s, 9H).

MS-ESI : 693.3 ([M+Na]+, 100%). *(Sole peak above 15% intensity)*

Optimization of reaction parameters for the (3+2) cyclization of substrates of type 4.012.

General procedure for optimization reactions:

In a reaction tube under air is prepared a solution of the yne-alkynyl sulfide substrate (0.05 mmol) and all indicated additives in the indicated solvent (0.50 mL, 0.1 M). The indicated catalyst is added last, and the reaction mixture is stirred at the indicated temperature. At the end of the reported time, the reaction mixture is evaporated to dryness (unless it is DCM), and resuspended in DCM or EtOAc. The suspension is then filtered through a small pad of silica, and eluted with either DCM or EtOAc, to remove the majority of inorganic species. The mixture was then evaporated under reduced pressure to produce a crude that is redissolved in $CDCl_3$ and directly analyzed by ^{1}H NMR analysis using 2.0 µL of 1,2-DBE as NMR standard.

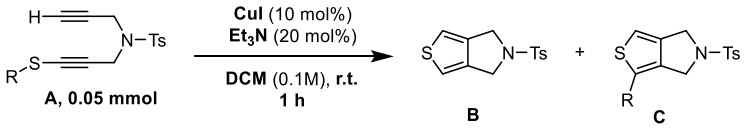

Substrate	R	Catalyst	Consumption A (%)	Yield B (%)	Yield C (%)
4.012a	tBu	CuI	61	22	11
4.012b	Bn	CuI	56	6	4
4.012c	Pr	CuI	76	2	0

Table SI-6.4-1. Evaluation of the S-alkyl substituent.

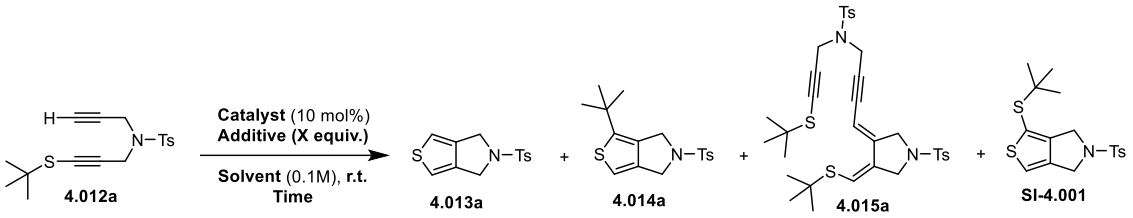

Catalyst	Additive	(X eq.)	Solvent	Time	Cons. 4.012a (%)	Yield 4.013a (%)	Yield 4.014a (%)	Yield 4.015a (%)	Yield SI-4.001 (%)
AgOAc	-	-	DCM	4 h	84	61	15	0	0
AgOPiv	-	-	DCM	1.5 h	100	82	14	0	0
AgOAc	-	-	AcOH	5 min	100	quant.	0	0	0
AgOAc	-	-	EtOH	4 h	100	quant.	2	0	0
AgOTf	-	-	AcOH	3 h	100	0	0	0	0
AgOTf	NaOAc	1.0	AcOH	5 min	100	99	0	0	0
AgOTf	NaOAc	1.0	DCM	1 h	19	1	0	0	0
AgOTf	Et_3N AcOH	0.2 1.0	DCM	1 h	100	quant.	2	0	0
AgOTf	-	-	DCM	1 h	44	1	0	0	0
AgOTf	-	-	DCM	2 h	45	1	0	0	0
AgOTf	Et_3N	0.2	DCM	1 h	98	96	0	0	0
$AgNO_3$	Et_3N	0.2	acetone	3 h	94	83	0	0	0
AgI	Et_3N	0.2	DCM	6 days	6	2	0	0	0
CuOTf[a]	Et_3N	0.2	DCM	1 h	93	47	8	7	0
CuTC	-	-	AcOH	4 h	100	80	7	4	0
IPrCuOTf	Et_3N	0.2	DCM	1 h	13	15	1	0	0
(DMS)AuCl	Et_3N	0.2	DCM	13 h	47	13	5	0	0
$IPrAuNTf_2$	Et_3N	0.2	DCM	17 h	11	0	0	0	0
CuOAc	-	-	AcOH	1 h	100	80	7	6	0
CuOAc	Na-Asc	1.0	AcOH	10 min	100	89	7	3	0
CuI (5 mol%)	Et_3N	1.5	DCM	1 h	100	44	11	12	0
CuI (5 mol%)	Et_3N	0.05	DCM	1 h	60	22	15	2	0
CuI	Et_3N	0.2	DCM	1 h	61	22	11	3	0
Ph_3PCuI	Et_3N	0.05	DCM	4 h	100	46	19	2	1
CuCl	Et_3N	0.2	DCM	1 h	100	20	11	10	1
IPrCuCl	Et_3N	0.1	DCM	41 h	75	56	2	0	0
IPrCuCl	Et_3N AgOTf	0.2 0.1	DCM	1 h	100	91	4	0	0
IPrCuOTf	Et_3N	0.2	DCM	1 h	13	15	1	0	0
IPrCuI	Et_3N	0.2	DCM	3 h	71	38	2	2	1
$Cu(OTf)_2$	Et_3N	0.2	DCM	1 h	6	0	2	0	0
$Cu(OAc)_2$	Et_3N	0.05	DCM	1 h	57	22	9	6	0
$Cu(OAc)_2$	Et_3N	0.2	DCM	1 h	57	23	12	3	0

CuI	Et_3N TMEDA	0.2 0.1	DCM	1 h	100	46	19	4	0
CuI	Et_3N dtbbpy	0.2 0.1	DCM	1 h	100	18	4	1	6
CuI	Et_3N 1,10-phen	0.2 0.1	DCM	1 h	100	14	3	0	6

Table SI-6.4-2. Evaluation of various reaction parameters for substrate **4.012a**. [a]as the $[(CuOTf)_2 \cdot benzene]$ complex

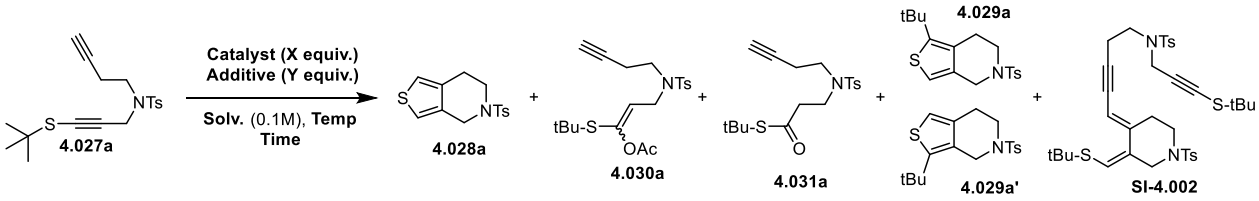

Cat. (X eq.)	Add. (Y eq.)	Solv.	Temp	Time	Cons. 4.027a (%)	4.028a (%)	4.030a (%)	4.031a (%)	4.029a,a' (%)	SI-4.002 (%)
AgOAc (0.1)	-	AcOH	r.t.	22 h	0	0	0	0	0	0
AgOAc (0.1)	-	AcOH	80 °C	7 h	100	0	74	17	0	0
-	-	AcOH	100 °C	3 h	100	0	87	14	0	0
CuOAc (0.1)	Na-Asc (1.0)	AcOH	100 °C	3 h	98	6	72	10	1 (1:1)	0
CuOAc (1.0)	Na-Asc (2.0)	AcOH	100 °C	5 min	100	81	0	0	2 (3:4)	0
CuOAc (0.1)	Na-Asc (1.0)	TFE	80 °C	15 min	100	89	0	0	12 (1:1)	1
CuOAc (0.1)	Na-Asc (1.0) + AcOH (1.0)	EtOH	80 °C	15 min	100	90	0	0	7 (2:1)	1

Table SI-6.4-3. Evaluation of various reaction parameters for substrate **4.027a**.

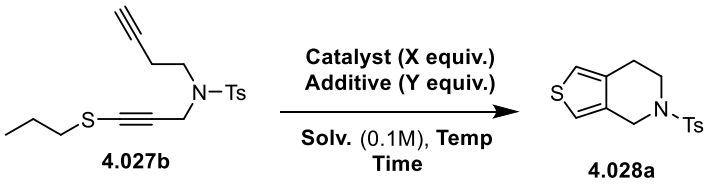

Cat. (X eq.)	Add. (Y eq.)	Solv.	Temp	Time	Cons. 4.027b (%)	4.028a (%)
CuOAc (0.1)	Na-Asc (1.0)	TFE	80 °C	15 min	100	99

	+ AcOH (1.0)					
CuOAc (0.1)	Na-Asc (1.0) + AcOH (1.0)	EtOH	80 °C	15 min	100	87
CuOAc (0.1)	Na-Asc (0.2) + AcOH (1.0)	TFE	80 °C	30 min	98	97
CuOAc (0.1)	Na-Asc (0.2)	TFE	80 °C	30 min	100	80
$Cu(OAc)_2$ (0.1)	Na-Asc (0.2) + AcOH (1.0)	TFE	80 °C	30 min	99	97

Table SI-6.4-4. Evaluation of various reaction parameters for substrate **4.027b**.

6.4.2. Building blocks synthesis

Functionalized bromoalkynes

Preparation of functionalized bromoalkynes:

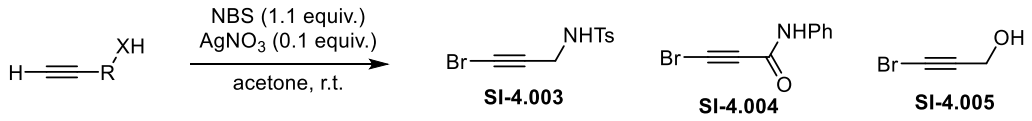

S-alkyl alkynyl sulfide building blocks

*Standard procedure **SP8**: Collins et al.'s method – C-S coupling between alkyl thiols and bromoalkynes*[35]

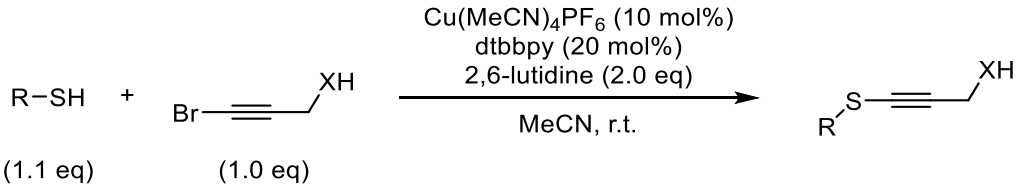

In a round-bottom flask equipped with a stir bar was added the bromoalkyne (1.05 mmol, 1.0 equiv.), 4,4'-di-tert-butyl-2,2'-bipyridine (56.4 mg, 0.210 mmol, 0.2 equiv.), 2,6-lutidine (0.24 mL, 2.10 mmol, 2.0 equiv.) and MeCN (10 mL, 0.1 M). The flask was capped with a septum and the solution was purged with N_2 for 5-10 minutes. The thiol (1.16 mmol, 1.1 equiv.) was added to the solution via syringe.[36] $Cu(MeCN)_4PF_6$ (39.1 mg, 0.105 mmol, 0.1 equiv.) was directly added as a solid (rapidly removing/replacing septum) to the reaction mixture, which immediately took a deep brownish-red

[35] Godin, É.; Santandrea, J.; Caron, A.; Collins, S.K. Org. Lett. **2020**, 22 *(15)*, 5905–5909.
[36] Due to the volatility of small thiols such as tBuSH, it is added after N_2 purging to avoid loss during degassing.

colour. Upon reaction completion (about 15 min, followed by TLC), the reaction took a pale greenish colour. The residual thiol was quenched simply by removing the septum and stirring the reaction under open air for a few hours.[37] The reaction mixture was then concentrated under reduced pressure. The concentrate was filtered through a silica pad (~15mL gel/mmol), eluting with DCM,[38] then concentrated to produce a crude. The crude was purified by either trituration or silica gel chromatography using the indicated eluent system to yield the desired alkynyl sulfide.

SI-4.006

Using standard procedure ***SP8*** with *tert*-butyl thiol and 5.21 mmol of bromoalkyne **SI-4.003**. Solvent system = Hexanes/acetone 4:1. Produced 948 mg (61% yield) of a white solid.

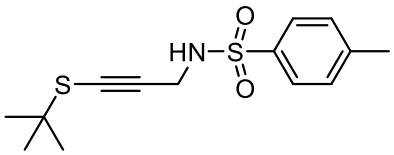

^{1}H NMR (400 MHz, $CDCl_3$) δ 7.77 (d, *J* = 8.4 Hz, 2H), 7.31 (d, *J* = 7.9 Hz, 2H), 4.51 (t, *J* = 5.7 Hz, 1H), 4.01 (d, *J* = 5.9 Hz, 2H), 2.43 (s, 3H), 1.29 (s, 9H).

^{13}C NMR (101 MHz, $CDCl_3$) δ 143.9, 136.8, 129.9, 127.5, 91.0, 75.1, 47.9, 34.6, 30.3, 21.7.

SI-4.007

Using standard procedure ***SP8*** with *tert*-butyl thiol and 2.00 mmol of bromoalkyne **SI-4.004**. Triturated using hexanes/DCM. Produced 398 mg (85% yield) of a beige solid.

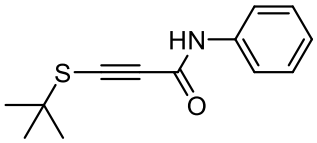

^{1}H NMR (400 MHz, $CDCl_3$) δ 7.51 (d, *J* = 7.5 Hz, 2H), 7.40 – 7.29 (m, 3H), 7.12 (t, *J* = 7.6 Hz, 1H), 1.50 (s, 9H).

^{13}C NMR (101 MHz, $CDCl_3$) δ 150.7, 137.6, 129.2, 124.7, 120.0, 93.0, 81.8, 50.2, 30.6.

<u>S-Aryl alkynyl sulfide building blocks</u>

[37] Likely due either by loss through evaporation or oxidation to the disulfide in the presence of [Cu] and O_2.
[38] This was found to be an excellent and simple way of separating the dtbbpy ligand and lutidine from the product.

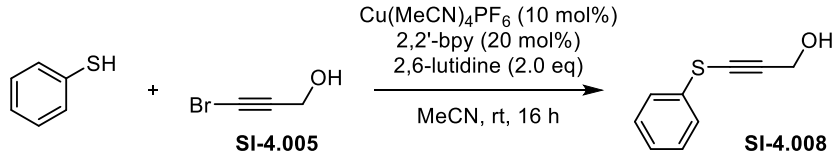

[39]In a flame-dried round bottom flask was added 2,2'-bipyridine[40] (1.16 g, 7.40 mmol, 0.20 equiv.). Three vacuum/N_2 purge cycles were performed to refill the flask with N_2 atmosphere. Thiophenol (4.00 mL, 38.8 mol, 1.05 equiv.), the bromoalkyne **SI-4.005** (5.00 g, 37.0 mmol, 1.00 equiv.), 2.6-lutidine (8.60 mL, 74.0 mmol, 2.00 equiv.), and MeCN (74.0 mL, 0.5 M) were all added to the flask via syringe. The mixture is then degassed with N_2, then $Cu(MeCN)_4PF_6$ (1.38 g, 3.70 mmol, 0.10 equiv.) was added quickly. The mixture is stirred overnight at room temperature then quenched with water and diluted with ethyl acetate. The organic phase was washed three times with 2.5% HCl aq. solution, three times with 10% NH_3 aq. solution, then once with brine. The organic phase was then dried over Mg SO_4, filtered, and concentrated under reduced pressure to produce a crude. The crude was then purified by silica gel chromatography using hexanes/EtOAc 8:2 as the eluent system to yield 4.51 g (74% yield) of **SI-4.008** as a light yellow oil.

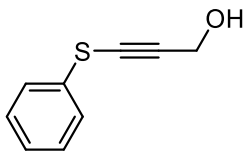

^{1}H NMR (400 MHz, $CDCl_3$) δ 7.44 (dd, *J* = 8.5, 1.2 Hz, 2H), 7.35 (t, *J* = 7.6 Hz, 2H), 7.24 (t, *J* = 7.3 Hz, 1H), 4.51 (s, 2H), 1.71 (s, 1H).

^{13}C NMR (101 MHz, $CDCl_3$) δ 132.4, 129.4, 126.9, 126.6, 97.4, 73.4, 52.2.

S-alkynyl alkynyl sulfide building blocks

SI-4.010

[39] Godin, É.; Santandrea, J.; Caron, A.; Collins, S.K. Org. Lett. **2020**, 22 *(15)*, 5905–5909.
[40] At this point in the project, 2,2'-bipyridine was used instead of 4,4'-di-tert-butyl-2,2'-bipyridine as it is less expensive and we have found that similar yields can be obtained using either ligands. Reaction times tend however to be longer, requiring overnight stirring (seemingly due to solubility issues of the [Cu] complex).

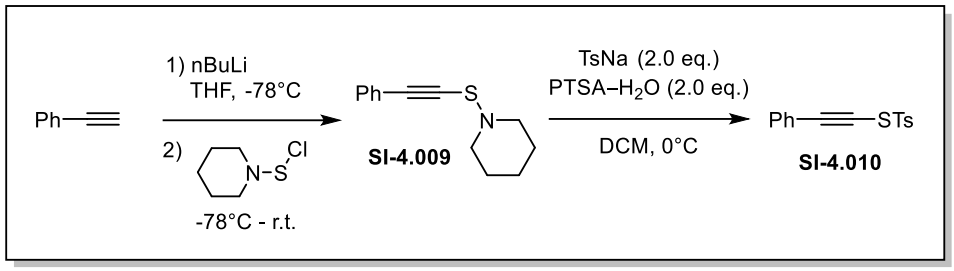

In a flame-dried round bottom flask equipped with a stir bar under N_2 atmosphere was added a solution of phenylacetylene (0.24 mL, 2.21 mmol, 1.0 equiv.) in dry THF (22 mL, 0.1 M) via syringe. The stirred solution was cooled to -78 °C, after which nBuLi (1.1 mL, 2.5 M in hexanes, 2.65 mmol, 1.2 equiv.) was added dropwise. The solution was stirred at -78 °C for 15 min. Then, the *N*-piperidine sulfenyl chloride (368 mg, 2.43 mmol, 1.1 equiv.) was added dropwise as a solution in dry THF (1.0 mL). The reaction solution was stirred at -78 °C for an additional 30 minutes, quenched at -78 °C with H_2O, and then warmed to room temperature. The mixture was diluted with Et_2O, washed once with H_2O, and then once with brine. The organic phase was then dried over $MgSO_4$, filtered and concentrated. The crude product was purified by silica gel chromatography (solvent system = Hexanes/DCM 9:1), producing 356 mg (74% yield) of **SI-4.009** as a pale brown oil.

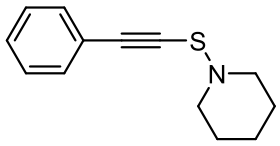

^{1}H NMR (600 MHz, $CDCl_3$) δ 7.49 – 7.43 (m, 2H), 7.36 – 7.29 (m, 3H), 2.99 (t, *J* = 5.6 Hz, 4H), 1.67 (p, *J* = 5.8 Hz, 4H), 1.44 – 1.37 (m, 2H).

^{13}C NMR (151 MHz, $CDCl_3$) δ 131.6, 128.6, 128.5, 123.3, 107.2, 77.3, 57.4, 27.2, 22.9.

A suspension of amino alkynyl sulfide **SI-4.009** (332 mg, 1.53 mmol, 1.0 equiv.) and sodium p-toluenesulfinate (545 mg, 3.06 mmol, 2.0 equiv.) in DCM (15 mL, 0.1 M) was cooled to 0 °C. With vigorous stirring of the suspension, PTSA-H_2O (582 mg, 3.06 mmol, 2.0 equiv.) was added at once. After 5 min at 0 °C, the reaction showed completion by TLC analysis. The suspension was diluted with more DCM. The mixture was then washed twice with H_2O, once with $NaHCO_3$ aq. sat., and once with brine. The organic phase was then dried over $MgSO_4$, filtered and concentrated. The crude product was purified by silica gel chromatography (solvent system = Hexanes/EtOAc 9:1), producing 336 mg (76% yield) of **SI-4.010** as a beige solid.

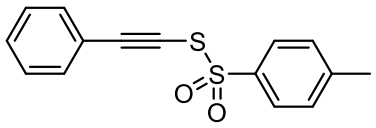

^{1}H NMR (600 MHz, $CDCl_3$) δ 7.89 (d, *J* = 8.4 Hz, 2H), 7.45 – 7.32 (m, 7H), 2.48 (s, 3H).

^{13}C NMR (151 MHz, $CDCl_3$) δ 146.1, 140.6, 132.3, 130.0 (x2), 128.7, 128.1, 121.9, 107.4, 71.7, 22.0.

Other alkynyl building blocks

4.035

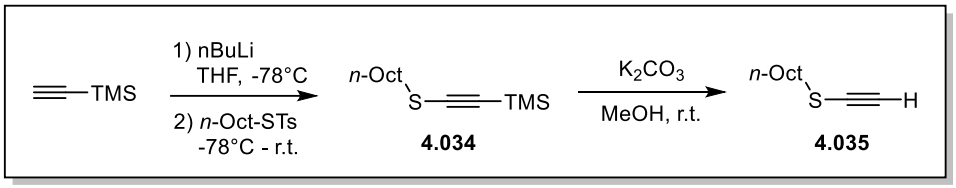

In a flame-dried round bottom flask equipped with a stir bar under N_2 atmosphere was added a solution of trimethylsilylacetylene (1.60 mL, 11.6 mmol, 1.2 equiv.) in dry THF (30 mL, 0.4 M) via syringe. The stirred solution was cooled to -78 °C, after which nBuLi (5.0 mL, 2.3 M in hexanes, 11.6 mmol, 1.2 equiv.) was added dropwise. The solution was stirred at -78 °C for 15 min. Then, (S)-*n*-octyl *p*-tolylthiosulfonate[41] (2.90 g, 9.65 mmol, 1.0 equiv.) was added dropwise. The reaction was then warmed to room temperature, stirred for 30 min, and quenched with NH_4Cl aq. sat. The mixture was then extracted with Et_2O. The organic phase was directly concentrated to provide a crude product **4.034**.

The crude mixture was redissolved in MeOH (100mL, 0.1 M) to which was added K_2CO_3 (2.67 g, 19.3 mmol, 2.0 equiv.). The mixture was stirred vigorously at room temperature for 1 hour. Then, the mixture was concentrated under reduced pressure to remove the majority of the volatiles. The mixture was redissolved in hexanes, washed once with H_2O, then once with brine. The organic phase was dried over $MgSO_4$, filtered and concentrated to directly provide alkynyl sulfide **4.035** (1.43 g, 87% over 2 steps) as a pale yellow oil without any need for additional purification.

[41] Prepared as reported in: *Phosphorus Sulfur Silicon Relat. Elem.* **2015**, *190*, 1934-1941.

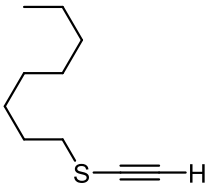

^{1}H NMR (400 MHz, $CDCl_3$) δ 2.75 (s, 1H), 2.73 (t, *J* = 7.8 Hz, 2H), 1.74 (p, *J* = 7.3 Hz, 2H), 1.48 – 1.19 (m, 10H), 0.88 (t, *J* = 6.7 Hz, 3H).

^{13}C NMR (101 MHz, $CDCl_3$) δ 81.9, 74.9, 35.3, 31.9, 29.3 (x2), 29.2, 28.4, 22.8, 14.2.

6.4.3. Yne-alkynyl sulfide substrates synthesis

*Standard procedure **SP9**: Propargylation*

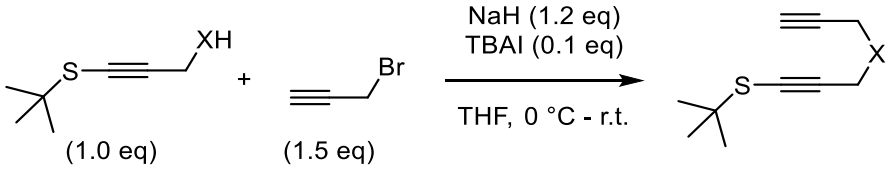

In a flame-dried round bottom flask equipped with a stir bar was added the functionalized alkynyl sulfide derivative (1.00 mmol, 1.0 equiv.) and tetra-*n*-butylammonium iodide (36.9 mg, 0.100 mmol, 0.1 equiv.). The flask was put under three cycles of vacuum/N_2 purge. Dry THF (10 mL, 0.1 M) and propargyl bromide (0.17 mL, 80% w/w toluene sol., 1.50 mmol, 1.5 equiv.) were added via syringe, and the mixture was cooled to 0 °C. NaH (48 mg, 60% w/w, 1.20 mmol, 1.2 equiv.) was rapidly added as a solid, and the mixture was stirred at 0 °C for 15 min, or until evolution of most of the H_2. The mixture was then warmed to room temperature, and stirred to completion (followed by TLC). The reaction mixture was then quenched with saturated aq. NH_4Cl, and diluted with Et_2O. The organic phase was washed sequentially with H_2O and brine, then dried over $MgSO_4$, filtered and concentrated to produce a crude. The crude was purified by silica gel chromatography using the indicated eluent system to yield the desired yne-alkynyl sulfide.

4.016c

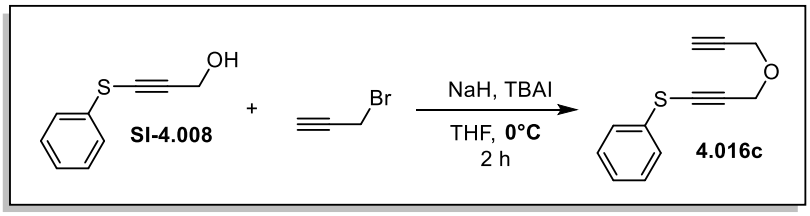

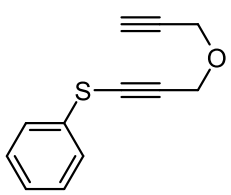

Using standard procedure ***SP9*** (<u>at 0 °C only</u>) with 22.2 mmol of alkynyl sulfide **SI-4.008**. Reaction time = 2 h. Solvent system = Hexanes/Et_2O 98:2. Produced 2.80 g (62% yield) of a pale yellow oil.

^{1}H NMR (400 MHz, $CDCl_3$) δ 7.46 – 7.41 (m, 2H), 7.38 – 7.31 (m, 2H), 7.27 – 7.21 (m, 1H), 4.51 (s, 2H), 4.31 (d, *J* = 2.4 Hz, 2H), 2.48 (t, *J* = 2.4 Hz, 1H).

^{13}C NMR (101 MHz, $CDCl_3$) δ 132.3, 129.4, 126.9, 126.6, 94.6, 79.0, 75.3, 74.6, 57.7, 56.5.

HRMS-EI : Calculated for $C_{12}H_{10}OS$ [M-H]$^+$: 201.0374; found: 201.0368.

4.012a

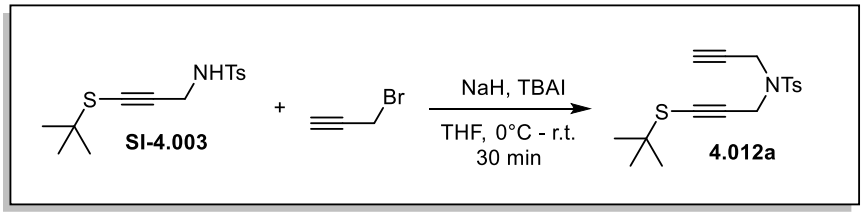

Using standard procedure ***SP9*** with 1.45 mmol of alkynyl sulfide **SI-4.003**. Reaction time = 30 min.

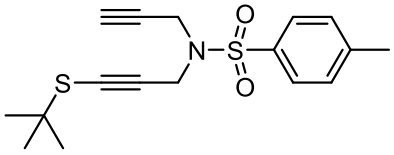

Solvent system = Hexanes/Et_2O 4:1. Produced 435 mg (90% yield) of a white solid.

^{1}H NMR (400 MHz, $CDCl_3$) δ 7.71 (d, *J* = 8.4 Hz, 2H), 7.29 (d, *J* = 8.3 Hz, 2H), 4.34 (s, 2H), 4.15 (d, *J* = 2.2 Hz, 2H), 2.42 (s, 3H), 2.14 (t, *J* = 2.3 Hz, 1H), 1.31 (s, 9H).

^{13}C NMR (101 MHz, $CDCl_3$) δ 144.0, 135.3, 129.8, 128.0, 89.3, 76.5, 76.3, 74.0, 48.0, 37.9, 36.4, 30.3, 21.7.

HRMS-EI : Calculated for $C_{13}H_{12}NO_2S_2$ [M-C_4H_9]: 278.0309; found: 278.0330.

4.012i

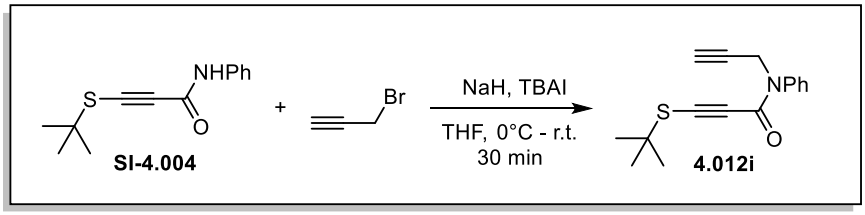

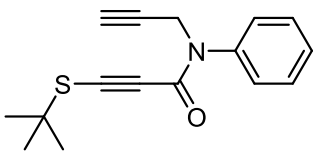

Using standard procedure ***SP9*** with 0.626 mmol of alkynyl sulfide **SI-4.004**. Reaction time = 30 min. Solvent system = Hexanes/Et_2O 7:3. Produced 160 mg (94% yield) of a pale yellow oil.

^{1}H NMR (400 MHz, $CDCl_3$) δ 7.48 – 7.31 (m, 5H), 4.52 (d, *J* = 2.5 Hz, 2H), 2.22 (t, *J* = 2.5 Hz, 1H), 1.08 (s, 9H).

^{13}C NMR (101 MHz, $CDCl_3$) δ 153.3, 141.1, 129.6, 129.0, 128.9, 92.1, 88.6, 78.5, 72.6, 49.6, 37.8, 30.3.

HRMS-EI : Calculated for $C_{12}H_8NOS$ [M-C_4H_9]: 214.0327; found: 214.0351.

4.027d

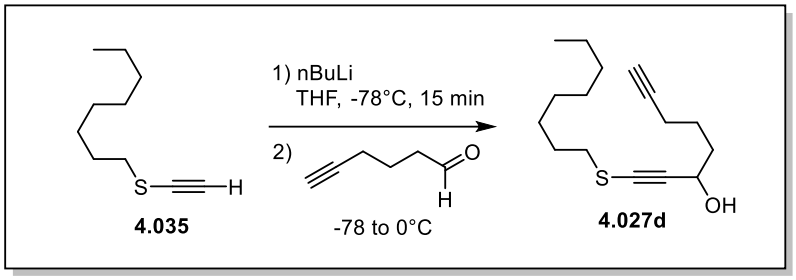

In a flame-dried round bottom flask equipped with a stir bar under N_2 atmosphere was added a solution of alkyne **4.035** (1.43 g, 8.40 mmol, 1.1 equiv.) in dry THF (30 mL, 0.3 M) via syringe. The stirred solution was cooled to -78 °C, after which nBuLi (3.7 mL, 2.3 M in hexanes, 8.4 mmol, 1.1 equiv.) was added dropwise. The solution was stirred at -78 °C for 15 min. Then, hex-5-ynal[42] (807 mg, 7.64 mmol, 1.0 equiv.) was added via syringe. The solution was then warmed to 0 °C, stirred for 10 min, and quenched with NH_4Cl aq. sat. The mixture was diluted with Et_2O, washed once with H_2O, and then once with brine. The organic phase was then dried over $MgSO_4$, filtered and concentrated to produce a crude. The crude product was purified by silica gel chromatography. Solvent system = Hexanes/EtOAc 17:3. Produced 1.49 g (74% yield) of **4.027d** a pale yellow oil.

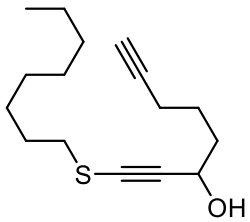

^{1}H NMR (400 MHz, $CDCl_3$) δ 4.55 – 4.46 (m, 1H), 2.70 (t, *J* = 7.3 Hz, 2H), 2.25 (td, *J* = 6.9, 2.6 Hz, 2H), 1.96 (t, *J* = 2.6 Hz, 1H), 1.90 – 1.77 (m, 3H), 1.76 – 1.65 (m, 4H), 1.46 – 1.35 (m, 2H), 1.35 – 1.20 (m, 8H), 0.87 (t, *J* = 6.8 Hz, 3H).

[42] Prepared as previously described in: *Org. Lett.* **2010**, *12*, 2330-2333.

^{13}C NMR (101 MHz, $CDCl_3$) δ 94.4, 84.1, 76.2, 68.9, 63.0, 36.8, 35.6, 31.9, 29.4, 29.3, 29.2, 28.4, 24.3, 22.8, 18.2, 14.2.

HRMS-EI : Calculated for $C_{16}H_{26}OS$ [M]: 266.1704; found: 266.1684.

4.065

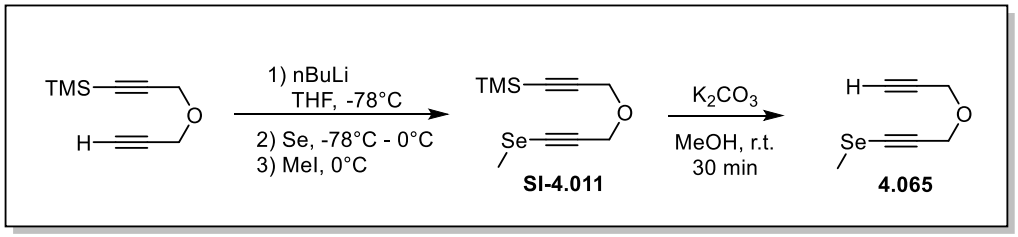

In a flame-dried round bottom flask equipped with a stir bar under N_2 atmosphere was added a solution of trimethylsilyl-protected dipropargyl ether[43] (159 mg, 0.851 mmol, 1.0 equiv.) in dry THF (5.0 mL, 0.1 M) via syringe. The stirred solution was cooled to -78 °C, after which nBuLi (0.37 mL, 2.5 M in hexanes, 0.55 mmol, 1.1 equiv.) was added dropwise. The solution was stirred at -78 °C for 15 min. Then, black selenium powder (100 mesh) (67.2 mg, 0.851 mmol, 1.0 equiv.) was directly added. The reaction solution was then warmed to 0 °C and stirred for 20 min (after which consumption of the alkyne could be observed by TLC). Then, methyl iodide (64 µL, 1.0 mmol, 1.2 equiv.) was added via syringe, and the mixture was stirred at 0 °C for an additional 5 min (after which full consumption of the intermediate alkynyl selenide salt was indirectly observed by TLC). The mixture was then quenched with NH_4Cl aq. sat. The mixture was diluted with Et_2O, washed once with H_2O, and then once with brine. The organic phase was then dried over $MgSO_4$, filtered and concentrated to produce **SI-4.011** as a crude mixture.

The crude was redissolved in MeOH (8.0 mL, 0.1 M), to which was added K_2CO_3 (213 mg, 1.54 mmol, 2.0 equiv.). The reaction mixture was stirred at room temperature for 30 min (after which completion was seen by TLC analysis). The mixture was then diluted with Et_2O, filtered through celite, and carefully concentrated under reduced pressure (the product seems to be slightly volatile!). The crude product was finally purified by silica gel chromatography (solvent system = Hexanes/Et_2O 49:1→19:1), producing 89.3 mg (56% yield over 2 steps) of **4.065** as a pale yellow oil.

[43] Prepared as previously described in: *Org. Lett.* **2007**, *9*, 505-508.

^{1}H NMR (300 MHz, $CDCl_3$) δ 4.37 (s, 2H), 4.25 (d, *J* = 2.4 Hz, 2H), 2.44 (t, *J* = 2.4 Hz, 1H), 2.30 (s, 3H).

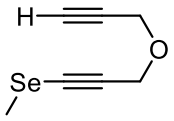

^{13}C NMR (76 MHz, $CDCl_3$) δ 94.4, 79.1, 75.0, 69.6, 57.8, 56.4, 9.6.

^{77}Se NMR (57 MHz, $CDCl_3$) δ 73.3.

HRMS-EI : Calculated for C_7H_8OSe [M]: 187.9740; found: 187.9758.

4.025

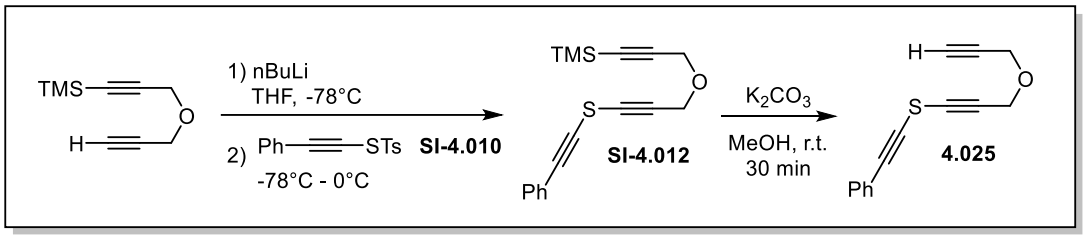

In a flame-dried round bottom flask equipped with a stir bar under N_2 atmosphere was added a solution of trimethylsilyl-protected dipropargyl ether (91.0 mg, 0.547 mmol, 1.1 equiv.) in dry THF (5.0 mL, 0.1 M) via syringe. The stirred solution was cooled to -78 °C, after which nBuLi (0.22 mL, 2.5 M in hexanes, 0.55 mmol, 1.1 equiv.) was added dropwise. The solution was stirred at -78 °C for 15 min. Then, the thiosulfonate **SI-4.010** (143 mg, 0.497 mmol, 1.0 equiv.) was added dropwise via syringe as a solution in dry THF (1.0 mL). The reaction solution was then warmed to 0 °C, stirred for 10 min, and quenched with NH_4Cl aq. sat. The mixture was diluted with Et_2O, washed once with H_2O, and then once with brine. The organic phase was then dried over $MgSO_4$, filtered and concentrated to produce **SI-4.012** as a crude mixture.

The crude was redissolved in MeOH (5.0 mL, 0.1 M), to which was added K_2CO_3 (137 mg, 0.994 mmol, 2.0 equiv.). The reaction mixture was stirred at room temperature for 30 min (after which completion was seen by TLC analysis). The mixture was then concentrated under reduced pressure, and diluted with Et_2O. The solution was washed once with H_2O, then once with brine. The organic phase was then dried over $MgSO_4$, filtered, and concentrated. The crude product was finally purified by silica gel chromatography (solvent system = Hexanes/EtOAc 49:1→19:1), producing 70.7 mg (63% yield over 2 steps) of **4.025** as a pale yellow oil.

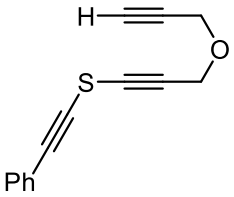

^{1}H NMR (400 MHz, $CDCl_3$) δ 7.51 – 7.42 (m, 2H), 7.39 – 7.29 (m, 3H), 4.41 (s, 2H), 4.28 (d, *J* = 2.4 Hz, 2H), 2.47 (t, *J* = 2.4 Hz, 1H).

^{13}C NMR (101 MHz, $CDCl_3$) δ 132.1, 129.3, 128.5, 122.2, 95.0, 91.7, 78.8, 75.4, 71.5, 71.2, 57.5, 56.7.

HRMS-EI : Calculated for $C_{14}H_{10}OS$ [M]: 226.0452; found: 226.0452.

6.4.4. Copper- or silver-catalyzed (3+2) procedures

<u>Using S-alkyl alkynyl sulfides</u>

*Standard procedure **SP10a**: Silver-catalyzed yne-alkynyl sulfide (3+2) cyclization*

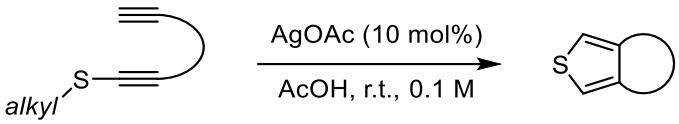

In a reaction tube equipped with a stir bar was dissolved the yne-alkynyl sulfide substrate (0.200 mmol, 1.0 equiv.) in glacial acetic acid (2.0 mL, 0.1 M). AgOAc (3.3 mg, 0.020 mmol, 0.1 equiv.) was added, and the reaction mixture was stirred at room temperature to completion (followed by TLC, first analysis always being done after 5 minutes). The solution was then concentrated under reduced pressure to produce a crude. The crude was purified by silica gel chromatography using the indicated eluent system to yield the desired thiophene product.

*Standard procedure **SP10b**: Copper-catalyzed yne-alkynyl sulfide (3+2) cyclization at 80 °C*

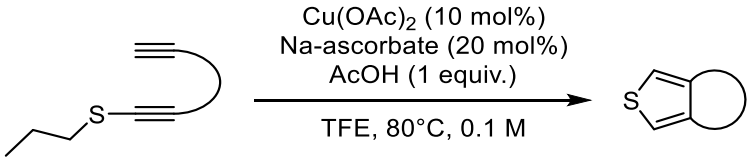

In a sealed reaction tube equipped with a stir bar was added the yne-alkynyl sulfide substrate (0.100 mmol, 1.0 equiv.), copper(II) acetate (1.8 mg, 0.010 mmol, 0.1 equiv.), sodium ascorbate (4.0 mg, 0.020 mmol, 0.2 equiv.), glacial acetic acid (5.7 µL, 0.10 mmol, 1.0 equiv.) and TFE (1.0 mL, 0.1M). The reaction mixture was stirred and heated in an oil bath set to 80 °C to completion (followed by

TLC, first analysis always being done after 5 minutes). The mixture was then concentrated under reduced pressure to produce a crude. The crude was purified by silica gel chromatography using the indicated eluent system to yield the desired thiophene product.

Notes:

- *At small scale, a sealed tube and higher oil bath temperature were used to maintain higher reaction rates. At larger scales, it would be recommended to use a set-up and/or conditions better suited to handle or avoid pressure buildups.*
- *Copper(II) acetate granules are poorly soluble in TFE at room temperature, but dissolve in the reaction mixture within a few minutes.*

(7a)

Using standard procedure ***SP10a*** with 0.200 mmol of yne-alkynyl sulfide **4.012a**. Reaction time = 5 min. Solvent system = Hexanes/Et_2O 7:3. Produced 52.9 mg (95% yield) of a white solid.

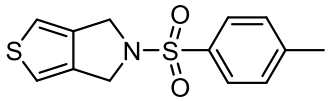

^{1}H NMR (400 MHz, $CDCl_3$) δ 7.75 (d, *J* = 8.3 Hz, 2H), 7.32 (d, *J* = 8.0 Hz, 2H), 6.88 (s, 2H), 4.39 (s, 4H), 2.41 (s, 3H).

^{13}C NMR (101 MHz, $CDCl_3$) δ 143.9, 140.2, 133.9, 130.0, 127.7, 115.4, 49.1, 21.6.

HRMS-EI : Calculated for $C_{13}H_{13}NO_2S_2$ [M]: 279.0388; found: 279.0383.

(7i)

Using standard procedure ***SP10a*** with 0.210 mmol of yne-alkynyl sulfide **4.012i**. Reaction time = 5 min. Solvent system = Hexanes/EtOAc gradient of 17:3 → 4:1. Produced 36.4 mg (81% yield) of **4.013i** as a white solid. The rest of the mass balance seems to have gone to a diene by-product **4.064**, of which an analytically pure fraction was isolated alongside.

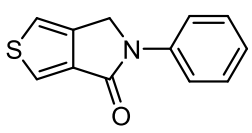

^{1}H NMR (400 MHz, $CDCl_3$) δ 7.84 (d, *J* = 2.4 Hz, 1H), 7.81 – 7.73 (m, 2H), 7.46 – 7.36 (m, 2H), 7.22 – 7.13 (m, 1H), 4.75 (d, *J* = 1.2 Hz, 2H).

^{13}C NMR (101 MHz, $CDCl_3$) δ 162.4, 140.1, 140.0, 139.4, 129.2, 124.8, 123.1, 119.8, 116.4, 48.2.

HRMS-EI : Calculated for $C_{12}H_9NOS$ [M]: 215.0405; found: 215.0430.

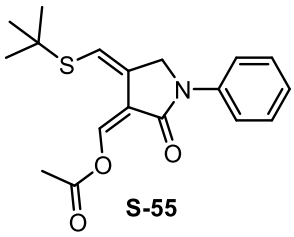

S-55

^{1}H NMR (400 MHz, $CDCl_3$) δ 7.84 – 7.76 (m, 3H), 7.72 (s, 1H), 7.45 – 7.35 (m, 2H), 7.20 – 7.12 (m, 1H), 4.53 (d, *J* = 2.5 Hz, 2H), 2.26 (s, 3H), 1.52 (s, 9H).

^{13}C NMR (101 MHz, $CDCl_3$) δ 167.0, 166.1, 139.5, 132.1, 131.0, 129.1, 124.6, 122.0, 119.4, 116.0, 47.6, 47.1, 31.2, 20.8.

COSY, **HSQC**, **HMBC** and **NOESY** experiments were also done and the spectra are provided.

4.028d

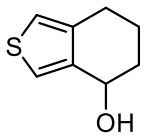

Using standard procedure ***SP10b*** with 0.0938 mmol of yne-alkynyl sulfide **4.027d**. Reaction time = 15 min. Solvent system = Hexanes/EtOAc 9:1→17:3. Produced 11.4 mg (79% yield) of a beige solid.

^{1}H NMR (400 MHz, $CDCl_3$) δ 7.31 (d, *J* = 2.9 Hz, 1H), 6.89 (dt, *J* = 2.9, 1.4 Hz, 1H), 4.86 – 4.79 (m, 1H), 2.81 – 2.62 (m, 2H), 2.07 – 1.89 (m, 2H), 1.83 – 1.63 (m, 3H).

^{13}C NMR (101 MHz, $CDCl_3$) δ 142.0, 138.1, 122.4, 119.7, 66.9, 33.3, 25.8, 20.1.

HRMS-EI : Calculated for $C_8H_{10}OS$ [M]: 154.0452; found: 154.0466.

<u>Using S-aryl alkynyl sulfides</u>

*Standard procedure **SP11**: Silver-catalyzed yne-(S-aryl)alkynyl sulfide (3+2) cyclization/rearrangement sequence*

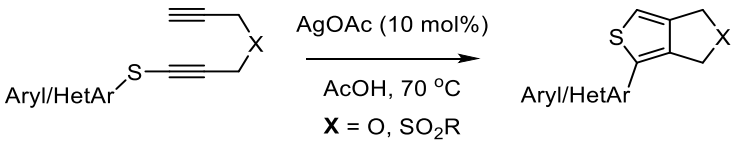

In a sealed reaction vial was added a solution of yne-alkynyl sulfide (0.0500 – 0.200 mmol, 1.0 equiv.) in acetic acid (0.05-0.2 M). AgOAc (0.1 equiv.) was then added to the mixture. The solution was

heated in an oil bath at 70 °C for the indicated time. Upon completion (determined by TLC – see below), the mixture is evaporated under reduced pressure to produce a crude. The crude was then purified by silica gel chromatography using the indicated eluent system (unless otherwise noted) to yield the desired 2-substituted thiophene.

Following the reaction by TLC (ex. derivative **4.016a**): The TLCs are stained with a para-anisaldehyde (PA) based staining solution where both the thiophenium intermediate (ex. **4.017a-OAc**) and the neutral 2-substituted thiophene (ex. **4.018a**) typically stain as bright blue/purple color. The reaction is determined to be completed when the thiophenium intermediate (ex. **4.017a-OAc**) is consumed.

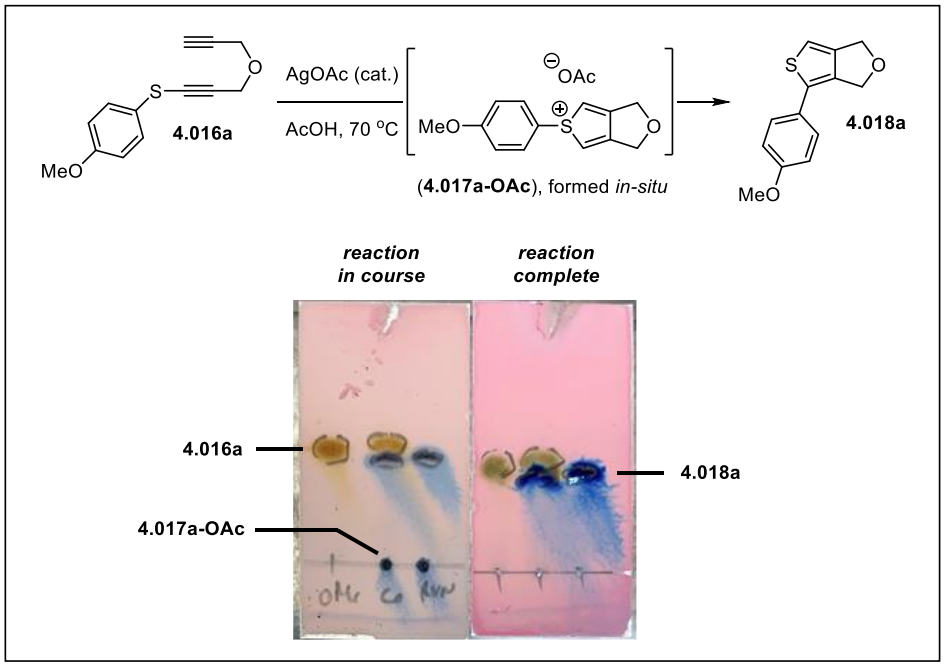

4.018c

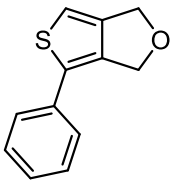

Using standard procedure ***SP11*** with 0.205 mmol of alkynyl sulfide **4.016c** in AcOH (1.0 mL, 0.2 M). Reaction time = 3 h. Solvent system = Hexanes/Et_2O 95:5. Produced 38.2 mg (92% yield) of a white solid.

^{1}H NMR (300 MHz, $CDCl_3$) δ 7.44 – 7.34 (m, 2H), 7.32 – 7.22 (m, 2H), 6.79 (t, *J* = 1.4 Hz, 1H), 5.05 (s, 2H), 4.84 – 4.87 (m, 2H).

^{13}C NMR (76 MHz, $CDCl_3$) : δ 146.7, 141.4, 133.8, 132.2, 129.2, 127.4, 126.0, 111.6, 69.1, 68.1.

Data matches that as previously reported.[44]

Using an S-alkynyl alkynyl sulfide

4.026

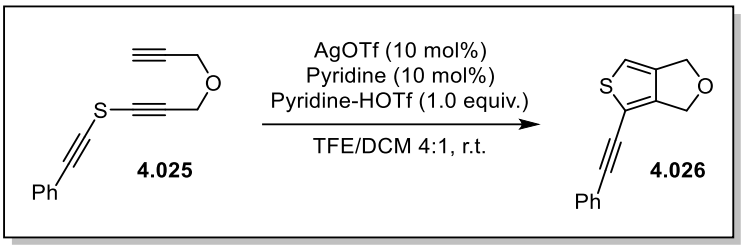

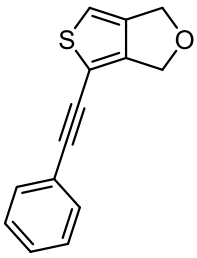

To a solution of yne-alkynyl sulfide **4.025** (14.7 mg, 0.0650 mmol, 1.0 equiv.), pyridine (0.5 µL, 0.0065 mmol, 0.1 equiv.) and pyridinium triflate (14.9 mg, 0.0650 mmol, 1.0 equiv.) in a 4:1 mixture of TFE:DCM (0.65 mL, 0.1 M) was added silver triflate (1.7 mg, 0.065 mmol, 0.1 equiv.). The reaction mixture was stirred at room temperature for 29 hours (until consumption of substrate, as observed by TLC analysis). The mixture was then concentrated under reduced pressure to produce a crude. The crude was purified by flash chromatography (Hexanes/EtOAc 9:1) to produce **4.026** (4.8 mg, 33% yield) as a white solid.

^{1}H NMR (400 MHz, $CDCl_3$) δ 7.53 – 7.44 (m, 2H), 7.40 – 7.30 (m, 3H), 6.79 (t, *J* = 1.4 Hz, 1H), 4.93 (t, *J* = 1.3 Hz, 2H), 4.84 (q, *J* = 1.0 Hz, 2H).

^{13}C NMR (101 MHz, $CDCl_3$) δ 149.4, 145.4, 131.6, 128.8, 128.5, 122.8, 114.6, 111.9, 95.1, 81.0, 68.7, 68.6.

HRMS-EI : Calculated for $C_{14}H_{10}OS$ [M]: 226.0452; found: 226.0463.

[44] *Angew. Chem. Int. Ed.* **2022**, *61*, e202205963

6.4.5. Scaled-up (3+2) cycloaddition of 4.028d and product derivatizations

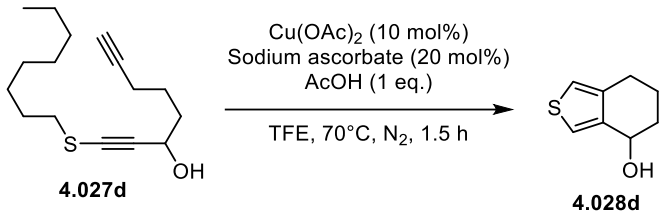

4.027d **4.028d**

In a round-bottom flask was prepared a suspension of yne-alkynyl sulfide **4.027d** (1.54 g, 5.61 mmol, 1.0 equiv.), sodium ascorbate (222 mg, 1.12 mmol, 0.2 equiv.) and glacial acetic acid (0.32 mL, 5.61 mmol, 1.0 equiv.) in TFE (50 mL, 0.1M). The suspension was purged with N_2 gas for 10 min, followed by addition of copper(II) acetate (102 mg, 0.561 mmol, 0.1 equiv.). The reaction mixture was then heated in an oil bath at 70 °C for 1.5h (reaction completion monitored by TLC). The mixture was concentrated under reduced pressure, and directly loaded on a silica gel column for purification. Solvent system = Hexanes/EtOAc 9:1→3:1. Produced 670 mg (77% yield) of **4.028d** as a beige solid.

Several visual indicators provide some information on reaction development:

t = 0	5 min	8 min	30 min	1.5 h
Reaction mixture added to heated oil bath.	*$Cu(OAc)_2$ granules solubilize as reaction heats up, mixture takes a green colour*	*Cu^{II} (green) turns to active Cu^{I} (yellow) as it gets reduced by ascorbate*		*The mixture slowly takes on a darker brown hue as the reaction proceeds*

4.037, 4.038 & 4.040

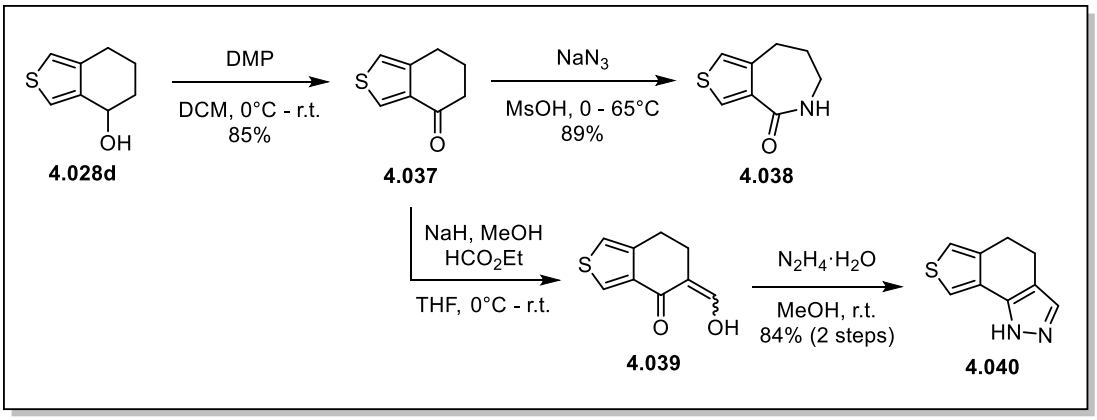

To a solution of alcohol **4.028d** (403 mg, 2.61 mmol, 1.0 equiv.) in DCM (12 mL, 0.2M) cooled to 0 °C was added Dess-Martin periodinane (1.22 g, 2.87 mmol, 1.1 equiv.). The mixture was brought to room temperature and stirred for 15 min. The reaction mixture was then filtered through celite, concentrated under reduced pressure, and directly purified via flash chromatography (eluent system = Hex/EtOAc 9:1) to produce ketone **4.037** (339 mg, 85% yield) as a pale yellow oil.

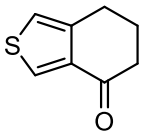

^{1}H NMR (400 MHz, $CDCl_3$) δ 8.13 (d, *J* = 3.1 Hz, 1H), 7.01 (dt, *J* = 3.2, 1.6 Hz, 1H), 2.87 (t, *J* = 6.1 Hz, 2H), 2.59 – 2.51 (m, 2H), 2.07 (p, *J* = 6.4 Hz, 2H).

^{13}C NMR (101 MHz, $CDCl_3$) δ 194.4, 142.6, 137.9, 131.0, 120.4, 39.4, 25.9, 24.0.

HRMS-EI : Calculated for C_8H_8OS [M]: 152.0296; found: 152.0282.

To a solution of ketone **4.037** (57.1 mg, 0.375 mmol, 1.0 equiv.) in methanesulfonic acid (1 mL, 0.3M) cooled to 0 °C was added sodium azide (26.8 mg, 0.412 mmol, 1.1 equiv.). The mixture was heated in an oil bath to 65 °C for 1.5 h. Upon completion, the mixture was cooled to room temperature and diluted with 15 mL of 1M aq. NaOH, and slowly reacidified to a pH of 7 using 2.5% aq. HCl. This was extracted 3 times with EtOAc. The combined organic phases were dried over $MgSO_4$, filtered, and evaporated to produce lactam **4.038** (55.8 mg, 89% yield) as a beige solid without any need for purification.

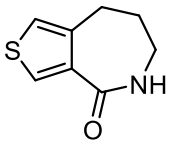

^{1}H NMR (400 MHz, $CDCl_3$) δ 7.92 (d, *J* = 3.2 Hz, 1H), 6.99 (d, *J* = 3.2 Hz, 1H), 6.45 (broad s, 1H), 3.21 (q, *J* = 6.2 Hz, 2H), 2.90 (t, *J* = 7.2 Hz, 2H), 1.96 (p, *J* = 6.8 Hz, 2H).

^{13}C NMR (101 MHz, $CDCl_3$) δ 169.8, 138.8, 137.1, 131.1, 121.6, 40.8, 28.8, 25.7.

HRMS-EI : Calculated for C_8H_9NOS [M]: 167.0405; found: 167.0389.

In a flame-dried round bottom flask under N_2 atmosphere was cooled a suspension of NaH (35.6 mg, 60% w/w in mineral oil, 0.890 mmol, 2.0 equiv.) in dry THF (4.0 mL) to 0 °C. Ethyl formate (0.18 mL, 2.22 mmol, 5.0 equiv.), a solution of ketone **4.038** (67.7 mg, 0.445 mmol, 1.0 equiv.) in THF (1.0 mL), and MeOH (40 µL, 0.98 mmol, 2.2 equiv.) were sequentially added to the cooled solution. The reaction mixture was then warmed to room temperature and stirred for 30 min (after which TLC analysis showed completion). The mixture was quenched with MeOH, then water, and concentrated under reduced pressure to remove volatiles. The mixture was redissolved in H_2O, acidified with HCl 2.5% aq., and extracted twice with Et_2O. The organic phase was dried over Na_2SO_4, filtered, and evaporated to produce the crude intermediate **4.039** which was used in the next step without purification.

The crude vinylogous ester **4.039** from above was dissolved in MeOH (4.0 mL) at room temperature, to which $N_2H_4 \cdot H_2O$ (0.11 mL, 2.22 mmol, 5.0 equiv.) was added. The reaction mixture was stirred at room temperature for 10 min (after which MS analysis showed completion). The mixture was diluted with H_2O and extracted twice with EtOAc. The organic phase was dried over $MgSO_4$, filtered, and evaporated. The obtained crude was purified via flash chromatography (eluent system = Hex/EtOAc 3:7) to produce pyrazole **4.040** (66.2 mg, 84% yield over 2 steps) as a beige solid.

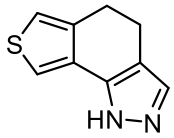

^{1}H NMR (400 MHz, $CDCl_3$) δ 8.69 (broad s, 1H), 7.50 (d, *J* = 2.8 Hz, 1H), 7.43 (broad s, 1H), 7.03 (dt, *J* = 2.7, 1.3 Hz, 1H), 2.92 (t, *J* = 7.0 Hz, 2H), 2.79 (t, *J* = 7.3 Hz, 2H).

^{13}C NMR (101 MHz, $CDCl_3$) δ 143.9, 138.9, 130.8, 128.4, 119.8, 116.7, 115.9, 26.0, 20.1.

HRMS-EI : Calculated for $C_9H_8N_2S$ [M]: 176.0408; found: 176.0422.

4.043

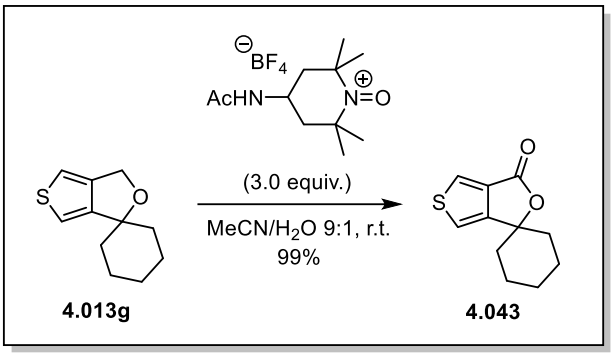

To a solution of thiophene **4.013g** (28.0 mg, 0.144 mmol, 1.0 equiv.) in 9:1 MeCN/H_2O (0.5 mL, 0.3M) stirred at room temperature was added Bobbitt's salt (130 mg, 0.432 mmol, 3.0 equiv.) all at once. The reaction mixture was stirred at room temperature for 20 hours until completion. The mixture was diluted with H_2O and extracted three times with Et_2O. The combined organic fractions were washed once with H_2O, then once with brine. The organic phase was then dried over $MgSO_4$, filtered and concentrated under reduced pressure to produce lactone **4.043** (29.9 mg, 99% yield) as a pale yellow solid without any need for further purification.

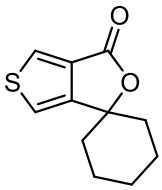

^{1}H NMR (400 MHz, $CDCl_3$) δ 7.88 (d, *J* = 2.3 Hz, 1H), 7.10 (d, *J* = 2.3 Hz, 1H), 2.06 – 1.47 (m, 10H).

^{13}C NMR (101 MHz, $CDCl_3$) δ 163.1, 155.2, 133.5, 126.1, 115.2, 86.1, 36.8, 24.6, 22.7.

HRMS-EI : Calculated for $C_{11}H_{12}O_2S$ [M]: 208.0558; found: 208.0542.

4.066

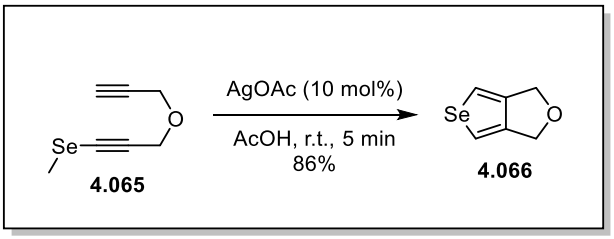

Using standard procedure ***SP9a*** with 0.183 mmol of yne-alkynyl selenide **4.065**. Reaction time = 5 min. Due to the product's volatility, the reaction mixture was simply worked up. Upon completion, the mixture was diluted with NaOH 2.0M aq. until a pH of ~7 was reached. The mixture was then

extracted with Et_2O three times. The combined organic phases were then washed once with brine. The organic phase was dried over $MgSO_4$, filtered, and concentrated (carefully at room temperature, the product is slightly volatile!) to produce 27.4 mg (86% yield) of **4.066** as a pale yellow solid.

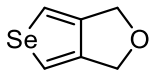

^{1}H NMR (300 MHz, $CDCl_3$) δ 7.51 (t, *J* = 0.9 Hz, 2H), 4.76 (d, *J* = 0.9 Hz, 4H).

^{13}C NMR (76 MHz, $CDCl_3$) δ 148.2, 116.6, 68.6.

^{77}Se NMR (57 MHz, $CDCl_3$) δ 745.5.

HRMS-EI : Calculated for C_6H_6OSe [M]: 173.9584; found: 173.9563.

6.4.6. NMR observation of a thiophenium salt

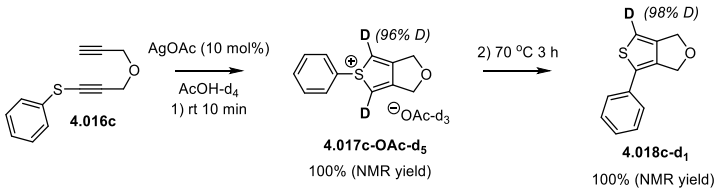

In a sealed NMR tube was added the yne-alkynyl sulfide substrate **4.016c** (10.3 mg, 0.0509 mmol, 1.0 equiv.) and deuterated acetic acid (0.5 mL, 0.1 M). 2.0 µL of mesitylene was added as internal NMR standard. AgOAc (0.8 mg, 5.09 x 10^{-3} mmol, 0.1 equiv.) was then added to the NMR tube. The solution was analyzed by ^{1}H NMR experiment before addition of the catalyst (0 min), after 10 min at room temperature, and followed while heating at 70 °C until consumption of the thiophenium intermediate (**4.017c-OAc-d$_5$**) is seen (3 h).

The ratio of ^{1}H NMR signal integration between the thiophenium α-hydrogens and either of the H_2 groups in a pure sample of thiophenium triflate salt **4.017c-OTf** is 1.94 : 2.00. The ratio of ^{1}H NMR signal integration between the thiophene α-hydrogen and either of the CH_2 groups in a pure sample of thiophene **4.018c** is 0.92 : 2.00. Obtained ratios in each spectrum are set against these respective ratios in order to determine the ratio of deuteration.

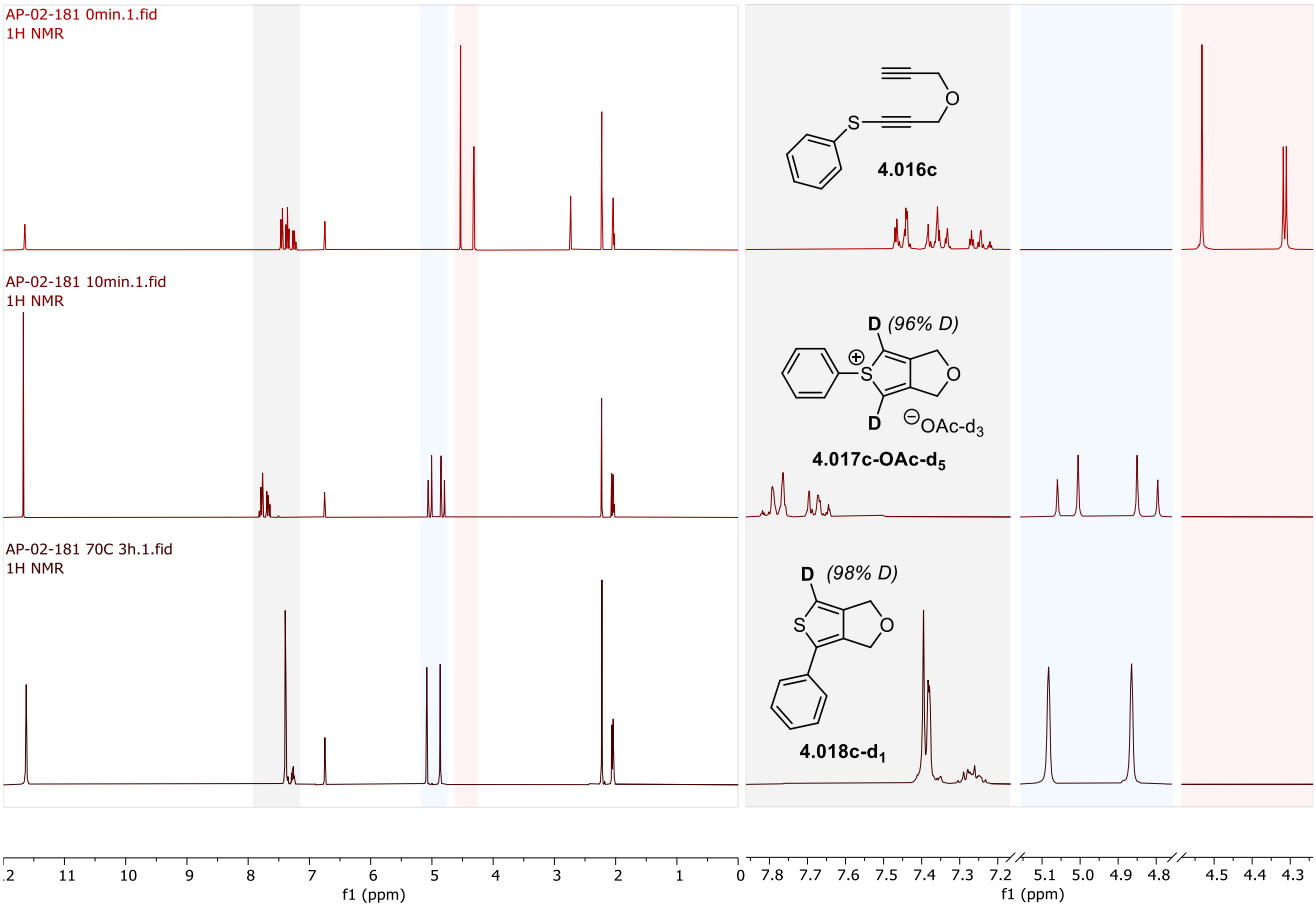

Figure SI-6.4-5 : NMR spectra overlap taken at time 0 min (top), after 10 min at room temperature (middle) and after 3 h of heating at 70 °C (bottom).[45]

6.4.7. Stoichiometric kinetic studies using an S-Aryl substrate

Collection of kinetic data

A solution containing **4.016a** (11.6 mg, 0.0500 mmol, 1.0 equiv.), triethylamine (13.9µL, 0.100 mmol, 2.0 equiv.) and *N*,*N*-dimethylacetamide (4.6µL, 0.050 mmol) in $CDCl_3$ (0.60 mL, 0.083 M) was prepared in a screw-cap NMR tube under air. To the tube was added silver(I) triflate (14.1 mg, 0.0550

[45] Increase in the signal for AcOH is seen by NMR after formation of the thiophenium intermediate **4.017c-OAc-d_5** (middle spectra) which is consistent with protic exchange between the terminal alkyne and solvent via the formation of an initial silver-acetylide.

mmol, 1.1 equiv.), the tube was vigorously shaken until homogeneous, and subsequent ^{1}H NMR analyses were immediately begun.

^{1}H NMR spectra were collected every 60 seconds for a total of 80 minutes. Using the MestreNova software, concentration data was extracted from the stacked spectra, using an internal dimethylacetamide signal as integration standard.

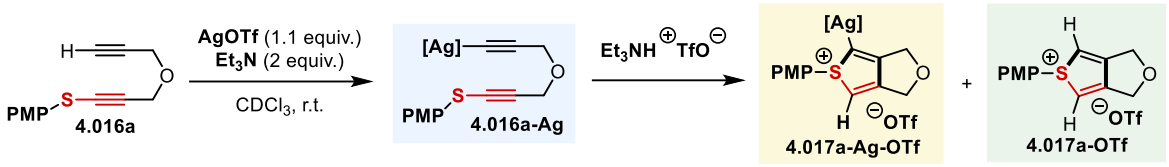

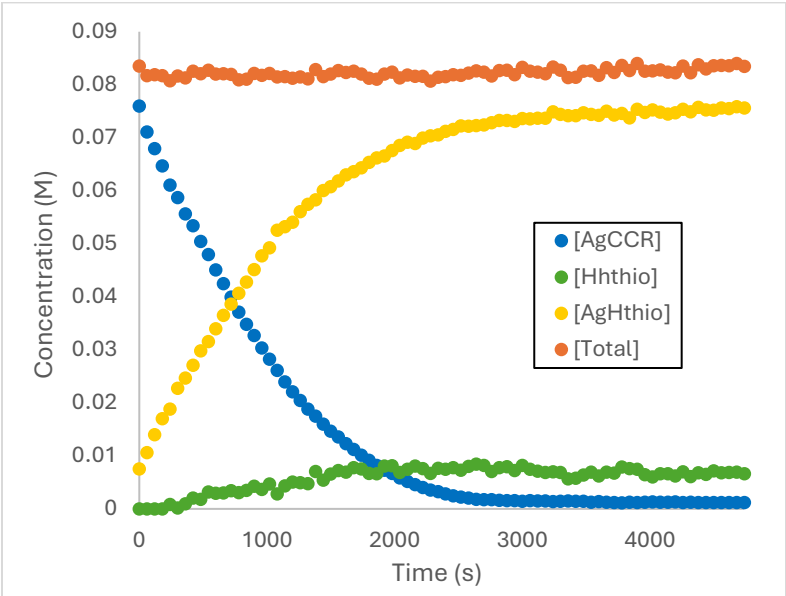

Figure SI-6.4-6. Kinetic data collected from ^{1}H NMR analysis during reaction.

Observations and preliminary conclusions from the stoichiometric kinetic experiment:

Apart from Et_3N and its triflate salt, only three species can be observed in significant amounts by NMR: **4.016a-Ag**, **4.017a-Ag-OTf** and **4.017a-OTf**. Their summed mass balance remains constant throughout the experiment.

Silver acetylide **4.016a-Ag** undergoes stoichiometric conversion to silver-bound thiophenium **4.017a-Ag-OTf**.

The sequential formation of protodemetalated thiophenium **4.017a-OTf** plateaus, presumably due to depletion of available "protic sources".

Model fitting using COPASI

Procedure for COPASI modelling:

Three models were evaluated using the COPASI software to distinguish between:

1) Implication of a "mono" silver intermediate **4.016a-Ag**

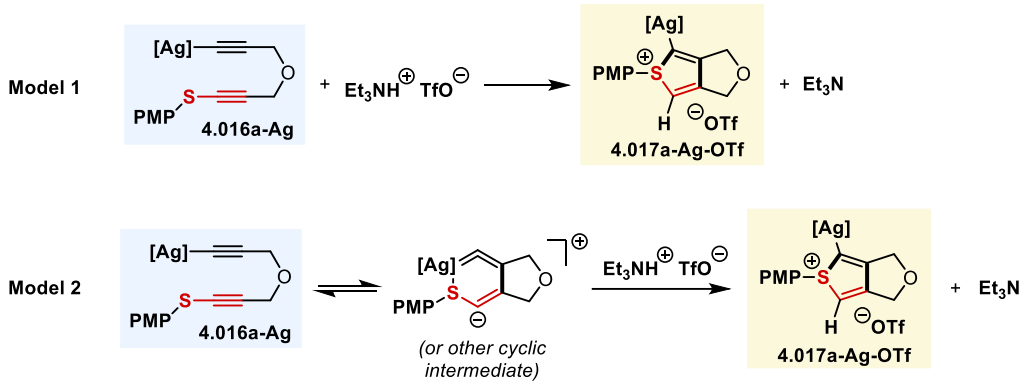

2) Implication of a bis-silver intermediate (**4.045**)

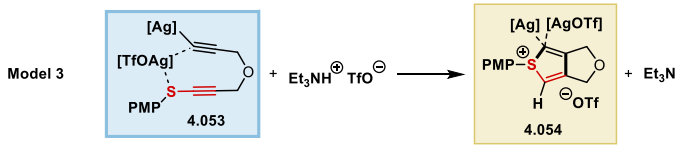

In each case, the model was constructed with a minimum set of reactions that would participate in the formation of the three observed species. The set of reactions are described below. Initial concentrations for each species in the model were based on the collected experimental NMR data. Using the parameter estimation function in COPASI (genetic algorithm, number of generations = 200, population size = 20), all rate constant values from the model were optimized against the concentration values that were experimentally obtained. Time course data for both the experiment and the model were then plotted on the same graph in order to qualitatively observe correlation.

Model 1 : Monosilver - Bimolecular reaction

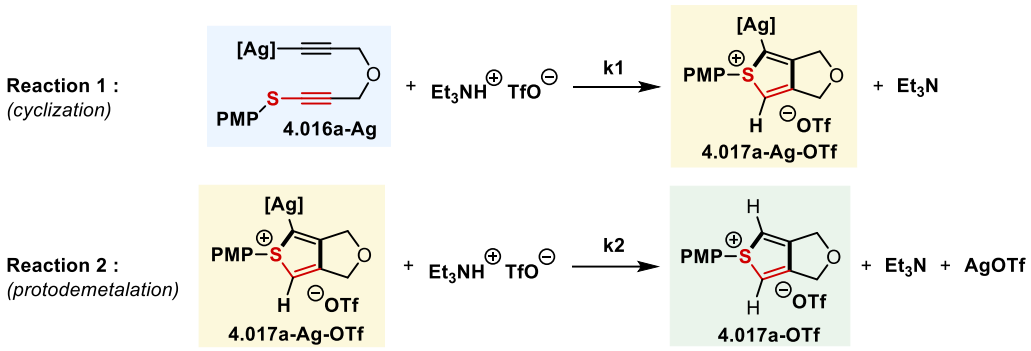

Figure SI-6.4-7. Schematic representation of the Model 1 investigated in model fitting.

COPASI model fitting			
Initial concentrations (M) (from experimental NMR data)			
[4.016a-Ag]$_0$	**[4.017a-Ag-OTf]$_0$**	**[4.017a-OTf]$_0$**	**[Et$_3$NHOTf]$_0$**
0.0760	0.0076	0.0000	0.0850

Optimized parameter fitting		
k1 (L/mol · s)	**k2 (L/mol · s)**	**Model R^2**
2.63e-2	1.74e-3	0.957043

Table SI-6.4-5. Input values for the COPASI Model 1 and the resulting optimized parameters.

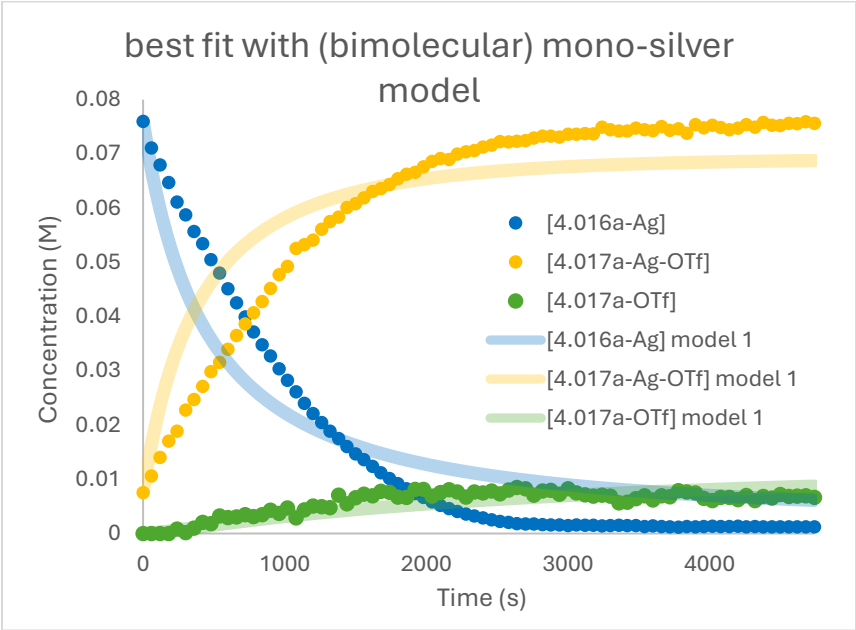

Figure SI-6.4-8. Superposition of experimental data with fitted data from the COPASI Model 1.

Model 2 : Monosilver - Unimolecular reaction

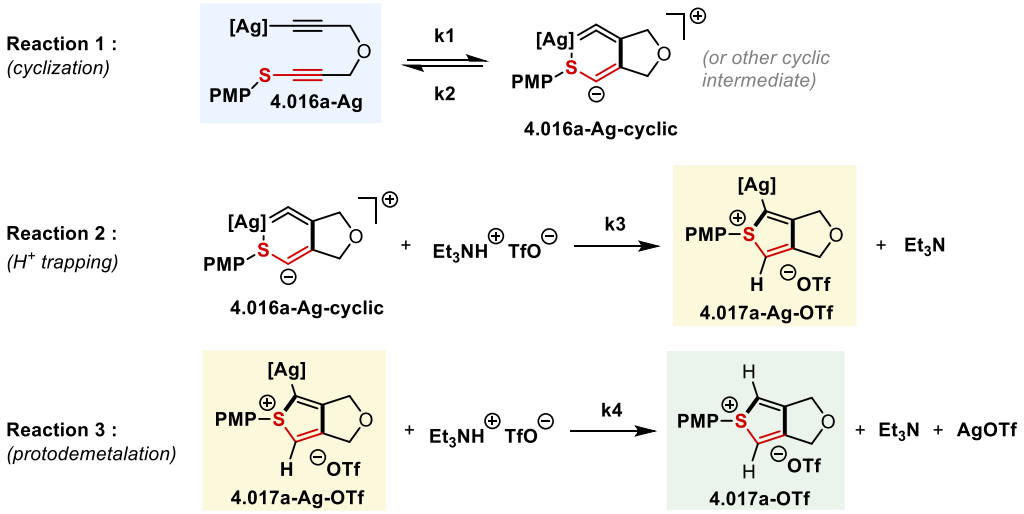

Figure SI-6.4-9. Schematic representation of the Model 2 investigated in model fitting.

	COPASI model fitting			
Initial concentrations (M) (from experimental NMR data)				
[4.016a-Ag]$_0$	**[4.016a-Ag-cyclic]$_0$**	**[4.017a-Ag-OTf]$_0$**	**[4.017a-OTf]$_0$**	**[Et_3NHOTf]$_0$**
0.0760	0.0000	0.0076	0.0000	0.0850

Optimized parameter fitting				
k1 (1/s)	**k2 (1/s)**	**k3 (L/mol·s)**	**k3 (L/mol·s)**	**Model R^2**
1.07e-3	1.48e-2	3.35e+2	2.16e-3	0.994192

Table SI-6.4-6. Input values for the COPASI Model 2 and the resulting optimized parameters.

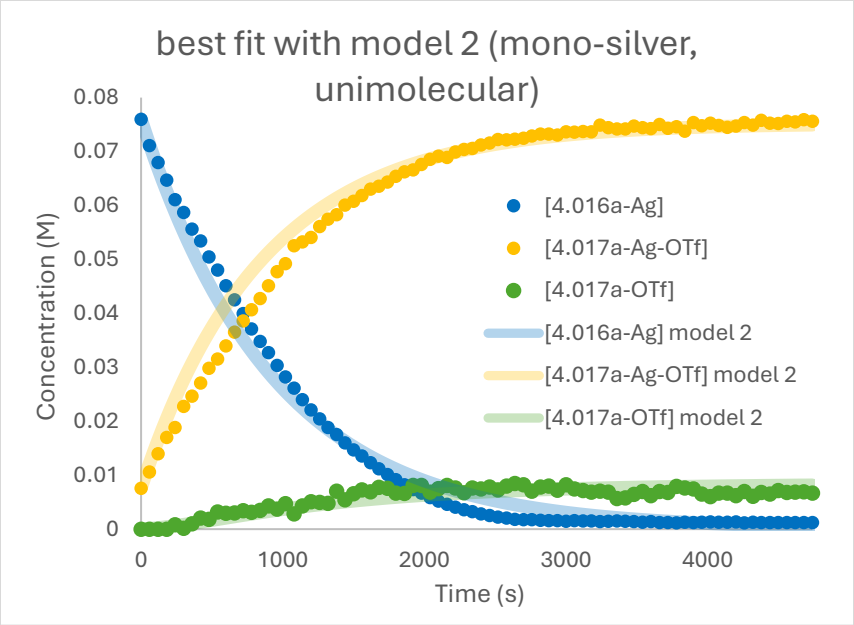

Figure SI-6.4-10. Superposition of experimental data with fitted data from the COPASI Model 2.

Model 3 : Bis-silver catalyzed reaction

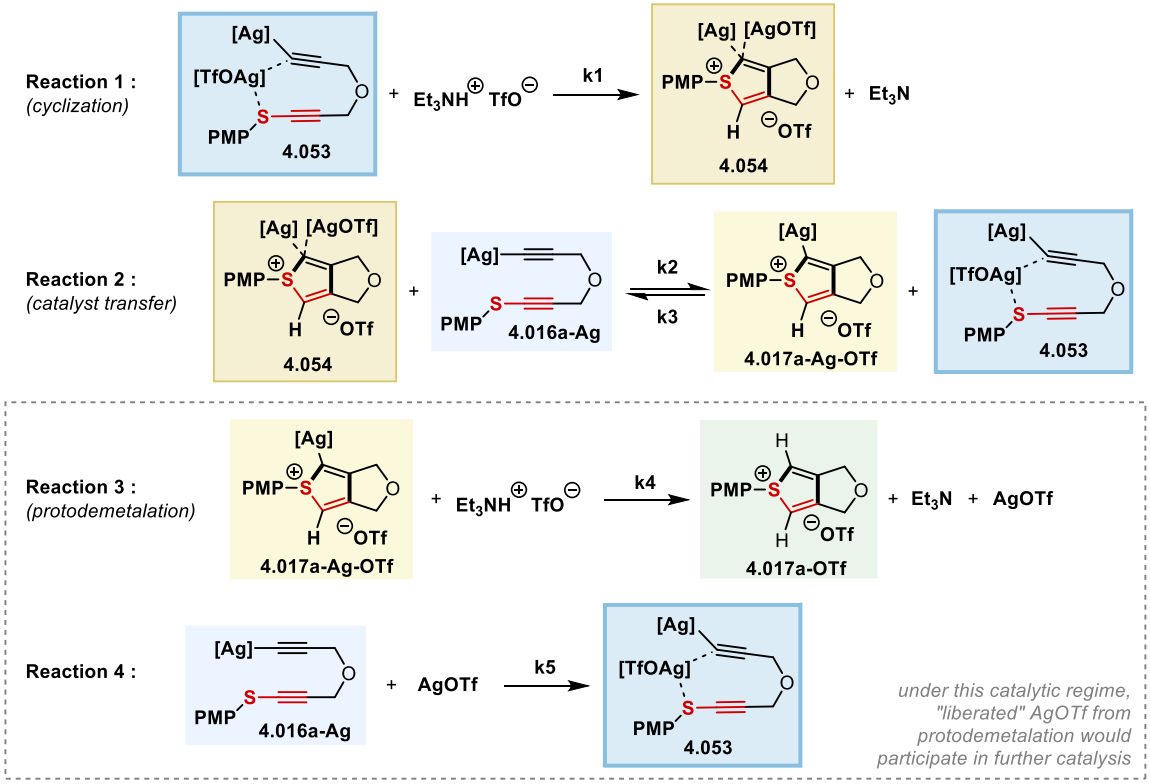

Figure SI-6.4-11. Schematic representation of the Model 3 investigated in model fitting.

COPASI model fitting			
Initial concentrations (M) (from experimental data)			
[4.016a-Ag]$_0$ (+ **[4.053]$_0$**)	**[4.017a-Ag-OTf]$_0$** (+ **[4.054]$_0$**)	**[4.017a-OTf]$_0$**	**[$Et_3NHOTf]_0$**
0.0760 (+ 0.0000)	0.0000 (+ 0.0076)	0.0000	0.0850

Optimized parameter fitting					
k1 (L/mol · s)	**k2 (L/mol · s)**	**k3 (L/mol · s)**	**k4 (L/mol · s)**	**k5 (L/mol · s)**	**Model R^2**
1.54e3	9.82e-2	1.65e-4	3.75e-3	3.86e4	0.998874

Table SI-6.4-7. Input values for the COPASI Model 3 and the resulting optimized parameters.

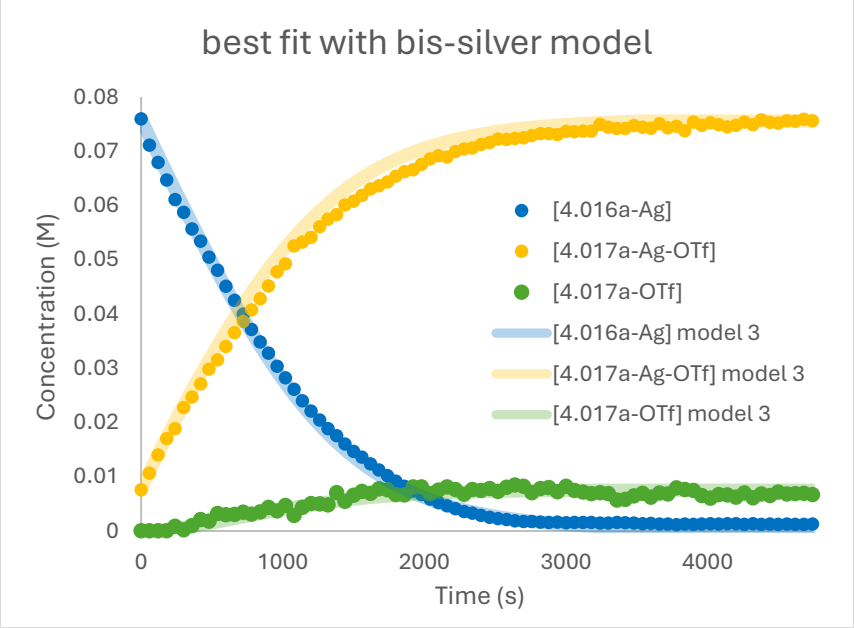

Figure SI-6.4-12. Superposition of experimental data with fitted data from the COPASI Model 3.

Conclusions and considerations from the COPASI modelling:

The COPASI modelling was used in order to compare the plausibility of the three investigated models. It was not used to calculate exact values for the rate constants. Other factors such as ligation and solvation of silver species by triethylamine may provide a more accurate picture of the medium, but were not studied here to keep the models as minimal as possible.

Nevertheless, it can be concluded that the cyclization process is unlikely described by the "mono" silver acetylide, as the bimolecular and unimolecular kinetics from models 1 and 2 were much less successfully fitted to the experimental data in comparison to bis-silver model 3.

6.4.8. Optimization for the formation of the thiophenium triflate salt

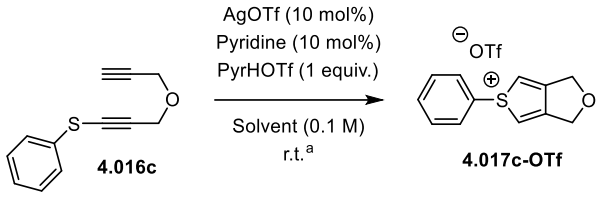

Entry	Solvent	Time	Conv. (%)[b]	Yield 14a-OTf (%)[b]
1	**DCM**	4 h	29	6
2	**MeCN**	4 h	18	0
3	**TFE**	4 h	89	67
4	**TFE : DCM (10 : 1)**	4 h	100	89
5	**MeOH : DCM (10 : 1)**	4 h	44	29
6	**MeOH : DCM (10 : 1)**	24 h	92	52

Table SI-6.4-8. Evaluation of various reaction parameters for obtaining the thiophenium triflate salt **4.017c-OTf**.[a] All reactions are performed in sealed reaction tubes at the 0.06 mmol scale in the indicated solvent (0.1 M). [b] Yields and consumptions are assessed by ^{1}H-NMR analysis after the indicated time with 2.0 µL of mesitylene as NMR standard.

Full procedure for entries 1-6 : Alkynyl sulfide **4.016c** (12.1 mg, 0.0600 mmol, 1.0 equiv.) is dissolved in the reaction solvent (0.6 mL, 0.1 M) and transferred to an amber vial. Pyridine (0.5 µL, 6.00 x 10^{-3} mmol, 0.1 equiv.) and PyrHOTf (13.8 mg, 0.0600 mmol, 1.0 equiv.) are then added to the mixture followed by AgOTf (1.5 mg, 6.00 x 10^{-3} mmol, 0.1 equiv.). The reaction is stirred for 4 h (or 24 h for entry 6). MeOH (1 mL) is then added to the mixture and NaCl (s) is added in excess to quench the reaction. Filtration through a celite pad with MeOH affords a crude upon evaporation under reduced pressure.

The crude is analyzed by ^{1}H NMR in DMSO-d_6 and the yields are assessed with the addition of 2.0 µL of mesitylene as internal standard.

6.4.9. Scale-up and isolation of a thiophenium triflate salt

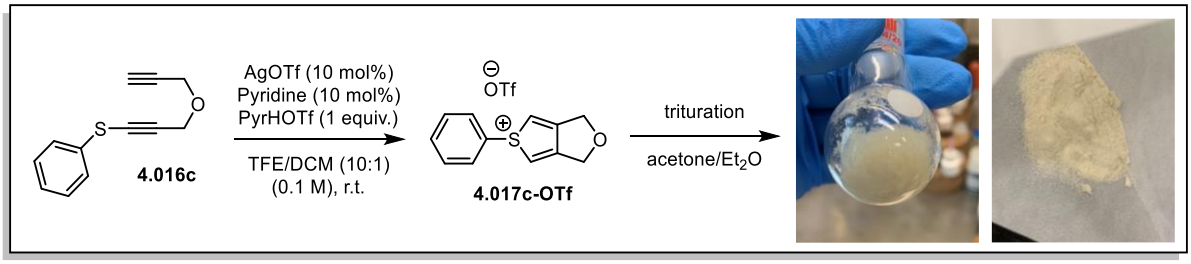

In a round bottom flask was added a solution of yne-alkynyl sulfide substrate **4.016c** (708 mg, 3.50 mmol, 1.0 equiv.) in trifluoroethanol : dichloromethane (10 : 1) (35.0 mL, 0.1 M). Pyridinium triflate (802 mg, 3.50 mmol, 1.0 equiv.) and pyridine (28.0 µL, 0.350 mmol, 0.1 equiv.) were then added to the solution. AgOTf (90.0 mg, 0.350 mmol, 0.1 equiv.) was then quickly added to the reaction mixture, and the flask was covered with aluminum foil. The mixture was stirred at room temperature for 4 hours. The reaction mixture was then concentrated under reduced pressure at **<u>room temperature</u>** to remove the volatiles. The crude was then diluted with acetone (approx. 10 mL), then diethyl ether is added to precipitate the thiophenium that is in solution. Diethyl ether is added until precipitation of the thiophenium salt stops (approx. 10 mL). The supernatant solution was then carefully removed using a glass pipette and the salt was subsequently washed with diethyl ether several times. The resulting precipitate was dried under vacuum yielding 1.06 g (86% yield) of **4.017c-OTf** as an off-white solid.

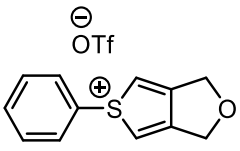

^{1}H NMR (600 MHz, DMSO-d_6) δ 7.80 – 7.75 (m, 3H), 7.72 – 7.66 (m, 2H), 7.56 (q, *J* = 1.7 Hz, 2H), 4.89 (dd, *J* = 16.2, 1.4 Hz, 2H), 4.72 (dd, *J* = 16.2, 1.7 Hz, 2H).

^{13}C NMR (151 MHz, DMSO-d_6) δ 161.8, 134.4, 131.0, 130.6, 120.7 (q, *J* = 322.3 Hz), 121.6, 118.1, 66.5.

^{19}F NMR (282 MHz, DMSO-d_6) δ -77.8.

COSY, **HSQC** and **HMBC** experiments were also done, and the spectra are provided.

HRMS-ESI : Calculated for $C_{12}H_{11}OS^+$ [M-OTf]$^+$: 203.0525 ; found: 203.0507.

6.4.10. DFT studies

General methodology for calculation of potential energy surfaces:

Using the Gaussian16 software,[46] structural optimization and vibrational frequency calculations for minima and maxima along the potential energy surface were carried out at the PBE0/def2SVP level of theory,[47] using GD3 (BJ)[48] as correction for empirical dispersion and the SMD solvation model (acetic acid).[49] Vibrational frequency calculations were performed at the gas phase, 1 atm, and 298.15 K. Normal modes of vibration were analyzed to assure either 0 (minima) or 1 (maxima) imaginary frequencies were obtained. Intrinsic reaction coordinate (IRC) calculations were performed on each transition state structure to assign connectivity (dotted lines) to the indicated minima.

Free energy corrections at the def2SVP level basis set were applied to electronic energies from single point calculations at the def2TZVP basis set.

Table SI-6.4-9. Potential energy surface data for the copper-catalyzed cyclization.

Coordinate	Negative frequencies	EE (Hartrees) (def2SVP)	Thermal Free Energy Correction (Hartrees) (def2SVP)	EE (Hartrees) (def2TZVP)	EE (def2TZVP) + Thermal Free Energy Correction (def2SVP)	ΔG (kcal/mol)
4.048-A	**0**	-2383.368891	0.081619	-2384.133537	-2384.051918	0.0
4.049-A	**1**	-2383.343283	0.081675	-2384.107962	-2384.026287	16.1
4.050-A	**0**	-2383.359925	0.084061	-2384.121902	-2384.037841	8.8
4.048-B	**0**	-4251.614265	0.122045	-4252.868029	-4252.745984	0.0
4.049-B	**1**	-4251.595135	0.123215	-4252.84907	-4252.725855	12.6
4.050-B	**0**	-4251.618464	0.127563	-4252.870376	-4252.742813	2.0
4.048-C	**0**	-4251.577175	0.123244	-4252.839469	-4252.716225	0.0
4.049-C	**1**	-4251.554075	0.120372	-4252.815459	-4252.695087	13.3

[46] Frisch, M. J.; Trucks, G. W.; Schlegel, H. B.; Scuseria, G. E.; Robb, M. A.; Cheeseman, J. R.; Scalmani, G.; Barone, V.; Petersson, G. A.; Nakatsuji, H.et al. *Gaussian 16 Rev. C.01* Wallingford, CT, 2016.

[47] The PBE0 functional with GD3(BJ) correction has been shown to perform well in a benchmarking study of transition metals reaction barrier heights (Iron, M.A.; Janes, T. J. Phys. Chem. A **2019**, 123 (*17)*, 3761–3781), and a similar methodology has been used recently to evaluate the mechanism of a copper-catalyzed (3+2) cycloaddition (Héron, J.; Balcells, D. ACS Catal. **2022**, 12 *(8)*, 4744–4753).

[48] Grimme, S.; Ehrlich, S.; Goerigk, L. *J. Comput. Chem.* **2011,** *32* (7), 1456.

[49] Marenich, A. V.; Cramer, C. J.; Truhlar, D. G. *The Journal of Physical Chemistry B* **2009,** *113* (18), 6378.

4.050-C	**0**	-4251.594462	0.123893	-4252.853357	-4252.729464	-8.3
4.048-D	**0**	-4480.298047	0.174873	-4481.814125	-4481.639252	0.0
4.049-D	**1**	-4480.283946	0.177332	-4481.798493	-4481.621161	11.4
4.050-D	**0**	-4480.333919	0.181435	-4481.848411	-4481.666976	-17.4
4.050-D'	**0**	-4480.372365	0.182461	-4481.875757	-4481.693296	-33.9
4.051-D	**1**	-4480.357703	0.181059	-4481.863843	-4481.682784	-27.3
4.052-D	**0**	-4480.378349	0.181444	-4481.885187	-4481.703743	-40.5
4.048-E	**0**	-2612.05301	0.131188	-2613.079293	-2612.948105	0.0
4.049-E	**1**	-2612.034872	0.13363	-2613.059538	-2612.925908	13.9
4.050-E	**0**	-2612.078018	0.136349	-2613.101869	-2612.96552	-10.9

Table SI-6.4-10. Supplementary potential energy surface data for the silver-catalyzed cyclization.

Coordinate	Negative frequencies	EE (Hartrees) (def2SVP)	Thermal Free Energy Correction (Hartrees) (def2SVP)	EE (Hartrees) (def2TZVP)	EE (def2TZVP) + Thermal Free Energy Correction (def2SVP)	ΔG (kcal/mol)
Ag-4.048-A	**0**	-890.263915	0.078886	-890.820826	-890.74194	0.0
Ag-4.049-A	**1**	-890.235474	0.080347	-890.793134	-890.712787	18.3
Ag-4.050-A	**0**	-890.24576	0.082243	-890.802574	-890.720331	13.6
Ag-4.048-B	**0**	-1265.382033	0.117884	-1266.232477	-1266.114593	0.0
Ag-4.049-B	**1**	-1265.356575	0.117688	-1266.207405	-1266.089717	15.6
Ag-4.050-B	**0**	-1265.370346	0.121106	-1266.220148	-1266.099042	9.8
Ag-4.048-D	**0**	-1494.065827	0.170094	-1495.178306	-1495.008212	0.0
Ag-4.049-D	**1**	-1494.044302	0.171161	-1495.155986	-1494.984825	14.7
Ag-4.050-D-pre H	**0**	-1494.067338	0.173285	-1495.176800	-1495.003515	2.9
Ag-4.050-D-TS H	**1**	-1494.066981	0.171391	-1495.176674	-1495.005283	1.8
Ag-4.050-D-post H	**0**	-1494.076078	0.175289	-1495.190036	-1495.014747	-4.1

6.4.11. Cartesian coordinates for the obtained minima/maxima

4.048-A

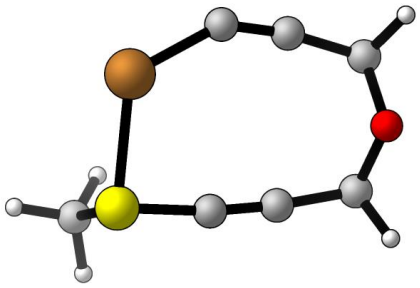

Atom type	X	Y	Z
C	2.40430600	1.61389400	-0.01392700
C	3.02170500	-0.66427900	0.44315500
H	3.85353400	-1.31928400	0.13576600
H	2.59994400	1.85351700	1.05059500
H	2.81218800	2.44643200	-0.60965200
H	3.22803000	-0.35484900	1.48721500
C	1.73993100	-1.36395900	0.36042400
C	0.95180400	1.54061600	-0.19913800
C	0.58909500	-1.78510700	0.21649800
C	-0.24805100	1.37633000	-0.31359700
S	-1.87344400	0.94090100	-0.50435600
C	-2.55857000	1.32731300	1.13369500
H	-1.96547300	0.83683900	1.91625400
H	-3.58452300	0.93255200	1.13152900
H	-2.57829400	2.41588700	1.27768800
O	3.10991400	0.46679300	-0.41495300
Cu	-1.19554900	-1.30581800	-0.16423200

4.049-A

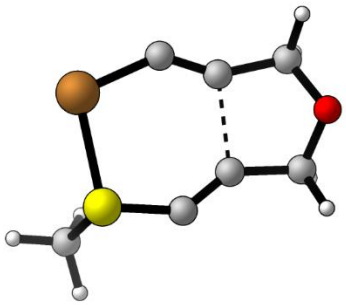

Atom type	X	Y	Z
C	2.62676700	1.33933500	0.03336400
C	2.88159400	-0.91705200	0.35413800
H	3.36902200	-1.79606000	-0.09329900
H	2.81273800	1.68137500	1.07307200
H	2.90738700	2.15301000	-0.65122200
H	3.12096500	-0.90664200	1.43742000
C	1.41046500	-0.97249600	0.17554600
C	1.17399000	1.01889300	-0.09318300
C	0.33476100	-1.63381600	0.13867300
C	0.03880600	1.54639100	-0.27929400
S	-1.55172800	1.04086300	-0.53623800
C	-2.43423400	1.74836000	0.87858700
H	-1.98697800	1.40058500	1.81932800
H	-3.47635600	1.40574800	0.80476700
H	-2.40135900	2.84494600	0.82011900
O	3.41290500	0.22409200	-0.27830400
Cu	-1.48323800	-1.31059300	-0.05692800

4.050-A

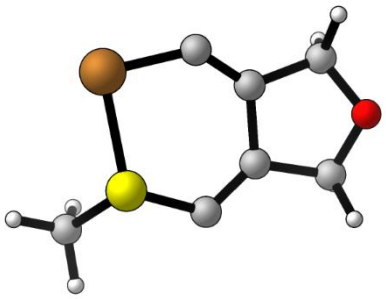

Atom type	X	Y	Z
C	2.69263000	1.24415900	0.05602600
C	2.72774500	-1.01866200	0.31152500
H	3.07049200	-1.92836600	-0.20116000
H	2.88642800	1.65825300	1.06727900
H	2.98061200	2.00191600	-0.68706500
H	2.86959700	-1.15260000	1.40333200
C	1.26688000	-0.69162800	0.04648800
C	1.23162000	0.83077900	-0.04606400
C	0.26637800	-1.52785600	-0.08719300
C	0.18399900	1.65164300	-0.13785600
S	-1.35526500	0.98348500	-0.48353000
C	-2.48314800	1.86019100	0.62241700
H	-2.21631600	1.68054200	1.67248700
H	-3.50002100	1.49532000	0.41840100
H	-2.42198000	2.93431600	0.39799400
O	3.45614800	0.08209000	-0.16680400
Cu	-1.55001300	-1.28184900	0.01405500

4.048-B

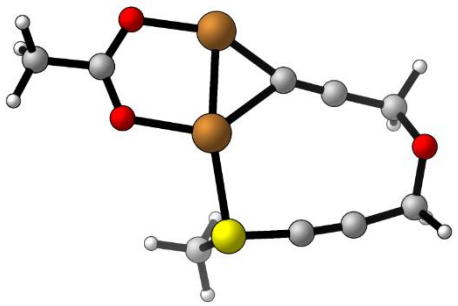

Atom type	X	Y	Z
C	4.45743400	-0.12978800	-0.14936100
C	3.11893500	-1.97863100	0.54038100
H	3.24031300	-3.07386100	0.49047900
H	4.94058300	-0.04649800	0.84488200
H	5.22897200	0.09406400	-0.90281100
H	3.40295700	-1.67360400	1.56670600
C	1.71561500	-1.64627300	0.28976600
C	3.37976700	0.85138600	-0.22155000
C	0.51807200	-1.39572200	0.10910100
C	2.38061000	1.54571800	-0.24620000
S	0.90335600	2.33606400	-0.40757500
C	0.57173200	2.92222800	1.27994800
Cu	-1.35720700	-1.71725200	0.07257400
H	0.68684000	2.09746300	1.99495000
H	-0.47236900	3.26632400	1.26993900
H	1.24329900	3.75567100	1.52622900
O	4.03900400	-1.45097400	-0.39701200
Cu	-0.45852000	0.41036300	-0.25910300
O	-2.42095200	0.99845700	-0.14807200
C	-3.35792100	0.16218100	-0.05597000
C	-4.76980700	0.68208500	-0.00594400
H	-5.14473500	0.58444800	1.02580500
H	-4.81870200	1.73696300	-0.30368100
H	-5.42190500	0.07246800	-0.64765000
O	-3.21424100	-1.09370800	0.02316900

4.049-B

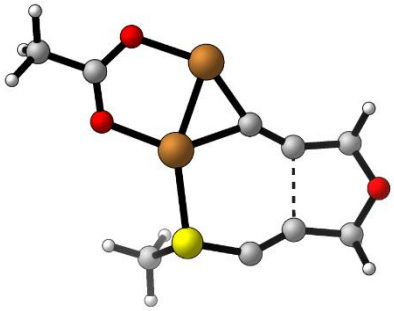

Atom type	X	Y	Z
C	4.34510400	-0.17600800	0.05025100
C	3.04676500	-2.04394400	0.39299800
H	2.88818600	-3.06101700	0.00422200
H	4.73084900	-0.01329200	1.07809500
H	5.07655100	0.23879400	-0.65931200
H	3.19442700	-2.11684300	1.49052300
C	1.86878400	-1.18690700	0.11770400
C	3.04120600	0.52451400	-0.06298900
C	0.61802800	-1.05640700	0.00603800
C	2.44282800	1.62175400	-0.19527400
S	0.91805800	2.24471600	-0.49979800
C	0.55170900	3.23704500	0.97188900
Cu	-1.17988900	-1.74096000	0.03034400
H	0.68807300	2.63285200	1.87836300
H	-0.50007300	3.54290400	0.87638800
H	1.20040300	4.12335200	0.99259600
O	4.20592800	-1.54219100	-0.22776200
Cu	-0.59324500	0.49766800	-0.17943900
O	-2.52979400	0.94419300	-0.07664100
C	-3.37098900	0.00422100	0.00463900
C	-4.82100700	0.39284100	0.10077800
H	-5.04650100	0.63260700	1.15302700
H	-5.02101900	1.29348300	-0.49530900
H	-5.47415900	-0.43173100	-0.21231000
O	-3.09355100	-1.22747100	0.04165800

4.050-B

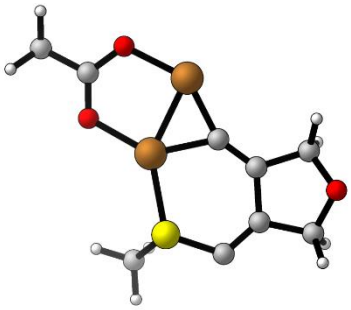

Atom type	X	Y	Z
C	4.26359700	-0.41489500	0.08349000
C	2.76254800	-2.10975200	0.33857500
H	2.40369500	-3.01217700	-0.17647200
H	4.69462800	-0.23413500	1.08986300
H	4.97877300	-0.04790500	-0.66717300
H	2.77426000	-2.30792500	1.43013000
C	1.90434500	-0.88151900	0.07502400
C	2.90288300	0.25204900	-0.01501500
C	0.59425300	-0.84975400	-0.01979200
C	2.66398700	1.56078400	-0.11042800
S	1.08378600	2.08523000	-0.46726400
C	0.76363100	3.42819800	0.69702900
Cu	-1.12258000	-1.65656900	-0.01379200
H	0.84388300	3.06835300	1.73135700
H	-0.25252400	3.79744600	0.49830900
H	1.49535900	4.22758000	0.51492100
O	4.04578800	-1.78997700	-0.13361800
Cu	-0.63796200	0.61972900	-0.11127900
O	-2.61727600	0.94096400	-0.02085700
C	-3.40457400	-0.04673700	0.02335900
C	-4.87323000	0.24677800	0.14106400
H	-5.09994000	0.45373000	1.19997700
H	-5.13562800	1.14402800	-0.43546000
H	-5.47602200	-0.61182600	-0.18068900
O	-3.05050800	-1.26140900	0.00681100

4.048-C

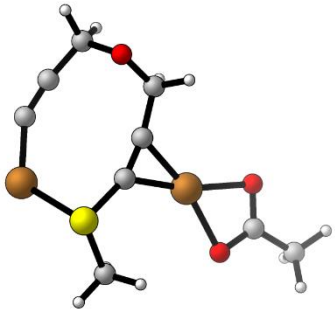

Atom type	X	Y	Z
C	-0.54626700	2.50386800	0.39928900
C	-2.82769800	2.84524400	-0.23176600
H	-3.69430700	3.37798700	0.19244600
H	-0.31425800	2.84442000	-0.62785100
H	0.15608300	3.02352600	1.07111900
H	-2.48289000	3.43364100	-1.10491900
C	-3.18143300	1.48505100	-0.62441100
C	-0.26319300	1.05141300	0.48207600
C	-3.31525100	0.27522900	-0.82287700
C	-0.25621100	-0.19545300	0.60967100
S	-0.87517400	-1.76481700	0.94802500
C	0.42189400	-2.83002100	0.26985500
H	0.58547200	-2.61042700	-0.79294100
H	0.05333600	-3.85859000	0.39003900
H	1.34925800	-2.69575800	0.84192500
O	-1.83573200	2.88561100	0.78800000
Cu	-2.67724900	-1.46397100	-0.49616400
O	3.33628100	1.27233600	-0.31691900
C	3.90495900	0.14278500	-0.32240000
C	5.35553400	0.03430400	-0.67918100
H	5.43032700	-0.15148900	-1.76335200
H	5.88700200	0.96811400	-0.45500200
H	5.82161200	-0.81377900	-0.16030100
O	3.23747600	-0.90030400	-0.06711400
Cu	1.55838500	0.31858400	0.13503200

4.049-C

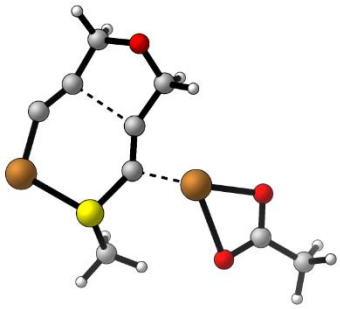

Atom type	X	Y	Z
C	0.51856500	2.62070900	-0.13625900
C	2.73915400	2.83340200	0.42933300
H	3.67061100	3.30909400	0.08734300
H	0.10171300	2.88372000	0.85722300
H	-0.20922500	2.91788500	-0.90492600
H	2.57353500	3.12580500	1.48611800
C	2.82537400	1.36737300	0.32510700
C	0.72549900	1.13887000	-0.17321700
C	3.33276400	0.22097500	0.34530500
C	0.21614900	-0.01386700	-0.39126900
S	0.76336400	-1.61759500	-0.67474600
C	-0.29267100	-2.59207100	0.42512600
H	-0.12758600	-2.29973300	1.47079300
H	-0.00275200	-3.64212200	0.27745700
H	-1.34578300	-2.44807100	0.14700300
O	1.70031800	3.32421400	-0.38707600
Cu	2.97950100	-1.59626800	0.14990600
O	-3.51305000	1.02971900	0.18535200
C	-4.03632800	-0.13014200	0.15838400
C	-5.52069600	-0.23284300	0.38338500
H	-5.79243400	0.28295500	1.31661700
H	-6.04718800	0.28284900	-0.43493600
H	-5.84603800	-1.27979900	0.42440900
O	-3.35333100	-1.15529200	-0.05594300
Cu	-1.63146800	0.41990100	-0.15215400

4.050-C

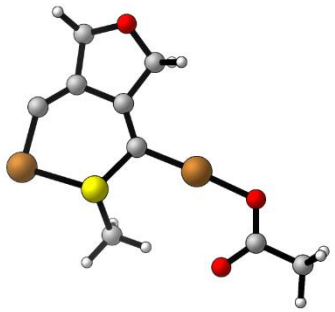

Atom type	X	Y	Z
C	1.08296100	2.74423700	0.10139800
C	3.32028400	2.35033200	0.30103900
H	4.26479700	2.50931400	-0.23745600
H	0.73301200	3.01151200	1.11959200
H	0.37650900	3.16581700	-0.62811500
H	3.50672000	2.45318200	1.38888000
C	2.69497100	0.98450700	0.04782900
C	1.22743600	1.23665500	-0.01001000
C	3.30523400	-0.16896800	-0.10403600
C	0.21275400	0.35791300	-0.09578100
S	0.59356100	-1.31998500	-0.44836400
C	-0.47880600	-2.25462700	0.66582000
H	-0.26055900	-2.00192600	1.71192500
H	-0.28331300	-3.32076500	0.48111400
H	-1.52676100	-2.01689900	0.42222700
O	2.36538800	3.27407900	-0.14923400
Cu	2.78578600	-1.92236000	-0.00871600
O	-3.55262700	0.90478700	-0.01273800
C	-4.22587600	-0.18588600	0.01077700
C	-5.72720800	-0.00654200	-0.00165900
H	-6.03330400	0.62715700	0.84501400
H	-6.02583500	0.52145200	-0.92087300
H	-6.24467900	-0.97286200	0.05150000
O	-3.73519000	-1.32267900	0.03709200
Cu	-1.65111800	0.67920600	-0.04484300

4.048-D

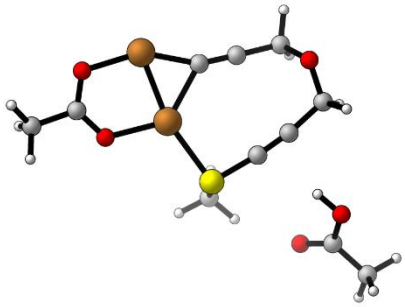

Atom type	X	Y	Z
C	-2.70466500	2.56112000	-0.31473800
C	-0.71454600	3.44331300	0.65320500
H	-0.27490600	4.45300300	0.71419900
H	-3.30102200	2.69942300	0.60957600
H	-3.37479900	2.76290100	-1.16499100
H	-1.22037200	3.25844900	1.62104800
C	0.35716300	2.46981700	0.44786600
C	-2.24498700	1.17459100	-0.35021800
C	1.27820700	1.66254300	0.27608300
C	-1.72905900	0.07163500	-0.30038800
S	-0.87410700	-1.37699900	-0.30167000
C	-1.20218500	-2.00874800	1.36955100
Cu	3.07423300	1.08240200	0.03982800
H	-0.87958700	-1.27448800	2.11873000
H	-0.60765200	-2.92879800	1.45923700
H	-2.27404400	-2.22794000	1.45573700
O	-1.66617300	3.50480600	-0.39431900
Cu	1.26671700	-0.41106800	0.02509100
O	2.75462900	-1.80404400	-0.14870600
C	3.97072200	-1.49137400	-0.24359300
C	4.97109600	-2.61034000	-0.35937700
H	5.28679400	-2.89978900	0.65668100
H	4.52029100	-3.49026000	-0.83695200
H	5.86384600	-2.28561800	-0.91016000
O	4.42840700	-0.31083300	-0.21952000
O	-4.92021600	-0.23400300	-0.85258800
C	-5.24595200	-1.24307400	-0.04769100
C	-6.70164300	-1.57096000	-0.10625300
H	-7.29219500	-0.68332800	0.16710200
H	-6.97681500	-1.83929600	-1.13767800
H	-6.92935800	-2.40054100	0.57252700
O	-4.43243800	-1.81601200	0.64373400
H	-3.96061300	-0.05087700	-0.75650000

4.049-D

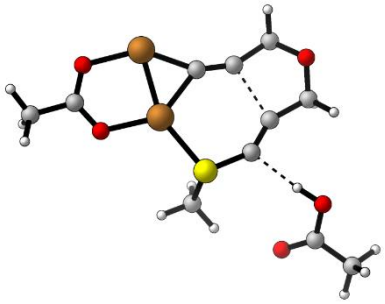

Atom type	X	Y	Z
C	-2.61866200	2.57033800	0.13555100
C	-0.56815900	3.58512700	0.40005400
H	0.04161800	4.40357100	-0.01163600
H	-2.95140900	2.61399000	1.19313500
H	-3.51342700	2.57825500	-0.50534300
H	-0.64578800	3.73616000	1.49634300
C	0.07219400	2.27902400	0.13678100
C	-1.85924800	1.31251100	-0.05300600
C	1.05885600	1.50752400	0.02191700
C	-1.85954200	0.07337300	-0.24512700
S	-0.85170600	-1.23025700	-0.59095700
C	-1.10499100	-2.33791300	0.82007500
Cu	2.94804600	1.13619500	0.06573900
H	-0.85959600	-1.81999700	1.75647000
H	-0.42173500	-3.18467200	0.66385700
H	-2.15088000	-2.67235400	0.81993700
O	-1.83947200	3.68394800	-0.19925300
Cu	1.29765900	-0.45290200	-0.17658000
O	2.74604300	-1.83139200	-0.08640900
C	3.95177100	-1.46403600	0.00777200
C	4.99540500	-2.54356200	0.08238700
H	5.04249100	-2.91055200	1.12083100
H	4.71821300	-3.39292800	-0.55671700
H	5.98500800	-2.15814900	-0.19418100
O	4.34525900	-0.26427400	0.07126200
O	-4.73626000	-0.20244600	-0.49237600
C	-5.17134300	-1.32107100	0.07154800
C	-6.66125000	-1.44126100	0.03297600
H	-7.11767200	-0.57153300	0.52927900
H	-7.00270300	-1.43487900	-1.01347900
H	-6.97810600	-2.36758500	0.52562800
O	-4.42945300	-2.14911800	0.55795400
H	-3.74330500	-0.16477600	-0.42941100

4.050-D

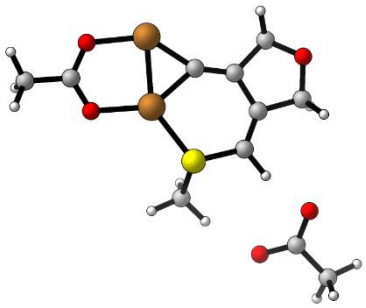

Atom type	X	Y	Z
C	-2.42347300	2.68537200	0.03179700
C	-0.30621600	3.47376500	0.33712600
H	0.45507500	4.09633200	-0.15312200
H	-2.87818800	2.70640100	1.04225900
H	-3.23225800	2.70426300	-0.71163000
H	-0.25200700	3.63489900	1.43239400
C	-0.14811200	1.98154100	0.06190800
C	-1.52178100	1.47728300	-0.09026200
C	0.97402400	1.29690800	-0.00883500
C	-1.92076200	0.21353400	-0.27137300
S	-0.83307600	-1.12132800	-0.56023400
C	-1.35705600	-2.32401500	0.68277400
Cu	2.85640000	1.12951300	0.12157300
H	-1.10297000	-1.96814200	1.68967400
H	-0.83354400	-3.26295100	0.45620000
H	-2.45081800	-2.43962300	0.56963300
O	-1.57355100	3.79371500	-0.17190900
Cu	1.32132000	-0.57342500	-0.14866100
O	2.79072700	-1.90612100	-0.07983200
C	3.97301000	-1.46623700	0.00924400
C	5.08693500	-2.46905800	0.04003600
H	5.18076400	-2.84860300	1.07076500
H	4.85327300	-3.32389600	-0.60849100
H	6.04037300	-2.00951200	-0.24875000
O	4.27540900	-0.24066600	0.10699900
O	-4.86476900	-0.05609700	-0.30620000
C	-5.25656800	-1.19465200	0.06068100
C	-6.76414600	-1.39869900	0.17089100
H	-7.27790600	-0.45693500	0.41195300
H	-7.14515500	-1.74820300	-0.80352300
H	-7.00482300	-2.16768100	0.91916300
O	-4.52576800	-2.18083400	0.31018000
H	-3.00801200	-0.03608700	-0.33506700

4.050-D′

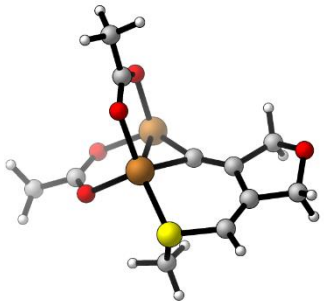

Atom type	X	Y	Z
C	4.44757000	0.41583100	-0.15937500
C	2.90962300	1.57634200	-1.37411800
H	2.41581400	2.55715500	-1.41164400
H	4.98415600	-0.19372300	-0.91491800
H	5.09778900	0.53000800	0.72030900
H	3.07772000	1.21928000	-2.40992700
C	2.12347600	0.52763300	-0.59632200
C	3.11951900	-0.22769300	0.15674500
C	0.80633200	0.37937500	-0.59192500
C	2.89978500	-1.27124700	0.97442900
S	1.30932400	-1.98155400	1.21289500
C	1.07381000	-2.98909300	-0.27678300
Cu	-0.92093100	0.73372100	-1.23712600
H	1.21205200	-2.38496700	-1.18340600
H	0.03774400	-3.35309700	-0.22841400
H	1.77559500	-3.83365800	-0.25246900
O	4.12182100	1.68943500	-0.66759900
Cu	-0.34325100	-0.43497600	0.75924000
O	-1.93627800	-1.70119500	0.31112600
C	-2.71511000	-1.39965800	-0.63267300
C	-3.98723600	-2.19415600	-0.77167900
H	-3.88609800	-3.18602700	-0.31209500
H	-4.79022600	-1.65231000	-0.24527500
H	-4.28040900	-2.28329600	-1.82651700
O	-2.52709400	-0.46500500	-1.46099200
O	-1.73011200	2.33950000	-0.21646100
C	-1.72417900	2.19234300	1.03475000
C	-2.22510300	3.34519300	1.86879200
H	-2.96462400	3.93820500	1.31413700
H	-2.64864700	2.98834600	2.81719700
H	-1.36994100	4.00029100	2.10409100
O	-1.30680300	1.17279400	1.65013400
H	3.70798000	-1.71838800	1.56058400

4.051-D

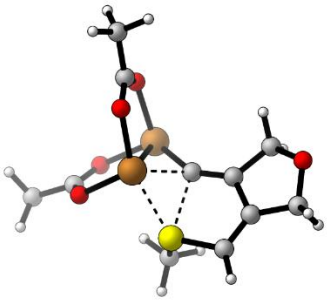

Atom type	X	Y	Z
C	-4.55711600	0.26624700	-0.05794200
C	-2.96146600	1.47697800	1.10075700
H	-2.45683900	2.45031800	1.01220000
H	-5.16942000	-0.30404400	0.66951900
H	-5.14688000	0.38438200	-0.98012200
H	-3.08672900	1.24468400	2.17732700
C	-2.23199100	0.35736300	0.39665000
C	-3.24529000	-0.42289400	-0.27557800
C	-0.91272000	0.07597800	0.37416100
C	-2.87257700	-1.55890400	-0.90245400
S	-1.13965300	-1.80670700	-0.84328000
C	-0.84288300	-2.82855200	0.61486700
Cu	0.75209200	0.39251000	1.25583000
H	-1.54149600	-2.53924600	1.41069800
H	0.19105800	-2.62572900	0.92640600
H	-0.96427700	-3.88421600	0.33838900
O	-4.21346800	1.54404500	0.44210900
Cu	0.55683500	-0.10888900	-1.04896800
O	2.07864200	-1.46250200	-0.81644600
C	2.67518900	-1.52778000	0.29404300
C	3.92678100	-2.36656300	0.35286400
H	3.85371800	-3.22650000	-0.32676100
H	4.77390200	-1.74586900	0.01730000
H	4.13288400	-2.69991000	1.37850300
O	2.32394100	-0.93326600	1.34860600
O	1.68130800	2.16003600	0.72128600
C	1.68705600	2.47377500	-0.49759400
C	2.18298000	3.85276000	-0.85757000
H	2.89791600	4.22056400	-0.10950200
H	2.63470600	3.85917400	-1.85869500
H	1.32043700	4.53961000	-0.87164600
O	1.28470300	1.74531900	-1.44823600
H	-3.49217900	-2.21042300	-1.52192800

4.052-D

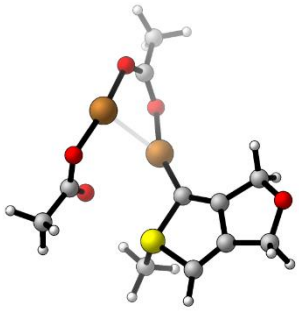

Atom type	X	Y	Z
C	4.52458100	-1.59611100	-0.75828200
C	2.41139800	-2.57554100	-0.51901300
H	1.64280900	-2.92229300	-1.22711500
H	5.21350700	-1.89074000	0.05848200
H	5.13652200	-1.28969700	-1.62141700
H	2.35993900	-3.21972200	0.38147500
C	2.27248400	-1.12998200	-0.14969900
C	3.59173200	-0.53237900	-0.28362000
C	1.25029200	-0.34920900	0.29242800
C	3.65627200	0.76985700	0.05809200
S	1.99642700	1.27697000	0.39604300
C	1.97137800	1.68350700	2.14710700
Cu	-0.57809200	-0.59784700	0.69885400
H	2.37027100	0.84078900	2.72582900
H	0.91660300	1.88769100	2.37302000
H	2.57402100	2.59194200	2.28324300
O	3.68558600	-2.67225600	-1.14236200
Cu	-2.16245900	0.41919900	-1.06857700
O	-1.27494700	2.07737100	-1.32692400
C	-0.80498500	2.63353200	-0.27797900
C	-0.19670100	3.99884600	-0.49325000
H	0.55459300	3.94990600	-1.29594000
H	-0.97940000	4.69760100	-0.82840700
H	0.26102000	4.38267800	0.42767100
O	-0.82143300	2.12831700	0.85755300
O	-2.24340700	-1.46773700	1.23762000
C	-3.16810000	-1.67006800	0.40677900
C	-4.22324300	-2.67373600	0.77581900
H	-4.55619300	-2.50291500	1.80966200
H	-5.07692800	-2.63096000	0.08846400
H	-3.78033500	-3.68196900	0.73922300
O	-3.25717200	-1.10340400	-0.71833400
H	4.47708200	1.48634300	0.02037800

Ag-4.048-A

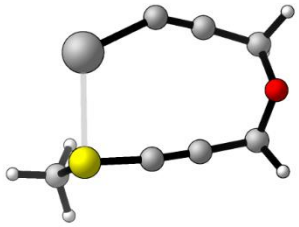

Atom type	X	Y	Z
C	2.89335600	1.42266200	-0.08338000
C	3.15525300	-0.89613400	0.46689900
H	3.88006200	-1.68241300	0.19990300
H	3.15960400	1.67344600	0.96285300
H	3.40652500	2.15355400	-0.72904500
H	3.40100500	-0.56893900	1.49641600
C	1.78858000	-1.41659600	0.41164200
C	1.44372300	1.57562700	-0.23064600
C	0.61172300	-1.76752000	0.31273300
C	0.23326300	1.65659800	-0.32400900
S	-1.44656400	1.58340600	-0.49048400
C	-2.00220400	2.10142900	1.16067200
H	-1.54788400	1.46936200	1.93459900
H	-3.09455500	1.97839300	1.16487000
H	-1.74633600	3.15779700	1.31814700
O	3.39941100	0.16248700	-0.44583100
Ag	-1.28193300	-1.08238300	-0.11099600

Ag-4.049-A

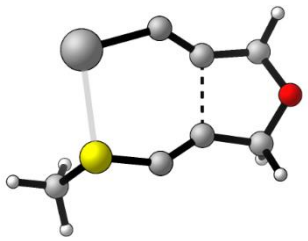

Atom type	X	Y	Z
C	3.09425400	1.08523800	-0.09469600
C	3.00186100	-1.13071100	0.45266700
H	3.35863900	-2.11750700	0.12541800
H	3.36679600	1.53515700	0.88240800
H	3.44364000	1.75637700	-0.89265200
H	3.19711500	-1.03344700	1.54027700
C	1.53915900	-0.98092000	0.20272500
C	1.60310700	0.94720800	-0.12640800
C	0.43118300	-1.59369700	0.15606800
C	0.57143900	1.66453000	-0.28219400
S	-1.08491500	1.56577600	-0.51351800
C	-1.75596400	2.44571100	0.92239900
H	-1.40554500	1.98374500	1.85450900
H	-2.85060800	2.37466500	0.85038500
H	-1.44952300	3.49946700	0.87367300
O	3.71164700	-0.15722200	-0.26982100
Ag	-1.50862300	-0.98760100	-0.04771300

Ag-4.050-A

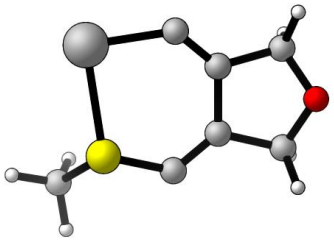

Atom type	X	Y	Z
C	3.14559600	0.99513800	-0.01016100
C	2.87998800	-1.22687400	0.37370200
H	3.10301100	-2.20918000	-0.06387900
H	3.41335500	1.43291800	0.97306000
H	3.51154500	1.66657500	-0.80019100
H	2.99995700	-1.28813900	1.47421700
C	1.46560500	-0.73933800	0.07222500
C	1.63740100	0.78678000	-0.05929200
C	0.40354100	-1.48848700	-0.05789800
C	0.72238500	1.74015000	-0.14775900
S	-0.90963200	1.46432500	-0.48746000
C	-1.79704200	2.52347500	0.67955100
H	-1.55971800	2.24456200	1.71446700
H	-2.87170700	2.39593700	0.48582600
H	-1.50537000	3.56581300	0.49004400
O	3.73719800	-0.26782000	-0.18153400
Ag	-1.55700800	-0.94979100	-0.00264100

Ag-4.048-B

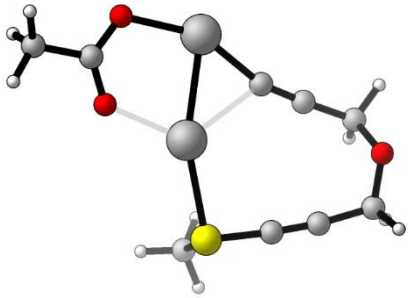

Atom type	X	Y	Z
C	4.62350100	-0.80836400	-0.52303000
C	3.08860400	-2.28203100	0.55064900
H	3.08003100	-3.37699600	0.68373500
H	5.31642500	-0.77711300	0.34167000
H	5.24296700	-0.77898700	-1.43315200
H	3.52684700	-1.85433600	1.47236900
C	1.70571300	-1.82763500	0.38919800
C	3.76463800	0.36901200	-0.46323500
C	0.52124000	-1.50727400	0.26851500
C	2.96070500	1.27474600	-0.34840400
S	1.75140500	2.44517200	-0.29119700
C	1.87659800	3.04952700	1.41736900
H	1.78285300	2.21720200	2.12628800
H	1.04210300	3.75322000	1.54715800
H	2.83216900	3.57454100	1.54832500
O	3.92264900	-2.02788300	-0.56256300
O	-2.44200300	1.33018400	-0.23770300
C	-3.46580000	0.60566000	-0.20210900
C	-4.81384700	1.27601400	-0.28803700
H	-5.22069900	1.36962100	0.73212900
H	-4.73072300	2.27972400	-0.72389000
H	-5.51526700	0.66046500	-0.86798800
O	-3.47740100	-0.65588200	-0.06925700
Ag	-1.53022300	-1.54112600	0.13704400
Ag	-0.19261200	0.76965000	-0.10761500

Ag-4.049-B

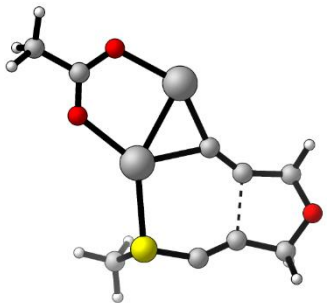

Atom type	X	Y	Z
C	4.54462800	-0.71036300	-0.15086600
C	3.01468300	-2.32307500	0.38772900
H	2.64933800	-3.30936300	0.06848200
H	5.06790300	-0.56399500	0.81637100
H	5.23123800	-0.42343500	-0.96079600
H	3.22440200	-2.36501400	1.47614900
C	1.98156400	-1.27698600	0.13503500
C	3.33737600	0.16315700	-0.14211900
C	0.74276100	-1.03741500	0.07702000
C	2.96301900	1.36116000	-0.22944100
S	1.65709800	2.37464900	-0.41681200
C	1.64073200	3.33395300	1.12334100
H	1.61423700	2.66044700	1.98941000
H	0.73187800	3.95156400	1.09258200
H	2.52920100	3.97875000	1.15456700
O	4.18464800	-2.04927300	-0.33708400
O	-2.57997300	1.24807000	-0.12395800
C	-3.49180800	0.38058300	-0.06240700
C	-4.91245800	0.88898200	-0.06030100
H	-5.13702400	1.29116900	0.94096900
H	-5.02317400	1.71403600	-0.77785200
H	-5.62595500	0.08619500	-0.28512800
O	-3.33084600	-0.86978200	0.02417500
Ag	-1.27637400	-1.62902400	0.09190700
Ag	-0.35956700	0.85611300	-0.13060400

Ag-4.050-B

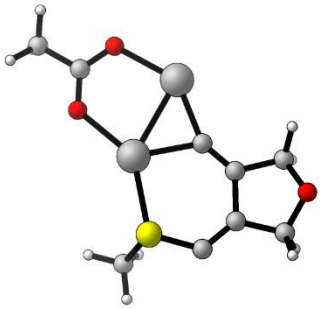

Atom type	X	Y	Z
C	4.46120200	-0.81827800	-0.01192100
C	2.78904500	-2.31395100	0.33453600
H	2.29983900	-3.17928400	-0.13256400
H	4.94342900	-0.69199400	0.97884400
H	5.18524000	-0.53591400	-0.78936600
H	2.84156000	-2.47893700	1.42967000
C	2.05248200	-0.99942400	0.08364100
C	3.19211100	0.01641400	-0.05360500
C	0.75648800	-0.85356400	0.02471200
C	3.10922900	1.33202400	-0.14718800
S	1.70047200	2.19615200	-0.44357900
C	1.65000000	3.44135200	0.86900100
H	1.64836200	2.95807400	1.85455400
H	0.73067500	4.02655000	0.72540900
H	2.52877800	4.09173300	0.76055900
O	4.06597500	-2.15099800	-0.21907300
O	-2.61366700	1.21557300	-0.05719000
C	-3.48733200	0.30789400	-0.01304200
C	-4.92719600	0.74988500	0.04559000
H	-5.17046800	0.99440100	1.09262300
H	-5.07759300	1.65907600	-0.55207500
H	-5.60186900	-0.04876000	-0.28837400
O	-3.26854200	-0.93647400	0.01822400
Ag	-1.18983100	-1.61708600	0.04185800
Ag	-0.39701600	0.93342000	-0.09947600

Ag-4.048-D

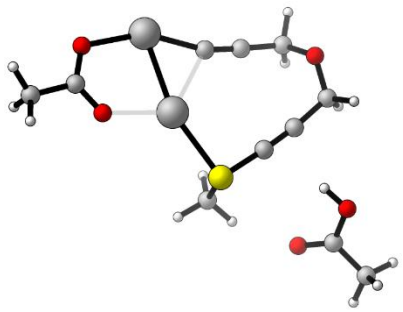

Atom type	X	Y	Z
C	-3.05083300	2.60624500	-0.41584400
C	-1.05392400	3.44285700	0.57724400
H	-0.63547300	4.45915700	0.66882400
H	-3.66375900	2.81587300	0.48352100
H	-3.68635300	2.80434700	-1.29317000
H	-1.58727400	3.23249300	1.52373400
C	0.05429400	2.50200000	0.40062500
C	-2.67007900	1.19626100	-0.38475100
C	1.02907900	1.75794300	0.27324300
C	-2.24526000	0.05816000	-0.29116500
S	-1.56051500	-1.47922400	-0.25762500
C	-1.86637800	-1.99667200	1.45677100
H	-1.42473200	-1.27639900	2.15676300
H	-1.37914700	-2.97650200	1.56130900
H	-2.95109600	-2.08672200	1.59605600
O	-1.96272400	3.49035500	-0.50572600
O	2.73751100	-1.95133600	-0.32432700
C	3.95707700	-1.66427900	-0.24682800
C	4.95010200	-2.79555000	-0.33961000
H	5.09079200	-3.21446900	0.67039700
H	4.56749400	-3.59667600	-0.98591500
H	5.92429100	-2.43975100	-0.69975000
O	4.43554700	-0.50429100	-0.06431200
O	-5.46820200	-0.07544700	-0.76350900
C	-5.83858100	-1.07967600	0.02834900
C	-7.29999100	-1.37041000	-0.06516400
H	-7.87504700	-0.46861700	0.19425200
H	-7.55622500	-1.63195700	-1.10322900
H	-7.56437600	-2.19448000	0.60697600
O	-5.05522700	-1.67675100	0.73395300
H	-4.50449100	0.07025600	-0.65612600
Ag	2.95124000	1.03434700	0.15192900
Ag	0.85568300	-0.60946400	-0.13421600

Ag-4.049-D

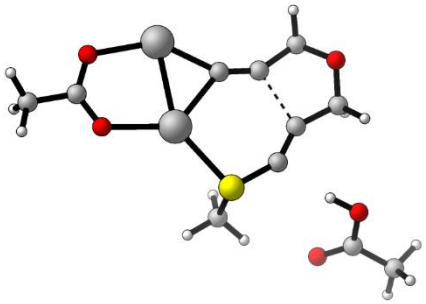

Atom type	X	Y	Z
C	-3.06296400	2.41284700	-0.15697600
C	-1.07277500	3.41096400	0.36613300
H	-0.40093600	4.22051500	0.04696500
H	-3.55351800	2.43934800	0.83763200
H	-3.84792400	2.39965600	-0.92744500
H	-1.26197200	3.52413900	1.45280500
C	-0.43613900	2.08772800	0.12488000
C	-2.24658400	1.16891500	-0.21975300
C	0.61941600	1.40328700	0.08368000
C	-2.29406300	-0.07846700	-0.36845400
S	-1.41279700	-1.48918700	-0.55675000
C	-1.77413800	-2.39004700	0.97655900
H	-1.43942500	-1.80802800	1.84473200
H	-1.22294800	-3.33890800	0.91370500
H	-2.85655200	-2.57082000	1.01924600
O	-2.26500000	3.54104900	-0.36391800
O	2.91918100	-1.90894400	-0.19527000
C	4.07534900	-1.43451400	-0.03993100
C	5.22387200	-2.41221100	-0.01986900
H	5.37686300	-2.74276000	1.02069600
H	4.99516500	-3.29825400	-0.62666300
H	6.15161500	-1.93610700	-0.36364700
O	4.36633200	-0.21653800	0.13429500
O	-5.21700200	-0.12918300	-0.62236000
C	-5.75022300	-1.04977800	0.17237200
C	-7.24256600	-0.97982200	0.20813600
H	-7.55937200	0.02197900	0.53554700
H	-7.64114200	-1.13136700	-0.80668700
H	-7.64027500	-1.74327000	0.88634400
O	-5.08359200	-1.85267400	0.79063800
H	-4.22860400	-0.20254900	-0.58837700
Ag	2.71379000	1.21376300	0.20069200
Ag	0.98279100	-0.75226700	-0.22291700

Ag-4.050-D-pre H

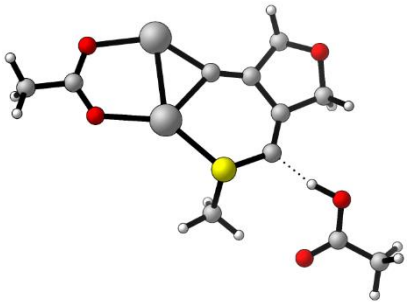

Atom type	X	Y	Z
C	-2.86885300	2.59321900	0.03275300
C	-0.75330200	3.34493800	0.36652400
H	0.02425300	3.96814500	-0.09534100
H	-3.34005700	2.63638100	1.03557900
H	-3.66373000	2.62308900	-0.72556200
H	-0.72782700	3.48870700	1.46512200
C	-0.58553300	1.84921700	0.08367500
C	-1.99933800	1.34886800	-0.05911400
C	0.56463200	1.23345300	0.01219500
C	-2.43913300	0.10079700	-0.19678300
S	-1.42197600	-1.22966000	-0.51387600
C	-1.92439700	-2.44930500	0.72234800
H	-1.67592700	-2.09589200	1.73158700
H	-1.39076600	-3.38286900	0.49608700
H	-3.01186400	-2.58270200	0.61681400
O	-2.00139400	3.68278700	-0.16907300
O	2.89765000	-1.94596500	-0.01449900
C	4.05062100	-1.43692300	0.01666000
C	5.21748600	-2.38791700	0.07484400
H	5.37199400	-2.68012300	1.12648000
H	5.00240900	-3.30048400	-0.49713600
H	6.13609100	-1.91002100	-0.28874400
O	4.31691000	-0.20148200	0.03476900
O	-5.10923000	0.05286700	-0.27738500
C	-5.72693400	-1.05322000	0.05526900
C	-7.22216000	-0.91902500	0.04396200
H	-7.52688300	-0.10367300	0.71751000
H	-7.55825800	-0.64590200	-0.96817700
H	-7.69327800	-1.85967000	0.35313900
O	-5.15814500	-2.09438300	0.34315700
H	-4.05018700	-0.05531800	-0.24673300
Ag	2.64862900	1.20211200	0.04768500
Ag	0.95585500	-0.85573600	-0.10616100

Ag-4.050-D-TS H

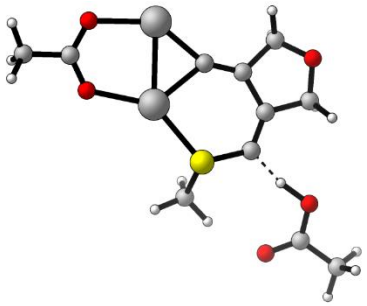

Atom type	X	Y	Z
C	-2.87601000	2.58533600	0.06405800
C	-0.75909900	3.34519700	0.36600000
H	0.01237400	3.96823500	-0.10609700
H	-3.32688600	2.62913800	1.07597000
H	-3.68559900	2.61101600	-0.67829200
H	-0.72085900	3.48856400	1.46411500
C	-0.59658600	1.84703200	0.08371800
C	-2.00177000	1.34602900	-0.04369600
C	0.55593200	1.23633500	0.00023500
C	-2.44567100	0.09723800	-0.18724400
S	-1.42184300	-1.24040000	-0.51036200
C	-1.93271100	-2.45629300	0.72561700
H	-1.66706000	-2.11263100	1.73382000
H	-1.41935300	-3.39833000	0.48818700
H	-3.02465900	-2.56629600	0.62812400
O	-2.01378600	3.67648900	-0.15617200
O	2.88636000	-1.93671200	0.00229200
C	4.04043800	-1.42925800	0.03029600
C	5.20245300	-2.38540400	0.08924600
H	5.26963400	-2.78856900	1.11266200
H	5.03064500	-3.23425800	-0.58718800
H	6.14644500	-1.88299000	-0.15560200
O	4.30715200	-0.19397200	0.03850500
O	-5.03833200	0.04150400	-0.27579300
C	-5.66880400	-1.04561500	0.04482800
C	-7.16880100	-0.90483600	0.02549100
H	-7.47388800	-0.09134900	0.70137600
H	-7.49811300	-0.62414600	-0.98691300
H	-7.65003700	-1.84354300	0.32668700
O	-5.12589100	-2.10677800	0.33763200
H	-3.87947300	-0.06205000	-0.23490400
Ag	2.63760800	1.20382200	0.03557900
Ag	0.94571300	-0.85286900	-0.10747600

Ag-4.050-D-post H

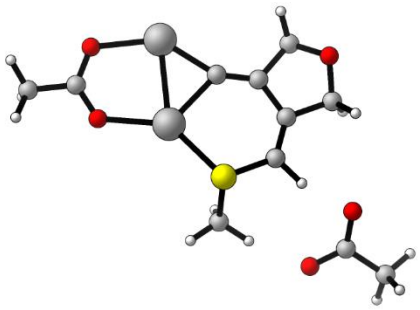

Atom type	X	Y	Z
C	-2.83834000	2.58055800	-0.02234000
C	-0.73721000	3.34939000	0.37176000
H	0.04344200	3.99939100	-0.04536700
H	-3.31103300	2.56746100	0.97944100
H	-3.63137800	2.63083000	-0.78015600
H	-0.73158000	3.42756900	1.47654300
C	-0.56607100	1.86228500	0.01765400
C	-1.94032800	1.36773100	-0.16880800
C	0.59072000	1.25652200	-0.06322600
C	-2.36577300	0.12091200	-0.39387200
S	-1.36463900	-1.26111100	-0.72862500
C	-2.02394400	-2.48196700	0.43047600
H	-1.72840700	-2.23270800	1.45772900
H	-1.61778500	-3.45794000	0.13160100
H	-3.12660900	-2.45712100	0.32786600
O	-1.97815400	3.68792000	-0.17196600
O	2.87674500	-1.93290000	0.05170200
C	4.03188000	-1.44109500	0.15925100
C	5.18114300	-2.40216600	0.29667400
H	5.27811700	-2.67156900	1.36122500
H	4.98526100	-3.32430000	-0.26624400
H	6.12231200	-1.94060700	-0.02808100
O	4.30867000	-0.20696800	0.19389400
O	-5.26596800	0.09721900	-0.26536400
C	-5.75902500	-0.96899800	0.19147300
C	-7.24598000	-0.94053100	0.52584900
H	-7.54214300	0.04350100	0.91780200
H	-7.81959800	-1.11218800	-0.40038500
H	-7.50878800	-1.73175100	1.24209400
O	-5.14846300	-2.04816000	0.36228800
H	-3.47140100	-0.07146500	-0.44159000
Ag	2.65472000	1.18177400	0.09438300
Ag	0.95355100	-0.84313700	-0.17328200

6.4.12. X-Ray Data

CCDC deposition number: 2260026

ORTEP drawing of K1392_FP (**4.017c-OTf**):

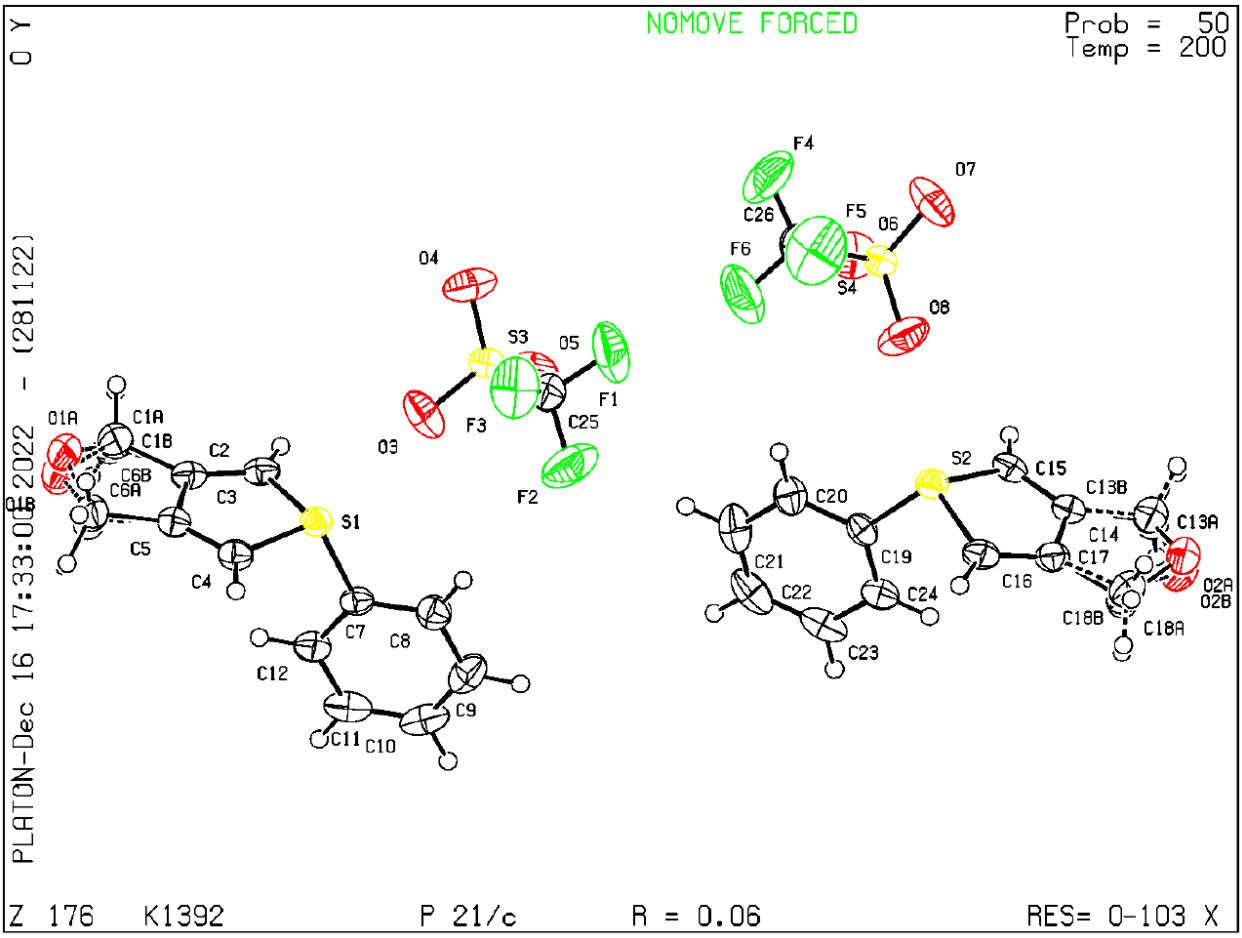

6.4.13. NMR Spectra

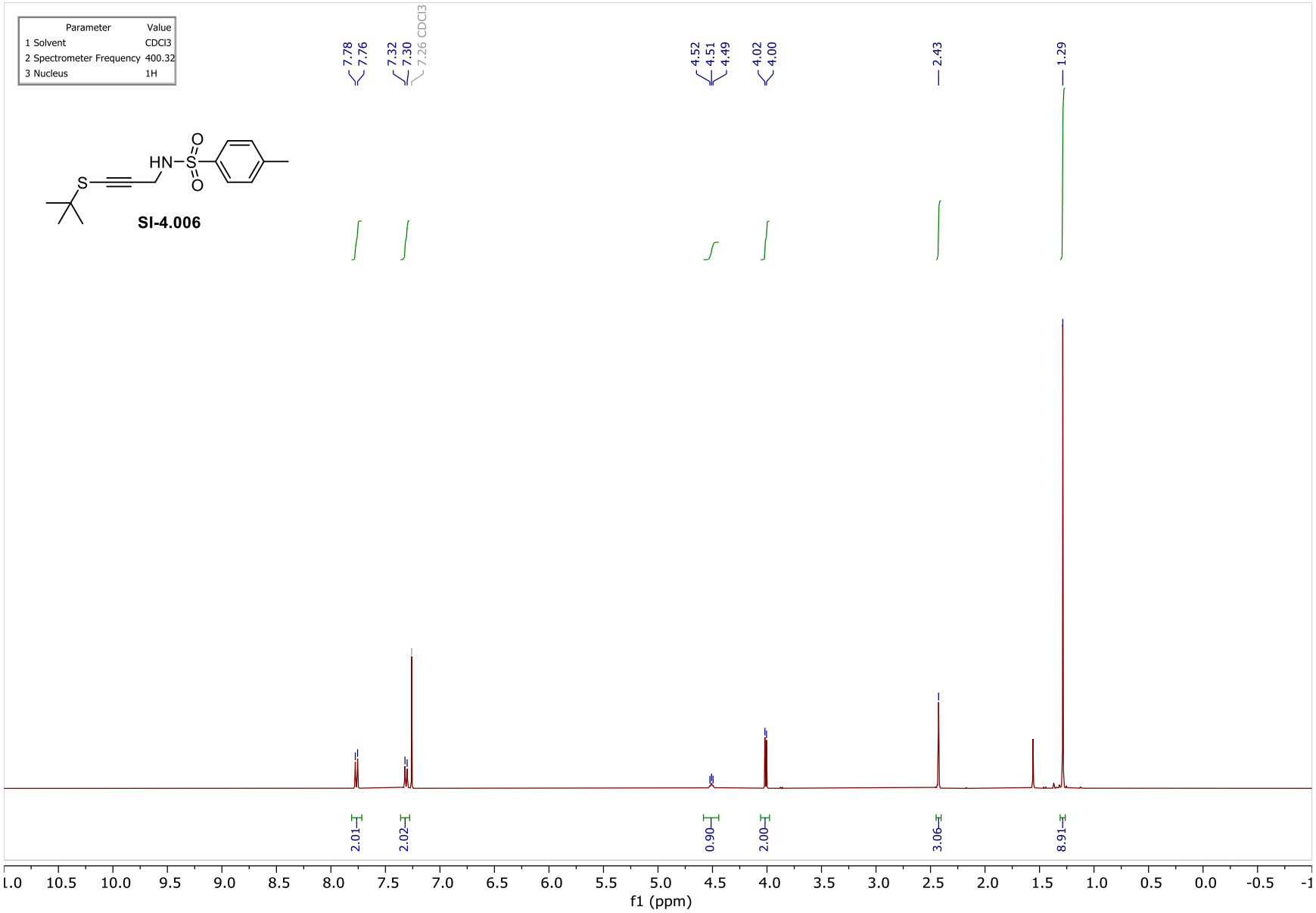
Parameter Value
1 Solvent CDCl3
2 Spectrometer Frequency 400.32
3 Nucleus 1H
SI-4.006
7.78
7.76
7.32
7.30
7.26 CDCl3
4.52
4.51
4.49
4.02
4.00
2.43
1.29
2.01
2.02
0.90
2.00
3.06
8.91
f1 (ppm)

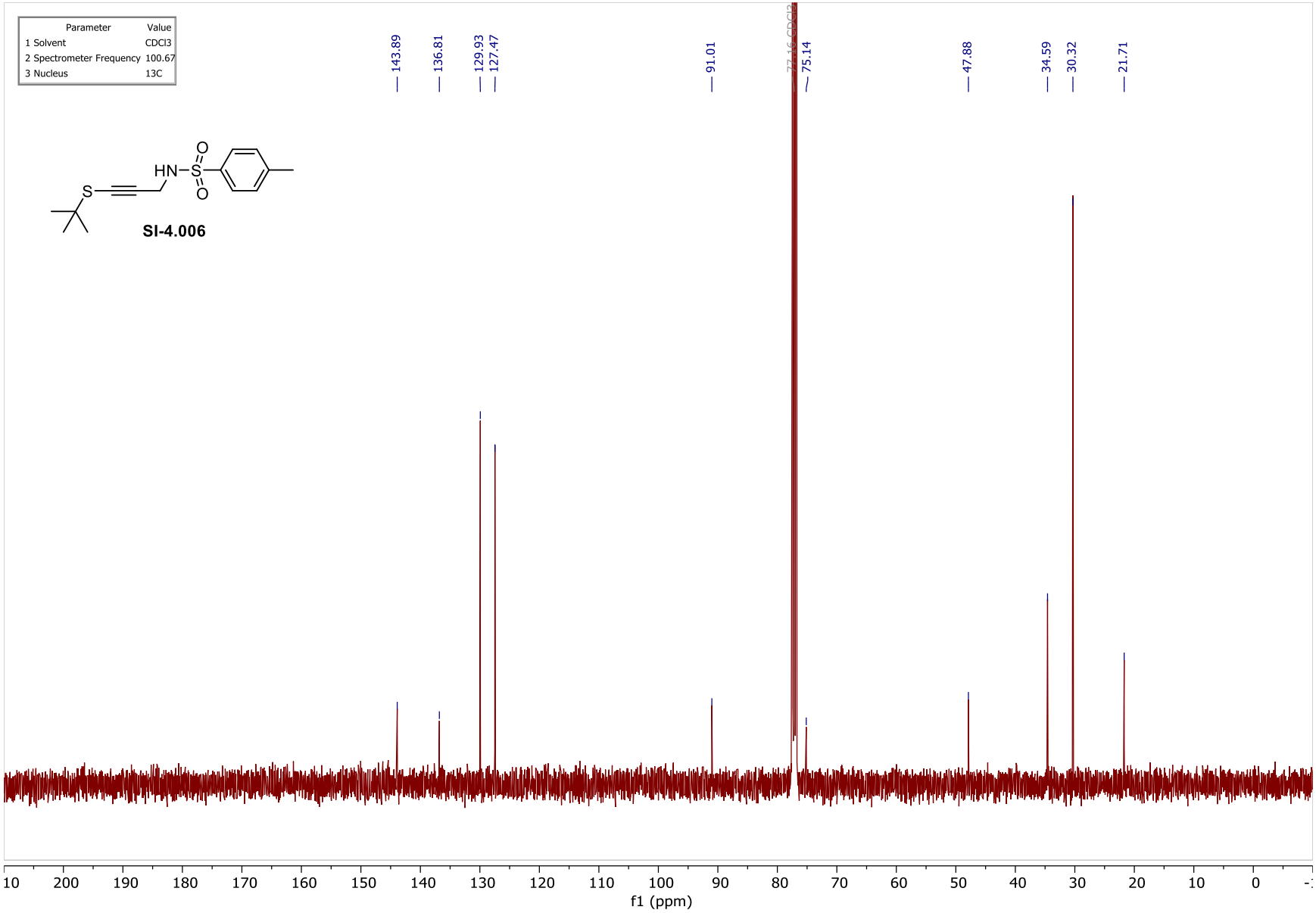
Parameter Value
1 Solvent CDCl3
2 Spectrometer Frequency 100.67
3 Nucleus 13C
143.89
136.81
129.93
127.47
91.01
77.16 CDCl3
75.14
47.88
34.59
30.32
21.71
HN
S
O
O
S
SI-4.006
10 200 190 180 170 160 150 140 130 120 110 100 90 80 70 60 50 40 30 20 10 0
f1 (ppm)

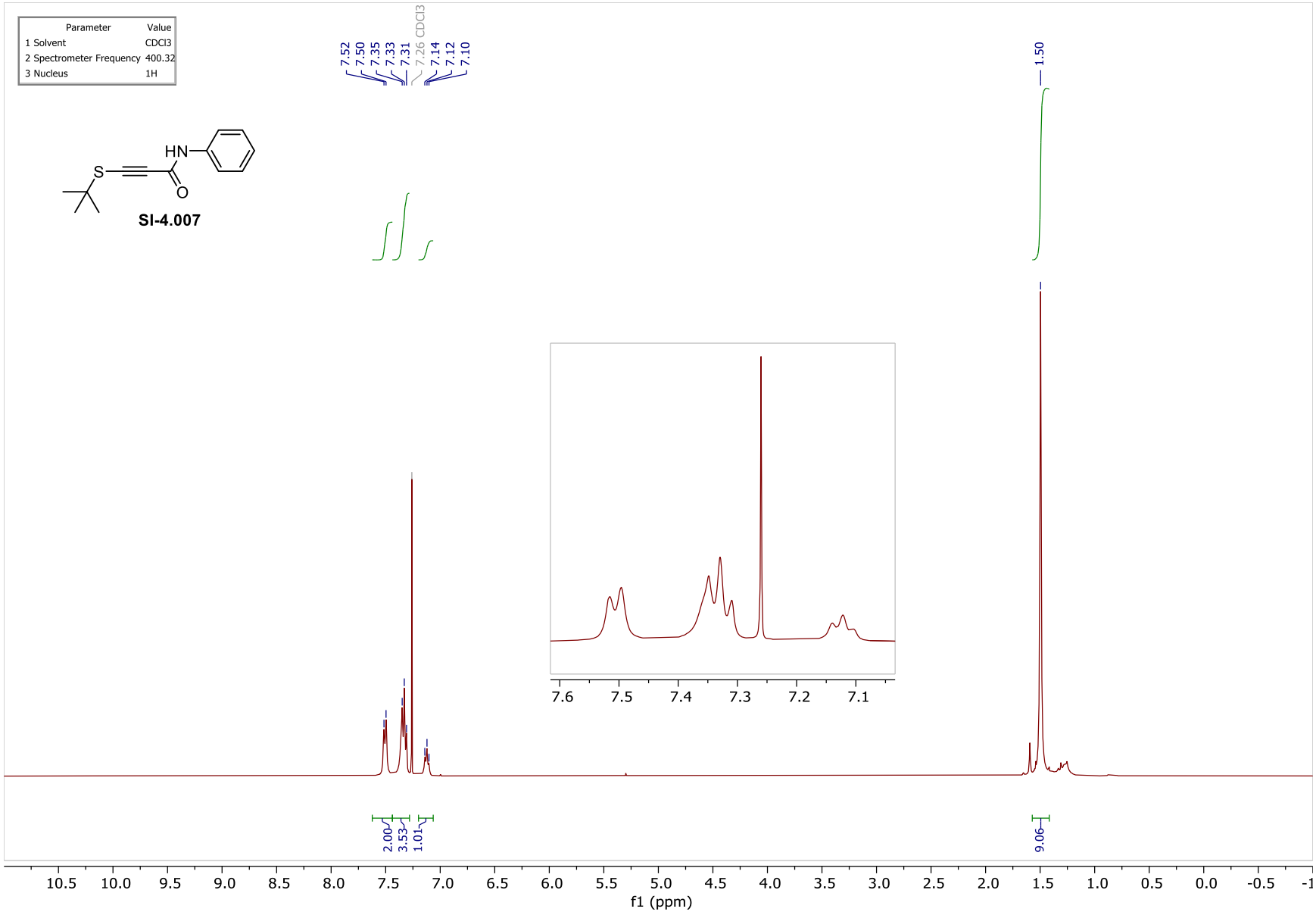
Parameter Value
1 Solvent CDCl3
2 Spectrometer Frequency 400.32
3 Nucleus 1H
HN
S
O
SI-4.007
7.52
7.50
7.35
7.33
7.31
7.26 CDCl3
7.14
7.12
7.10
1.50
2.00
3.53
1.01
9.06
f1 (ppm)

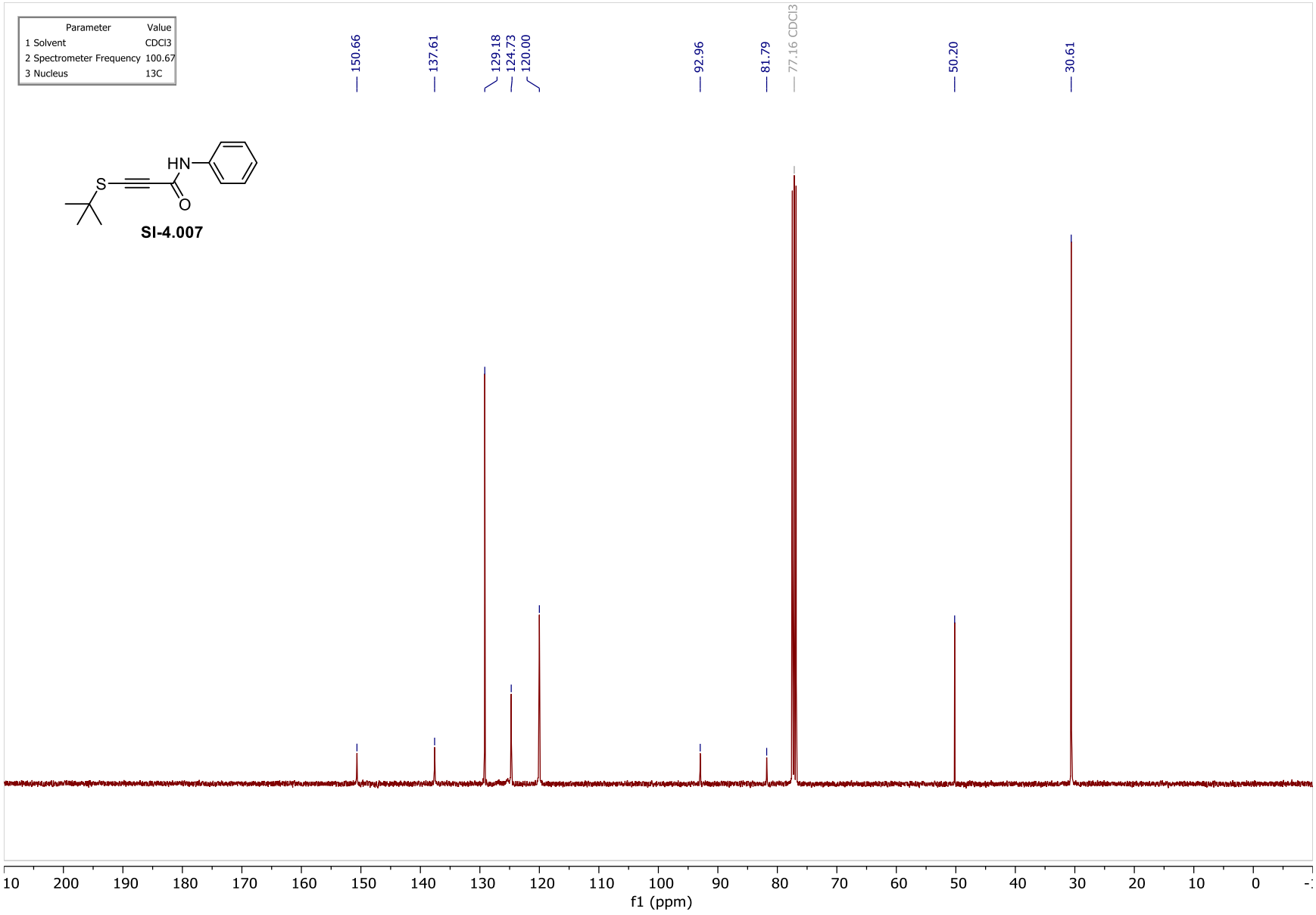
Parameter Value
1 Solvent CDCl3
2 Spectrometer Frequency 100.67
3 Nucleus 13C
150.66
137.61
129.18
124.73
120.00
92.96
81.79
77.16 CDCl3
50.20
30.61
HN
S
O
SI-4.007
f1 (ppm)

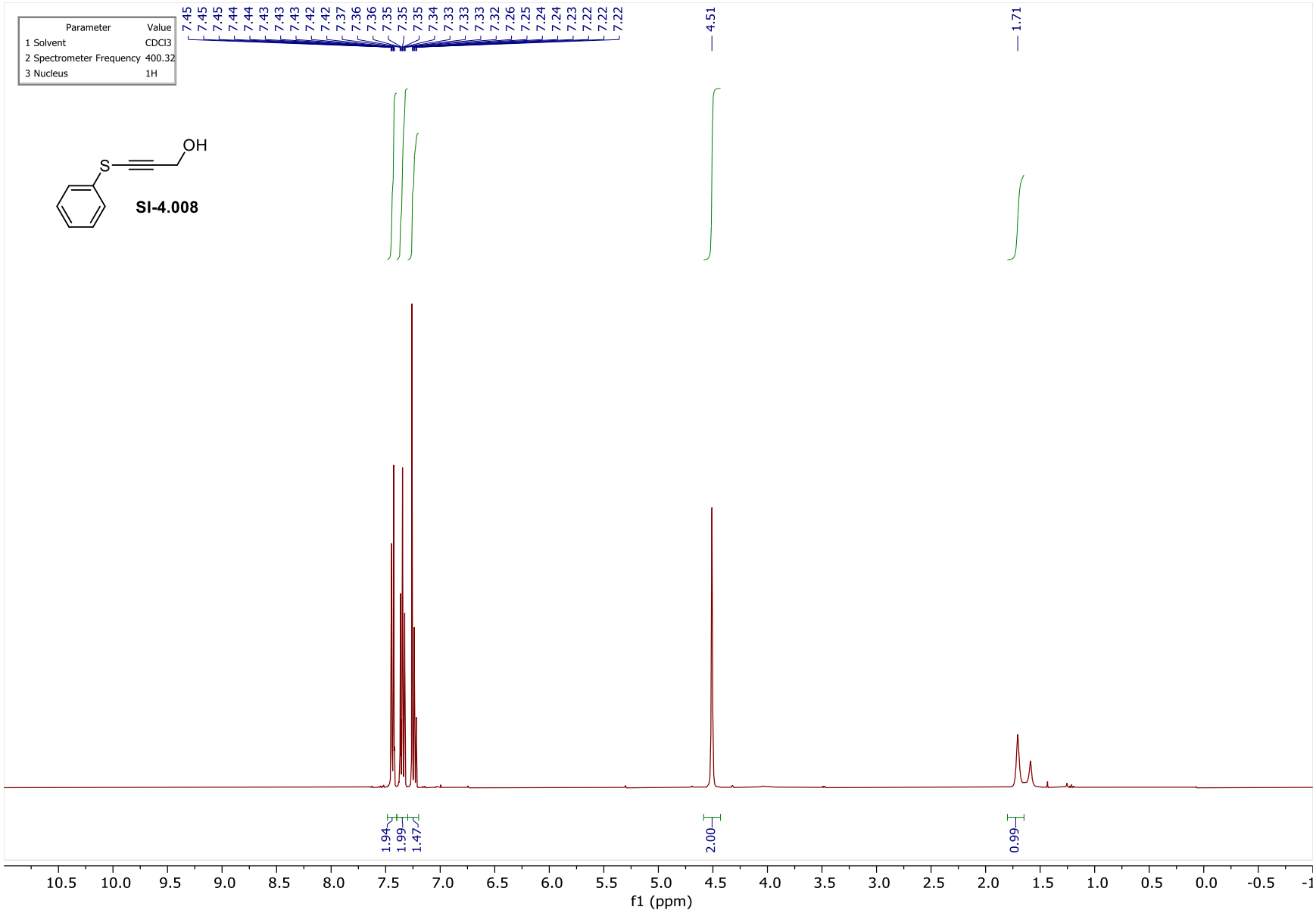
Parameter Value
1 Solvent CDCl3
2 Spectrometer Frequency 400.32
3 Nucleus 1H
OH
S
SI-4.008
7.45 7.45 7.45 7.44 7.44 7.43 7.43 7.43 7.42 7.42 7.37 7.36 7.36 7.35 7.35 7.35 7.34 7.33 7.33 7.33 7.32 7.26 7.25 7.24 7.24 7.23 7.22 7.22 7.22
4.51
1.71
1.94
1.99
1.47
2.00
0.99
10.5 10.0 9.5 9.0 8.5 8.0 7.5 7.0 6.5 6.0 5.5 5.0 4.5 4.0 3.5 3.0 2.5 2.0 1.5 1.0 0.5 0.0 -0.5 -1
f1 (ppm)

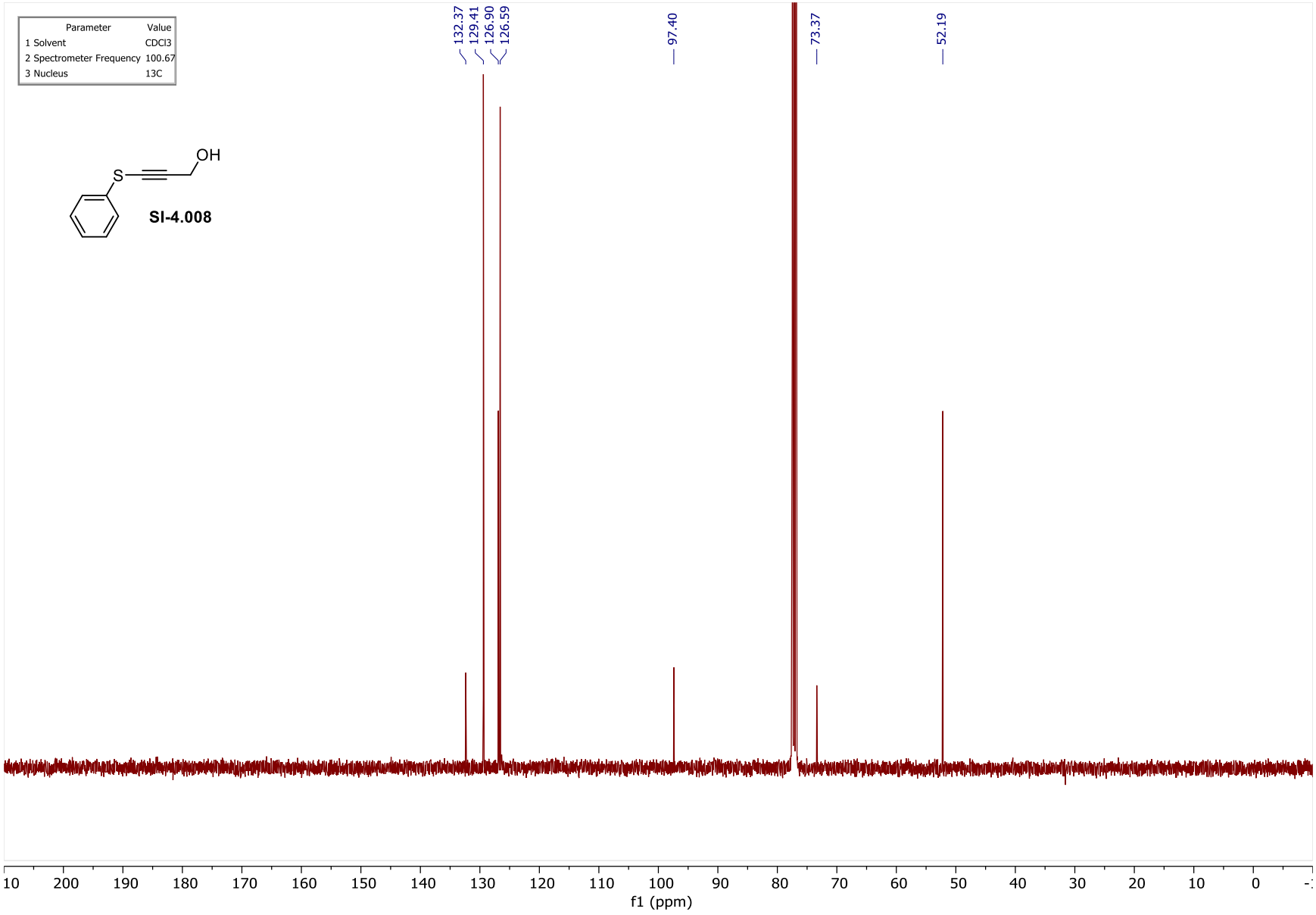
Parameter Value
1 Solvent CDCl3
2 Spectrometer Frequency 100.67
3 Nucleus 13C
OH
S
SI-4.008
132.37
129.41
126.90
126.59
97.40
73.37
52.19
f1 (ppm)

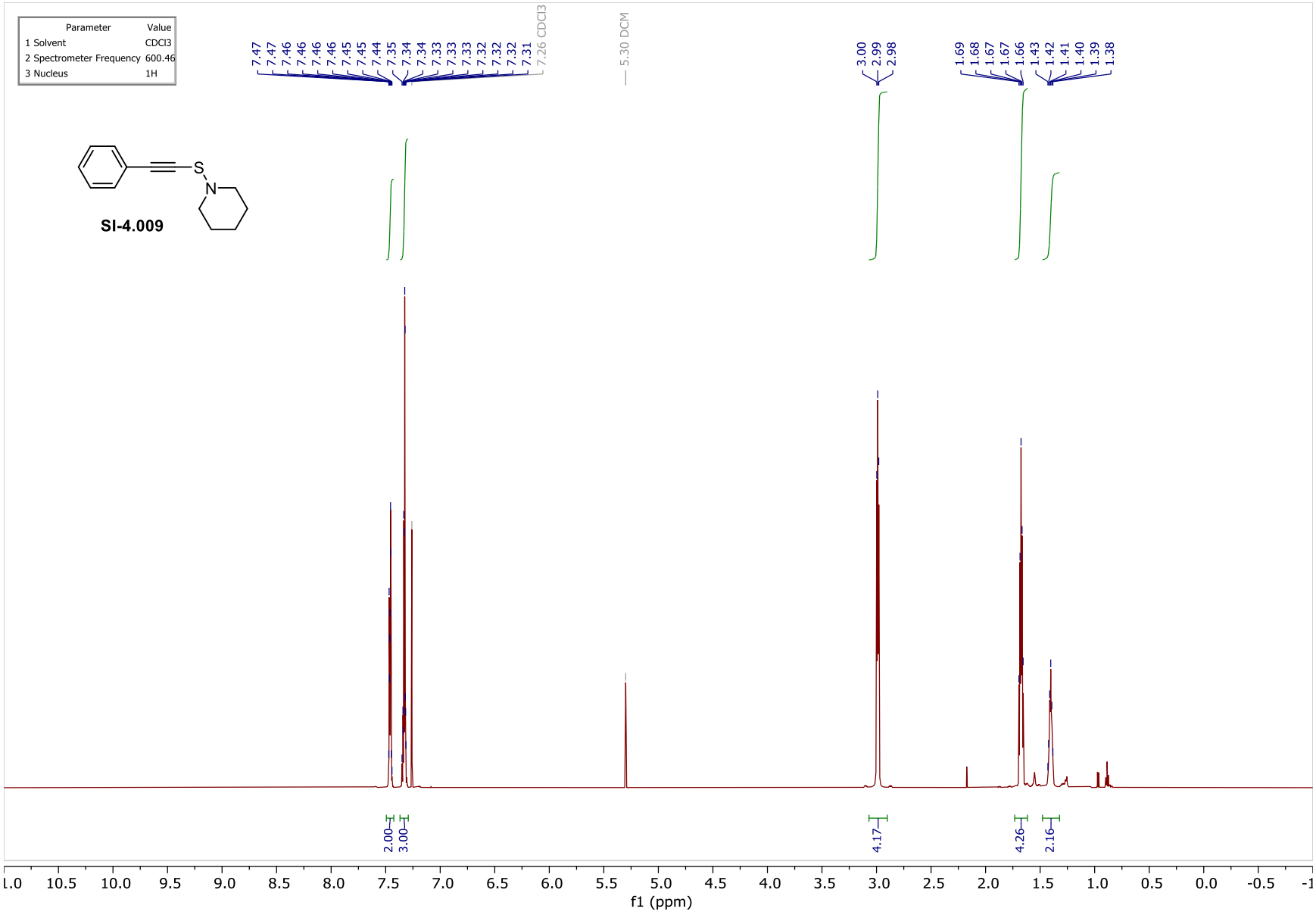
Parameter Value
1 Solvent CDCl3
2 Spectrometer Frequency 600.46
3 Nucleus 1H
SI-4.009
7.47 7.47 7.46 7.46 7.46 7.46 7.45 7.45 7.44 7.35 7.34 7.34 7.33 7.33 7.33 7.32 7.32 7.32 7.31
7.26 CDCl3
5.30 DCM
3.00 2.99 2.98
1.69 1.68 1.67 1.67 1.66 1.43 1.42 1.41 1.40 1.39 1.38
2.00
3.00
4.17
4.26
2.16
f1 (ppm)

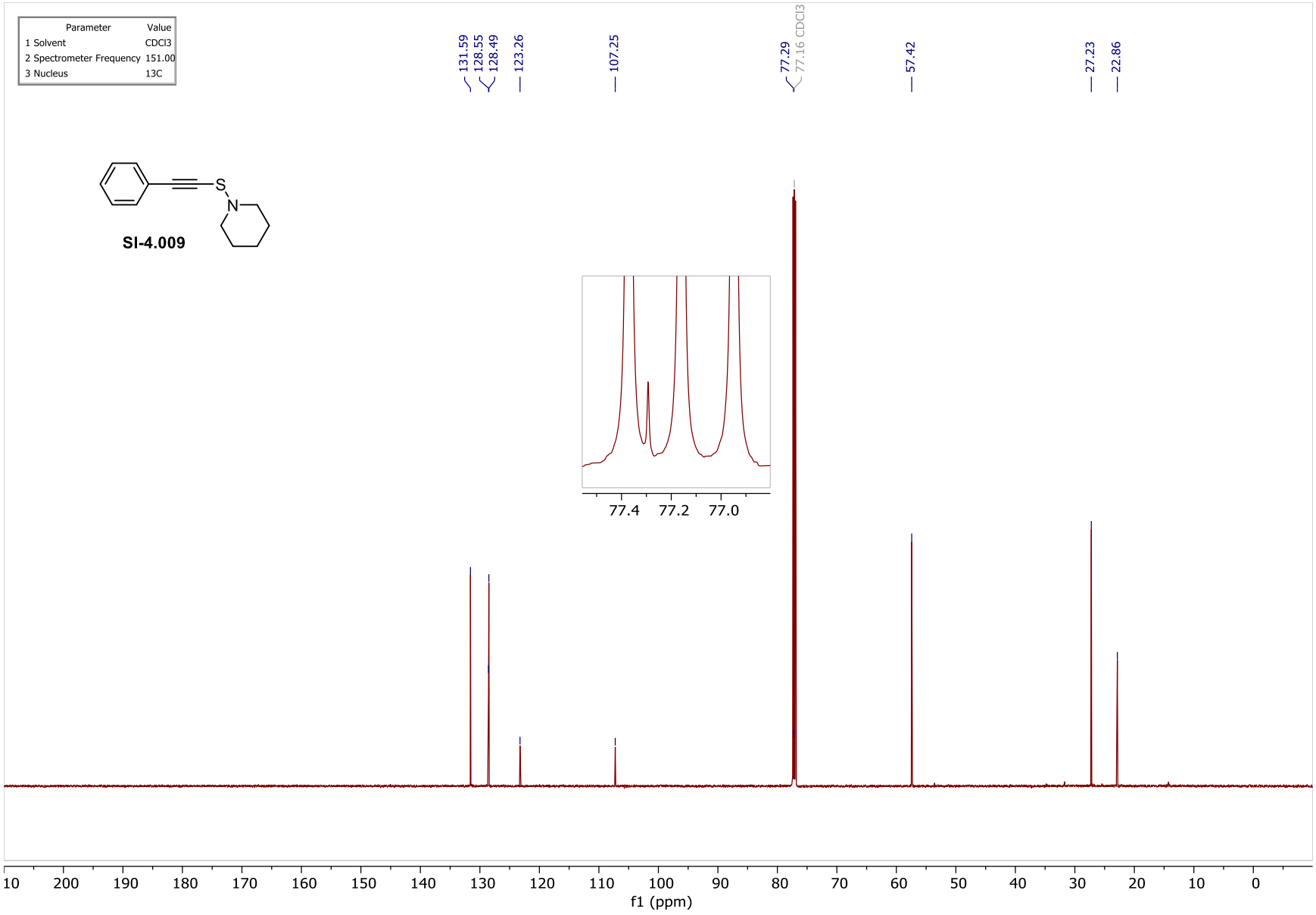
Parameter Value
1 Solvent CDCl3
2 Spectrometer Frequency 151.00
3 Nucleus 13C
131.59
128.55
128.49
123.26
107.25
77.29
77.16 CDCl3
57.42
27.23
22.86
SI-4.009
77.4
77.2
77.0
f1 (ppm)

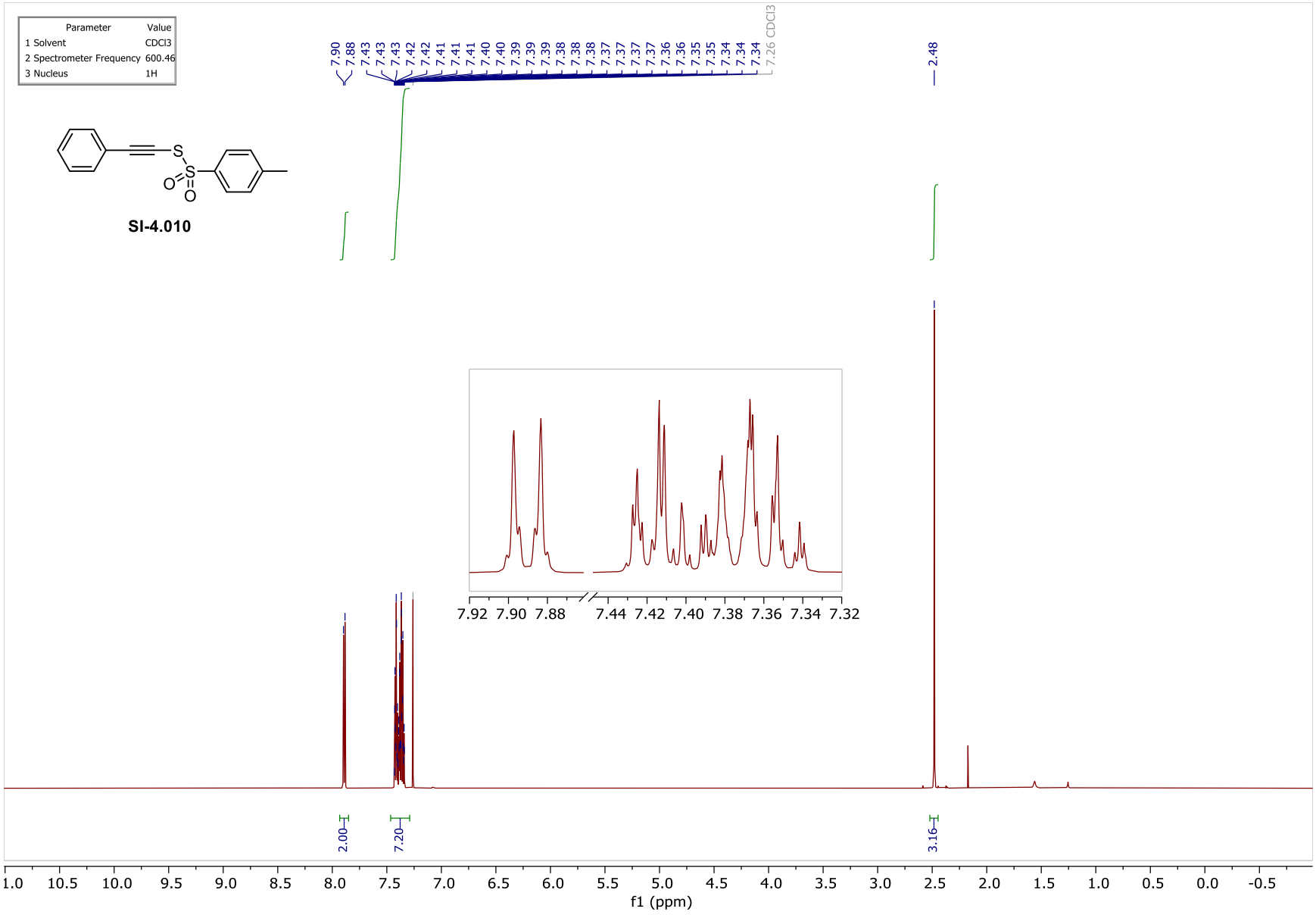
Parameter Value
1 Solvent CDCl3
2 Spectrometer Frequency 600.46
3 Nucleus 1H
SI-4.010
7.90 7.88 7.43 7.43 7.42 7.42 7.41 7.41 7.40 7.40 7.39 7.39 7.39 7.38 7.38 7.37 7.37 7.37 7.36 7.36 7.35 7.35 7.34 7.34 7.34 7.26 CDCl3
2.48
7.92 7.90 7.88 7.44 7.42 7.40 7.38 7.36 7.34 7.32
2.00
7.20
3.16
1.0 10.5 10.0 9.5 9.0 8.5 8.0 7.5 7.0 6.5 6.0 5.5 5.0 4.5 4.0 3.5 3.0 2.5 2.0 1.5 1.0 0.5 0.0 -0.5
f1 (ppm)

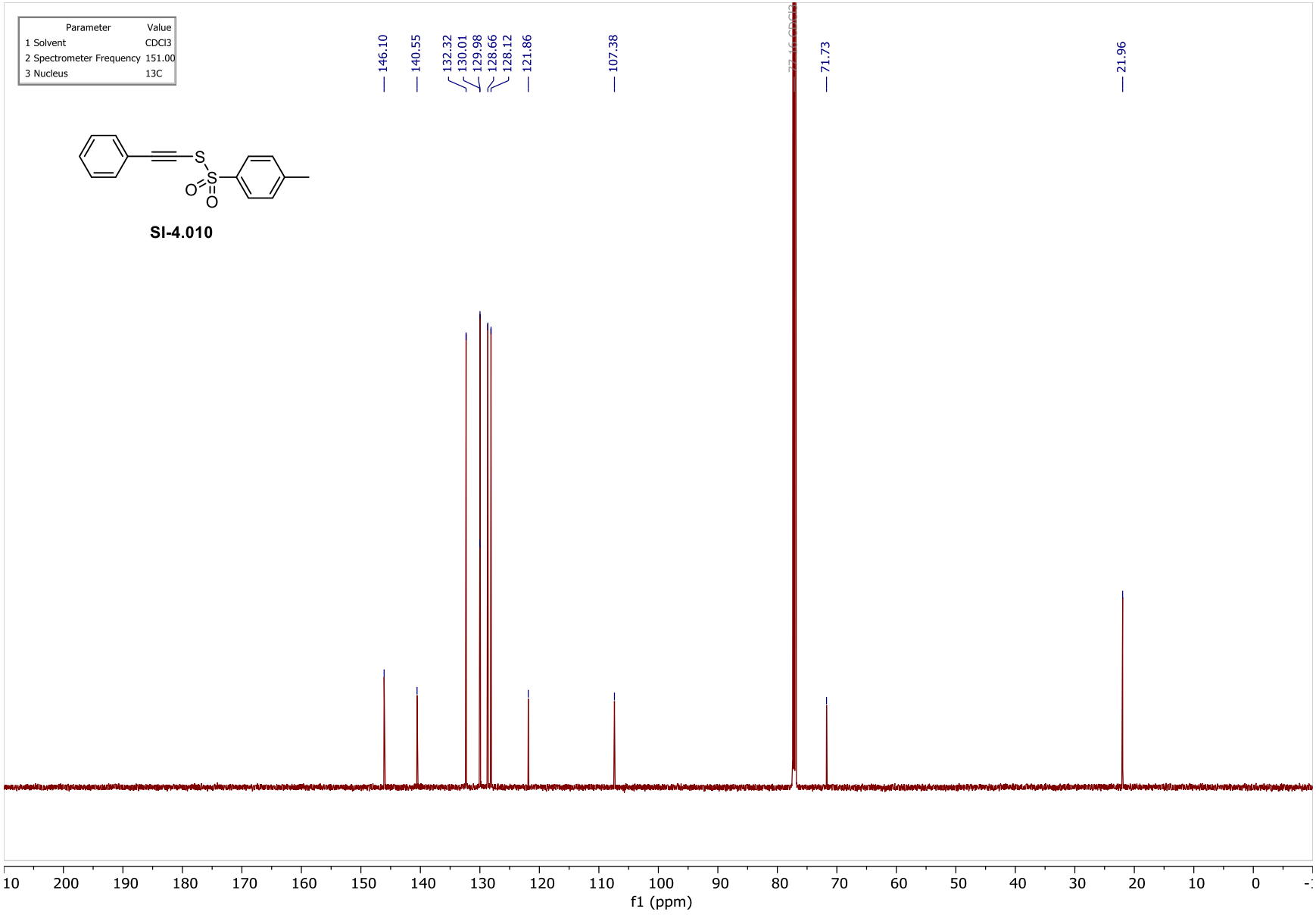
Parameter Value
1 Solvent CDCl3
2 Spectrometer Frequency 151.00
3 Nucleus 13C
SI-4.010
146.10
140.55
132.32
130.01
129.98
128.66
128.12
121.86
107.38
77.16
71.73
21.96
f1 (ppm)

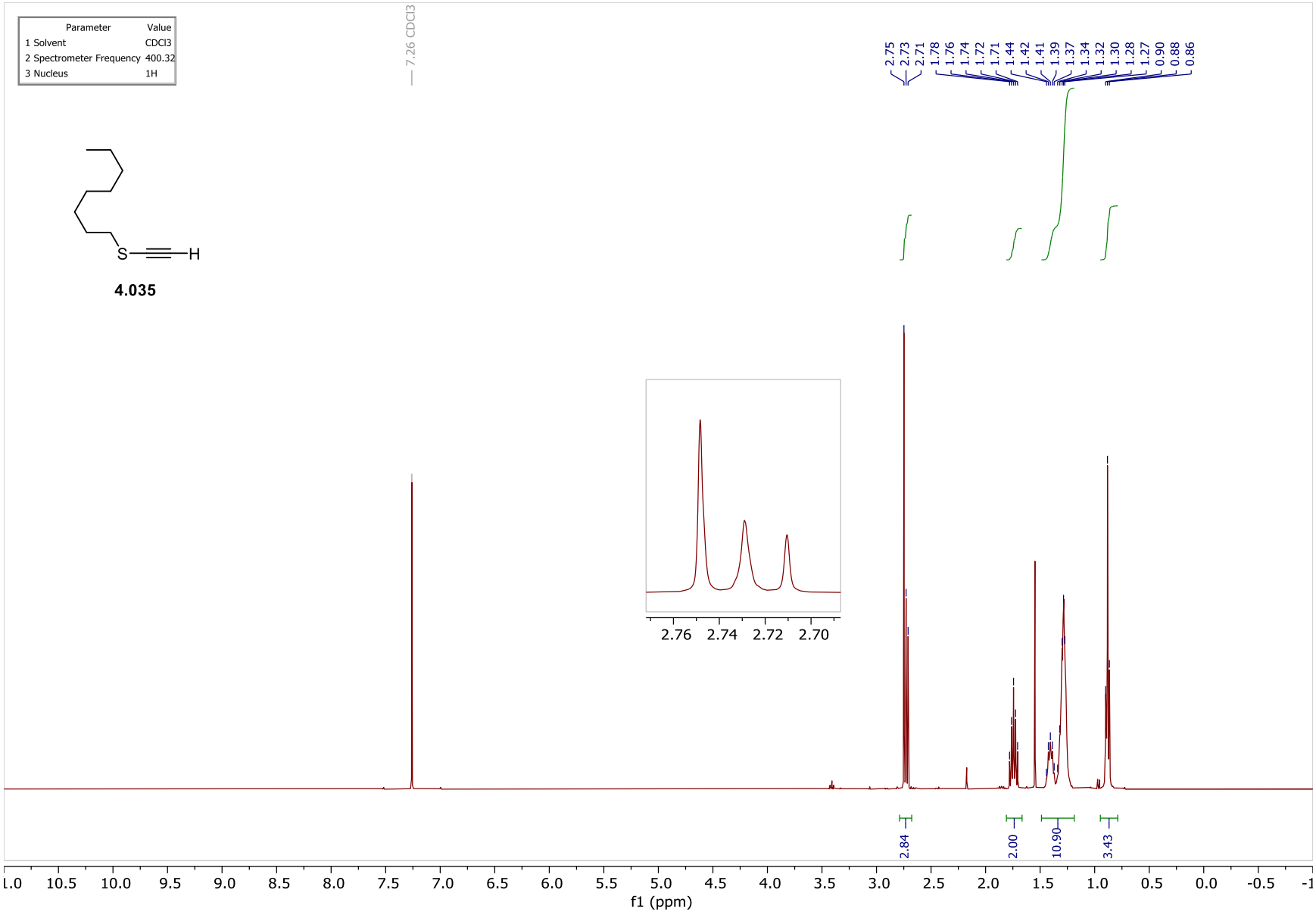
Parameter Value
1 Solvent CDCl3
2 Spectrometer Frequency 400.32
3 Nucleus 1H
7.26 CDCl3
2.75 2.73 2.71 1.78 1.76 1.74 1.72 1.71 1.44 1.42 1.41 1.39 1.37 1.34 1.32 1.30 1.28 1.27 0.90 0.88 0.86
S H
4.035
2.76 2.74 2.72 2.70
2.84 2.00 10.90 3.43
f1 (ppm)

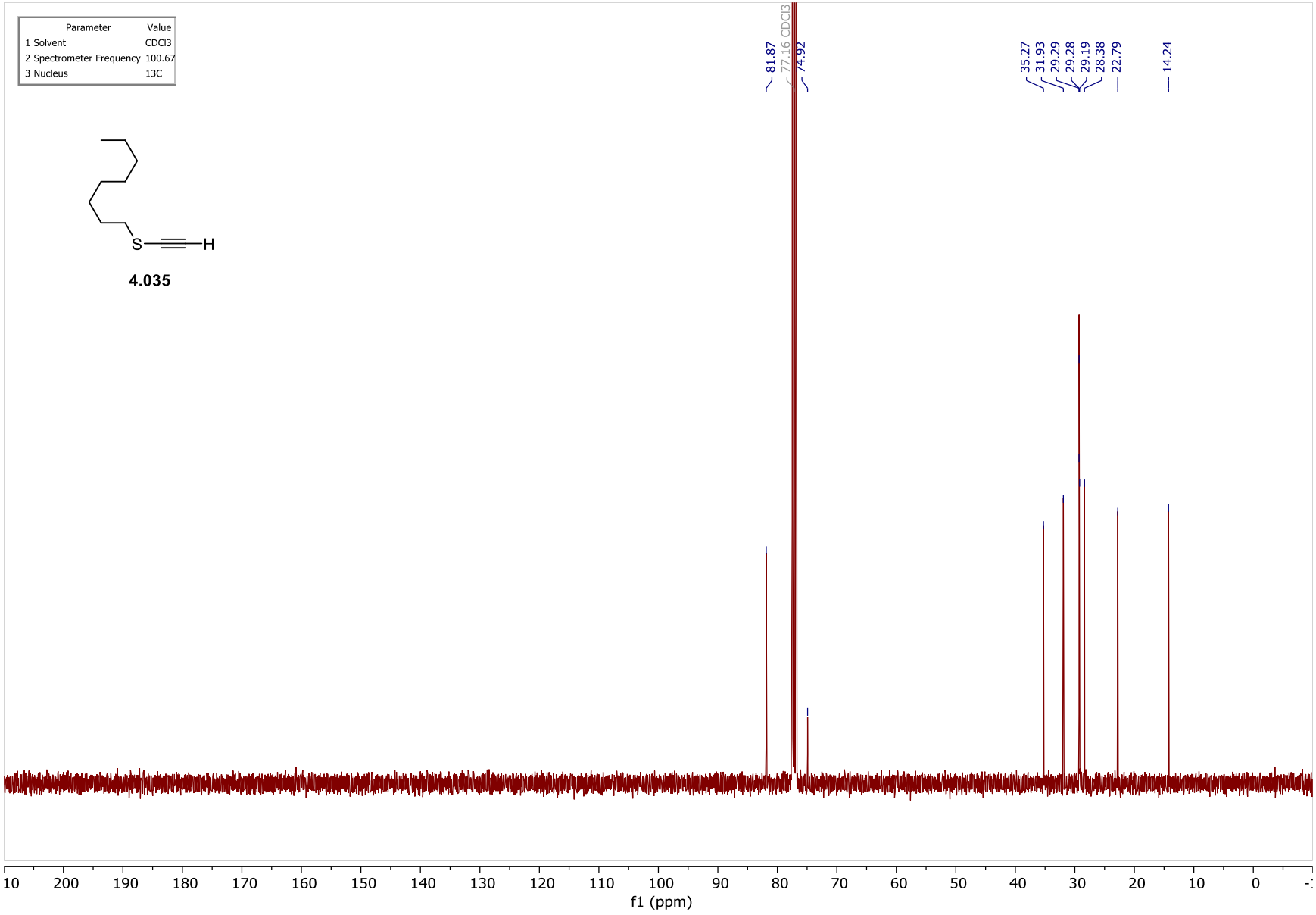
Parameter Value
1 Solvent CDCl3
2 Spectrometer Frequency 100.67
3 Nucleus 13C
S
H
4.035
81.87
77.16 CDCl3
74.92
35.27
31.93
29.29
29.28
29.19
28.38
22.79
14.24
f1 (ppm)

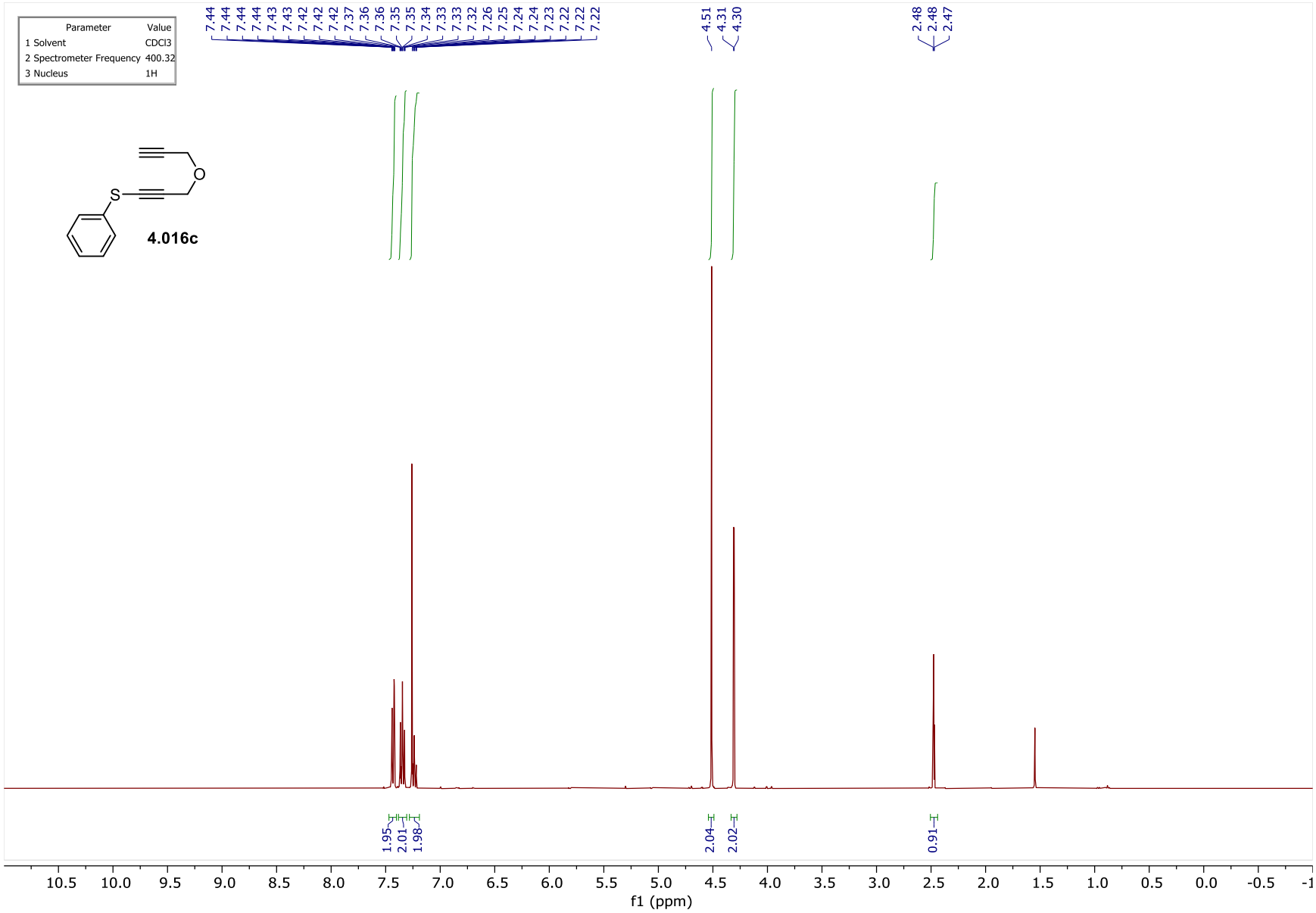
Parameter Value
1 Solvent CDCl3
2 Spectrometer Frequency 400.32
3 Nucleus 1H
4.016c
7.44 7.44 7.44 7.44 7.43 7.43 7.42 7.42 7.42 7.37 7.36 7.36 7.35 7.35 7.34 7.33 7.33 7.32 7.26 7.25 7.24 7.24 7.23 7.22 7.22 7.22
4.51 4.31 4.30
2.48 2.48 2.47
1.95 2.01 1.98 2.04 2.02 0.91
10.5 10.0 9.5 9.0 8.5 8.0 7.5 7.0 6.5 6.0 5.5 5.0 4.5 4.0 3.5 3.0 2.5 2.0 1.5 1.0 0.5 0.0 -0.5 -1
f1 (ppm)

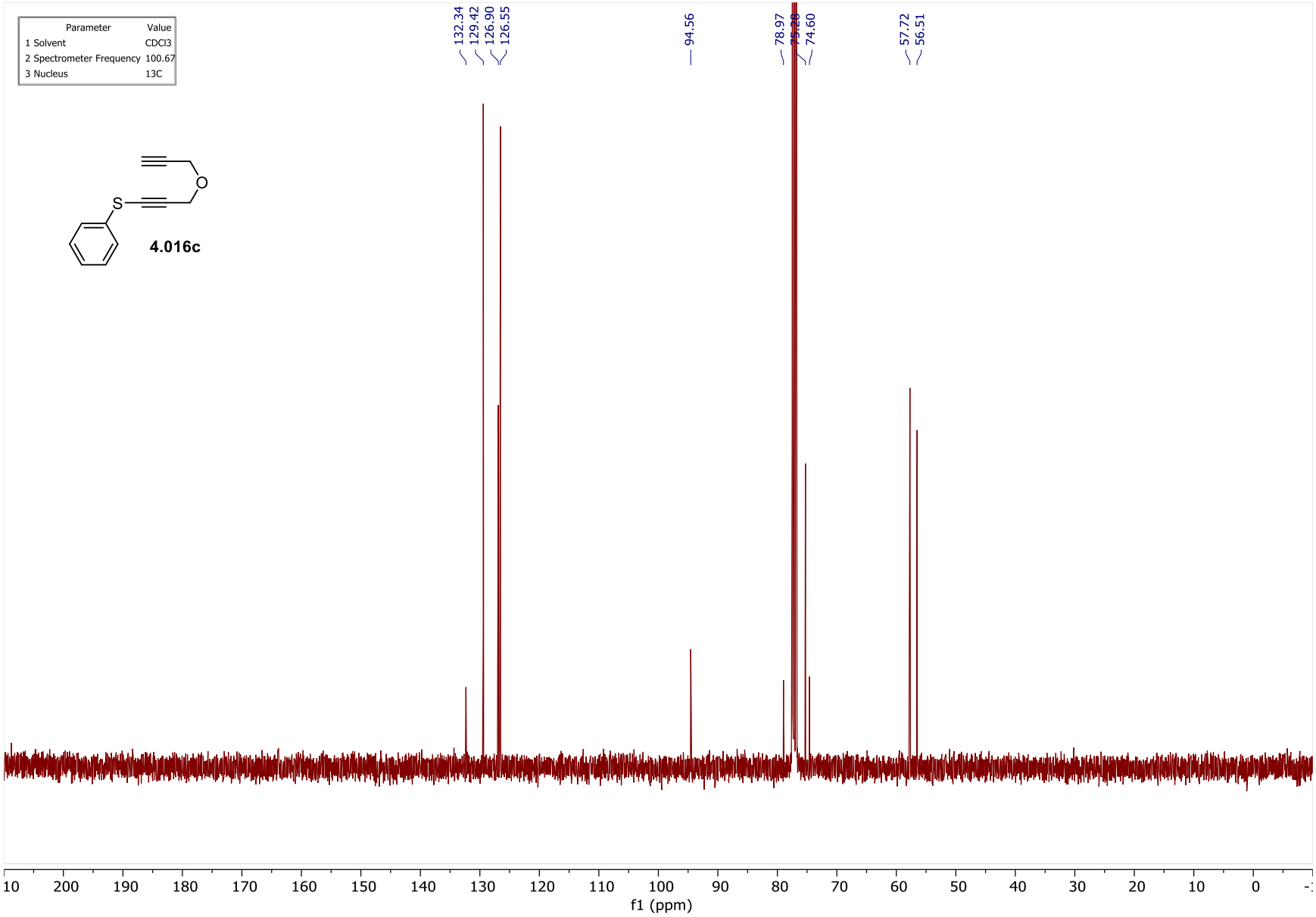
Parameter Value
1 Solvent CDCl3
2 Spectrometer Frequency 100.67
3 Nucleus 13C
4.016c
132.34
129.42
126.90
126.55
94.56
78.97
75.28
74.60
57.72
56.51
f1 (ppm)

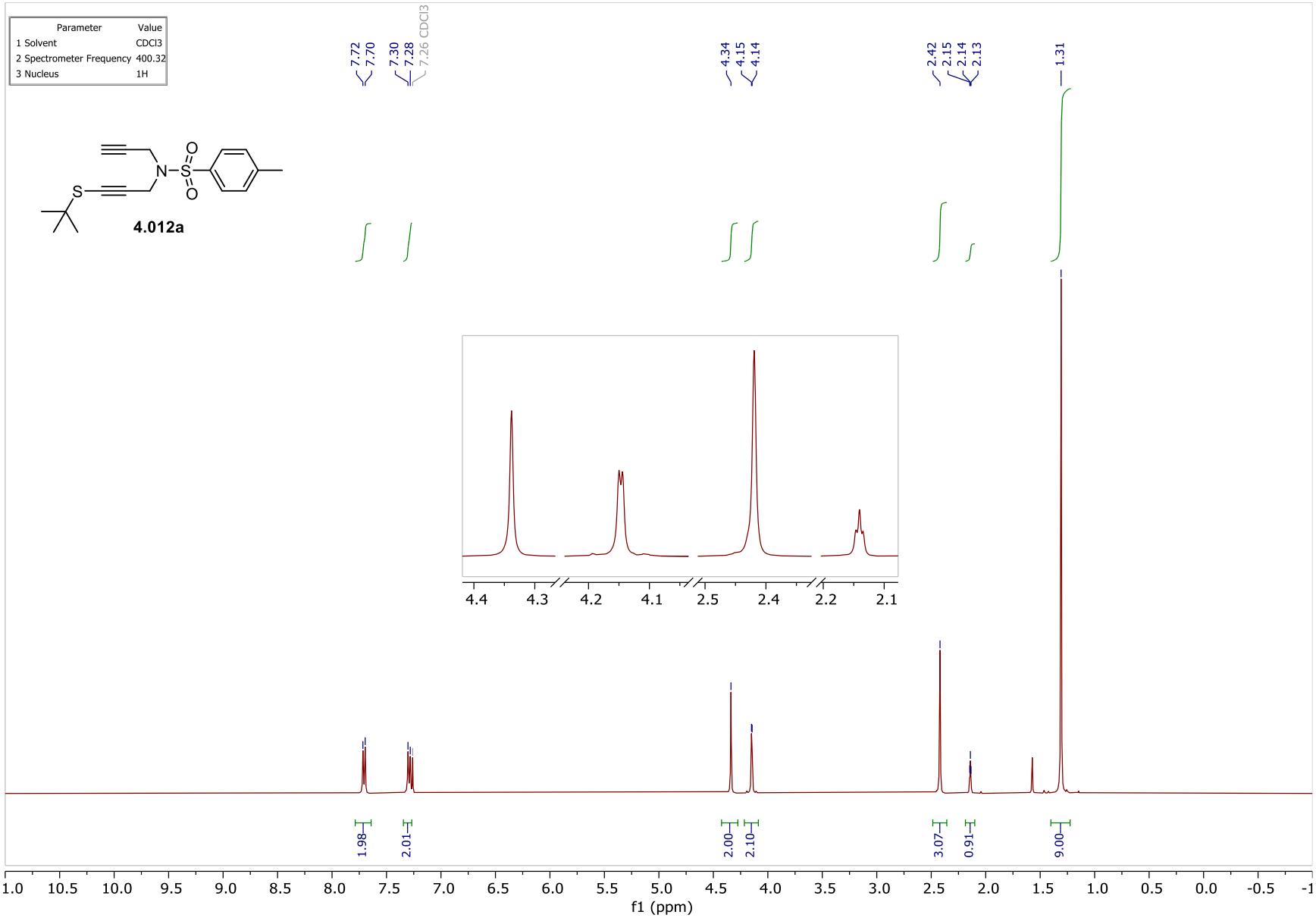
Parameter Value
1 Solvent CDCl3
2 Spectrometer Frequency 400.32
3 Nucleus 1H
4.012a
7.72
7.70
7.30
7.28
7.26 CDCl3
4.34
4.15
4.14
2.42
2.15
2.14
2.13
1.31
1.98
2.01
2.00
2.10
3.07
0.91
9.00
f1 (ppm)

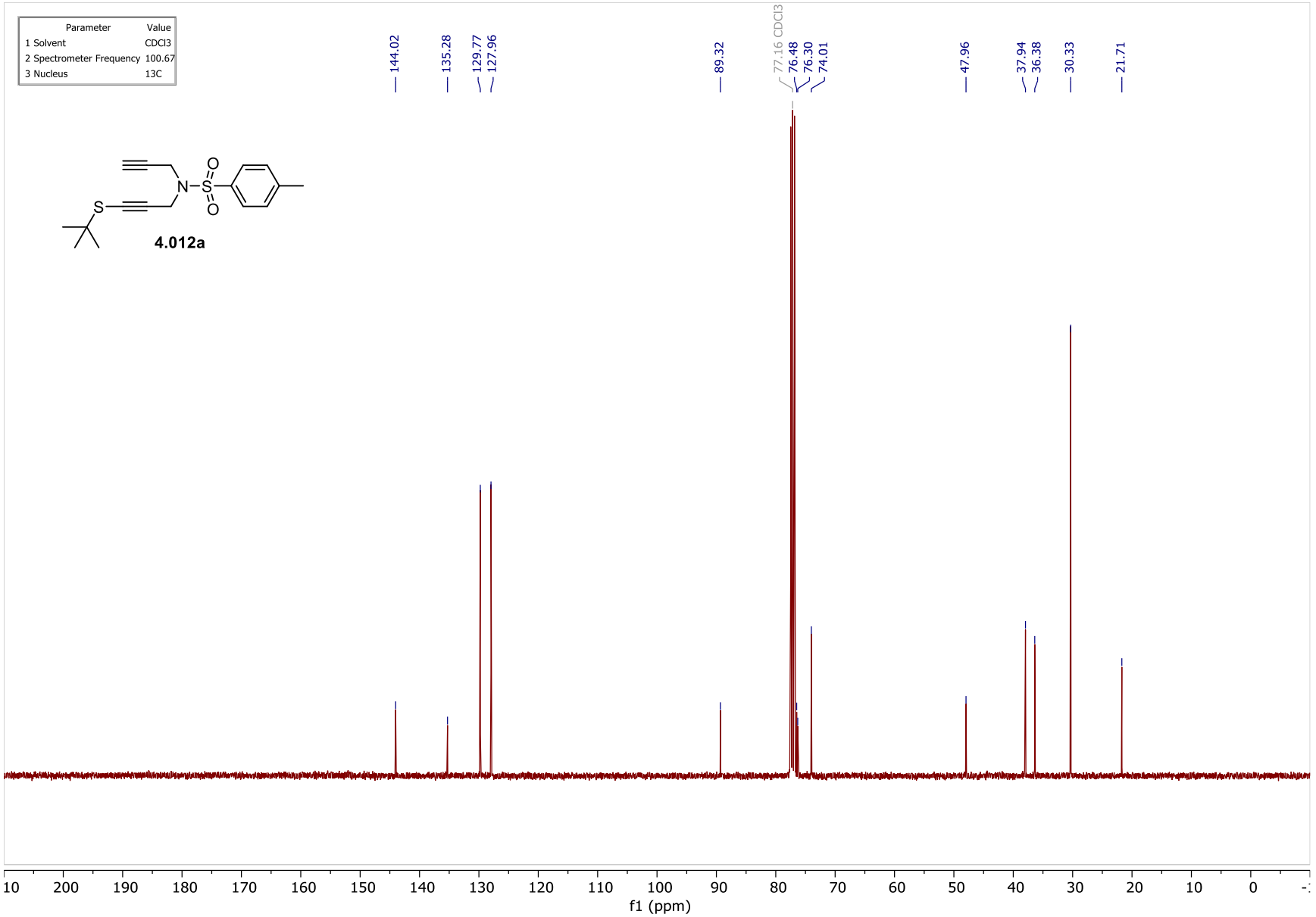
Parameter Value
1 Solvent CDCl3
2 Spectrometer Frequency 100.67
3 Nucleus 13C
144.02
135.28
129.77
127.96
89.32
77.16 CDCl3
76.48
76.30
74.01
47.96
37.94
36.38
30.33
21.71
4.012a
f1 (ppm)

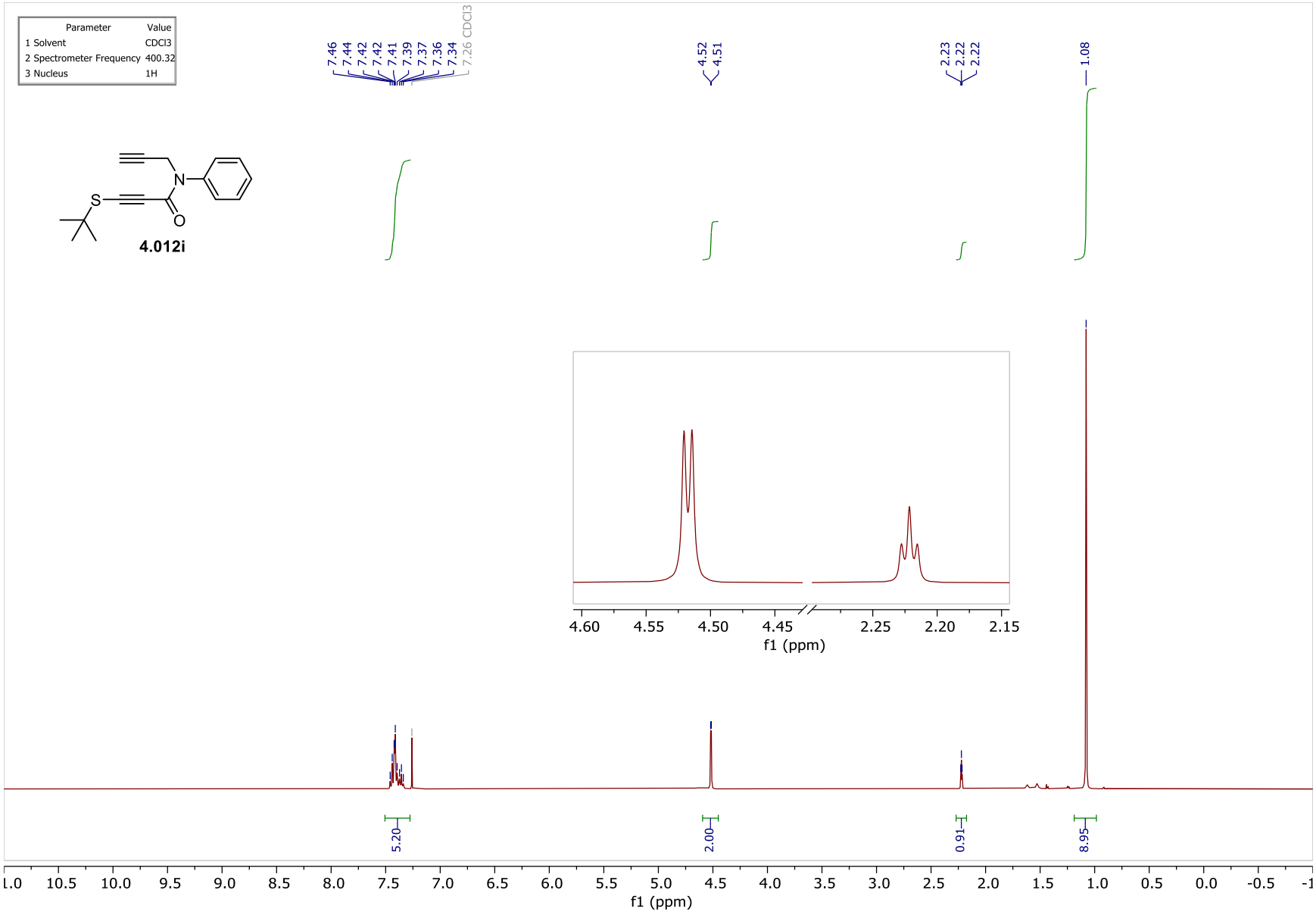
Parameter Value
1 Solvent CDCl3
2 Spectrometer Frequency 400.32
3 Nucleus 1H
7.46
7.44
7.42
7.42
7.41
7.39
7.37
7.36
7.34
7.26 CDCl3
4.52
4.51
2.23
2.22
2.22
1.08
4.012i
4.60
4.55
4.50
4.45
2.25
2.20
2.15
f1 (ppm)
5.20
2.00
0.91
8.95
f1 (ppm)

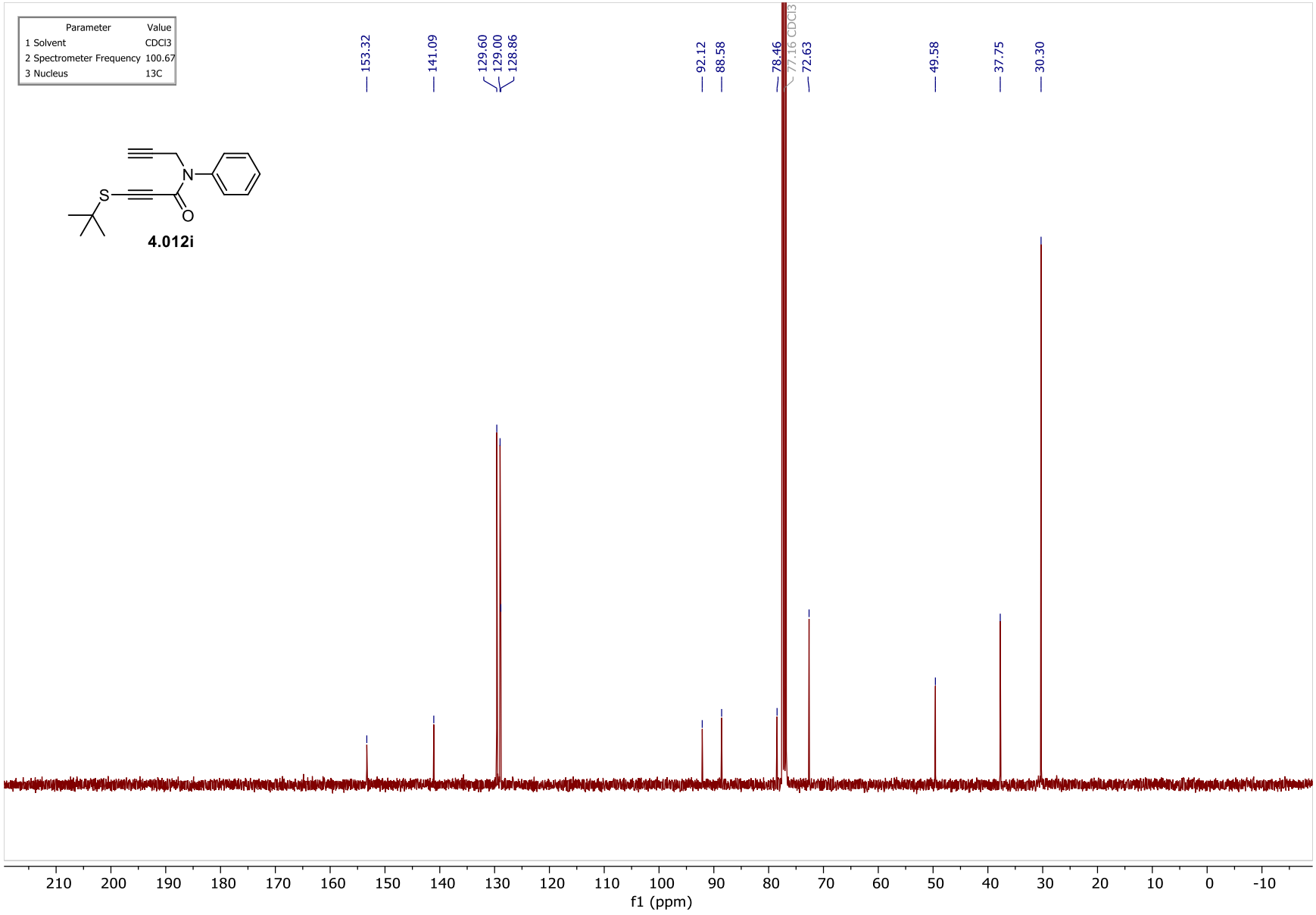
Parameter Value
1 Solvent CDCl3
2 Spectrometer Frequency 100.67
3 Nucleus 13C
153.32
141.09
129.60
129.00
128.86
92.12
88.58
78.46
77.16 CDCl3
72.63
49.58
37.75
30.30
N
S
O
4.012i
210 200 190 180 170 160 150 140 130 120 110 100 90 80 70 60 50 40 30 20 10 0 -10
f1 (ppm)

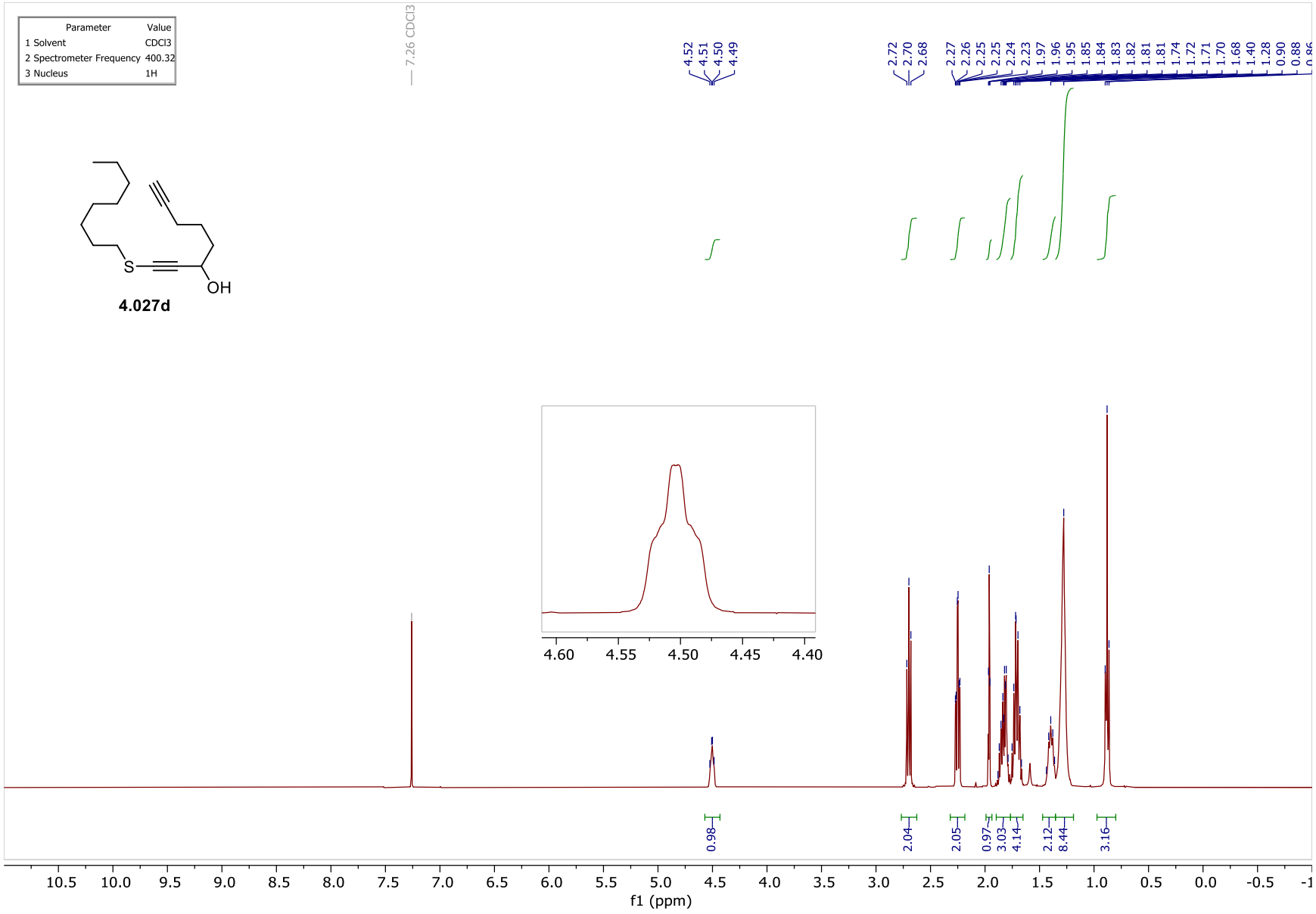
Parameter Value
1 Solvent CDCl3
2 Spectrometer Frequency 400.32
3 Nucleus 1H
7.26 CDCl3
4.52 4.51 4.50 4.49
2.72 2.70 2.68
2.27 2.26 2.25 2.25 2.24 2.23 1.97 1.96 1.95 1.85 1.84 1.83 1.82 1.81 1.81 1.74 1.72 1.71 1.70 1.68 1.40 1.28 0.90 0.88
S
OH
4.027d
4.60 4.55 4.50 4.45 4.40
0.98 2.04 2.05 0.97 3.03 4.14 2.12 8.44 3.16
10.5 10.0 9.5 9.0 8.5 8.0 7.5 7.0 6.5 6.0 5.5 5.0 4.5 4.0 3.5 3.0 2.5 2.0 1.5 1.0 0.5 0.0 -0.5 -1
f1 (ppm)

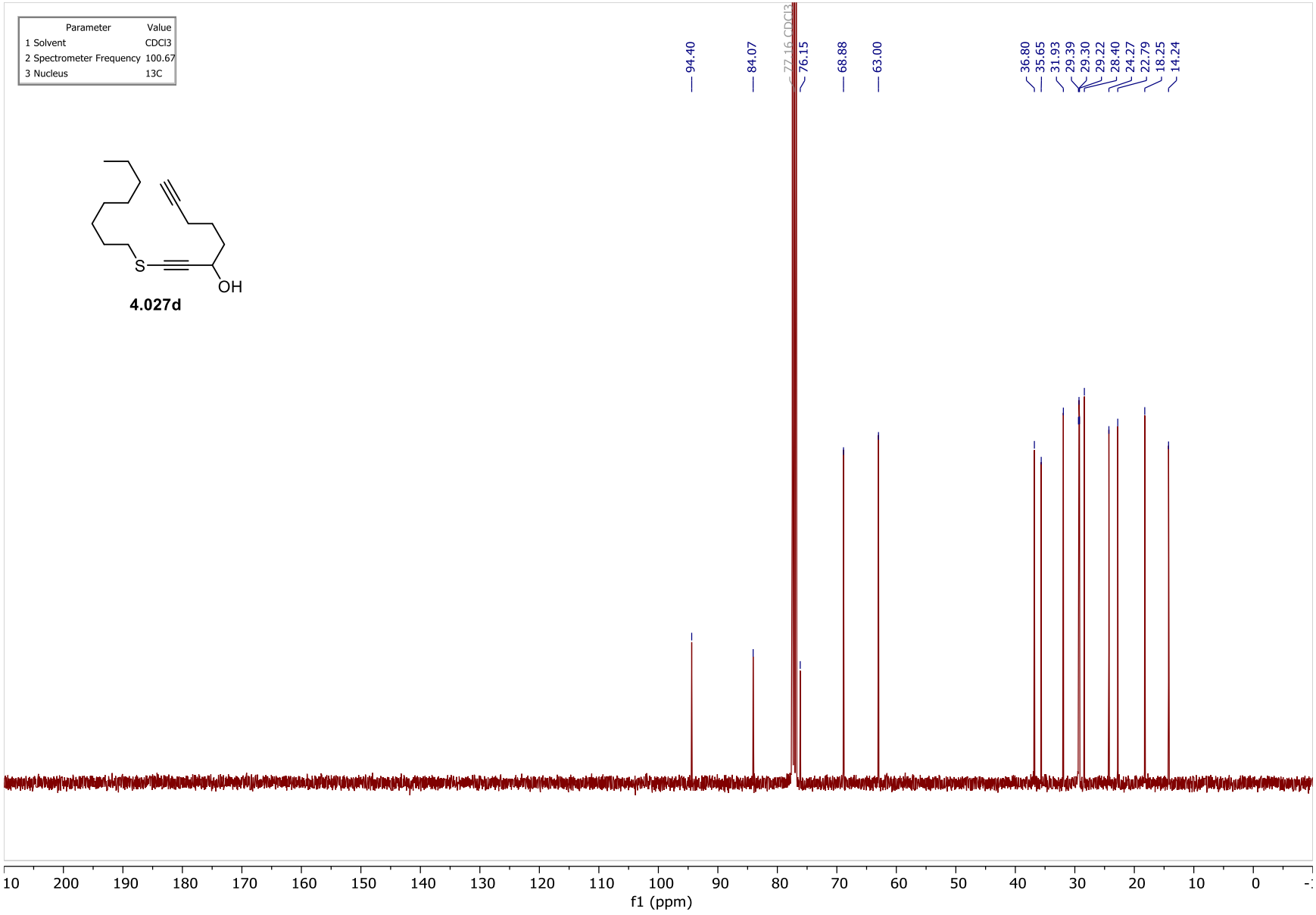
Parameter Value
1 Solvent CDCl3
2 Spectrometer Frequency 100.67
3 Nucleus 13C
94.40
84.07
77.16 CDCl3
76.15
68.88
63.00
36.80
35.65
31.93
29.39
29.30
29.22
28.40
24.27
22.79
18.25
14.24
S
OH
4.027d
f1 (ppm)

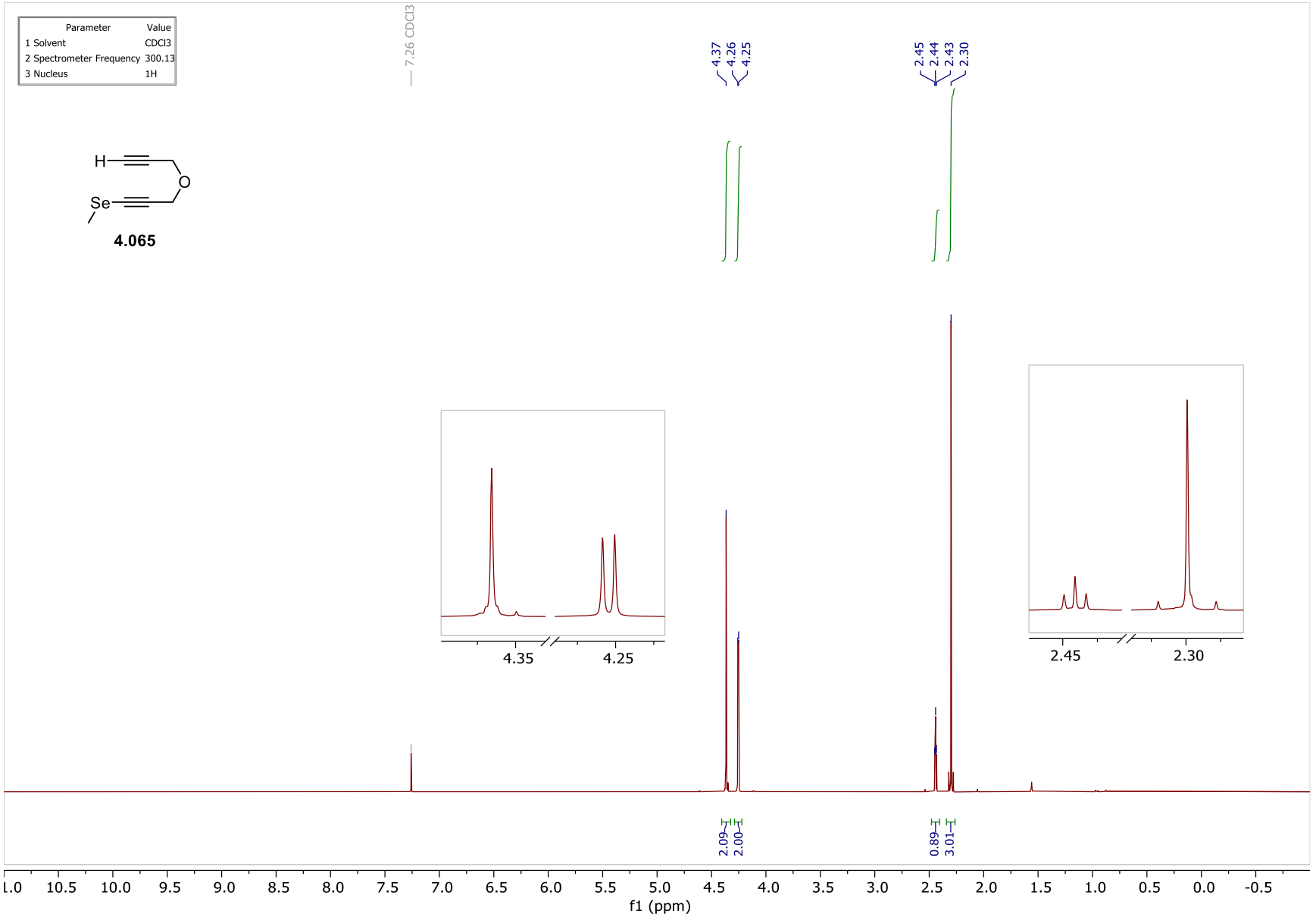
Parameter Value
1 Solvent CDCl3
2 Spectrometer Frequency 300.13
3 Nucleus 1H
7.26 CDCl3
4.37
4.26
4.25
2.45
2.44
2.43
2.30
H
O
Se
4.065
4.35
4.25
2.45
2.30
2.09
2.00
0.89
3.01
f1 (ppm)

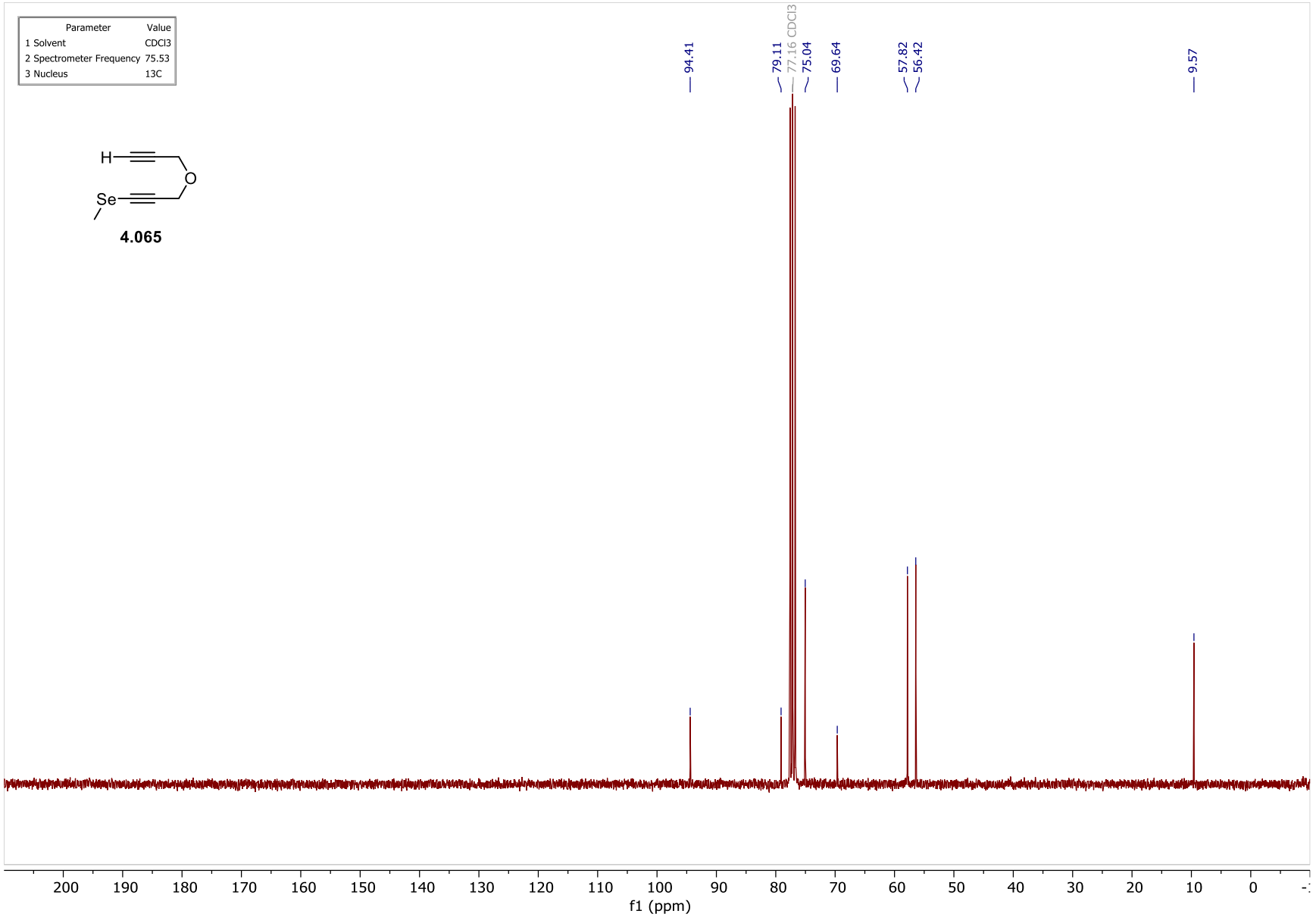
Parameter Value
1 Solvent CDCl3
2 Spectrometer Frequency 75.53
3 Nucleus 13C
H
O
Se
4.065
94.41
79.11
77.16 CDCl3
75.04
69.64
57.82
56.42
9.57
200 190 180 170 160 150 140 130 120 110 100 90 80 70 60 50 40 30 20 10 0
f1 (ppm)

Parameter	Value
1 Comment	77Se NMR with inverse gated 1H decoupling
2 Solvent	CDCl3
3 Spectrometer Frequency	57.32
4 Nucleus	77Se

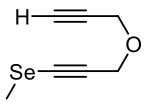

4.065

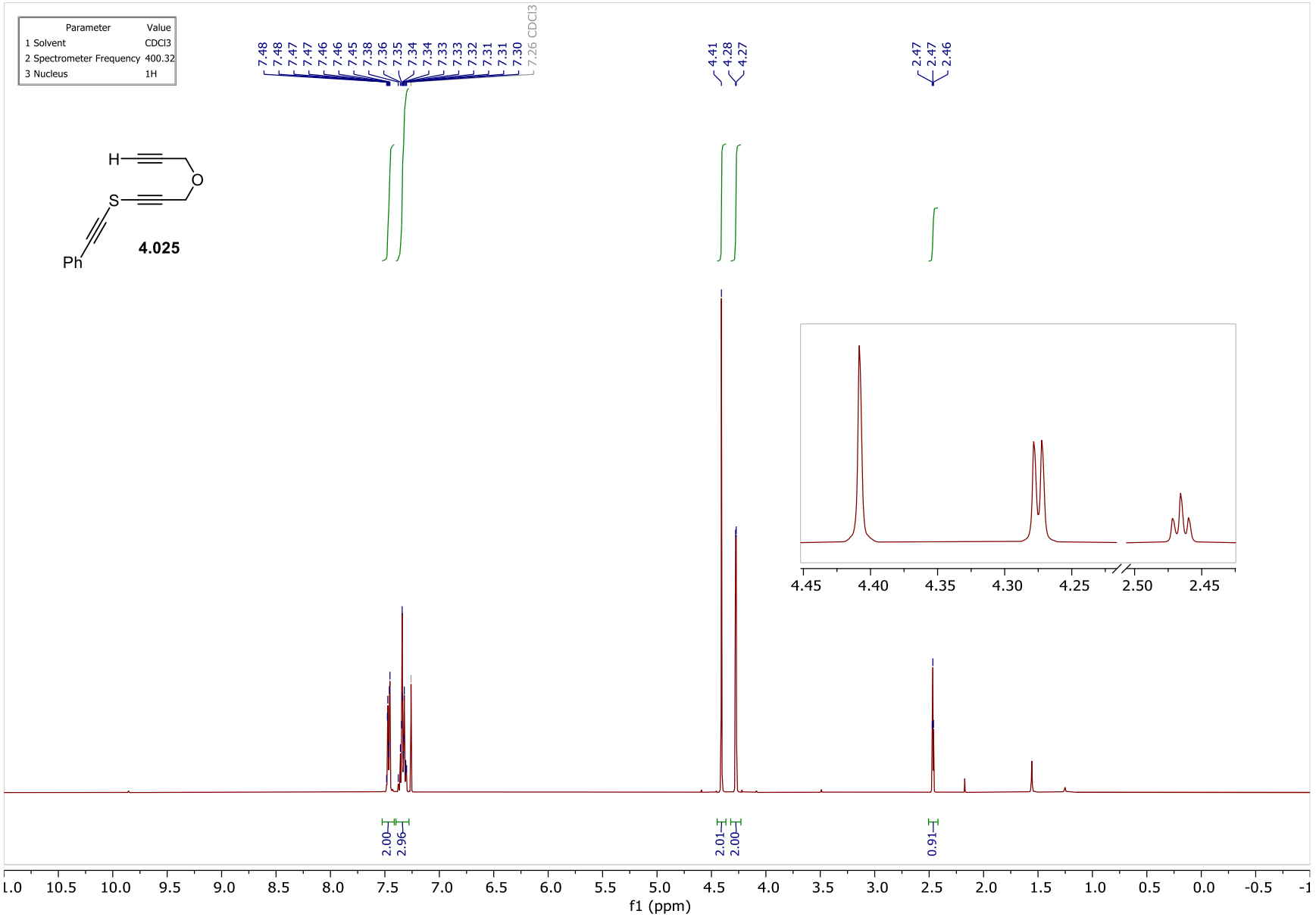
Parameter Value
1 Solvent CDCl3
2 Spectrometer Frequency 400.32
3 Nucleus 1H
7.48 7.48 7.47 7.47 7.46 7.46 7.45 7.38 7.36 7.35 7.34 7.34 7.33 7.32 7.31 7.31 7.30 7.26 CDCl3
4.41 4.28 4.27
2.47 2.47 2.46
H
O
S
Ph
4.025
4.45 4.40 4.35 4.30 4.25 2.50 2.45
2.00 2.96 2.01 2.00 0.91
f1 (ppm)

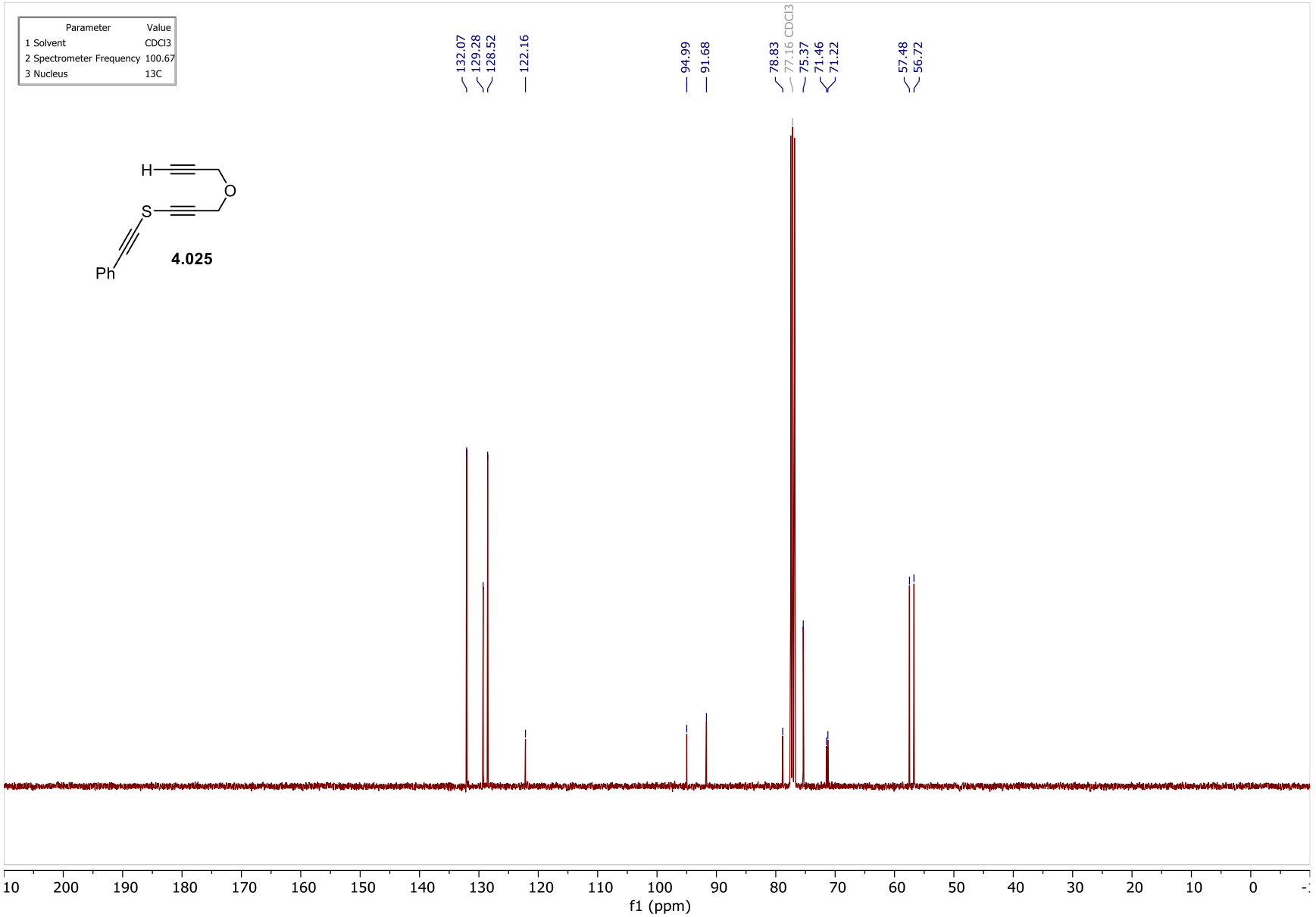
Parameter Value
1 Solvent CDCl3
2 Spectrometer Frequency 100.67
3 Nucleus 13C
132.07
129.28
128.52
122.16
94.99
91.68
78.83
77.16 CDCl3
75.37
71.46
71.22
57.48
56.72
H
O
S
Ph
4.025
f1 (ppm)

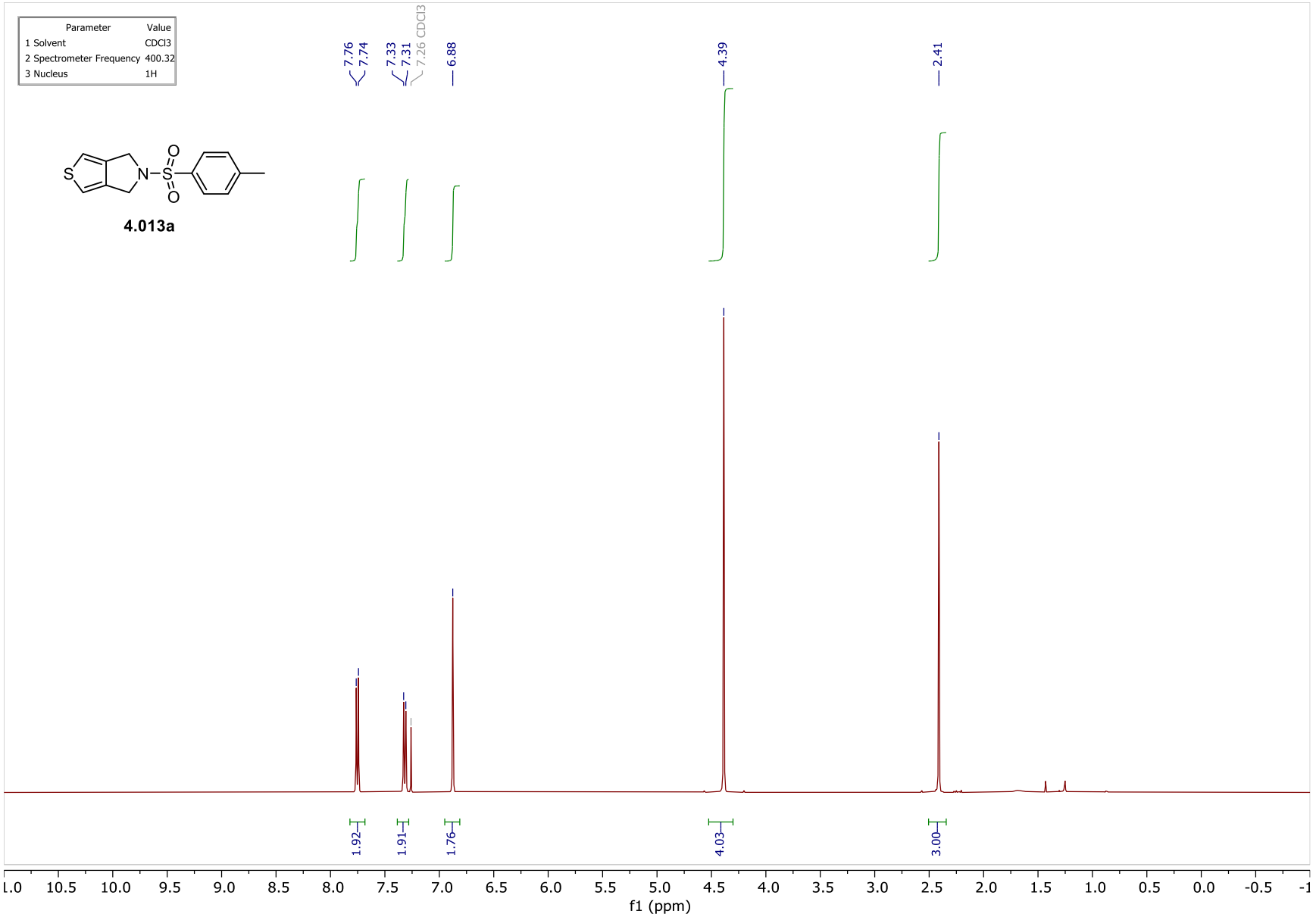
Parameter Value
1 Solvent CDCl3
2 Spectrometer Frequency 400.32
3 Nucleus 1H
4.013a
7.76
7.74
7.33
7.31
7.26 CDCl3
6.88
4.39
2.41
1.92
1.91
1.76
4.03
3.00
f1 (ppm)

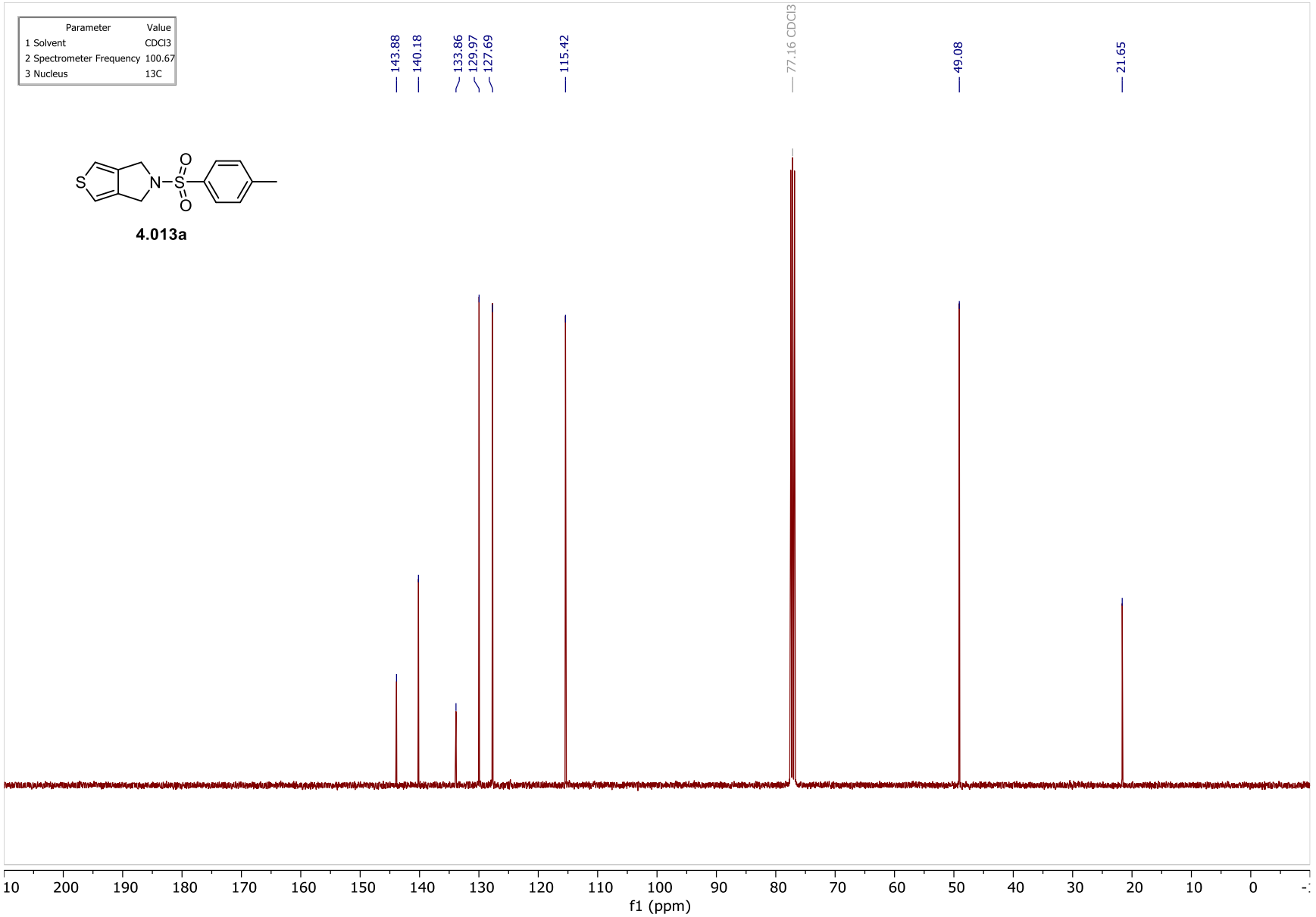
Parameter Value
1 Solvent CDCl3
2 Spectrometer Frequency 100.67
3 Nucleus 13C
143.88
140.18
133.86
129.97
127.69
115.42
77.16 CDCl3
49.08
21.65
4.013a
f1 (ppm)

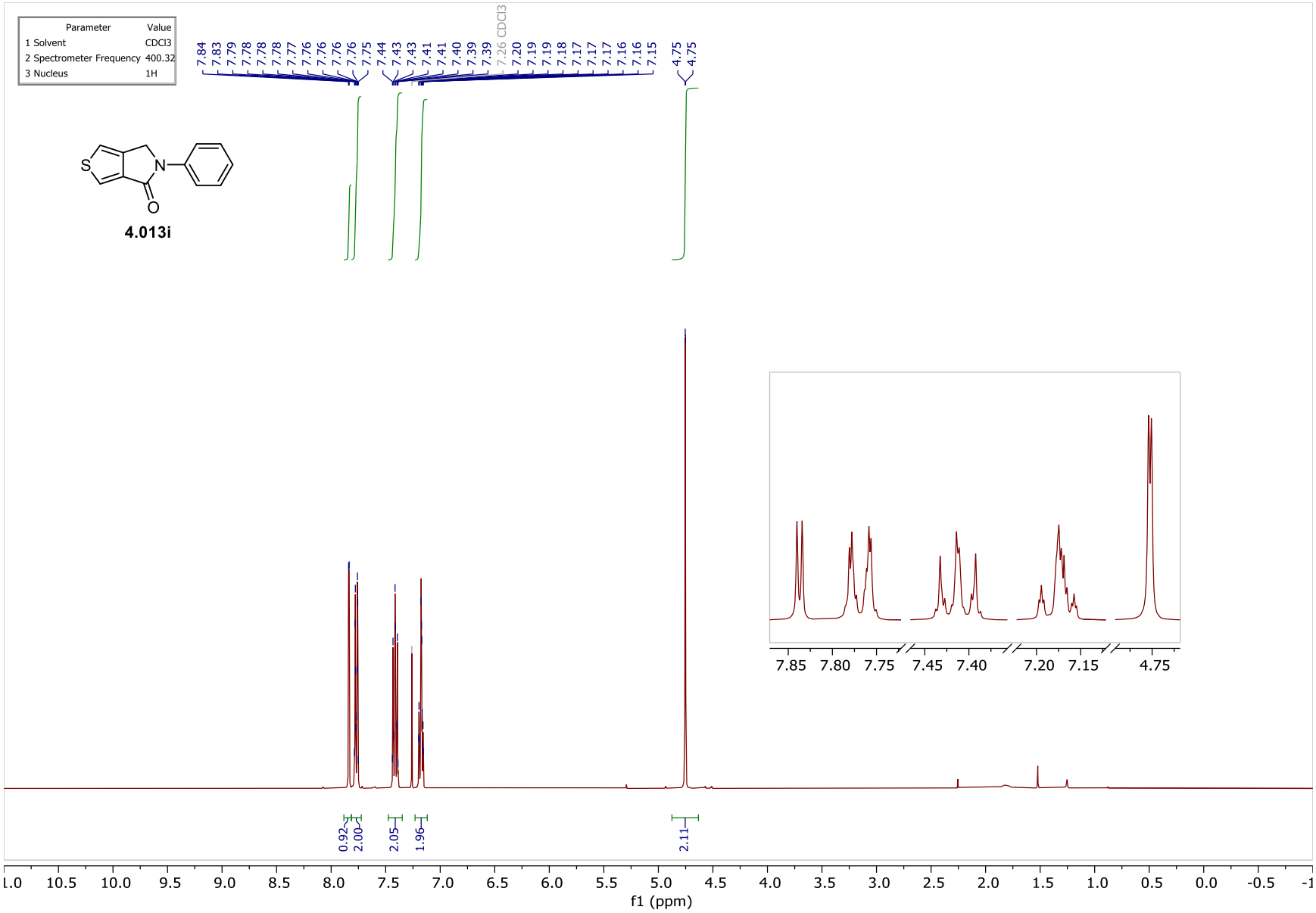
Parameter Value
1 Solvent CDCl3
2 Spectrometer Frequency 400.32
3 Nucleus 1H
4.013i
7.84 7.83 7.79 7.78 7.78 7.78 7.77 7.76 7.76 7.76 7.76 7.75 7.44 7.43 7.43 7.41 7.41 7.40 7.39 7.39 7.26 CDCl3 7.20 7.19 7.19 7.18 7.17 7.17 7.17 7.16 7.16 7.15 4.75 4.75
0.92 2.00 2.05 1.96 2.11
7.85 7.80 7.75 7.45 7.40 7.20 7.15 4.75
f1 (ppm)

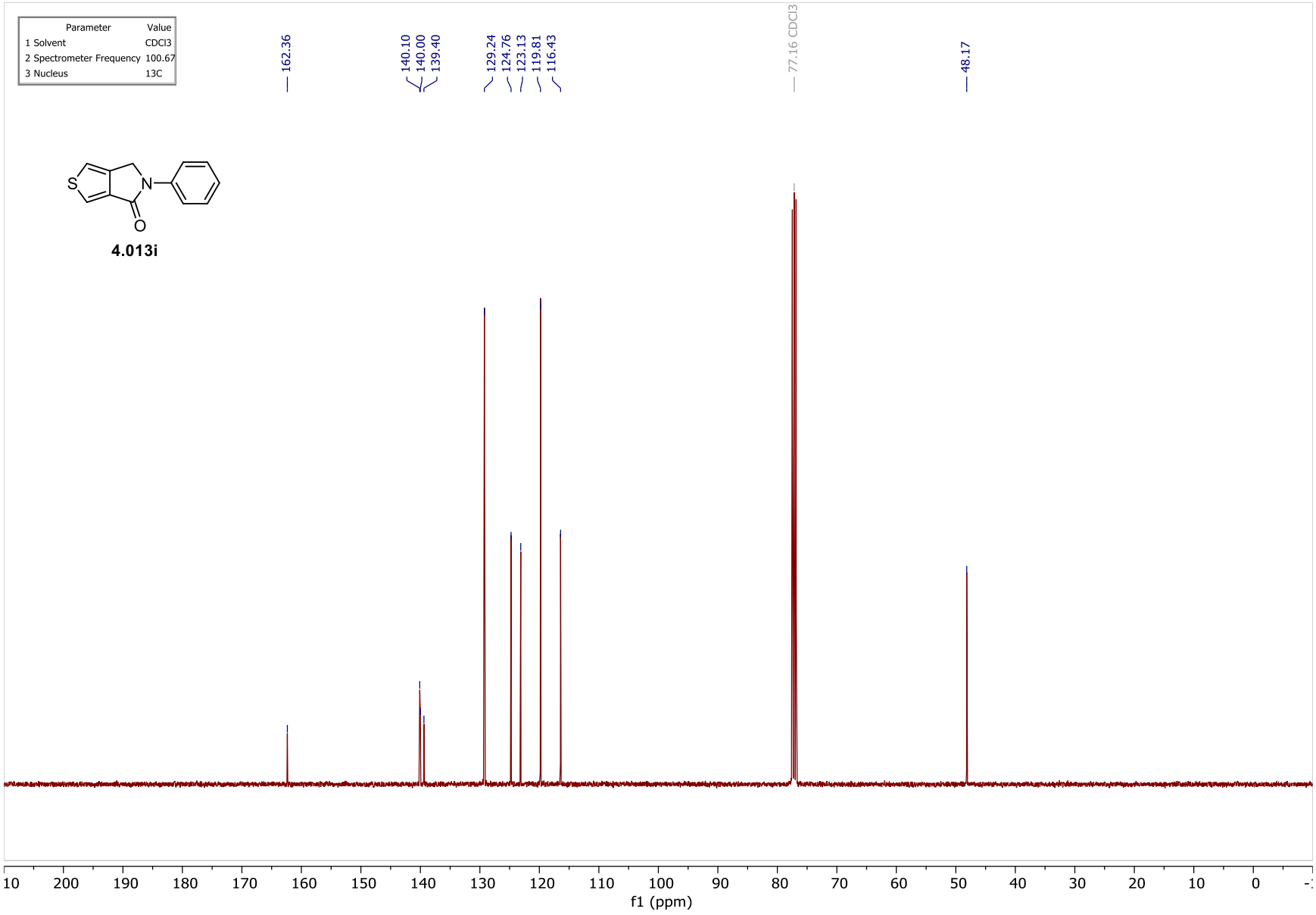
Parameter Value
1 Solvent CDCl3
2 Spectrometer Frequency 100.67
3 Nucleus 13C
162.36
140.10
140.00
139.40
129.24
124.76
123.13
119.81
116.43
77.16 CDCl3
48.17
S
N
O
4.013i
f1 (ppm)

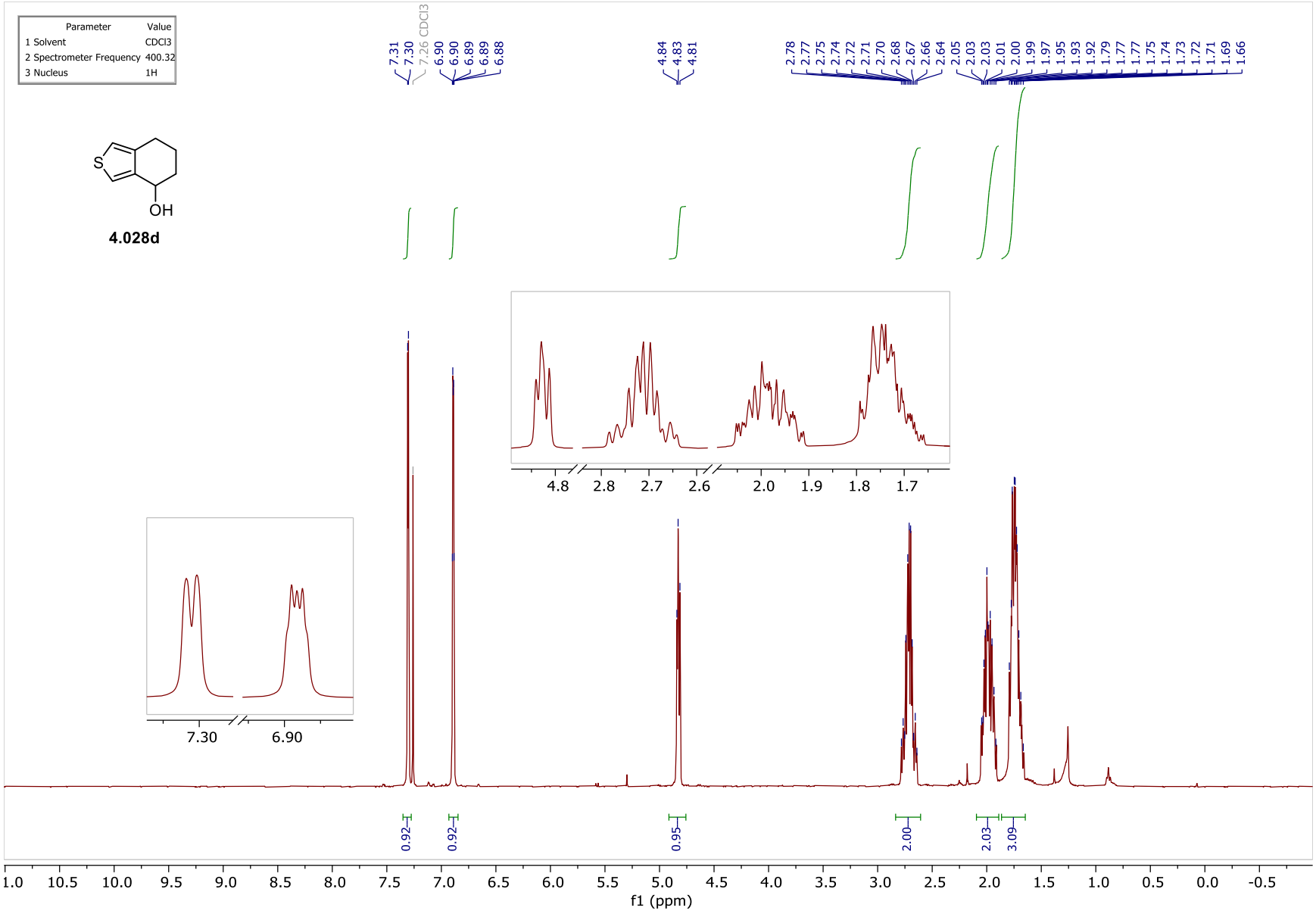
Parameter Value
1 Solvent CDCl3
2 Spectrometer Frequency 400.32
3 Nucleus 1H
S
OH
4.028d
7.31
7.30
7.26 CDCl3
6.90
6.90
6.89
6.89
6.88
4.84
4.83
4.81
2.78
2.77
2.75
2.74
2.72
2.71
2.70
2.68
2.67
2.66
2.64
2.05
2.03
2.03
2.01
2.00
1.99
1.97
1.95
1.93
1.92
1.79
1.77
1.77
1.75
1.74
1.73
1.72
1.71
1.69
1.66
4.8
2.8
2.7
2.6
2.0
1.9
1.8
1.7
7.30
6.90
0.92
0.92
0.95
2.00
2.03
3.09
1.0
10.5
10.0
9.5
9.0
8.5
8.0
7.5
7.0
6.5
6.0
5.5
5.0
4.5
4.0
3.5
3.0
2.5
2.0
1.5
1.0
0.5
0.0
-0.5
f1 (ppm)

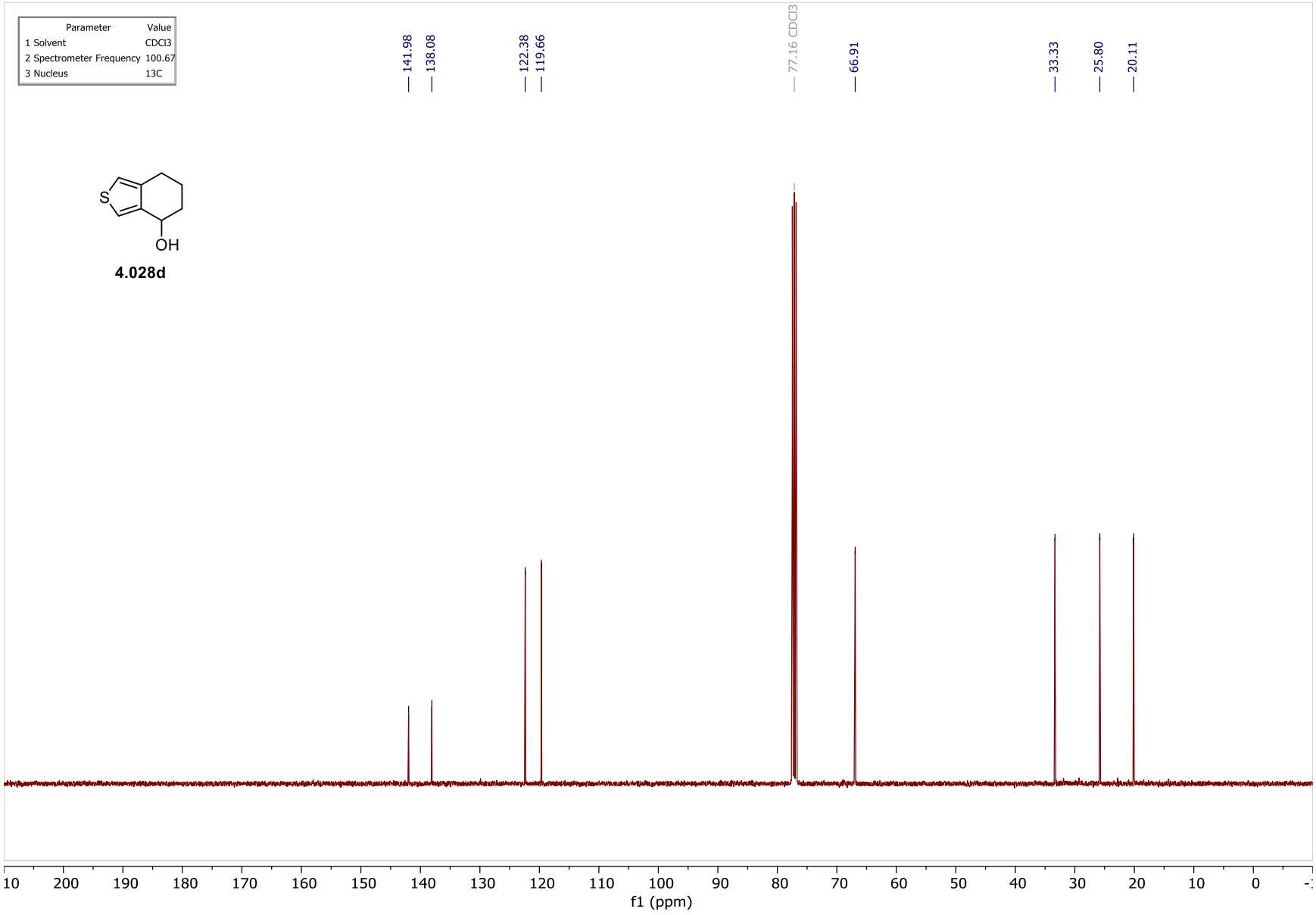
Parameter Value
1 Solvent CDCl3
2 Spectrometer Frequency 100.67
3 Nucleus 13C
141.98
138.08
122.38
119.66
77.16 CDCl3
66.91
33.33
25.80
20.11
S
OH
4.028d
f1 (ppm)

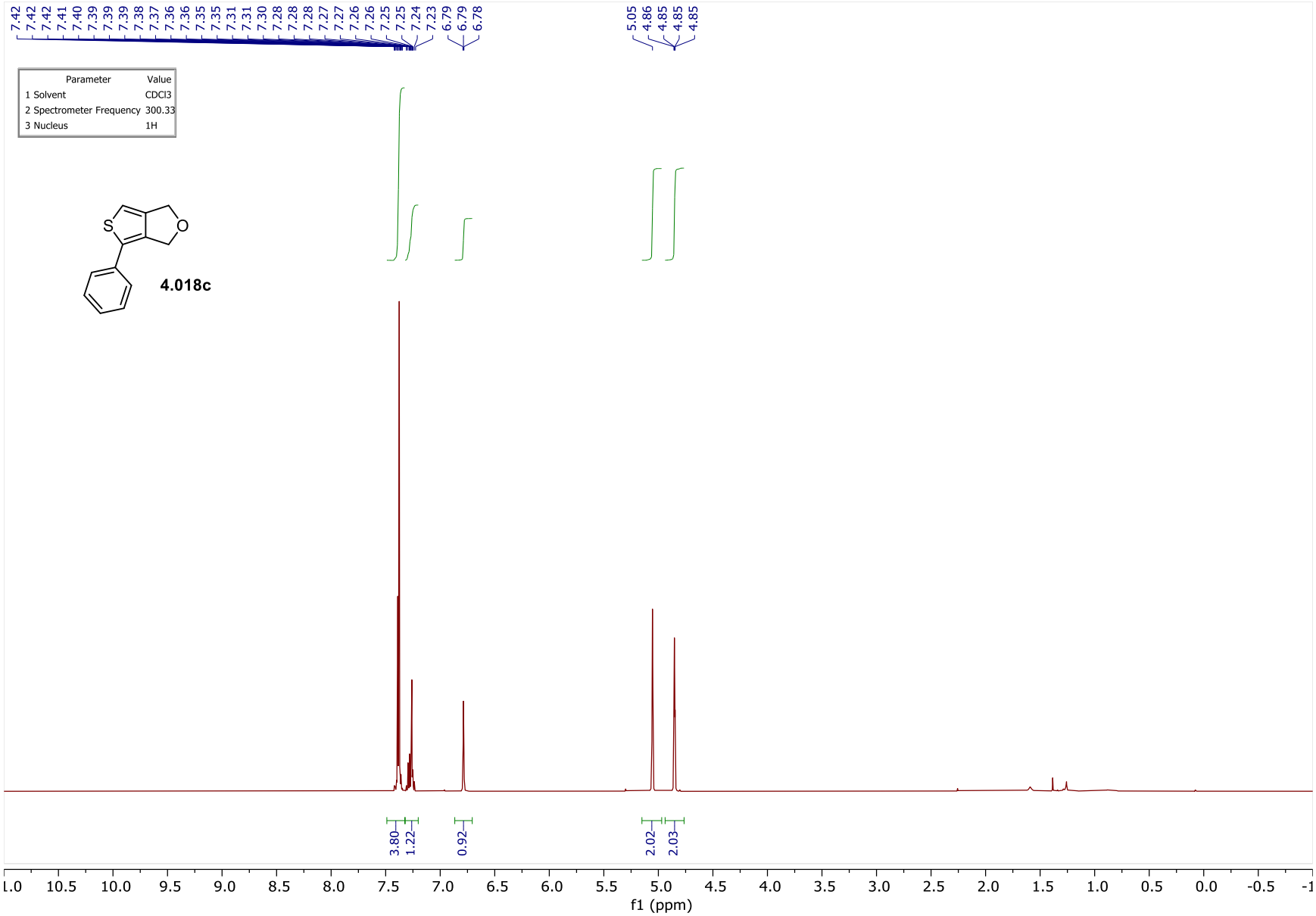
7.42 7.42 7.42 7.41 7.40 7.39 7.39 7.39 7.38 7.37 7.36 7.36 7.35 7.35 7.31 7.31 7.30 7.28 7.28 7.28 7.27 7.27 7.26 7.26 7.25 7.25 7.24 7.23 6.79 6.79 6.78
5.05 4.86 4.85 4.85 4.85
Parameter Value
1 Solvent CDCl3
2 Spectrometer Frequency 300.33
3 Nucleus 1H
S
O
4.018c
3.80 1.22 0.92 2.02 2.03
f1 (ppm)

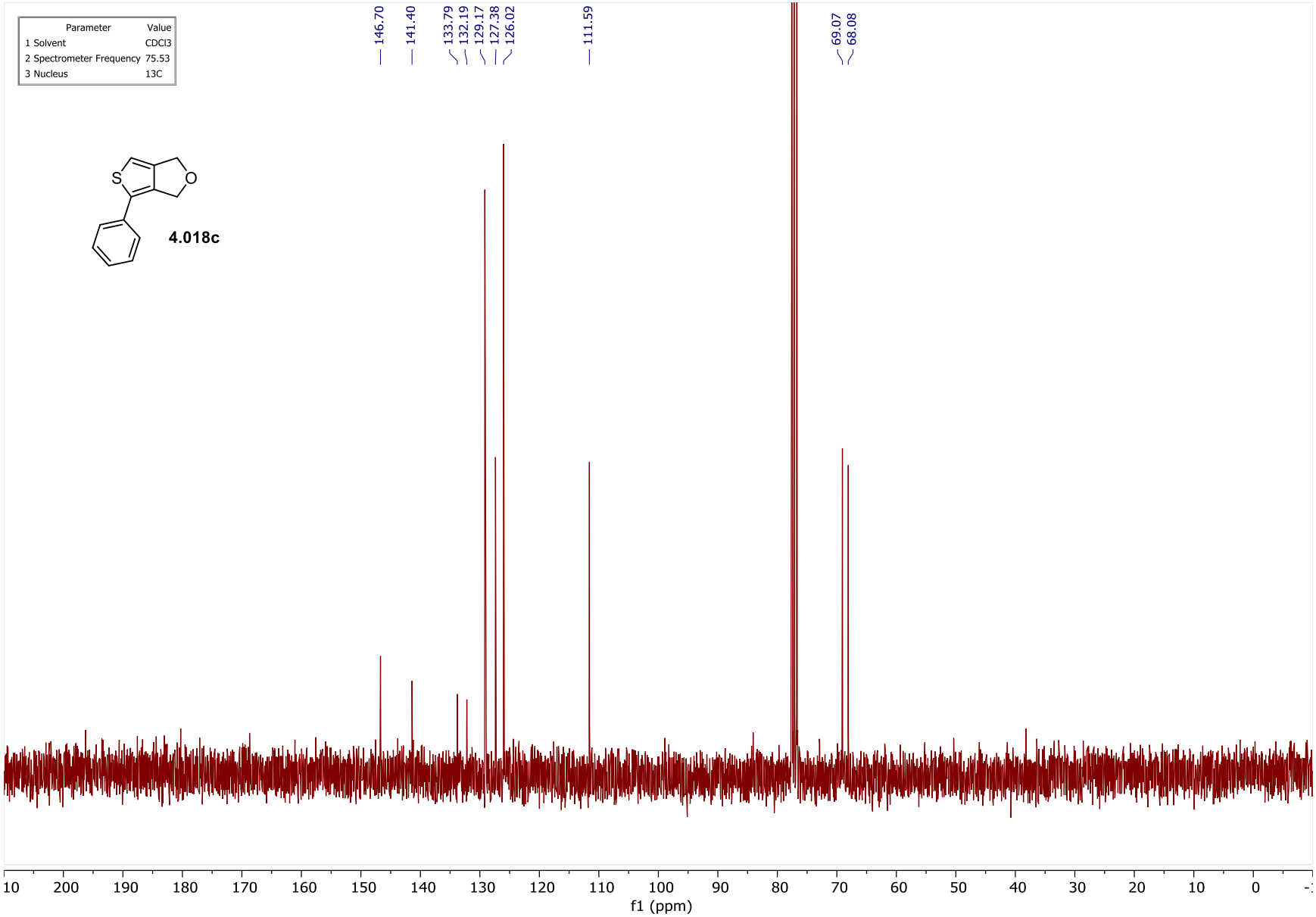
Parameter Value
1 Solvent CDCl3
2 Spectrometer Frequency 75.53
3 Nucleus 13C
146.70
141.40
133.79
132.19
129.17
127.38
126.02
111.59
69.07
68.08
S
O
4.018c
f1 (ppm)

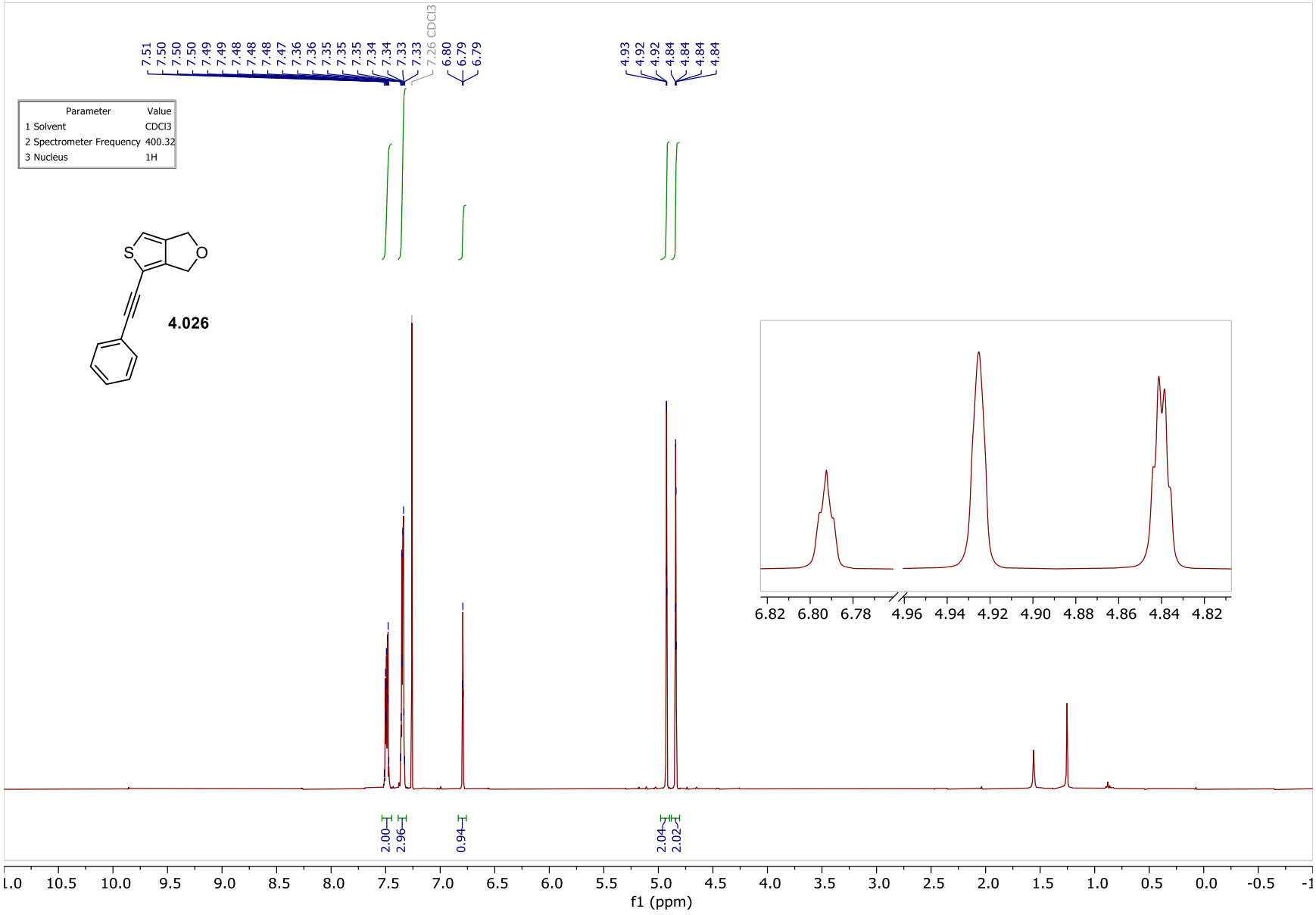
7.51 7.50 7.50 7.50 7.49 7.49 7.48 7.48 7.48 7.47 7.36 7.36 7.35 7.35 7.35 7.34 7.34 7.33 7.33 7.26 CDCl3 6.80 6.79 6.79
4.93 4.92 4.92 4.84 4.84 4.84 4.84
Parameter Value
1 Solvent CDCl3
2 Spectrometer Frequency 400.32
3 Nucleus 1H
S
O
4.026
6.82 6.80 6.78 4.96 4.94 4.92 4.90 4.88 4.86 4.84 4.82
2.00 2.96 0.94 2.04 2.02
f1 (ppm)

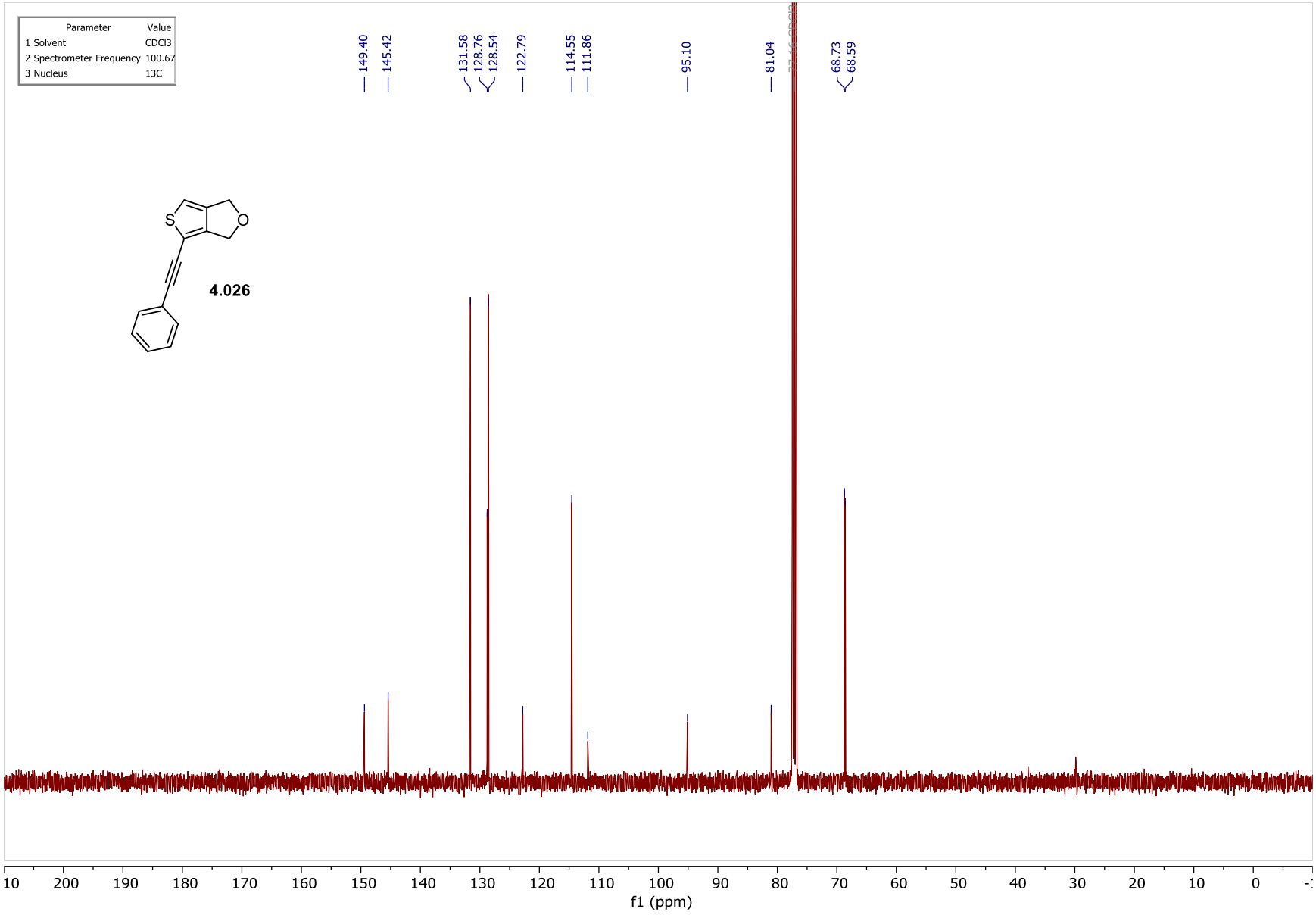
Parameter Value
1 Solvent CDCl3
2 Spectrometer Frequency 100.67
3 Nucleus 13C
149.40
145.42
131.58
128.76
128.54
122.79
114.55
111.86
95.10
81.04
68.73
68.59
S
O
4.026
f1 (ppm)

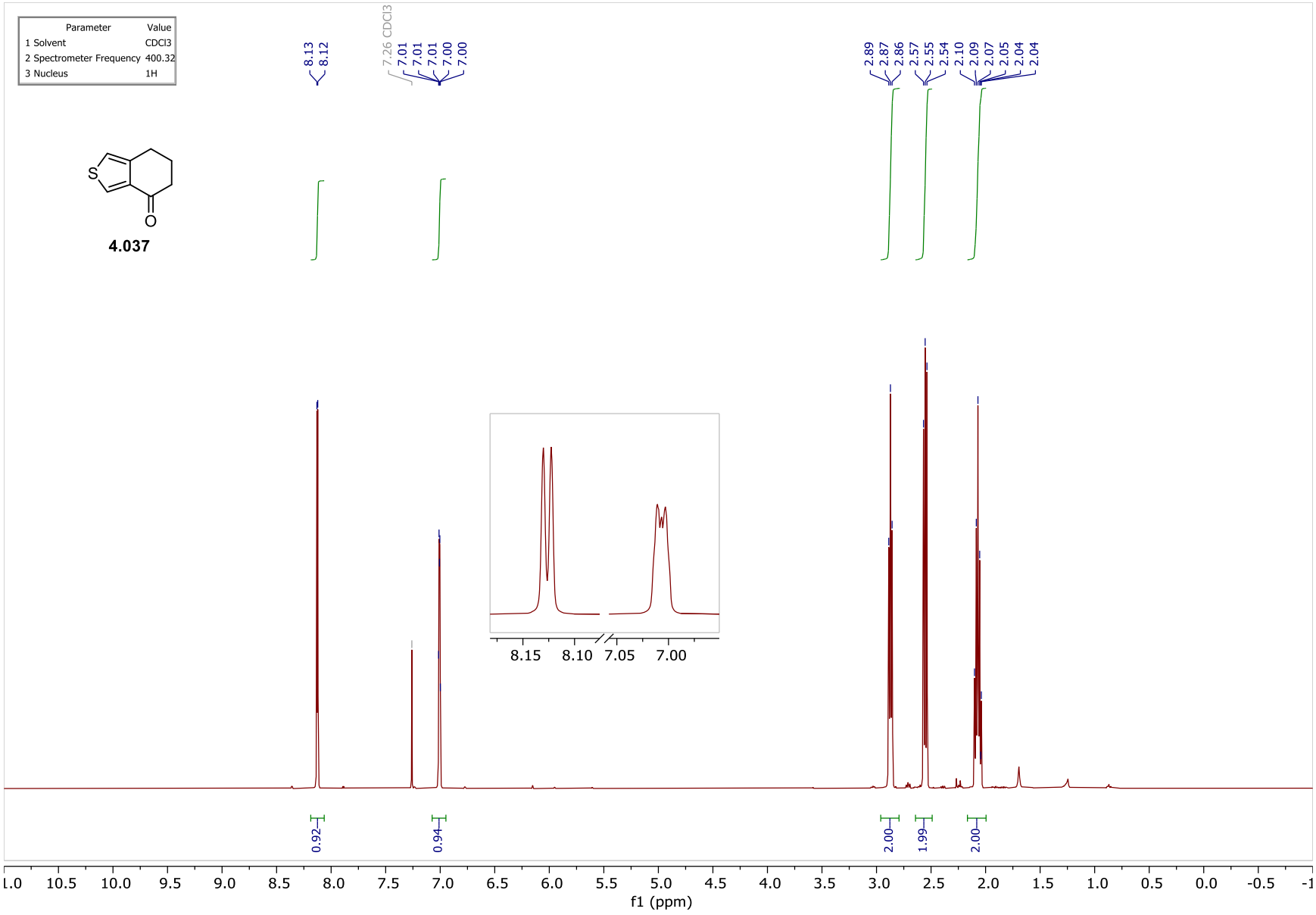
Parameter Value
1 Solvent CDCl3
2 Spectrometer Frequency 400.32
3 Nucleus 1H
4.037
8.13
8.12
7.26 CDCl3
7.01
7.01
7.01
7.00
7.00
2.89
2.87
2.86
2.57
2.55
2.54
2.10
2.09
2.07
2.05
2.04
2.04
8.15
8.10
7.05
7.00
0.92
0.94
2.00
1.99
2.00
f1 (ppm)

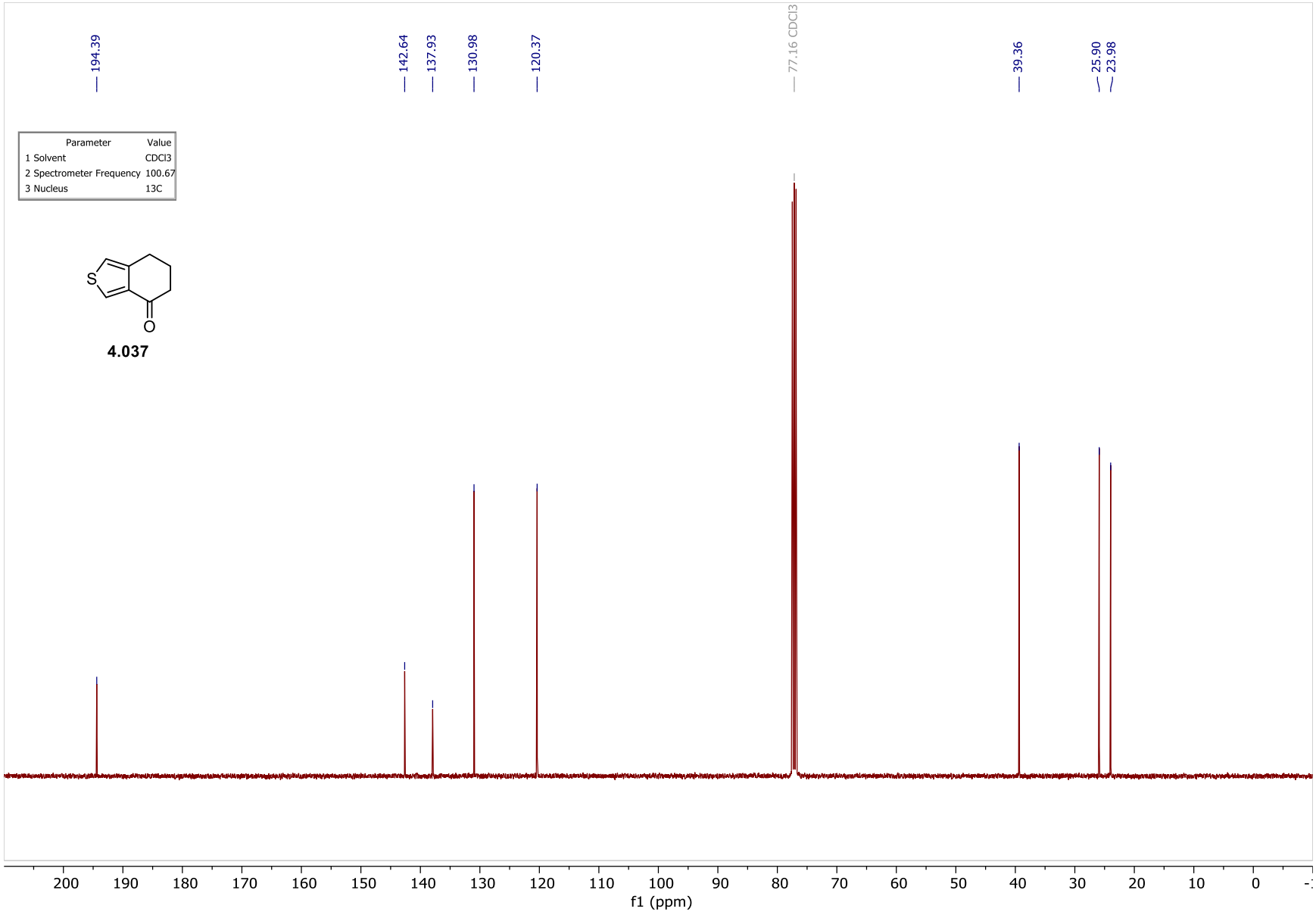
194.39
142.64
137.93
130.98
120.37
77.16 CDCl3
39.36
25.90
23.98
Parameter Value
1 Solvent CDCl3
2 Spectrometer Frequency 100.67
3 Nucleus 13C
S
O
4.037
200 190 180 170 160 150 140 130 120 110 100 90 80 70 60 50 40 30 20 10 0
f1 (ppm)

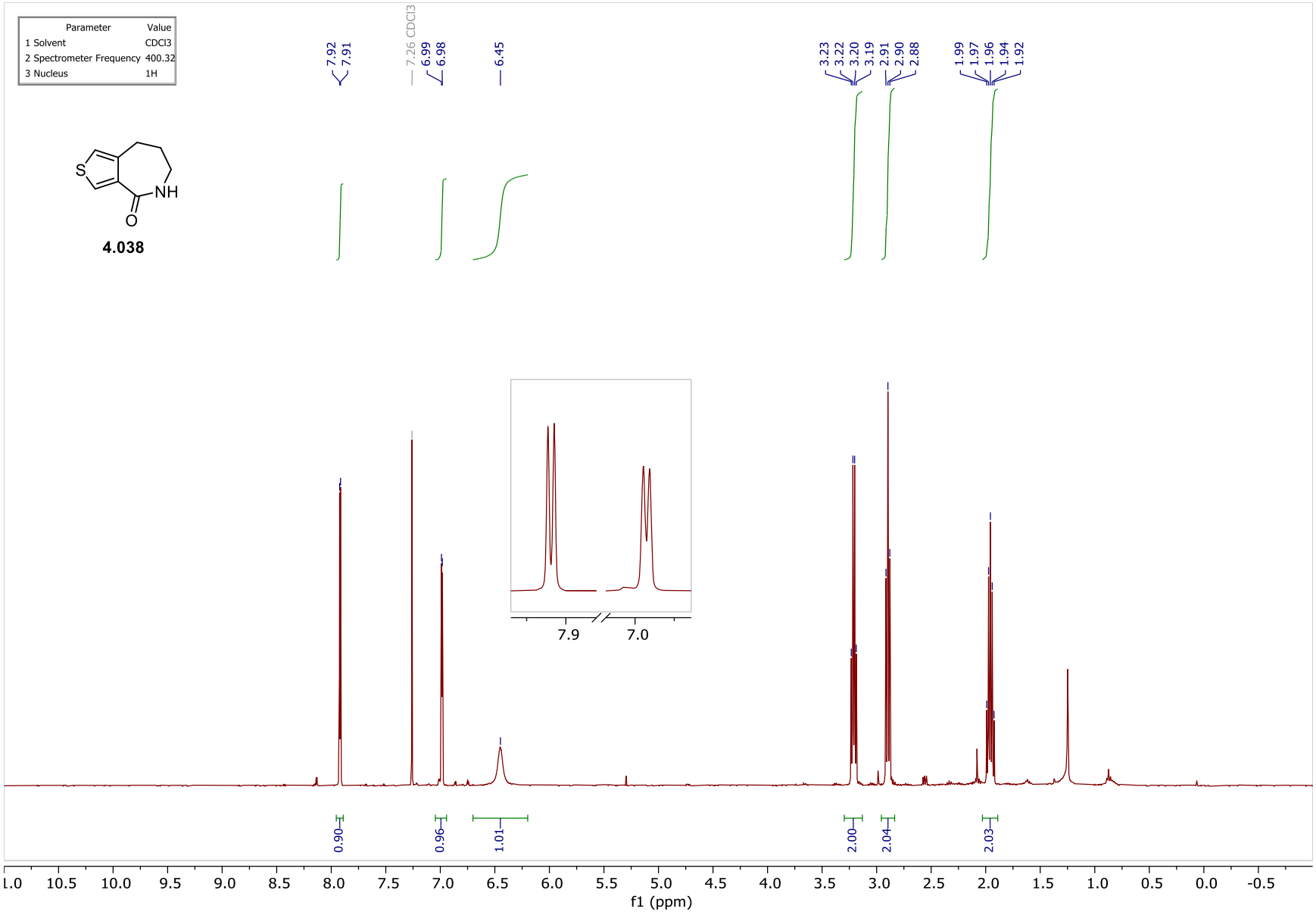
Parameter Value
1 Solvent CDCl3
2 Spectrometer Frequency 400.32
3 Nucleus 1H
4.038
7.92
7.91
7.26 CDCl3
6.99
6.98
6.45
3.23
3.22
3.20
3.19
2.91
2.90
2.88
1.99
1.97
1.96
1.94
1.92
7.9
7.0
0.90
0.96
1.01
2.00
2.04
2.03
f1 (ppm)

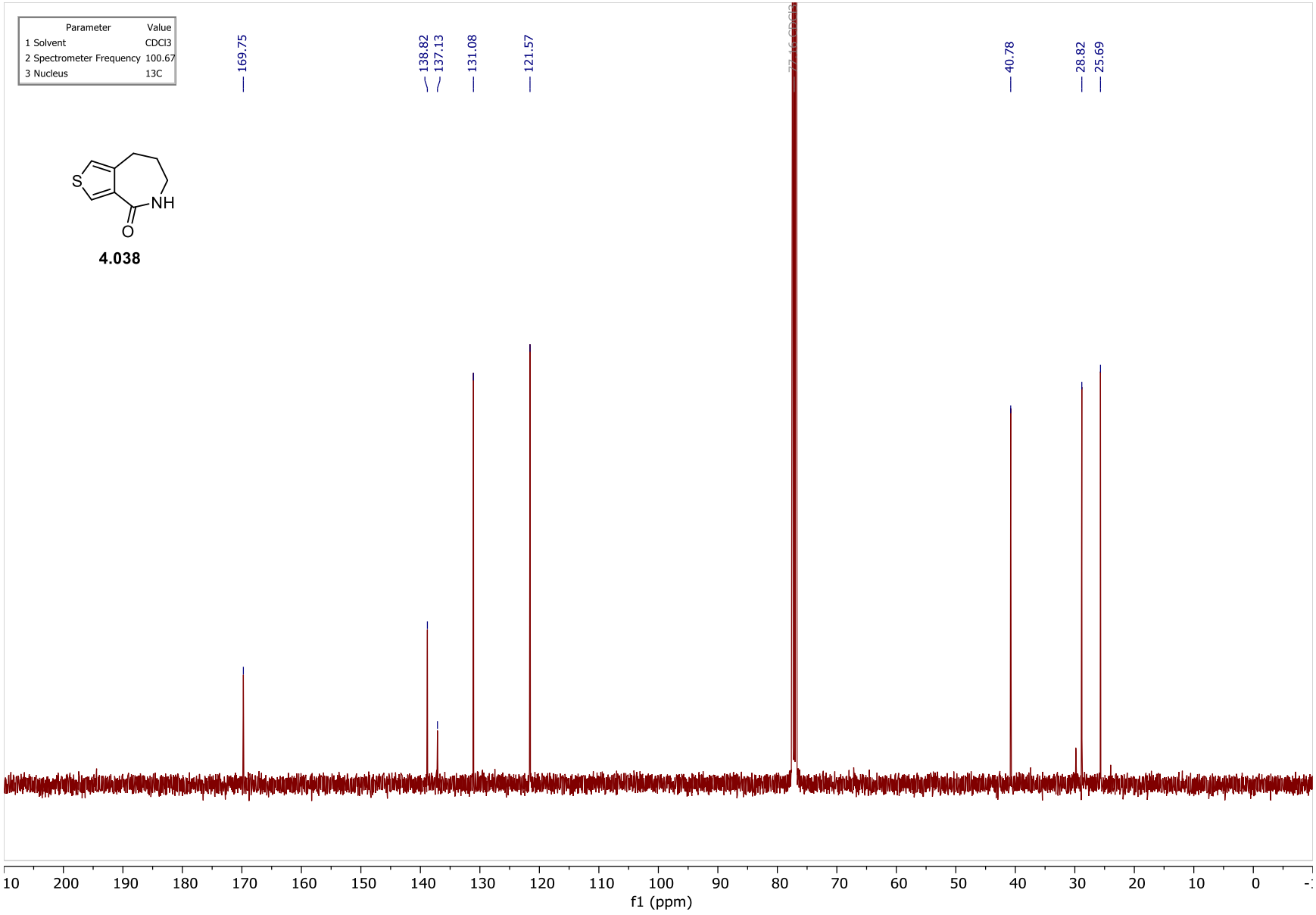
Parameter Value
1 Solvent CDCl3
2 Spectrometer Frequency 100.67
3 Nucleus 13C
169.75
138.82
137.13
131.08
121.57
40.78
28.82
25.69
S
NH
O
4.038
f1 (ppm)

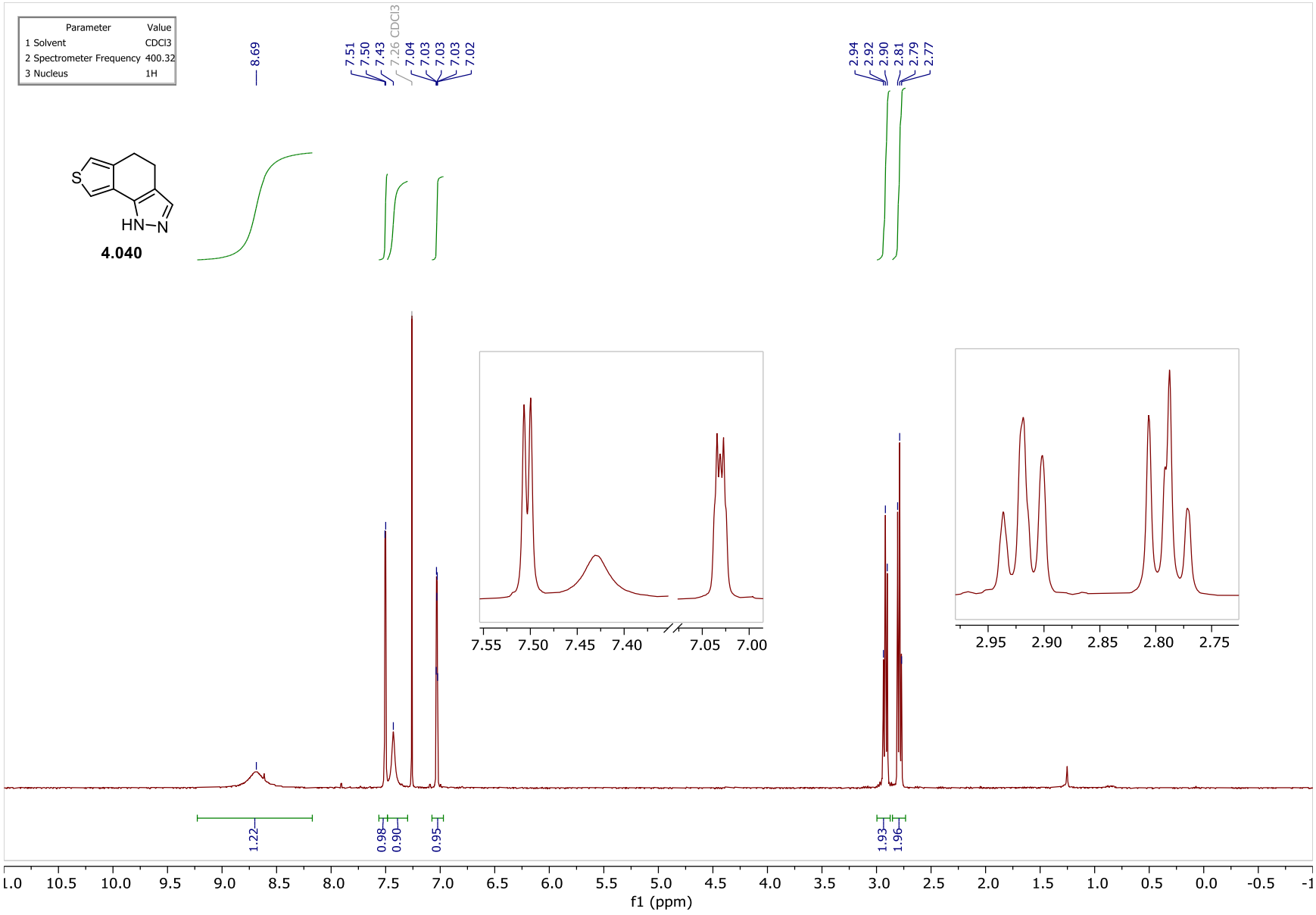
Parameter Value
1 Solvent CDCl3
2 Spectrometer Frequency 400.32
3 Nucleus 1H
8.69
7.51
7.50
7.43
7.26 CDCl3
7.04
7.03
7.03
7.03
7.02
2.94
2.92
2.90
2.81
2.79
2.77
S
HN–N
4.040
7.55 7.50 7.45 7.40 7.05 7.00
2.95 2.90 2.85 2.80 2.75
1.22
0.98
0.90
0.95
1.93
1.96
f1 (ppm)

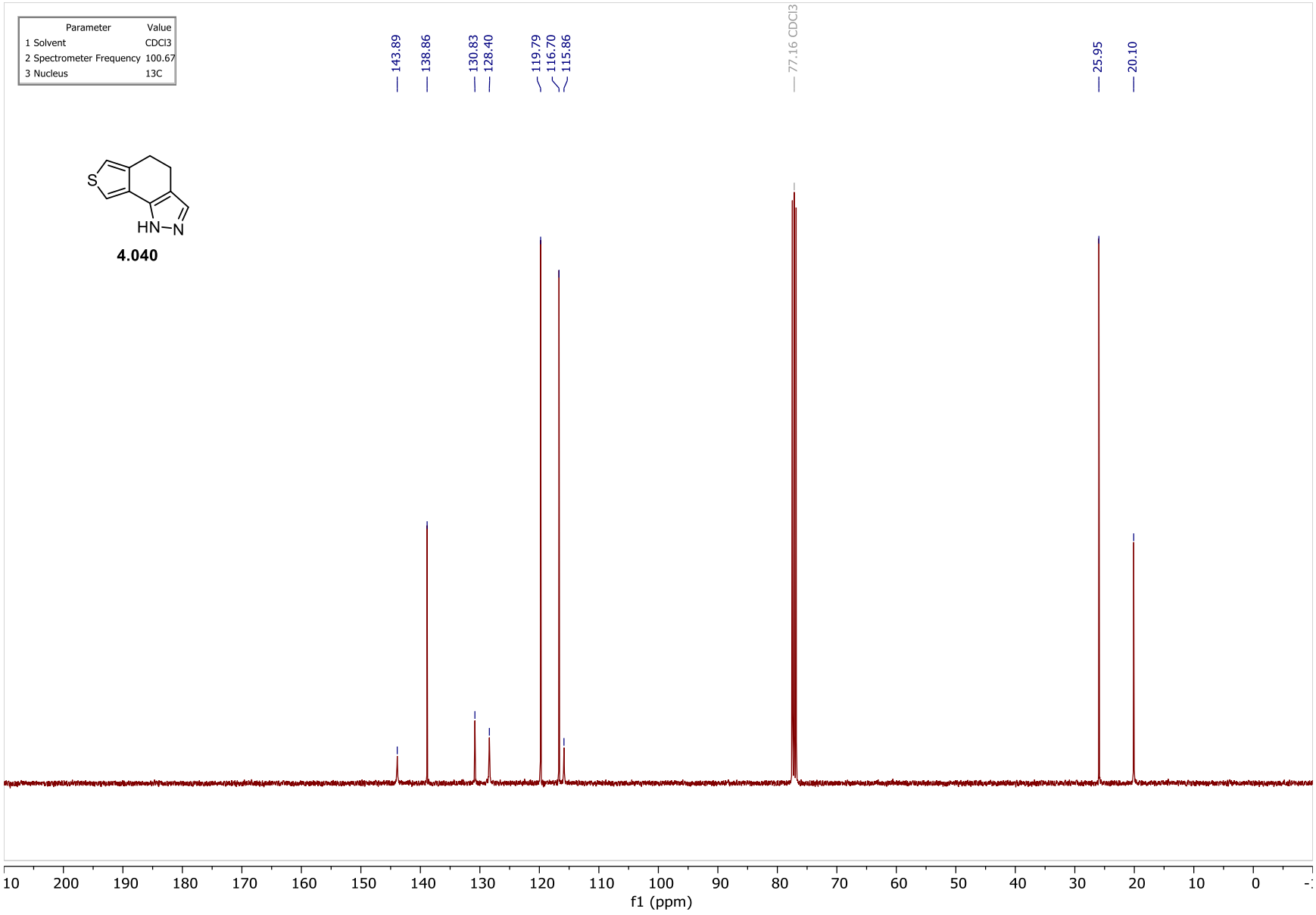
Parameter Value
1 Solvent CDCl3
2 Spectrometer Frequency 100.67
3 Nucleus 13C
143.89
138.86
130.83
128.40
119.79
116.70
115.86
77.16 CDCl3
25.95
20.10
S
HN–N
4.040
f1 (ppm)

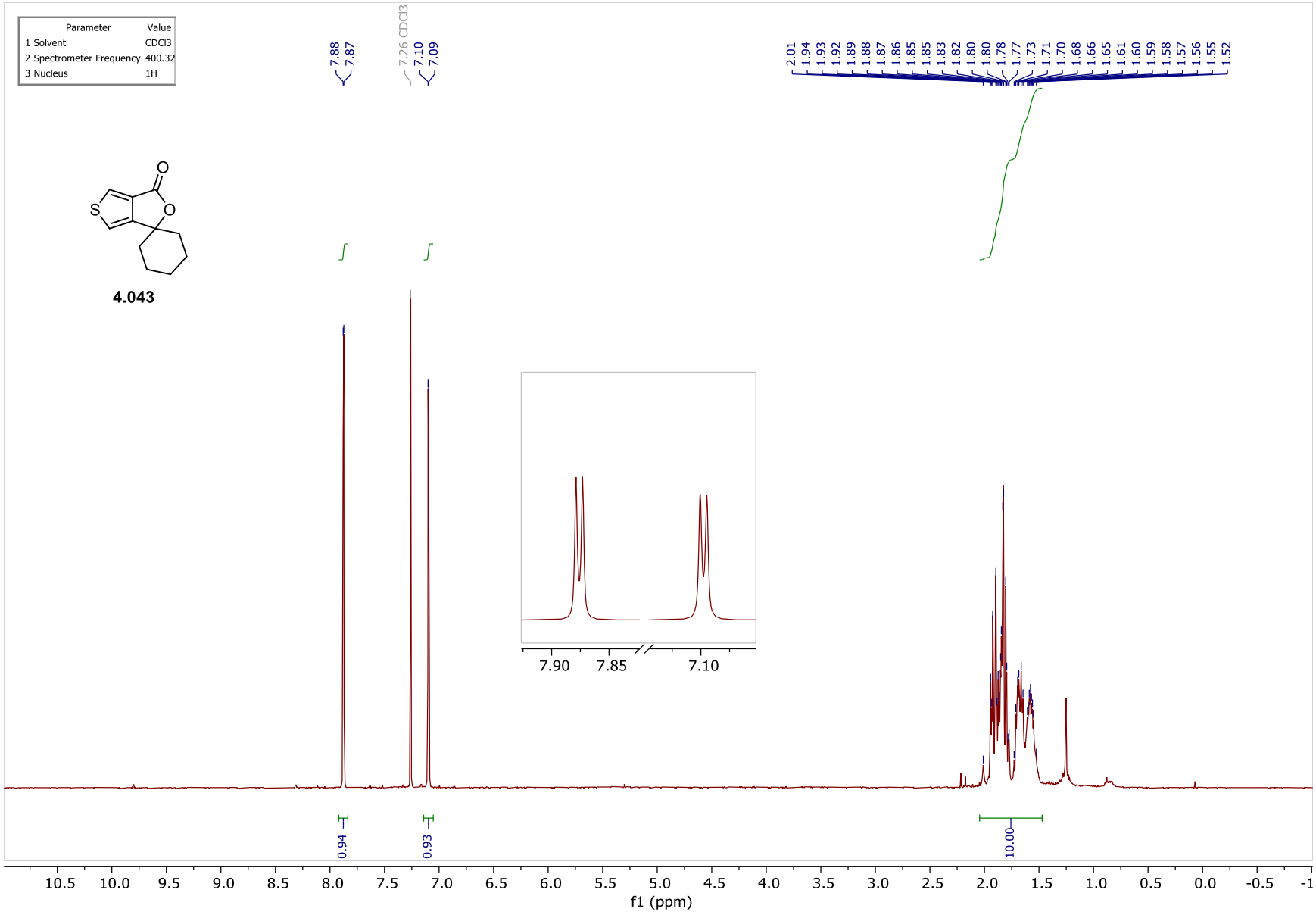
Parameter Value
1 Solvent CDCl3
2 Spectrometer Frequency 400.32
3 Nucleus 1H
7.88
7.87
7.26 CDCl3
7.10
7.09
2.01
1.94
1.93
1.92
1.89
1.88
1.87
1.86
1.85
1.85
1.83
1.82
1.80
1.80
1.78
1.77
1.73
1.71
1.70
1.68
1.66
1.65
1.61
1.60
1.59
1.58
1.57
1.56
1.55
1.52
O
S
O
4.043
7.90
7.85
7.10
0.94
0.93
10.00
10.5 10.0 9.5 9.0 8.5 8.0 7.5 7.0 6.5 6.0 5.5 5.0 4.5 4.0 3.5 3.0 2.5 2.0 1.5 1.0 0.5 0.0 -0.5 -1
f1 (ppm)

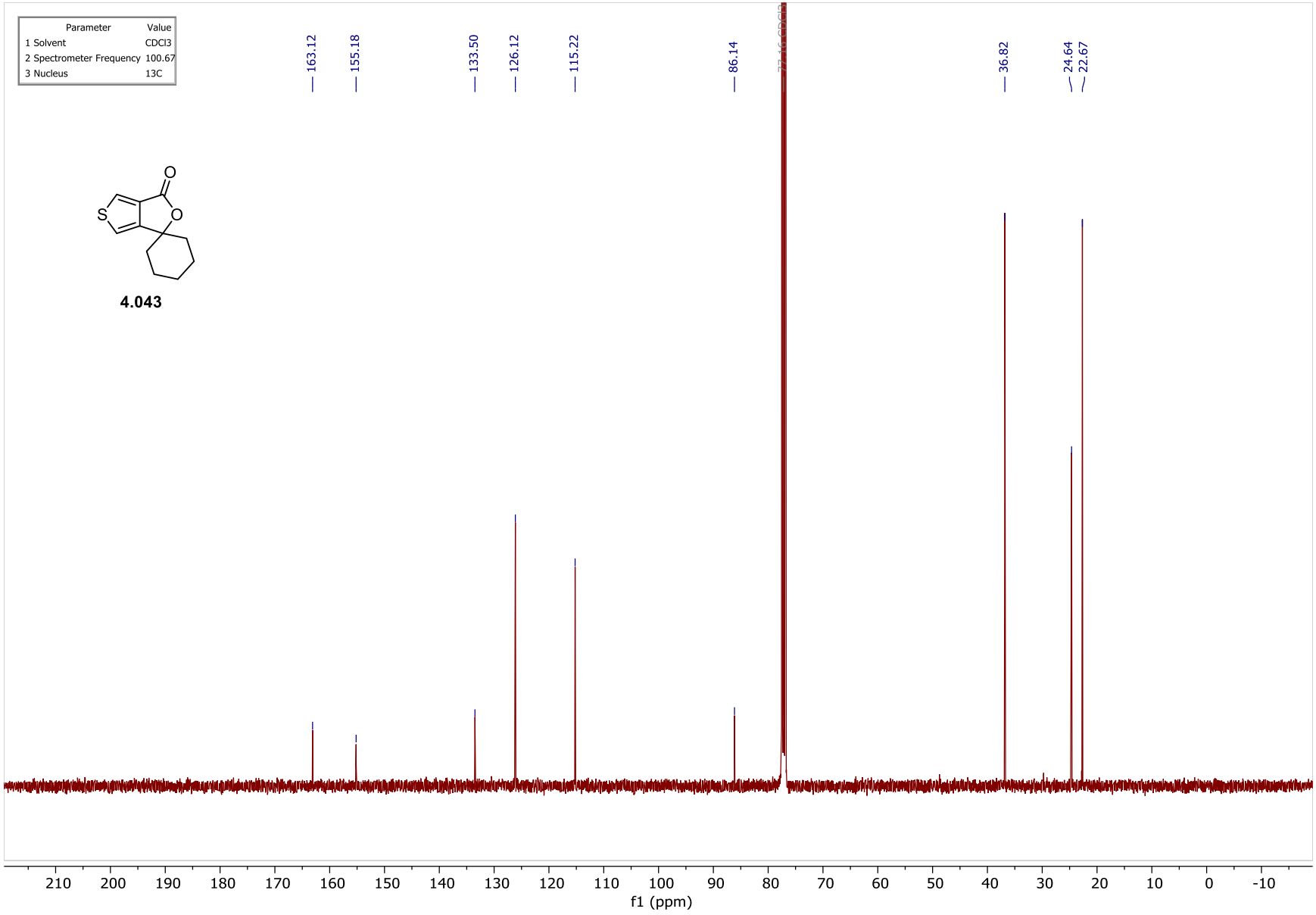
Parameter Value
1 Solvent CDCl3
2 Spectrometer Frequency 100.67
3 Nucleus 13C
163.12
155.18
133.50
126.12
115.22
86.14
77.16
36.82
24.64
22.67
O
S
O
4.043
210 200 190 180 170 160 150 140 130 120 110 100 90 80 70 60 50 40 30 20 10 0 -10
f1 (ppm)

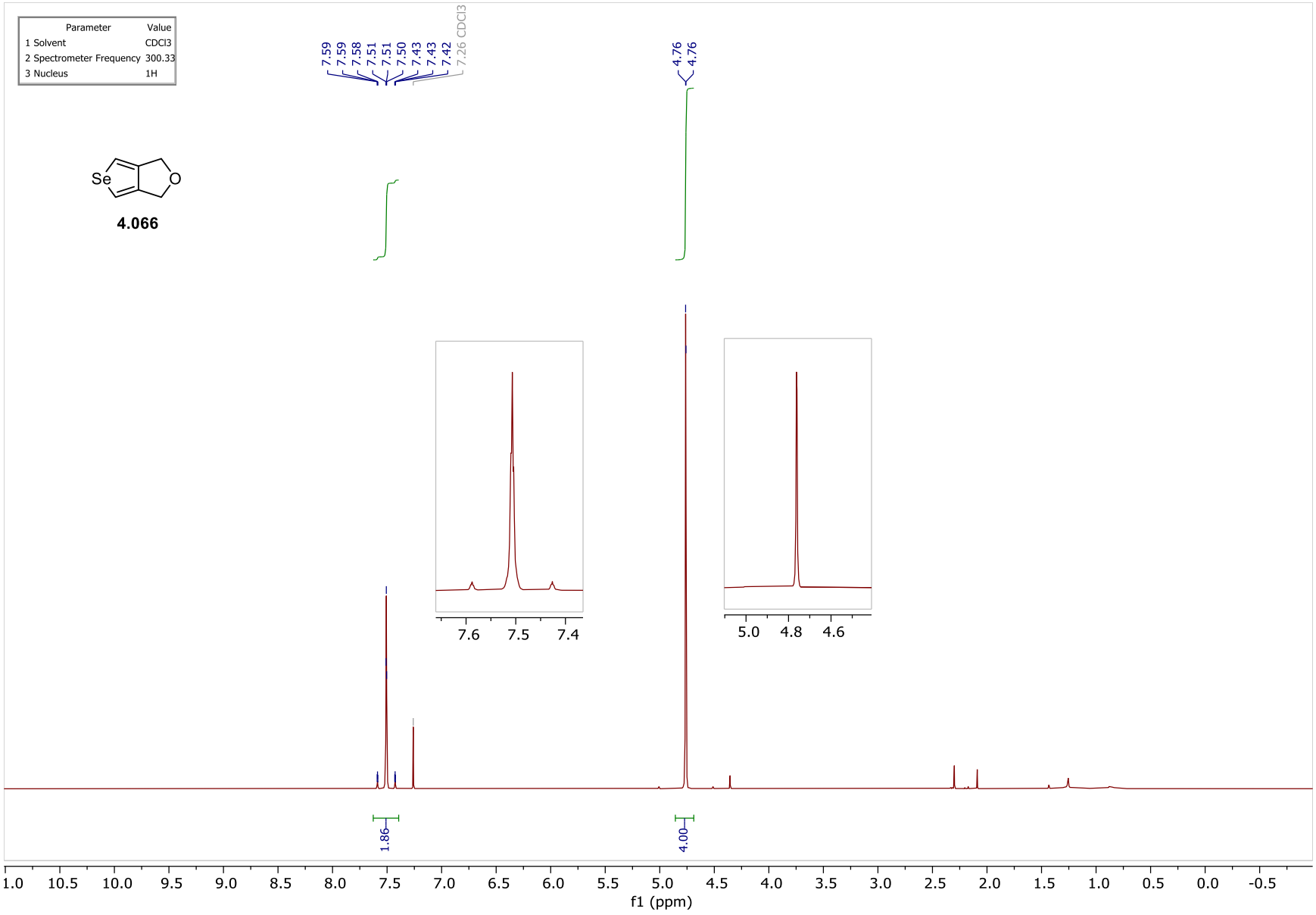
Parameter Value
1 Solvent CDCl3
2 Spectrometer Frequency 300.33
3 Nucleus 1H
7.59
7.59
7.58
7.51
7.51
7.50
7.43
7.43
7.42
7.26 CDCl3
4.76
4.76
Se
O
4.066
7.6
7.5
7.4
5.0
4.8
4.6
1.86
4.00
1.0 10.5 10.0 9.5 9.0 8.5 8.0 7.5 7.0 6.5 6.0 5.5 5.0 4.5 4.0 3.5 3.0 2.5 2.0 1.5 1.0 0.5 0.0 -0.5
f1 (ppm)

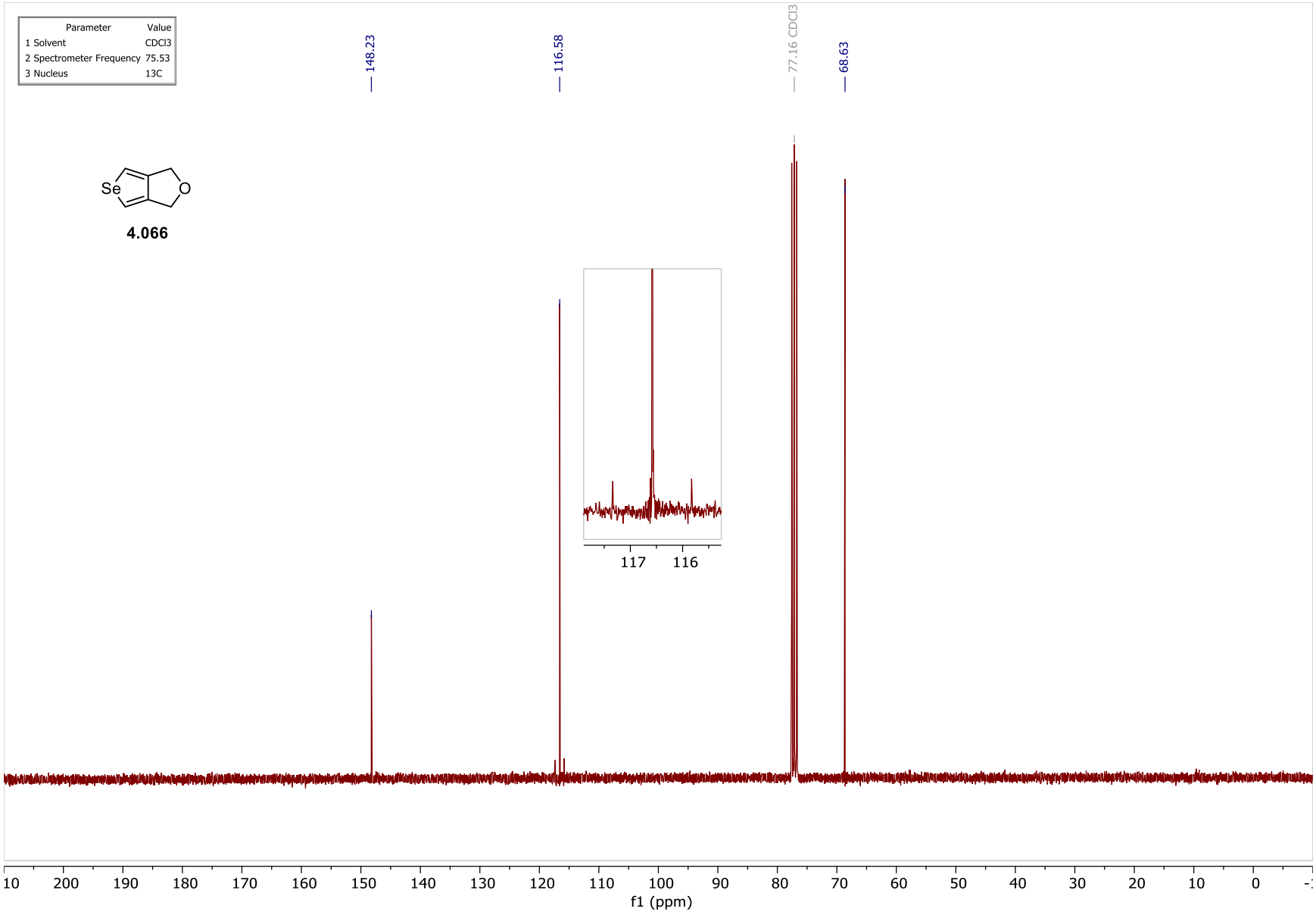
Parameter Value
1 Solvent CDCl3
2 Spectrometer Frequency 75.53
3 Nucleus 13C
148.23
116.58
77.16 CDCl3
68.63
Se
O
4.066
117
116
f1 (ppm)

Parameter	Value
1 Comment	77Se NMR with inverse gated 1H decoupling
2 Solvent	CDCl3
3 Spectrometer Frequency	57.32
4 Nucleus	77Se

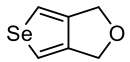

4.066

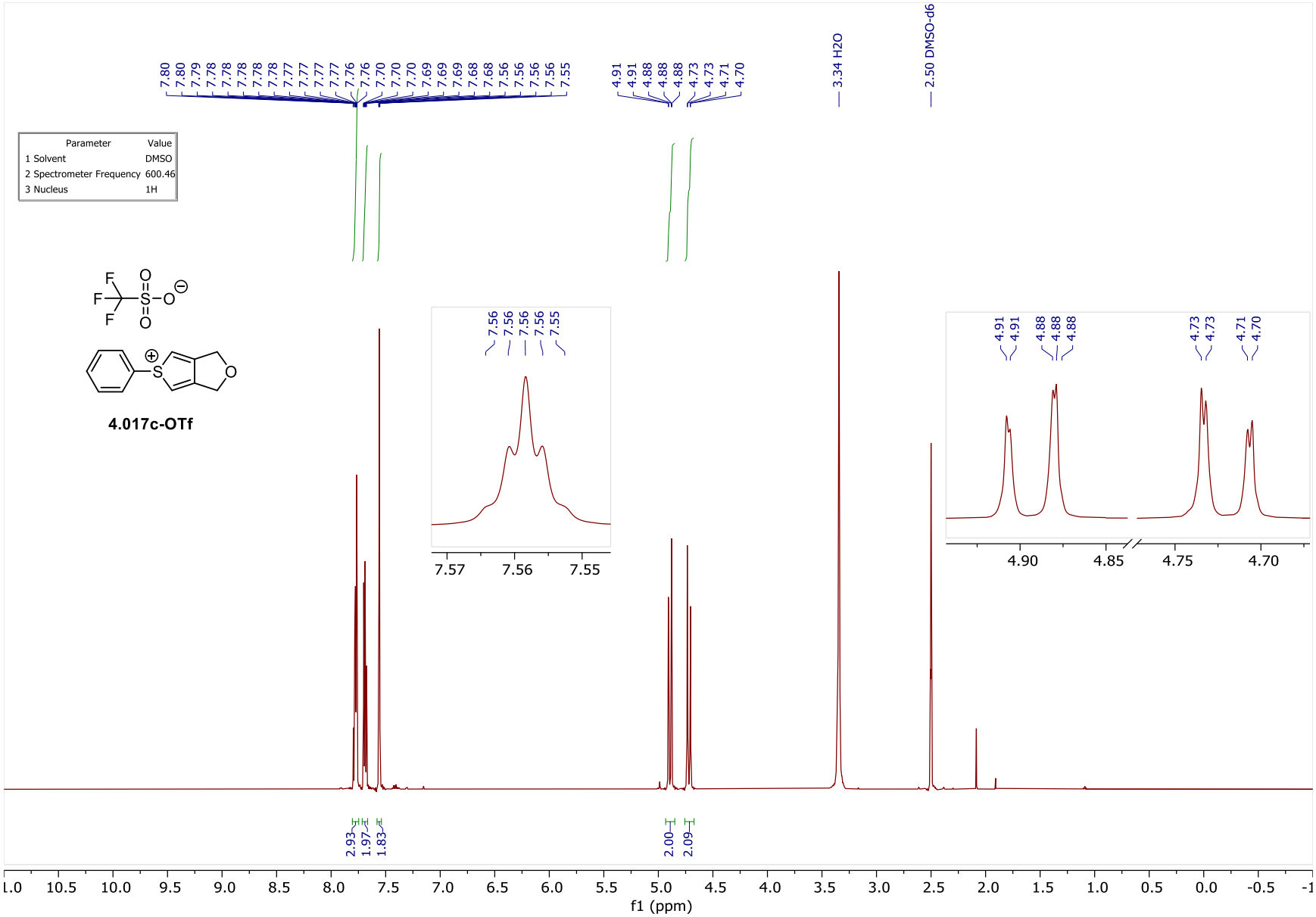
Parameter Value
1 Solvent DMSO
2 Spectrometer Frequency 600.46
3 Nucleus 1H
4.017c-OTf
3.34 H2O
2.50 DMSO-d6
f1 (ppm)

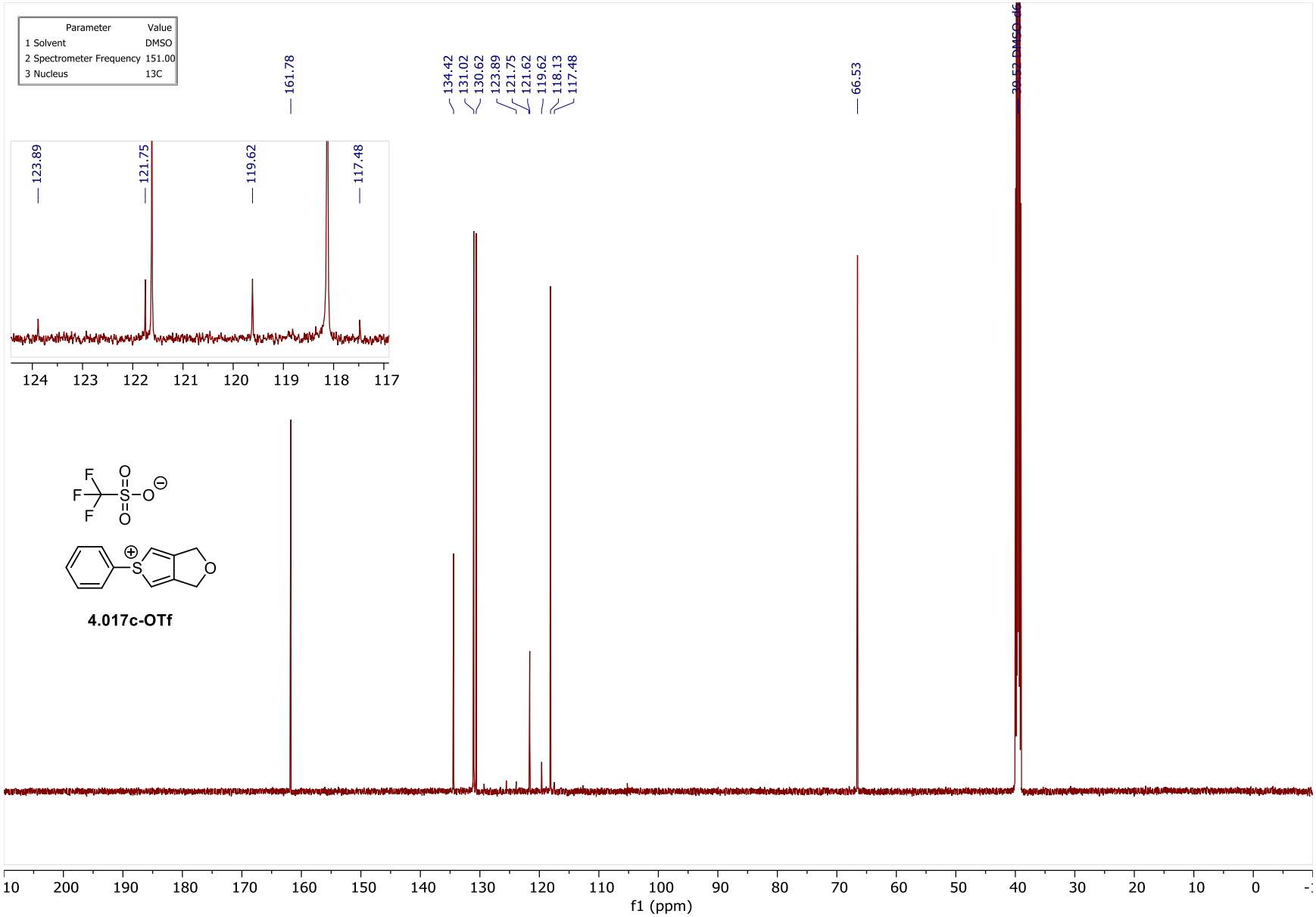
Parameter Value
1 Solvent DMSO
2 Spectrometer Frequency 151.00
3 Nucleus 13C
161.78
134.42
131.02
130.62
123.89
121.75
121.62
119.62
118.13
117.48
66.53
39.52 DMSO-d6
123.89
121.75
119.62
117.48
124 123 122 121 120 119 118 117
4.017c-OTf
f1 (ppm)

Parameter	Value
1 Solvent	DMSO
2 Spectrometer Frequency	282.38
3 Nucleus	19F

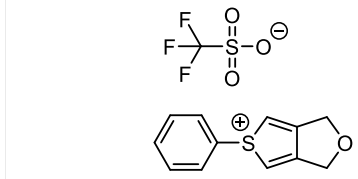

4.017c-OTf

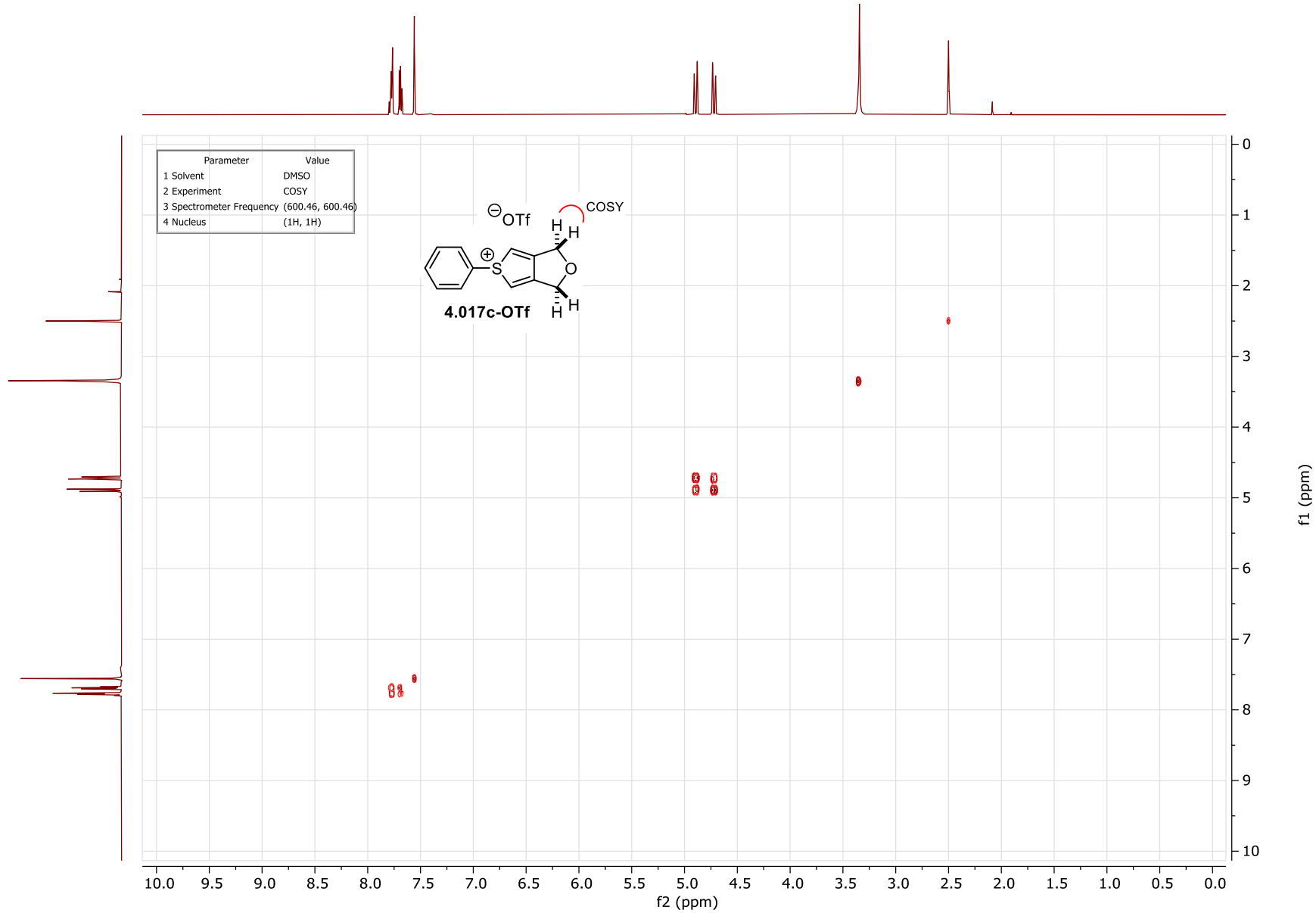
Parameter Value
1 Solvent DMSO
2 Experiment COSY
3 Spectrometer Frequency (600.46, 600.46)
4 Nucleus (1H, 1H)
⊖OTf
COSY
4.017c-OTf
f2 (ppm)
f1 (ppm)

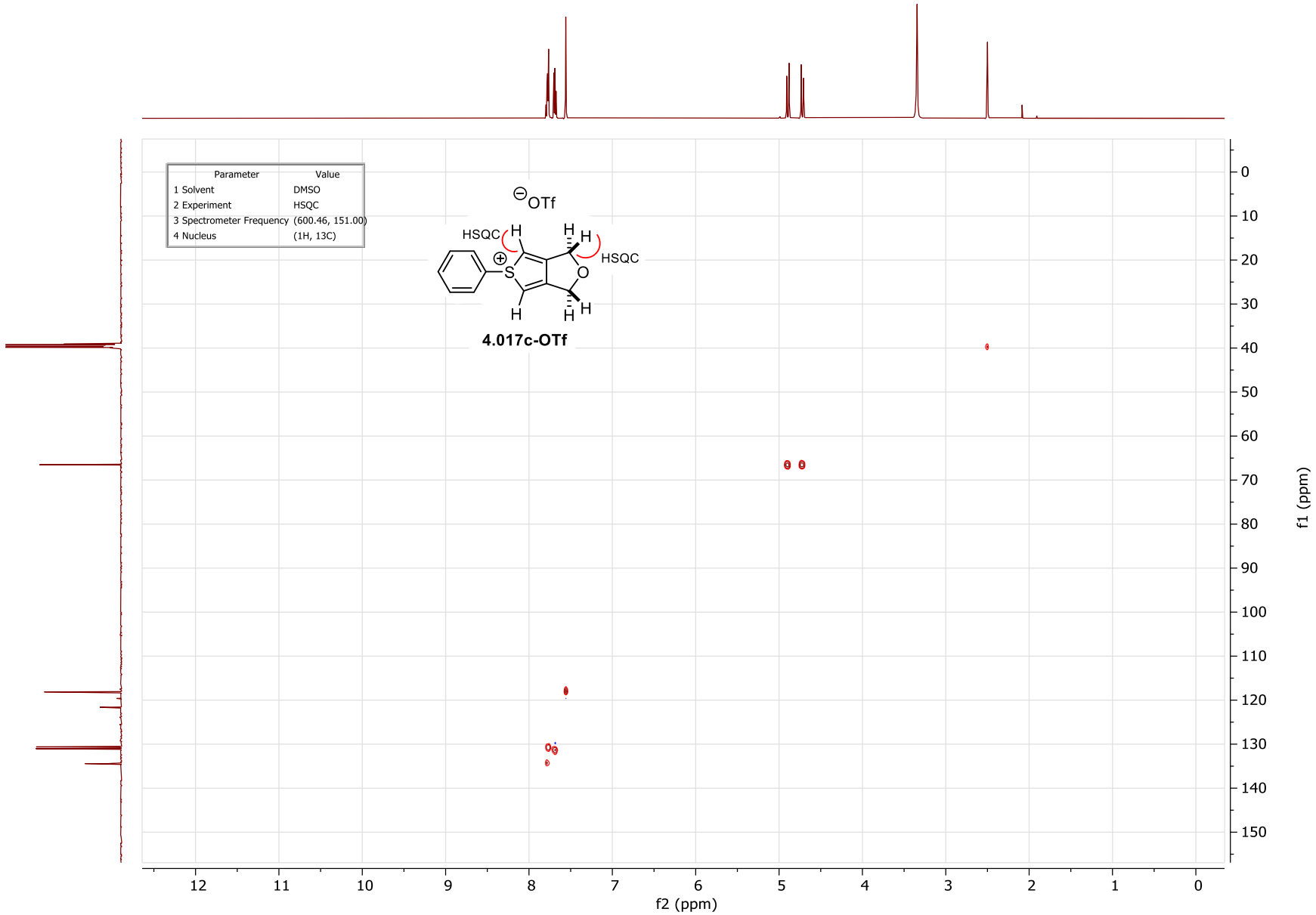
Parameter Value
1 Solvent DMSO
2 Experiment HSQC
3 Spectrometer Frequency (600.46, 151.00)
4 Nucleus (1H, 13C)
⊖OTf
HSQC
HSQC
4.017c-OTf
f2 (ppm)
f1 (ppm)

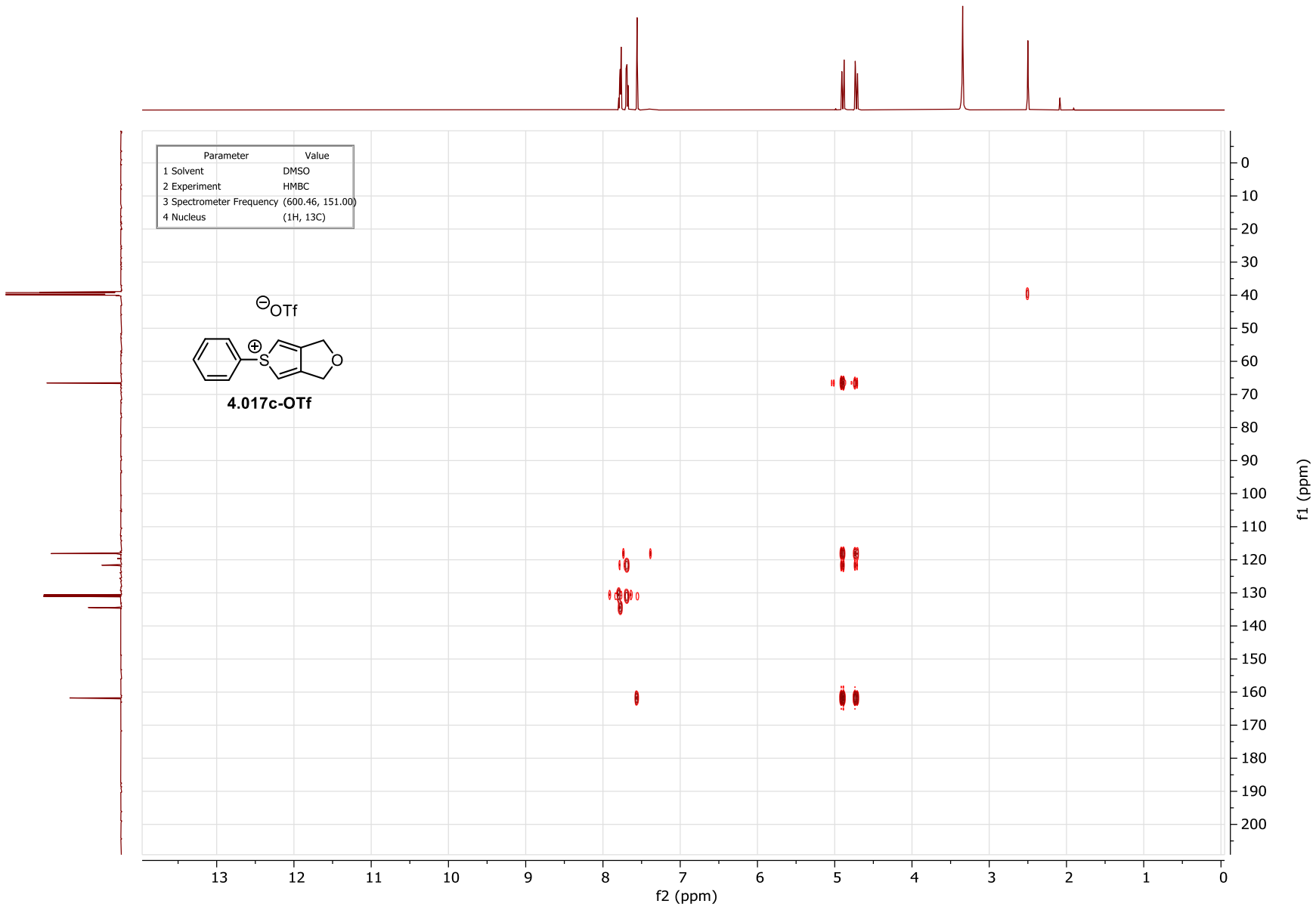
Parameter Value
1 Solvent DMSO
2 Experiment HMBC
3 Spectrometer Frequency (600.46, 151.00)
4 Nucleus (1H, 13C)
⊖OTf
S
O
4.017c-OTf
f2 (ppm)
f1 (ppm)

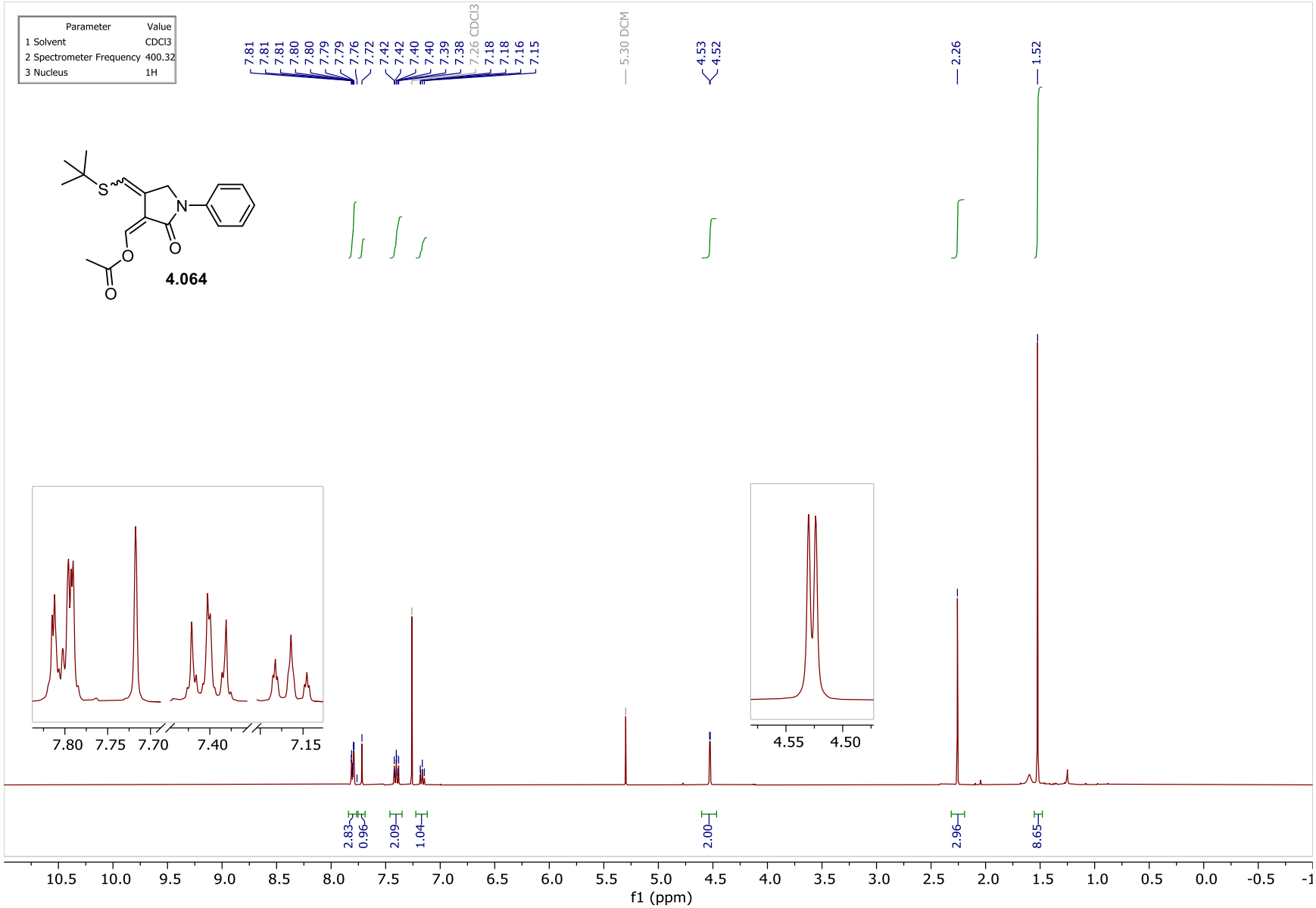
Parameter Value
1 Solvent CDCl3
2 Spectrometer Frequency 400.32
3 Nucleus 1H
7.81 7.81 7.81 7.80 7.80 7.79 7.79 7.76 7.72 7.42 7.42 7.40 7.40 7.39 7.38 7.26 CDCl3 7.18 7.18 7.16 7.15
5.30 DCM
4.53 4.52
2.26
1.52
4.064
7.80 7.75 7.70 7.40 7.15
4.55 4.50
2.83 0.96 2.09 1.04 2.00 2.96 8.65
10.5 10.0 9.5 9.0 8.5 8.0 7.5 7.0 6.5 6.0 5.5 5.0 4.5 4.0 3.5 3.0 2.5 2.0 1.5 1.0 0.5 0.0 -0.5 -1
f1 (ppm)

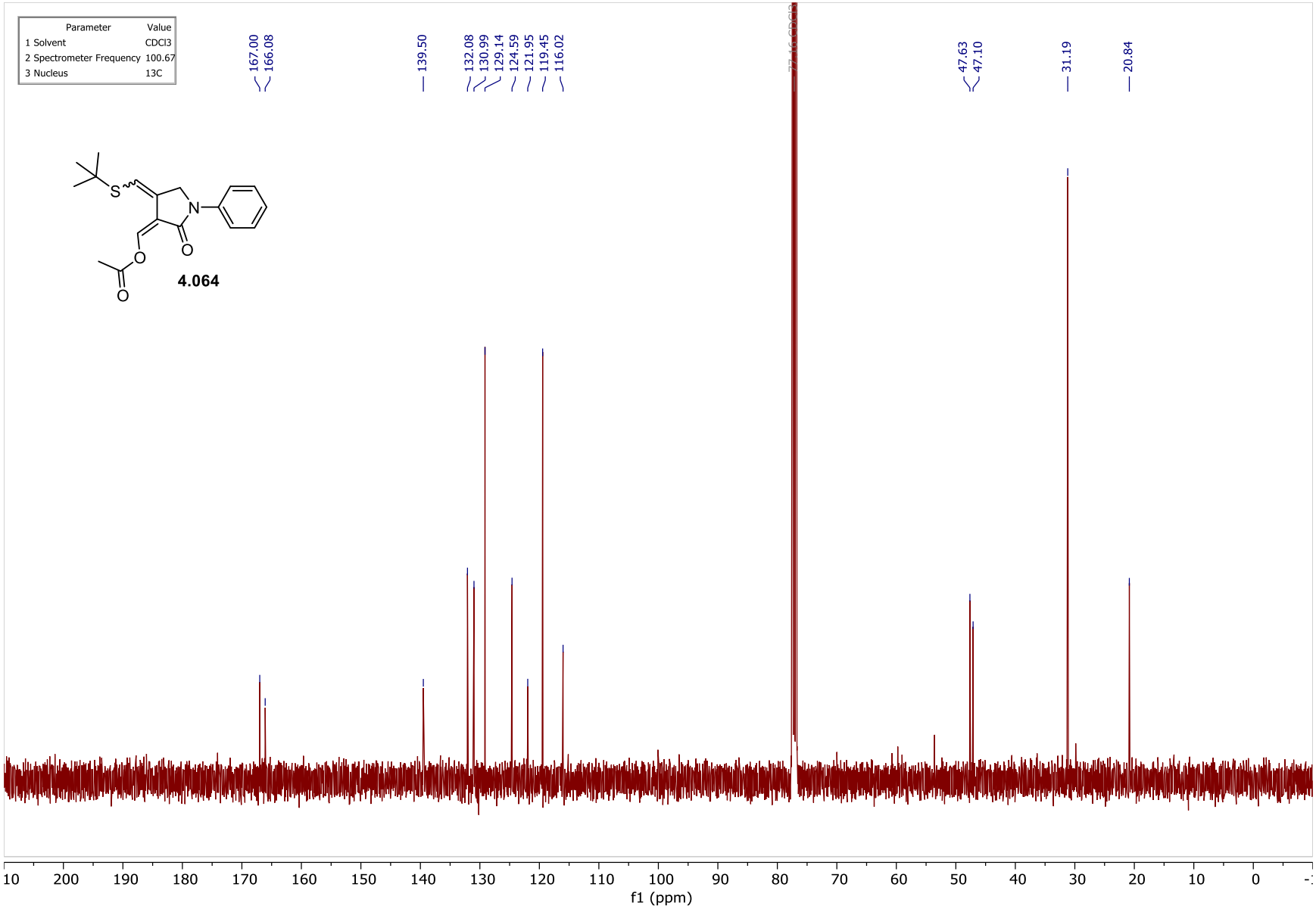
Parameter Value
1 Solvent CDCl3
2 Spectrometer Frequency 100.67
3 Nucleus 13C
167.00
166.08
139.50
132.08
130.99
129.14
124.59
121.95
119.45
116.02
47.63
47.10
31.19
20.84
4.064
f1 (ppm)

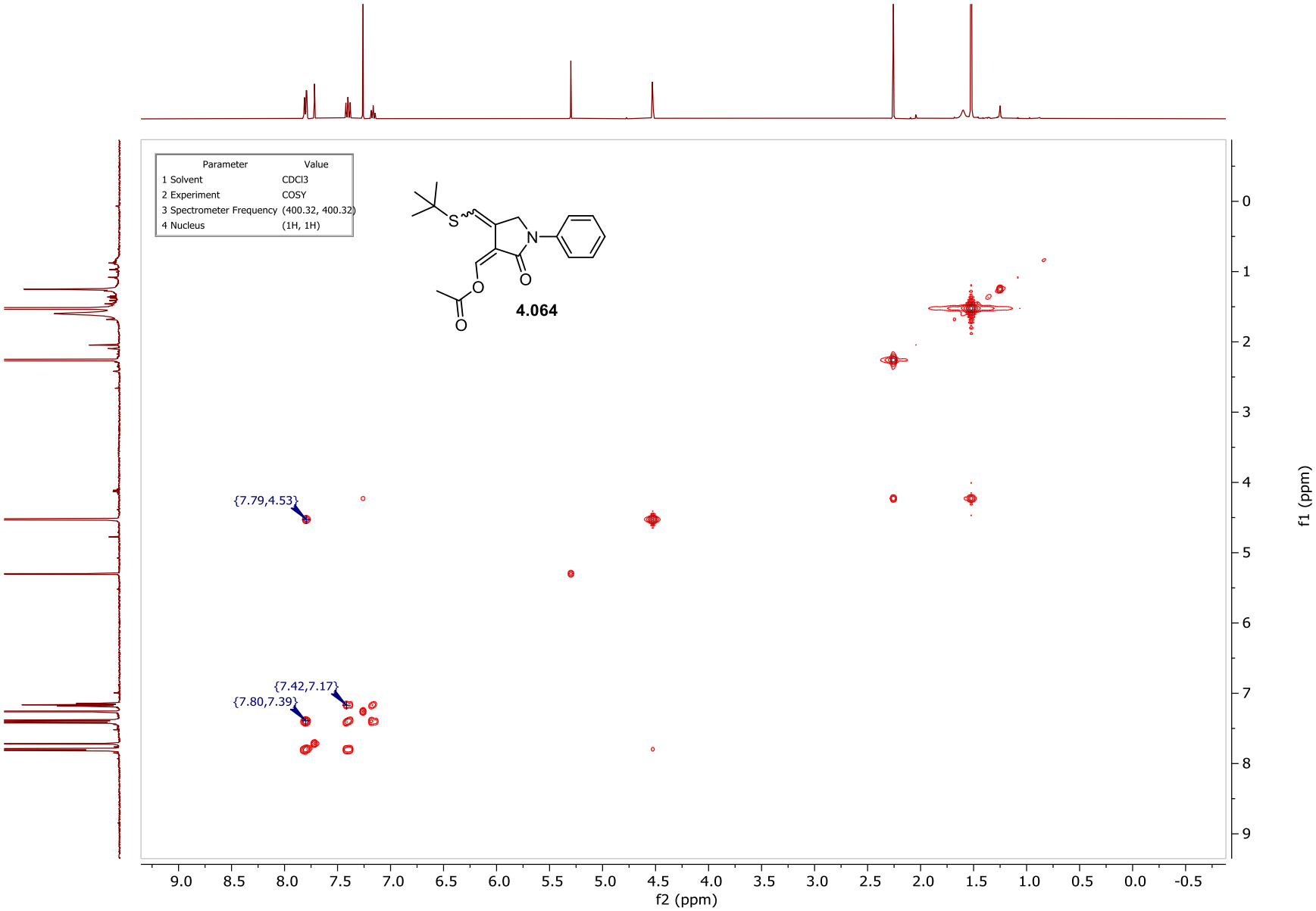
Parameter Value
1 Solvent CDCl3
2 Experiment COSY
3 Spectrometer Frequency (400.32, 400.32)
4 Nucleus (1H, 1H)
4.064
{7.79,4.53}
{7.42,7.17}
{7.80,7.39}
f2 (ppm)
f1 (ppm)

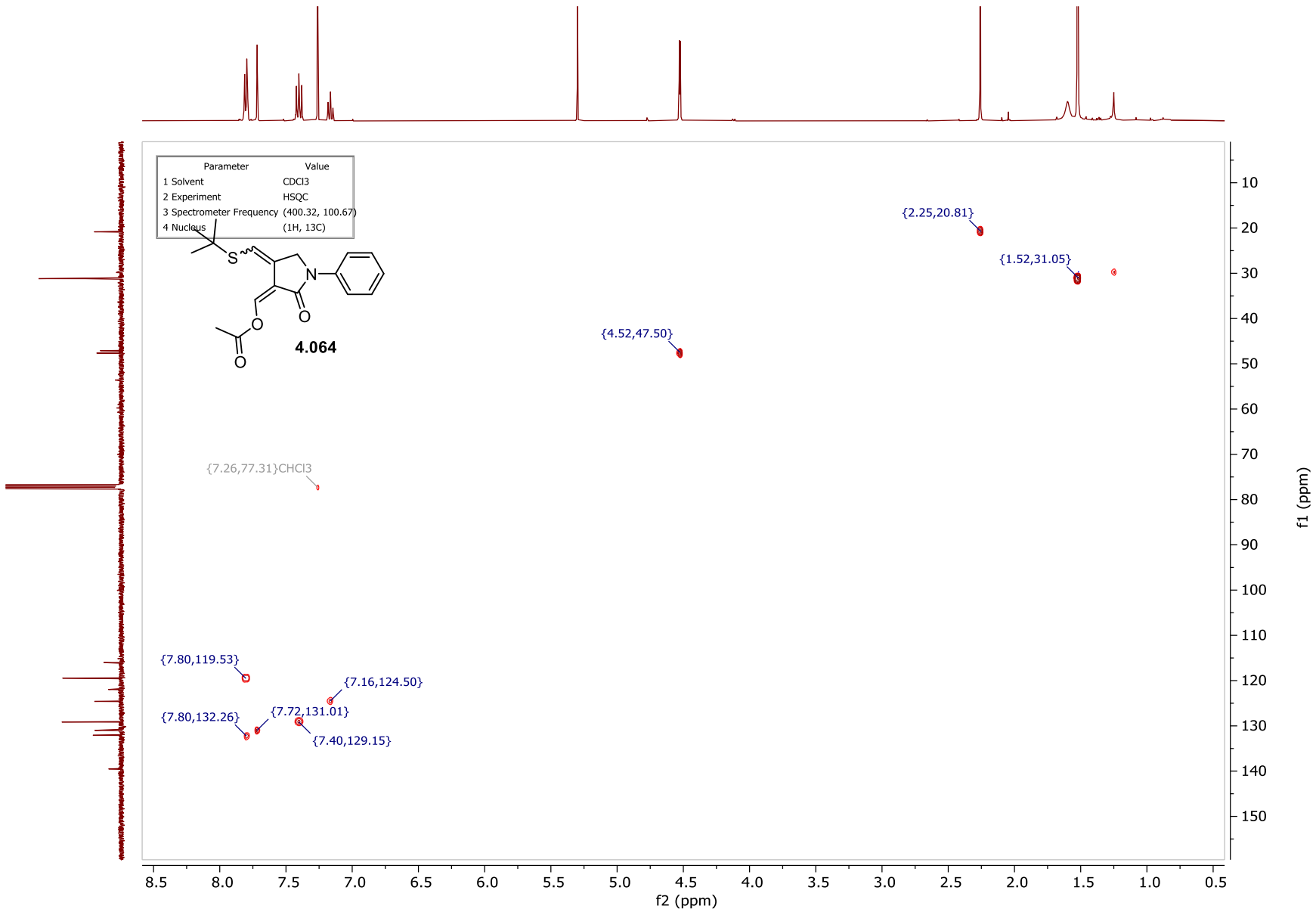
Parameter Value
1 Solvent CDCl3
2 Experiment HSQC
3 Spectrometer Frequency (400.32, 100.67)
4 Nucleus (1H, 13C)
4.064
{2.25,20.81}
{1.52,31.05}
{4.52,47.50}
{7.26,77.31}CHCl3
{7.80,119.53}
{7.16,124.50}
{7.80,132.26}
{7.72,131.01}
{7.40,129.15}
f2 (ppm)
f1 (ppm)

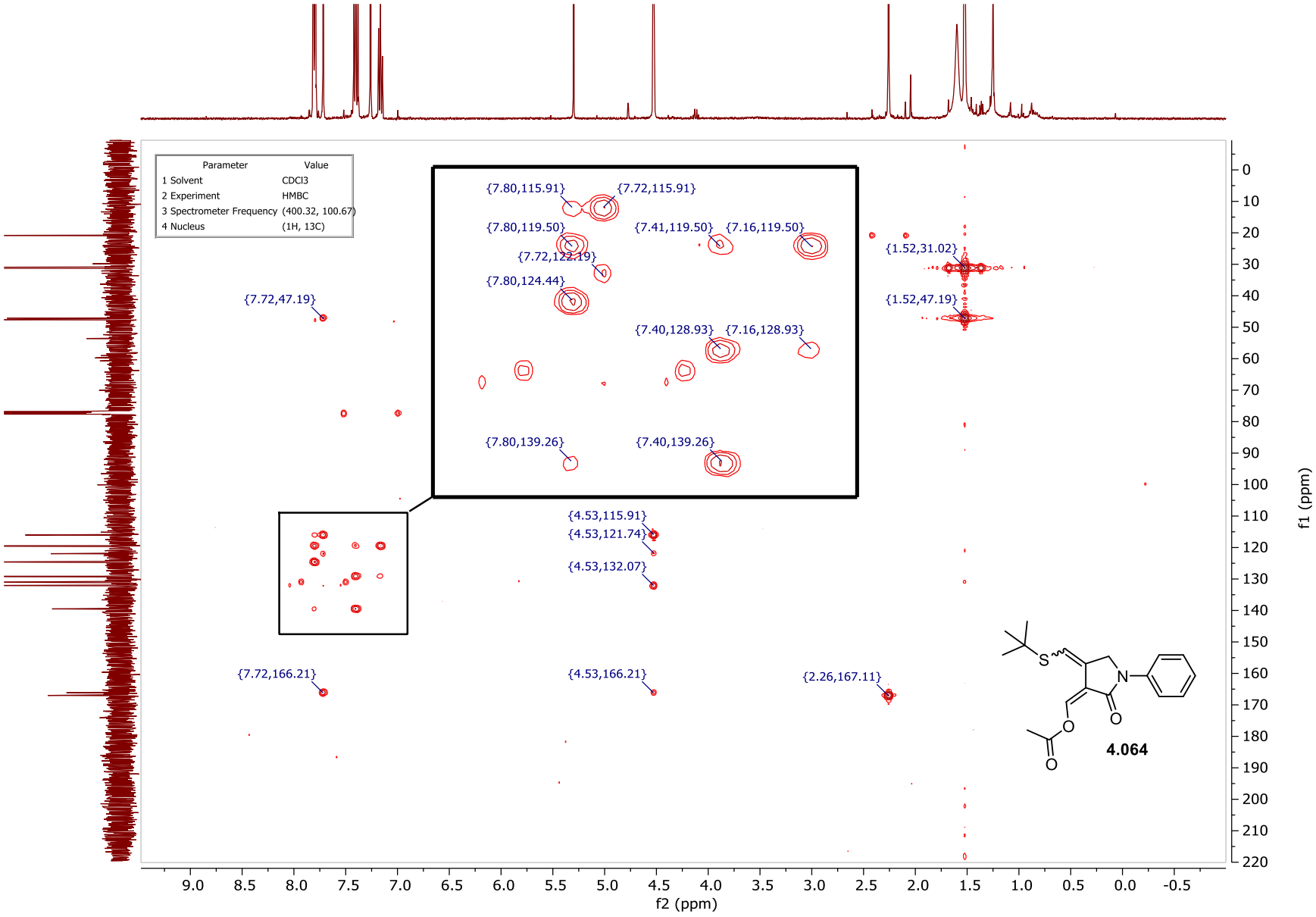
Parameter Value
1 Solvent CDCl3
2 Experiment HMBC
3 Spectrometer Frequency (400.32, 100.67)
4 Nucleus (1H, 13C)
{7.80,115.91}
{7.72,115.91}
{7.80,119.50}
{7.41,119.50}
{7.16,119.50}
{7.72,122.19}
{7.80,124.44}
{7.72,47.19}
{7.40,128.93}
{7.16,128.93}
{7.80,139.26}
{7.40,139.26}
{1.52,31.02}
{1.52,47.19}
{4.53,115.91}
{4.53,121.74}
{4.53,132.07}
{7.72,166.21}
{4.53,166.21}
{2.26,167.11}
4.064
f2 (ppm)
f1 (ppm)

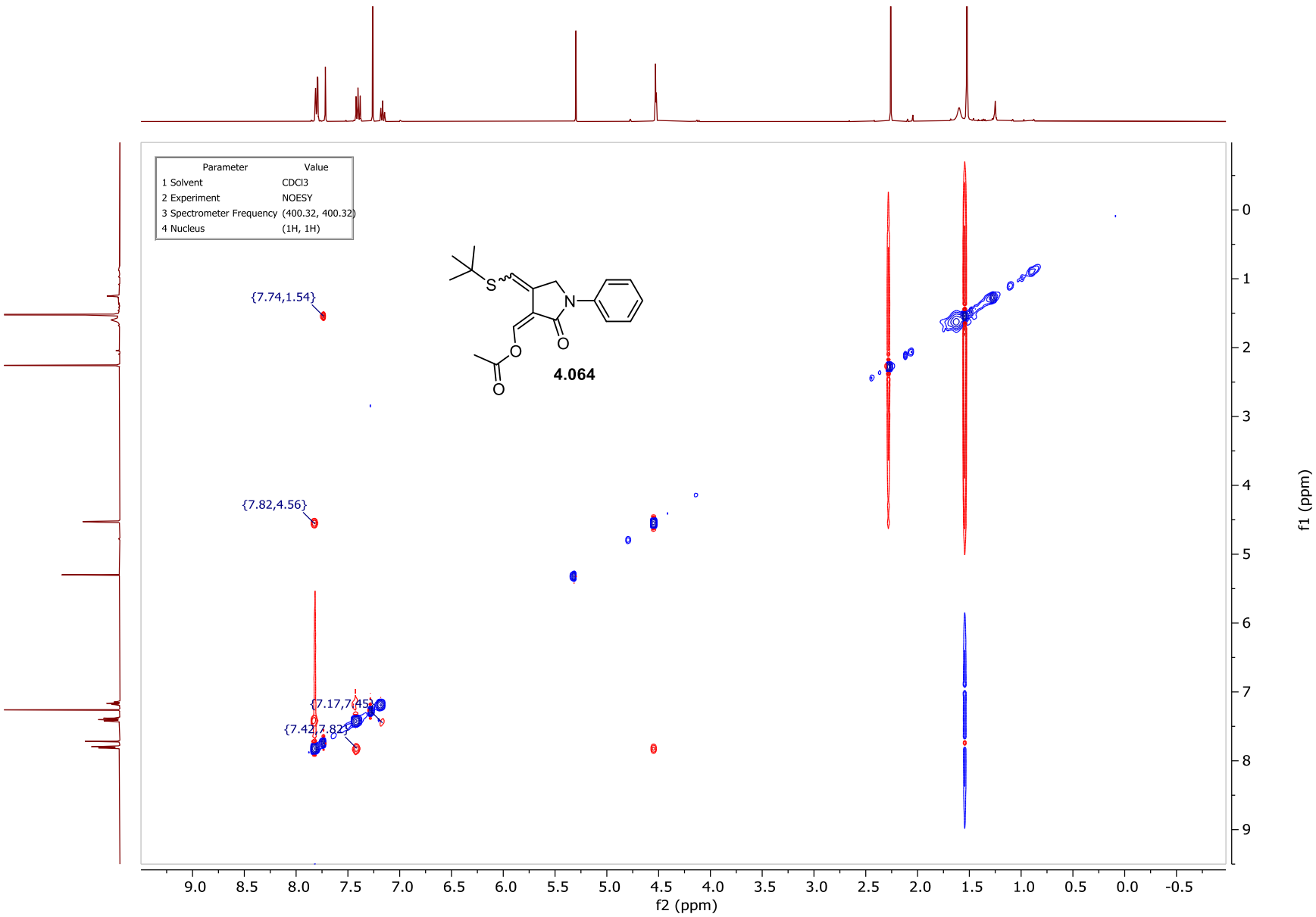
Parameter Value
1 Solvent CDCl3
2 Experiment NOESY
3 Spectrometer Frequency (400.32, 400.32)
4 Nucleus (1H, 1H)
{7.74,1.54}
{7.82,4.56}
{7.17,7.45}
{7.42,7.82}
4.064
f2 (ppm)
f1 (ppm)

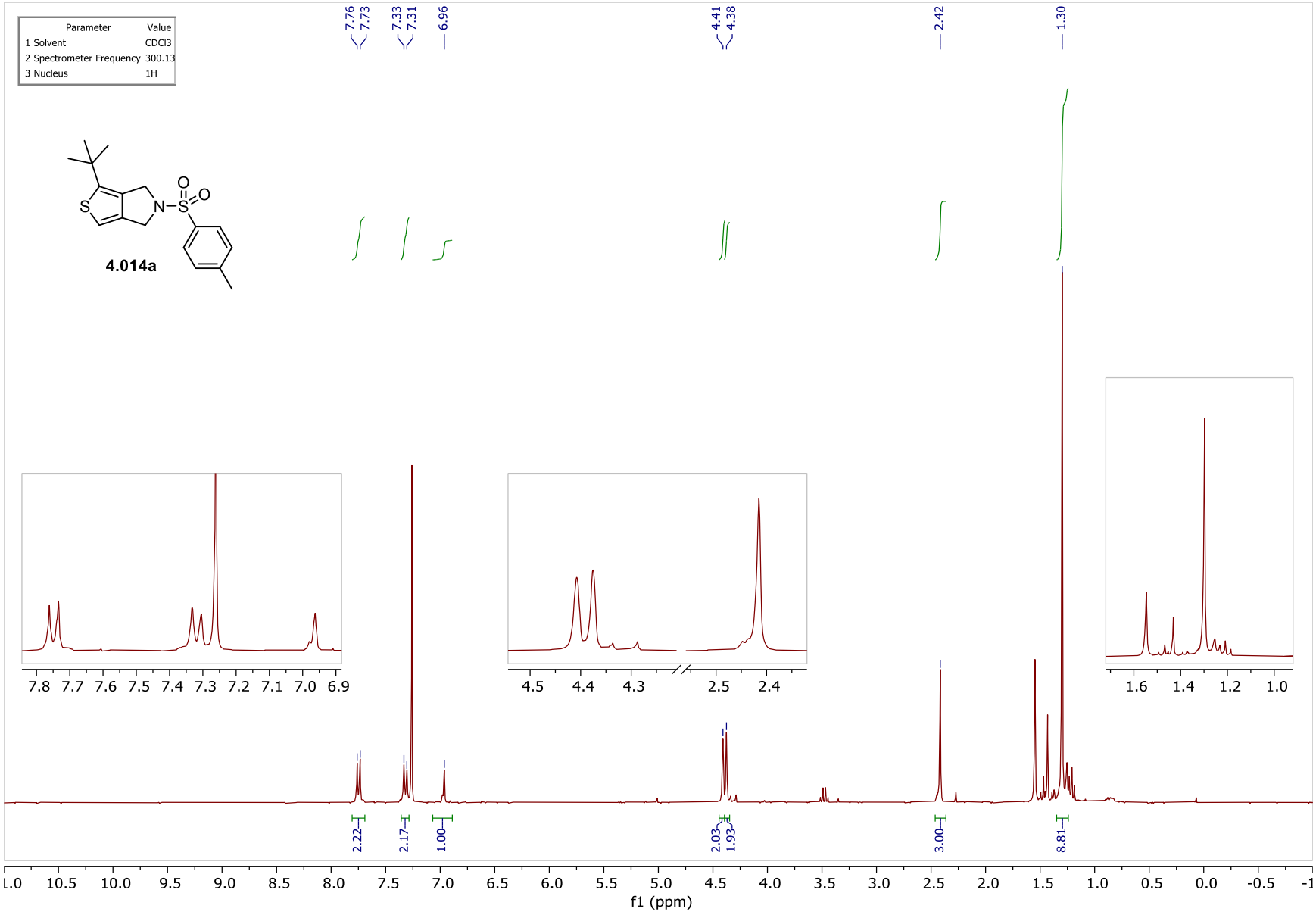
Parameter Value
1 Solvent CDCl3
2 Spectrometer Frequency 300.13
3 Nucleus 1H
4.014a
7.76
7.73
7.33
7.31
6.96
4.41
4.38
2.42
1.30
2.22
2.17
1.00
2.03
1.93
3.00
8.81
f1 (ppm)

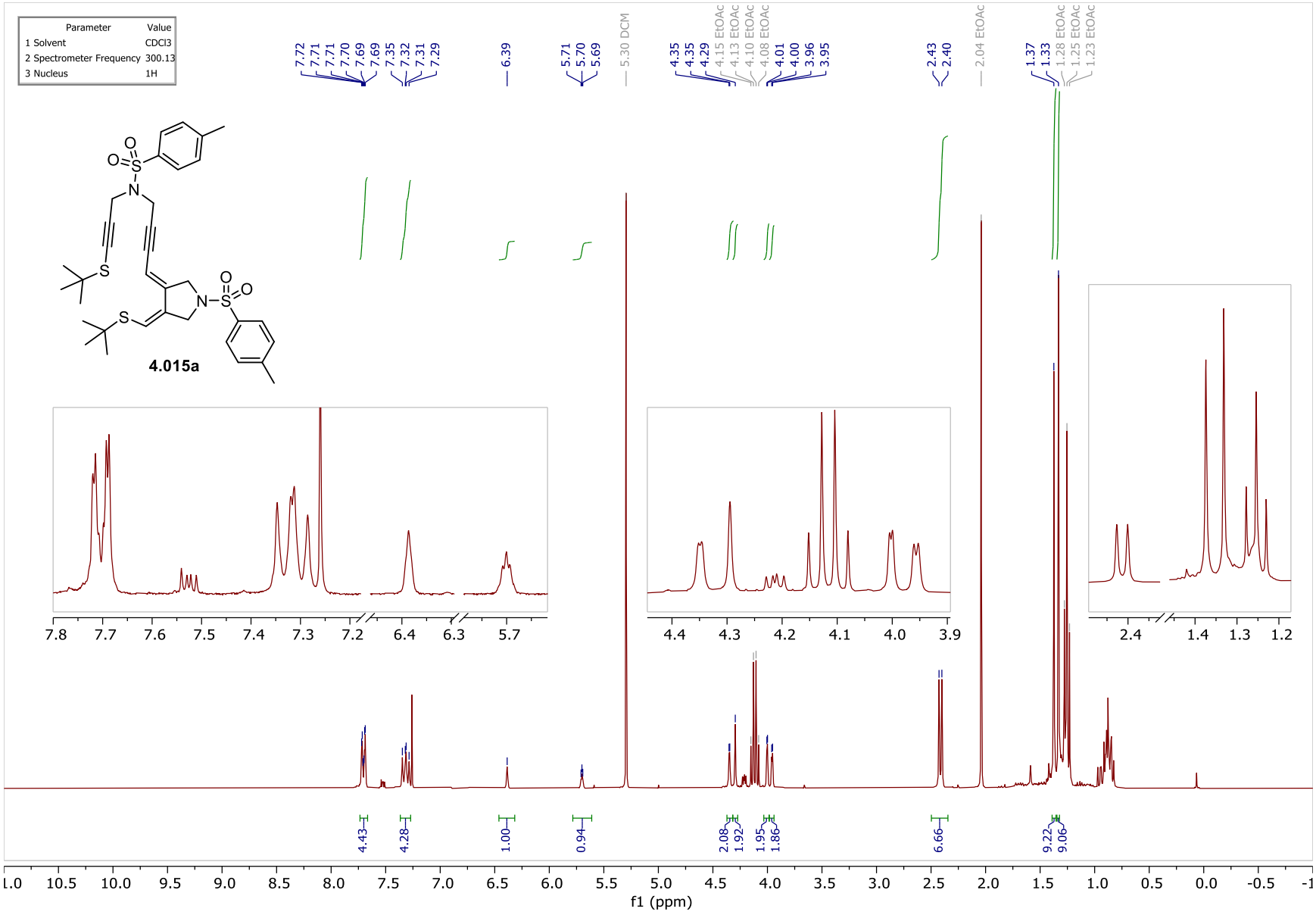
Parameter Value
1 Solvent CDCl3
2 Spectrometer Frequency 300.13
3 Nucleus 1H
4.015a
f1 (ppm)